Green Chemistry and Sustainable Technology

Marcel Schlaf
Z. Conrad Zhang *Editors*

Reaction Pathways and Mechanisms in Thermocatalytic Biomass Conversion I

Cellulose Structure, Depolymerization and Conversion by Heterogeneous Catalysts

Springer

Green Chemistry and Sustainable Technology

Aims and Scope

The series *Green Chemistry and Sustainable Technology* aims to present cutting-edge research and important advances in green chemistry, green chemical engineering and sustainable industrial technology. The scope of coverage includes (but is not limited to):

- Environmentally benign chemical synthesis and processes (green catalysis, green solvents and reagents, atom-economy synthetic methods etc.)
- Green chemicals and energy produced from renewable resources (biomass, carbon dioxide etc.)
- Novel materials and technologies for energy production and storage (biofuels and bioenergies, hydrogen, fuel cells, solar cells, lithium-ion batteries etc.)
- Green chemical engineering processes (process integration, materials diversity, energy saving, waste minimization, efficient separation processes etc.)
- Green technologies for environmental sustainability (carbon dioxide capture, waste and harmful chemicals treatment, pollution prevention, environmental redemption etc.)

The series *Green Chemistry and Sustainable Technology* is intended to provide an accessible reference resource for postgraduate students, academic researchers and industrial professionals who are interested in green chemistry and technologies for sustainable development.

More information about this series at http://www.springer.com/series/11661

Marcel Schlaf • Z. Conrad Zhang
Editors

Reaction Pathways and Mechanisms in Thermocatalytic Biomass Conversion I

Cellulose Structure, Depolymerization and Conversion by Heterogeneous Catalysts

Springer

Editors
Marcel Schlaf
Department of Chemistry
University of Guelph
Guelph, ON, Canada

Z. Conrad Zhang
Dalian National Laboratory for
Clean Energy
Dalian Institute of Chemical Physics
Chinese Academy of Sciences
Dalian, China

ISSN 2196-6982 ISSN 2196-6990 (electronic)
Green Chemistry and Sustainable Technology
ISBN 978-981-287-687-4 ISBN 978-981-287-688-1 (eBook)
DOI 10.1007/978-981-287-688-1

Library of Congress Control Number: 2015951980

Springer Singapore Heidelberg New York Dordrecht London

Printed on acid-free paper

Springer Science+Business Media Singapore Pte Ltd. is part of Springer Science+Business Media (www.springer.com)

Preface

Short carbon chain molecules (C_2–C_9) obtained either directly from sugars, the hydrolysis of starch, or preferably by the controlled breakup of lignocellulosic biomass into soluble components are the only conceivable sustainable source of carbon on the planet that could ultimately replace the fossil hydrocarbons that currently form the base of the chemical industry and hence our technological civilization at large. In particular, the production of polymer components and polymers that are chemically or at least functionally equivalent to those derived from the refining of crude oil would offer ecologic and environmental as well as economic advantages.

The use of sugars, starch, and ultimately lignocellulosic biomass, i.e., forestry (e.g., wood and bark chips, etc.) and agricultural (e.g., straws, husks, stovers, etc.) residues, as a renewable carbon resource will, however, require careful life-cycle analyses of the processes involved. This in turn is critically dependent on a deep and detailed understanding of the mass and energy flows in these processes and hence their mechanisms at the molecular level. Almost "by definition" these processes will have to be catalytic in nature to be ecologically sustainable and economically viable.

The development of new catalysts and catalytic processes that are specifically designed for and adapted to the unique properties of the biomass-derived carbon substrates poses a unique challenge. Due to the abundance of oxygen-containing functional groups, the pentose and hexose sugars and their furanic condensates obtainable from (hemi-)cellulose as well as the phenol propanoid units of lignin are characterized by a high polarity and reactivity that is very different – one could say almost opposite – to that of the traditionally employed alkane and arene sources available from refined crude oil. The fundamental study of the reaction cascades and mechanisms involved in the transformation of oxygenated biomass to value-added chemicals is the first step to meet this challenge.

Focusing on the use of thermochemical and acid-/base- or metal-catalyzed processes only, the two volumes of this book attempt to give an overview of and insights into the specific aspects of this challenge as perceived and formulated by expert contributors research-active in this field.

Volume I is comprised of chapters that address the nanoscale structure of lignocellulose, the application of acid-base reactions and catalysts to the depolymerization of cellulose, the use of heterogeneous hydrogenation catalysts for its direct conversion to polyols, as well as chapters that explore pathways for the metal-catalyzed dehydration and oxidation of sugars and sugar alcohols to furans and carboxylic acids, respectively.

The chapters of Volume II cover the hydrodeoxygenation of sugar-derived substrates by homogenous catalysts systems; the valorization of carboxylic acids, notably lactic acid and its derivatives; a theoretical approach to the elucidation of the conversion pathways of sugars and sugars condensates and their decomposition to humins as well as mechanistic and practical aspects of the conversion and pyrolysis of lignin to functionalized monocyclic aromatics and the pyrolysis of biomass to synthesis gas.

We hope that the insights provided by the different and varied perspectives offered here will convince the readers that a switch to renewable biomass as a key carbon source for the chemical industry will be feasible and does indeed offer a way forward to a more sustainable future.

Guelph, Canada — Marcel Schlaf
Dalian, China — Z. Conrad Zhang

Contents

Contributors

Rik De Clercq Center for Surface Chemistry and Catalysis, Leuven, Belgium

Eva Díaz Department of Chemical and Environmental Engineering, University of Oviedo, Oviedo, Spain

Shi-You Ding Department of Plant Biology, Michigan State University, East Lansing, MI, USA

Michiel Dusselier Center for Surface Chemistry and Catalysis, Leuven, Belgium

Laura Faba Department of Chemical and Environmental Engineering, University of Oviedo, Oviedo, Spain

Atsushi Fukuoka Catalysis Research Center, Hokkaido University, Kita-ku, Sapporo, Hokkaido, Japan

Hirokazu Kobayashi Catalysis Research Center, Hokkaido University, Kita-ku, Sapporo, Hokkaido, Japan

Adam F. Lee European Bioenergy Research Institute, School of Engineering & Applied Science, Aston University, Birmingham, UK

Huixiang Li State Key Laboratory of Catalysis, Dalian National Laboratory for Clean Energy, Dalian Institute of Chemical Physics, Chinese Academy of Sciences, Dalian, Liaoning, China

College of Chemistry and Chemical Engineering, University of Chinese Academy of Sciences, Beijing, China

Ning Li State Key Laboratory of Catalysis, Dalian Institute of Chemical Physics, Chinese Academy of Sciences, Dalian, China

Hongfei Lin Department of Chemical and Materials Engineering, University of Nevada, Reno, NV, USA

Yoshinao Nakagawa Department of Applied Chemistry, School of Engineering, Tohoku University, Sendai, Japan

Salvador Ordóñez Department of Chemical and Environmental Engineering, University of Oviedo, Oviedo, Spain

Jifeng Pang State Key Laboratory of Catalysis, Dalian Institute of Chemical Physics, Chinese Academy of Sciences, Dalian, China

Bert F. Sels Center for Surface Chemistry and Catalysis, Leuven, Belgium

Ji Su Department of Chemical and Materials Engineering, University of Nevada, Reno, NV, USA

Zhijun Tai European Bioenergy Research Institute, School of Engineering & Applied Science, Aston University, Birmingham, UK

Masazumi Tamura Department of Applied Chemistry, School of Engineering, Tohoku University, Sendai, Japan

Keiichi Tomishige Department of Applied Chemistry, School of Engineering, Tohoku University, Sendai, Japan

Aiqin Wang State Key Laboratory of Catalysis, Dalian Institute of Chemical Physics, Chinese Academy of Sciences, Dalian, China

Karen Wilson European Bioenergy Research Institute, School of Engineering & Applied Science, Aston University, Birmingham, UK

Mizuho Yabushita Catalysis Research Center, Hokkaido University, Kita-ku, Sapporo, Hokkaido, Japan

Lisha Yang Department of Chemical and Materials Engineering, University of Nevada, Reno, NV, USA

Xiaokun Yang Department of Chemical and Materials Engineering, University of Nevada, Reno, NV, USA

Tao Zhang State Key Laboratory of Catalysis, Dalian Institute of Chemical Physics, Chinese Academy of Sciences, Dalian, China

Z. Conrad Zhang State Key Laboratory of Catalysis, Dalian National Laboratory for Clean Energy, Dalian Institute of Chemical Physics, Chinese Academy of Sciences, Dalian, Liaoning, China

Mingyuan Zheng State Key Laboratory of Catalysis, Dalian Institute of Chemical Physics, Chinese Academy of Sciences, Dalian, China

Chapter 1
Nanoscale Structure of Biomass

Shi-You Ding

Abstract Plant biomass is a renewable source that can be processed to produce biofuels and biomaterials. The plant cell walls are the major material in biomass. Depending on plant species and the time of harvest, biomass varies in its anatomical structure and chemical composition. This chapter summarizes general structure of the plant cell walls in different plant tissues and plant species, and updates are given from new findings in in situ imaging at nanoscale resolution and real-time changes during biomass deconstruction processes. The physicochemical properties of biomass that affect the efficiency of thermochemical pretreatment and enzymatic hydrolysis are also discussed.

Keywords Plant cell walls • Cellulose • Lignin • Microfibrils • Macrofibrils

1.1 Introduction

Plant biomass has recently got much attention due to its potential to be used as a renewable and sustainable source for producing biofuels and biomaterials. Over the past few decades, conversion technologies have been developed using thermal, chemical, and/or biochemical processes to produce simple sugars, which can then be fermented by microbes to produce ethanol or other chemicals. The major challenge yet to overcome in commercializing these technologies to industrial scale production of biofuels and biomaterials is the relative high cost of current state-of-the-art conversion processes. One of the most promising techniques developed today is the biochemical platform that includes three major steps: thermochemical pretreatment, enzymatic hydrolysis, and microbial fermentation [1]. The efficiency of each these steps can be significantly affected by the source of plant biomass, i.e., plant species, such as grass or wood, and their harvest conditions, such as green plant, dry stover/straw, or wood chip.

S.-Y. Ding (✉)
Department of Plant Biology, Michigan State University, East Lansing, MI 48824, USA
e-mail: SDing@msu.edu

M. Schlaf, Z.C. Zhang (eds.), *Reaction Pathways and Mechanisms in Thermocatalytic Biomass Conversion I*, Green Chemistry and Sustainable Technology, DOI 10.1007/978-981-287-688-1_1

Biomass solids (particles) are composed of primarily the plant cell walls, in which the structural polysaccharides (mainly cellulose and hemicelluloses) and lignins are cross-linked to form complex networks. A deeper understanding of plant cell wall structure and their changes during conversion is critical to further improve the process.

This chapter provides a background of the discussion on plant cell wall features that affect the efficiency of biomass conversion processes. Plant biomass may contain significant amount of extractable materials (extractives), which is out of the scope of this chapter. In this context, only the insoluble structures are discussed. In particular, the nanoscale structures of the plant cell walls based on advanced imaging techniques are reviewed, to provide new insights into the improvement of the state-of-the-art biomass conversion technology toward a cost-effective solution of biomass to biofuels production.

1.2 General Plant Anatomy and Plant Cell Wall Structure

A mature plant body has three vegetative organs: stem, leaf, and root. In a vascular plant, these organs are composed of three tissue systems: the dermal, the vascular, and the ground. The relative distribution of the vascular and ground tissues varies in plant organs. Although biomass may contain stem, leaf, and root, the majority of the material is the stem. Figure 1.1 shows the stem structure of three example plants, representing the major types of biomass currently used in the conversion processes. Corn stover represents an agricultural by-product from annual crops, which are left residues after harvest of cereal grain; similar biomass includes straw from rice, wheat, barley, oats, etc. They are normally dry and dead plants. Switchgrass represents a perennial grass that can be used as an energy crop, which is normally harvested as wet green plant. Poplar is a fast-growing energy crop widely available on fallow lands to provide an ample supply of biomass [2–4]. It has also been regarded as a model hardwood species for breeding modified genotypes for bioenergy applications [5].

In each plant tissue, a variety of cell types arranged differently to facilitate their function. During plant development, cell walls are deposited layer by layer. The first layer formed outside of the protoplast is the primary wall (PW), which is flexible to allow cell expanding and elongating. In many cell types, additional wall layers are deposited from the outside of the protoplast inward to enhance the mechanical property of the cell wall, which is called secondary wall (SW). In some cell types, the secondary wall may undergo lignification to further strengthen the mechanical property in supporting tissues and in water conducting elements. The cell is permanently dead when the wall is fully lignified. The triangle region formed by three contiguous cells is called cell corner, and middle lamella refers to the area between the PWs of two cells.

Although plant biomass contains all these types of cell walls, the relative amount and anatomical arrangement vary significantly in different plant species and harvest

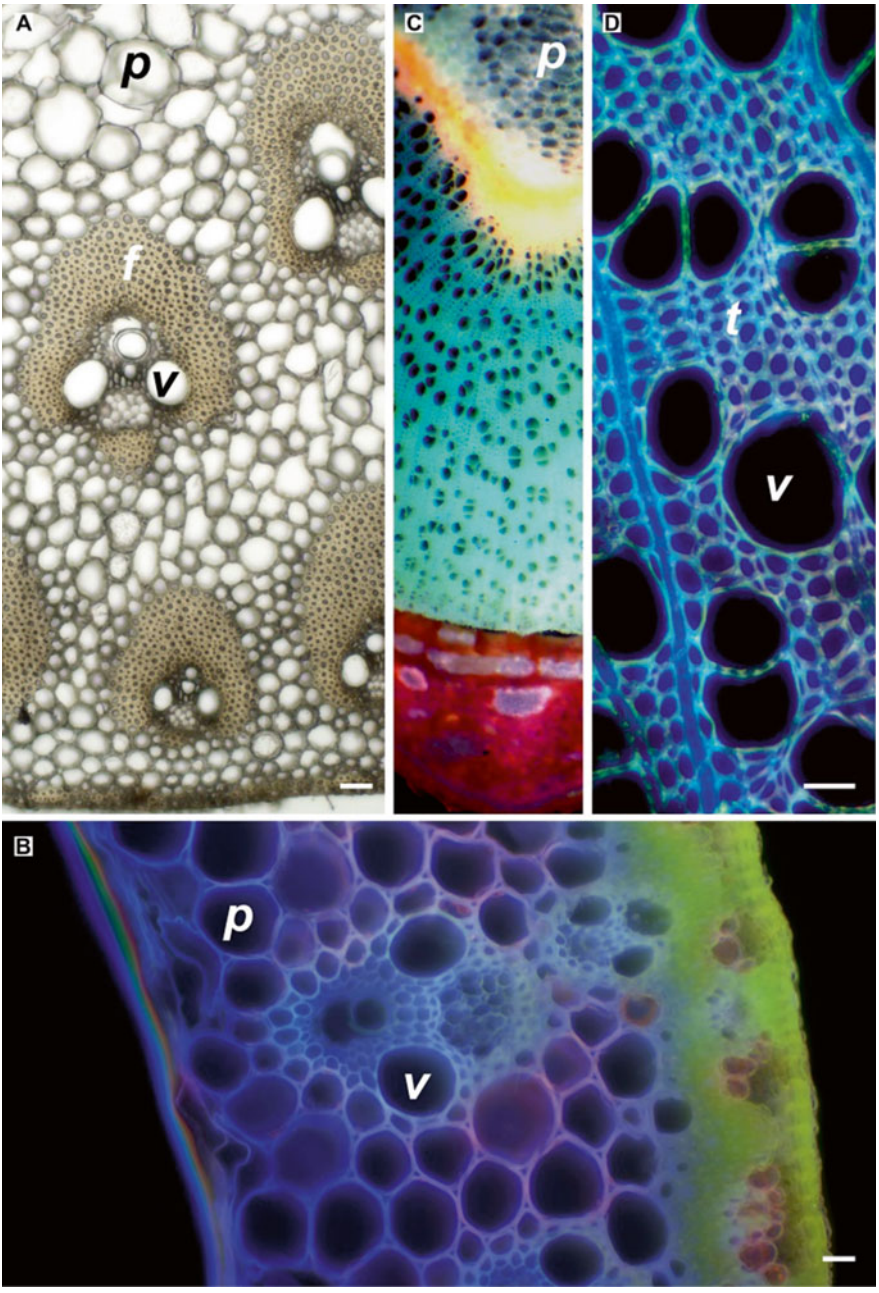

Fig. 1.1 Cross section of plant stems from representative biomass feedstock. (**a**) Field-dry corn stover. (**b**) Switchgrass, green plant. (**c**) One-year poplar. (**d**) Zoom-in of (**c**) showing the xylem tissue. *p* parenchyma, *v* vessel, *f* fiber, *t* tracheid. *Bar* = 50 μm

time. Based on the wall thickness and level of lignification, there are generally three types of walls in a mature plant. The PW is thin (approximately 100 nm) and non-lignified, and the cell normally retains active protoplasts and can be induced to resume meristematic activity. There are two types of SWs. The parenchyma-type secondary wall (pSW) is in the ground tissue (i.e., parenchyma and collenchyma); the wall can be significantly thickened to function as supporting tissue. These cells are normally active and the wall remains non-lignified during vegetative growth. After plant starts reproductive growth, the thickened wall of parenchyma and collenchyma in stem may be partially lignified from the side of the cell corner and middle lamella to reinforce the stem to handle heavy seeds, such as in grass plants. Full lignification only occurs in sclerenchyma fibers and tracheary elements (tracheids and vessels), which is called sclerenchyma-type secondary wall (sSW). The sSW is thick normally ranges from 5 to 10 μm, and the innermost side of the sSW is further covered by a unique layer of substance formed largely by lignin precursors, called warty layer [6].

1.2.1 Corn Stover

Maize (*Zea mays*) is a typical monocotyledonous plant, which is well studied in anatomy [7]. The stem contains scattered vascular bundles surrounded by ground parenchyma (Fig. 1.1a). Full lignified walls are the majority of biomass material, including a few layers of vascular bundle sheath fibers, two to four large vessel elements and tracheids between them, and the sclerenchyma fibers in the rind area under epidermis. The parenchyma walls are partially lignified, which is different from living plant. When maize undergoes vegetative growth, these parenchyma walls may be thickened, but are non-lignified. Lignification of parenchyma walls may occur after productive growth, particularly in the cells close to the rind area, resulting higher lignin content in these walls compared with that in pith parenchyma (in the middle of the stem). Non-lignified walls only exist in one layer of parenchyma around the vascular bundle sheath, a few cells that connect the stomata (in epidermis) to the vascular bundle, and cells in the phloem tissue.

1.2.2 Switchgrass

Biomass feedstock can be obtained from agricultural residues and forestry wastes; another potential source is dedicated energy crops – plants that can grow on marginal lands. The perennial grass, switchgrass (*Panicum virgatum*), is one of the popular candidates for this purpose. Research has shown that biomass yield reaches the maximum when switchgrass grows up to anthesis (flowering or productive growth) [7]. Figure 1.1b shows the cross-section of switchgrass stem, which is similar with maize in vascular bundle arrangement, and cell types, except the center pith

area is destroyed and forms large empty air space. Most of parenchyma cell walls between vascular bundles are thickened and partially lignified. Since the plant is harvested in green, there are chlorenchyma tissues (green cells) that can be seen under the epidermis, which are non-lignified.

1.2.3 Poplar

Fast-growing trees have also been considered to be a great potential to be used as biomass feedstock. Woody crops have some advantages, especially hybrid poplar (*Populus* spp.), for its ability to produce a significant amount of biomass in a short period of time and its relative high-cellulose and low-lignin contents [8]. The anatomy of wood plant is dramatically different from monocotyledonous grasses. The vascular tissue is arranged as ring structure (Fig. 1.1c). The majority of biomass is the secondary xylem tissues, containing predominantly tracheary elements (tracheids and vessels) (Fig. 1.1d), which have thick secondary walls and fully lignified. There are non-lignified walls in the pith and axial parenchyma and phloem tissue, but in terms of biomass, they are negligible.

1.3 Cellulose, Hemicelluloses, and Lignin

There are three major structural polymers that constitute the plant cell walls. Cellulose is the most abundant biopolymer on earth; it accounts for 40–50 % of the dry weight of the plant cell walls and is the major sugar source for biofuels production. The chemical composition of cellulose is simple containing a number of linear β-(1,4)-glucan chains. It often forms a fibril structure, called cellulose elementary fibril (CEF), in which the glucan chains are packed in parallel through intra- and inter-hydrogen bond networks. The exact number of glucan chains in a given CEF is still under debating [9]; a 36-chain model of the CEF in higher plants is widely accepted, which is deduced from a proposed model of rosettes (terminal synthesizing complexes) that contain 36 cellulose synthases [6, 10, 11]. In this CEF model, the 36 chains form a hexagonal shape in cross section, containing three layers: 18 surface chains, 12 transition chains, and 6 core chains (Fig. 1.2). Based on the crystalline structure of cellulose [12, 13], the CEF has two hydrophobic faces, or planar faces formed by glucose rings, and four hydrophilic faces formed by hydroxyls. Imaging studies on cell walls from different cell types using atomic force microscopy (AFM) have revealed a uniform structure of CEF with dimensions measured at 3×5 nm, which is consistent with the proposed 36-chain model [6]. In many cases, several CEFs may form large bundles, called macrofibrils, in which the CEFs interact through hydrophilic faces to form ribbonlike structure. The number of the CEF in the macrofibril varies in different cell types and cell wall layers (Fig. 1.3), which is a result of cellulose synthases, cell elongating and expanding during development [11].

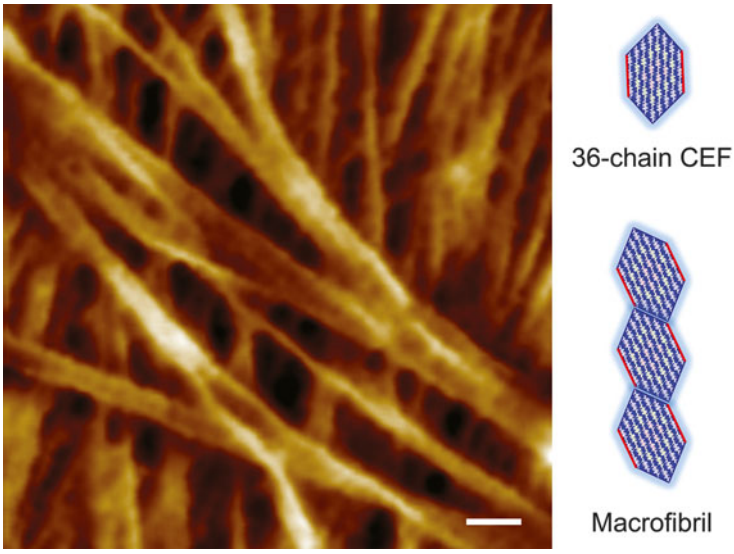

Fig. 1.2 Cellulose elementary fibril and macrofibril. In higher plant, cellulose is synthesized by a membrane-associated complex, called rosettes, that is proposed to contain 36 cellulose synthase isoforms, catalyzing the synthesis of 36-chain cellulose elementary fibril (*CEF*). In the CEF, the two hydrophobic faces are highlighted with *red lines*, and three layers of cellulose chains are illustrated in different color, i.e., 18 surface chains (*blue*), 12 transition chains (*green*), and 6 core chains (*pink*). *Left*: Atomic force micrograph of parenchyma cell wall from maize (Reprinted from Ding et al. [11], with permission from AAAS), showing the CEFs and the macrofibrils in the inner wall surface. *Bar* = 10 nm

The arrangement of the CEFs/macrofibrils is different in cell types. Normally, in the primary wall, the CEFs form large ribbonlike macrofibrils (Fig. 1.3a) that appear to be disorganized. In the thickened secondary walls, the CEFs/macrofibrils form layers. They appear to be parallel with different orientation in each layer (Fig. 1.3b–d).

Hemicelluloses are a class of branched or unbranched polysaccharides, composed of a wide variety of sugar residues linked with different glycosidic bonds, and sometimes including sugar acids and noncarbohydrate subunits. In contrast to the insoluble fibrillar cellulose, the heterogeneous structure of hemicelluloses makes them normally soluble and relatively easy to be chemically and enzymatically hydrolyzed. Some hemicelluloses, such as xyloglucan, have the same backbone structure as cellulose, i.e., β-(1,4)-glucan, which may facilitate the interaction

Fig. 1.3 (continued) wall after lignin removal. **e** Schematic illustration of the secondary cell wall showing the interaction between the CEF, hemicelluloses (*H*), and lignins (*L*). *Bar* = 50 nm (**a**–**d**) and 2 nm (**e**) (**a**–**d**) are from Ding et al. [11], reprinted with permission from AAAS, and **e** from Zeng et al. [14], Reprinted with publication with permission from Elsevier

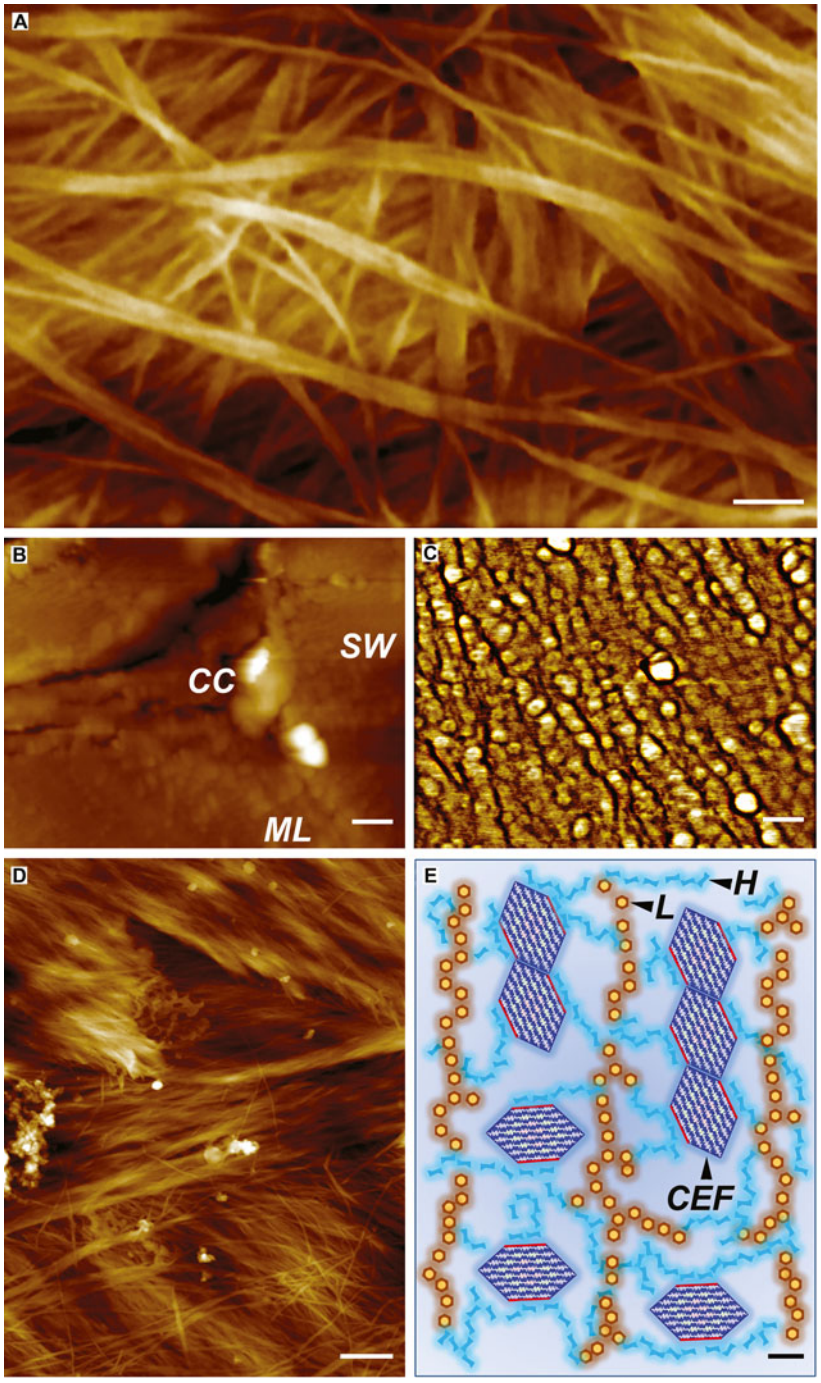

Fig. 1.3 Cellulose elementary fibrils (*CEFs*) and macrofibrils in primary and secondary cell walls. (**a**) Ribbonlike macrofibrils in untreated maize primary wall. (**b**) Cross section of fiber cell walls showing the cell corner (*CC*) and middle lamella (*ML*) area. (**c**) Zoom-in structure of (**b**) in the secondary wall (*SW*) area showing the "ends" of the CEFs and macrofibrils. (**d**) Layers of secondary

between cellulose and hemicelluloses, and serve as bridge between the CEFs. The branching and side groups of hemicelluloses may also form covalent bonds to other cell wall polymers, such as pectin and lignins in lignified walls.

Lignins are the second abundant natural material next to cellulose, which include many organic polymeric substances containing aromatic alcohols in the plant cell wall. Due to their hydrophobic nature when polymerized, it is believed that lignin is evolved during transition of plants to the land habitat with limited water supply, by sealing the pores of the cell walls, especially in water conducting elements, such as vessels and tracheids. Lignins may also function as mechanical support and protection of structural polysaccharides against natural microbial attack. In spite of their overall abundance, the structure of native lignins is poorly understood. What we know today is that lignins are highly branched polymers consisting primarily of three units: guaiacyl (G), sinapyl (S), and p-hydroxyphenyl (H) units. Lignins form covalent bonds with hemicelluloses and pectins, but no direct interaction with cellulose (Fig. 1.3e). Lignins have unique strong aromatic Raman vibration band at 1600 cm^{-1} [15–18], which can be semi-quantified using stimulated Raman scattering microscopy (Fig. 1.4).

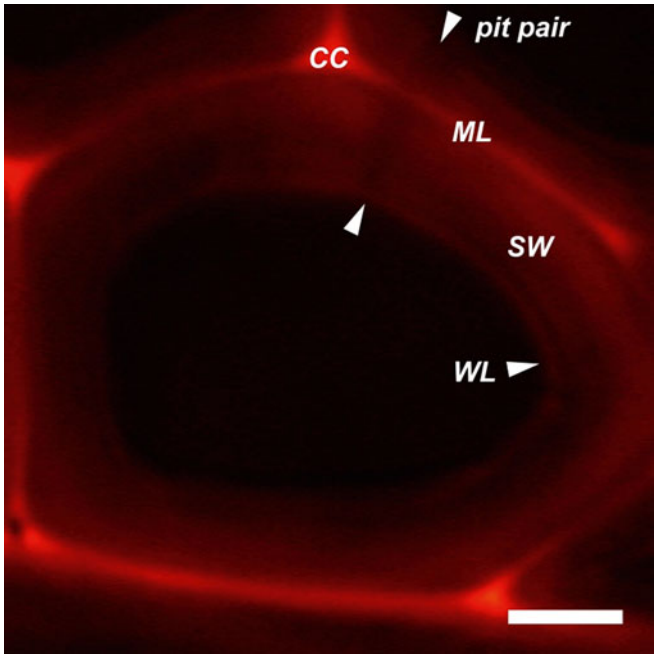

Fig. 1.4 Fully lignified poplar tracheid cell wall. The image was taken by stimulated Raman scattering microscopy based on the aryl ring stretch at 1600 cm^{-1} of lignins (From Zeng et al. [14], reprinted with publication with permission from Elsevier). Lignins are unevenly distributed in cell wall layers, highest lignin content in the cell corner (*CC*) and middle lamella (*ML*) areas; the warty layer (*WL*) also has relatively high-lignin content, and the secondary wall (*SW*) has a gradient lignin distribution from outside (*high*) to inner side (*low*)

1.4 Pretreatment

Although there are various amounts of non-lignified cell walls in biomass, the majority of biomass materials are fully lignified sclerenchyma-type secondary walls. Lignin content differs in cell wall layers; highly concentrated lignins in the cell corner, compound middle lamellae areas, and warty layer are observed. The sSWs are sealed completely, except the pit pair (Fig. 1.4). Inside the wall, lignins form networks between cellulose microfibrils. Such lignin shield at the tissue and microfibril levels must be broken down to allow efficient cellulase enzymes access to cell wall polysaccharides during saccharification process. Currently, many pretreatment technologies have been developed using alkaline or acid chemicals, and sometimes at elevated temperatures. Most of these thermochemical processes hydrolyze hemicelluloses or break down the linkage between hemicelluloses and lignins; under high pressure lignins are also extruded from the cellulose/cellulose microfibril network and redeposit on cell wall surface as lignin-carbohydrate complexes, such as the lignin droplets seen after dilute acid pretreatment [14]. Other pretreatment may aim to depolymerize lignins to produce small molecules that can be later solubilized by solvents. Nevertheless, the efficiency of pretreatment primarily relies on the change of lignins in the cell walls – either break down or delocalizes them from the microfibril network (Fig. 1.5).

The anatomical structure of plant tissue (Fig. 1.6) may affect the efficiency of thermochemical pretreatment. Biomass material can be considered as bundles of thick-wall straws (fully lignified fibers and tracheary elements) and thin-wall boxes (non- or partially lignified parenchyma). Pretreatment is normally performed under conditions of high temperature and short time, and the issue of mass and heat transfer, especially when pretreatment under aqueous conditions, is well known. There are two pathways for pretreatment chemicals to penetrate into the cell walls. The first pathway is through intercellular air spaces and the natural porosity of the cell walls, such as pit pairs. The second pathway is through the broken surfaces. Biomass particles (sub-inches) are normally significantly larger than a single plant cell that ranges from tens to several hundred micrometers; therefore, most of the cells in biomass particles are unbroken and sometimes fill with air. Pretreatment chemicals may bypass some of these cells, resulting ununiformed pretreatment. Pre-impregnation is a process to allow predelivery of water or pretreatment chemicals to the plant cell walls for relatively long times, sometimes with the use of moderate temperature and/or vacuum to squeeze out air bubbles in dry biomass [19]. In this circumstance, pretreatment chemicals can be transferred in the open spaces between tissues and plant cells (intercellular air space) and have limited penetration in the cell walls through pores where normally are not secondary thickened and not heavily lignified, such as the pits in tracheary elements and the pit fields in parenchyma that have pores to allow limited liquid transfer. Pre-impregnation significantly increases the interaction between biomass and pretreatment chemicals and thus increases the efficiency of thermochemical pretreatment.

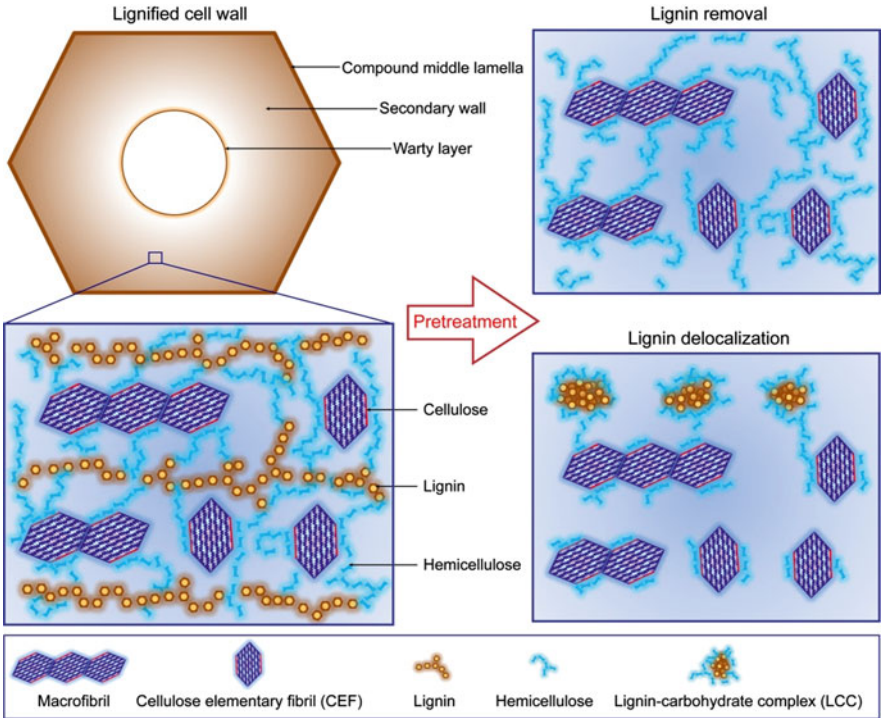

Fig. 1.5 Diagram of lignified cell wall and changes by pretreatment. The majority of cell wall material is the secondary wall, which is sealed by two condensed lignin layers, the warty layer in the lumen side and the compound middle lamella including the middle lamella original primary wall layers. Depending on the chemicals used in the pretreatment process, lignins may be bleached or delocalized from inside of the secondary wall and form lignin-carbohydrate complexes (Reprinted from Zeng et al. [14] with publication with permission from Elsevier)

1.5 Enzyme Hydrolysis

Both pretreatment and enzymatic hydrolysis can be called deconstruction process, which deconstruct and fractionate the cell wall polymers to produce fermentable sugars and value-added by-products. The pretreatment chemicals are normally small simple molecules, which can access the plant cell wall polymers in any available surface; whereas cellulase enzymes are large biomolecules composed of a mixture of carbohydrate-active enzymes, the specific molecular interactions between enzymes and their targeted substrates are critical in catalytic activities. Many enzymes contain a carbohydrate-binding module that specifically binds to the surface of cellulose (primarily the planar faces) [20] or to a glycan chain (hemicelluloses or amorphous cellulose) [21]. The catalytic domain has also a channel or a binding surface which specifically interacts with the substrate to facilitate bond

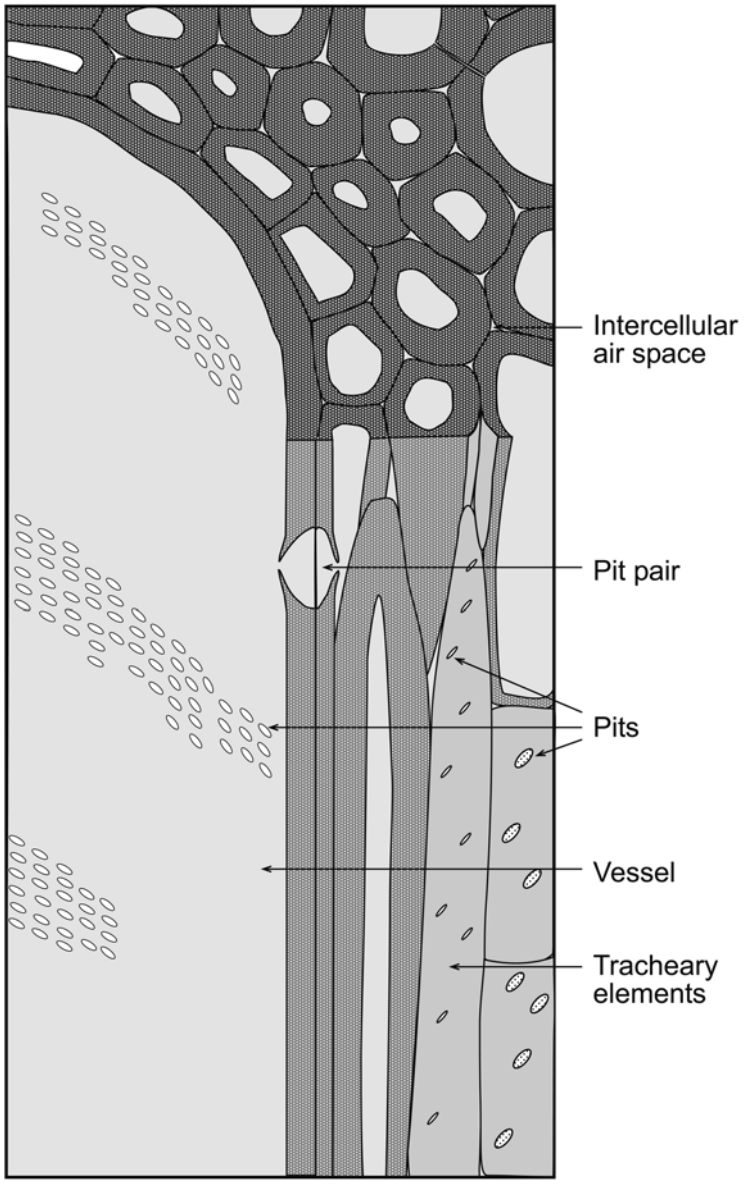

Fig. 1.6 Diagrams of major types of secondary cell walls. Vessel members are large in cell diameter and have simple or scalariform perforation plate at the end. Other tracheary elements, such as tracheids and fibers, are elongated cells. There are various types of pits in these walls

cleavage. Therefore, the heterogeneous structure of plant cell wall polymers requires synergistic reactions of multiple enzymes. In some anaerobic bacteria, a multi-protein complex was discovered, termed cellulosomes [22], containing many enzymes organized by a non-catalytic scaffold in protein. The cellulosomes have super activity when digesting pure cellulose due to the proximity of these enzymes in the complex and perhaps other unknown cofactors.

The accessibility of polysaccharides (cellulose and hemicelluloses) to enzymes determines the digestibility of biomass. Plant cell walls are readily digestible by enzymes when there is no lignin presented, such as non-lignified primary walls [11]. Enzymes can also bind to the innermost side of partially lignified parenchyma secondary walls and broken surfaces of fully lignified secondary walls; all these together accounts for approximately 10 % of digestibility in untreated biomass. After adequate pretreatment, over 90 % of conversion can be achieved. It has been revealed that enzyme digestion always starts from the innermost side of the cell walls (Fig. 1.7) [11]; that is because cell wall lignification starts from the cell corner and middle lamella area forming a gradient lignin concentration toward the cell lumen side. The porosity of the cell walls is also important for enzyme binding; the pore size of microfibril network is approximately 10 nm (Figs. 1.2 and 1.3) when lignin is removed, which allows sufficient penetration for free enzymes, such as fungal enzyme systems, but not for large enzyme complexes, such as cellulosomes (Fig. 1.7).

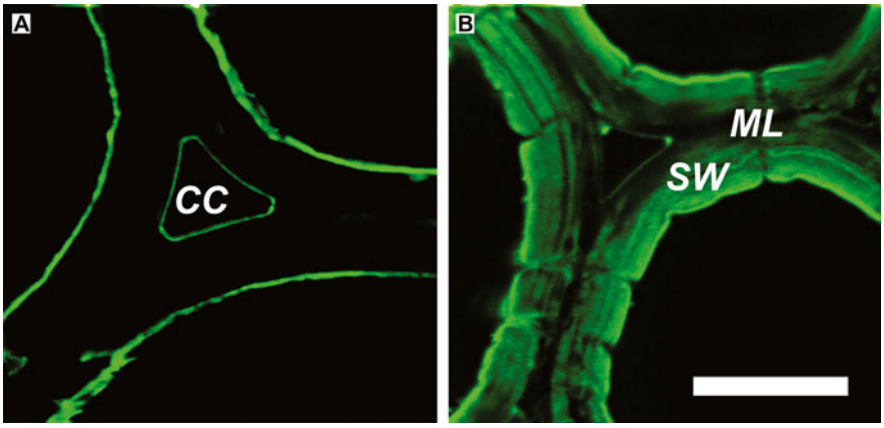

Fig. 1.7 Binding of cellulase enzymes to the secondary cell walls after lignin removal. (**a**) Dye-labeled cellulosomes (showing in *green*), because of their large size, only bind to wall surface. (**b**) Dye-labeled fungal cellulases (showing in *green*) penetrate into the inside of walls (Reprinted from Ding et al. [11], with permission from AAAS)

1.6 Conclusion

Plant biomass consists of various types of the plant cell walls that are composed of three major classes of polymers, cellulose, hemicelluloses, and lignins. These polymers are covalently linked by a variety of chemical bonds and are non-covalently interacted each other to form complex architectures. In order to effectively break down plant cell wall architectures, pretreatment and enzymatic hydrolysis processes have been developed to deconstruct these polymers to produce simple fermentable sugars and fractionate lignins as value-added by-products. Based on current understanding, especially recent new findings obtained by advanced imaging, the anatomy of plant tissue and ultrastructure of different types of cell walls affect the deconstruction process differently to some extent. Further, improvement of pretreatment must be made to achieve the ultimate goal of the process, which would minimize sugar degradation and maximize the yield of fermentable sugars, as well as a clean fractionation of lignins.

References

1. Himmel ME, Ding S-Y, Johnson DK, Adney WS, Nimlos MR, Brady JW, Foust TD (2007) Biomass recalcitrance: engineering plants and enzymes for biofuels production. Science 315(5813):804–807. doi:10.1126/science.1137016
2. Sannigrahi P, Ragauskas AJ, Tuskan GA (2010) Poplar as a feedstock for biofuels: a review of compositional characteristics. Biofuels Bioprod Biorefin 4(2):209–226. doi:10.1002/bbb.206
3. Wyman CE, Dale BE, Elander RT, Holtzapple M, Ladisch MR, Lee YY, Mitchinson C, Saddler JN (2009) Comparative sugar recovery and fermentation data following pretreatment of poplar wood by leading technologies. Biotechnol Prog 25(2):333–339. doi:10.1002/btpr.142
4. Guo M, Littlewood J, Joyce J, Murphy R (2014) The environmental profile of bioethanol produced from current and potential future poplar feedstocks in the EU. Green Chem 16(11):4680–4695. doi:10.1039/c4gc01124d
5. Tuskan GA, DiFazio S, Jansson S, Bohlmann J, Grigoriev I, Hellsten U, Putnam N, Ralph S, Rombauts S, Salamov A, Schein J, Sterck L, Aerts A, Bhalerao RR, Bhalerao RP, Blaudez D, Boerjan W, Brun A, Brunner A, Busov V, Campbell M, Carlson J, Chalot M, Chapman J, Chen G-L, Cooper D, Coutinho PM, Couturier J, Covert S, Cronk Q, Cunningham R, Davis J, Degroeve S, Déjardin A, de Pamphilis C, Detter J, Dirks B, Dubchak I, Duplessis S, Ehlting J, Ellis B, Gendler K, Goodstein D, Gribskov M, Grimwood J, Groover A, Gunter L, Hamberger B, Heinze B, Helariutta Y, Henrissat B, Holligan D, Holt R, Huang W, Islam-Faridi N, Jones S, Jones-Rhoades M, Jorgensen R, Joshi C, Kangasjärvi J, Karlsson J, Kelleher C, Kirkpatrick R, Kirst M, Kohler A, Kalluri U, Larimer F, Leebens-Mack J, Leplé J-C, Locascio P, Lou Y, Lucas S, Martin F, Montanini B, Napoli C, Nelson DR, Nelson C, Nieminen K, Nilsson O, Pereda V, Peter G, Philippe R, Pilate G, Poliakov A, Razumovskaya J, Richardson P, Rinaldi C, Ritland K, Rouzé P, Ryaboy D, Schmutz J, Schrader J, Segerman B, Shin H, Siddiqui A, Sterky F, Terry A, Tsai C-J, Uberbacher E, Unneberg P, Vahala J, Wall K, Wessler S, Yang G, Yin T, Douglas C, Marra M, Sandberg G, Van de Peer Y, Rokhsar D (2006) The genome of black cottonwood, Populus trichocarpa (Torr. & Gray). Science 313(5793):1596–1604. doi:10.1126/science.1128691
6. Evert RF (2006) Esau's plant anatomy: meristems, cells, and tissues of the plant body: their structure, function, and development. Wiley, Hoboken

7. Vogel KP, Brejda JJ, Walters DT, Buxton DR (2002) Switchgrass biomass production in the Midwest USA: harvest and nitrogen management. Agron J 94(3):413–420
8. Sannigrahi P, Ragauskas AJ, Tuskan GA (2010) Poplar as a feedstock for biofuels: a review of compositional characteristics. Biofuel Bioprod Biorefin 4(2):209–226. doi:10.1002/bbb.206
9. Fernandes AN, Thomas LH, Altaner CM, Callow P, Forsyth VT, Apperley DC, Kennedy CJ, Jarvis MC (2011) Nanostructure of cellulose microfibrils in spruce wood. Proc Natl Acad Sci U S A 108(47):E1195–E1203. doi:10.1073/pnas.1108942108
10. Ding SY, Himmel ME (2006) The maize primary cell wall microfibril: a new model derived from direct visualization. J Agric Food Chem 54(3):597–606. doi:10.1021/jf051851z
11. Ding SY, Liu YS, Zeng YN, Himmel ME, Baker JO, Bayer EA (2012) How does plant cell wall nanoscale architecture correlate with enzymatic digestibility? Science 338(6110):1055–1060. doi:10.1126/science.1227491
12. Nishiyama Y, Langan P, Chanzy H (2002) Crystal structure and hydrogen-bonding system in cellulose Iβ from synchrotron X-ray and neutron fiber diffraction. J Am Chem Soc 124(31):9074–9082
13. Nishiyama Y, Sugiyama J, Chanzy H, Langan P (2003) Crystal structure and hydrogen bonding system in cellulose Iα, from synchrotron X-ray and neutron fiber diffraction. J Am Chem Soc 125(47):14300–14306. doi:10.1021/Ja037055w
14. Zeng YN, Zhao S, Yang SH, Ding SY (2014) Lignin plays a negative role in the biochemical process for producing lignocellulosic biofuels. Curr Opin Biotechnol 27:38–45. doi:10.1016/j.copbio.2013.09.008
15. Zeng Y, Saar BG, Friedrich MG, Chen F, Liu Y-S, Dixon RA, Himmel ME, Xie XS, Ding S-Y (2010) Imaging lignin-downregulated alfalfa using coherent anti-stokes Raman scattering microscopy. Bioenerg Res 3(3):272–277. doi:10.1007/s12155-010-9079-1
16. Saar BG, Zeng YN, Freudiger CW, Liu YS, Himmel ME, Xie XS, Ding SY (2010) Label-free, real-time monitoring of biomass processing with stimulated Raman scattering microscopy. Angew Chem-Int Edit 49(32):5476–5479. doi:10.1002/anie.201000900
17. Zeng Y, Himmel ME, Ding S-Y (2012) Coherent Raman microscopy analysis of plant cell walls. In: Himmel ME (ed) Biomass conversion, vol 908, Methods in molecular biology. Humana Press, New York, pp 49–60. doi:10.1007/978-1-61779-956-3_5
18. Zeng Y, Zhao S, Yang S, Ding S-Y (2014) Lignin plays a negative role in the biochemical process for producing lignocellulosic biofuels. Curr Opin Biotechnol 27:38–45
19. Kazi KMF, Jollez P, Chornet E (1998) Preimpregnation: an important step for biomass refining processes. Biomass Bioenerg 15(2):125–141. doi:10.1016/S0961-9534(98)00008-7
20. Xu Q, Tucker MP, Arenkiel P, Ai X, Rumbles G, Sugiyama J, Himmel ME, Ding SY (2009) Labeling the planar face of crystalline cellulose using quantum dots directed by type-I carbohydrate-binding modules. Cellulose 16(1):19–26. doi:10.1007/s10570-008-9234-4
21. Boraston AB, Bolam DN, Gilbert HJ, Davies GJ (2004) Carbohydrate-binding modules: fine-tuning polysaccharide recognition. Biochem J 382:769–781
22. Lamed R, Setter E, Kenig R, Bayer EA (1983) The cellulosome – a discrete cell-surface organelle of Clostridium-thermocellum which exhibits separate antigenic, cellulose-binding and various cellulolytic activities. Biotechnol Bioeng 13:163–181

Chapter 2
Depolymerization of Cellulosic Biomass Catalyzed by Activated Carbons

Hirokazu Kobayashi, Mizuho Yabushita, and Atsushi Fukuoka

Abstract Efficient hydrolysis of cellulosic biomass to glucose is a grand challenge for the realization of a nonfood biorefinery. In recent years, solid catalysts have attracted significant attention for biomass conversion, as they can be separated from product solutions and their functions can be designed. In this chapter, we describe activated carbons that can hydrolyze cellulose and real biomass to glucose in yields up to 88 % in the presence of a trace amount of hydrochloric acid. Creating contacts between the solid catalyst and the solid substrate by ball-milling is the key to realizing the potential of this catalytic system. Activated carbon adsorbs cellulosic molecules by van der Waals forces, CH–π hydrogen bonds, and hydrophobic interactions between the polyaromatic surface of the carbon and the axial planes of glucans, namely, hydrophobic groups. Subsequently, the weakly acidic groups of the carbon surface such as carboxylic acids cleave the glycosidic bonds of cellulose via oxocarbenium intermediates, for which the salicylic acid structure is especially effective.

Keywords Cellulose • Hydrolysis • Activated carbon • Ball-milling • Depolymerization

2.1 Introduction

Efficient hydrolysis of cellulosic biomass to glucose (Fig. 2.1) is a grand challenge for the realization of a nonfood biorefinery, as cellulose is the most abundant inedible biomass and glucose is a versatile precursor to chemicals [1, 2]. In recent years, enzymatic hydrolysis of cellulose has been widely studied at up to a 10^5-ton-per-year scale in the USA (DuPont, KL Energy, Poet, and Cobalt Technologies), Japan (a project of New Energy and Industrial Technology Development Organization), Taiwan (Institute of Nuclear Energy Research), etc.

H. Kobayashi • M. Yabushita • A. Fukuoka (✉)
Catalysis Research Center, Hokkaido University,
Kita 21 Nishi 10, Kita-ku, Sapporo, Hokkaido 001-0021, Japan
e-mail: fukuoka@cat.hokudai.ac.jp

M. Schlaf, Z.C. Zhang (eds.), *Reaction Pathways and Mechanisms in Thermocatalytic Biomass Conversion I*, Green Chemistry and Sustainable Technology, DOI 10.1007/978-981-287-688-1_2

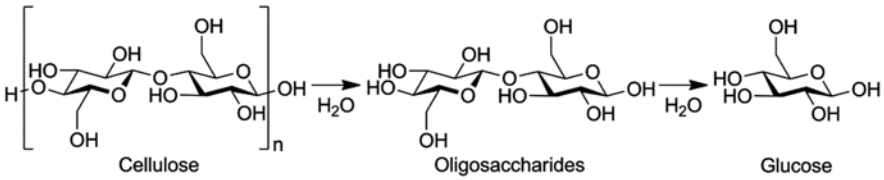

Fig. 2.1 Hydrolysis of cellulose to glucose

However, the high cost of enzymes has remained an issue for the establishment of economical processes.

Another potential strategy to depolymerize cellulose is the utilization of solid catalysts, because they can be separated from product solutions and their functions can be designed [3]. Solid strong acids such as sulfonated carbons have been intensively studied by many groups to hydrolyze cellulose [4–12], whereas little research has focused on weakly acidic solid catalysts. However, weak acids may also be useful, as cellulase enzymes selectively hydrolyze cellulose using weak acids/bases [13]. Moreover, weak acids can survive in the presence of salts potentially derived from biomass, whereas solid strong acids readily cause cation exchange, namely, proton leaching [14]. Solid weak acids are worthwhile to investigate for the hydrolysis of cellulose.

We have focused on activated carbons because they are ubiquitous materials bearing weakly acidic oxygenated groups such as carboxylic acids and phenols. Moreover, carbon is stable under the harsh aqueous conditions required for the conversion of cellulose. In this chapter, we describe the catalysis of activated carbons for the hydrolysis of cellulose and real biomass and discuss the reaction mechanism.

2.2 Hydrolysis of Cellulose by Activated Carbons

2.2.1 Catalytic Activities of Carbons

Various carbons were tested for the hydrolysis of ball-milled cellulose in water with the following temperature program: r.t. to 503 K in 18 min and then a rapid cool down to r.t. by blowing air [15]. The concentration of cellulose used here was 8.1 g in 1 L of water, denoted 8.1 g L^{-1}, and the weight-based ratio of substrate to catalyst (S/C) was 6.5. As shown in Table 2.1, alkali-activated carbon K26 gave the highest conversion of cellulose (60 %) with the formation of sugar products such as glucose (36 % yield), soluble oligosaccharides (2.5 %), fructose (2.7 %), and mannose (2.6 %). K26 was reusable three times without significant loss of activity. Other alkali-activated carbons K20 and MSP20 also had good catalytic activities (glucose yields of 35 % and 26 %, respectively). A mesoporous carbon CMK-3 [16] reproducibly afforded 12–16 % yields of glucose over several tests [15, 17, 18], and

Table 2.1 Hydrolysis of cellulose by various carbon catalysts

Catalyst	Acid amount[a]/ μmol g^{-1}	Conv./%	Yield based on carbon/%						
			Glc	Olg	Frc	Man	Lev	HMF	Others
None	–	28	4.6	15	0.5	0.6	0.2	1.8	5
K26[b]	880	60	36	2.5	2.7	2.6	2.1	3.4	11
K20[b]	1010	59	35	1.7	1.9	1.3	2.7	2.9	14
MSP20[c]	450	50	26	6.3	1.7	1.6	1.6	2.1	11
CMK-3[d]	410	52	12	25	0.9	0.8	0.7	2.5	10
BP2000[e]	160	37	6.4	12	0.5	0.5	0.3	1.8	16
XC72[e]	75	35	5.8	19	0.6	0.9	0.2	1.9	7
GO[f]	–	–[g]	58	1.5	0.5	2.5	3.1	11	–[g]

Reaction conditions: ball-milled cellulose, 8.1 g L^{-1}; S/C = 6.5; solvent, water 40 mL; r.t. to 503 K in 18 min and then cooled down to r.t. *Products*: *Glc* glucose, *Olg* water-soluble oligosaccharides, *Frc* fructose, *Man* mannose, *Lev* levoglucosan, *HMF* 5-hydroxymethylfurfural, others (conversion) – (total yield of the shown products)

[a]Total amount of surface acidic groups quantified by the Boehm titration [20]

[b]Alkali-activated carbon synthesized in Showa Denko

[c]Commercial alkali-activated carbon, Kansai Coke and Chemicals

[d]Mesoporous carbon [16]

[e]Commercial carbon black, Cabot

[f]Commercial graphene oxide, G-22, EM Japan

[g]Cannot be determined due to the decomposition of catalyst

another group also verified the catalytic activity of a mesoporous carbon [19]. Carbon blacks BP2000 and XC72 provided similar glucose yields (5.8–6.4 %) to that of a blank experiment without catalyst (4.6 %). Thus, the catalytic activity greatly depended on the types of carbons. In addition, good yields of glucose (50–60 %) were obtained by using graphene oxides, but graphene oxides became black precipitates having low activity after the reaction. The reaction temperature of 503 K is high enough to decompose oxygenated groups of graphene oxide to CO and CO_2 [11], which induce its aggregation. Thus, we studied the catalysis of more typical carbon materials for the hydrolysis of cellulose.

In order to identify the active sites, the surface acidic groups on carbons were quantified by the Boehm titration using $NaHCO_3$, Na_2CO_3, and NaOH [20]. The most active catalyst K26 had 270 μmol g^{-1} of carboxylic acids, 310 μmol g^{-1} of lactones, and 310 μmol g^{-1} of phenols, whereas an inactive catalyst XC72 possessed only 75 μmol g^{-1} of acidic groups in total. Figure 2.2 shows a plot of yields of glucose against the total amounts of acidic groups on the carbons, showing a fairly good correlation. It was also found that the activity of K26 decreased by reducing the amount of oxygenated groups. We and Chung et al., respectively, showed that the catalytic activity of such carbons was maintained after treating the materials with sodium acetate/acetic acid buffer of pH 4.0–4.1 [14]. If the carbon catalysts were strong acids, they would be deactivated by the treatment due to ion exchange with Na^+. Thus, major active sites of carbons such as K26 are not strong acids but weak ones.

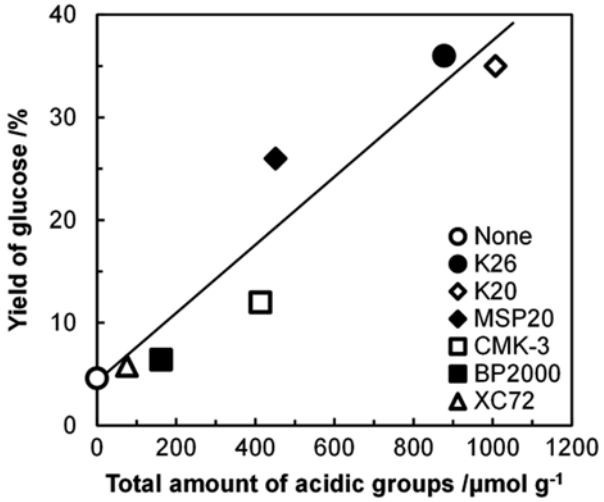

Fig. 2.2 Correlation between total acid amounts on carbons and glucose yields (cellulose, 8.1 g L^{-1}; S/C = 6.5; solvent, water; r.t. to 503 K in 18 min and cooled down to r.t.)

2.2.2 Mix-Milling for the Hydrolysis of Cellulose by Activated Carbon

The yield of glucose was at most 36 % in the screening tests, which must be improved for practical use of activated carbon catalysts. The hydrolysis of solid cellulose by solid catalysts is hampered by their limited collisions and therefore requires severe reaction conditions that may lead to the degradation of glucose. This degradation must be avoided while accelerating the hydrolysis of cellulose. Thus, we conceived of ball-milling cellulose and carbon together to improve their contact, denoted as mix-milling hereafter [15]. The mix-milled sample containing cellulose and K26 was used in a reaction at 418 K for 24 h, and 72 % yield of glucose was achieved (Table 2.2). On the other hand, individually milled cellulose gave only 17 % yield of glucose, thus showing that the mix-milling pretreatment dramatically improved the yield of glucose.

The effect of mix-milling was quantitatively analyzed in a kinetic study [21]. We have hypothesized that the catalytic conversion of cellulose consists of three pseudo-first-order reactions: hydrolysis of solid cellulose to soluble oligomers (k_1), that of soluble oligomers to glucose (k_2), and decomposition of glucose to by-products (k_3). When the mix-milling was used as a pretreatment, k_1 (0.17 h^{-1}) was as high as k_2 (0.16 h^{-1}) at 418 K, showing that solid cellulose was hydrolyzed similarly as soluble oligosaccharides in this system. Moreover, k_1 and k_2 were both *ca.* ten times greater than k_3 (0.017 h^{-1}), thus giving a good yield of glucose (72 %). In the case of individual milling, k_1 was as low as 0.013 h^{-1}, but k_2 and k_3 were 0.16 and 0.017 h^{-1}, respectively. In summary, the mix-milling improves k_1 by 13-fold but keeps k_2 and

Table 2.2 Effect of mix-milling and trace HCl on the hydrolysis of cellulose by K26

Milling pretreatment	Reaction temp./K	Reaction time/h	Solvent	Yield based on carbon/%					
				Glc	Olg	Frc	Man	Lev	HMF
Individual	418	24	Water	17	6.7	1.1	0.9	0.2	0.8
Mix	418	24	Water	72	2.8	1.4	1.5	1.4	4.9
Mix	453	0.33	Water	20	70	0.6	0.7	0.7	1.0
Mix	453	0.33	120 ppm HCl	88	2.7	1.5	1.5	3.0	1.7

Reaction conditions: Cellulose, 8.1 g L^{-1}; S/C = 6.5. *Products*: *Glc* glucose, *Olg* water-soluble oligosaccharides, *Frc* fructose, *Man* mannose, *Le*v levoglucosan, *HMF* 5-hydroxymethylfurfural

k_3 constant, indicating that the mix-milling pretreatment selectively improves the rate constant of the solid-solid reaction.

Pristine, mix-milled, and individually milled cellulose samples were characterized by several physicochemical methods. X-ray diffraction and ^{13}C nuclear magnetic resonance spectroscopy indicated that the pristine cellulose was in the cellulose I form with 80 % crystallinity, whereas the milled ones were in amorphous form with less than 5 % crystallinities. Median diameters of secondary particles were 63 μm for the pristine cellulose, 37 μm for the mix-milled one, and 33 μm for the individually milled one; both the milling pretreatments decreased the particle sizes almost by half. The polymerization degree of pristine cellulose (1240), determined by viscometry with parameters reported elsewhere [22], was also reduced to half by the milling pretreatments (690 for mix-milled and 640 for individually milled). Thus, the mix-milling and the individual milling changed the nature of cellulose in a similar way. Therefore, the origin of the specific effect of the mix-milling can be ascribed to enhanced contact between cellulose and the carbon catalyst.

2.2.3 *Combination of Activated Carbon and Trace Hydrochloric Acid*

The productivity of glucose was improved by optimizing the reaction conditions of cellulose hydrolysis. First, the reaction temperature was increased to shorten the reaction time to a more practical range. At 453 K, 20 % yield of glucose and 70 % yield of oligomers, 90 % yield in total, were obtained within 0.33 h. The hydrolysis of cellulose was remarkably rapid and that of oligosaccharides was the rate-determining step under these conditions. As indicated in the kinetic study described in the previous section, increasing reaction time causes the decomposition of glucose in addition to the hydrolysis of oligosaccharides. Therefore, the second step was the acceleration of the hydrolysis of oligosaccharides, for which trace soluble acid was used as a solvent instead of pure water for the reaction of a mix-milled sample containing cellulose and K26. Optimized conditions (120 ppm HCl; 453 K; 0.33 h) gave an 88 % yield of glucose with 90 % selectivity (Table 2.2), which is one

of the best records ever achieved with solid catalysts. Accordingly, we concluded that trace HCl efficiently transformed soluble oligosaccharides into glucose. Economic costs of a trace amount of HCl and its neutralization are low, and some stainless steel reactors are tolerant to low concentrations of HCl. We believe that combining *trace* HCl with a solid catalyst is a prospective method for the conversion of cellulose. Sels et al. also proposed the use of *trace* HCl with a solid catalyst as an efficient methodology for the conversion of cellulose [23].

Reuse experiments of K26 were carried out using a high concentration of cellulose (200 g L^{-1}) at S/C = 6.5 in 120 ppm HCl to evaluate productivity and durability of the catalyst (Fig. 2.3). Glucose was produced in 71 % yield with a concentration of 160 g L^{-1} in the first run. Although the yield of glucose was lower than that under a diluted condition (88 % yield at 8.1 g L^{-1}), our catalytic system still functioned well under the concentrated condition. Next, the catalyst was reused according to the following procedure. The reaction mixture was separated by centrifugation into hydrolysate and solid residue containing K26 and unreacted cellulose. The solid was washed with water, dried, and mix-milled with fresh cellulose, the amount of which was the same as that consumed in the previous reaction. The mix-milled sample was used for the next hydrolysis reaction. The yields of glucose in the second to fourth reactions were 72 %, 70 %, and 67 %, respectively, which indicated good reusability of K26.

The combination of activated carbon and HCl was applied to conversion of bagasse pulp as an example of real biomass. The bagasse sample was composed of cellulose (59 wt%), hemicellulose (27 wt%; xylan 25 wt% and arabinan 2 wt%), lignin (9 wt%), and others (5 wt%). The bagasse pulp and a commercial activated carbon bearing a relatively large amount of oxygenated groups among inexpensive

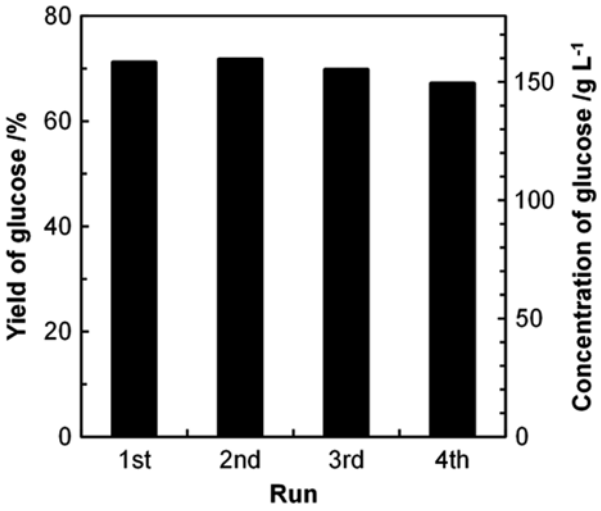

Fig. 2.3 Reuse tests of K26 in the hydrolysis of cellulose (cellulose, 200 g L^{-1}; S/C = 6.5; 0.012 % HCl aq.; r.t. to 473 K in 16 min, 473 K for 2 min, and 423 K for 60 min)

ones (BA50, Ajinomoto Fine-Techno) were mix-milled, and the mixture was used for a two-step reaction in order to selectively hydrolyze hemicellulose and cellulose. The first hydrolysis conditions at 453 K for 1 min gave glucose in 1.9 % yield based on the cellulose content and pentoses in 76 % yield based on the amount of hemicellulose, and most of the cellulose fraction remained as a solid together with BA50 in this step. Subsequently, the second hydrolysis at 483 K for 2 min using the solid residue in the first reaction afforded glucose in 74 % yield and pentoses in 16 % yield. These results clearly show that our catalytic system is applicable to the hydrolysis of real biomass.

2.3 Mechanistic Study of the Hydrolysis of Cellulose by Activated Carbon

2.3.1 Elementary Steps of Hydrolytic Reactions

Hydrolysis of cellulose by solid catalysts occurs after adsorption of the cellulose molecule on the surface of the catalyst followed by dissociation of the glycosidic bonds by the active sites. Katz et al. found that cellulose molecules grafted on silica via ether bonds were converted to oligosaccharides by surface silanol groups (pK_a*ca.* 7) in trace hydrochloric acid at pH 4 [24, 25]. The catalytic activity correlated with the density of surface OH groups [26]. In contrast, free cellulose cannot be depolymerized by the catalysts under the same conditions. These results indicate that even weak acids can hydrolyze glycosidic bonds of cellulose by attracting the molecule to active sites. Therefore, we studied the adsorption of cellulosic molecules on K26 and the hydrolysis step by oxygenated groups.

2.3.2 Adsorption of Cellulosic Molecules on Activated Carbon

Cellobiose was adsorbed onto K26 in water at 296 K to elucidate the manner of adsorption [27]. A Langmuir-type adsorption isotherm was obtained, and the adsorption equilibrium constant (K_{ads}) was calculated to be 5660 M^{-1} and the adsorption capacity (C_{ads}) to be 412 mg g^{-1}. Two driving forces behind the adsorption can be hypothesized based on interactions of hydrophobic and hydrophilic groups. The polyaromatic surface of carbon may interact with the hydrophobic plane of cellobiose (axial plane consists of C–H groups) via van der Waals forces and CH–π hydrogen bonds [28], whereas oxygenated groups of carbon possibly form OH–O hydrogen bonds with hydroxyl groups on the equatorial plane of cellobiose [29, 30]. To clarify which is the predominant force for the adsorption, K26 was deoxygenated at 1273 K under He flow. This treatment removed *ca.* 99 % of the oxygenated groups from K26, but this material similarly adsorbed cellobiose (K_{ads} = 5270 M^{-1},

Table 2.3 Enthalpy and entropy changes for the adsorption of β-glucans on K26

Adsorbate	ΔH°_{ads}/ kJ mol^{-1}	ΔS°_{ads}/ J K^{-1} mol^{-1}
Glucose	−8.4 ± 1.2	+16.5 ± 3.8
Cellobiose	−14.1 ± 1.9	+23.5 ± 3.4
Cellotriose	−20.2 ± 0.8	+32.2 ± 3.3

C_{ads} = 342 mg g^{-1}). The slight decrease in C_{ads} was due to the reduction of surface area by the heat treatment. It is thus concluded that the major driving force for the adsorption is the interaction between hydrophobic groups. The two-dimensional polyaromatic surface and flatly arrayed CH groups of cellobiose are well fitted to each other.

The adsorption enthalpy (ΔH°_{ads}) and entropy (ΔS°_{ads}) of cellobiose on K26 were calculated from the van't Hoff plot to quantitatively evaluate the driving forces (Table 2.3). ΔH°_{ads} was −14.1 kJ mol^{-1}, and accordingly, the value divided by the number of CH groups presenting on one side of cellobiose (5) was −2.8 kJ mol^{-1}.

This value is reasonable for the CH–π interactions [28, 31]. In contrast, ΔS°_{ads} of +23.5 J K^{-1} mol^{-1} is surprising, as the adsorption usually decreases the freedom of adsorbate. This positive entropy change is ascribed to the hydrophobic interaction (a review article is available for general hydrophobic interactions [32]). The adsorption of cellobiose onto K26 with hydrophobic groups releases water molecules restricted around the lipophilic surface, which increases freedom of the water molecules. Consequently, the adsorption of cellobiose onto K26 is driven by both enthalpy and entropy. The positive entropy change provides strong adsorption even at the high temperatures required for the conversion of cellulose, as demonstrated in a high-temperature adsorption experiment in which 230 mg of cellobiose adsorbed onto 1 g of K26 at 413 K within 10 min.

The thermodynamics of adsorption of glucose, cellobiose, and cellotriose were compared to clarify the effect of chain length. ΔH°_{ads} value linearly decreased from −8.4 kJ mol^{-1} (glucose) to −14.1 kJ mol^{-1} (cellobiose) and −20.2 kJ mol^{-1} (cellotriose), which was due to the increase in the number of CH groups. Similarly, ΔS°_{ads} was elevated from +16.5 J K^{-1} mol^{-1} to +23.5 and +32.2 J K^{-1} mol^{-1} with increasing chain length, owing to the increase in adsorption in cross-sectional area. The longer the cellulosic molecule becomes, the stronger the molecule and carbon interact. Thus, K26 has a strong interaction with cellulose on the interface.

2.3.3 Hydrolysis of Glycosidic Bonds by Oxygenated Groups

The role of oxygenated groups was studied in the hydrolysis of cellobiose by aromatic compounds as model catalysts at 443 K (Table 2.4) [15]. Phenol (pK_a = 10) and benzoic acid (pK_a = 4.2) provided low turnover frequencies (TOFs) of 0 and 4.5 h^{-1}, respectively. Salicylic acid (pK_a = 3.0), having phenolic and carboxylic groups in vicinal positions, gave a high TOF of 28 h^{-1}, whereas *m*-hydroxybenzoic

Table 2.4 Hydrolysis of cellobiose by molecular catalysts

Catalyst	pK_a	TOF[a]/h^{-1}
Phenol	10	0
Benzoic acid	4.2	4.5
Salicylic acid	3.0	28
m-Hydroxybenzoic acid	4.1	5.6
p-Hydroxybenzoic acid	4.6	2.2
o-Chlorobenzoic acid	2.9	17

[a]Initial rate method with reaction conditions of cellobiose 50 mM, catalyst 0.5 mM, and water solvent at 443 K for 10 min

acid (pK_a = 4.1) and *p*-hydroxybenzoic acid (pK_a = 4.6) were almost inactive (TOF = 5.7, 2.4 h^{-1}, respectively). Additionally, *o*-chlorobenzoic acid (pK_a = 2.9, TOF = 17 h^{-1}) was significantly more active than benzoic acid, but less active than salicylic acid. Hence, the catalytic activity is determined by two factors. One is the acidity of the catalyst; strong acids can easily activate glycosidic bonds. The other is its structure; vicinal oxygenated groups are effective for the hydrolysis. Hara et al. have proposed that phenols form hydrogen bonds with hydroxyl groups of glucans [4]. Thus, we assume that the hydrogen bonding between the phenol and cellobiose increases the frequency factor of scission of glycosidic bonds by the neighboring carboxylic acid. Recently, it has been proposed that a high local density of surface weak-acid sites cooperatively works for the hydrolysis of glycosidic bonds, as change of the density strongly affects the catalytic activity of carbons [33].

Controlled experiments were conducted to clarify the dissociation mechanism of glycosidic bonds: S_N1 or S_N2. First, the methanolysis of cellobiose by K26 gave a mixture of α- and β-methylglucose from the nonreducing end glucose unit, and we observed that isomerization of methylglucose was limited under the reaction conditions. These results indicate that the reaction intermediates should be oxocarbenium ions (S_N1). Second, the hydrolysis of cellobiose by K26 was performed in the presence of tetraethylammonium chloride or bromide as nucleophiles. The ratio of nucleophilicity of water, Cl^-, and Br^- is 1:1000:10,000 in water. However, chloroglucose or bromoglucose was not detected, and these reactions provided similar conversion rates of cellobiose. This result indicates that dissociation of glycosidic bonds by S_N2 reaction is negligible in this catalytic system. Therefore, it is concluded that the hydrolysis proceeds by the S_N1 mechanism.

2.3.4 Proposed Reaction Mechanism

Figure 2.4 shows the proposed reaction mechanism for the hydrolysis of cellulose by activated carbons. We hypothesized that the salicylic acid structure was the active site. Carbon adsorbs a cellulose molecule by van der Waals forces, CH–π hydrogen bonds, and hydrophobic interactions. Next, phenolic and carboxylic

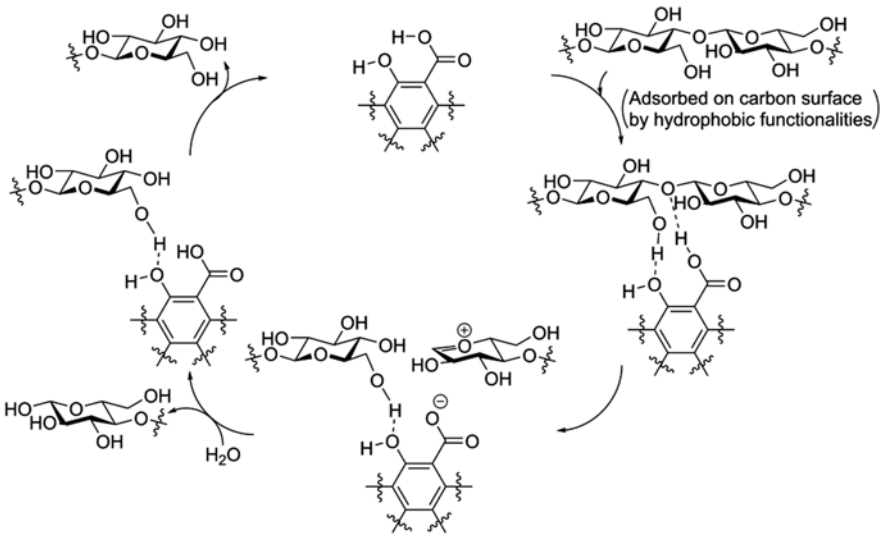

Fig. 2.4 Proposed reaction mechanism for the hydrolysis of cellulose by activated carbon catalysts

groups of carbon form OH–O hydrogen bonds with the cellulose molecule to attract a glycosidic bond to the carboxylic group. The oxygen atom of the glycosidic bond is protonated, and subsequently scission of the glycosidic bond occurs with formation of an oxocarbenium ion. A water molecule rapidly reacts with the cation to form a sugar residue and regenerates the carboxylic acid of carbon. Finally, the remaining cellulose molecule desorbs from carbon, and the catalyst is regenerated.

It is known that cellulase adsorbs onto cellulose by a hydrophobic aromatic amino acid residue and that the enzyme hydrolyzes glycosidic bonds by a carboxylic acid and a carboxylate [13, 34]. Thus, our activated carbon catalyst and cellulase function similarly in the hydrolysis of cellulose.

2.4 Summary

Activated carbons can hydrolyze cellulose and real biomass to glucose in high yields with good productivity. Creating contacts between the solid catalyst and the solid substrate by ball-milling is the key to realizing the potential of this catalytic system. Activated carbon adsorbs cellulose by hydrophobic functionality and cleaves glycosidic bonds by weakly acidic groups such as carboxylic acids, for which the salicylic acid structure is especially effective.

References

1. Gallezot P (2012) Conversion of biomass to selected chemical products. Chem Soc Rev 41:1538–1558. doi:10.1039/C1CS15147A
2. Kobayashi H, Fukuoka A (2013) Synthesis and utilisation of sugar compounds derived from lignocellulosic biomass. Green Chem 15:1740–1763. doi:10.1039/c3gc00060e
3. Fukuoka A, Dhepe PL (2006) Catalytic conversion of cellulose into sugar alcohols. Angew Chem Int Ed 45:5161–5163. doi:10.1002/anie.200601921
4. Suganuma S, Nakajima K, Kitano M, Yamaguchi D, Kato H, Hayashi S, Hara M (2008) Hydrolysis of cellulose by amorphous carbon bearing SO_3H, COOH, and OH groups. J Am Chem Soc 130:12787–12793. doi:10.1021/ja803983h
5. Onda A, Ochi T, Yanagisawa K (2008) Selective hydrolysis of cellulose into glucose over solid acid catalysts. Green Chem 10:1033–1037. doi:10.1039/b808471h
6. Rinaldi R, Palkovits R, Schüth F (2008) Depolymerization of cellulose using solid catalysts in ionic liquids. Angew Chem Int Ed 47:8047–8050. doi:10.1002/anie.200802879
7. Rinaldi R, Meine N, vom Stein J, Palkovits R, Schüth F (2010) Which controls the depolymerization of cellulose in ionic liquids: the solid acid catalyst or cellulose? ChemSusChem 3:266–276. doi:10.1002/cssc.200900281
8. Van de Vyver S, Peng L, Geboers J, Schepers H, de Clippel F, Gommes CJ, Goderis B, Jacobs PA, Sels BF (2010) Sulfonated silica/carbon nanocomposites as novel catalysts for hydrolysis of cellulose to glucose. Green Chem 12:1560–1563. doi:10.1039/c0gc00235f
9. Pang J, Wang A, Zheng M, Zhang T (2010) Hydrolysis of cellulose into glucose over carbons sulfonated at elevated temperatures. Chem Commun 46:6935–6937. doi:10.1039/c0cc02014a
10. Wang H, Zhang C, He H, Wang L (2012) Glucose production from hydrolysis of cellulose over a novel silica catalyst under hydrothermal conditions. J Environ Sci 24:473–478. doi:10.1016/S1001-0742(11)60795-X
11. Zhao X, Wang J, Chen C, Huang Y, Wang A, Zhang T (2014) Graphene oxide for cellulose hydrolysis: how it works as a highly active catalyst? Chem Commun 50:3439–3442. doi:10.1039/c3cc49634a
12. Hick SM, Griebel C, Restrepo DT, Truitt JH, Buker EJ, Bylda C, Blair RG (2010) Mechanocatalysis for biomass-derived chemicals and fuels. Green Chem 12:468–474. doi:10.1039/b923079c
13. Zechel DL, Withers SG (2000) Glycosidase mechanisms: anatomy of a finely tuned catalyst. Acc Chem Res 33:11–18. doi:10.1021/ar970172
14. Chung PW, Charmot A, Olatunji-Ojo OA, Durkin KA, Katz A (2014) Hydrolysis catalysis of *Miscanthus* xylan to xylose using weak-acid surface sites. ACS Catal 4:302–310. doi:10.1021/cs400939p
15. Kobayashi H, Yabushita M, Komanoya T, Hara K, Fujita I, Fukuoka A (2013) High-yielding one-pot synthesis of glucose from cellulose using simple activated carbons and trace hydrochloric acid. ACS Catal 3:581–587. doi:10.1021/cs300845f
16. Jun S, Joo SH, Ryoo R, Kruk M, Jaroniec M, Liu Z, Ohsuna T, Terasaki O (2000) Synthesis of new, nanoporous carbon with hexagonally ordered mesostructure. J Am Chem Soc 122:10712–10713. doi:10.1021/ja002261e
17. Kobayashi H, Komanoya T, Hara K, Fukuoka A (2010) Water-tolerant mesoporous-carbon-supported ruthenium catalysts for the hydrolysis of cellulose to glucose. ChemSusChem 3:440–443. doi:10.1002/cssc.200900296
18. Komanoya T, Kobayashi H, Hara K, Chun WJ, Fukuoka A (2011) Catalysis and characterization of carbon-supported ruthenium for cellulose hydrolysis. Appl Catal A Gen 407:188–194. doi:10.1016/j.apcata.2011.08.039
19. Pang J, Wang A, Zheng M, Zhang Y, Huang Y, Chen X, Zhang T (2012) Catalytic conversion of cellulose to hexitols with mesoporous carbon supported Ni-based bimetallic catalysts. Green Chem 14:614–617. doi:10.1039/c2gc16364k

20. Boehm HP (1994) Some aspects of the surface chemistry of carbon blacks and other carbons. Carbon 32:759–769. doi:10.1016/0008-6223(94)90031-0
21. Yabushita M, Kobayashi H, Hara K, Fukuoka A (2014) Quantitative evaluation of ball-milling effects on the hydrolysis of cellulose catalysed by activated carbon. Catal Sci Technol 4:2312–2317. doi:10.1039/C4CY00175C
22. McCormick CL, Callais PA, Hutchinson BH Jr (1985) Solution studies of cellulose in lithium chloride and N, N-dimethylacetamide. Macromolecules 18:2394–2401. doi:10.1021/ma00154a010
23. Geboers J, Van de Vyver S, Carpentier K, Jacobs P, Sels B (2011) Efficient hydrolytic hydrogenation of cellulose in the presence of Ru-loaded zeolites and trace amounts of mineral acid. Chem Commun 47:5590–5592. doi:10.1039/c1cc10422e
24. Gazit OM, Charmot A, Katz A (2011) Grafted cellulose strands on the surface of silica: effect of environment on reactivity. Chem Commun 47:376–378. doi:10.1039/c0cc02105a
25. Gazit OM, Katz A (2012) Grafted poly(1→4-β-glucan) strands on silica: a comparative study of surface reactivity as a function of grafting density. Langmuir 28:431–437. doi:10.1021/la2036482
26. Gazit OM, Katz A (2013) Understanding the role of defect sites in glucan hydrolysis on surfaces. J Am Chem Soc 135:4398–4402. doi:10.1021/ja311918z
27. Yabushita M, Kobayashi H, Hasegawa J, Hara K, Fukuoka A (2014) Entropically favored adsorption of cellulosic molecules onto carbon materials through hydrophobic functionalities. ChemSusChem 7:1443–1450. doi:10.1002/cssc.201301296
28. Chung PW, Charmot A, Gazit OM, Katz A (2012) Glucan adsorption on mesoporous carbon nanoparticles: effect of chain length and internal surface. Langmuir 28:15222–15232. doi:10.1021/la3030364
29. Bul S, Verykios X, Mutharasan R (1985) In situ removal of ethanol from fermentation broths. 1. Selective adsorption characteristics. Ind Eng Chem Process Des Dev 24:1209–1213. doi:10.1021/i200031a052
30. Kitano M, Yamaguchi D, Suganuma S, Nakajima K, Kato H, Hayashi S, Hara M (2009) Adsorption-enhanced hydrolysis of β-1,4-glucan on graphene-based amorphous carbon bearing SO_3H, COOH, and OH groups. Langmuir 25:5068–5075. doi:10.1021/la8040506
31. Tsuzuki S, Honda K, Uchimaru T, Mikami M, Tanabe K (2000) The magnitude of the CH/p interaction between benzene and some model hydrocarbons. J Am Chem Soc 122:3746–3753. doi:10.1021/ja993972j
32. Franks F (1975) The hydrophobic interaction. In: Franks F (ed) Water a comprehensive treatise, vol 4. Plenum Press, New York
33. Charmot A, Chung PW, Katz A (2014) Catalytic hydrolysis of cellulose to glucose using weak-acid surface sites on postsynthetically modified carbon. ACS Sustain Chem Eng 2:2866–2872. doi:10.1021/sc500669q
34. Tormo J, Lamed R, Chirino AJ, Morag E, Bayer EA, Shoham Y, Steitz TA (1996) Crystal structure of a bacterial family-III cellulose-binding domain: a general mechanism for attachment to cellulose. EMBO J 15:5739–5751

Chapter 3
Advances in the Conversion of Short-Chain Carbohydrates: A Mechanistic Insight

Rik De Clercq, Michiel Dusselier, and Bert F. Sels

Abstract This chapter discusses recent insights in the conversion of short carbohydrates, viz., sugars containing four or less carbon atoms. Rather than summarizing product yields from such sugars and reported catalysts for the conversions, the focus lies on understanding the underlying mechanisms. These short carbohydrates can lead to a broad spectrum of products, ranging from platform chemicals such as lactic acid and ethylene glycol to high-value chemicals such as α-hydroxy-γ-butyrolactone and even fuels. Different synthesis strategies of these short carbohydrates include (1) a *top-down* approach from mono- or polysaccharides and (2) a selective *bottom-up* synthesis route from formaldehyde. Lewis acids play a major role in carbohydrate chemistry, and among these, Sn-based catalysts often show the highest activity. Whether dioses, trioses, or tetroses are used as substrate, Sn is able to convert them efficiently into α-hydroxy acids or esters, which are useful building blocks for renewable polyesters. Other reaction types such as isomerization, hydrogenation, and cross couplings are discussed briefly as well. Glycerol and glyoxal are no sugars, but their chemistry shows great resemblance to that of carbohydrates. Therefore, these compounds are also briefly accounted for in this chapter.

Keywords Catalysis • Carbohydrates • Lewis acids • α-Hydroxy acids • Polymer building blocks • Formaldehyde

3.1 Introduction

The imminent decline in fossil resources along with rising environmental concerns like global warming has greatly increased interest to use renewable raw materials in the chemical industry [1–3]. As the end of cheap oil is estimated to be around 2040 at the latest, an increase in the use of such renewable feedstock for chemicals is

R. De Clercq (✉) • M. Dusselier • B.F. Sels (✉)
Center for Surface Chemistry and Catalysis,
Leuven Chem&Tech, KU Leuven, Celestijnenlaan 200F, Leuven 3001, Belgium
e-mail: rik.declercq@biw.kuleuven.be; bert.sels@biw.kuleuven.be

M. Schlaf, Z.C. Zhang (eds.), *Reaction Pathways and Mechanisms in Thermocatalytic Biomass Conversion I*, Green Chemistry and Sustainable Technology, DOI 10.1007/978-981-287-688-1_3

needed to meet future product demands [2, 4, 5]. Carbohydrates are by far the most important class of biomass-derived compounds in terms of volume, representing roughly 75 % of the annually renewable biomass of about 200 billion tons. However, currently only ca. 4 % is exploited by the chemical industry [6]. The majority of the annually renewable carbohydrates exist as high-molecular-weight polysaccharides, such as starch and (hemi)cellulose, made up of C_5 (pentose) and C_6 (hexose) sugar units linked via glycosidic bonds [7]. Until now, scientists have mainly focused on these polysaccharides or their constituent pentose and hexose building units for the production of chemicals and fuels. In particular, the conversion of cellulose and glucose to platform chemicals like polyols, lactic acid, levulinic acid, or 5-hydroxymethylfurfural and biofuels has been widely investigated [8–36].

The conversion of short sugars, viz., sugars with four or less carbon atoms, has been investigated to a lesser extent. Nevertheless, there is an increasing interest in using these compounds, as they not only show great potential to be converted into renewable platform chemicals such as lactic acid [9] but also into specialty chemicals such as α-hydroxy-γ-butyrolactone [37], green solvents such as alkyl lactates [38], and new C_4-α-hydroxy acids, suitable as functionalizable polymer building blocks [39, 40]. Therefore, this contribution will focus on recent insights on the catalytic transformations of C_2-, C_3-, and C_4-sugars (dioses, trioses, and tetroses, respectively), but will also include formaldehyde (CH_2O), though often not recognized as a real sugar.

Short-chain sugars can be used directly for producing chemicals but are, due to their rare nature, often very expensive. Until now, practical applications of these small carbohydrates were limited, as well as their large-scale production. Nevertheless, two major strategies to selectively produce these compounds and their related products can be distinguished. The first one is the *top-down* approach, where large mono- or polysaccharides are selectively converted into smaller carbohydrates via thermal treatment or catalysis, before subsequent conversion to the final products. In this respect, glycolaldehyde (C_2) and erythrose (C_4) can be made in high yields (up to 63 %) by the conversion of glucose under supercritical hydrothermal conditions in the absence of a catalyst [41]. The second approach is the *bottom-up* strategy. Here, small compounds such as formaldehyde undergo C-C coupling forming larger substances, before ultimately converting to end products. For example, dihydroxyacetone (C_3) can be selectively made from formaldehyde (up to 85 % yield) using a thiazolium catalyst [42, 43]. Formaldehyde can in turn be produced from renewable methanol, obtained by gasification of biomass through syngas [44, 45].

Short-chain carbohydrates can also be purified from complex bio-oils obtained by the pyrolysis of biomass. Indeed, small carbohydrates often comprise non-negligible fractions of the product stream. Glycolaldehyde, for example, is a major by-product in bio-oils (up to 5–13 wt.%), obtained by pyrolysis of cellulose [46–48]. A successful valorization of those yet unused oxygenate side streams to valuable chemicals could increase the viability of such pyrolytic processes. The different strategies for the production of small carbohydrates are visualized in Fig. 3.1.

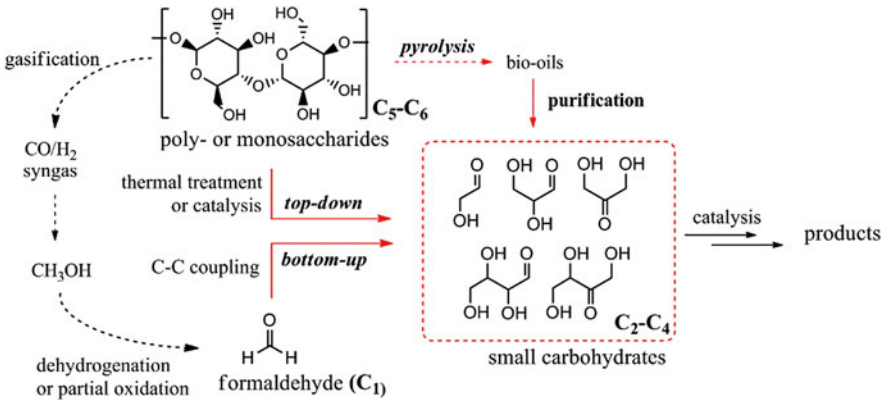

Fig. 3.1 Schematic overview of different synthesis procedures of small carbohydrates

This chapter will try to guide the reader through the recent progresses and obtained insights in the catalytic conversion of short carbohydrates or sugar-like compounds with four or less carbon atoms in the backbone. Also, the lessons learned from reactions with these short sugars are useful to those studying the conversion of pentoses, hexoses, and (hemi)cellulose, because they often appear as intermediates in a series of cascade reactions in one-pot catalytic approaches. Usually, each of those steps still favors its own optimal catalytic environment.

3.2 New Platform Chemicals from Three-Carbon Sugars

3.2.1 Lewis Acid-Catalyzed Synthesis of Lactic Acid or Alkyl Lactates

Lactic acid (LA) is considered to be one of the top carbohydrate-derived platform chemicals [8, 49, 50]. It can serve as a precursor for the synthesis of a wide range of chemicals such as acrylic acid, pyruvic acid, and propylene glycol, but currently finds its main uses in the food industry, in the biopolymer industry, and as a green solvent [9, 10, 38]. The current dominant production process comprises the fermentation of a suitable carbohydrate source by microorganisms, with an estimated annual production capacity of over 0.5 Mton.yr^{-1} [9, 51, 52]. Unfortunately, this process suffers from huge gypsum waste issues (around 1 $kg_{CaSO4}.kg^{-1}{}_{LA}$) and requires a laborious multistep purification work-up to isolate the pure acid. Therefore many research groups are actively exploring alternative ways for producing LA.

A promising alternative route is the chemocatalytic conversion of carbohydrates into LA or alkyl lactates, as evidenced by the huge amount of publications on this topic over the past decade [53–71]. Generally, the three-carbon-containing LA or

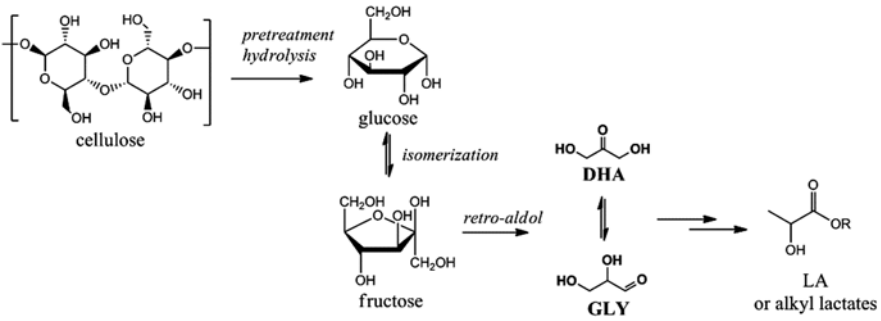

Fig. 3.2 Cascade reaction from cellulose to LA or alkyl lactates

its esters can be produced in high yields from trioses, i.e., dihydroxyacetone (DHA) and glyceraldehyde (GLY). From an economical point of view, the direct conversion of low-value cellulose or refined mono- and disaccharide syrups of, e.g., glucose and sucrose into highly priced lactic acid or lactates is more desirable. However, this in turn implies that more reaction steps are needed, i.e., hydrolysis, isomerization, and retro-aldol. Nonetheless, insight in the conversion of trioses into LA or alkyl lactates is highly informative as they are intermediates in this multistep process as seen in Fig. 3.2, which shows the cellulose-to-LA cascade. For the sake of simplicity, this section will only focus on the catalytic mechanism of converting trioses. The reader is kindly referred to some recent reviews for more information on the direct conversion of cellulose into LA or similar molecules [8, 10].

Hayashi and coworkers were the first to report a fast and selective conversion of trioses to alkyl lactates in alcoholic solvents in 2005 [53, 54]. Using Lewis acidic Sn salts, viz., $SnCl_2$ and $SnCl_4.5H_2O$, alkyl lactate yields of over 80 % were attained after 1 h at 90 °C using 10 mol% of catalyst. While Sn halides are by far the most active catalysts in alcoholic solvents, Al^{3+}- and Cr^{3+}-based halides are superior in water, likely due to the tendency of Sn to form insoluble Sn (hydr)oxides in water [54]. However in water, slightly higher temperatures are needed, yielding up to 90 % of LA after 90 min at 140 °C using 5 mol% of $AlCl_3.6H_2O$ [61]. Recently, the use of lanthanide triflates, alkaline metal earth hydroxides, and $ErCl_3$ has also been suggested [66, 67, 72]. Lanthanide-based catalysts were shown to be recyclable, but high reaction temperatures (240 °C) are required to achieve high LA yields up to 90 % after 30 min, albeit this temperature dependence was only investigated starting from cellulose. The use of alkaline metal earth hydroxides such as $Ca(OH)_2$ suffers from serious limitations, as long reaction times of up to 66 h are needed to achieve mediocre LA yields (59 %) in the form of their corresponding metal salts, requiring an extra purification step to produce the free acid. The generally accepted mechanism for the conversion of trioses to LA or alkyl lactates in water or alcohols, respectively, is schematically shown in Fig. 3.3 for Sn halides, but is equally valid for heterogeneous Lewis acid catalysts.

Both triose isomers, viz., DHA and GLY, can interconvert via a ketose-aldose isomerization in the presence of Lewis acidic Sn [73]. The first reaction step is the

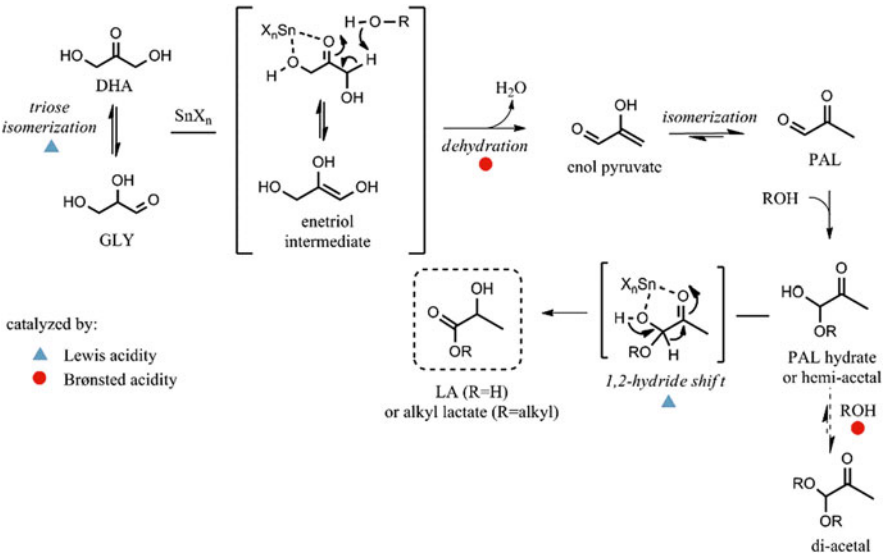

Fig. 3.3 Mechanism for the conversion of trioses to alkyl lactates or lactic acid in alcohols (R = alkyl) or water (R = H), respectively. Note that in water, Sn halides are not stable, and other metals are used, e.g., Al^{3+}

dehydration of a triose via an enetriol intermediate, forming enol pyruvate which rapidly isomerizes to pyruvic aldehyde (PAL). There is no consensus yet on which triose is the ultimate starting material, as both can be converted to alkyl lactates in similar yields [9, 54]. Nonetheless, it is suggested that due to the higher thermodynamic stability of DHA, GLY rapidly isomerizes to DHA prior to dehydration [59, 69, 73]. After rapid isomerization of enol pyruvate to PAL, a nucleophilic attack by alcohol or water on the electrophilic aldehyde carbonyl forms the corresponding hemiacetal or hydrate of PAL, respectively. Lastly, this hemiacetal or hydrate is converted to alkyl lactate or lactic acid, respectively, as the final product. This reaction was proven to occur by a Lewis acid-catalyzed 1,2-hydride shift. The mechanism can be regarded as a formal internal Cannizzaro reaction, or as the combination of a Meerwein-Ponndorf-Verley reduction and Oppenauer oxidation; see Fig. 3.4 [57, 60].

In the presence of strong Brønsted acidity, the hemiacetal of PAL can reversibly incorporate a second alcohol molecule forming the dialkyl acetal as a side product. This side reaction is seen in Fig. 3.3. Still, due to the higher thermodynamic stability of alkyl lactate, the dialkyl acetal can eventually transform to the final product, albeit over longer reaction times and/or at elevated temperatures [60].

The early reports on the conversion of DHA to lactic acid or its esters have invoked a great interest in using heterogeneous catalysts. In 2007, Sels and coworkers reported, for the first time, the use of heterogeneous catalysts for the conversion of sugars like trioses to alkyl lactates using Y zeolites [55]. Three years later, two independent research groups simultaneously investigated the use of H-USY zeolites

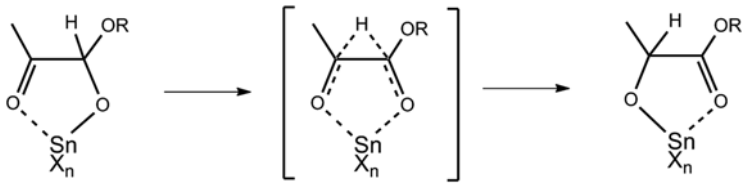

Fig. 3.4 Sn-catalyzed 1,2-hydride shift of PAL hemiacetal to alkyl lactate

for this reaction, along with H-beta, H-ZSM-5, H-MOR, H-montmorillonite, and sulfated zirconia [59, 60]. Both studies confirmed the superior activity of H-USY zeolites, yielding up to 91–96 % alkyl lactate at elevated temperatures (115–120 °C) after 3–24 h. Interestingly, the selectivity to alkyl lactates was correlated to the amount of extra-framework Al (EFAl) species in the zeolite. Whereas framework Al species are associated with Brønsted acidity, EFAl usually displays Lewis acid properties. EFAl may occur in different forms, e.g., $Al(OH)^{2+}$, $Al(OH)_2^{+}$, $Al(OH)_3$, AlO(OH), and Al_2O_3. In general, the lactate yields greatly increase with an increasing amount of EFAl, whereas the dialkyl acetal of LA was the major by-product when the H-USY zeolites contained large amounts of framework Al, due to strong Brønsted acidity. While Lewis acidity is needed to catalyze the final 1,2-hydride shift, Brønsted acidity catalyzes the initial dehydration of the triose as well as the unwanted acetalization of PAL hemiacetal; see Fig. 3.3. Thus, a suitable catalyst should, ideally, contain a high density of Lewis acidic sites in the presence of some weak Brønsted acid sites, which are able to catalyze the initial dehydration step, but are not strong enough to catalyze the unwanted acetalization of PAL hemiacetal.

With this insight, many research groups have attempted alternative methods to incorporate Lewis and Brønsted acidity in heterogeneous catalysts for triose isomerization to LA or alkyl lactates. In this respect, Dapsens et al. have investigated the desilication of MFI-type (ZSM-5) zeolites in a solution of alkali metal hydroxides [74]. The desilication of zeolites introduces mesopores, on which surface Lewis acid sites are generated. Though the true nature of these Lewis acid sites is still the topic of discussion, they are not equivalent to the sites of EFAl obtained by steaming Y zeolites to form H-USY. The density of Lewis acid sites in the catalyst can be tuned by altering conditions during the desilication step. The best catalyst was obtained after desilication in 0.5 M NaOH, achieving a selectivity towards LA exceeding 90 % at 90 % conversion after 6 h at 140 °C.

Next to dealumination or desilication, Lewis acidic zeolites can be obtained by incorporating heteroatoms in the framework. In 2009, Taarning and coworkers have investigated the use of beta zeolites substituted with Lewis acidic heteroatoms such as Sn, Ti, and Zr in the zeolite framework [57]. Sn-beta proved to be very active, yielding >99 % methyl lactate or 90 % lactic acid in methanol and water, respectively, after 24 h at 80 °C. The Lewis acidity likely originates from isolated Sn centers tetrahedrally coordinated in the zeolite framework [57]. Since then, other Sn-based zeolites have been proposed, such as Sn-MWW [65] and Sn-MFI [75],

though the activity of Sn-Beta remained unsurpassed. As an alternative to Sn-zeolites, Ga-zeolites have also been proposed [69, 74, 76]. In analogy to Sn-beta, the Lewis acid sites likely originate from tetrahedrally coordinated gallium species [76]. Different topologies (e.g., MFI, MOR, FER, BEA, and FAU) were tested, but Ga-USY (FAU) proved to be most active, yielding 82 % ethyl lactate for full conversion after 24 h at 85 °C, which is the highest activity reported so far for any tin-free catalyst [76].

Next to zeolites, other materials have also been investigated. One example is Sn-montmorillonite, which converted DHA selectively to ethyl lactate (97 % yield) after 15 h at 150 °C, despite the strong Brønsted acidity of the catalyst [62]. In the same year, Li et al. proposed substituted mesoporous MCM-41 materials, along with transition metal-free oxides, such as Ga_2O_3. Despite the high selectivity of these metal oxides, the catalytic activity was low, yielding only 39 % ethyl lactate after 6 h at 90 °C with Ga_2O_3. Sn-MCM-41, on the other hand, was very active, yielding 98 % ethyl lactate under the same conditions. The great activity was attributed to the presence of Lewis acid sites (as tetrahedrally coordinated tin in the silica framework) together with weak Brønsted acidity, apparently generated by introducing Sn in the silica framework. In Sn-MCM-41, the amount of Brønsted acidity and Lewis acidity were thus somehow correlated to the presence of Sn, and therefore, direct proof of this elegant bifunctional catalysis was still lacking [63].

Later, De Clippel et al. proposed a simple carbon-silica composite design, in which the number of Brønsted acid sites could be altered independently from the Lewis acid sites. Lewis acidity was provided by grafting mesoporous MCM-41 with Sn^{4+}, while Brønsted acidity was introduced by an active carbon phase, located in the mesopores of the MCM structure and obtained by polymerizing impregnated furfuryl alcohol in the mesopores, followed by pyrolysis. A clear correlation was found between the amount of Brønsted acid sites and rate of the reaction. For the first time, it was proven that Sn is crucial for the selectivity towards alkyl lactates by catalyzing the 1,2-hydride shift, whereas the Brønsted acid sites determine the reaction rate, by catalyzing the rate-determining initial dehydration of the triose. This can be seen in Fig. 3.5, which indicates that by altering the amount of Brønsted acid sites (displayed by total amount of CO_x evolution in temperature programmed desorption (TPD)), the conversion rate can be significantly enhanced, while the high selectivity towards ethyl lactate is preserved.

In a very recent publication, Dijkmans et al. were able to synthesize Sn-beta zeolite with Al in the framework. Their procedure involves partial dealumination of a commercial Al-containing beta zeolite in acid solution, followed by grafting with Sn chloride in dry isopropanol [77, 78]. The presence of Brønsted acidity clearly accelerated the rate-determining dehydration step, presented by a linear increase in the conversion rate of DHA with the content of framework Al. Too high contents of Al are detrimental for the selectivity as a lot of side products appear. An ideal atomic ratio of Al to Sn was suggested to convert DHA to ethyl lactate in ethanol. Materials containing moderate amounts of Al (0.3 wt.% Al) and Sn (1.6 wt.%) show the highest ethyl lactate (ELA) productivity, leading to a record value of 2113 g ELA.kg $catalyst^{-1}.h^{-1}$ at 363 K [78].

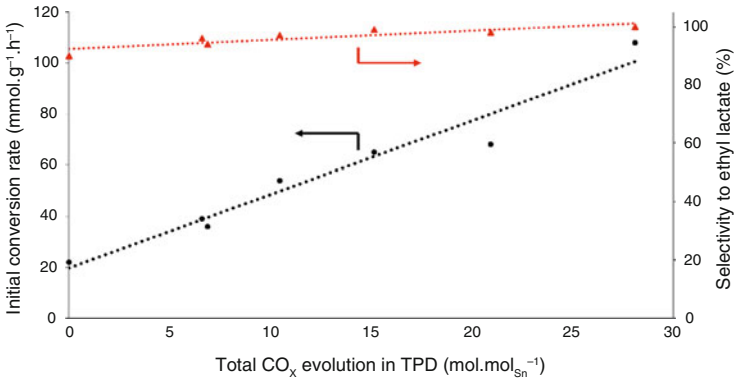

Fig. 3.5 Initial conversion rate (*circles*) and selectivity (*triangles*) of DHA to ethyl lactate for different amounts of Brønsted acid sites per Sn site in carbon-silica composite materials (displayed by total amount of CO_x evolution during TPD) (Based on data from [64])

Thus, it is clear that when designing a heterogeneous catalyst for triose isomerization to lactic acid or alkyl lactates, special care should be taken regarding the amount and type of Lewis and Brønsted acid sites in the material. For more extensive reviews with tabulated yields obtained by the different catalysts proposed so far for the production of alkyl lactates, the reader is referred to our previous work [8, 9].

3.2.2 Direct Conversion of Glycerol to Lactic Acid or Its Esters

Glycerol (GLC) is no sugar; however, its chemistry resembles certain similarities to that of trioses, especially in the production of LA from GLC, where trioses are intermediary products. Besides, GLC provides an interesting raw material as it is not only available in excessive amounts as a waste product in soap and detergent industry but also as a side product in biodiesel manufacturing [9, 79–81]. Therefore, the conversion of GLC towards LA will also be briefly discussed. The strategy is to mildly oxidize GLC to DHA or GLY before subsequent conversion to LA or its esters. This could be achieved in a two-step process. The first step, the oxidation of glycerol to DHA, is however difficult, and it is hard not to end up with the overoxidation product glyceric acid (even though it has been reported to proceed selectively with certain gold catalysts [82]). The GLC to lactate conversion can also be pursued in a one-pot approach, by using two catalytic functions. This cascade is presented in Fig. 3.6.

The first attempts for the one-pot approach typically made use of a heterogeneous oxidation catalyst (e.g., Au-Pt on TiO_2 or CeO_2) in the presence of a base [83–86]. Here, the supported metal is the active site for the oxidation of GLC, whereas the base catalyzes lactic acid formation in the form of a salt. In the presence of bases, LA is formed via rehydration of PAL by the action of hydroxide ions,

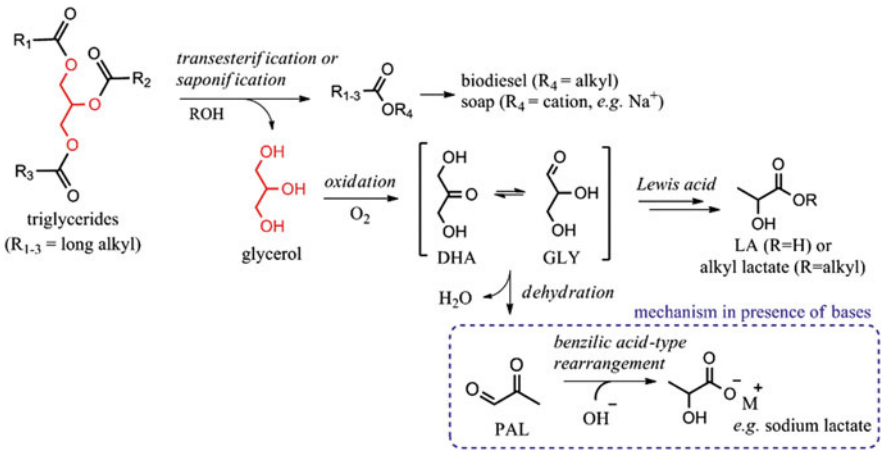

Fig. 3.6 Strategy for the conversion of surplus glycerol from the biodiesel/soap industries to lactic acid (R = H) or alkyl lactates (R = alkyl)

followed by a benzilic acid-type rearrangement. This mechanism is shown in the box in Fig. 3.6. Typically, selectivities to LA around 80 % can be attained for high glycerol conversions (>98 %) using Au or Au-Pt on TiO_2 or CeO_2 at 90–100 °C for 30 min. However, relatively large amounts of base are needed, usually a NaOH to glycerol ratio of 4:1 is used [84–86]. As base is used, additional steps are required to purify and isolate the acid form.

Very recently, researchers have successfully circumvented the need for a base by using a bifunctional catalyst containing both oxidation activity for glycerol oxidation and Lewis acidity for lactic acid formation, e.g., Au/USY [87] or Pt/Sn-MFI [88]. This way, glycerol is oxidized via dehydrogenation by the metallic Au or Pt catalyst, while the Lewis acidic extra-framework Al or framework Sn converts the triose to lactic acid or its esters via a 1,2-hydride shift (*vide supra*). Yields of up to 73 % were reached using these bifunctional catalysts in the absence of a base at 100–160 °C after 10–24 h in water.

3.2.3 Hydrogenation of Trioses to 1,2-Propylene Glycol

Next to making lactic acid or esters, trioses can be hydrogenated to short-chain polyols such as propylene glycol (PG), an important chemical used, for example, as an antifreeze agent or as a precursor for polyesters. This way, an alternative synthesis route is provided for the current method, which involves the hydration of propylene oxide. Though not much literature exists on this matter, two reaction routes can be distinguished: (i) hydrogenation to glycerol and subsequent hydrogenolysis or (ii) dehydration to PAL followed by hydrogenation; see Fig. 3.7 [89, 90]. At higher temperatures (>200 °C), the latter mechanism is dominant.

One patented way for producing PG from DHA comprises the use of a hydrogenation catalyst at temperatures above 200 °C in a continuous flow reactor, following reaction (ii) in Fig. 3.7 [89]. When using a Co-Cu catalyst at 210 °C and 150 bar H_2, 89 % PG yield can be achieved when pumping 50 ml of 20 wt.% DHA solution over 50 ml of catalyst per hour. In Ooms' work on the conversion of carbohydrates to ethylene glycol with a nickel-tungsten carbide catalyst, route (i) was encountered, producing 54–66 % glycerol, but only 18–25 % PG [90]. However, it is worthy to note that these experiments were conducted as a study of the conversion of intermediates in a cascade reaction of larger sugars (e.g., glucose) towards ethylene glycol, and reaction conditions for the hydrogenation of trioses to propylene glycol were thus not optimized in this system.

An alternative method for the production of PG is by the direct hydrogenation of GLC, a reaction that has been investigated in much larger extent. In summary, GLC is transformed to PG by an elimination reaction followed by reduction in acidic or basic conditions. Under alkaline conditions, PG is formed from GLY, whereas under acidic conditions, acetol is the key intermediate. Both reactions are sketched in Fig. 3.8. A more detailed discussion of the hydrogenation of GLC is outside of the scope of this work. More information on the hydrogenation/hydrogenolysis of GLC is available in recent reviews [79, 91].

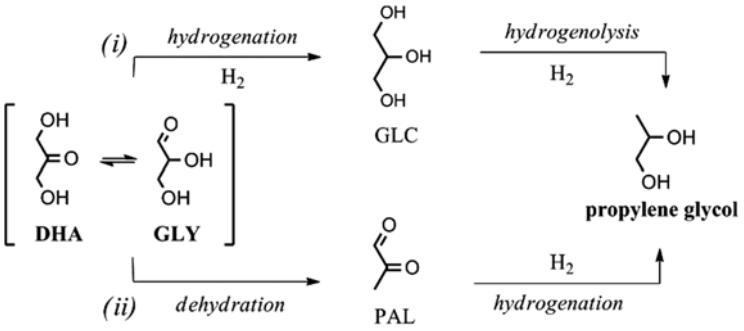

Fig. 3.7 Two different reaction pathways to 1,2-propylene glycol via the hydrogenation of trioses

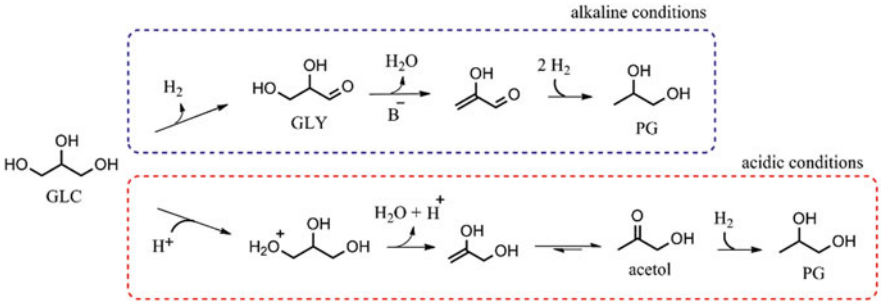

Fig. 3.8 Mechanisms of the hydrogenation of glycerol towards PG under alkaline (*top*) and acidic (*bottom*) conditions

3.3 The Chemistry of Tetroses: Rare Sugars to High-Value Chemicals

3.3.1 Catalytic Synthesis of Functional C_4-α-Hydroxy Esters

Back in 2010, traces of two new C_4-α-hydroxy esters were found in a study on the conversion of (hemi)cellulosic sugars to alkyl lactates with Lewis acidic zeolites in methanol. They were identified to be methyl vinyl glycolate (MVG) and methyl-4-methoxy-2-hydroxybutanoate (MMHB) [58, 92]. These compounds are similar to lactic acid esters, but they contain an extra terminal ether or vinyl group. Their origin was attributed to the conversion of tetroses resulting from the retro-aldol splitting of glucose; see Fig. 3.9. On the other hand, as discussed above, the retro-aldol reaction of fructose leads to the two trioses, DHA and GLY, which can subsequently be converted to lactic acid or lactates.

Interested by this finding, Dusselier et al. were the first to explore the mechanism of the formation of MVG and MMHB by the conversion of erythrulose (ERU) and erythrose (ERO), the keto- and aldotetroses, respectively, with soluble Lewis acid catalysts [39]. In analogy with Hayashi's work on trioses, Sn salts, viz., $SnCl_4.5H_2O$, were the most active catalysts, yielding up to 83 % MMHB in methanol after 1 h at 80 °C. The proposed reaction pathway is given in Fig. 3.10 and displays some notable similarities to the Sn-catalyzed conversion of trioses.

Tetroses can isomerize between the keto and aldo form by the action of Sn, prior to dehydrating twice, forming the suggested highly reactive intermediate vinyl glyoxal. The terminal carbonyl group of vinyl glyoxal can easily incorporate methanol from the solvent, forming a hemiacetal. This intermediate plays a prominent role in the product selectivity, as two different pathways can be followed from here. The formation of MVG suggests a Sn-catalyzed 1,2-hydride shift, trapping the vinyl bond in the final product. In the parallel route to MMHB, the vinyl group can be subjected to a nucleophilic (1,4-)addition of methanol, forming a terminal methoxy group in 1-hydroxy-1,4-dimethoxybutan-2-one (1-HDMBO). Lastly, a 1,2-hydride

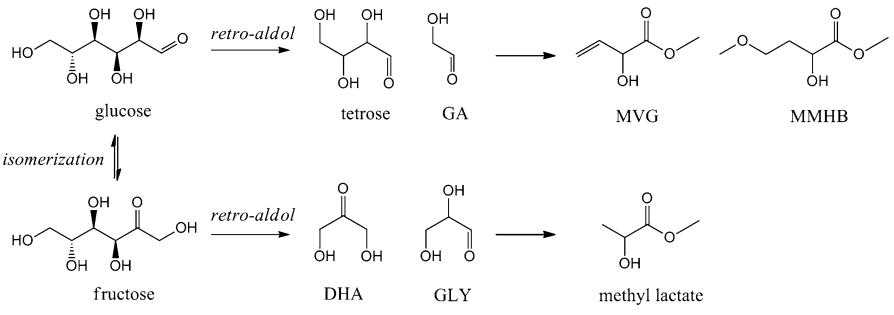

Fig. 3.9 Retro-aldol splitting of hexoses to smaller sugars and subsequent conversion to different α-hydroxy esters in methanol

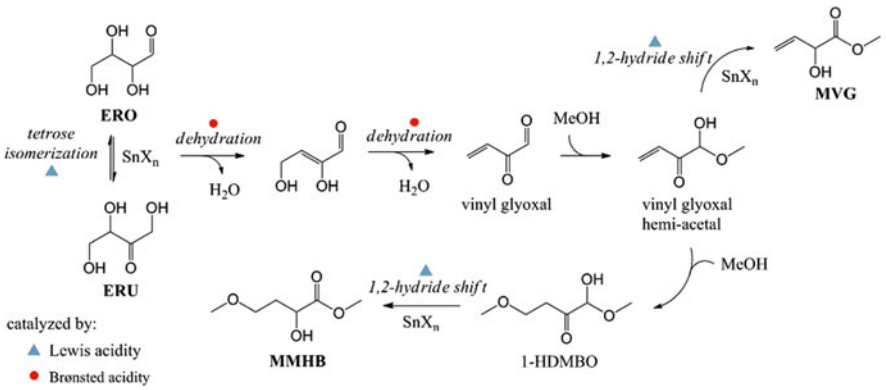

Fig. 3.10 Mechanism for the Sn-catalyzed conversion of tetroses ERU and ERO to MVG and MMHB in methanol, as proposed by [39]

shift results in MMHB as the final product. While the dehydration and methanol addition reactions may be catalyzed by Brønsted acidity, the presence of Sn^{2+} or Sn^{4+} was proven to be crucial for the final 1,2-hydride shift. The mechanism of the 1,2-hydride shift has been discussed previously (Fig. 3.4).

3.3.2 *Role of New C_4-α-Hydroxy Esters in the Biopolymer Industry*

The polymer of lactic acid, polylactic acid (PLA), has been considered a promising substitute for certain petrochemical-based plastics [93, 94]. PLA finds its use in numerous applications ranging from industrial packaging and coatings to biocompatible materials for medical applications [9, 10]. With an annual production of 187 kton, it is currently produced on a mediocre scale [95, 96]. Despite its interesting properties, PLA suffers from a few limitations on top of its slightly expensive production, such as lacking reactive side groups and being too hydrophobic for certain applications [97, 98]. The incorporation of functional α-hydroxy compounds such as MVG or MMHB might offer an innovative solution to this problem. As a proof of concept, Dusselier et al. have successfully incorporated up to 12 mol% of the corresponding acid of MVG in the PLA backbone [40]. The built-in vinyl groups were further functionalized via thiol-ene reactions, e.g., with thioglycerol or benzylmercaptan. With thioglycerol, the hydrophilicity of the polymer increased significantly, proving the value of these new accessible building blocks to obtain new renewable polyesters and properties. The general strategy is shown schematically for MVG in Fig. 3.11.

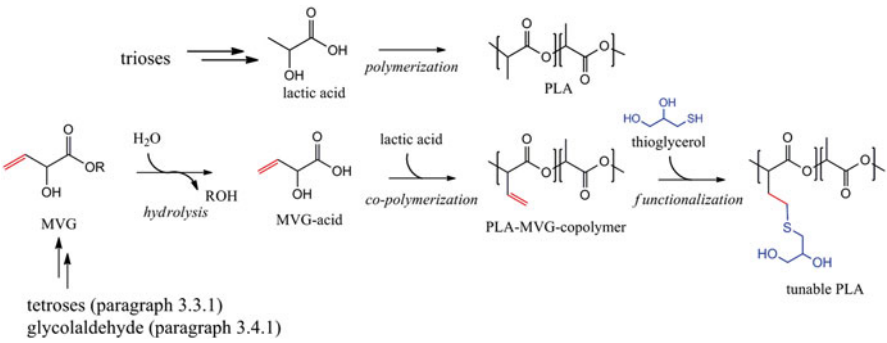

Fig. 3.11 The strategy of tuning PLA properties by incorporating functional C_4-α-hydroxy acids in the PLA backbone via copolymerization, as demonstrated by [40]

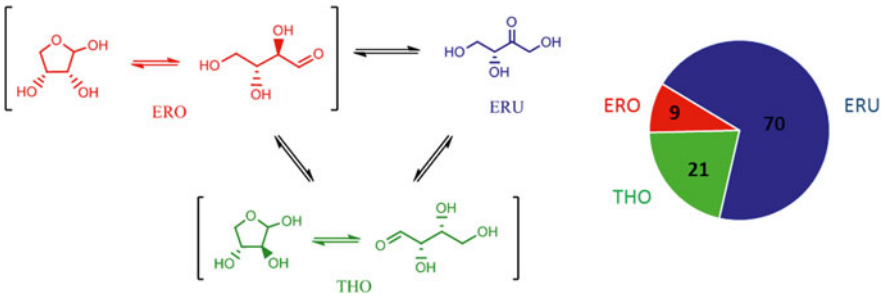

Fig. 3.12 H-USY-catalyzed isomerization of tetroses in aqueous medium (*left*) and distribution ratio of the total tetrose amounts at equilibrium (*right*)

3.3.3 Isomerization of Tetroses in Aqueous Media

In line of studies on the isomerization of pentoses [92, 99, 100] and hexoses [92, 101–103], Saravanamurugan et al. studied the zeolite-catalyzed isomerization of tetrose sugars in aqueous media [104]. H-USY (Si/Al = 6) was shown to be an effective catalyst for the conversion of ERO into ERU. After 3 h at 120 °C, 39 % ERU yield was obtained for 52 % ERO conversion. Threose (THO), an epimer of ERO, was only detected in trace amounts. It was shown that a thermodynamic equilibrium exists between the three tetrose isomers. After long reaction times (ca. 24 h), the total amount of tetroses converges to a distribution ratio of ERO:ERU:THO = 9:70:21, irrespective of which tetrose is the starting material; see Fig. 3.12. Furthermore, during the time needed to attain this equilibrium, the total tetrose yield decreases significantly (below 25 % after 24 h). This means that quantitative conversions of one isomer to another cannot happen in this system since the tetroses degrade or form other products. The strong decrease in total tetrose yield after longer reaction times might be attributed to the high temperatures used compared to pentose [92] and hexose [103] isomerization experiments, even though the tetrose

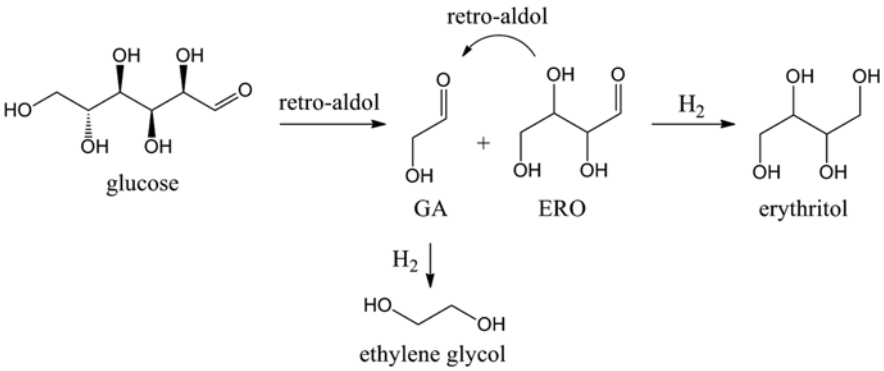

Fig. 3.13 Hydrogenation of ERO and GA to erythritol and ethylene glycol, as proposed by [90]

sugars are thermally less stable than the larger (often cyclic) sugars. In alcoholic media, the tetroses seemed to degrade rapidly, preserving only a limited total tetrose yield (27 %) after 1 h at 80 °C in methanol. This is in correspondence with our earlier work [39] which showed the rapid conversion of tetroses in alcoholic media after 1 h at 90 °C in the presence of Brønsted and Lewis acids, both sites that are also present in the H-USY zeolites used in Saravanamurugan's work.

3.3.4 Hydrogenation of Tetroses

In analogy with trioses, tetroses can be hydrogenated to erythritol or ethylene glycol. Both electrochemical [105, 106] and catalytic methods have been suggested. Though not a lot of literature exists on the latter, Ooms et al. have yielded 49 % ethylene glycol and 10 % erythritol from the hydrogenation of ERO using nickel-tungsten carbide catalysts after 3 h at 245 °C [90]. This experiment was in function of a larger study on the direct hydrogenolysis of glucose, where high temperatures were used in order to catalyze the retro-aldol splitting of glucose to GA and ERO. The mechanism is schematically shown in Fig. 3.13.

3.4 Valorization of C_2-Sugars

Glycolaldehyde, the two-carbon sugar, is rare in nature, but is said to have had a major role in the *origin of life* as a precursor for the prebiotic synthesis of riboses, building blocks of DNA [107, 108]. Recently, the presence of GA was shown in interstellar space [109]. No large-scale production processes are employed at the moment, but recently there is an increasing interest in producing GA. As such, GA can be produced selectively by converting glucose uncatalytically in supercritical water.

This way, up to 64 % GA yield (at >99 % conversion) was obtained when converting glucose at 450 °C, 35 MPa, and a contact time of 0.25 s [41]. Furthermore, GA is often encountered as a by-product in bio-oils obtained from the pyrolysis of biomass [46–48]. Indeed, pyrolysis oil can contain up to 5–13 wt.% GA [46, 47, 110]. Considering the availability of the feedstock, these are non-negligible amounts which are now considered as unwanted side oxygenates.

Attempts to isolate GA from pyrolysis oil via extraction have already been made, though with an overall GA yield of 17 %, too many GA is lost in the process [111]. More recently, a purification process based on reactive extraction was proposed [112]. Here, a biphasic system is used, in which GA in the aqueous phase reacts with an amine in the organic phase according to a Schiff-base reaction, forming an imine. The subsequent hydrolysis of this imine then releases GA again. With this method, a much higher recovery of GA can be realized, e.g., 94 % when using 2-ethylaniline in 1-octanol as the organic phase. However, the hydrolysis of the imines requires the use of anti-solvents, catalysts, and extra purification steps, which can hamper applications at a larger scale. Nevertheless, the valorization of such oxygenate side streams in bio-oils to high-value chemicals can be a major strategy to increase the viability of the future biorefineries. Therefore, this section will briefly discuss the opportunities regarding the catalytic conversion of GA.

3.4.1 Synthesis of C_4-α-Hydroxy Esters from Glycolaldehyde

The origin of C_4-α-hydroxy esters was attributed to tetroses resulting from the retro-aldol reaction of glucose. Next to ERO, this reaction produces an equimolar amount of GA (*vide infra*). To study the fate of GA, Holm et al. were the first to study its conversion with Sn-beta catalysts [92]. After 16 h in methanol, four major products were identified, viz., MVG, MMHB, methyl lactate (MLA), and glycolaldehyde dimethylacetal (GADMA). At higher temperatures (160 °C), MVG and MLA are the preferred products with 27 % and 16 % yield, respectively. At lower temperatures (100 °C), the selectivity to MMHB rises (26 % yield), whereas the selectivity to MVG and MLA decreases (13 and 4 % yield, respectively). The presence of both C_4- and C_3-compounds suggests Sn-beta zeolites can simultaneously catalyze aldol and retro-aldol reactions. A proposed reaction pathway is given in Fig. 3.14.

To study the Sn-catalyzed origin of these products from GA, Dusselier and coworkers used homogeneous Sn halide catalysts for the conversion of GA in alcoholic media [40]. Analogous to the conversion of trioses [54] and tetroses [39] in alcohols, Sn^{2+} and Sn^{4+} halides were the most active catalysts, yielding 55–58 % MMHB after 1 h at 90 °C in methanol. In contrast to heterogeneous Sn-beta catalysts, no methyl lactate was observed when using homogeneous Sn halides. This indicates that, when using Sn halides, intermediately formed tetroses convert too fast to undergo a second aldol addition to higher sugars that in turn could lead to MLA (Fig. 3.14). The proposed reaction mechanism for the conversion of GA to MMHB is shown in Fig. 3.15.

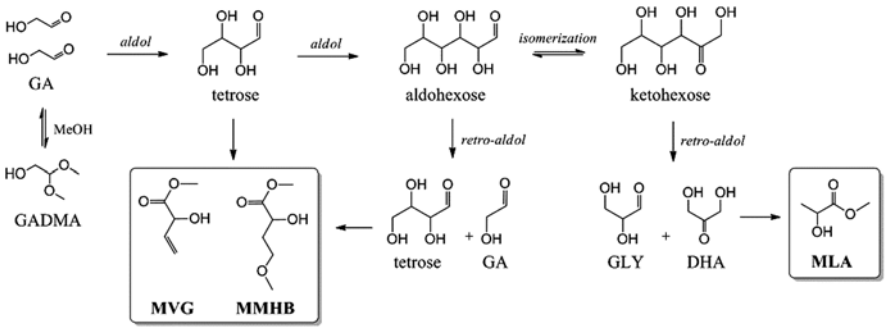

Fig. 3.14 Reaction pathway for the conversion of GA with Sn-beta in methanol as proposed by [92]

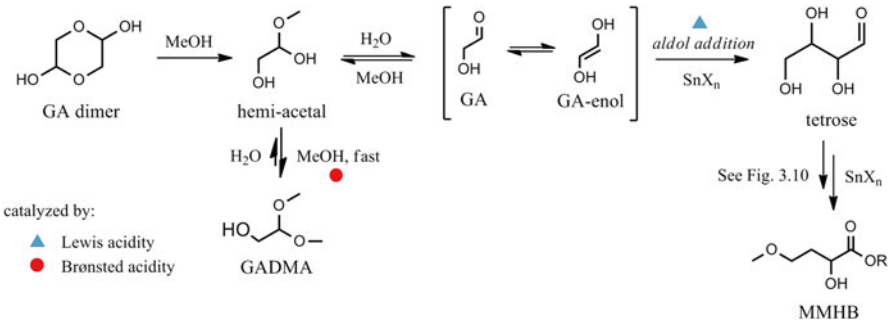

Fig. 3.15 Reaction pathway for the conversion of GA to MMHB in methanol in the presence of Sn halides as proposed by [40]

When dissolving the substrate (the dimer of GA) in methanol in the presence of Sn halides, GADMA is formed very fast in near-quantitative amounts. This means that GADMA can formally be viewed as the starting point of the reaction. In order for an aldol reaction to be possible, GA should be present in its unprotected monomeric form. Consequently, the first two steps in the reaction are the double hydrolysis of GADMA via its hemiacetal, forming free GA. This free GA is in equilibrium with its enol, which can attack the carbonyl of another GA, forming a tetrose via aldol addition. In the absence of SnX_n, no C_4-compounds were detected, hinting to the crucial role of Sn for the aldol reaction. Once the tetrose is formed, its conversion to MMHB goes according to the same mechanism as previously discussed for the Sn-catalyzed conversion of tetroses (Sect. 3.3).

The rate-determining step in the cascade was proven to be the first reaction, the hydrolysis of GADMA to its hemiacetal. Consequently, the reaction kinetics could be enhanced significantly (up to 4.5 times, to a rate of 3.7 $mol_{MMHB}.mol_{Sn}.h^{-1}$) by adding small aliquots of water to the reaction medium. Further investigation revealed that the ratio of Lewis acidic Sn centers over Brønsted acidity, coming from the

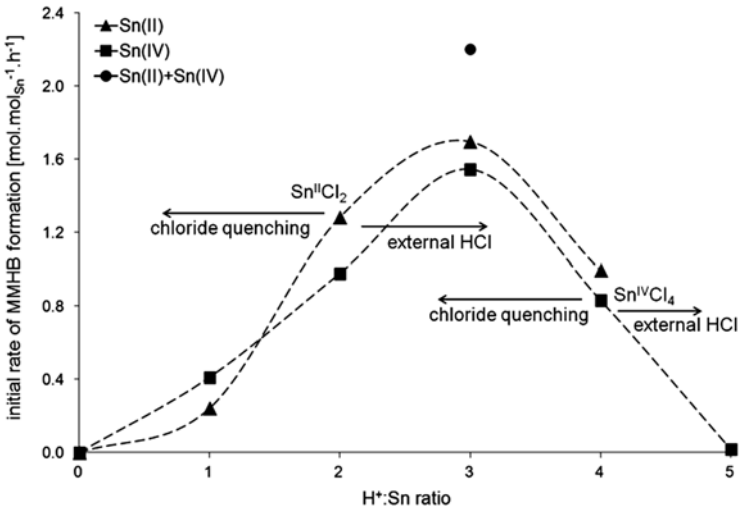

Fig. 3.16 Initial rate of MMHB formation in function of the H^+:Sn ratio in the reaction mixture (Reprinted with permission from [40]. Copyright 2013, American Chemical Society)

presence of (partially) dissociated Cl^- ligands, also has a major impact on the reaction kinetics. This ratio can be described as H^+:Sn and can be altered by carefully quenching H^+ or adding external HCl. Optimally, a ratio of H^+:Sn = 3 is used, as seen in Fig. 3.16. Interestingly, this optimum is irrespective of the oxidation state of Sn. An alternative to the tedious quenching or acidification manipulations is the use of equimolar amounts of $SnCl_4.5H_2O$ and $SnCl_2.2H_2O$, also mounting to a H^+:Sn = 3 ratio as seen as the dot in Fig. 3.16. These findings indicate the importance of balancing multiple active sites in cascade biomass chemistry and can be highly informative in the future to design heterogeneous catalysts with the ideal balance of Lewis and Brønsted acid sites.

3.4.2 Lewis Acid-Catalyzed Conversion of Glyoxal to Glycolic Acid

Even though glyoxal (GLX) is not a sugar, technically, the chemistry of this two-carbon dialdehyde is much related to that of the small saccharides. Analogue to the conversion of trioses to lactic acid, GLX can be converted by Lewis acids to glycolic acid (GLA), a two-carbon α-hydroxy acid. Like PLA, polymers of GLA, e.g., polyglycolide or copolymers thereof, are extensively studied for their biocompatibility, mostly in the medical field [113, 114]. GLA is currently produced by carbonylation of formaldehyde in the presence of H_2SO_4 at high temperature and pressure. Recently, a new route to synthesize GLA was proposed based on the heterogeneously catalyzed isomerization of GLX in water under mild conditions [115].

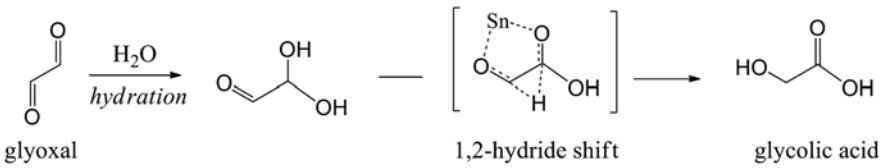

Fig. 3.17 Sn-catalyzed conversion of glyoxal to glycolic acid in water via a 1,2-hydride shift

As with GA, bio-oils from the pyrolysis of biomass can contain ca. 2–3 wt.% of GLX, which can be easily recovered by water extraction followed by chromatographic purification [116]. The isomerization of GLX to GLA could thus provide an attractive route to valorize a side oxygenate stream to high-value chemicals. The isomerization of GLX to GLA or corresponding esters is efficiently catalyzed by Lewis acidic zeolites in water and alcohols, respectively. Again, Sn-based zeotype catalysts seemed superior for this reaction. Indeed, during batch experiments, Sn-MFI yields 91 % GLA after 18 h at 90 °C, whereas a commercial USY with extra-framework Al (e.g., CBV600) only yields 62 % [115]. As in the conversion of trioses and tetroses, the mechanism was shown to occur via a 1,2-hydride shift, in agreement with earlier performed theoretical studies; see Fig. 3.17 [117]. The authors have also investigated this isomerization reaction in continuous flow mode. For this, an aqueous solution of 2 wt.% GLX was sent through a catalytic bed of Sn-MFI (0.5 cm^3) with a flow of 0.3 $cm^3.min^{-1}$ during 8 h at 90 °C. During this experiment, the GLX conversion and selectivity towards GLA remained stable at 40 and 96 %, respectively, proving the potential of such continuous processes in the valorization of GLX to GLA.

3.5 Prebiotic Mechanisms as Inspiration for the Selective *Bottom-Up* Synthesis of Carbohydrates

Although not officially considered as a sugar [118], formaldehyde (CH_2O) abides by the theoretical sugar structural formula ($C_nH_{2n}O_n$). It has likely played a major role in the prebiotic synthesis of carbohydrates, a crucial step in the *origin of life* [107]. In 1861, Butlerow reported the synthesis of a sugary substance when heating an aqueous solution of formaldehyde in the presence of a base, a reaction now generally known as the formose reaction [119]. This nonselective reaction comprises the conversion of formaldehyde to a complex mixture of compounds, ranging from C_2-C_8 carbohydrates to polyols and polyhydroxy acids [120–122]. In fact, due to the complexity of the formose product, Weiss stated it can be regarded as the carbohydrate analogue of petroleum [123]. Researchers have been devoting much time in elucidating the underlying mechanism to apply this for a selective *bottom-up* synthesis of larger carbohydrates [121]. However, due to many different reactions occurring simultaneously, e.g., (retro)-aldol, isomerizations, and Cannizzaro reactions,

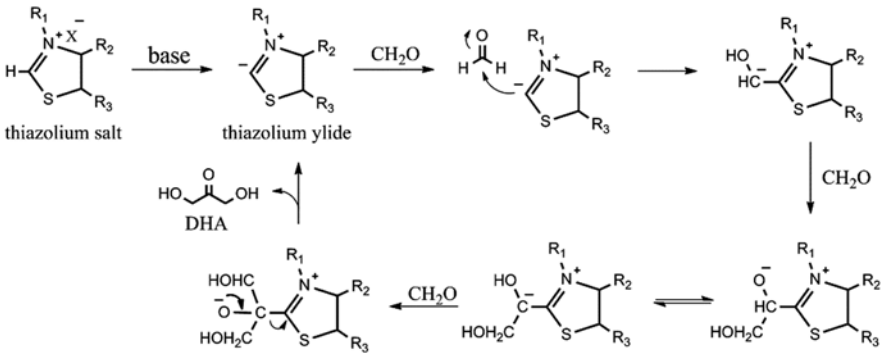

Fig. 3.18 Mechanism for the selective conversion of formaldehyde to DHA catalyzed by a thiazolium ylide, as proposed by [43]

successful attempts are limited. Nevertheless, one remarkable attempt is the selective formation of DHA from formaldehyde, catalyzed by thiazolium salts, reported by Matsumoto et al. after earlier exploration by Castells and coworkers [42, 43, 124]. These catalysts efficiently catalyze the acyloin condensation of formaldehyde to DHA in different solvents. The presence of a base is needed to deprotonate the C_2-carbon of the thiazolium ring, forming an ylide, the active species. After screening different bases and solvents, selectivities up to 91 % were achieved for 94 % formaldehyde conversion after 1 h at 100 °C. The most active and selective catalytic system was obtained when using 3-ethylbenzothiazolium bromide in the presence of tetraethylammonium hydroxide. The mechanism is based on the nucleophilic attack of a carbanion on the electrophilic formaldehyde; see Fig. 3.18. Recently, a similar strategy was reported for the selective conversion of formaldehyde to glycolaldehyde using N-heterocyclic carbene catalysts [125].

In light of finding heterogeneous catalysts for the selective conversion of formaldehyde to carbohydrates, efforts have been made to immobilize a thiazolium-based catalyst on cation-exchange resins [126] or zeolites [127], with reasonable success. The impregnated zeolites showed lower formaldehyde conversions along with pore blockage caused by the products, resulting in a rapid decrease of activity when reused, though the latter can be partly solved by washing the zeolite with water between each run. However, the catalytic activity was only assessed by comparing the conversion of formaldehyde, but no data was mentioned on the influence on the selectivity towards DHA. Nevertheless, it was mentioned that the main product in the reaction remained DHA (no yields were given). The decrease in activity between each run of the thiazolium-impregnated zeolites with and without intermediate washing is shown in Fig. 3.19.

The selective synthesis of DHA via thiazolium catalysts was recently used as a linking strategy to produce fuels from formaldehyde. Deng and coworkers (2013) have proposed a multistep process, comprising (1) the synthesis of formaldehyde from biomass, (2) the thiazolium-catalyzed formation of DHA, (3) the base-catalyzed aldol condensation of DHA to dendroketose, and (4) the dehydration

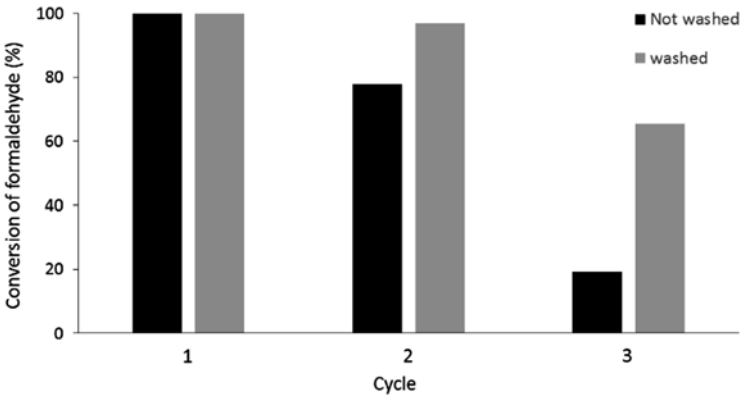

Fig. 3.19 Decrease in activity of thiazolium-impregnated zeolites for DHA production with each reuse cycle, without (*black*) and with (*gray*) washing between each use (Based on data from [127])

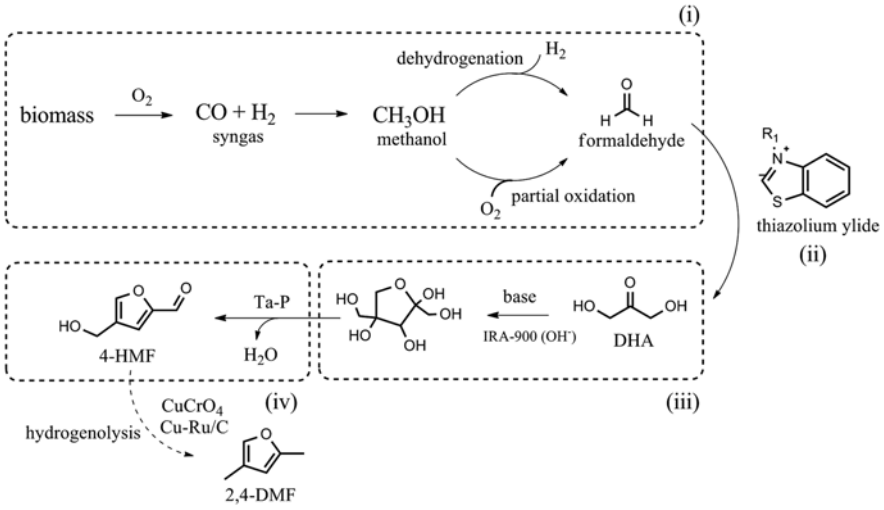

Fig. 3.20 Strategy for the conversion of biomass to 2,4-DMF via the selective synthesis of DHA from formaldehyde, as proposed by [45]

of dendroketose to 4-hydroxymethylfurfural (4-HMF) catalyzed by tantalum phosphates [45, 121]. 4-HMF can then further be converted to 2,4-dimethylfuran (2,4-DMF) or C_9-C_{15} branched-chain alkanes for use as a high-energy-density liquid fuels. Formaldehyde can be acquired by the oxidation of methanol, synthesized from syngas via the gasification of biomass, or by steam reforming of natural gas or liquid hydrocarbons. A schematic overview of the suggested process is shown in Fig. 3.20. Such approaches might inspire scientists to consider the use of cheap formaldehyde as starting substrate for carbohydrates, from which high-value

chemicals or fuels can be synthesized. Formaldehyde is cheap, having a production cost of around 0.38 $.kg^{-1} [45]. The production of carbohydrates, which would otherwise be difficult to obtain (e.g., trioses), from such a cheap precursor would thus be highly desirable. Insight in prebiotic mechanisms such as the formose reaction might provide the missing link between formaldehyde and workable carbohydrates.

3.6 Cross Coupling of Small Carbohydrates

The aldol reaction is a powerful and well-known tool for producing C-C bonds in organic chemistry. Its mechanism proceeds via the nucleophilic addition of an enol or enolate to an electrophilic carbonyl group, producing a new β-hydroxy carbonyl compound. In Matsumoto's work on DHA formation, formaldehyde fulfills both roles. When different electrophilic and nucleophilic compounds are used, a wide range of products can be formed. Due to the intrinsically high electrophilicity of formaldehyde, it is commonly used as a one-carbon electrophile [128]. Recently, Yamaguchi et al. have successfully exploited this in their attempt to couple formaldehyde to triose sugars, forming α-hydroxy-γ-butyrolactone (HBL), a cyclic C_4-α-hydroxy ester that finds its use as a synthetic intermediate in pharmaceutical chemistry [37, 129]. A similar approach was followed earlier for the coupling of formaldehyde to GA with *D-fructose-6-phosphate aldolase* [130]. In Yamaguchi's work, Sn halides were the most active catalysts, yielding up to 70 % HBL after 3 h at 140 °C in 1,4-dioxane when using 14 mol% $SnCl_4$. The proposed reaction mechanism is shown in Fig. 3.21. As a side reaction, the triose sugars can convert to lactic acid. In a standard reaction in the absence of formaldehyde, up to 24 % LA is formed this way. However, by using an excess amount of formaldehyde, the selectivity can be steered towards HBL, e.g., when a formaldehyde to DHA ratio of 3:1 is used,

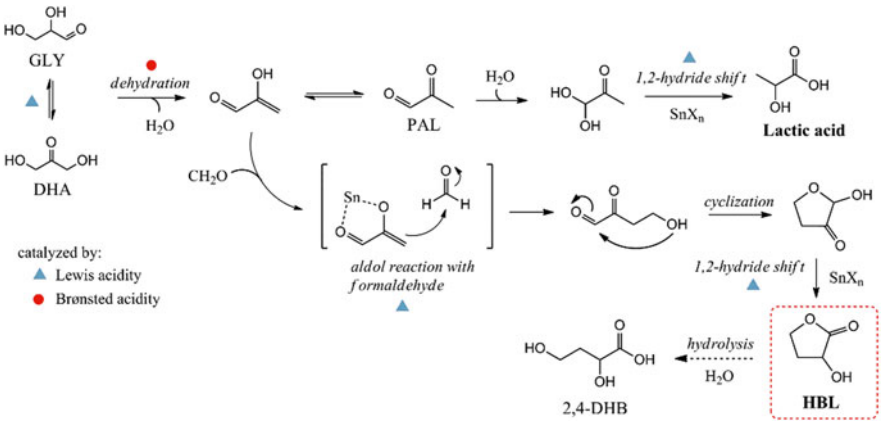

Fig. 3.21 Reaction pathway for the synthesis of HBL from trioses and formaldehyde, as proposed by [37]

70 % HBL is obtained with only 5 % of LA [37, 129]. Simultaneously, Van de Vyver et al. investigated the use of solid Lewis acids for the same reaction [131]. Under similar reaction conditions (3 h at 140 °C in 1,4-dioxane), up to 68 % HBL yield was attained using a Sn-beta catalyst. Via a continuous reaction experiment in a packed-bed flow reactor, an average productivity of 18.1 g HBL per g catalyst per h was calculated. It was proposed that the formation of HBL by solid Lewis acids proceeds via soft enolization of DHA to a Sn-enolate intermediate, followed by an aldol addition of formaldehyde generating erythrulose as an intermediate species [131].

In the work on the Sn-catalyzed conversion of tetroses, HBL was encountered as a side product. In 1,4-dioxane, the cyclization of the C_4-intermediate is most pronounced, whereas in alcohols the conversion to MMHB and MVG is preferred [39]. Note that when one would hydrolyze HBL, 2,4-dihydroxybutyric acid (2,4-DHB) is obtained, which is essentially MMHB but with the methoxy groups replaced by hydroxyl groups. 2,4-DHB could serve as an interesting α-hydroxy acid, due to the terminal alcohol group. Just as the terminal vinyl group in MVG, the terminal alcohol in 2,4-DHB could provide extra functionality when this compound is built in a polyester backbone, such as that of PLA.

3.7 Summary, Conclusions, Outlook

Carbohydrates, the largest available renewable carbon feedstock, will likely play a major role in future biorefineries. Until now, scientists have mainly focused on the direct conversion of poly- or monosaccharides such as (hemi)cellulose or glucose. However, it is clear that shorter sugars, such as glycolaldehyde, trioses, or tetroses, have tremendous potential in the chemical industry. For instance, trioses can be readily converted to lactic acid, a major bio-derived platform chemical, in high yields. Moreover, more specialized, high-value compounds can be targeted as well, such as α-hydroxy-γ-butyrolactone or recently discovered four-carbon α-hydroxy esters, of which the potential as functionalizable polyester building blocks has been demonstrated.

Unfortunately, large-scale production processes of short carbohydrates are still lacking, but reasonable attempts for selectively obtaining them have already been made, such as the retro-aldol splitting of glucose to erythrose and glycolaldehyde in supercritical water or via purification from pyrolytic bio-oils. From a practical point of view, the direct use of poly- or monosaccharides might remain more interesting. Nevertheless, the insights provided in this chapter remain very useful, as short sugars are intermediates in the cascade reaction departing from, e.g., cellulose or glucose.

Instead of using poly- or monosaccharides, a new and innovative approach is to use formose-like reactions, starting with cheap formaldehyde, to link the selective synthesis of carbohydrates to their conversion to chemicals. This *bottom-up* strategy has recently been used to make 4-hydroxymethylfurfural from formaldehyde with intermediary triose formation. Such out-of-the-box thinking can shine a new light on future carbohydrate-related research, although the sustainable production of

formaldehyde could then be an issue. Indeed, formaldehyde is made from syngas, which can be obtained in a renewable way via gasification of biomass, but it is currently produced from steam reforming of natural gas or liquid hydrocarbons.

In the chemistry of short carbohydrates, Lewis acids, mainly Sn, play a major role. When acids or esters are the desired product, they determine the product selectivity by catalyzing the 1,2-hydride shift, the final reaction. Brønsted acidity on the other hand has a major effect on reaction kinetics. For both homogeneous and heterogeneous catalysts, it was shown that optimal ratios of Lewis/Brønsted acid sites exist. This information is vital for future catalyst design. Since the elucidation of the role of Lewis acids in carbohydrate chemistry, researchers are actively and successfully exploring different Lewis acidic materials, mainly Sn based, as a catalyst for sugar chemistry, but the use of other elements is currently under exploration. Due to the toxicity and limited availability of Sn, Sn-free catalysts, e.g., gallium-based zeolites, have also been suggested, but until now, the activity of Sn catalysts still remains unsurpassed. Rare earth elements are investigated as well.

It is clear that, over the past decades, the knowledge on carbohydrate conversion chemistry has expanded rapidly. Many challenges remain, but the potential of carbohydrates, whatever their size, is undoubtedly promising. With the help of the insights provided in this chapter, it is now up to researchers and industry to assess the possibilities of carbohydrates in the chemical processes of future biorefineries.

Acknowledgments R.D.C. acknowledges the agency for Innovation by Science and Technology in Flanders (IWT) and the Industrial Research Fund (IOF) (grant ZKC8139) for funding.

References

1. Ragauskas AJ, Williams CK, Davison BH, Britovsek G, Cairney J, Eckert CA, Frederick WJ, Hallett JP, Leak DJ, Liotta CL, Mielenz JR, Murphy R, Templer R, Tschaplinski T (2006) The path forward for biofuels and biomaterials. Science 311:484–489
2. Shafiee S, Topal E (2009) When will fossil fuel reserves be diminished? Energy Policy 37:181–189
3. Geboers JA, Van de Vyver S, Ooms R, Op de Beeck B, Jacobs PA, Sels BF (2011) Chemocatalytic conversion of cellulose: opportunities, advances and pitfalls. Catal Sci Technol 1:714–726
4. Vennestrøm PNR, Osmundsen CM, Christensen CH, Taarning E (2011) Beyond petrochemicals: the renewable chemicals industry. Angew Chem Int Ed Engl 50:10502–10509
5. Lipinsky ES (1981) Chemicals from biomass: petrochemical substitution options. Science 212:1465–1471
6. Lichtenthaler FW, Peters S (2004) Carbohydrates as green raw materials for the chemical industry. C R Chim 7:65–90
7. Lynd LR, Wyman CE, Gerngross TU (1999) Biocommodity engineering. Biotechnol Prog 15:777–193
8. Dusselier M, Mascal M, Sels B (2014) Top chemical opportunities from carbohydrate biomass: a chemist's view of the biorefinery. In: Nicholas KM (ed) Selective catalysis for renewable feedstocks and chemicals. Springer International Publishing, Cham, Switzerland, pp 1–40
9. Dusselier M, Van Wouwe P, Dewaele A, Makshina E, Sels BF (2013) Lactic acid as a platform chemical in the biobased economy: the role of chemocatalysis. Energy Environ Sci 6:1415–1442

10. Dusselier M, Sels BF (2014) Selective catalysis for cellulose conversion to lactic acid and other α-hydroxy acids. In: Nicholas KM (ed) Selective catalysis for renewable feedstocks and chemicals. Springer International Publishing, Cham, Switzerland, pp 85–125
11. Van de Vyver S, Thomas J, Geboers J, Keyzer S, Smet M, Dehaen W, Jacobs PA, Sels BF (2011) Catalytic production of levulinic acid from cellulose and other biomass-derived carbohydrates with sulfonated hyperbranched poly(arylene oxindole)s. Energy Environ Sci 4:3601–3610
12. Mäki-Arvela P, Simakova IL, Salmi T, Murzin DY (2014) Production of lactic acid/lactates from biomass and their catalytic transformations to commodities. Chem Rev 114:1909–1971
13. Corma A, Iborra S, Velty A (2007) Chemical routes for the transformation of biomass into chemicals. Chem Rev 107:2411–2502
14. Zhang Q, Jérôme F (2013) Mechanocatalytic deconstruction of cellulose: an emerging entry into biorefinery. ChemSusChem 6:2042–2044
15. Carrasquillo-Flores R, Käldström M, Schüth F, Dumesic JA, Rinaldi R (2013) Mechanocatalytic depolymerization of dry (ligno)cellulose as an entry process for high-yield production of furfurals. ACS Catal 3:993–997
16. Meine N, Rinaldi R, Schüth F (2012) Solvent-free catalytic depolymerization of cellulose to water-soluble oligosaccharides. ChemSusChem 5:1322
17. Gliozzi G, Innorta A, Mancini A, Bortolo R, Perego C, Ricci M, Cavani F (2014) Zr/P/O catalyst for the direct acid chemo-hydrolysis of non-pretreated microcrystalline cellulose and softwood sawdust. Appl Catal B Environ 145:24–33
18. Climent MJ, Corma A, Iborra S (2014) Conversion of biomass platform molecules into fuel additives and liquid hydrocarbon fuels. Green Chem 16:516–547
19. Ruppert AM, Weinberg K, Palkovits R (2012) Hydrogenolysis goes bio: from carbohydrates and sugar alcohols to platform chemicals. Angew Chem Int Ed 51:2513
20. Kobayashi H, Fukuoka A (2013) Synthesis and utilisation of sugar compounds derived from lignocellulosic biomass. Green Chem 15:1740–1763
21. Yabushita M, Kobayashi H, Fukuoka A (2014) Catalytic transformation of cellulose into platform chemicals. Appl Catal B Environ 145:1–9
22. Gallezot P (2012) Conversion of biomass to selected chemical products. Chem Soc Rev 41:1538–1558
23. Wang T, Nolte MW, Shanks BH (2014) Catalytic dehydration of C6 carbohydrates for the production of hydroxymethylfurfural (HMF) as a versatile platform chemical. Green Chem 16:548–572
24. Zhang J, Liu X, Sun M, Ma X, Han Y (2012) Direct conversion of cellulose to glycolic acid with a phosphomolybdic acid catalyst in a water medium. ACS Catal 2:1698–1702
25. Weingarten R, Conner WC, Huber GW (2012) Production of levulinic acid from cellulose by hydrothermal decomposition combined with aqueous phase dehydration with a solid acid catalyst. Energy Environ Sci 5:7559–7574
26. Corma A, de la Torre O, Renz M (2012) Production of high quality diesel from cellulose and hemicellulose by the Sylvan process: catalysts and process variables. Energy Environ Sci 5:6328–6344
27. Corma A, de la Torre O, Renz M, Villandier N (2011) Production of high-quality diesel from biomass waste products. Angew Chem Int Ed 50:2375–2378
28. Huber GW, Corma A (2007) Synergies between bio- and oil refineries for the production of fuels from biomass. Angew Chem Int Ed 46:7184–7201
29. Han J, Sen SM, Alonso DM, Dumesic JA, Maravelias CT (2014) A strategy for the simultaneous catalytic conversion of hemicellulose and cellulose from lignocellulosic biomass to liquid transportation fuels. Green Chem 16:653–661
30. Serrano-Ruiz JC, Dumesic JA (2011) Catalytic routes for the conversion of biomass into liquid hydrocarbon transportation fuels. Energy Environ Sci 4:83–99

31. Kunkes EL, Simonetti DA, West RM, Serrano-Ruiz JC, Gärtner CA, Dumesic JA (2008) Catalytic conversion of biomass to monofunctional hydrocarbons and targeted liquid-fuel classes. Science 322:417–421
32. Huber GW, Chheda J, Barett C, Dumesic JA (2005) Production of liquid alkanes by aqueous-phase processing of biomass-derived carbohydrates. Science 308(80):1446–1450
33. Mascal M, Nikitin EB (2008) Direct, high-yield conversion of cellulose into biofuel. Angew Chem Int Ed 47:7924–7926
34. Chen K, Tamura M, Yuan Z, Nakagawa Y, Tomishige K (2013) One-pot conversion of sugar and sugar polyols to n-alkanes without C–C dissociation over the Ir-ReOx/SiO2 catalyst combined with H-ZSM-5. ChemSusChem 6:613–621
35. Roman-Leshkov Y, Barrett CJ, Liu ZY, Dumesic JA (2007) Production of dimethylfuran for liquid fuels from biomass-derived carbohydrates. Nature 447:982–985
36. Liu S, Tamura M, Nakagawa Y, Tomishige K (2014) One-pot conversion of cellulose into n-hexane over the Ir-ReOx/SiO2 catalyst combined with HZSM-5. ACS Sustain Chem Eng 2:1819–1827
37. Yamaguchi S, Motokura K, Sakamoto Y, Miyaji A, Baba T (2014) Tin-catalyzed conversion of biomass-derived triose sugar and formaldehyde to α-hydroxy-γ-butyrolactone. Chem Commun 50:4600–4602
38. Pereira CSM, Silva VMTM, Rodrigues AE (2011) Ethyl lactate as a solvent: properties, applications and production processes – a review. Green Chem 13:2658–2671
39. Dusselier M, Wouwe V, De Clippel F, Dijkmans J, Gammon W, Sels BF (2013) Mechanistic insight into the conversion of tetrose sugars to novel alpha-hydroxy acid platform molecules. ChemCatChem 5:569–575
40. Dusselier M, Van Wouwe P, De Smet S, De Clercq R, Verbelen L, Van Puyvelde P, Du Prez FE, Sels BF (2013) Toward functional polyester building blocks from renewable glycolaldehyde with Sn cascade catalysis. ACS Catal 3:1786–1800
41. Sasaki M, Goto K, Tajima K, Adschiri T, Arai K (2002) Rapid and selective retro-aldol condensation of glucose to glycolaldehyde in supercritical water. Green Chem 4:285–287
42. Matsumoto T, Inoue S (1983) Selective formation of triose from formaldehyde catalysed by ethylbenzothiazolium bromide. J Chem Soc Chem Commun 4:171–172
43. Matsumoto T, Yamamoto H, Inoue S (1984) Selective formation of triose from formaldehyde catalyzed by thiazolium salt. J Am Chem Soc 106:4829–4832
44. Dolan GA (2010) Methanol production and utilization. In: Vertès AA, Qureshi N, Blaschek HP, Yukawa H (eds) Biomass to Biofuels. Blackwell Publishing Ltd., Oxford, UK, pp 435–455
45. Deng J, Pan T, Xu Q, Chen M-Y, Zhang Y, Guo Q-X, Fu Y (2013) Linked strategy for the production of fuels via formose reaction. Sci Rep 3:1244
46. Diebold JP, Czernik S, Diebold J, Meier D, Oasmaa A, Peacocke C, Piskorz J, Radlein D (2003) Fast pyrolysis of biomass: a handbook. CPL Scientific Publishing, Newbury
47. Mohan D, Pittman CU, Steele PH (2006) Pyrolysis of wood/biomass for Bio-oil: a critical review. Energy Fuel 20:848–889
48. Vinu R, Broadbelt LJ (2012) A mechanistic model of fast pyrolysis of glucose-based carbohydrates to predict bio-oil composition. Energy Environ Sci 5:9808–9826
49. Bozell JJ, Petersen GR (2010) Technology development for the production of biobased products from biorefinery carbohydrates—the US Department of Energy's "Top 10" revisited. Green Chem 12:539–554
50. Werpy T, Petersen G (2004) Top value added chemicals from biomass. Volume I – Results of screening for potential candidates from sugars and synthesis gas. https://www1.eere.energy.gov/bioenergy/pdfs/35523.pdf. Accessed 2 Jun 2014
51. Castillo Martinez FA, Balciunas EM, Salgado JM, Domínguez González JM, Converti A, de S Oliveira RP (2013) Lactic acid properties, applications and production: a review. Trends Food Sci Technol 30:70–83

52. Nattrass L, Higson A (2010) NNFCC renewable chemicals factsheet: lactic acid. http://www.nnfcc.co.uk/publications/nnfcc-renewable-chemicals-factsheet-lactic-acid. Accessed 3 Jun 2014
53. Eriksen J, Mønsted O, Mønsted L (1998) Mechanism of lactic acid formation catalyzed by tetraamine rhodium(III) complexes. Transit Met Chem 23:783–787
54. Hayashi Y, Sasaki Y (2005) Tin-catalyzed conversion of trioses to alkyl lactates in alcohol solution. Chem Commun (Camb) 21:2716–2718
55. Janssen KPF, Paul JS, Sels BF, Jacobs PA (2007) Glyoxylase biomimics: zeolite catalyzed conversion of trioses. Stud Surf Sci Catal 170:1222–1227
56. Taarning E, Madsen AT, Marchetti JM, Egeblad K, Christensen CH (2008) Oxidation of glycerol and propanediols in methanol over heterogeneous gold catalysts. Green Chem 10:408–414
57. Taarning E, Saravanamurugan S, Holm MS, Xiong J, West RM, Christensen CH (2009) Zeolite-catalyzed isomerization of triose sugars. ChemSusChem 2:625–627
58. Holm MS, Saravanamurugan S, Taarning E (2010) Conversion of sugars to lactic acid derivatives using heterogeneous zeotype catalysts. Science 328:602–605
59. West RM, Holm MS, Saravanamurugan S, Xiong J, Beversdorf Z, Taarning E, Christensen CH (2010) Zeolite H-USY for the production of lactic acid and methyl lactate from C3-sugars. J Catal 269:122–130
60. Pescarmona PP, Janssen KPF, Delaet C, Stroobants C, Houthoofd K, Philippaerts A, De Jonghe C, Paul JS, Jacobs PA, Sels v (2010) Zeolite-catalysed conversion of C3 sugars to alkyl lactates. Green Chem 12:1083–1089
61. Rasrendra CB, Fachri BA, Makertihartha IGBN, Adisasmito S, Heeres HJ (2011) Catalytic conversion of dihydroxyacetone to lactic acid using metal salts in water. ChemSusChem 4:768–777
62. Wang J, Masui Y, Onaka M (2011) Conversion of triose sugars with alcohols to alkyl lactates catalyzed by Brønsted acid tin ion-exchanged montmorillonite. Appl Catal B Environ 107:135–139
63. Li L, Stroobants C, Lin K, Jacobs PA, Sels BF, Pescarmona PP (2011) Selective conversion of trioses to lactates over Lewis acid heterogeneous catalysts. Green Chem 13:1175–1181
64. De Clippel F, Dusselier M, Van Rompaey R, Vanelderen P, Dijkmans J, Makshina E, Giebeler L, Oswald S, Baron GV, Denayer JFM, Pescarmona PP, Jacobs PA, Sels BF (2012) Fast and selective sugar conversion to alkyl lactate and lactic acid with bifunctional carbon-silica catalysts. J Am Chem Soc 134:10089–10101
65. Guo Q, Fan F, Pidko EA, van der Graaff WNP, Feng Z, Li C, Hensen EJM (2013) Highly active and recyclable Sn-MWW zeolite catalyst for sugar conversion to methyl lactate and lactic acid. ChemSusChem 6:1352–1356
66. Wang F-F, Liu C-L, Dong W-S (2013) Highly efficient production of lactic acid from cellulose using lanthanide triflate catalysts. Green Chem 15:2091–2095
67. Lux S, Siebenhofer M (2013) Synthesis of lactic acid from dihydroxyacetone: use of alkaline-earth metal hydroxides. Catal Sci Technol 3:1380–1385
68. Zhou L, Wu L, Li H, Yang X, Su Y, Lu T, Xu J (2014) A facile and efficient method to improve the selectivity of methyl lactate in the chemocatalytic conversion of glucose catalyzed by homogeneous Lewis acid. J Mol Catal A Chem 388–389:74–80
69. Dapsens PY, Kusema BT, Mondelli C, Pérez-Ramírez J (2014) Gallium-modified zeolites for the selective conversion of bio-based dihydroxyacetone into C1–C4 alkyl lactates. J Mol Catal A Chem 388–389:141–147
70. Huan FL, Bi R, Liu YH, Li WS, Zhou XP (2014) The synthesis of methyl lactate and other methyl oxygenates from cellulose. Catal Commun 49:78–81
71. Li L, Collard X, Bertrand A, Sels BF, Pescarmona PP, Aprile C (2014) Extra-small porous Sn-silicate nanoparticles as catalysts for the synthesis of lactates. J Catal 314:56–65
72. Lei X, Wang F-F, Liu C-L, Yang R-Z, Dong W-S (2014) One-pot catalytic conversion of carbohydrate biomass to lactic acid using an ErCl3 catalyst. Appl Catal A Gen 482:78–83

73. Assary RS, Curtiss LA (2011) Theoretical study of 1,2-hydride shift associated with the isomerization of glyceraldehyde to dihydroxy acetone by Lewis acid active site models. J Phys Chem A 115:8754–8760
74. Dapsens PY, Mondelli C, Pérez-Ramírez J (2013) Highly selective Lewis acid sites in desilicated MFI zeolites for dihydroxyacetone isomerization to lactic acid. ChemSusChem 6:831–839
75. Lew CM, Rajabbeigi N, Tsapatsis M (2012) Tin-containing zeolite for the isomerization of cellulosic sugars. Microporous Mesoporous Mater 153:55–58
76. Dapsens PY, Menart MJ, Mondelli C, Pérez-Ramírez J (2014) Production of bio-derived ethyl lactate on GaUSY zeolites prepared by post-synthetic galliation. Green Chem 16:589–593
77. Dijkmans J, Gabriëls D, Dusselier M, de Clippel F, Vanelderen P, Houthoofd K, Malfliet A, Pontikes Y, Sels BF (2013) Productive sugar isomerization with highly active Sn in dealuminated β zeolites. Green Chem 15:2777–2785
78. Dijkmans J, Dusselier M, Gabriëls D, Houthoofd K, Magusin PCMM, Huang S, Pontikes Y, Trekels M, Vantomme A, Giebeler L, Oswald S, Sels BF (2015) Cooperative catalysis for multistep biomass conversion with Sn/Al beta zeolite. ACS Catal 5:928–940
79. Ten Dam J, Hanefeld U (2011) Renewable chemicals: dehydroxylation of glycerol and polyols. ChemSusChem 4:1017–1034
80. Sels BF, D'Hondt E, Jacobs P (2007) Catalytic transformation of glycerol. In: Centi G, van Santen RA (eds) Catalysis for renewables from feedstock to energy production. Wiley-VCH Verlag GmbH & Co. KGaA, Weinheim, Germany, pp 223–255
81. Fan Y, Zhou C, Zhu X (2009) Selective catalysis of lactic acid to produce commodity chemicals. Catal Rev 51:293–324
82. Dimitratos N, Lopez-Sanchez JA, Meenakshisundaram S, Anthonykutty JM, Brett G, Carley AF, Taylor SH, Knight DW, Hutchings GJ (2009) Selective formation of lactate by oxidation of 1,2-propanediol using gold palladium alloy supported nanocrystals. Green Chem 11:1209–1216
83. Long Y-D, Guo F, Fang Z, Tian X-F, Jiang L-Q, Zhang F (2011) Production of biodiesel and lactic acid from rapeseed oil using sodium silicate as catalyst. Bioresour Technol 102:6884–6886
84. Purushothaman RKP, van Haveren J, van Es DS, Melián-Cabrera I, Meeldijk JD, Heeres HJ (2014) An efficient one pot conversion of glycerol to lactic acid using bimetallic gold-platinum catalysts on a nanocrystalline CeO2 support. Appl Catal B Environ 147:92–100
85. Shen Y, Zhang S, Li H, Ren Y, Liu H (2010) Efficient synthesis of lactic acid by aerobic oxidation of glycerol on Au-Pt/TiO2 catalysts. Chemistry 16:7368–7371
86. Lakshmanan P, Upare PP, Le N-T, Hwang YK, Hwang DW, Lee U-H, Kim HR, Chang J-S (2013) Facile synthesis of CeO2-supported gold nanoparticle catalysts for selective oxidation of glycerol into lactic acid. Appl Catal A Gen 468:260–268
87. Pazhavelikkakath Purushothaman RK, van Haveren J, Melián-Cabrera I, van Eck ERH, Heeres HJ (2014) Base-free, one-pot chemocatalytic conversion of glycerol to methyl lactate using supported gold catalysts. ChemSusChem 7:1140–1147
88. Cho HJ, Chang C-C, Fan W (2014) Base free, one-pot synthesis of lactic acid from glycerol using a bifunctional Pt/Sn-MFI catalyst. Green Chem 16:3428–3433
89. Gehrer E, Harder W (1994) Manufacture of 1,2-propyleneglycol. US 5,306,847 A
90. Ooms R, Dusselier M, Geboers J, Op de Beeck B, Verhaeven R, Gobechiya E, Martens J, Redl A, Sels BF (2014) Conversion of sugars to ethylene glycol with nickel tungsten carbide in a fed-batch reactor: high productivity and reaction network elucidation. Green Chem 16:695–707
91. Nakagawa Y, Tomishige K (2011) Heterogeneous catalysis of the glycerol hydrogenolysis. Catal Sci Technol 1:179–190
92. Holm MS, Pagán-Torres YJ, Saravanamurugan S, Riisager A, Dumesic J, Taarning E (2012) Sn-beta catalysed conversion of hemicellulosic sugars. Green Chem 14:702–706

93. Henton DE, Gruber P, Lunt J, Randall Jed (2005) Polylactic acid technology. In: Mohanty AK, Misra MM, Drzal LT (eds) Natural fibers, biopolymers and biocomposites. CRC Press, Boca Raton, Florida, pp 527–578
94. Shen L, Worrell E, Patel M (2010) Present and future development in plastics from biomass. Biofuels Bioprod Biorefin 4:25–40
95. European bioplastics – driving the evolution of plastics (2012). http://en.european-bioplastics.org/multimedia/. Accessed 25 May 2014
96. Chemical business focus: a monthly roundup and analysis of the key factors shaping world chemical markets (2014). http://www.tecnon.co.uk/Chemical_Business_Focus.aspx. Accessed 20 May 2014
97. Auras R, Lim L-T, Selke SEM, Tsuji H (eds) (2010) Poly(lactic acid): synthesis, structures, properties, processing, and applications. Wiley, New York
98. Rasal RM, Janorkar AV, Hirt DE (2010) Poly(lactic acid) modifications. Prog Polym Sci 35:338–356
99. Choudhary V, Pinar AB, Sandler SI, Vlachos DG, Lobo RF (2011) Xylose isomerization to xylulose and its dehydration to furfural in aqueous media. ACS Catal 1:1724–1728
100. Choudhary V, Caratzoulas S, Vlachos DG (2013) Insights into the isomerization of xylose to xylulose and lyxose by a Lewis acid catalyst. Carbohydr Res 368:89–95
101. Moliner M, Román-Leshkov Y, Davis ME (2010) Tin-containing zeolites are highly active catalysts for the isomerization of glucose in water. Proc Natl Acad Sci U S A 107:6164–6168
102. Román-Leshkov Y, Moliner M, Labinger JA, Davis ME (2010) Mechanism of glucose isomerization using a solid Lewis acid catalyst in water. Angew Chem 122:9138–9141
103. Saravanamurugan S, Paniagua M, Melero JA, Riisager A (2013) Efficient isomerization of glucose to fructose over zeolites in consecutive reactions in alcohol and aqueous media. J Am Chem Soc 135:5246–5249
104. Saravanamurugan S, Riisager A (2014) Zeolite-catalyzed isomerization of tetroses in aqueous medium. Catal Sci Technol 4:3186–3190
105. Stapley J, Atherton DM, Genders DJ, Kendall PM (2012) Methods for the electrolytic production of erythritol. WO 2012167012 (A2)
106. Stapley JA, Genders DJ, Atherton DM, Kendall PM (2011) Methods for the electrolytic production of erythrose or erythritol. US 7,955,489 B2
107. Benner SA, Kim H-J, Kim M-J, Ricardo A (2010) Planetary organic chemistry and the origins of biomolecules. Cold Spring Harb Perspect Biol 2:1–21
108. Simonov AN, Pestunova OP, Matvienko LG, Snytnikov VN, Snytnikova OA, Tsentalovich YP, Parmon VN (2007) Possible prebiotic synthesis of monosaccharides from formaldehyde in presence of phosphates. Adv Space Res 40:1634–1640
109. Hollis JM, Lovas FJ, Jewell PR (2000) Interstellar glycolaldehyde: the first sugar. Astrophys J 107–110
110. Balat M, Balat M, Kırtay E, Balat H (2009) Main routes for the thermo-conversion of biomass into fuels and chemicals. Part 1: Pyrolysis systems. Energy Convers Manag 50:3147–3157
111. Vitasari CR, Meindersma GW, de Haan AB (2012) Laboratory scale conceptual process development for the isolation of renewable glycolaldehyde from pyrolysis oil to produce fermentation feedstock. Green Chem 14:321–325
112. Vitasari CR, Meindersma GW, de Haan AB (2012) Renewable glycolaldehyde isolation from pyrolysis oil-derived aqueous solution by reactive extraction with primary amines. Sep Purif Technol 95:103–108
113. Gilding DK, Reed AM (1979) Biodegradable polymers for use in surgery—polyglycolic/poly(actic acid) homo- and copolymers: 1. Polymer (Guildf) 20:1459–1464
114. Seyednejad H, Ghassemi AH, van Nostrum CF, Vermonden T, Hennink WE (2011) Functional aliphatic polyesters for biomedical and pharmaceutical applications. J Control Release 152:168–176

115. Dapsens PY, Mondelli C, Kusema BT, Verel R, Pérez-Ramírez J (2014) A continuous process for glyoxal valorisation using tailored Lewis-acid zeolite catalysts. Green Chem 16:1176–1186
116. Sipilä K, Kuoppala E, Fagernäs L, Oasmaa A (1998) Characterization of biomass-based flash pyrolysis oils. Biomass Bioenergy 14:103–113
117. Ohshima T, Yamamoto Y, Takaki U, Inoue Y, Saeki T, Itou K, Maegawa Y, Iwasaki T, Mashima K (2009) Theoretical study of Al(III)-catalyzed conversion of glyoxal to glycolic acid: dual activated 1,2-hydride shift mechanism by protonated Al(OH)3 species. Chem Commun (Camb) 19:2688–2690
118. McNaught AD (1996) Nomenclature of carbohydrates. Pure Appl Chem 68:1919–2008
119. Butlerow A (1861) Bildung einer zuckerartigen Substanz durch Synthese. Justus Liebigs Ann Chem 120:295–298
120. Partridge RD, Weiss AH, Todd D (1972) Branched-chain carbohydrate structures resulting from formaldehyde condensation. Carbohydr Res 24:29–44
121. Delidovich IV, Simonov AN, Taran OP (2014) Catalytic formation of monosaccharides: from the formose reaction towards selective synthesis. ChemsusChem Minirev 7:1833–1846
122. Kim H-J, Ricardo A, Illangkoon HI, Kim MJ, Carrigan MA, Frye F, Benner SA (2011) Synthesis of carbohydrates in mineral-guided prebiotic cycles. J Am Chem Soc 133:9457–9468
123. Weiss A (1970) Homogeneously catalyzed formaldehyde condensation to carbohydrates. J Catal 16:332–347
124. Castells J, López-Calahorra F, Geijo F (1983) The formoin reaction. Carbohydr Res 116:197–207
125. Vetter AJ, Janka ME, Zoeller JR (2009) Coupling of formaldehyde to glycoaldehyde using N-heterocyclic carbene catalysts. US7498469 B1
126. Tajima H, Niitsu T, Inoue H (1999) Polymerization of formaldehyde by an immobilized thiamine catalyst on cation-exchange resin. J Chem Eng Japan 32:776–782
127. Tajima H, Tabata K, Niitsu T, Inoue H (2002) The formose reaction on a synthetic zeolite impregnated with thiazolium catalyst. J Chem Eng Japan 35:564–568
128. Zhang J, Xing C, Tiwari B, Chi YR (2013) Catalytic activation of carbohydrates as formaldehyde equivalents for Stetter reaction with enones. J Am Chem Soc 135:8113–8116
129. Yamaguchi S, Matsuo T, Motokura K, Sakamoto Y, Miyaji A, Baba T (2015) Mechanistic studies on the cascade conversion of 1,3-dihydroxyacetone and formaldehyde into α-hydroxy-γ-butyrolactone. ChemSusChem 8:853–860
130. Garrabou X, Castillo JA, Guérard-Hélaine C, Parella T, Joglar J, Lemaire M, Clapés P (2009) Asymmetric self- and cross-aldol reactions of glycolaldehyde catalyzed by D-fructose-6-phosphate aldolase. Angew Chem Int Ed 48:5521–5525
131. Van de Vyver S, Odermatt C, Romero K, Prasomsri T, Roman-Leshkov Y (2015) Solid Lewis acids catalyze the carbon–carbon coupling between carbohydrates and formaldehyde. ACS Catal 5:972–977

Chapter 4
Differentiation of the Coordination Chemistry of Metal Chlorides in Catalytic Conversion of Glucose in Ionic Liquids

Huixiang Li and Z. Conrad Zhang

Abstract Catalytic aldose isomerization to ketose is an important reaction for the utilization of cellulosic biomass. However, a fundamental understanding and knowledge base involved in this reaction remains lacking in the literature. In this chapter, we provide a focused review of the most studied solvent-based catalytic system involving metal halides for glucose isomerization to fructose and further to 5-hydroxymethhylfurfral (5-HMF). Results from studies by different physical techniques are critically reviewed. A differentiation of the coordination chemistry of different metal chlorides obtained by various physical techniques is established to rationalize the drastically different catalytic pathways by the metal chloride catalysts. The performance of metal chloride catalysts for the isomerization of aldose to ketose is found to correlate with their coordination chemistry. Solvents play an important role in determining the coordination structures for the metal ions, which critically affect the catalysis of the metal chloride precursors. Undesired side products are related to the reaction pathways corresponding to the nature of the coordination of metal ions with different oxygen sources in the substrates and the products.

Keywords Glucose isomerization • 5-Hydroxymethylfurfural metal chlorides • Cellulosic biomass • Platform chemicals

H. Li
State Key Laboratory of Catalysis, Dalian National Laboratory for Clean Energy, Dalian Institute of Chemical Physics, Chinese Academy of Sciences,
457 Zhongshan Road, Dalian 116023, Liaoning, China

College of Chemistry and Chemical Engineering, University of Chinese Academy of Sciences, Beijing 10049, China

Z.C. Zhang (✉)
State Key Laboratory of Catalysis, Dalian National Laboratory for Clean Energy, Dalian Institute of Chemical Physics, Chinese Academy of Sciences,
457 Zhongshan Road, Dalian 116023, Liaoning, China
e-mail: zczhang@yahoo.com

M. Schlaf, Z.C. Zhang (eds.), *Reaction Pathways and Mechanisms in Thermocatalytic Biomass Conversion I*, Green Chemistry and Sustainable Technology, DOI 10.1007/978-981-287-688-1_4

4.1 Introduction

Cellulose, polymers of β-D-glucose, is a sustainable feedstock for the production of liquid fuels and chemicals, e.g., 2, 5-dimethylfuran, propyl levulinate, furfural, and 5-hydroxymethylfurfural (5-HMF) [1–5]. In the past few years, massive interests in research on catalytic conversion of carbohydrates to biofuels and biochemicals have emerged, as evidenced by the rapid increase in the number of publications (Fig. 4.1). Among carbohydrates, glucose as the most abundant biomolecule received the highest attention. Remarkable progress has been made in the catalytic conversion of glucose [5–10], especially to furanics, highlighted by 5-HMF as a potentially versatile platform chemical [11, 12].

A large number of chemicals can be derived from 5-HMF, e.g., 6-hexanediol, adipic acid, levulinic acid, 2,5-dimethylfuran, and 5-hydroxymethylfuroic acid [11, 12], which may be applied for new material synthesis, food additives, and medicine intermediates [12, 13]. However, achieving a highly isolated 5-HMF yield from glucose has been a key challenge. The synthesis of 5-HMF from carbohydrates by a combination of different solvents [4, 14, 15], catalysts [16–18], and process conditions [19] has been broadly studied. However, a fundamental understanding and the knowledge base involved in the catalytic transformations of carbohydrates remain lacking in the literature. In this chapter, we provide a focused review of the most studied solvent-based catalytic systems involving metal chlorides for glucose conversion. Results from studies by different physical techniques are critically reviewed. A differentiation of the coordination chemistry of different metal chlorides obtained by various physical technologies is established to rationalize the drastically different catalytic pathways observed by the metal chloride catalysts.

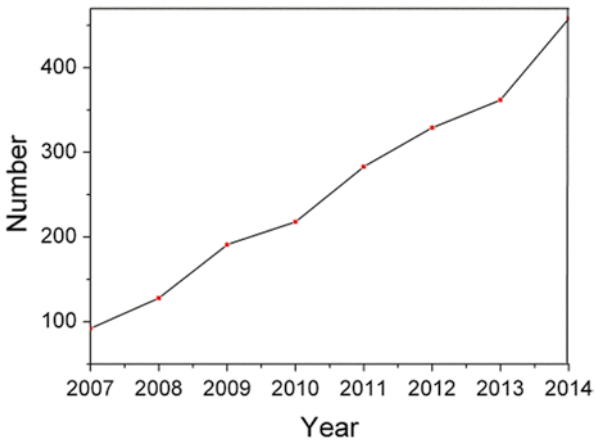

Fig. 4.1 The number of publications related to the synthesis of chemicals, particularly 5-HMF, from the conversion of monosaccharides each year from 2007 to 2013 (Source: Web of Science)

4.2 Analytical Techniques Applied to Characterize Carbohydrate Conversions to 5-HMF

Various physical techniques and methods, e.g., NMR spectroscopy, UV–vis spectrophotometry, density functional theory, X-ray absorption spectroscopy, and infrared spectroscopy with far infrared in particular, have been used to characterize the reaction intermediates, pathways and kinetics, anomer distribution, side products, and coordination chemistry of metal ions with carbohydrates in the process of catalytic reactions. While there were only a limited number of focused physical studies on the fundamental mechanisms involved in carbohydrate conversions, a preliminary picture of the mechanistic pathways has emerged. These studies also illustrate the potential of extending these physical techniques for broader fundamental researches. It should be emphasized that there remain many unanswered questions in this new research field, and considerable fundamental researches are needed to gain detailed mechanistic insights on the catalyzed conversions of carbohydrates. Areas needing further research will be pointed out.

4.3 Equilibrium Anomer Distribution, Reaction Pathway, and Kinetics in Glucose Hydrothermal Conversion

The kinetics of fundamental steps of main reactions and side reactions in the conversion of glucose determine the yield of 5-HMF. It has been established that glucose isomerization to fructose (K_1 of Eq. 4.1) is a critical step that precedes the formation of 5-HMF through fructose dehydration (K_2 of Eq. 4.1) [20, 21]:

$$\mathrm{D-glucose} \underset{k_{-1}}{\overset{k_{+1}}{\rightleftharpoons}} \mathrm{D-fructose} \xrightarrow{k_2} \mathrm{5-HMF} \tag{4.1}$$

where k_{+1}, k_{-1}, and k_2 are defined as the rate constants for the forward and backward transformation of D-glucose into D-fructose and the conversion of D-fructose into 5-HMF, respectively. The equilibrium distributions of multiple structural anomers of D-glucose and D-fructose are dependent on the nature of solvents. Important to the catalysis, the isomerization of only the open chain anomer of D-glucose to the open chain anomer of D-fructose determines K_1 (Eq. 4.1). Therefore, the concentration of open chain anomer of D-glucose is an important parameter for the isomerization of glucose to fructose.

In an aqueous system consisting of 0.02 M glucose, the kinetics of D-glucose hydrothermolysis reaction were measured at a temperature range of 120–160 °C by applying time-resolved in situ ^{13}C NMR spectroscopy and the site-selective ^{13}C-labeling technique [20]. The distribution of various anomers of D-glucose and D-fructose in this system was also quantitatively determined. In the proposed reaction pathways as shown in Fig. 4.2, all species generated through the reaction were

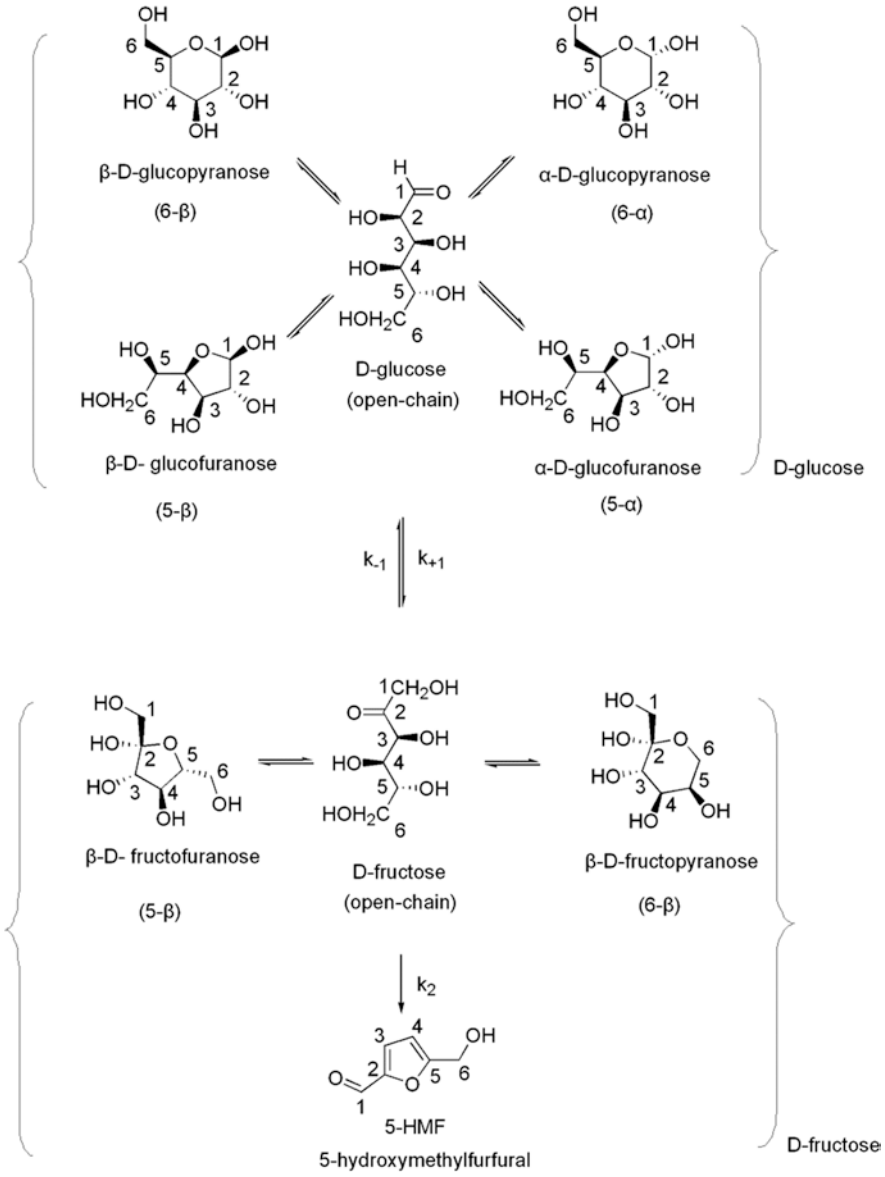

Fig. 4.2 Reaction pathways for the hydrothermolysis of D-glucose. Curly braces mean that all the isomers of each sugar are collectively treated in the kinetic analysis. For D-fructose, the configurations of 6-α and 5-α forms are omitted here for brevity (Reproduced with permission from Ref. [20]. Copyright 2011, ACS)

quantitatively analyzed. At 100 °C in water, the fractions of the chain and ring anomers for D-glucose are in the following order:

$$6-\beta(54\ \%) > 6-\alpha(44\ \%) >> 5-\beta(1\ \%) > 5-\alpha(0.5\ \%) > \text{chain}(0.04\ \%)$$

The numbers in the parentheses are the fraction (%) of the preceding anomers normalized by the overall D-glucose isomers. The numbers 6 and 5 stand for pyranose and furanose ring structures, respectively. For D-fructose, the isomers are in the following order:

$$6-\beta(48\ \%) > 5-\beta(36\ \%) > 5-\alpha(8\ \%) > \text{chain}(5\ \%) > 6-\alpha(4\ \%)$$

The following anomer distributions in water are observed:

1. For D-glucose, the pyranose forms, 6-β and 6-α, dominate, accounting for 98 % of the total glucose.
2. For D-fructose, the β types, 6-β and 5-β, prevail, accounting for 84 % of the total fructose.
3. The fraction of the chain form of D-glucose is a factor of ~100 smaller than that of D-fructose.
4. The furanose forms, 5-β and 5-α, are more preferable in D-fructose than in D-glucose.

However, it should be noted that the rates of mutarotation for D-glucose and D-fructose are several order of magnitude less in aprotic solvents than that in water at the same temperature [22]. In 1-ethyl-3-methylimidazolium chloride ([EMIM]Cl) ionic liquid, it was found that mutarotation of α-D-glucose did not take place even at 90 °C [23]. The equilibrated anomer distributions for fructose and glucose are also markedly different in other solvent than that in water [24]. For example, the β-D-fructopyranose is the dominant anomer of D-fructose configuration at 6β: 5β: 5α: 6α ratio of 1:3:1.3: trace in DMSO.

In the reaction scheme (Eq. 4.1), D-glucose, a six-carbon aldose, is reversibly (the rate constants are denoted as k_{+1} and k_{-1}, respectively) and rather slowly transformed into D-fructose, a six-carbon ketose, as the first step via the open chain isomer and successively transformed (k_2) into 5-hydroxymethylfurfural (5-HMF). When compared with the value of k_{+1}, k_{-1} is one order of magnitude larger and k_2 is on the same order. According to the Arrhenius activation energy, the energy barrier ($Ea_{,2} = 100$ kJ mol^{-1}) associated with k_2 is remarkably smaller than those associated with k_{+1} ($Ea_{,+1} = 143$ kJ mol^{-1}) and k_{-1} ($Ea_{,-1} = 134$ kJ mol^{-1}). The high k_{-1} value relative to that of k_{+1} and k_2, together with the two orders of magnitude lower open chain glucose concentration (0.04 %) than that of open chain fructose (5 %), indicates that the equilibrium of glucose conversion to 5-HMF is highly unfavorable in aqueous solvent. With fructose as the feed, continuous removal of 5-HMF product from the reaction phase to an extraction phase is one effective strategy for the production of 5-HMF from fructose [25–28]. Without an extraction phase, a general curve corresponding to an equilibrium between glucose and fructose was established in the presence of an effective glucose isomerization catalyst, for example, $CrCl_3$ [29]. This general curve, which also extends to other catalysts, is a characteristic of aqueous solvent. It should be noted that the kinetic study ignored the effects of side reactions, such as the oligomerization of glucose and fructose, which would change the rate constants. Because

the ^{13}C NMR spectroscopic study requires a long accumulation time of 20 h due to the lower natural abundance of ^{13}C, unstable intermediates and products may not be registered. Another limitation of this physical characterization technique is that the strong solvent signals of most nonaqueous solvents and ionic liquids may shadow the weak signals of the carbohydrate substrates.

4.4 Metal Halide Catalyzed Glucose Conversion to 5-HMF

Other studies confirmed the role of fructose in the process of converting glucose to 5-HMF and investigated the mechanism [30–32].

In nonaqueous solvent, the dehydration of fructose to 5-HMF is obviously favored. Numerous solvents, particularly ionic liquids, and process conditions have been studied for this reaction. The ionic liquid 1-butyl-3-methylimidazolium chloride ([BMIM]Cl) is one of such solvents studied for the conversion of fructose. Mineral acids, HCl and H_2SO_4, are efficient catalysts for the selective formation of 5-HMF in yields up to 97 % when the fructose concentration was 10 % in the ionic liquid [33]. A 5-HMF yield of 51 % was obtained from a high concentration (67 wt.%) of fructose in [BMIM]Cl. Solid acid resins also effectively catalyze this dehydration reaction in [BMIM]Cl [34].

While the mutarotation of glucose in a pure aprotic ionic liquid, e.g., [BMIM]Cl, does not take place even at 80 °C, transition metal chlorides, e.g., $CuCl_2$ and $CrCl_2$, were found to rapidly catalyze the mutarotation in the solvent [23]. Importantly, chromium chlorides, $CrCl_2$ and $CrCl_3$, were first discovered to be the most effective in catalyzing the isomerization of glucose to fructose in the ionic liquid solvent. The chromium chlorides are also effective catalysts for the same reaction in other solvents, including aqueous phase [15]. Adding $CrCl_2$ to 1-ethyl-3-methylimidazolium chloride ([EMIM]Cl) results in the formation of $[EMIM]^+CrCl_3^-$. The amount of $CrCl_2$ used was in catalytic amount. The key roles of the chromium chlorides in the ionic liquid solvent were proposed to include (1) proton transfer to form open chain glucose which is a key part of the mutarotation mechanism and (2) facilitating a formal hydride transfer, leading to isomerization of glucose to fructose [23]. A chromium enolate was suggested to be the key intermediate. Once fructose is formed, dehydration of fructofuranose is rapid in the presence of the catalyst in this solvent. As $CrCl_3{\cdot}6H_2O$ is also active in catalyzing the isomerization of glucose to fructose in water, the chromium complex formation with the substrate was probed by UV–vis spectrophotometry [29]. Two weak absorption peaks at 417 nm and 582.5 nm were attributed to the *d–d* transitions of Cr complexes formed in water at room temperature. The peak 582.5 nm showed a blue shift with the addition of reactant glucose, indicating Cr complexes formation with glucose. The replacement of a Cr–Cl by a Cr–O bond and hydrolysis of $CrCl_3{\cdot}6H_2O$ can be expected to form hydrochloric acid (HCl) as a by-product. Using a similar concentration of protonic acid as would be expected from the hydrolysis of $CrCl_3{\cdot}6H_2O$ did not show catalytic effect for glucose conversion. Evidently, through coordination of glucose to the Cr(III) ions by replacing a fraction of the Cr–Cl bonds, the chromium coordination

complex played the critical role of hydride transfer for the transformation of glucose to fructose.

The information from the UV–vis spectrophotometry characterization is however rather limited and offers little insight to the nature of the coordination bond between Cr(III) and the carbohydrates.

The hydride transfer mechanism was confirmed by ^{1}H NMR study in the chromium (III)-catalyzed isomerization of glucose in aqueous solvent [35]. It was found that 5-HMF produced from deuterium isotope-labeled glucose-2-D in the presence of H_2O contained 33 % C-1 deuterium incorporation, while unlabeled glucose in the presence of D_2O produced 5-HMF with <5 % deuterium incorporation. The results are consistent with a hydride transfer mechanism in the isomerization of glucose to fructose. However, ^{1}H and ^{13}C NMR are not capable of probing the coordination chemistry involved by the Cr(III) ions. The coordination structure of Cr(III) with glucose/fructose that is essential to enable the hydride transfer was not considered in this study.

The catalytic effect of some metal chlorides for the isomerization of aldose to ketose has also been found to be solvent specific. The property of solvents affects the reaction pathway in glucose conversion and the prevalent coordination structure of metal ions for some metal chloride precursors. A change in the metal ion coordination may occur from that of the precursor during the dissolution of the metal chloride precursor to a solvent. The solubility of a metal chloride under study in an ionic liquid solvent is dependent on the properties of both the solute and the solvent. When a metal chloride precursor is in hydrated form, dehydration environment or conditions in a solvent, particularly an ionic liquid, may cause dehydration of the precursor upon dissolution, which consequently induces a change from the original coordination structure of the metal chloride precursor. In addition, coordination strength of a solvent itself should be considered. Furthermore, a solvent may promote side reactions such as oligomerization favoring humin formation during the process of glucose conversion. Therefore, study of the coordination structure of catalytic metal chloride species should take into account the solvent property and the influence of the solvent for potential side reactions.

$SnCl_4{\cdot}5H_2O$ provides an intriguing example of solvent specificity for its performance in catalyzing glucose conversion to fructose and subsequent conversion to 5-HMF [17]. It is an efficient catalyst for converting glucose to 5-HMF in 61 % yield in [EMIM][BF_4] ionic liquid at 100 °C, but its performance is very poor in ionic liquids with alternate cations, e.g., [Bpyr][BF_4] or anions [BMIM]Cl, under same reaction conditions. Remarkably, its performance is even sensitive to a small variation in ionic liquid of similar cation, e.g., [BMIM][BF_4]. For the $SnCl_4{\cdot}5H_2O$/[EMIM][BF_4] catalyst/solvent system, ethylene glycol was found to inhibit the catalyst performance, but ethanol and 1,3-propanediol did not. It was therefore proposed that the five-membered-ring chelate structure may be more stable than the acyclic and six-membered-ring chelate structures (Fig. 4.3a). Thus for glucose conversion in this system, the formation of a five-membered-ring chelate structure with the Sn(IV) ion by the two neighboring hydroxyl oxygen in glucose was proposed to play an important role in the catalytic reaction.

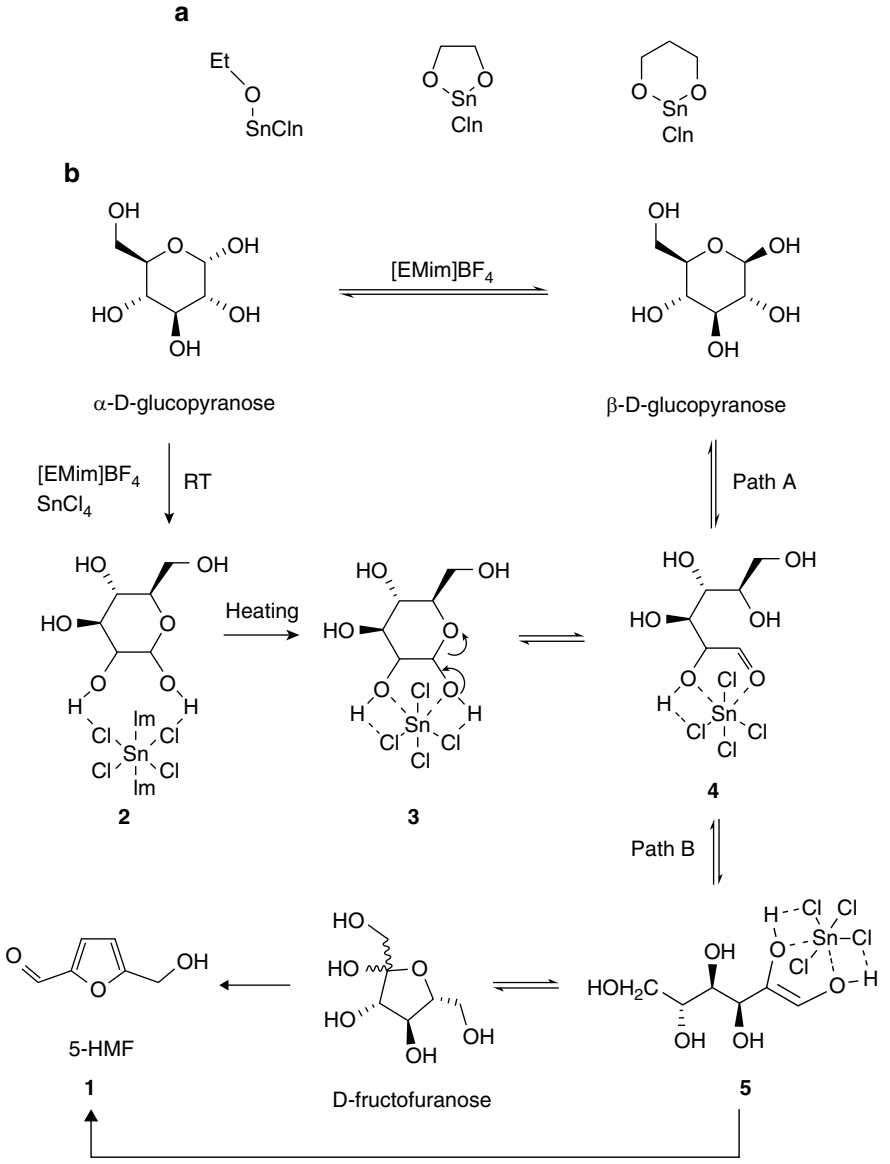

Fig. 4.3 (**a**) The coordination type of $SnCl_n$ with various oxygenated chemicals; (**b**) proposed processes of glucose conversion to produce HMF catalyzed by SnCl4 in $[EMIM]BF_4$ (Reproduced with permission from Ref. [17]. Copyright 2009, Royal Society of Chemistry)

Results of ^{1}H NMR spectroscopy applied to follow the change in glucose substrate support the coordination of the hydroxyl oxygen with Sn(IV) based on the disappearance of the glucose OH ^{1}H NMR peaks in the presence of the Sn(IV) catalyst in [EMIM][BF_4] [17]. The ^{1}H NMR spectrum of this system at a reaction temperature of 80 and 100 °C showed a chemical shift of 4.9 ppm, which indicated the formation of complex 4 in Fig. 4.3b. Formation of the five-membered-ring chelate complex of Sn and glucose was proposed to play a key role in the mechanistic pathway for the formation of HMF.

While NMR spectroscopy, as an ex situ tool, is informative in characterizing possible changes that may occur in the carbohydrate substrate, it cannot provide information on the metal ion coordination structure. The structure of the Sn complex in the processes of glucose conversion (Fig. 4.3b) is just inferred and speculative. This point is particularly relevant for this discussion when the coordination structure of Sn(IV) is known to be sensitive to the moisture content [36]. $SnCl_4{\cdot}5H_2O$ was determined to exist in the coordination structure of $[SnCl_4(H_2O)_2]{\cdot}3H_2O$, which has two types of water molecules in the structure [36]. Two of the six coordination bonds to Sn(IV) would be expected to be Sn–O bonds before Sn(IV) in $SnCl_4{\cdot}5H_2O$ exchanges ligands with glucose in the inert solvent. However, because the [EMIM][BF_4] solvent is water deficient, $[SnCl_4(H_2O)_2]{\cdot}3H_2O$ could partially dehydrate at least by losing water in its outer coordination sphere. The Sn(IV) coordination becomes even more uncertain in $SnCl_4{\cdot}xH_2O$ (x = 2,3,4). In addition, the coordination of the water molecules with Sn(IV) is expected to change at different temperatures [36], which raises additional uncertainty about the metal ion coordination.

Density functional theory (DFT) calculations were applied to study the complete catalytic cycle of glucose conversion to 5-hydroxymethylfurfural (5-HMF) by metal chlorides of the same oxidation states ($CrCl_3$, WCl_3, $MoCl_3$, and $FeCl_3$) in 1-butyl-3-methylimidazolium chloride ([BMIM]Cl) ionic liquid; the isomerization of glucopyranose to fructofuranose and subsequent dehydrations of fructofuranose to the final product 5-HMF were included [37–39]. Energy profiles and Gibbs free energy profiles at 353 K for the glucopyranose isomerization and the fructofuranose dehydration catalyzed by [BMIM]/MCl_3 (M = Cr, Mo, W and Fe) indicate that the metal centers exerted significant influences on the stabilities of the intermediates as well as the energy barriers associated with each elementary reaction step. The overall free energy barriers at 353 K indicate that the reaction activities of the entire processes over different MCl_3 active sites decrease in the order of WCl_3> $MoCl_3$> $CrCl_3$> $FeCl_3$, suggesting that WCl_3 could be a promising catalyst at low temperatures. However, in this DFT calculation, the mechanism of hydride transfer is not explained. In addition, the selectivity of these catalysts in glucose conversion was not taken into account as well as the coordination characteristic of the metal complexes particularly with competing molecules that are either formed as a product (e.g., 5-HMF) or as a side product (e.g., H_2O).

4.5 Mechanistic Pathway in Aldose–Ketose Isomerization: Hydride Transfer by Binuclear Complexes Based on DFT and EXAFS Study

Detailed analysis of structures and coordination properties of metal chlorides and their complexes with glucose in ionic liquids by a combined density functional theory (DFT) and in situ extended X-ray absorption fine structure spectroscopy (EXAFS) study has been proved to be feasible [40–44]. The EXAFS measurement of chromium compounds $CrCl_3{\cdot}6H_2O$ and $CrCl_2$ dissolved in [EMIM]Cl at 80 °C showed that Cr^{3+} and Cr^{2+} are coordinated by six and four chlorine atoms at an average bond length of 2.35 Å and 2.39 Å, respectively [40, 41]. The replacement of part of these chlorine anions in Cr(III) by oxygen upon addition of glucose at 80 °C evidences the coordination of glucose to the Cr(III) center as determined by X-ray absorption spectroscopy. Glucose is not converted into $CrCl_2$/[EMIM]Cl/glucose under these conditions. Thus Cr(III) shows notable activity compared to Cr^{2+}. The results of model DFT calculations are in qualitative agreement with the experimental differences [40, 41]. The estimated overall activation barrier for the Cr(III)-catalyzed glucose isomerization equals 66 kJ mol^{-1}. This compares favorably to the barrier of 93 kJ mol^{-1} for Cr(II).

The results of more detailed DFT calculations on glucose to fructose isomerization in [EMIM]Cl that involves three reaction steps—(1) ring opening, (2) hydrogen transfer between C2 and C1, and (3) ring closure—are summarized in Fig. 4.4 [42]. The calculations indicate that ring opening is rather easy for Cr(III). The mononuclear Cr complexes are preferred at this stage over their binuclear forms. The isomerization of glucose to fructose proceeds through a 1,2-H shift of the open form of glucose and requires the deprotonation of the O_2–H group (Fig. 4.4). At this step the formation of binuclear complexes (Fig. 4.5) was proposed to be favorable for Cr(II) and Cr(III).

Similarly, the reactivity of the same valence state of $CrCl_2$, $CuCl_2$, and $FeCl_2$ catalysts toward glucose activation in dialkylimidazolium chloride ionic liquids was also studied with the combined density functional theory (DFT) and in situ extended X-ray absorption spectroscopy (EXAFS) [42]. In the same way, the model DFT calculations suggested that the overall free energy barrier for the Cu(II) catalytic reaction is a little higher than the barrier computed for the case of chromium(II) catalyst. The key H shift step of the isomerization reaction involves the migration of the negative charge from the O_2 site of carbohydrate to O_1. The coordination with a single cationic center was suggested not sufficient to promote the H shift reaction. The overall free energy barrier for the H shift for a mononuclear sugar–Cr complex is rather high. And this barrier decreases strongly when the deprotonated glucose intermediate interacted with two Cr(II) or two Cu(II) centers. The metal cations are surrounded by four Cl ligands at a distance of 2.28 Å and 2.32 Å, respectively, for Cu^{2+} and Fe^{2+} as determined by X-ray absorption spectroscopy. The addition of sugar at 80 °C and the subsequent heating of the solution at 100 °C did not result in any notable change of the coordination environment of Fe centers. Thus, iron(II)

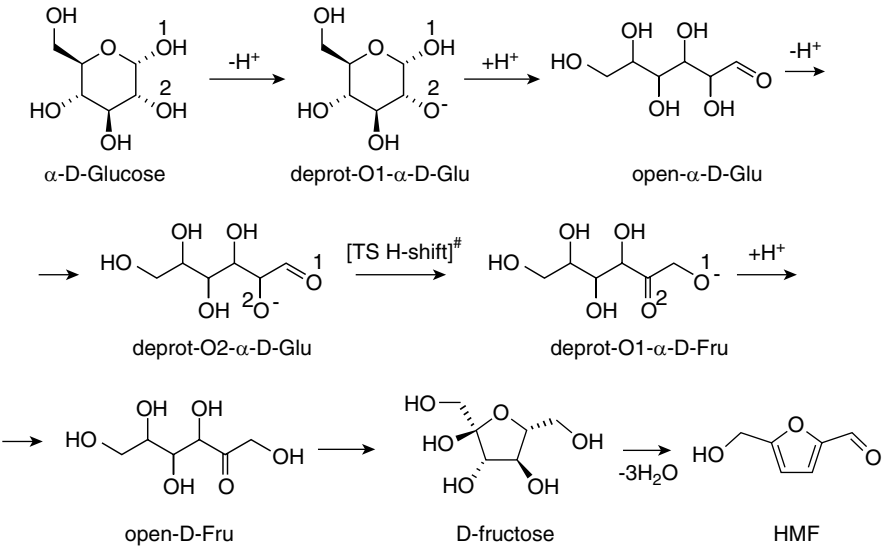

Fig. 4.4 Mechanism of glucose to fructose isomerization as a first step toward the selective glucose dehydration to HMF (Reproduced with permission from Ref. [42]. Copyright 2011, John Wiley and Sons)

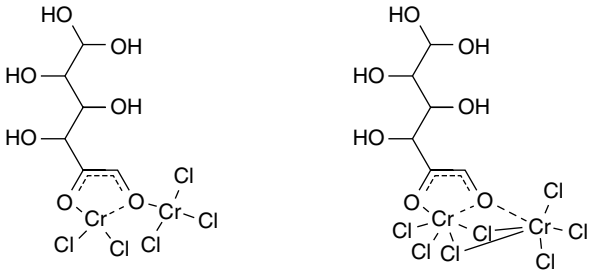

Fig. 4.5 The binuclear coordination complexes of Cr(II) and Cr(III) with the deprotonated sugar (Reproduced with permission from Ref. [41]. Copyright 2011, John Wiley and Sons)

chloride complexes are unable to coordinate glucose as well as to promote its direct deprotonation. The formation of hydrogen bonded complexes between $CuCl_4^{2-}$ and glucose is preferred for the Cu^{2+} complexes. And $CuCl_2$ could activate other hydroxyl groups of the sugar molecule. This could lead to condensation-type side reactions instead of the desirable ring opening and isomerization to fructose. Exchange of Cl^- ligands by a hydroxyl group of glucose is only favorable for $CrCl_4^{2-}$.

Thus the combined DFT and EXAFS could provide the detailed analysis of the coordination structure of metal chlorides and the complexes with glucose in ionic liquids and the energy profiles and Gibbs free energy profiles for the whole reaction process. However it is important to understand the differences in the coordination chemistry of

the metal chlorides involved in the reaction mechanism, particularly related to the effect of different oxygen sources on the coordination chemistry of the metal chlorides.

4.6 Differentiation of Metal Chloride Catalysts by In Situ Far-Infrared Spectroscopy: Effect of Oxygen Sources on the Coordination Chemistry and on Catalysis

4.6.1 The Introduction of Far-Infrared Spectroscopy (FIR)

Fourier transform infrared spectroscopy is suited to study the absorption of chemical bonds or groups in the 10–12,500 cm^{-1} spectral region. It is divided into three segments, near infrared (NIR), middle infrared (MIR), and FIR (Fig. 4.6). MIR spectroscopy has been widely applied in the study of various areas [45–50], including chemical researches, food safety, environmental monitoring, materials, etc. However it becomes of limited use for structural investigation of inorganic compounds, such as metal oxides or salts, which are inactive in the MIR region. FIR offers great advantages in the characterization of those inorganic compounds [51–54], as well as coordination complexes [55], lattice vibrations [56, 57], hydrogen bonds [58, 59], and the skeleton vibration of ring molecule [58], due to the lower energy in the FIR than the MIR spectral region. Just as with MIR, FIR analysis also suffers from the interference of water vapor in the air especially in low frequency [60, 61]. In order to reduce the interference of water, several methods may be adopted [60], such as background subtraction, reduction in moisture level by purging with dry inert gases, resolution reduction, and isolation of the workplace from the air with a physical barrier. In addition, the spectral information of far infrared below 200 cm^{-1} may be neglected as there is little meaningful absorption by most compounds of interest, but the absorption of water is very intense in this region [55].

As far-infrared spectroscopy analyzes the weakest energy, it remains much less developed and the least applied in the infrared region. Therefore, the library of FIR spectra is considerably limited in offering meaningful references for new studies using this spectral tool. In addition, it is known that the peak absorption wave number shifts for different solvents and cations [62, 63]. The spectral analysis and peak identification must be taken with great care, particularly in the choice of appropriate reference substances and in spectral background subtraction.

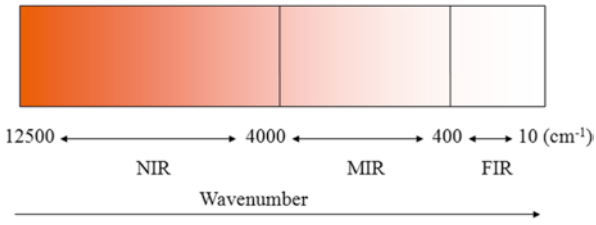

Fig. 4.6 The regions of infrared spectra

4.6.2 *The Application of FIR in Glucose Conversion Catalyzed by Metal Chlorides in 1-Butyl-3-Methylimidazolium Chloride ([BMIM]Cl)*

Because the metal atomic mass is typically quite high in metal chloride compounds, the absorption peak corresponding to the stretching vibration of a metal chloride compound lies in the FIR spectra region. And the absorption intensity shows viable correlation to the concentration of the compounds according to the Bouguer–Lambert–Beer law [64, 65]. Careful calibration and measurement of the absorption intensity may be used to analyze the concentration of metal complexes as potential catalysts. Therefore FIR spectroscopy offers the unique potential as a tool in the study of the coordination chemistry of metal complexes in catalytic reaction systems.

Most recently, we have developed an in situ FIR spectroscopy tool and successfully applied it to the study of the coordination chemistry of metal chlorides in [BMIM]Cl [55]. The metal chlorides that showed strikingly different catalytic performances in the conversion of glucose to 5-HMF in [EMIM]Cl, as shown in Fig. 4.7, were subjected to this original FIR study. Figure 4.7 shows that $CrCl_3$, $CrCl_2$, and VCl_3 represented a group with high glucose conversion and 5-HMF yield. In contrast, $PtCl_2$ showed inefficient glucose conversion. And similar to other tested catalysts, $ZrCl_4$, $MoCl_5$, $NbCl_5$, $CuCl_2$, and $FeCl_3$ all showed poor 5-HMF selectivity. Four representative metal chlorides, $CrCl_3$, VCl_3, $PtCl_2$, and $FeCl_3$, were studied by in situ FIR in order to understand the distinctively different characteristics of the catalysts in correlation to their coordination chemistries.

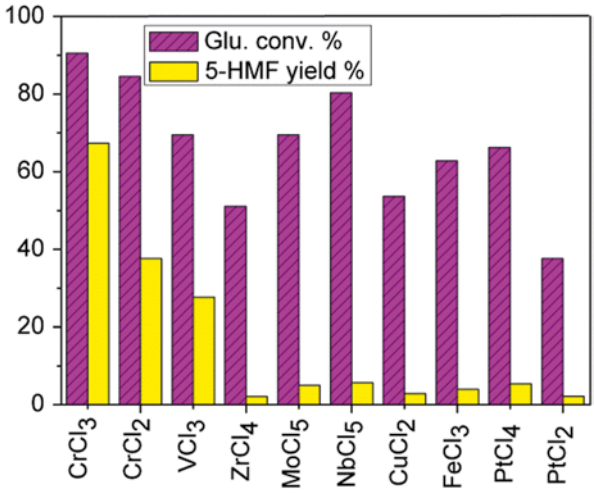

Fig. 4.7 The catalytic characteristics of metal chlorides for glucose conversion to 5-HMF in [BMIM]Cl; reaction at 96 °C (Reproduced with permission from Ref. [55]. Copyright 2014, ACS)

4.6.3 The Coordination Characteristics of Metal Chlorides in Glucose Conversion to 5-HMF in [BMIM]Cl

Because of the shortage of sufficient and reliable references in the literature, the FIR spectra of pure substances or nonreactive mixed system were first analyzed for identification of the absorption peak (Fig. 4.8). In the metal chlorides/[BMIM]Cl system, metal chlorides dissolved in [BMIM]Cl are dominated by metal–Cl bonds. The intense absorption bands at 302 cm^{-1}, 287 cm^{-1}, 311 cm^{-1}, and 381 cm^{-1} for the MCl_X/[BMIM]Cl (M=Cr, V, Pt, Fe; X=2, 3) systems are ascribed to the strong stretch vibrations of M–Cl bonds in the $[CrCl_6]^{3-}$, $[VCl_6]^{3-}$, $[PtCl_4]^{2-}$, and $[FeCl_4]^-$ anions.

Then in situ far-infrared spectroscopy was employed to follow the variation trend of metal–Cl complexes in the process of the glucose conversion catalyzed by the metal chlorides in [BMIM]Cl (Figs. 4.9 and 4.10).

The dissolved MCl_X (M=Cr, V, Pt, Fe; X=2, 3) was found to form new M complexes in MCl_X/[BMIM]Cl/glucose reaction system under typical reaction conditions, as shown in Fig. 4.9. With increasing time, the absorbance of M–Cl (M=Cr, V, Pt, Fe) bands at 302 cm^{-1}, 287 cm^{-1}, 311 cm^{-1}, and 381 cm^{-1} all decreased gradually in varying degrees.

The absorbance of Cr–Cl band at 302 cm^{-1} decreased gradually at the beginning (Fig. 4.9a) and then showed a limited restoration (Fig. 4.10) after an extended period of reaction, due to the consumption of glucose. Meanwhile, the peak intensity at 497 cm^{-1} increased gradually (Fig. 4.9a) and then decreased slowly (Fig. 4.10). The peak at 497 cm^{-1} was attributed to the absorption of Cr–O (from glucose) coordination bond in this spectral region. The absorption peaks of glucose, fructose, and 5-HMF in [BMIM]Cl as well as the $CrCl_3$/[BMIM]Cl and $CrCl_3$/[BMIM]Cl/5-HMF systems (Fig. 4.8) do not lie at 497 cm^{-1}. Though the coordination between fructose with chromium is similar to that between glucose with chromium, the amount of fructose during the reaction is known to be very low [41]. In addition, in situ far-infrared spectra of the VCl_3/[BMIM]Cl/glucose system (Fig. 4.9b) indicate that the V–Cl bond absorbance declined much more than the Cr–Cl bond absorbance in the $CrCl_3$/[BMIM]Cl/glucose system with time and with concomitant change in V–O bond FIR absorbance. The spectra in Fig. 4.9c show the FIR features of the $PtCl_2$/[BMIM]Cl/glucose system. Both the glucose absorption peak at 554 cm^{-1} and the Pt–Cl stretch vibration band at near 310 cm^{-1} showed a less pronounced change in 80 min compared to that in $CrCl_3$/[BMIM]Cl/glucose (Fig. 4.9a). Evidently, replacement of Pt–Cl bond by Pt–O bond is not favored as indicated by the FIR spectra. As a result, $PtCl_2$ displays rather low catalytic activity for glucose conversion (Fig. 4.7). In the $FeCl_3$/[BMIM]Cl/glucose system, the absorbance of the anion $[FeCl_4]^-$ at 381 cm^{-1} decreased sharply, and the absorbance of $[FeCl_4]^{2-}$ [66] at near 310 cm^{-1} increased gradually at the same time. Neither the absorbance at 381 cm^{-1} or 310 cm^{-1} was restored, even after 2 h (Fig. 4.9d).

As discussed above, the previous mechanism studies [40, 41, 43] have shown that the metal ions coordinate with the oxygen atoms of glucose and then catalyze the isomerization of glucose to fructose, which is the rate-controlling step in glucose conversion to HMF reaction. In order to clarify the coordination strength of the

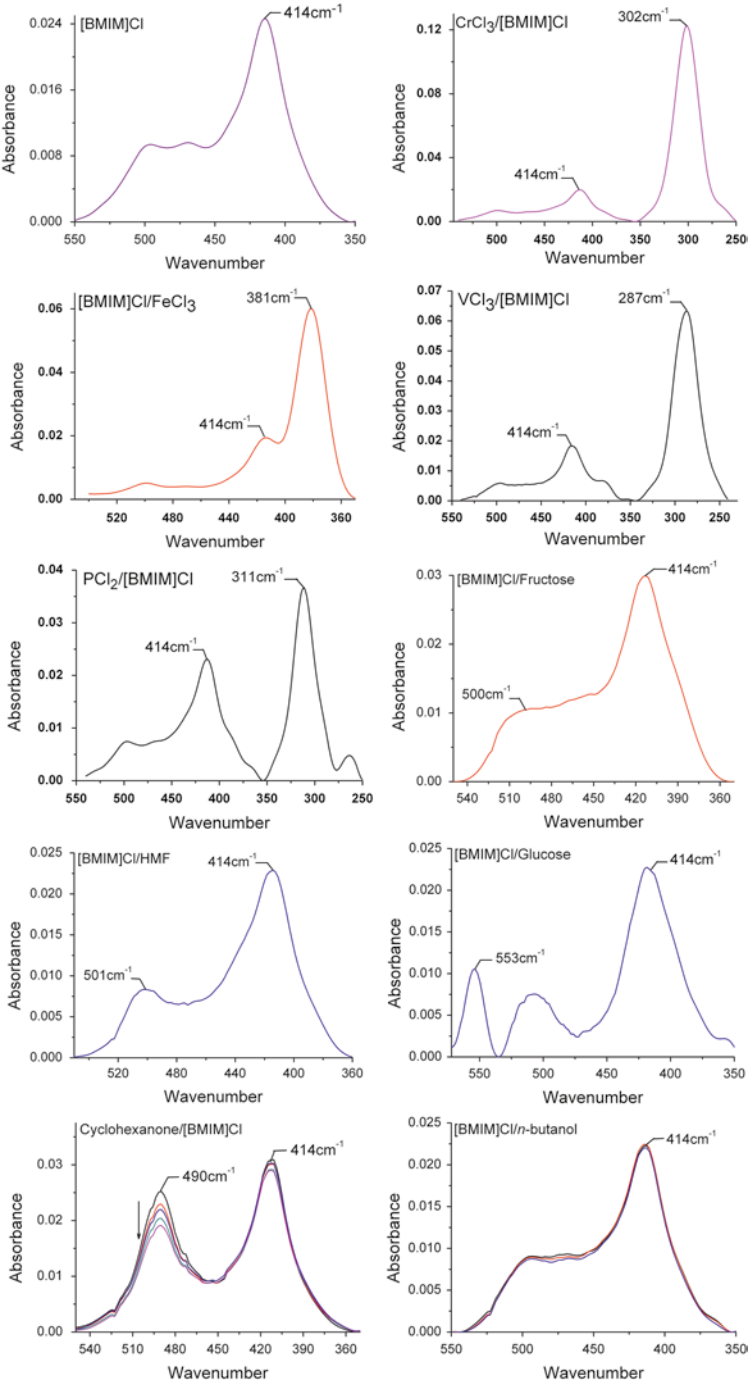

Fig. 4.8 The far-infrared background spectra were recorded for all the reaction systems. The far-infrared background spectra of [BMIM]Cl, metal–Cl bond in the homogeneous metal chloride/[BMIM]Cl systems, [BMIM]Cl/fructose, [BMIM]Cl/glucose and [BMIM]Cl/5-HMF, and [BMIM]Cl/$CrCl_3$ and the spectra of [BMIM]Cl/cyclohexanone and [BMIM]Cl/*n*-butanol system were all recorded at 100 °C. The downward *arrows* indicate that intensity decreases with time (Reproduced with permission from Ref. [55]. Copyright 2014, ACS)

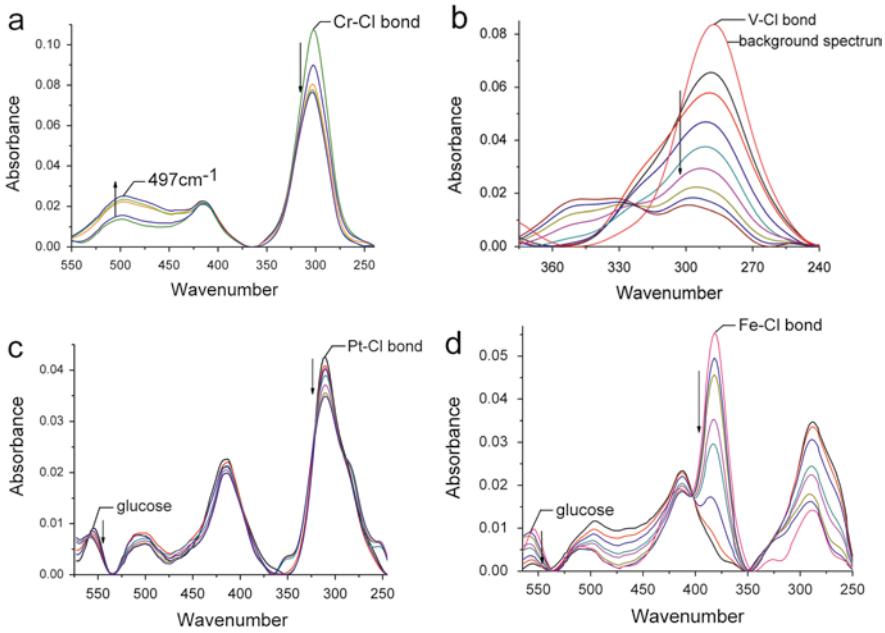

Fig. 4.9 The far-infrared spectra of metal chlorides/[BMIM]Cl/glucose, recorded at 100 °C. (**a**) $CrCl_3$/[BMIM]Cl/glucose, about 30 min; (**b**) VCl_3/[BMIM]Cl/glucose, about 60 min; (**c**) $PtCl_2$/[BMIM]Cl/glucose, about 80 min; and (**d**) $FeCl_3$/[BMIM]Cl/glucose, about 60 min. The *arrows* indicate that intensity changes with time (Reproduced with permission from Ref. [55]. Copyright 2014, ACS)

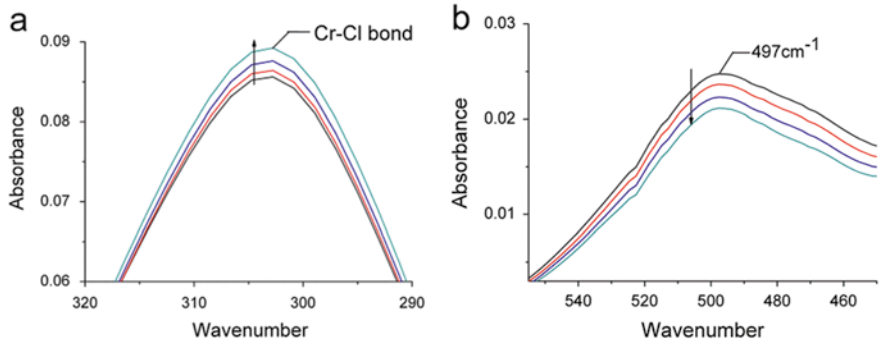

Fig. 4.10 The trend of the peak absorbance at 303 cm^{-1} (**a**) and 497 cm^{-1} (**b**) in the $CrCl_3$/[BMIM]Cl/glucose reaction system. The spectra were recorded for 30 min after the reaction started for 30 min (Reproduced with permission from Ref. [55]. Copyright 2014, ACS)

different types of oxygen in glucose molecule to the metal ions in the MCl_3/[BMIM]Cl/glucose reaction system (M=Cr, V, Fe), model compounds with either a carbonyl or a hydroxyl group only were studied for their coordination with the metal ions and their impact on glucose conversion as a result of the coordination. Cyclohexanone and *n*-butanol were selected for having a carbonyl group and a hydroxyl group, respectively, in the study. Glycolaldehyde was also studied as a model compound to probe the coordination chemistry of metal chlorides with the end group of glucose. In addition, the coordination strength of water and HMF as the products to metal ions was also studied.

4.6.4 The Mechanism of Metal Chlorides in the Process of Glucose Conversion

Cyclohexanone, n-butyl alcohol, and glycolaldehyde were first evaluated as additives to study their effect on the performance of MCl_3-catalyzed glucose conversion to 5-HMF. Striking differences were observed for different MCl_3-catalyst systems. When cyclohexanone and n-butyl alcohol were separately added to the reaction system, the glucose conversion and 5-HMF yield showed a negligible change compared with the results of the $CrCl_3$/[BMIM]Cl/glucose system in Fig. 4.11a. The results indicate that cyclohexanone and n-butyl alcohol are not competitive against glucose in the coordination with Cr(III) ion. However, adding glycolaldehyde dramatically suppressed the glucose conversion and 5-HMF yield (Fig. 4.11a). Evidently, glycolaldehyde competes strongly with glucose for the coordination with Cr(III) ion. In addition, previous study has established that addition of glycerol to the reaction system did not affect the glucose isomerization by chromium chloride catalysts [23], suggesting that glycerol is a weaker ligand to the Cr(III) catalyst than glucose. Ethylene glycol was also verified not to inhibit the glucose conversion. It can therefore be unambiguously concluded that the coordination of glucose with $CrCl_3$ responsible for the desired catalysis is mainly via the "glycolaldehyde" end group, possibly with enolate di-oxygen coordination to the metal ion [23, 40, 41].

Glycolaldehyde was further used as a model compound to quantify how many Cr–Cl bonds of the $[CrCl6]^3$ [41] anion in [BMIM]Cl were replaced. When excess glycolaldehyde and glucose were added to the $CrCl_3$/[BMIM]Cl system, respectively, the Cr–Cl bond absorbance at about 302 cm^{-1} was reduced by nearly one-half in both systems (Fig. 4.11b, c). Roughly near half of Cr–Cl bonds in BMIM]Cl/$CrCl_3$ system were replaced due to the formation of Cr–O (coming from glucose or glycolaldehyde) coordination bonds and Cr–Cl–Cr bridged bond [41]. There exists a little blue shift of the Cr–Cl bond absorption wave number, which appears consistent with the EXAFS analysis results [41] in which the length of Cr–Cl bond was shortened due to the trans effect. In addition, an isosbestic point was observed in Fig. 4.11b and less pronounced in Fig. 4.11c. The stronger isosbestic point due to increased coordination by glycolaldehyde to Cr(III) ions as shown in Fig. 4.11b occurs when the Cr–Cl absorption band at 302 cm^{-1} is decreased over one-half of

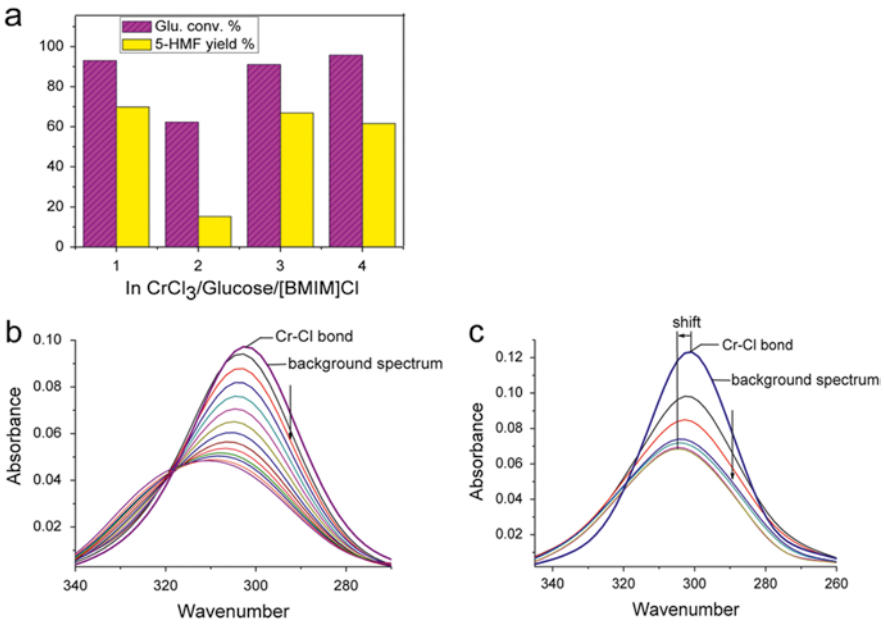

Fig. 4.11 (**a**) The effect of different probing model compounds on glucose conversion: *1* = none, *2* = glycolaldehyde, *3* = *n*- butanol, *4* = cyclohexanone; (**b**) FIR spectra of the Cr–Cl stretch vibration in the $CrCl_3$/[BMIM]Cl/glycolaldehyde system with excess glycolaldehyde; the FIR spectra were recorded at 80 °C; (**c**) FIR spectra of the Cr–Cl stretch vibration in the $CrCl_3$/[BMIM]Cl/glucose system with excess glucose; the far-infrared spectra were recorded at 100 °C. The background spectra in (**b**) and (**c**) for the $CrCl_3$/[BMIM]Cl system were recorded before addition of glycolaldehyde or glucose. The downward *arrows* indicate that intensity decreases with time (Reproduced with permission from Ref. [55]. Copyright 2014, ACS)

the original Cr–Cl band intensity. The less pronounced isosbestic point in Fig. 4.11c appears consistent with a slightly less than one-half decrease in the intensity of the original Cr–Cl absorption band.

Because the catalytic reaction of metal chlorides for glucose conversion is mainly via the "glycolaldehyde" end group, the authors simulated the self-condensation of glucose and fructose catalyzed by metal chloride with glycolaldehyde as a model compound. The results show that VCl_3 condensed the glycolaldehyde much more rapidly than $CrCl_3$. It is therefore evident that VCl_3 favors the condensation of glucose or fructose to humins especially at the first stage of the reaction [55].

4.6.5 The Coordination Characteristic of Metal Atoms to the Hydroxyl Oxygen

When the model compound *n*-butanol was added to the MCl_3/[BMIM]Cl (M=Cr, V) system, the M–Cl band in MCl_3 (M=Cr, V) complex absorbance at 302 cm^{-1} and 287 cm^{-1}, respectively, decreased in response to the added *n*-butanol, but it was then

recovered when *n*-butanol was evaporated (as indicated by the upward arrows in Fig. 4.12a, b). However, the absorbance of the Fe–Cl bonds decreased gradually in the $FeCl_3$/[BMIM]Cl system. And the evaporation of *n*-butyl alcohol does not restore the lost Fe–Cl bonds even after an extended period of time (Fig. 4.12c). According to the correlation of the absorbance and the concentration, the chloride ions in MCl_3 (M=V, Cr, Fe) complex were replaced by oxygen atoms of n-butyl alcohol as added model compound, leading to the decrease of the absorbance and concentration in the MCl_3 absorption band. And then the concentration of $CrCl_3$ and VCl_3 complex increased because the weaker coordination between Cr(III) and V(III) ions and the hydroxyl oxygen would prompt the restoration from the M–O complex to M–Cl complex with the evaporation of *n*-butyl alcohol. Similarly it is concluded that the stronger coordination between Fe(III) and the hydroxyl oxygen caused the continuous decrease of the $FeCl_3$ complex absorbance and concentration. In the reaction system, the reagent glucose, intermediate product fructose, and the product HMF are all hydroxyl

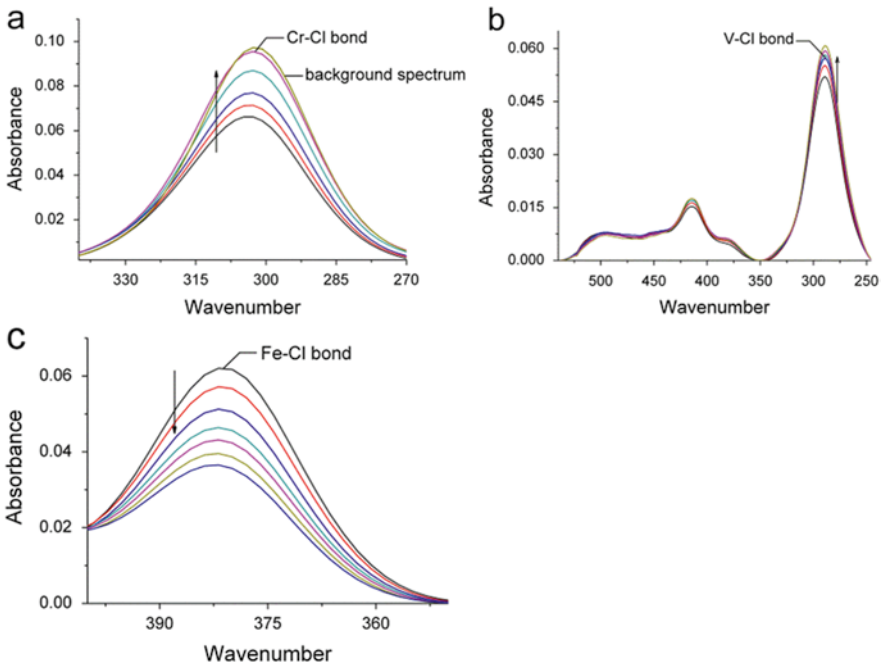

Fig. 4.12 (**a**) FIR spectra of the Cr–Cl stretch vibration in the $CrCl_3$/[BMIM]Cl/*n*-butanol system; (**b**) far-infrared spectra of the V–Cl stretch vibration in the VCl_3/[BMIM]Cl/*n*-butyl alcohol system; (**c**) far-infrared spectra of the Fe–Cl stretch vibration in the $FeCl_3$/[BMIM]Cl/*n*-butyl alcohol system. The far-infrared spectra in (**a**), (**b**), and (**c**) were recorded at 100 °C immediately after adding the model compounds. The background spectra of MCl_3/[BMIM]Cl system were taken before addition of model compounds (M=Cr, V, Fe). The *arrows* in (**a**), (**b**) and (**c**) represent the variation trend of the M–Cl coordination bond during evaporation of the model compound (Reproduced with permission from Ref. [55]. Copyright 2014, ACS)

compounds. Thus the stronger coordination of the iron atoms to the single hydroxyl oxygen atoms could interfere with the coordination of the metal atom to the glycolaldehyde end group of glucose and then affect the catalytic selectivity to some extent.

4.6.6 *The Coordination Characteristic of Metal Atoms to the Ketonic Oxygen*

The Cr–Cl band in $CrCl_3$ complex absorbance at 302 cm^{-1} decreased in response to the added cyclohexanone and restored gradually with the vaporization of the model compound at 100 °C (Fig. 4.13a). The coordination of Cr(III) to the oxygen from cyclohexanone is so weak that a temperature of 100 °C was sufficient to disrupt the $Cr–O_{carbonyl}$ coordination bond and to reverse to the more stable $[CrCl_6]^{3-}$ complex. However the coordination characteristic of V(III) and Fe(III) with cyclohexanone shows a strong contrast to that of chromium. The coordination of V(III) and Fe(III)

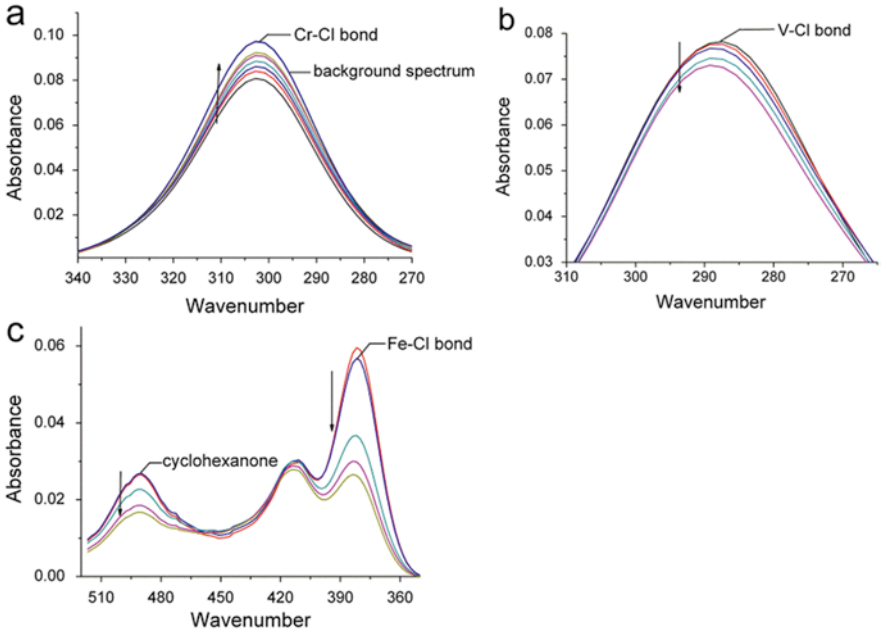

Fig. 4.13 (**a**) FIR spectra of the Cr–Cl stretch vibration in the $CrCl_3$/[BMIM]Cl/cyclohexanone system; (**b**) far-infrared spectra of the V–Cl stretch vibration in the VCl_3/[BMIM]Cl/cyclohexanone system; **(c)** far-infrared spectra of the $FeCl_3$/[BMIMCl]/cyclohexanone system. The far-infrared spectra in **(a)**, **(b)**, and (**c**) were recorded at 100 °C immediately after adding the model compounds. And the *arrows* represent the variation trend of the M–Cl coordination bond during evaporation of the model compound (Reproduced with permission from Ref. [55]. Copyright 2014, ACS)

ions to the carbonyl oxygen from cyclohexanone is much stronger. Thus $FeCl_3$ and VCl_3 tend to form strong coordination bonds with the carbonyl oxygen from cyclohexanone.

The catalytic performances of the metal (V, Cr, and Fe) chlorides in glucose conversion and 5-HMF yield reflect a clear response to the coordination strength of the metal ions with the carbonyl oxygen of cyclohexanone. The HMF yield in the $FeCl_3$ catalytic reaction is rather low, about 2.4 %, due to the addition of cyclohexanone. When nearly the same amounts of cyclohexanone were added to the MCl_3/[BMIM]Cl/glucose system (M=Cr, V), respectively, the yield of 5-HMF was suppressed in the VCl_3 catalytic system, but the 5-HMF yield in the $CrCl_3$ system was little affected (Fig. 4.14a). Evidently, the coordination chemistry of MCl_3 (M=Cr, V) with the carbonyl oxygen of cyclohexanone is correlated with their catalytic performance in glucose conversion. The stronger coordination of vanadium atoms with the carbonyl oxygen would favor the formation of the possible intermediate as proposed in Fig. 4.15a, c and the subsequent consumption of 5-HMF to produce undesired side products (Fig. 4.15b). For the $CrCl_3$ catalyst, the coordination of Cr(III) with the carbonyl oxygen is very weak and the impact of carbonyl oxygen does not inhibit the performance of the $CrCl_3$ catalyst. Thus it is the coordination strength of metal ions with the carbonyl oxygen as revealed by in situ FIR that contributed to the change in 5-HMF yield in the MCl_3/[BMIM]Cl/glucose (M=Cr, V) system with the addition of cyclohexanone. And the stronger coordination of V(III) to carbonyl oxygen could also explain the results that the V–Cl bond absorbance declined much more than the Cr–Cl bond absorbance in the MCl_3/[BMIM]Cl/glucose (M=V, Cr) reaction system with time and VCl_3 was found to condense the glycolaldehyde much more rapidly than $CrCl_3$.

4.6.7 The Coordination Characteristic of Metal Atoms to the Oxygen Atoms of 5-HMF and Water

The absorbance and concentration of M–Cl bonds in MCl_X complex (M=Cr, V, Fe) present different trends with the addition of same amount of 5-HMF (Fig. 4.16a–c). With increasing time, the absorbance of Cr–Cl bonds at 302 cm^{-1} in $[CrCl_6]^{3-}$ complex showed only a little decreased in 60 min. The absorbance of Fe–Cl and V–Cl bonds in $[FeCl_4]^-$, $[VCl_6]^{3-}$ appeared a sharp decline an hour later. The MCl_3 (M=Fe, V) catalysts therefore may be expected to have strong coordination with the product 5-HMF in the process of glucose conversion. However, the coordination of Cr atom to 5-HMF is rather weak. The results on the 5-HMF conversion in the presence of glycolaldehyde in [BMIM]Cl/MCl_3 (M=Cr, V), as shown Fig. 4.16d, are in excellent conformity to what one would expect based on the coordination chemistry. The VCl_3 catalyst converts the 5-HMF faster than $CrCl_3$ catalyst. Thus, in the process of glucose conversion, one may expect that glucose could also react with the formed product 5-HMF, resulting in humins formation in the presence of VCl_3 catalyst. The

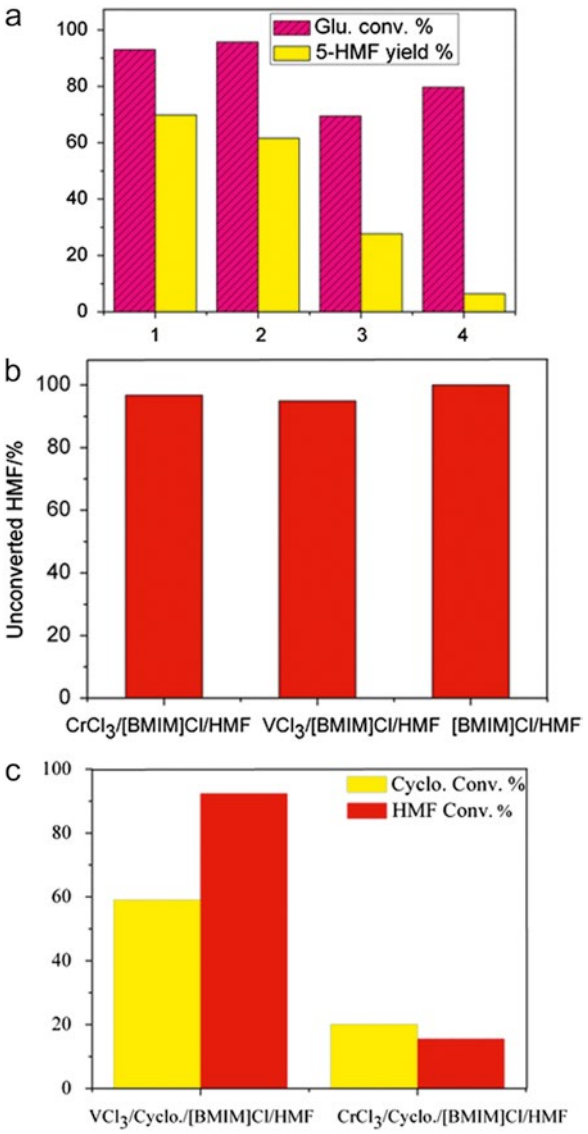

Fig. 4.14 (**a**) The effect of cyclohexanone on glucose conversion and 5-HMF yield in the $CrCl_3$/[BMIM]Cl/glucose and VCl_3/[BMIM]Cl/glucose systems: *1* = $CrCl_3$/[BMIM]Cl/glucose, *2* = $CrCl_3$/[BMIM]Cl/glucose/cyclohexanone, *3* = VCl_3/[BMIM]Cl/glucose, *4* = VCl_3/[BMIM]Cl/glucose/cyclohexanone; (**b**) the unconverted 5-HMF in pure [BMIM]Cl and in [BMIM]Cl containing $CrCl_3$ or VCl_3 reacted at 96 °C; (**c**) the 5-HMF and cyclohexanone conversion in [BMIM]Cl containing VCl_3 or $CrCl_3$ (Reproduced with permission from Ref. [55]. Copyright 2014, ACS)

reaction between glucose and 5-HMF possibly occurred at a common V(III) site via the multiple V–O coordination bonds (Fig. 4.16e), which partly contributed to the lower catalytic efficiency of VCl_3 than $CrCl_3$.

The coordination characteristics of metal ions to the product water are shown in Fig. 4.17. When the approximately equal amount of water was individually added to the MCl_3/[BMIM]Cl system (M=Cr, V, Fe), the M–Cl (M=Cr, V) absorbance band intensity

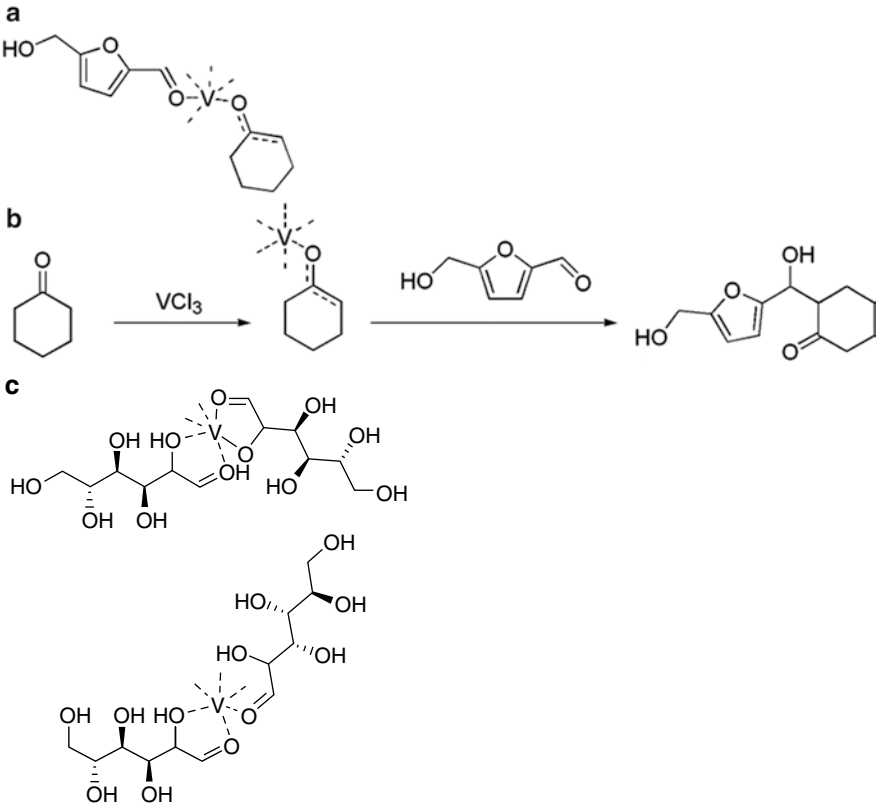

Fig. 4.15 (**a**) Proposed coordination structure of vanadium with carbonyl compounds. (**b**) Proposed reaction of 5-HMF with cyclohexanone in [BMIM]Cl containing VCl_3. Only simplified complex forms of the metal ions with the compounds are shown. (**c**) Proposed coordination structures between vanadium and the oxygen atoms of glucose (Reproduced with permission from Ref. [55]. Copyright 2014, ACS)

decreased in response to the added water, but it was then restored with the evaporation of water (as indicated by the upward arrows in Fig. 4.17a, b). The coordination of chromium and vanadium atom to the oxygen atom from water is weak and reversible. However the absorbance of Fe–Cl bond decreased sharply and did not recover due to strong coordination of $Fe–O_{water}$ (Fig. 4.17c). Thus, the coordination sites of Fe(III) are fully blocked by the presence of water. Consequently, the catalytic activity of $FeCl_3$ was almost lost completely with the addition of some amount of water (Fig. 4.17d), in strong contrast to that of $CrCl_3$ catalysis.

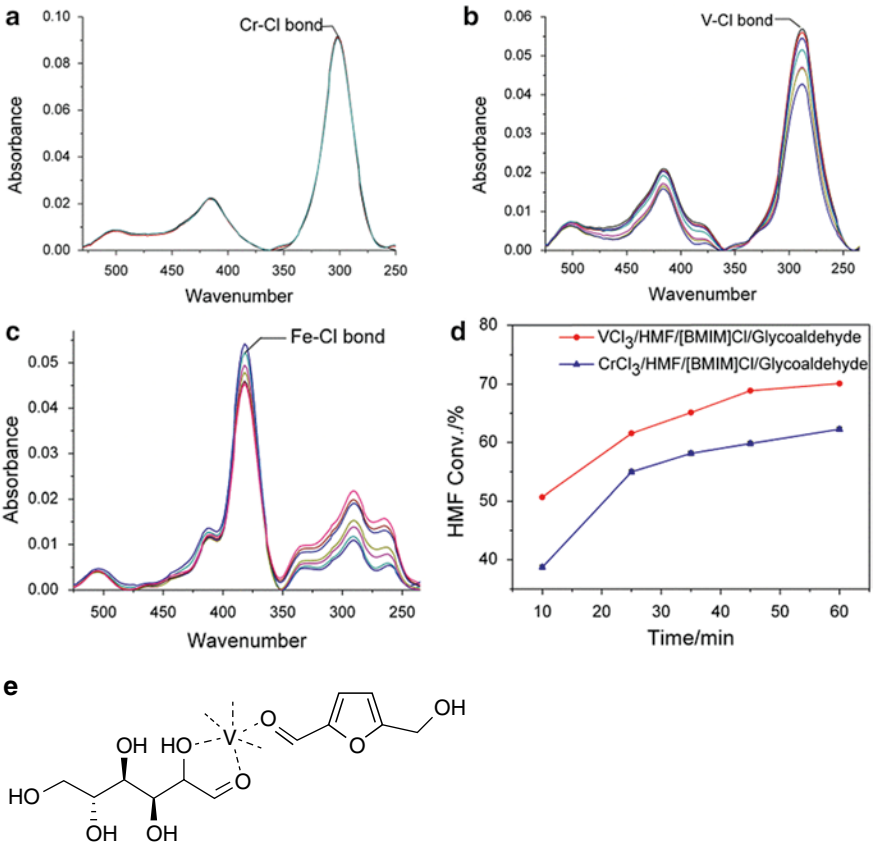

Fig. 4.16 (**a**) Far-infrared spectra of $CrCl_3$/5-HMF/[BMIM]Cl system for 1 h; (**b**) far-infrared spectra of the VCl_3/5-HMF/[BMIM]Cl system for 90 min; (**c**) far-infrared spectra of the $FeCl_3$/5-HMF/[BMIM]Cl system for 65 min. The far-infrared spectra in (**a**), (**b**), and (**c**) were recorded at 100 °C immediately after adding the model compound 5-HMF, with approximately equal molar amounts of glucose and MCl_3 catalytic amounts; (**d**) the 5-HMF conversion in [BMIM]Cl/glycolaldehyde containing $CrCl_3$ and VCl_3; (**e**) proposed coordination structures between vanadium and the oxygen atoms of glucose and 5-HMF (Reproduced with permission from Ref. [55]. Copyright 2014, ACS)

4.6.8 Correlation of the Coordination Chemistry of Metal Chlorides with Their Catalytic Performance in Glucose Conversion

By using in situ far-infrared spectroscopy and a combination of well-selected model compounds of different oxygen sources, cyclohexanone, *n*-butanol, glycolaldehyde, and deionized water, the distinctively different coordination chemistries of four classes of representative catalysts, $CrCl_3$, $PtCl_2$, $FeCl_3$, and VCl_3, with oxygen of

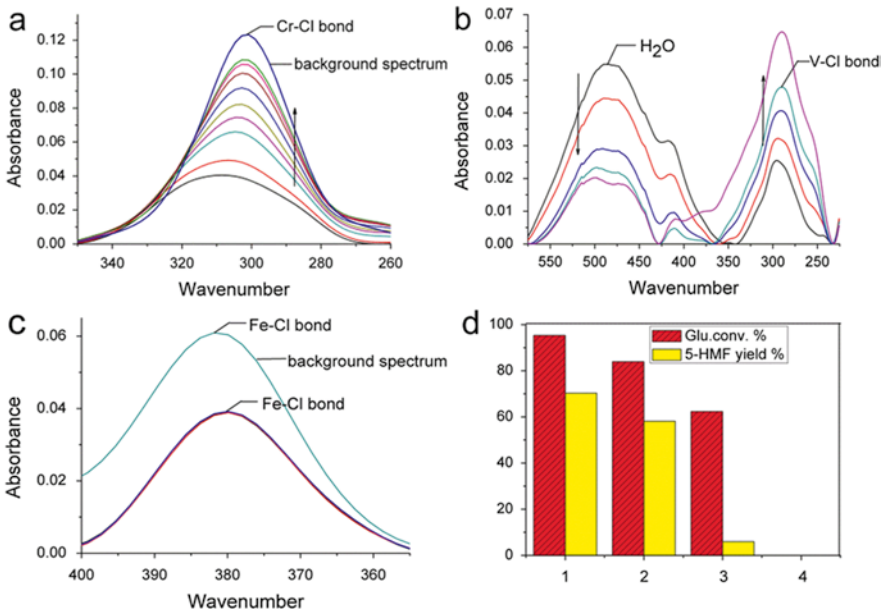

Fig. 4.17 (**a**) FIR spectra of the Cr–Cl stretch vibration in the $CrCl_3$/[BMIM]Cl/water system. The background spectra of $CrCl_3$/[BMIM]Cl system were taken before the addition of the model compound, water; (**b**) far-infrared spectra of the VCl_3/[BMIMCl]/water system; (**c**) far-infrared spectra of the Fe–Cl stretch vibration in $FeCl_3$/[BMIM]Cl, before and after the addition of a drop of water. The spectra in (**a**), (**b**), and (**c**) were recorded at 100 °C and the *arrows* represent the recovery of the M–Cl coordination bond during evaporation of water; (**d**) the effect of water on glucose conversion and HMF yield in the MCl_3/[BMIM]Cl/glucose (M=Cr, Fe): *1* = $CrCl_3$/[BMIM]Cl/glucose, *2* = $CrCl_3$/[BMIM]Cl/H_2O/glucose, *3* = $FeCl_3$/[BMIM]Cl/glucose, *4* = $FeCl_3$/[BMIM]Cl/H_2O/glucose (Reproduced with permission from Ref. [55]. Copyright 2014, ACS)

different sources (Fig. 4.18a) were found to be well correlated to the catalytic performances of the metal chlorides (Fig. 4.18b).

Furthermore, the experimental results on the coordination strengths of metal ions with oxygen of different sources achieved by the FIR studies may be rationalized by the crystal field theory. $CrCl_3$, VCl_3, $PtCl_2$, and $FeCl_3$ favor to be in the form of $[CrCl_6]^{3-}$, $[VCl_6]^{3-}$, $[PtCl_4]^{2-}$, and $[FeCl_4]^{-}$, respectively, in [BMIM]Cl. The geometry configuration of $[CrCl_6]^{3-}$ and $[VCl_6]^{3-}$ is octahedron, $[PtCl_4]^{2-}$ is quadrate, and $[FeCl_4]^{-}$ is tetrahedron [66]. The outermost electron configurations of Cr^{3+}, V^{3+}, Pt^{2+}, and Fe^{3+} are $3d^34s^0$, $3d^24s^0$, $5d^86s^0$, and $3d^54s^0$, respectively. Thus the crystal field stabilization energy (CFSE) can be calculated according to the crystal field theory [67, 68]. CFSE ($[CrCl_6]^{3-}$) = 12Dq, CFSE ($[VCl_6]^{3-}$) = 8Dq, CFSE ($[PtCl_4]^{2-}$) = 14.56Dq, CFSE ($[FeCl_4]^{-}$) = 0Dq, and Δ = 10Dq are the octahedral crystal field splitting energy. Then the values of CFSE may be used to reflect the relative energetic order in replacing the metal–Cl bonds by the metal–O bonds. The CFSE of $[FeCl_4]^{-}$ is the lowest among the four metal chloride anions, indicating that

a

O \ M^{n+}	$CrCl_3$	VCl_3	$FeCl_3$	$PtCl_2$
	Strong	Strong	Strong	Negligible
$-CH_2OH$	Weak, Reversible	Weak, Reversible	Strong	Negligible
-C=O	Weak, Reversible	Strong	Strong	Negligible
H_2O	Weak, Reversible	Weak, Reversible	Very Strong	Negligible

b

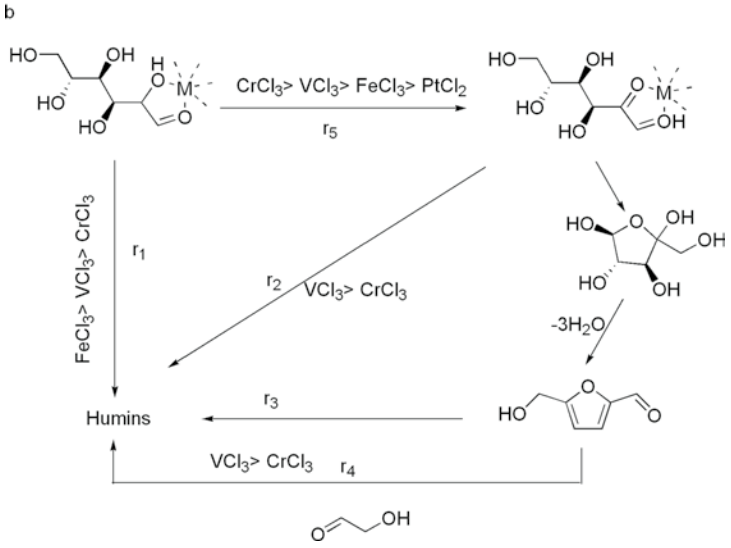

Fig. 4.18 (**a**) The distinctively different coordination chemistry of metal ion with oxygen of different sources. (**b**) Overall glucose conversion pathways in the presence of metal chloride catalyst. The complexes of the metal ions with the compounds are only shown in simplified form (Reproduced with permission from Ref. [55]. Copyright 2014, ACS)

the coordination of the iron with an oxygen atom is in optimum and the coordination strength of the iron center to the oxygen is the strongest. The CFSE of $[PtCl_4]^{2-}$ is the highest; the coordination of Pt in with oxygen is unfavorable. And the theoretical analysis is consistent with the FIR results (Fig. 4.18). Therefore changing of geometry configuration [40, 41] before and after the catalytic reaction on the coordination strength may not dominate based on the CFSE. In addition, the chelating effect of metal ions by the glycolaldehyde structure of glucose could stabilize the metal complex. Thus the coordination strength of metal ion by the glycolaldehyde structure would be expected to be more stable than other single-oxygen molecules, consistent with those obtained by the experiments.

New mechanistic insights have been further established by correlating the coordination chemistries of the metal chlorides with their drastically different catalytic characteristics in glucose conversion through the FIR spectroscopy study. The superior performance of $CrCl_3$ catalyst for the formation of 5-HMF from glucose among the studied metal chlorides can be ascribed to preferential coordination of $CrCl_3$ with the glycolaldehyde group of glucose. Water generated during the reaction makes little difference for the $CrCl_3$ catalytic activity due to the reversible interaction between chromium ion and water. In addition, the relatively weaker interactions of Cr(III) with individual oxygen atoms in the hydroxyl group of alcohols and in the carbonyl group of ketones with respect to that of glycolaldehyde group made $CrCl_3$ uniquely superior for selective aldose isomerization. Isolated hydroxy and carbonyl in 5-HMF do not inhibit the catalytic activity of $CrCl_3$ for the reaction, which also explains the stability of 5-HMF in the chromium chloride/ionic liquid systems.

References

1. Ragauskas AJ, Williams CK, Davison BH, Britovsek G, Cairney J, Eckert CA, Frederick WJ Jr, Hallett JP, Leak DJ, Liotta CL, Mielenz JR, Richard M, Templer R, Tschaplinski T (2006) The path forward for biofuels and biomaterials. Science 311:484
2. Mamman AS, Lee J-M, Kim Y-C, Hwang IT, Park N-J, Hwang YK, Chang J-S, Hwang J-S (2008) Furfural: hemicellulose/xylose derived biochemical. Biofuels Bioprod Biorefin 2(5):438–454. doi:10.1002/bbb.95
3. Tong X, Ma Y, Li Y (2010) Biomass into chemicals: conversion of sugars to furan derivatives by catalytic processes. Appl Catal Gen 385(1–2):1–13. doi:10.1016/j.apcata.2010.06.049
4. Zhang ZC (2013) Catalytic transformation of carbohydrates and lignin in ionic liquids. Wiley Interdiscip Rev Energy Environ 2(6):655–672. doi:10.1002/wene.67
5. Corma A, Iborra S, Velty A (2007) Chemical routes for the transformation of biomass into chemicals. Chem Rev 107(6):2411–2502. doi:10.1021/cr050989d
6. Grande PM, Bergs C, Dominguez de Maria P (2012) Chemo-enzymatic conversion of glucose into 5-hydroxymethylfurfural in seawater. ChemSusChem 5(7):1203–1206. doi:10.1002/cssc.201200065
7. Hernández M, Lima E, Guzmán A, Vera M, Novelo O, Lara V (2014) A small change in the surface polarity of cellulose causes a significant improvement in its conversion to glucose and subsequent catalytic oxidation. Appl Catal Environ 144:528–537. doi:10.1016/j.apcatb.2013.07.061
8. Yang G, Pidko EA, Hensen EJ (2013) The mechanism of glucose isomerization to fructose over Sn-BEA zeolite: a periodic density functional theory study. ChemSusChem 6(9):1688–1696. doi:10.1002/cssc.201300342
9. Zhang J, Cao Y, Li H, Ma X (2014) Kinetic studies on chromium-catalyzed conversion of glucose into 5-hydroxymethylfurfural in alkylimidazolium chloride ionic liquid. Chem Eng J 237:55–61. doi:10.1016/j.cej.2013.10.007
10. He J, Zhang Y, Chen EY (2013) Chromium(0) nanoparticles as effective catalyst for the conversion of glucose into 5-hydroxymethylfurfural. ChemSusChem 6(1):61–64. doi:10.1002/cssc.201200795
11. Lewkowski J (2001) Synthesis, chemistry and applications of 5-hydroxymethylfurfural and its derivatives. ARKIVOC i:17
12. van Putten RJ, van der Waal JC, de Jong E, Rasrendra CB, Heeres HJ, de Vries JG (2013) Hydroxymethylfurfural, a versatile platform chemical made from renewable resources. Chem Rev 113(3):1499–1597. doi:10.1021/cr300182k

13. Kuster BFM (1990) 5-Hydroxymethylfurfural (HMF). A review focussing on its manufacture. Starch 42:314
14. Ståhlberg T, Fu W, Woodley JM, Riisager A (2011) Synthesis of 5-(Hydroxymethyl)furfural in ionic liquids: paving the way to renewable chemicals. ChemSusChem 4(4):451–458. doi:10.1002/cssc.201000374
15. Choudhary V, Mushrif SH, Ho C, Anderko A, Nikolakis V, Marinkovic NS, Frenkel AI, Sandler SI, Vlachos DG (2013) Insights into the interplay of Lewis and Bronsted acid catalysts in glucose and fructose conversion to 5-(hydroxymethyl)furfural and levulinic acid in aqueous media. J Am Chem Soc 135(10):3997–4006. doi:10.1021/ja3122763
16. Ståhlberg T, Sørensen MG, Riisager A (2010) Direct conversion of glucose to 5-(hydroxymethyl)furfural in ionic liquids with lanthanide catalysts. Green Chem 12(2):321. doi:10.1039/b916354a
17. Hu S, Zhang Z, Song J, Zhou Y, Han B (2009) Efficient conversion of glucose into 5-hydroxymethylfurfural catalyzed by a common Lewis acid SnCl4 in an ionic liquid. Green Chem 11(11):1746. doi:10.1039/b914601f
18. Kim B, Jeong J, Lee D, Kim S, Yoon H-J, Lee Y-S, Cho JK (2011) Direct transformation of cellulose into 5-hydroxymethyl-2-furfural using a combination of metal chlorides in imidazolium ionic liquid. Green Chem 13(6):1503. doi:10.1039/c1gc15152e
19. Nikolla E, Román-Leshkov Y, Moliner M, Davis ME (2011) "One-Pot" synthesis of 5-(hydroxymethyl)furfural from carbohydrates using tin-beta zeolite. ACS Catal 1(4):408–410. doi:10.1021/cs2000544
20. Kimura H, Nakahara M, Matubayasi N (2011) In situ kinetic study on hydrothermal transformation of D-glucose into 5-hydroxymethylfurfural through D-fructose with 13C NMR. J Phys Chem A 115(48):14013–14021. doi:10.1021/jp206355e
21. Antal MJ Jr, Mok WSL, Richards GN (1990) Mechanism of formation of 5-(hydroxymethyl)-2-furaldehyde from d-fructose and sucrose. Carbohydr Res 199(1):91–109. doi:10.1016/0008-6215(90)84096-D
22. Poncini L, Richards GN (1980) Thermolysis of sucrose in dimethyl sulphoxide solution. Carbohydr Res 87(2):209–217. doi:10.1016/S0008-6215(00)85207-6
23. Zhao H, Holladay JE, Brown H, Zhang ZC (2007) Metal chlorides in ionic liquid solvents convert sugars to 5-hydroxymethylfurfural. Science 316(5831):1597–1600. doi:10.1126/science.1141199
24. Dais P, Perlin AS (1985) Stabilization of the β-furanose form, and kinetics of the automerization of d-fructose in dimethyl sulfoxide. Carbohydr Res 136:215–223. doi:10.1016/0008-6215(85)85198-3
25. Rigal L, Gaset A, Gorrichon JP (1981) Selective conversion of D-fructose to 5-hydroxymethyl-2-furancarboxaldehyde using a water-solvent-ion-exchange resin triphasic system. Ind Eng Chem Prod Res Dev 20(4):719–721. doi:10.1021/i300004a025
26. Román-Leshkov Y, Chheda JN, Dumesic JA (2006) Phase modifiers promote efficient production of hydroxymethylfurfural from fructose. Science 312(5782):1933–1937. doi:10.1126/science.1126337
27. Mercadier D, Rigal L, Gaset A, Gorrichon J-P (1981) Synthesis of 5-hydroxymethyl-2-furancarboxaldehyde catalysed by cationic exchange resins. Part 3. Kinetic approach of the D-fructose dehydration. J Chem Technol Biotechnol 31(1):503–508. doi:10.1002/jctb.503310167
28. Kuster BFM, Laurens J (1977) Preparation of 5-hydroxymethylfurfural part II. Dehydration of fructose in a tube reactor using polyethyleneglycol as solvent. Starch/Stärke 29(5):172–176. doi:10.1002/star.19770290507
29. Jia S, Liu K, Xu Z, Yan P, Xu W, Liu X, Zhang ZC (2014) Reaction media dominated product selectivity in the isomerization of glucose by chromium trichloride: from aqueous to non-aqueous systems. Catal Today 234:83–90. doi:10.1016/j.cattod.2014.02.038
30. Hu L, Sun Y, Lin L, Liu S (2012) Catalytic conversion of glucose into 5-hydroxymethylfurfural using double catalysts in ionic liquid. J Taiwan Inst Chem Eng 43(5):718–723. doi:10.1016/j.jtice.2012.04.001

31. Rajabbeigi N, Torres AI, Lew CM, Elyassi B, Ren L, Wang Z, Je Cho H, Fan W, Daoutidis P, Tsapatsis M (2014) On the kinetics of the isomerization of glucose to fructose using Sn-Beta. Chem Eng Sci 116:235–242. doi:10.1016/j.ces.2014.04.031
32. Despax S, Estrine B, Hoffmann N, Le Bras J, Marinkovic S, Muzart J (2013) Isomerization of d-glucose into d-fructose with a heterogeneous catalyst in organic solvents. Catal Commun 39:35–38. doi:10.1016/j.catcom.2013.05.004
33. Li C, Zhao ZK, Wang A, Zheng M, Zhang T (2010) Production of 5-hydroxymethylfurfural in ionic liquids under high fructose concentration conditions. Carbohydr Res 345(13): 1846–1850. doi:10.1016/j.carres.2010.07.003
34. Qi XH, Watanabe M, Aida TM, Smith RL Jr (2009) Efficient process for conversion of fructose to 5-hydroxymethylfurfural with ionic liquids. Green Chem 11(9):1327–1331 . doi:10.1039/B905975J
35. Binder JB, Cefali AV, Blank JJ, Raines RT (2010) Mechanistic insights on the conversion of sugars into 5-hydroxymethylfurfural. Energy Environ Sci 3(6):765. doi:10.1039/b923961h
36. Han JK, Lee KW, Eui LC (2000) Proton dynamics in SnCl4·5H2O. J Kor Phys Soc 37(5):L487–L489
37. Guan J, Cao Q, Guo X, Mu X (2011) The mechanism of glucose conversion to 5-hydroxymethylfurfural catalyzed by metal chlorides in ionic liquid: a theoretical study. Comput Theor Chem 963(2–3):453–462. doi:10.1016/j.comptc.2010.11.012
38. van Putten RJ, Soetedjo JN, Pidko EA, van der Waal JC, Hensen EJ, de Jong E, Heeres HJ (2013) Dehydration of different ketoses and aldoses to 5-hydroxymethylfurfural. ChemSusChem 6(9):1681–1687. doi:10.1002/cssc.201300345
39. Loerbroks C, van Rijn J, Ruby MP, Tong Q, Schuth F, Thiel W (2014) Reactivity of metal catalysts in glucose-fructose conversion. Chemistry 20(38):12298–12309. doi:10.1002/chem.201402437
40. Pidko EA, Degirmenci V, van Santen RA, Hensen EJ (2010) Glucose activation by transient Cr^{2+} dimers. Angew Chem 49(14):2530–2534. doi:10.1002/anie.201000250
41. Zhang Y, Pidko EA, Hensen EJ (2011) Molecular aspects of glucose dehydration by chromium chlorides in ionic liquids. Chemistry 17(19):5281–5288. doi:10.1002/chem.201003645
42. Pidko EA, Degirmenci V, Hensen EJM (2012) On the mechanism of Lewis acid catalyzed glucose transformations in ionic liquids. ChemCatChem 4(9):1263–1271. doi:10.1002/cctc.201200111
43. Pidko EA, Degirmenci V, van Santen RA, Hensen EJ (2010) Coordination properties of ionic liquid-mediated chromium(II) and copper(II) chlorides and their complexes with glucose. Inorg Chem 49(21):10081–10091. doi:10.1021/ic101402r
44. Yang G, Pidko EA, Hensen EJM (2012) Mechanism of Brønsted acid-catalyzed conversion of carbohydrates. J Catal 295:122–132. doi:10.1016/j.jcat.2012.08.002
45. Amir RM, Anjum FM, Khan MI, Khan MR, Pasha I, Nadeem M (2013) Application of Fourier transform infrared (FTIR) spectroscopy for the identification of wheat varieties. J Food Sci Technol 50(5):1018–1023. doi:10.1007/s13197-011-0424-y
46. Cozzolino D, Roumeliotis S, Eglinton J (2014) Evaluation of the use of attenuated total reflectance mid infrared spectroscopy to determine fatty acids in intact seeds of barley (Hordeum vulgare). LWT Food Sci Technol 56(2):478–483. doi:10.1016/j.lwt.2013.11.019
47. Lejeune J, Brubach JB, Roy P, Bleuzen A (2014) Application of the infrared spectroscopy to the structural study of Prussian blue analogues. C R Chim 17(6):534–540. doi:10.1016/j.crci.2014.01.017
48. Nasrazadani S, Springfield T (2013) Application of Fourier transform infrared spectroscopy in cement Alkali quantification. Mater Struct 47(10):1607–1615. doi:10.1617/s11527-013-0140-3
49. Zhu ZY, Zhang C, Liu F, Kong WW, He Y (2014) Producing area identification of Letinus edodes using mid-infrared spectroscopy. Spectrosc Spectr Anal 34(3):664–667. doi:10.3964/j.issn.1000-0593(2014)03-0664-04
50. Ruthenburg TC, Perlin PC, Liu V, McDade CE, Dillner AM (2014) Determination of organic matter and organic matter to organic carbon ratios by infrared spectroscopy with application to selected sites in the IMPROVE network. Atmos Environ 86:47–57. doi:10.1016/j.atmosenv.2013.12.034

51. Kendix EL, Prati S, Joseph E, Sciutto G, Mazzeo R (2009) ATR and transmission analysis of pigments by means of far infrared spectroscopy. Anal Bioanal Chem 394(4):1023–1032. doi:10.1007/s00216-009-2691-2
52. Vahur S, Teearu A, Leito I (2010) ATR-FT-IR spectroscopy in the region of 550–230 cm^{-1} for identification of inorganic pigments. Spectrochim Acta A Mol Biomol Spectrosc 75(3):1061–1072. doi:10.1016/j.saa.2009.12.056
53. Kendix E, Moscardi G, Mazzeo R, Baraldi P, Prati S, Joseph E, Capelli S (2008) Far infrared and Raman spectroscopy analysis of inorganic pigments. J Raman Spectrosc 39(8):1104–1112. doi:10.1002/jrs.1956
54. Zhang M, Moxon T (2014) Infrared absorption spectroscopy of SiO2-moganite. Am Mineral 99(4):671–680. doi:10.2138/am.2014.4589
55. Li HX, Xu WJ, Huang TY, Jia SY, Xu ZW, Yan PF, Liu XM, Zhang ZC (2014) Distinctive aldose isomerization characteristics and the coordination chemistry of metal chlorides in 1-Butyl-3-methylimidazolium chloride. ACS Catal 4(12):4446–4454. doi:10.1021/cs5012684
56. Brusentsova TN, Peale RE, Maukonen D, Harlow GE, Boesenberg JS, Ebel D (2010) Far infrared spectroscopy of carbonate minerals. Am Mineral 95(10):1515–1522. doi:10.2138/am.2010.3380
57. Kidchob T, Malfatti L, Marongiu D, Enzo S, Innocenzi P (2009) Formation of cerium titanate, $CeTi_2O_6$, in sol-gel films studied by XRD and FAR infrared spectroscopy. J Sol Gel Sci Technol 52(3):356–361. doi:10.1007/s10971-009-2047-6
58. Falconer RJ, Zakaria HA, Fan YY, Bradley AP, Middelberg APJ (2010) Far-infrared spectroscopy of protein higher-order structures. Appl Spectrosc 64(11):1259–1264. doi:10.1366/000370210793335025
59. Zhang F, Zhu X, Ding J, Qi Z, Wang M, Sun S, Bao J, Gao C (2014) Mechanism study of photocatalytic degradation of gaseous toluene on TiO2 with weak-bond adsorption analysis using in situ far infrared spectroscopy. Catal Lett 144(6):995–1000. doi:10.1007/s10562-014-1213-9
60. Withayachumnankul W, Fischer BM, Abbott D (2008) Numerical removal of water vapour effects from terahertz time-domain spectroscopy measurements. Proc R Soc A Math Phys 464(2097):2435–2456. doi:10.1098/rspa.2007.0294
61. Bernath PF (2002) The spectroscopy of water vapour: experiment, theory and applications. Phys Chem Chem Phys 4(9):1501–1509. doi:10.1039/b200372d
62. Eysel HH (1972) Hexamminmetall(III)-hexachlorochromate(III): Darstellung, Kristallgitter und Spektren. Z Anorg Allg Chem 390(2):210–216. doi:10.1002/zaac.19723900209
63. Fumino K, Fossog V, Stange P, Wittler K, Polet W, Hempelmann R, Ludwig R (2014) Ion pairing in protic ionic liquids probed by far-infrared spectroscopy: effects of solvent polarity and temperature. ChemPhysChem 15(12):2604–2609. doi:10.1002/cphc.201402205
64. Ricci RW, Ditzler MA, Nestor LP (1994) Discovering the Beer-Lambert law. J Chem Educ 71(11):983–985
65. Commoner B, Lipkin D (1949) The application of the Beer-Lambert law to optically anisotropic systems. Science 110(2845):41–43. doi:10.1126/science.110.2845.41-a
66. Avery JS, Burbridge CD, Goodgame DML (1968) Raman spectra of tetrahalo-anions of Fe^{III}, Mn^{II}, Fe^{II}, Cu^{II} and Zn^{II}. Spectrochim Acta A Mol Spectrosc 24(11):1726. doi:10.1016/0584-8539(68)80227-2
67. Landis CR, Weinhold F (2007) Valence and extra-valence orbitals in main group and transition metal bonding. J Comput Chem 28(1):198–203. doi:10.1002/jcc.20492
68. Schläfer HL, Gliemann G (1969) Basic principles of ligand field theory. Wiley Interscience, New York

Chapter 5
Base-Catalyzed Reactions in Biomass Conversion: Reaction Mechanisms and Catalyst Deactivation

Laura Faba, Eva Díaz, and Salvador Ordóñez

Abstract Although less studied than acid-catalyzed reactions, mainly because of their marginal interest in petrochemical processes, base-catalyzed reactions (either homogeneous or heterogeneous) play a key role in the upgrading of biomass-derived platform molecules. As in most of the chemical processes, the replacement of homogeneous catalysts by heterogeneous catalysts is of key interest. This article reviews the state of the art in the most important base-catalyzed reactions in the biofuel manufacture (biodiesel from triglycerides) and the upgrading of biomass-derived platform molecules (such as acetone, ethanol, furfural, 5-hydroxymethylfurfural, or acetic acid). Transesterification reactions, aldol condensation (alone or in combination with other reactions), and ketonization are the main reactions involved in these biorefinery processes. Reviewed are the most common catalysts proposed for these reactions (mainly heterogeneous), as well as the proposed mechanisms for these reactions, and the main factors governing catalyst deactivation when used in each of these reactions.

Keywords Base catalysis • Aldol condensation • Guerbet reaction • Ketonization • Decarboxylative condensation • Transesterification • Biodiesel • Reaction mechanism

5.1 Introduction

The conversion of renewable biomass feedstock into fuels and chemicals has emerged in the last years as the most promising opportunity to solve one of the most crucial environmental issues – global warming. At the same time, socioeconomic problems derived from the depletion of fossil fuels and the dependence on imported

L. Faba • E. Díaz • S. Ordóñez (✉)
Department of Chemical and Environmental Engineering, University of Oviedo, Julián Clavería s/n, 33006 Oviedo, Spain
e-mail: fabalaura@uniovi.es; diazfeva@uniovi.es; sordonez@uniovi.es

M. Schlaf, Z.C. Zhang (eds.), *Reaction Pathways and Mechanisms in Thermocatalytic Biomass Conversion I*, Green Chemistry and Sustainable Technology, DOI 10.1007/978-981-287-688-1_5

resources are also solved. Biomass can be transformed into a large variety of liquid fuels or fuel additives [1], being the only renewable feedstock with the internal capacity to be transformed into liquid energy carriers. This energy is essential for the transportation sector, accounting one-third of the global energy consumption [2]. Bioethanol and biodiesel have been the two first successful approaches to obtain liquid fuels from biomass (first-generation biofuels). Currently, they are industrially obtained from sugar fermentation and fatty acid transesterification, respectively. However, the specific nature of these fractions and competition with food industry have forced the development of alternative technologies that allow using the use of lignocellulosic biomass as raw material (second and third generation of biofuels). At the same time, as previous processes must be adapted to obtain same fuels from this feedstock, new technologies have to be developed to obtain alternative fuels or fuel additives. On the other hand, a large amount of chemicals presently consumed have a fossil origin. Consequently, the dependence on fossil resources can only be overcome if alternative processes are developed to obtain the same or substituting molecules from other feedstocks. Lignocellulose biomass is the most promising feedstock for this because more than 200 platform molecules can be obtained by the chemical transformation of this raw material [3].

Even if there are different thermochemical and biological processes (pyrolysis, gasification, fermentation, etc.), biomass conversion by catalytic processes plays a key role in this topic for several reasons, highlighting the possibility to develop a general process to obtain products selectively, both fuels and platform molecules. The development of catalytic technologies based on biomass requires important changes if compared to the traditional petrochemical industry. Petroleum and liquid fuels are chemically similar, and the required transformations are relatively simple processes, such as distillations, cracking, and isomerizations. These last reactions are usually catalyzed by acid materials, and most of them operate in the gas phase at high temperatures. On the other hand, the production of biofuels from biomass requires a different chemistry mainly focused on reactions to adjust the molecular weight and different oxygen removal steps. Most of these reactions are catalyzed by basic materials, and these catalysts have been much less studied until now. In addition, considering the properties of the raw material, these reactions are carried out in the liquid phase, so catalysts must be conditioned to avoid leaching problems.

The over-functionalization of lignocellulose biomass can be a disadvantage for its transformation into biofuels but is also a good opportunity to obtain a high flexibility for the production of a large variety of useful compounds by different reactions (polymerizations, hydrogenations, condensations, deoxygenations, etc.). Some of these reactions are new processes whereas others have been previously developed in organic chemistry but with more specific reactants. In this case, the high, and sometimes uncontrolled, reactivity of this feedstock implies an important issue, and the main challenge is now to design novel catalytic routes that allow controlling this reactivity in order to lead the synthesis to targeted chemicals with high yields.

Biomass-derived processes should follow the green chemistry principles, such as to use waste and by-products as raw materials, prevent the use of hazardous

compounds and minimize the energy consumption. The use of heterogeneous catalysts is a key point because of the several advantages versus the classical homogeneous catalysts; the direct separation of products and the catalyst allows saving energy in the recovery steps. Furthermore, the possibility of tuning the active properties of these materials makes it easier to obtain more active and selective materials, with a direct positive effect in the purification steps. However, the use of heterogeneous catalysts also has some disadvantages, such as a higher mechanism complexity, possible diffusional limitations and a high susceptibility to poisoning, coke deposition, and other deactivation mechanisms. The loss of activity is a common weak point in all these processes, and the implementation of these technologies on an industrial scale is conditioned by the development of selective and active materials.

The main base-catalyzed reactions in biomass conversion are discussed in this chapter (transesterification, condensation, and ketonization) with emphasis focused on the different reaction mechanisms proposed by the expert researchers. The discussion is mainly focused on processes catalyzed by heterogeneous materials, with special attention to the stability and the different deactivation causes identified as well as the possible solutions tagged in the literature.

5.2 Transesterification

Transesterification of fatty acids and vegetable oils with a short alcohol (usually methanol) is the most typical reaction to produce biodiesel. The general scheme of this reaction is summarized in Fig. 5.1.

This process can be catalyzed by acid or base materials, the latter ones being the most commonly used [4]. The equilibrium can be shifted by continuous removal of glycerine reaching almost complete triglyceride conversion when a pure fatty acid is used as the raw material. However, when lower-quality feedstock is used (waste oils), free fatty acids are present at levels ranging from 2 to 90 % [5]. These free fatty acids are obtained by hydrolysis at high temperatures during the primary uses

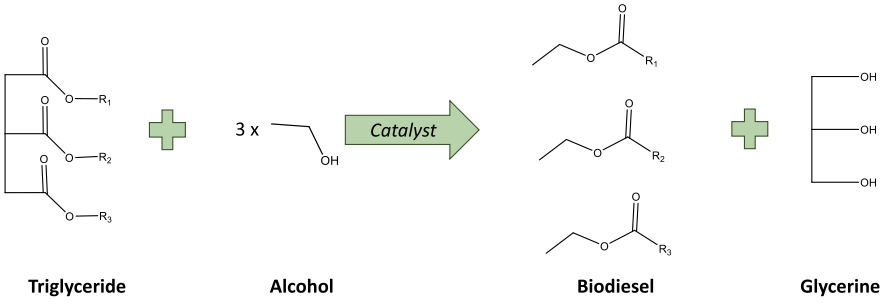

Fig. 5.1 General mechanism of the transesterification of fatty acids to obtain biodiesel

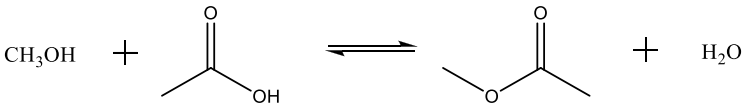

Fig. 5.2 Esterification of free fatty acids

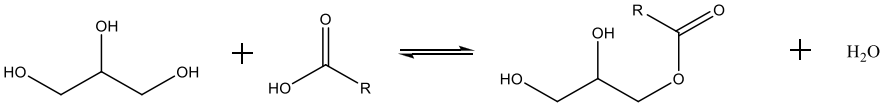

Fig. 5.3 Glycerolysis of free fatty acids

of these oils (cooking). Free fatty acids act as inhibitors of base catalysts. Under these conditions, a pretreatment of raw material is needed to remove these undesired compounds. Industrially, this pretreatment consist of an esterification with an acid catalyst starting with the protonation of the carbonyl oxygen of the free fatty acid, followed by a nucleophilic attack by the methanol oxygen on the partial positive charge of the carbonyl carbon atom in the protonated free fatty acid, followed by water elimination and finally deprotonation to yield the methyl ester (Fig. 5.2.) [6].

Another alternative is glycerolysis, i.e., the opposite reaction to transesterification that allows obtaining mono- and diglycerides in presence of zinc-based catalyst at temperatures above 200 °C and high pressures (Fig. 5.3). Once the free fatty acids are transformed, standard transesterification is carried out.

5.2.1 Transesterification Catalysts and Reaction Mechanisms

As previously indicated, this reaction can be both, acidic and basic, catalyzed. However, the basic catalysts are much more developed because they result in higher conversions at milder reaction conditions. The acidic reaction is a slower process that requires higher methanol concentrations. Reactions can be carried out even without any catalyst at temperatures higher than 240 °C and pressures above 78.5 bar [7]. Under basic conditions, when mixed with methanol, the base active site abstracts a proton from the alcohol to achieve equilibrium between the alcohol and the methoxide anion. This anion reacts with a fatty acid chain of the vegetable oil. The general reaction consists of a three-step nucleophilic attack on the carbonyl center by the methoxide anion, for the sequentially transesterification of each fatty acid from the glycerine backbone [8]:

$$\mathrm{TG} + \mathrm{MeOH} \leftrightarrow \mathrm{FAME} + \mathrm{DG} \tag{5.1}$$

$$\mathrm{DG} + \mathrm{MeOH} \leftrightarrow \mathrm{FAME} + \mathrm{MG} \tag{5.2}$$

$$\mathrm{MG} + \mathrm{MeOH} \leftrightarrow \mathrm{FAME} + \mathrm{G} \tag{5.3}$$

Where TG, DG, and MG identify triglyceride, diglyceride, and monoglyceride, respectively, methanol is labeled as MeOH, FAME indicates the fatty acid methyl ester or biodiesel, and G stands for glycerol.

Initially, this process was developed using homogeneous catalysts, mainly alkaline metal hydroxides such as KOH or NaOH. Reaction conditions were optimized using temperatures close to the boiling point of the alcohol and at molar ratios of alcohol/oil from 3:1 to 6:1 [9, 10]. The use of these catalysts, despite their high activity, has several drawbacks: they leave the process together with the glycerine in the polar product stream, increasing the costs of glycerine purification and making catalyst recycling very difficult. In some cases, homogeneous catalysts can be neutralized and removed as precipitated salts, but in other cases, catalysts form soaps with free fatty acids. Most of these drawbacks can be solved by using heterogeneous catalysts.

There are a large number of heterogeneous catalysts proposed for this process. Concerning the basic materials used, they are mainly divalent metal oxides with a substantial amount of covalent character, such as alkali metal oxides, alkaline earth metal oxides, transition metal oxides, and mixed metal oxides. Specific studies and results with these materials will be detailed below, but a common mechanism is accepted for all cases. This mechanism is summarized in Fig. 5.4. Active sites are associated to the pair M–O (where M is the metal) and its basicity. The key reaction step is the abstraction of H^+ from methanol to produce the anionic intermediate. It is accepted that this abstraction can be catalyzed by a Lewis or a Brønsted basic site, justifying the large variety of active metals proposed for this reaction [11]. In general, the higher the basicity of the M–O pair, the higher the abstraction capacity. The carbonyl group of the fatty acid is then attacked by the methoxide obtaining the FAME product.

Basic oxides of alkaline earth metals such as Mg, Be, Ca, and Sr are used by different researchers, obtaining good results [13–15]. There are several references about the activity of MgO, tested in different reaction conditions: from room temperature in batch configurations, needing longer times but with the economic advantage of working at these conditions [16], to supercritical conditions at 300 °C, obtaining more than 90 % of biodiesel in a very short time [17]. However, the most

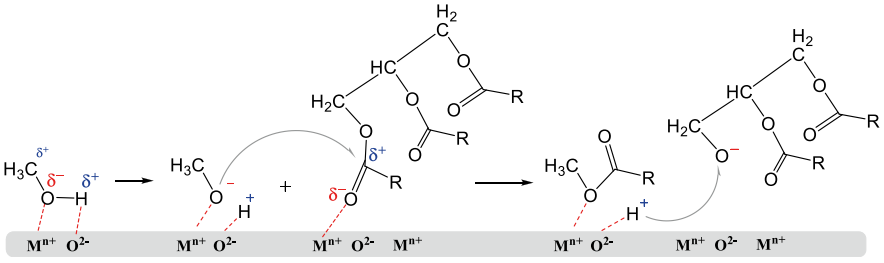

Fig. 5.4 General mechanism of transesterification catalyzed by solid basic materials (Reproduced from Manríquez-Ramírez et al. [12] by Manríquez-Ramírez, Copyright 2013, with permission from Elsevier)

widely used catalyst is CaO, with conversions higher than 90 %, relating its higher selectivity to its higher basicity [18]. This material shows good properties as a catalyst, highlighting its high basicity, low solubility in methanol, and low price. In a special effort to develop environment-friendly processes, CaO catalysts have been successfully obtained by thermal treatment of different waste materials, such as eggshell, mollusk shell, and bones, obtaining good activity at mild temperatures in less than 2 h [19, 20]. The reaction mechanism catalyzed by CaO was studied in detail [21, 22], identifying lack of stability as its main weakness, because of leaching and poisoning problems [21]. Stability limitations were also observed with other oxides, such as SrO or ZnO, catalysts that show good activity and have generated high interest in the last years [23–25]. Different procedures were tested to increase the activity and stability of these oxides: the synthesis modified by organometallic precursors [26], thermal activation treatments [27], and transesterification under ultrasonic conditions [28]. Stability was considerably improved, and their deactivation is negligible after 10 cycles [29], but these results are not enough for them to be considered good industrial catalysts. Deactivation causes are considered in more detail below.

Transition metal oxides, such as ZnO, ZrO_2, CuO, and TiO_2, also exhibit a good activity in this reaction, working under relatively mild conditions (low temperature and room pressure) with short reaction times [30, 31]. In most of these studies, ZnO is reported as the best alternative, obtaining almost complete conversion after 10 min [29]. Recently, studies focused on the development of active mixed metal oxides with at least two oxides in order to obtain a material with higher basicity, specific surface area, and pore volume. In this field, materials such as bentonite, kaolinite, CaO–CeO_2, and hydrotalcites have a promising future [32].

5.2.2 Transesterification Catalyst Deactivation

Despite the intense efforts to develop active heterogeneous catalysts, most of them present stability problems. In contrast to solid acid materials, the deactivation of basic catalysts has not yet been studied in detail, and there are few references on this topic. Concerning transesterification, there is no agreement about the main reasons for this loss of activity. Some papers indicate the leaching of the active phase into the oils and solvents involved in the reaction as the main cause [33, 34]. This leaching is more important at high conversions because these catalysts only present relevant solubility in water, but not in oil solvent [34]. Other researchers suggest that deactivation is mainly due to the strong adsorption of free fatty acids on the surface, and its subsequent reaction obtaining calcium soap [35]. Almerindo et al. [36] suggested that this poisoning is mainly related to the presence of hydrogen carbonate sites on the surface. Consequently, this deactivation can be prevented just by storing the catalyst under very dry air. Finally, other authors suggest that materials can suffer from sintering, decreasing the concentration of active sites on the surface, with an important effect on the activity [34, 36–38]. This process is mainly observed for

mixed oxides because high temperatures can favor the layered structure, with partial loss of activity [38]. The use of ultrasonication reactors has been proposed as an opportunity to prevent this deactivation [37].

Mouzu et al. [34] indicates in a review about transesterification catalyzed by CaO that all these deactivation pathways can coexist when CaO is used and propose working at milder temperatures, under sonication and with a prior acidic catalyzed step for free fatty acid esterification to avoid the deposition and catalyst deactivation.

5.3 Aldol Condensation

Aldol condensation is one of the most common reactions to form carbon–carbon bonds between two carbonylic compounds using a basic catalyst. This process, with its different variations, is an important starting point for several organic syntheses using different catalysts and reaction conditions. The general mechanism of this reaction involves the nucleophilic addition of a ketone enolate to an aldehyde to form a β-hydroxy ketone or aldol, as it is summarized in Fig. 5.5.

The high variability of this reaction makes it a good option to synthesize valuable compounds from different aldehydes, such as butanal [39, 40] or heptanal [41], amides, [42] and more complex compounds, e.g., the condensation of citral and acetone [43, 44]. However, this reaction has gained attention in the last years because of the development of new technologies to obtain chemicals and liquid fuels from biomass. Aldol condensation is the key step for valorization of different bio-platform molecules, such as acetone, ethanol, furfural, and 5-hydroxymethylfurfural (HMF). Considering the main aim of this chapter, the study of this reaction will be focused on the valorization of these compounds.

Acetone is maybe the most representative bio-platform that can be valorized by the aldol self-condensation obtaining different solvents, food additives, drugs, and fine chemicals. In this case, the role of the catalyst and the reaction conditions are critical in order to lead to the target compounds. Another important bio-platform molecule is ethanol. The production of this compound is increasing whereas its use as liquid biofuel is limited by the blend wall. Consequently, ethanol is considered as one of the cheapest, most abundant, and highest potential chemical product in biorefinery schemes. There are different alternatives to the chemical transformation of ethanol, condensation being one of the most promising ones.

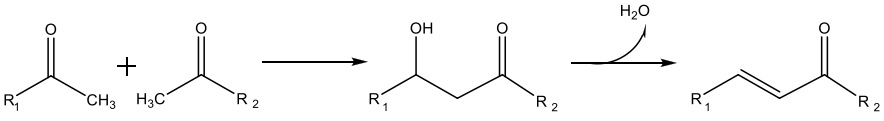

Fig. 5.5 General mechanism of aldol condensation

This reaction is also a good opportunity for the valorization of biomass into biofuels with similar properties as the mineral diesel. Biomass C5 and C6 sugars obtained from cellulose, hemicellulose, and starch fraction can be dehydrated yielding furan compounds (HMF and furfural). The direct hydrogenation of these derivatives results into very low-quality fuels because monomers of carbohydrate fraction have not enough length and their energy density is directly dependent on the number of carbons (diesel fraction corresponds from C8 to C15). Different alternative approaches have been proposed to solve this point, condensation being the most promising one. In fact, this reaction is the key stage in the aqueous-phase catalytic processing of biomass derivatives to biofuel obtaining, initially proposed by Dumesic and co-workers in 2005 [45].

Considering their particular mechanisms, catalysts, and optimum reaction conditions, the study of each process is presented independently.

5.3.1 Acetone Self-Condensation

Acetone is a very important compound in the organic chemistry because of its high reactivity. Chemically, acetone is the simplest ketone, and it is used as a common building block to obtain several plastics, paints, solvents, drugs, and other chemical intermediates. Currently, more than 90 % is industrially obtained directly or indirectly from the propylene by the cumene process [46]. However, acetone can be also obtained by a green process together with ethanol and butanol in the reaction known as ABE sugar fermentation [47] and as secondary product in biomass pyrolysis [48]. Acetone can be transformed into a large variety of valuable compounds by aldol condensation using one or two of its α-protons.

Catalytic self-condensation of acetone is a very complex reaction, and numerous products are possible via competitive self-condensation and cross-condensation between the same or different ketones that are formed in the reaction. The primary product of the reaction is diacetone alcohol that can be dehydrated obtaining mesityl oxide. Diacetone alcohol can be used in some paints, but the industrial value of mesityl oxide as intermediate to obtain methyl isobutyl ketone (MIBK) is much higher. These compounds can react again with the acetone, obtaining linear and cyclic compounds, such as phorones, isophorones, and mesitylene. These compounds are relevant in many different industries, with good properties as solvents and industrial building blocks to obtain plastics, polymers, adhesives, rubber and waxes [49, 50].

Even though aldol condensations can be catalyzed by acid or basic materials, the acetone self-condensation was mainly studied by using basic materials, with only few references on this reaction under acidic conditions [51, 52]. There is no complete agreement about the reaction network, but a generalized mechanism is summarized in Fig. 5.6.

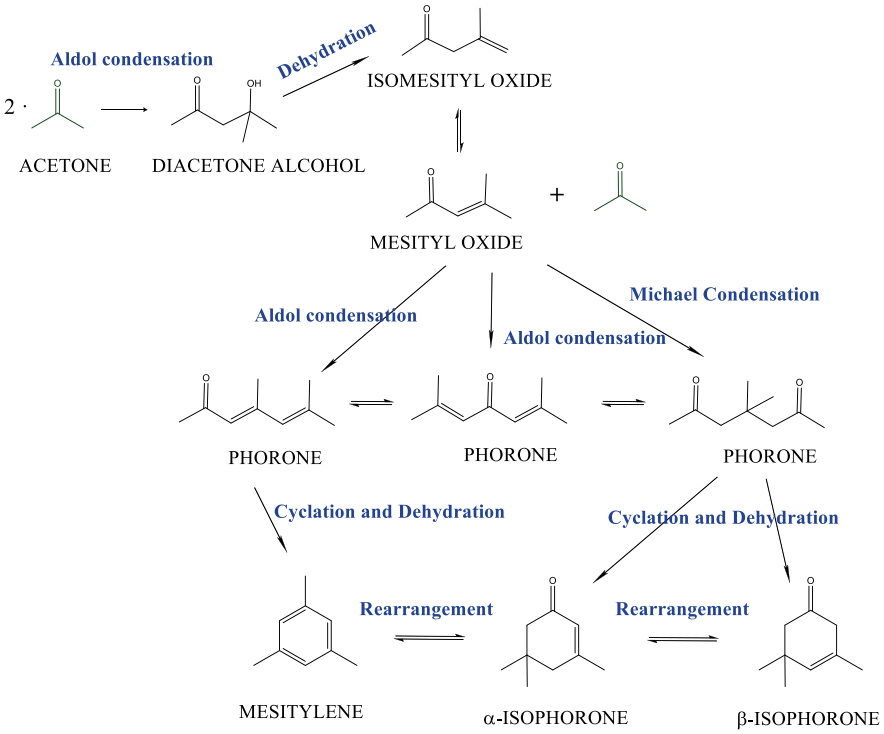

Fig. 5.6 Acetone self-condensation general network (Adapted from Ordóñez et al. [53] by Faba et al. with permission from Elsevier)

5.3.1.1 Acetone Self-Condensation Catalysts and Reaction Mechanism

When the reaction is carried out in the liquid phase, main products are the diacetone alcohol (DAA) and mesityl oxide (MO). Carrying out the reaction at higher temperatures in gas phase, the amount of chemicals obtained increases, and the role of the catalyst increases, conditioning the selectivity to phorones, isophorones, and mesitylene, as well as the relevance of side reactions of trimer polymerizations. Considering the different reaction conditions for each case, liquid-phase and gas-phase acetone self-condensation will be analyzed independently.

Acetone Self-Condensation in the Liquid Phase

The acetone self-condensation in the liquid phase catalyzed by homogeneous alkaline bases like NaOH or KOH is the industrial process to produce the diacetone alcohol (DAA). Considering the equilibrium between the acetone and the DAA, a maximum of 23 % is obtained at 0 °C, and the yield decreases further as the temperature increases [54]. The use of these homogeneous catalysts brings large waste

streams and promotes the corrosion of the installations. Consequently, the substitution by heterogeneous materials is compulsory in order to improve the process.

During the last years of the twentieth century, different heterogeneous materials were tested. Prodebarac et al. [55] focused their efforts on developing active anion-exchange resins with high selectivity to diacetone alcohol, trying to prevent mesityl oxide formation by adding water and using pore diffusion control. The role of H_2O in the diacetone alcohol and mesityl equilibrium was studied in detail using Mg–Al layered double hydroxides (LDH), identifying the formation of strong Brønsted basic sites (-OH) as the responsible site for diacetone alcohol formation [56]. Other researchers tried to optimize the behavior of different alkaline metal oxides, such as MgO, BaO, SrO, CaO, and La_2O_3 [57]. Good initial activity was obtained with these basic materials, but the evolution of selectivity at increased reaction times was plagued by two problems: the important leaching of the active phase (mainly in the case of MgO, that it is not stable in aqueous phase) and the high selectivity to mesityl oxide. In this study, the dehydration of diacetone alcohol was attributed to the presence of acid–base pairs. This hypothesis was corroborated studying the effect of different adsorbents: an increase of activity was observed under ammonia atmosphere and an almost complete inhibition when carbon dioxide is pre-adsorbed [57].

Concerning the reaction mechanism and kinetics of this reaction, almost all the studies confirm that acetone condensation proceeds faster over Brønsted basic sites compared with the Lewis ones, the equilibrium between diacetone alcohol and acetone being more displaced to the diacetone compound. On the other hand, mesityl oxide is obtained by alcohol dehydration, requiring acid sites to catalyze this step. Consequently, mesityl oxide is favored by solid catalysts with acid–base pairs, whereas diacetone alcohol is mainly obtained in the absence of acid sites. This hypothesis was confirmed with different catalysts, such as oxides [57], Mg–Al hydrotalcites [58], or hydrotalcites modified with rare earth elements such as La, Y, and Ce [59]. This mechanism is summarized in Fig. 5.7.

According to this model, the acetone self-condensation proceeds via a first initial activation step by H^+ abstraction at the α-position of carbonyl group of the acetone molecule. The second step consists of the aldol formation by reaction of the carbanion formed in the initial activation step with the carbonyl group of another acetone molecule to form the corresponding larger carbanion. Each step of this mechanism was corroborated by infrared spectroscopy and computational density functional theory (DFT) studies [60]. Despite the agreement in the mechanism, there is no good agreement concerning the kinetic model, with two main alternatives being suggested: Firstly, considering a reversible reaction of second order with respect to acetone and first order with respect to diacetone alcohol, being congruent with the reaction stoichiometry (Eq. 5.4) [55, 59]. Secondly, a first-order model considering that the diacetone alcohol reaction rate is controlled only by the enolate formation (Eq. 5.5) [61].

$$\frac{\mathrm{d}[\mathrm{DAA}]}{\mathrm{d}t} = k_1 \bullet [\mathrm{Ace}]^2 - k_2 \bullet [\mathrm{DAA}] \tag{5.4}$$

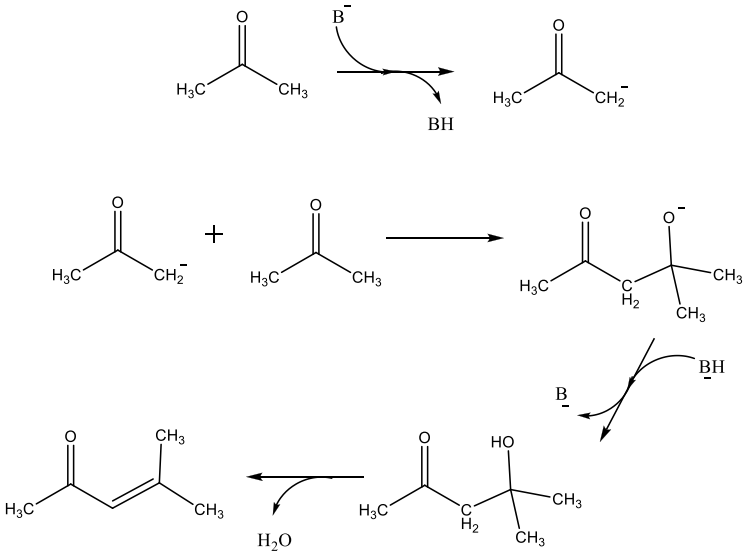

Fig. 5.7 Most accepted reaction mechanism of acetone self-condensation in liquid phase

$$\frac{\mathrm{d}[\mathrm{DAA}]}{\mathrm{d}t} = k_1 \bullet [\mathrm{Ace}] - k_2 \bullet [\mathrm{DAA}] \tag{5.5}$$

These two models consider the chemical reaction as the kinetic controlling step. However, other researchers also consider the other processes that involve a heterogeneous reaction: the transport of reactants to the reaction interface, including external diffusion and internal diffusion, the adsorption of reactants, the interface chemical reaction, the desorption of the product, and the transport of product away from the reaction interface. Considering all these processes, there are several kinetic models proposed, obtaining better results with one-dimensional diffusion models, i.e. the diffusion of acetone to or diacetone alcohol from the surface of the catalysts is the slowest step [62]. According to this model, an effective solid–liquid mass transfer rate is needed for avoiding the decomposition of diacetone alcohol into acetone and mesityl oxide [63].

Acetone Self-Condensation in Gas Phase

Acetone self-condensation in gas phase results in the formation of a large of number of valuable compounds by a complex reaction cascade which involves different condensation between mesityl oxide itself or with the acetone. Compounds such as isophorone and mesitylene, with many industrial applications, are obtained by these processes. The first examples of using heterogeneous catalysts for this reaction were reported by Apesteguía and co-workers, using MgO promoted with different alkali

or alkaline earth metal ions [64]. The promoter addition increases the activity of MgO because it increases the basicity. The highest selectivity to isophorone is obtained with Li/MgO working at 300 °C, reaching selectivities close to 40 %. In any case, mesityl oxide is always the main product, even at higher temperatures. The main drawback of this catalyst is the low acetone conversion despite the high temperatures. Subsequent studies tried to improve the activity by different activation procedures, combining different precursors, hydration, and thermal treatments [65]. The best results were obtained when periclase (MgO) was firstly hydrated to brucite ($Mg(OH)_2$) and secondly thermal treated to obtain a periclase phase (MgO) with a higher surface area and a better basicity distribution. Acetone conversion reached values up to 37 % at 500 °C, with selectivities of 32.8 and 20.7 % to isophorone and mesitylene, respectively.

As in the case of the reaction in the liquid phase, different mixed oxides are proposed giving good activity over a large range of temperatures. Examples are the studies on MgZr and MgAl mixed oxides [53, 65–68]. These two mixed oxides have a good balance between medium-strength basicity and weak acidity, promoting both, condensations and different dehydrations and rearrangements that imply acidity, with a positive effect in the isophorone and mesitylene selectivities. Isophorone selectivity was enhanced working at medium temperatures when MgAl is used as the catalyst, reaching more than 22 % at 500 °C [67]. The conversion increases when MgZr was used (with maximum of 33.5 % at 500 °C working at same conditions), with a global 39 % selectivity of the trimer family [66]. These better results suggest the use of MgZr to design a more active catalyst by supporting this active phase on different microporous and mesoporous materials, such as active carbons (AC) and high surface area graphites (HSAG) with different morphologies [66]. The conversion reached values of 54.3 % with a C9 selectivity of almost 50 % with MgZr/HSAG500, whereas worse results were obtained when microporous supports were used (because of diffusion limitations). The selectivity toward mesitylene is increased by tuning the basicity of properties using peroxo-routes for the synthesis of MgZr [68].

On the other hand, the desired basicity was also observed with other heterogeneous materials, and their activity in this reaction has been also reported in the last years. A good example is TiO_2, whose acid–base character can be tuned by preparing the titania doped with lithium or rubidium by the solgel method [69]. With the latter, mesitylene selectivity can reach almost 40 % at 300 °C. This selectivity can be close to 50 % when alkaline metals are used to dope the TiO_2, with 60 % of acetone conversion [70, 71].

As a general conclusion from all these studies, there is no doubt about the key role of the basicity in this reaction. Experimentally, this fact was corroborated observing an almost complete suppression of activity by co-feeding acetic acid with the acetone but being almost unaffected by presence of pyridine in the feed [64]. Figures 5.8, 5.9, and 5.10 illustrate the mechanism of different steps involved in the acetone gas-phase self-condensation.

The first step of the process is common to reactions in liquid and gas phase; medium-strength basic sites are needed to abstract the α-proton of acetone to obtain

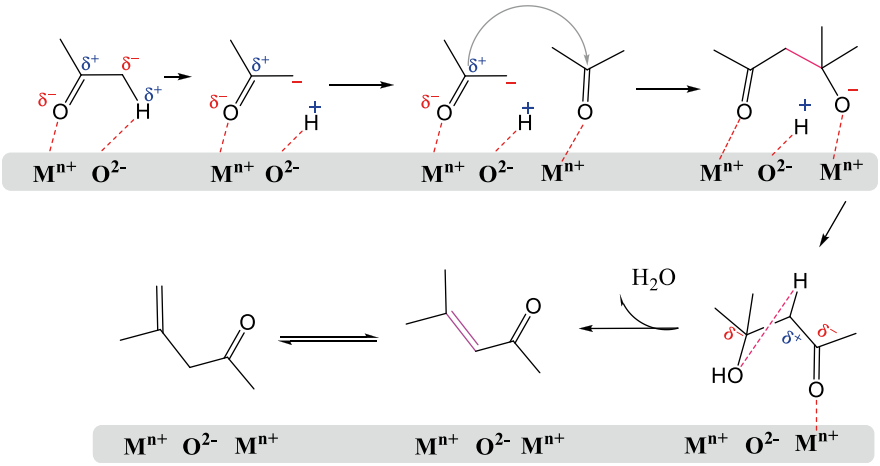

Fig. 5.8 Reaction mechanism for the acetone self-condensation: diacetone alcohol and mesityl oxide formation (Figure reproduced from [66] by Faba et al. with permission of Elsevier)

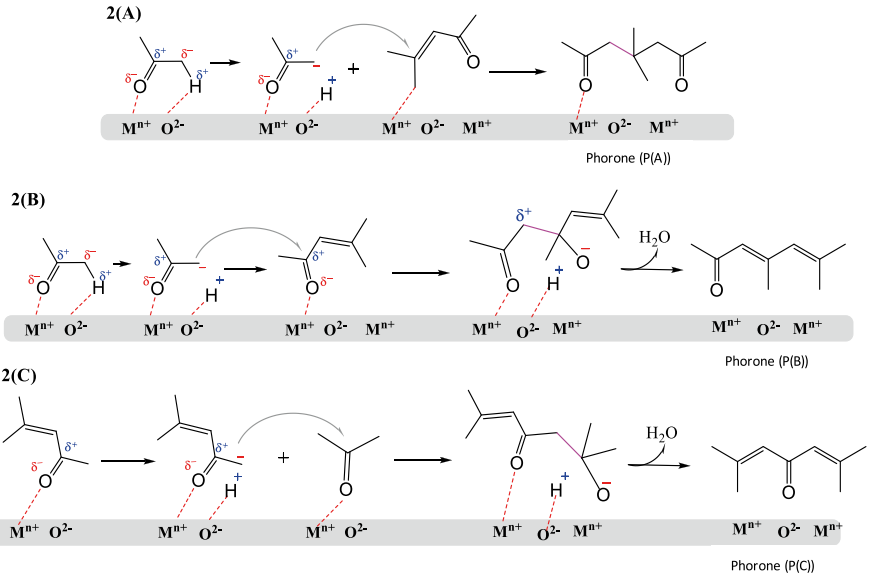

Fig. 5.9 Reaction mechanism for the second step in the gas-phase acetone condensation: linear trimmers formation by Michael addition (**2A**) or aldol condensation (**2B** and **2C**) (Figure reproduced from [66] by Faba et al. with permission of Elsevier)

the enolate that reacts with the second molecule of acetone. Diacetone alcohol is dehydrated when weak acid sites are present, giving mesityl oxide. According to this mechanism, diacetone alcohol cannot condense because it does not have any α-proton. On the contrary, mesityl oxide can react again with another acetone mol-

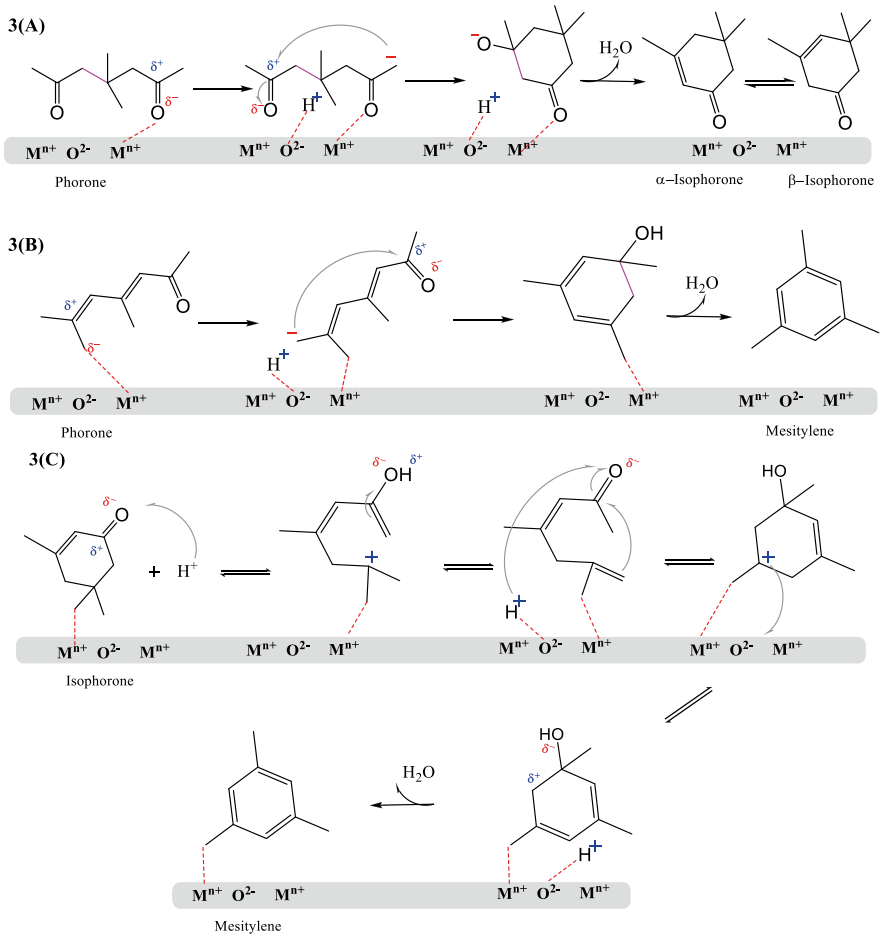

Fig. 5.10 Reaction mechanism for the third step in the gas-phase acetone self-condensation: cyclations of phorones, obtaining isophorones (**3A**) and mesitylene (**3B**). Isophorone rearrangement to mesitylene (**3C**) (Figure reproduced from [66] by Faba et al. with permission of Elsevier)

ecule if the temperature is enough to favor the abstraction of its α-proton (less acidic than the acetone one). Concerning phorone formation, three different possibilities are identified and detailed in Fig. 5.9. If mesityl oxide is adsorbed on monodentate sites (strongest) and enolate is formed by the acetone previously adsorbed on bidentate sites (medium strength), linear phorones are obtained by a Michael addition mechanism (2A). On the other hand, if mesityl oxide is also adsorbed on bidentate sites, enolate can be formed from both molecules, with two subsequent different aldol condensations (2B and 2C). These mechanisms were identified in previous studies using different oxide catalysts [51, 72]. Finally, two different possibilities of phorone cyclizations have been identified (Fig. 5.10). The intramolecular aldol condensation of the phorone isomer with two carbonyl groups, obtaining the isopho-

rones, is the most evident one. This reaction requires strong basic sites. The other possibility allows the formation of mesitylene by Michael addition reactions from phorone. The subsequent dehydrations are favored by the equilibrium in the acid–base pair.

The most controversial step is the equilibrium between isophorones and mesitylene. According to this mechanism, when the catalyst presents weak acid sites, mesitylene can also be formed from isophorones by dehydration (3C). This fact was also observed by other studies [71, 73], whereas other results do not identify this isomerization [69].

According to this mechanism, the reaction is limited by the ability to abstract the α-proton from the enolate of one of the reagents. Consequently, the kinetic rate only depends on one of the two molecules involved in each step of the reaction, and the expression of the kinetic rate has a first-order dependence, for both the direct and indirect reactions [61]. This model is opposite to the previous hypothesis of second-order models (stoichiometric relation) previously proposed [55, 59].

5.3.1.2 Acetone Self-Condensation Catalyst Deactivation

As previously mentioned, the use of solid bases has an important drawback because of their fast deactivation [74]. Despite the important efforts on developing active and selective solid catalysts to substitute the use of sodium hydroxide as the industrial catalyst for the acetone self-condensation, there are very few references on the studies of stability. First investigations of this problem date from 20 years ago, identifying possible deactivation causes but without the technology needed to conduct deeper studies. Thus, some authors suggest the blockage by coke deposition as the main reason [74–76], but others indicate a high influence of strong adsorption of water and -OH groups on the catalytic surface [77] and morphological changes that affect the distribution and strength of active sites [78]. After these first studies, there were no new references until the last few years, in which the petroleum depletion and the climate change have given impulse to study these processes again. Consequently, this problem is still not solved, and acetone self-condensation catalyzed by heterogeneous materials has not yet been implemented on an industrial scale.

Hydrotalcites undergo rapid deactivation even working in liquid phase, when oligomerizations are not relevant; a loss of more than 50 % of activity was observed in less than 1 h of continuous reaction [79]. A rapid deactivation is also observed when the active phase is supported on carbonaceous materials, with less than 15 % of conversion in second cycles [80]. Deactivation affects both the rate of reaction and the product selectivities, particularly at low values of time on stream [81]. Despite the relevance of this phenomenon, there is no good agreement on the reasons for and the mechanisms of deactivation. The most cited cause is coke formation and its subsequent deposition blocking the active sites [74–76]. This deactivation takes place on both basic and acidic sites, being more important with strong basic sites [74]. On the other hand, some authors indicate that the formation of water

during the reaction can justify the inactivity of basic sites, because deactivation is also observed at temperatures that are not high enough for coke formation [77]. This hypothesis suggests a reversible deactivation that can be preventing with simultaneous removal (adsorption on catalytic supports) of this water during the course of the reaction. An important role of morphological changes on the catalytic surface was also proposed; highlighting that the amount of -OH on the surface can modify the activity [78].

5.3.2 Alcohol Condensation: Guerbet Reaction

Alcohol coupling, also known as the Guerbet reaction, is a potentially important process to increase the value of short-chain alcohols. This reaction was previously developed by Marcel Guerbet, in the 1890s, for the study of the self-condensation of 1-butanol [82]. Today this reaction is applied to different self- and cross-condensations of different alcohols with more than one carbon atom (ethanol, propanol, butanol, etc.), for obtaining long-chain alcohols, mainly used as surfactants [83]. The Guerbet reaction involves a complex sequence of many different reactions (dehydrogenation, aldolization, dehydration, and hydrogenation), which makes the detailed study of its mechanism difficult. The general scheme of the mechanism is illustrated in Fig. 5.11.

Alcohol condensations have attracted high interest in the last few years because of both environmental concerns and the new economic opportunities seen in bio-based feedstock. In this context, main interest is focused on the ethanol condensation. Ethanol is one of the most important bio-platform molecules. It has many applications as biofuel, solvent, and as a starting material to produce different added-value chemicals [83]. Ethanol condensation takes place mainly in gas phase under basic conditions, and different compounds are simultaneously obtained, including acetaldehyde, ethylene, butadiene, butanol, and crotonaldehyde. Most of these compounds have high industrial value. 1-Butanol is of particular interest as a crucial building block for acrylic acid and acrylic esters and is widely used as solvent and additive to gasoline [84]. Butadiene is considered as the most important conjugated diene, being the raw material of a wide variety of synthetic rubbers and elastomer and polymer resins [85]. In order to obtain these compounds, ethanol must react by different mechanisms involved in the ethanol condensation in gas phase. The mechanism of this process is discussed in detail in the next sections, but the general network is illustrated in Fig. 5.12. Considering the different reactions, the selected catalyst and reaction conditions play a key role in the results.

5.3.2.1 Ethanol Condensation Catalysts and Reaction Mechanism

Different basic oxide catalysts have been tested for this reaction. In particular, MgO appears to be the standard material used in these reactions [87–89]. According to the results obtained, temperatures higher than 300 °C are needed to observe ethanol

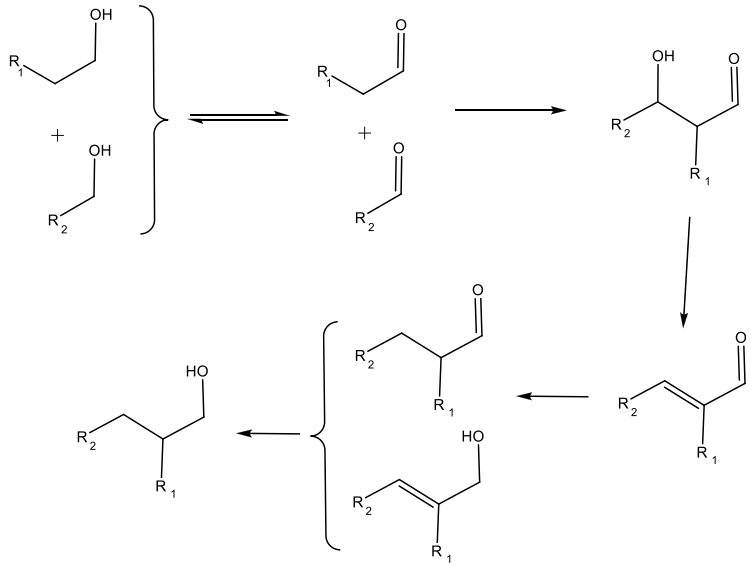

Fig. 5.11 General mechanism of Guerbet reaction

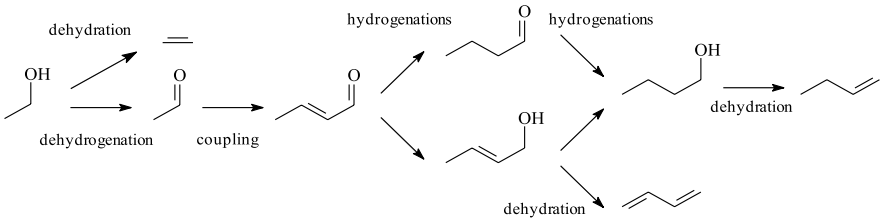

Fig. 5.12 Overall mechanism for ethanol condensation (Figure reproduced from [86] by León et al. with permission of Elsevier)

conversion, but only acetaldehyde can be observed at temperatures under 400 °C. The strong adsorption of ethanol on the MgO surface as well as the negligible concentration of products at lower temperatures was corroborated by DRIFT studies [90] and by using isotope transient analysis [89]. As general conclusions, it must be highlighted that higher temperatures increase the coupling rate as well as the hydrogenation and dehydration rates. On the other hand, the evolution of the aldehyde concentration suggests that, under basic conditions, most of the Guerbet reaction products are formed from a gas-phase aldehyde intermediate.

Many different promoters have been added to MgO to enhance its activity and selectivity to butan-1-ol, with the most promising results being obtained using alkali metals, such as Li, Na, K, and Cs [91, 92]. The addition of the alkali metal salt increases the basicity of the catalyst, increasing the selectivity to the dehydrogenated product, but without increasing the rate of the coupling step. Another approach to increase the activity of MgO is by preparing mixed oxides, in which Al incorpo-

rates Lewis acid sites. The activity of MgAl mixed oxide was studied by different researchers [53, 84, 88, 93], investigating the effect of Mg/Al ratio, the catalyst preparation method, and reaction temperature. As Al content increases, the rate of dehydration increases, because of the high acid site density (e.g., at 50 % ethanol conversion, selectivity to butan-1,3-diene reaches values of 12 %) [53]. This dehydration is more important as the temperature increases [53]. The key role of basic sites in this reaction, especially the strongest ones, was corroborated analyzing the influence of different preparation procedures (different distribution of these sites) and the catalytic activity [86].

As was explained above, the ethanol condensation involves a complex set of reactions involving both acid and basic sites. Consequently, an amphoteric catalyst can be a good alternative to MgO and MgAl mixed oxides. Zirconia (ZrO_2) is considered as an amphoteric oxide with both acid and basic sites on its surface. Lower values of ethanol conversion were obtained, and, due to this acidity, zirconia catalyzes the dehydration of ethanol preferentially over the dehydrogenation reaction, which is required for the coupling reaction [94, 95]. With the aim of modifying the acid–base character of zirconia, different amounts of Na were added. This promoter does not affect the ethanol conversion but has an important effect on the dehydration/dehydrogenation ratio. Considering the good properties of MgO and ZrO_2, MgZr mixed oxides were also suggested for ethanol coupling [90]. The activity of this mixed oxide is strongly influenced by the preparation method, in such a way that those prepared in strong basic medium present a lower rate of ethanol dehydration compared with those prepared by the rising pH precipitation method.

Another bifunctional material (with acid and base sites) used in the coupling of ethanol is the hydroxyapatite, $Ca_5(PO_4)_3OH$. Good results were reported by Ogo et al. [96, 97] and Tsuchida et al. [87], with the catalyst being more selective to dehydrogenation than other mixed oxides and obtaining a coupling rate 50 times higher than the rate obtained with MgAl. As in the case of MgZr and MgAl, results are strongly dependent on the composition of the catalyst, in such a way that best results were obtained with the stoichiometric ratio (Ca/P = 1.67). These results are congruent with the decrease in acidity at the Ca content increase.

There is no complete agreement about the reaction path of alcohol condensation, but the generally accepted mechanism consists of a sequence of different stages. The first step in the ethanol coupling reaction is the dehydrogenation of the ethanol to produce the acetaldehyde. Since the aldol condensation occurs between two carbonyl-containing molecules, both ethanol molecules must be dehydrogenated. The state of free hydrogen obtained is not clear and it depends on the catalyst. If the catalyst includes a transition metal, hydrogen can be released from the surface and coexist in the gas phase with the aldehyde in equilibrium with the alcohol. If the catalyst has an active metal (Pd, Pt, Rh, etc.), hydrogen can be chemisorbed [98]. If the catalyst is a mixed oxide, its behavior is not clear; hydrogen can remain adsorbed on the surface [87], it can desorb to gas phase, or it can be coupled to a hydrogenation step by the Meerwin–Ponndorf–Verley (MPV) reaction [99].

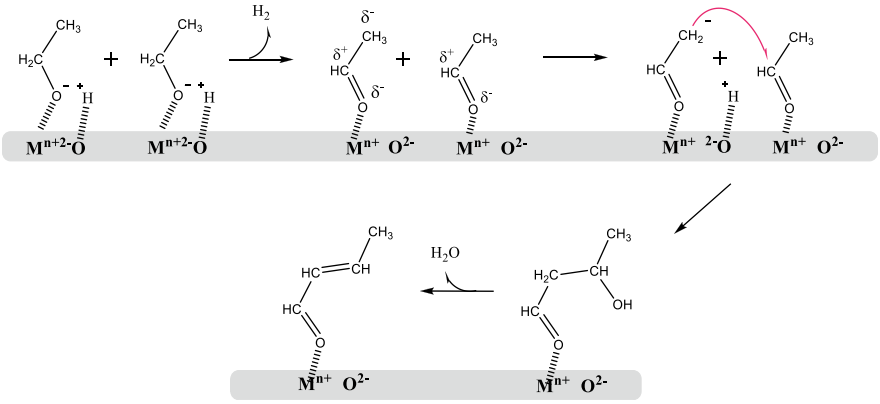

Fig. 5.13 Detailed mechanism of 2-butenal formation from ethanol condensation over a basic catalyst (Figure reproduced from [86] by León et al. with permission of Elsevier)

The main step of this process is the aldol condensation between two acetaldehyde molecules. The mechanism of this reaction was previously detailed and consists in the formation of a C-C bond between the α-carbon of one molecule and the carbonyl carbon of the another, being the abstraction of the α-proton the key step (with a key role of basic sites). As a consequence of this condensation, 3-hydroxybutanal is obtained. However, this intermediate is generally not observed because it is unstable and it is fast dehydrogenated over acid–base pairs, giving 2-butenal. This mechanism is illustrated in Fig. 5.13.

If the temperature is high enough, 2-butenal can react with hydrogen (obtained from an external source or the internal hydrogen released in the first step), yielding either butanal (hydrogenation of the double bond) or 2-buten-1-ol (hydrogenation of the carbonyl group). These compounds can also undergo second hydrogenations, giving 1-butanol. The presence of this alcohol even without any active metal and external hydrogen source is only justified by the Lebedev reaction [87, 88]. In parallel to this reaction, some authors observe the presence of different olefins, such as ethylene, 1-butene, and 1,3-butadiene. The existence of these compounds is explained by dehydration of ethanol, 1-butanol, and 2-buten-1-ol, respectively, and it is related to the presence of acid–base pairs in mixed oxides [86].

Different alternatives to this general mechanism consider the possibility of a coupling step without obtaining two molecules of acetaldehyde. Yang and Mend [100] and Ndou et al. [101] suggest that Guerbet reaction involves a direct surface coupling between the α-carbon of an aldehyde and one alcohol or even by a direct nucleophilic attack between two alcohols. However, the presence of C4 hydroxylic derivatives with the alcohol function in terminal position is incongruent with this mechanism.

Despite these mechanistic studies, data on the kinetics of the reaction to support these mechanistic studies are lacking, and they are required for a better understanding and for optimization of the process conditions.

5.3.2.2 Ethanol Condensation Catalyst Deactivation

There are no specific studies on the catalyst stability in the ethanol condensation. Most of the papers about this process indicate that the influence of deactivation is almost negligible during the time of the reported experiments [85, 86, 102]. However, there is an extensive list of side products that are obtained because of uncontrolled reactions at these temperatures [85]. This list includes hydrocarbons and oxygenated compounds such as aldehydes, ketones, alcohols, ethers, and esters. More attention should be paid to all by-products that are formed because they can produce oligomers and coke precursors that strongly affect to the catalytic stability. The presence of these oligomers is detected by TPO analyses of spent catalysts, corroborating this hypothesis [103]. Other reason suggested in the literature is the sintering and different morphological changes that the mixed oxides can undergo at reaction temperatures. The formation of more ordered structures strongly affect the amount of active sites exposed on the surface, obtaining a high decrease in catalytic activity [85]. The role of water molecules as deactivation agents by adsorption on the active sites was studied by Carlini and co-workers, without observing appreciable deactivation by this cause [102].

5.3.3 Condensation of Cellulose-Derived Aldehydes

Despite the self-condensation of acetone or ethanol, this reaction can be also useful to obtain liquid fuels with similar properties to petroleum diesel. In order to obtain this biofuel, it is needed to obtain linear hydrocarbons in the range C8–C15. This range cannot be obtained by the self-condensation of small molecules, but biomass can be transformed into the needed intermediates: the aldehydes. Dehydration of sugar carbohydrates leads to the formation of aldehydes such as furfural and hydroxymethylfurfural (HMF) [104]. These compounds are essential intermediates in biorefineries for production of liquid alkanes with fuel properties, and the study of their upgrading is a key of interest in the last years [45, 105].

As was previously introduced, these compounds are not long enough to be directly transformed into high-quality fuels, and their valorization requires aldol condensation as a key step followed by a complete hydrodeoxygenation [106]. The furanic aldehydes cannot undergo self-condensation because they do not have any α-proton. Consequently, they need to react with other molecules, generally acetone, glyceraldehyde, propanal, hexanone, or any derivative of these compounds [107–109]. These molecules, as well as the reaction conditions, determine the length of the final hydrocarbons, the C8–C15 count being the most common. This carbon count can, e.g., be obtained by the condensation of furfural or 5-hydroxymethylfurfural with acetone in a liquid-phase reaction, as it is illustrated in Figs. 5.14 and 5.15.

This reaction is the key step of an important alternative pathway to obtain diesel fuels from biomass. This process was first proposed by Dumesic and co-workers [45], and it is illustrated in Fig. 5.16, taking hemicellulose as model biomass constituent.

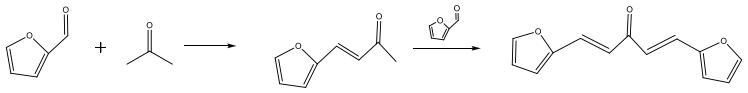

Fig 5.14 Furfural–acetone aldol condensation

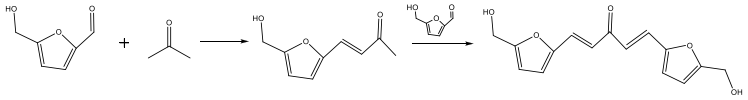

Fig. 5.15 HMF–acetone aldol condensation

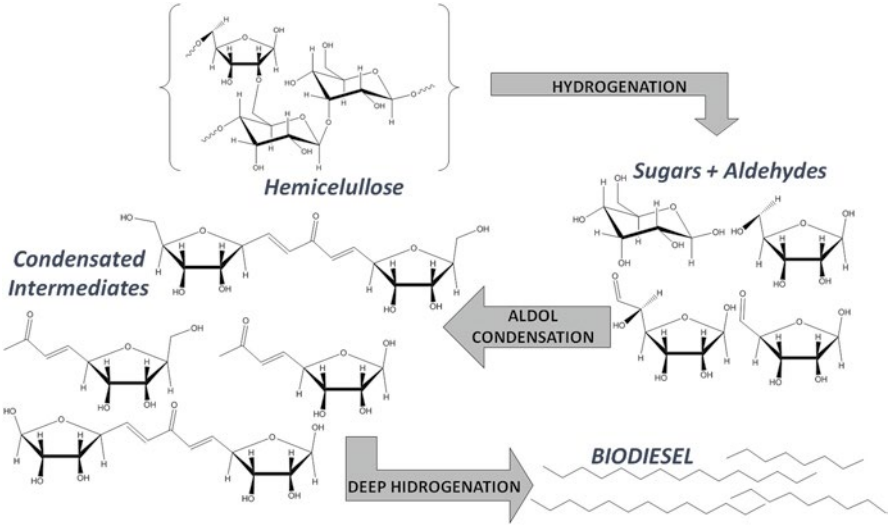

Fig. 5.16 Reaction pathway for renewable diesel from lignocellulosic biomass

5.3.3.1 Aldehyde Condensation Catalysts and Reaction Mechanisms

Despite the fact C6 sugars are more abundant than C5 in lignocellulose biomass, the aldol condensation of furfural has been much more studied than the aldolization of 5-HMF. The furfural–acetone aldol condensation was mainly catalyzed by basic materials, but there are some references proposing the use of acid catalysts, mainly zeolites, with good results [110–112]. Regarding the aldolization catalyzed by basic sites, this reaction was studied using homogeneous and heterogeneous catalysts. As to the first ones, good results were obtained by Dumesic et al. using NaOH as catalysts and obtaining up to 90 % of alkane yields when the aldolization is integrated in a complex system of reactors of aldolization, hydrogenation, and hydrodeoxygenation [47]. The presence of uncontrolled polymerization of dimer adducts generated by Michael addition reactions was identified as the main disadvantage of the use of this catalyst [113], as well as the need to neutralize the catalyst and remove

high volumes of water. Different alternatives have been proposed in order to prevent these disadvantages. One of these alternatives is the use of a biphasic catalytic system consisting of a reactive aqueous phase and an organic extracting phase, usually tetrahydrofuran (THF) that continuously extracts the hydrophobic phase [48, 114]. The use of NaCl improves the immiscibility between both phases, improving the results.

In any case, the use of homogeneous catalysts leads to high operation costs and serious environmental problems. Hence, the development of basic heterogeneous catalysts is again essential. In parallel with studies of acetone self-condensation, different mixed oxides have been studied in detail for the furfural–acetone cross-condensation, mainly those based on magnesium. Mg–Al layered double hydroxides (LDH) have been proposed obtaining almost complete furfural conversion and yield higher than 90 % of condensated adducts with selectivities to diacetone alcohol (the main by-product) less than 5 % [115, 116]. With those catalysts, temperatures close to 100 °C are needed, and the C13 adduct is favored by furfural/acetone initial ratio of 10:1. Similar activity was observed with MgAl mixed oxides, but working under milder conditions (50 °C) [53, 61, 117]. This catalyst was tested both in a batch and flow fixed bed and with different Mg/Al ratios, and the best results were obtained for Mg/Al = 3 [61, 117]. Characterization of these solid catalysts indicates that medium-strength basic sites associated mainly with MgO are responsible of their activity [117]. Consequently, MgO and other mixed oxides based on MgO were also considered.

Huang et al. [118] suggested MgO as a condensation catalyst, supporting the active phase on NaY to prevent the magnesium leaching. Working at 85 °C, almost complete conversion was obtained after 8 h in a batch reaction, without observing any side products. However, in order to increase the selectivity to C13 (most interesting compound), the initial ratio of furfural/acetone must be even higher than with the MgAl LDH, and the reaction rate at these conditions is strongly affected.

Considering that basicity is the key parameter in this reaction, MgO–ZrO_2 was considered by several researchers, because the stronger basicity of ZrO_2 and because the zirconia can stabilize the activity of MgO, preventing its leaching [61, 119–122]. Activity of MgZr and MgAl mixed oxides were compared at 50 °C, obtaining better results with MgZr, both in terms of conversion and C13 selectivity [61]. The influence of the preparation method and the activation temperature on the activity of this material were studied in detail, concluding that the activation temperature has the most important effect, in such a way that materials treated at temperatures under 600 °C showed a substantial decrease in the final activity [121]. Differences caused by the preparation method are less pronounced, but the coprecipitation method prevailed over alcogel and other procedures [120, 121].

The main advantage of the coprecipitation method is the better distribution of basic sites, increasing the concentration of medium strengths. However, the results obtained can be further enhanced by supporting the active phase on an inert support, in such a way that the presence of structural effects creates new basic sites, improving the basicity dispersion and the catalytic activity. High surface area graphites (HSAG) were proposed as one of the most promising because of their good properties: they have a

marked mesoporous character and moderate surface areas (100–500 m^2/g) caused by their disordered graphitic layers, and they have unsaturated valences at the edges of these layers, leading to the formation of oxygenated functional groups, which act as anchoring sites [123]. As it could be expected, MgZr/HSAG catalysts show higher basicity dispersion, observing an important increase in the C8 and C13 formation rate, whereas no side products were observed [122].

Other mixed oxides, such as Co–Al [124, 125] and Ca–Zr [61], were also tested. In the first case, good results are obtained in terms of conversion, selectivity, and reusability, but temperatures higher than 140 °C are needed. For the latter, the activity is very low, with the strong basicity being the main factor causing the bad results obtained and the high amount of by-products obtained. More complex catalysts, such as activated dolomites ($CaMg(CO_3)_2$) [126] or MCM-41 [127], were tested with good results, showing similar activity as with the homogeneous NaOH.

In addition to studies on furfural–acetone cross-condensation, there are several studies about the HMF-acetone condensation. This reaction was firstly proposed by Dumesic and co-workers using NaOH as catalyst in a biphasic system, investigating the effect of reagent ratio and reaction conditions on the final product distribution [128]. In further studies, this reaction was studied using several solid base catalysts such as MgO, CaO, La/ZrO_2, Y/ZrO_2, $MgO–Al_2O_3$, $MgO–ZrO_2$, and $MgO–TiO_2$ [113]. La/ZrO_2 and Y/ZrO_2 showed poor activity, whereas CaO was found to be active but leached into aqueous solution. For this reaction, best results were obtained with MgAl mixed oxide, with C15 selectivities 20 % higher than the selectivity obtained with MgZr (at similar conversion).

Concerning to the reaction mechanism, this process is, as all the condensations, conditioned by the ability to abstract the α-proton of one of the reagents, depending on both the basicity of the active site and the acidity of that proton [129]. A detailed study of the reaction mechanism was reported by Faba et al. [61] and corroborated by the theoretical studies of Chen et al. [130]. The proposed mechanism is illustrated in Fig. 5.17.

According to Fig. 5.17, the reaction begins with the abstraction of the α-proton from one acetone molecule previously adsorbed on a medium-strength basic site, forming a carbanion that consecutively attacks the carbonyl group of the also adsorbed furfural molecule. As product of this reaction, a β-hydroxyl ketone intermediate is expected to form, but this was never observed because of the high instability of this intermediate. It is assumed that this intermediate undergoes fast dehydration, obtaining the first condensated adduct (C8) and water, and regenerating the active site on the catalysts surface. In the same way, C13 is obtained by the abstraction of the α-proton from C8 adduct, forming a carbanion that consecutively attacks the carbonyl group of another adsorbed furfural molecule. Diacetone alcohol is the main by-product that can be generated in this reaction because the first part of both reactions (acetone self-condensation and furfural–acetone cross-condensation) is common to both reactions and is catalyzed by same type of active site [61]. This mechanism is in good agreement with the mechanism proposed by other researchers for same reaction [126, 131] and other aldolizations involving acetone, such as the citral–acetone condensation [43, 129] or the condensation of

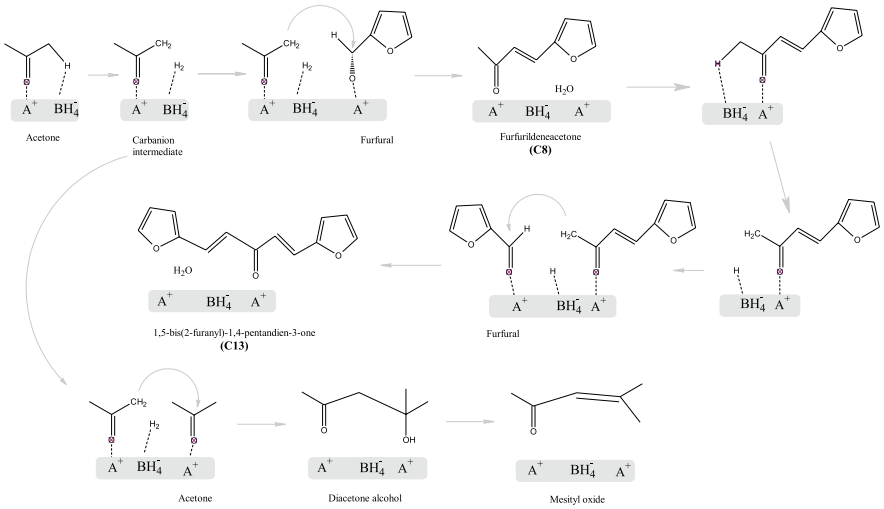

Fig. 5.17 Surface process for the furfural/acetone aldol condensation catalyzed by MgZr (Figure reproduced from [61] by Faba et al. with permission of Elsevier)

campholenic aldehyde [132]. Computational methods were also used to identify the mechanism [130]. All calculations were implemented with Gaussian 09 program, and the key role of Brønsted basicity and the abstraction of the α-proton were corroborated.

Despite the good agreement on the reaction mechanism, there are different kinetic models proposed in the literature. One model states that reaction can be represented by a sequence of elementary steps, and the rate-determining steps for the C8 and C13 formation only involve the enolate species, acetone and C8 derivatives, whereas the furfural concentration has no influence on the kinetic expressions [61, 126, 130]. This model has two main versions because the possible presence of equilibrium in both steps is still not clear, with some authors defending this hypothesis [61, 126] and other authors do not observe enough evidence for it [130]. On the contrary, other authors consider that furfural concentration also has influence in the kinetic rate, obtaining a second global order expression (first-order respect to acetone and respect to furfural) [126].

5.3.3.2 Aldehyde Condensation Catalyst Deactivation

As in other condensations, the instability of solid catalysts is the main drawback to their implementation in a larger scale. Most of the reports on these condensations mention results about stability of the catalysts, and most of them record a substantial decrease in their activity after few cycles or few hours in continuous mode [61, 117, 118, 120]. In general, several mechanisms can contribute to this deactivation: fouling and/or poisoning of the catalyst surface by heavy compounds derived from aldehydes, leaching of alkaline earth cations, or hydration of oxides.

Different heavy compounds are identified when Mg/Al is used as catalyst [117], corresponding to the oligomerization of C13 and C15 compounds. These compounds are not soluble and precipitate, blocking the active phase and BEING detected by TPO analyses. When Ca–Zr mixed oxides [61] and MgO/NaY [118] were used, the strongest basic sites were identified as the active phase that favor these side reactions. If the reaction times are not too long, most of the catalysts show good regeneration capability, and their catalytic activity are well recovered after calcination treatments [117, 118].

Other researches considered reactions in biphasic configurations, using organic solvents such as methanol [119] or hexane [104] to combine the reaction with an extraction that prevents the oligomerizations. With the same aim, bifunctional catalysts can play an important role: if the reaction is carried out under H_2 atmosphere and the catalyst combines the basic sites with a noble metal (generally Pd), condensed adducts can be partially hydrogenated, increasing their solubility in the aqueous phase and preventing their strong adsorption on basic sites that promote the oligomerization [113, 133]. Thus, the stability of these catalysts is strongly enhanced by combining the condensation with a partial hydrogenation.

5.4 Ketonization

Ketonization or ketonic decarboxylation is a reaction that converts two carboxylic acid molecules into a ketone, obtaining also carbon dioxide and water, as follows:

$$R_1COOH + R_2COOH \rightarrow R_1COR_2 + CO_2 + H_2O \tag{5.6}$$

Even though the first example of ketonization was reported in 1858 [134], this reaction has regained attention in recent years because of its potential applications in biomass conversion. A large variety of chemicals can be obtained by this process, with high industrial and technological importance. The reaction can be adapted to different conditions, under solid, liquid, and gas phase [135, 136]. In addition, ketonization can be carried out under catalytic, pyrolytic, or photolytic conditions, the catalytic ketonization being considered as the simplest, most economic, and most versatile [137].

Acetic acid is one of the most promising bio-platform molecules, mainly obtained by biomass fast pyrolysis [138]. It is part of the bio-oil, reaching values of 10 % (w/w), and it is one of the products that limit the direct use of bio-oil as biofuel [139]. Acetic acid is undesirable due to its high corrosiveness and the instability, so its conversion into acetone by ketonization (to direct use or to its transformation) has gained relevance in the last years. The study of acetic acid ketonization is presented in this chapter with main attention on the catalyst, the reaction mechanism, and the present knowledge on catalyst deactivation.

5.4.1 Acetic Acid Ketonization Catalysts and Reaction Mechanism

A large number of catalysts, including metal oxides, oxides with redox properties, and zeolites, have been found to be active for the ketonization of acetic acid. Metal oxides are the most referred in the literature. An active oxide catalyst for surface ketonization should be able to adsorb the carboxylic acid-forming surface carboxylates and to have adjacent coordinately unsaturated cation sites to allow the adsorbate–adsorbate interactions that lead to the formation of the ketone. FTIR and XRD studies corroborate that the most stable adsorption of acetic acid on the catalytic surface is by bridging bidentate configurations, concluding that a surface containing doubly unsaturated cations must be presented [140].

Amphoteric reducible metal oxides, such as CeO_2, TiO_2, and ZrO_2, have been reported to be the most active catalysts for ketonization, observing a high impact of the preparation and activation method [141–143]. Materials calcined at higher temperature gave significantly greater rates of ketonization, as did preparation methods that increase the surface area. The influence of crystal structure and bond strength between metal and oxygen were also studied by different authors, highlighting the role of these parameters to stabilize the β-keto acid intermediate [137, 144]. At appropriate reaction conditions, the activity of CeO_2 (amphoteric oxides) is almost double than the activity of a classical basic oxide (MgO) [145]. Other authors have tested the activity of different supported and unsupported rare earth oxides in the ketonization of acetic acid, obtaining total selectivity to acetone and conversions higher than 75 % at temperatures from 325 to 425 °C [146].

Despite the extensive efforts in studying this reaction, there is still no complete agreement about the reaction mechanism. Two different types of ketonization have been identified: the bulk ketonization and the surface one. It is generally accepted that the first one needs oxides with low lattice energies (i.e., very high basicity), whereas the second one implies the interaction with high lattice energetic materials [140]. However, other researchers disagree with this hypothesis, identifying a high relevance of the catalyst crystallinity and a secondary importance of the lattice energy [141]. The existence of two different mechanisms was confirmed by comparing the evolution of acetic acid, acetone, water, and CO_2 using different types of catalysts. When TiO_2, Al_2O_3, or ZrO_2 are used, the decrease in acid concentration occurred simultaneously with the appearance of reaction products, whereas in the case of using MgO, CaO, or SrO, the decrease in acid concentration occurred significantly before their formation [140]. Currently, the coexistence of both mechanisms is accepted, i.e., it is possible that, in some cases, they operate simultaneously on a given solid, depending on the reaction conditions. Some researchers [147, 148] have identified a temperature limit (around 400 °C) below which the reaction catalyzed by alkaline and alkaline earth oxides proceeds on the catalyst surface by interaction of two adsorbed molecules of acetic acid. At higher temperatures, the reaction would take place through the bulk acetate decomposition. In any case, metal–oxygen bond strengths are implicated as being important for determining the reaction pathway [144].

The acetic acid ketonization via bulk acetates is also known as pyrolytic route whereas ketonization that implies surface acetates is known as the actual catalytic process. Regarding the pyrolytic pathway, the ketonization implies obtaining stable intermediates (which can be easily analyzed) known as bulk acetates. Equation 5.7 illustrates this reaction, using MgO as the catalyst [135]:

$$2 \cdot CH_3COOH(g) + MgO(s) \rightarrow Mg(CH_3COO)_2(s) + H_2O \quad (5.7)$$

Reaction mechanisms are more difficult in the case of catalytic ketonization. Despite the different alternatives, all surface-catalyzed ketonization studies agree in the need for an α-hydrogen. The mechanism starts with the abstraction of this hydrogen by a basic site of the catalyst surface, which leads to the formation of a nucleophile that can attack another carboxylic acid to form a ketone. This mechanism was corroborated in the ketonization of different acids (acetic acid, propanoic acid, valeric acid, and their derivatives), by using isotopic compounds and with DFT approaches [144, 149, 150]. Discrepancies arise between the types of adsorption of AcOH on these catalysts, with two main alternatives: (a) non-dissociative adsorption in the form of hydrogen-bonded AcOH molecule, as is detailed in Eq. 5.8, or (b) dissociative adsorption in the form of acetate groups, as in Eq. 5.9 [135].

$$CH_3COOH(g) + Mg - OH(s) + O_2 - (s) \rightarrow CH_3COOH \cdots HO - Mg(s) \quad (5.8)$$

$$CH_3COOH(g) + Mg^{2+}(s) + O^{2-}(s) \rightarrow CH_3COO - \cdots Mg^{2+}(s) + HO^{-}(s) \quad (5.9)$$

DFT studies indicate that the dissociative mechanism is kinetically favored with a lower activation energy, mainly because of the formation of a reactive nucleophilic center that can easily couple with another adsorbed molecule [152]. This mechanism is known as the β-keto acid-based mechanism, because this intermediate has a crucial role in the reaction. This is at present the most accepted mechanism for the acetic acid ketonization. The β-keto acid is formed by coupling an enolate (enolized carboxylate) and a carboxylate. In the case of acetic acid ketonization, this reaction is between two molecules, but the ketonization of more complex compounds can be intramolecular [149]. The β-keto acid suffers decarboxylation by a mechanism that involves redistribution of six electrons, giving an enol that can be rapidly tautomerized to form the corresponding ketene [153]. Consequently, the catalyst undergoes consecutive reduction–oxidation cycles during the reaction, so basic materials with redox properties are particularly effective. The β-keto acid mechanism proposed is shown in Fig. 5.18.

Another alternative to this process is the ketene-based mechanism [156]. In this approach, a carboxylate intermediate is first formed on an unsaturated metal site and then dehydrated to a surface ketene intermediate. This compound couples with the alkyl group of an adsorbed carboxylate species to form the ketone. This mechanism is still not defined, but the existence of this intermediate was observed by FTIR combined with isotopic labeling studies [154]. Presently, it is considered more as a

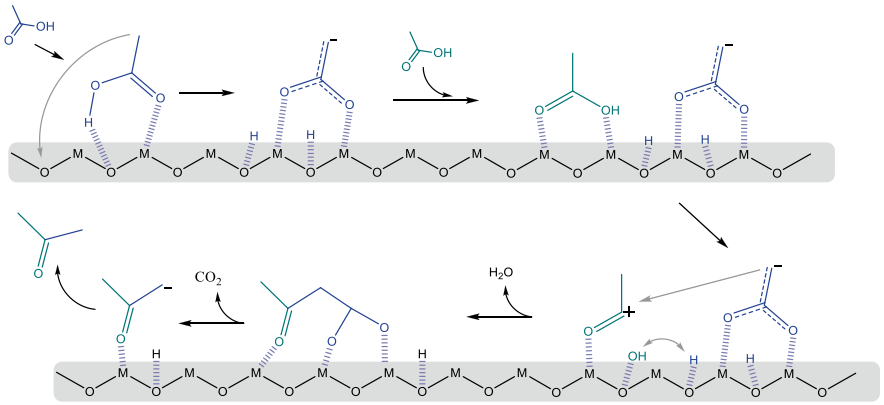

Fig. 5.18 Acetic acid ketonization mechanism via β-keto acid intermediate (Figure reproduced from [151] by Pulido et al. with permission of Wiley-VCH)

side reaction than an alternative mechanism to the main ketonization, in such a way that ethenone was identified during studies of acetic acid ketonization [142].

5.4.2 Acetic Acid Ketonization Catalyst Deactivation

Despite the high interest of this reaction, there are no specific studies on catalyst stability, and most of the studies indicate a negligible loss of activity during their experiments. However, some authors have analyzed their spent catalyst observing a significant modification of their crystalline structure [146, 155]. These structural changes can distort the positions of acid–base active sites, making the stabilization of adsorbed species more difficult. This effect is more relevant in ketonizations than in condensations because more than one active site is needed in intermediate stages.

On the other hand, CO_2 and acetone have affinity for surface Lewis base and acid sites, so they are considered by some authors as inhibitors of the ketonization, this deactivation being verified experimentally by Resasco and co-workers [140, 156].

Side reactions are not identified, as ketonization is considered to be a very selective process, but some catalysts favor acetone condensations and ketonizations at the same time, obtaining higher-molecular-weight compounds such as 4-methyl-3-penten-2-one, trimethylbenzene, and cyclohexanone as side products [146]. These compounds can form polymers and remain strongly adsorbed on the catalytic surface leading to the subsequent poisoning of these surfaces. In the last few years, ketonization via ketenes and bulk ketonization has been considered more as side reactions than as alternative mechanisms. Consequently, materials with higher tendency to increase the relevance of these processes at increasing reaction times can be considered as more affected by partial deactivation.

References

1. Huber GW, Iborra S, Corma A (2006) Synthesis of transportation fuels from biomass chemistry, catalyst and engineering. Chem Rev 106:4044–4098
2. EIA (2014) World Energy Outlook. http://www.iea.org/w/bookshop/477-World_Energy_Outlook_2014. Accessed Nov 2014
3. Corma A, de la Torre O, Renz M (2011) High-quality diesel from hexose-and pentose-derived biomass platform molecules. ChemSusChem 4:1574–1577
4. Ma FR, Hanna MA (1999) Biodiesel production: a review. Bioresour Technol 70:1–15
5. Canakci M, Van Gerpen J (2001) Biodiesel production from oils and fats with high free fatty acids. Trans ASAE 44:1429–1436
6. Navjot K, Ali A (2014) One-pot transesterification and esterification of waste cooking oil via ethanolysis using Sr:Zr mixed oxide as solid catalyst. RSC Adv 4:43671–43681
7. Tsai Y, Ling H, Lee M (2013) Biodiesel production with continuous supercritical process: non-catalytic transesterification and esterification with or without carbon dioxide. Bioresour Technol 145:362–369
8. Thanh LT, Okitsu J, Maeda Y (2014) Ultrasound assisted production of fatty acid methyl esters from transesterification of triglycerides with methanol in the presence of KOH catalyst: optimization, mechanism and kinetics. Ultrason Sonochem 21:467–471
9. Ghasemi M, Dehkordi AM (2014) Transesterification of waste cooking oil to biodiesel using KOH/gamma-Al_2O_3 catalyst in a new two-impinging-jets reactor. Ind Eng Chem Res 53:12238–12248
10. Hoda N (2010) Optimization of biodiesel production from cottonseed oil by transesterification using NaOH and methanol. Energy Source Part A 32:434–441
11. Boey PL, Maniam GP, Hamid SA (2011) Performance of calcium oxide as a heterogeneous catalyst in biodiesel production: a review. Chem Eng J 168:15–22
12. Manríquez-Ramírez M, Gómez R, Hernández-Cortez JG, Zúñiga-Moreno A, Reza-San Germán C, Flores-Valle SO (2013) Advances in the transesterification of triglycerides to biodiesel using MgO-NaOH, MgO-KOH and MgO-CeO_2 as solid basic catalysts. Catal Today 212:23–30
13. Zabeti M, Wan M, Wan D (2009) Activity of solid catalysts for biodiesel production: a review. Fuel Process Technol 90:422–427
14. Chouhan APS, Sarma AK (2011) Modern heterogeneous catalysts for biodiesel production: a comprehensive review. Renew Sustain Energy Rev 15:4378–4399
15. Salamatinia B, Mootabadi J, Bhatia S, Abdullah AZ (2010) Optimization of ultrasonic-assisted heterogeneous biodiesel production from palm oil: a response surface methodology approach. Fuel Process Technol 91:441–448
16. Dossin TF, Reyniers MF, Berger RJ, Marin GB (2006) Simulation of heterogeneously production. Appl Catal B 67:136–148
17. Tateno T, Sasaki T (2004) Process for producing fatty acid fuels comprising fatty acids esters, Uni. State Patent 6818026, November 16
18. Veljkovic VB, Stamenkovic OS, Todorovic ZB, Lazic ML, Skala DU (2009) Kinetics of sunflower oil methanolysis catalyzed by calcium oxide. Fuel 88:554–562
19. Boey PL, Maniam GP, Hamid SA (2009) Biodiesel production via transesterification of palm olein using waste mud crab shell as a heterogeneous catalyst. Bioresour Technol 100:6362–6368
20. Viriya-empikul N, Krasae P, Puttasawat B, Yoosuk B, Chollacoop N, Faung-Nawakij K (2010) Waste shells of mollusk and egg as biodiesel production catalysts. Bioresour Technol 101:3765–3767
21. Lam MK, Lee KT, Mohamed AR (2010) Homogeneous, heterogeneous and enzymatic catalysts for transesterification of high free fatty acid oil (waste cooking oil) to biodiesel: a review. Biotechnol Adv 28:500–518

22. Vujicic DJ, Comic D, Zarubica A, Micic R, Boskovic G (2010) Kinetics of biodiesel synthesis from sunflower oil over CaO heterogeneous catalyst. Fuel 89:2054–2061
23. Ilgen O (2011) Dolomite as a heterogeneous catalyst for transesterification of canola oil. Fuel Process Technol 92:452–455
24. Liu Y, Lotero E, Goodwin JG (2006) Effect of carbon chain length on esterification of carboxylic acids with methanol using acid catalysis. J Catal 243:221–228
25. Encinar JM, González JF, Pardal A, Martínez G (2010) Rape oil transesterification over heterogeneous catalysts. Fuel Process Technol 91:1530–1536
26. Liu R, Wnag X, Zhao X, Feng P (2006) Sulfonated ordered mesoporous carbon for catalytic preparation of biodiesel. Carbon 310:48–53
27. Grandos ML, Poves MD, Alonso D, Mariscal R, Galisteo FC, Moreno-Tost R (2007) Biodiesel from sunflower oil by using activated calcium oxide. Appl Catal B 73:317–326
28. Mootabadi H, Salamatinia B, Bhatia S, Abdullah AZ (2010) Ultrasonic-assisted biodiesel production process from palm oil using alkaline earth metal oxides as the heterogeneous catalysts. Fuel 89:1818–1825
29. Yoo SJ, Lee HS, Bambang V, Kim J, Kim JD, Lee YW (2010) Synthesis of biodiesel from rapeseed oil using supercritical methanol with metal oxide catalysts. Bioresour Technol 101:8686–8689
30. Silva RB, Lima AF, Santos SS, Oliveira JR, Chaves MH, Santos JR (2008) Catalysts of Cu(II) and Co(II) ions adsorbed in chitosan used in transesterification of soy bean and babassu oils – a new route for biodiesel syntheses. Bioresour Technol 99:6793–6798
31. Brito YC, Mello VM, Cesar C, Macedo CS, Meneghetti MR, Suárez AZ (2006) Fatty acid methyl esters preparation in the presence of maltolate and n-butoxide Ti(IV) and Zr(IV) complexes. Appl Catal A 351:24–28
32. Rashtizadeh E, Farzaneh F, Ghandi M (2010) A comparative study of KOH loaded on double aluminosilicate layers, microporous and mesoporous materials as catalyst for biodiesel production via transesterification of soybean oil. Fuel 89:3393–3398
33. Jin L, Zhang Y, Dombrowski JP, Chen CH, Pravatas A, Xy L, Perkins C, Suib SL (2011) ZnO/$La_2O_2CO_3$ layered composite: a new heterogeneous catalyst for the efficient ultra-fast microwave biofuel production. App Catal B 103:200–205
34. Kouzu M, Hidaka J (2012) Transesterification of vegetable oil into biodiesel catalyzed by CaO: A review. Fuel 93:1–12
35. Kouzu M, Kasuno T, Tajika M, Yamanaka S, Hidaka J (2008) Active phase of calcium oxide used as solid base catalyst for transesterification of soybean oil with refluxing methanol. Appl Catal A 334:357–365
36. Almerindo GI, Probst LFD, Campos CEM, Almeida RM, Meneghetti SMP, Meneghetti MR, Clacens JM, Fajardo HV (2011) Magnesium oxide prepared via metal-chitosan complexation method: application as catalyst for transesterification of soybean oil and catalyst deactivation studies. J Power Sources 196:8057–8063
37. Choedkiatsakul I, Ngaosuwan K, Assabumrungrat S (2013) Application of heterogeneous catalysts for transesterification of refined palm oil in ultrasound-assisted reactor. Fuel Process Technol 111:22–28
38. Chantrasa A, Phlernjai N, Goodwin JG (2011) Kinetics of hydrotalcite catalyzed transesterification of tricaprylin and methanol for biodiesel synthesis. Chem Eng J 168:333–340
39. Lee S, Varma A (2013) Kinetic study of biphasic aldol condensation of n-butyraldehyde using stirred cell. Chem Eng Sci 140:619–629
40. Hanna DG, Shylesh S, Li Y, Krishna S, Head-Gordon M, Bell AT (2014) Experimental and theoretical study of n-butanal self-condensation over Ti species supported on silica. ACS Catal 4:2908–2916
41. Yadav GP, Aduri P (2012) Aldol condensation of benzaldehyde with heptanal to jasminaldehyde over novel Mg-Al mixed oxide on hexagonal mesoporous silica. J Mol Catal A 355:142–154
42. Foo SW, Oishi S, Saito S (2012) Aldol condensation of amides using phosphazene-based catalysis. Tetrahedron Lett 53:5445–5448

43. Abelló S, Dhir S, Colet G, Pérez-Ramírez J (2007) Accelerated study of the citral-acetone condensation kinetics over activated Mg-Al hydrotalcite. Appl Catal A 325:121–129
44. Raju V, Radhakrishnana R, Jaenicke S, Chuah GK (2011) KF on γ-alumina: an efficient catalyst for the aldol condensation to pseudoionones. Catal Today 164:139–142
45. Huber GW, Chheda JN, Barret CJ, Dumesic JA (2005) Production of liquid alkanes by aqueous-phase processing of biomass-derived carbohydrates. Science 308:1446–1450
46. Sifniades S, Levy AB (2002) Acetone Ullmann's encyclopedia of industrial chemistry, 6th edn. Wiley-VCh, New York
47. Qureshi N, Ezeji TC (2008) Butanol, "a superior biofuel" production from agricultural residues (renewable biomass): recent progress in technology. Biofuels Bioprod Biorefin 2:319–330
48. Mansur D, Yoshikawa T, Norinaga K, Hayashi J, Tago T, Masuda T (2013) Production of ketones from pyroligneous acid of woody biomass pyrolysis over an iron-oxide catalyst. Fuel 103:130–134
49. Bej SK, Thompson LT (2004) Acetone condensation over molybdenum nitride and carbide catalysts. Appl Catal A 264:141–150
50. Weissermel K, Arpe HJ (1997) Industrial organic chemistry, 3rd ed. Wiley New York (USA)
51. Salvapati GS, Ramanamurty KV, Janardanarao M (1989) Selective catalytic self-condensation of acetone. J Molec Catal 54:9–30
52. Kikhtyanin O, Kubicka D, Cejka J (2015) Toward understanding of the role of Lewis acidity in aldol condensation of acetone and furfural using MOF and zeolite catalysts. Catal Today 243:158–162
53. Ordóñez S, Díaz E, León M, Faba L (2011) Hydrotalcite-derived mixed oxides as catalysts for different C-C bond formation reactions from bioorganic materials. Catal Today 167:71–76
54. Kustrowski P, Sulkowska D, Chmielarz L, Rafalska A, Dudk B, Dziembaj R (2005) Influence of thermal treatment conditions on the activity of hydrotalcite derived Mg-Al oxides in the aldol condensation of acetone. Microporous Mesoporous Mater 78:11–22
55. Podrebarac GG, Ng FTT, Rempel GL (1997) A kinetic study of the aldol condensation of acetone using an anion exchange resin catalyst. Chem Eng Sci 52:2991–3002
56. Tichit D, Bennani MN, Figueras F, Tessier R, Kervennal J (1998) Aldol condensation of acetone over layered double hydroxides of the meixnerite type. Appl Clay Sci 13:401–415
57. Zhang G, Hattori H, Tanabe K (1988) Aldol addition of acetone, catalyzed by solid base catalysts: magnesium oxide, calcium oxide, strontium oxide, barium oxide, lanthanum (IIII) oxide and zirconium oxide. Appl Catal A 382:272–276
58. Cota I, Ramírez E, Medina F, Sueiras JE, Layrac G, Tichit D (2010) Highly basic catalysts obtained by intercalation of La-containing anionic complexes in layered doublé hydroxides. Appl Catal A 382:272–276
59. Wang Z, Fongarland P, Lu G, Essayem N (2014) Reconstructed La-, Y-Ce-modified MgAl-hydrotalcite as a solid base catalyst for aldol condensation: investigation of water tolerance. J Catal 318:108–118
60. Gao J, Teplyakov AV (2014) Chemical transformations of acetone on ZnO powder. J Catal 319:136–141
61. Faba L, Díaz E, Ordóñez S (2012) Aqueous-phase furfural-acetone aldol condensation over basic mixed oxides. Appl Catal B 113–114:201–211
62. Lu Z, Zhang F, Lei X, Yang L, Xu S, Duan X (2008) In situ growth of layered double hydroxide films on anodic aluminum oxide/aluminum and its catalytic feature in aldol condensation of acetone. Chem Eng Sci 63:4055–4062
63. Huang C, Ng FTT, Rempel GL (2000) Application of catalytic distillation for the aldol condensation of acetone: the effect of the mass transfer and kinetic rates on the yield and selectivity. Chem Eng Sci 55:5919–5931
64. Di Cosimo JI, Díez VK, Apesteguía CR (1996) Base catalysis for the synthesis of α, β-unsaturated ketones from the vapor-phase aldol condensation of acetone. Appl Catal A 137:149–166

65. León M, Faba L, Díaz E, Bennici S, Vega A, Ordóñez S, Auroux A (2014) Consequences of MgO activation procedures on its catalytic performance for acetone self-condensation. Appl Catal B 147:796–804
66. Faba L, Díaz E, Ordóñez S (2013) Gas phase acetone self-condensation over unsupported and supported Mg-Zr mixed-oxides catalysts. Appl Catal B 142–143:387–395
67. Li Z, Xi W, Lu C (2015) Hydrotalcite-assisted cataluminescence: a new approach for sensing mesityl oxide in aldol condensation of acetone. Sensor Actuat B-Chem 207:598–503
68. Krivtsov I, Faba L, Díaz E, Ordóñez S, Avdin V, Khainakov S, García JR (2014) A new peroxo-route for the synthesis of Mg-Zr mixed oxides catalysts: application in the gas phase acetone self-condensation. Appl Catal A 477:26–33
69. Zamora M, López T, Gómez R, Asomoza M, Meléndrez R (2005) Acetone gas phase condensation of alkaline metals doped TiO_2 sol-gel catalysts. Appl Surf Sci 252:828–832
70. Zamora M, López T, Gómez R, Asomoza M, Meléndrez R (2005) Oligomerization of acetone over titania-doped catalysts (Li, Na, K and Cs): effect of the alkaline metal in activity and selectivity. Catal Today 107–108:289–293
71. Zamora M, López T, Asomoza M, Meléndrez R, Gómez R (2006) Alkaline doped TiO2 sol-gel catalysts: Effect of sintering on catalyst activity and selectivity for acetone condensation. Catal Today 116:234–238
72. Torok DS, Scott WJ (1993) Thermal conversion of phorone into isophorone via (trimethylsilyl)oxyhexatriene (soh) cyclization. Tetrahedron Lett 34:3067–3070
73. Kumar VS, Nagaraja BM, Shashikala V, Seetharamulu P, Padmasri AH, Raju BD, Rao KSR (2004) Role of acidic and basic sites of Al_2O_3 in predicting the reaction pathway of isophorone transformation. J Mol Catal A 223:283–288
74. Di Cosimo JI, Apesteguía CR (1998) Study of the catalyst deactivation in the base-catalyzed oligomerization of acetone. J Mol Catal 130:177–185
75. Diez VK, Apesteguía CR, Di Cosimo JI (2001) Deactivation of MgyAlOx mixed oxides during aldol condensation reactions of ketones. Stud Surf Sci Catal 139:303–310
76. Sugi Y, Matsuzaki T, Hanaoka T, Takeuchi K, Tokoro T, Takeuchi G (1991) Alkylation of biphenyl catalyzed by zeolites. Stud Surf Sci Catal 60:303–310
77. Talwalkar S, Mahajani S (2006) Synthesis of methyl isobutyl ketone from acetone over metal-doped ion exchange resin catalyst. Appl Catal A 302:140–148
78. Prinetto F, Tichit D, Teissier R, Coq B (2000) Mg- and Ni-containing layered double hydroxides as soda substitutes in the aldol condensation of acetone. Catal Today 55:103–116
79. Abelló S, Vijaya-Shankar D, Pérez-Ramírez J (2008) Stability, reutilization and scalability of activated hydrotalcites in aldol condensation. Appl Catal A 342:119–125
80. Winter F, Koot V, Jos van Dillen A, Geus JW, de Jong KP (2005) Hydrotalcites supported on carbon nanofibers as solid base catalysts for the synthesis of MIBK. J Catal 236:91–100
81. Rekoske JE, Barteau MA (2011) Kinetics, selectivity and deactivation in the aldol condensation of acetaldehyde on anatase titanium dioxide. Ind Eng Chem 50:41–51
82. Davis RJ (2013) Heterogeneous catalysts for the Guerbet coupling of alcohols. ACS Catal 3:1588–1600
83. Angelici C, Weckhuysen BM, Bruijnincx PCA (2013) Chemocatalytic conversion of ethanol into butadiene and other bulk chemicals. ChemSusChem 6:1595–1614
84. Marcu IC, Tanchoux N, Fajula F, Tichit D (2013) Catalytic conversion of ethanol into butanol over M-Mg-Al mixed oxide catalysts (M= Pd, Ag, Mn, Fe, Cu, Sm, Yb) obtained from LDH precursors. Catal Lett 143:23–30
85. Makshina EV, Dusselier M, Janssens W, Degrève J, Jacobs PA, Sels BF (2014) Review of old chemistry and new catalytic advances in the on-purpose synthesis of butadiene. Chem Soc Rev 43:7913–7953
86. León M, Diaz E, Ordóñez S (2011) Ethanol catalytic condensation over Mg-Al mixed oxides derived from hydrotalcites. Catal Today 164:436–442
87. Tsuchida T, Kubo J, Yoshioka T, Sakuma S, Takeguchi T, Ueda W (2008) Reaction of ethanol over hydroxyapatite affected by Ca/P ratio of catalyst. J Catal 259:183–189

88. Di Cosimo JI, Díez VK, Xu M, Iglesia E, Apesteguía CR (1998) Structure and surface and catalytic properties of Mg-Al basic oxides. J Catal 178:499–510
89. Birky TW, Kozlowski JT, Davis RJ (2013) Isotopic transient analysis of the ethanol coupling reaction over magnesia. J Catal 298:130–137
90. Kozlowski JT, Behrens M, Schlögl R, Davis RJ (2013) Influence of the precipitation method on acid-base-catalyzed reactions over Mg-Zr mixed oxides. ChemCatChem 5:1989–1997
91. Ndou AS, Plint N, Coville NJ (2003) Dimerisation of ethanol to butanol over solid-base catalysts. Appl Catal A 251:337–345
92. Ueda W, Kuwabara T, Ohshida T, Morikawa Y (1990) A low-pressure Guerbet reaction over magnesium oxide catalyst. J Chem Soc Chem Commun 22:1558–1559
93. Di Cosimo JI, Apesteguía CR, Ginés MJL, Iglesia E (2000) Structural requirements and reaction pathways in condensation reactions of alcohol son MgyAlOx catalysts. J Catal 290:261–275
94. Kozlowski JT, Davis RJ (2013) Sodium modification of zirconia catalysts for ethanol coupling to 1-butanol. J Energy Chem 22:58–64
95. Ordomsky VV, Sushkevich VL, Ivanova II (2010) Study of acetaldehyde condensation chemistry over magnesia and zirconia supported on silica. J Mol Catal A 333:85–93
96. Ogo S, Onda A, Iwasa Y, Hara K, Fukuoka A, Yanagisawa K (2012) 1-butanol synthesis from ethanol over strontium phosphate hydroxyapatite catalysts with various Sr/P ratios. J Catal 296:24–30
97. Ogo S, Onda A, Yanagisawa K (2011) Selective synthesis of 1-butanol from ethanol over strontium phosphate hydroxyapatite catalysts. Appl Catal A 402:188–195
98. Gines MJL, Iglesia E (1998) Bifunctional condensation reactions of alcohol son basic oxides modified by copper and potassium. J Catal 176:155–172
99. Di Cosimo JI, Acosta A, Apesteguía CR (2004) Gas-phase hydrogen transfer reduction of α, β-unsaturated ketones on Mg-based catalysts. J Mol Catal A 222:87–96
100. Yang C, Meng ZY (1993) Bimolecular condensation of ethanol to 1-butanol catalyzed by alkali cation zeolites. J Catal 142:37–44
101. Ndou AS, Coville NJ (2004) Self-condensation of propanol over solid-base catalysts. Appl Catal A 275:103–110
102. Carlini C, Flego C, Marchionna M, Noviello M, Galletti AMR, Sbrana G, Basile F, Vaccari A (2004) Guerbet condensation of methanol with n-propanol to isobutyl alcohol over heterogeneous copper chromite/Mg-Al mixed oxides catalysts. J Mol Catal A 220:215–220
103. Ramasamy KK, Wang Y (2014) Ethanol conversion to hydrocarbons on HZSM-5: effect of reaction conditions and Si/Al ratio on the product distributions. Catal Today 237:89–99
104. Lamminpää K, Ahola J, Tanskanen J (2015) Acid-catalysed xylose dehydration into furfural in the presence of kraft lignin. Bioresour Technol 177:94–101
105. Alonso DM, Bond JQ, Dumesic JA (2010) Catalytic conversion of biomass to biofuels. Green Chem 12:1493–1513
106. West RM, Liu ZY, Peter M, Dumesic JA (2008) Liquid alkanes with targeted molecular weights from biomass-derived carbohydrates. ChemSusChem 1:417–424
107. Amarasekara AS, Singh TB, Larkin E, Hasan MA, Fan HJ (2015) NaOH catalyse condensation reactions between levulinic acid and biomass derive furan-aldehydes in water. Ind Crop Prod 65:546–549
108. West RM, Liu ZY, Peter M, Gärtner CA, Dumesic JA (2008) Carbon-carbon bond formation for biomass-derived furfurals and ketones by aldol condensation in a biphasic system. J Mol Catal 296:18–27
109. James OO, Maity S, Usman LA, Ajanaku KO, Jani OO, Siyanbola TO, Sahu S, Chaubey R (2010) Towards the conversion of carbohydrate biomass feedstocks to biofuels via hydroxymethylfurfural. Energy Environ Sci 3:1833–1850
110. Kikhtyanin O, Kelbichová V, Vitvarová D, Kubu M, Kubicka D (2014) Aldol condensation of furfural and acetone on zeolites. Catal Today 227:154–162

111. Kikhtyanin O, Kubicka D, Cejka J (2015) Toward understanding of the role of Lewis acidity in aldol condensation of acetone and furfural using MOF and zeolite catalysts. Catal Today 243:158–162
112. Agirrezabal-Telleria I, Gandarias PL (2014) Heterogeneous acid-catalysts for the production of furan-derived compounds (furfural and hydroxymethylfurfural) from renewable carbohydrates: a review. Catal Today 234:42–58
113. Faba L, Díaz E, Ordóñez S (2013) Improvement of the stability of basic mixed oxides used as catalysts for aldol condensation of bio-derived compounds by palladium addition. Biomass Bioenergy 56:592–599
114. Xing R, Subrahmanyam AV, Olcay H, Qi W, van Walsu GP, Pendse H, Huber GW (2010) Production of jet and diesel fuel range alkanes from waste hemicellulose-derived aqueous solutions. Green Chem 12:1933–1946
115. Hora L, Kikhtyanin O, Capek L, Bortnovskiy O, Kubicka D (2015) Comparative study of physico-chemical properties of laboratory and industrially prepared layered double hydroxides and their behavior in aldol condensation of furfural and acetone. Catal Today 241:221–230
116. Hora L, Kelbichova V, Kikhtyanin O, Bortnovskiy O, Kubicka D (2014) Aldol condensation of furfural and acetone over Mg-Al layered double hydroxides and mixed oxides. Catal Today 223:138–147
117. Kikhtyanin O, Hora L, Kubicka D (2015) Unprecedented selectivities in aldol condensation over Mg-Al hydrotalcite in a fixed be reactor setup. Catal Commun 58:89–92
118. Huang X, Zhang Q, Wang T, Liu Q, Ma L, Zhang Q (2012) Production of jet fuel intermediates from furfural and acetone by aldol condensation over MgO/NaY. J Fuel Chem Technol 40:973–978
119. Shen W, Tompsett GA, Hammond KD, Xing R, Dogan F, Grey CD, Conner C, Auerbach SM, Huber GW (2011) Liquid phase aldol condensation reactions with MgO-ZrO2 and shape-selective nitrogen-substituted NaY. Appl Catal A 392:57–68
120. Sádaba I, Ojeda M, Mariscal R, Fierro JLG, López Granados M (2011) Catalytic and structural properties of co-precipitated Mg-Zr mixed oxides for furfural valorization via aqueous aldol condensation with acetone. Appl Catal B 101:638–648
121. Sádaba I, Ojeda M, Mariscal R, Richards R, López Granados M (2011) Mg-Zr mixed oxides for aqueous aldol condensation of furfural with acetone: Effect of preparation method and activation temperature. Catal Today 167:77–83
122. Faba L, Díaz E, Ordóñez S (2013) Improvement on the catalytic performance of Mg-Zr mixed oxides for furfural-acetone aldol condensation by supporting on mesoporous carbons. ChemSusChem 6:463–473
123. Díaz E, Ordóñez S, Bueres RF, Asedegbega-Nieto E, Sastre H (2010) High-surface área graphites as supports for hydrodechlorination catalysts: tuning support surface chemistry for an optimal performance. Appl Catal B 99:181–190
124. Xu W, Liu X, Ren J, Zhang P, Whang Y, Guo Y, Guo Y, Lu G (2010) A novel mesoporous Pd/cobalt aluminate bifunctional catalyst for aldol condensation and following hydrogenation. Catal Commun 11:721–726
125. Xu W, Liu X, Ren J, Liu H, Ma Y, Wang Y, Lu G (2011) Synthesis of nanosized mesoporous Co-Al spinel and its application as solid base catalyst. Microporous Mesoporous Mater 142:251–257
126. O'Neill RE, Vanoye L, De Bellefon C, Aiouache F (2014) Aldol-condensation of furfural by activated dolomite catalyst. Appl Catal B 144:46–56
127. Wang Q, Varela V, Ghosh A, Yeu S, Lunn JD, Shantz DF (2010) Catalytic properties of Dendron-OMS hybrids. J Catal 269:15–25
128. Chheda JN, Dumesic JA (2007) An overview of dehydration, aldol-condensation and hydrogenation processes for production of liquid alkanes from biomass-derived carbohydrates. Catal Today 123:59–70
129. Díez VK, Apesteguía CR, Di Cosimo JI (2006) Aldol condensation of citral with acetone on MgO and alkali-promoted MgO catalysts. J Catal 240:235–244

130. Chen S, Yang H, Hu C (2015) Theoretical study on the reaction mechanisms of the aldol-condensation of 5-hydroxymethylfurfural with acetone catalysed by MgO and MgO+. Catal Today 245:100–107
131. Fakhfakh N, Cognet P, Cabassud M, Lucchese Y, Días de los Ríos M (2008) Stoichio-kinetic modeling and optimization of chemical synthesis: application to the aldolic condensation of furfural on acetone. Chem Eng Process 47:349–362
132. Abelló S, Medina F, Tichit D, Pérez-Ramírez J, Sueiras JE, Salagre P, Cesteros Y (2007) Aldol condensation of campholenic aldehyde and MEK over actívate hydrotalcites. Appl Catal B 70:577–584
133. Faba L, Díaz E, Ordóñez S (2011) Performance of bifunctional Pd/MxNyO (M=Mg, Ca, N=Zr, Al) catalysts for aldolization-hydrogenation of furfural-acetone mixtures. Catal Today 164:451–456
134. Renz M (2005) Ketonization of carboxylic acids by decarboxylation: mechanism and scope. Eur J Org Chem 2005:979–988
135. Mekhemer GAH, Halawy SA, Mohamed MA, Zaki MI (2005) Ketonization of acetic acid vapour over polycrystalline magnesia: in situ Fourier transform infrared spectroscopy and kinetic studies. J Catal 230:109–122
136. Pham TN, Shi D, Sooknoi T, Resasco DE (2012) Aqueous-phase ketonization of acetic acid over Ru/TiO_2/carbon catalysts. J Catal 295:169–178
137. Hasan MA, Zaki MI, Pasupulety L (2003) Oxide-catalyzed conversion of acetic acid into acetone: and FTIR spectroscopic investigation. Appl Catal A 243:81–92
138. Phung TK, Casazza AA, Aliakbarian B, Finocchio E, Perego P, Busca G (2013) Catalytic conversion of ethyl acetate and acetic acid on alumina as models of vegetable oils conversion to biofuels. Chem Eng J 215:838–848
139. Yang X, Chatterjee S, Zhang Z, Zhu X, Pittman CU (2010) Reactions of phenol, water, acetic acid, methanol, and 2-hydroxymethylfuran with olefins as models for bio-oil upgrading. Ind Eng Chem Res 49:2003–2013
140. Pham TN, Sooknoi T, Crossley SP, Resasco DE (2013) Ketonization of carboxylic acids: mechanisms, catalysts, and implications for biomass conversion. ACS Catal 3:2456–2473
141. Snell RW, Shanks BH (2013) Ceria calcination temperature influence on acetic acid ketonization: mechanistic insights. Appl Catal A 451:86–93
142. Martinez R, Huff MC, Barteau MA (2004) Ketonization of acetic acid on titania-functionalized silica monoliths. J Catal 222:404–409
143. Pham TN, Shi D, Resasco DE (2014) Reaction kinetics and mechanism of ketonization of aliphatic carboxylic acids with different carbon chain lengths over Ru/TiO_2 catalyst. J Catal 314:149–158
144. Pestman R, Koster RM, Duijne A, Pieterse JAZ, Ponec V (1997) Reactions of carboxylic acids on oxides: 2. Bimolecular reaction of aliphatic acids to ketones. J Catal 168:265–272
145. Diebold U (2003) The surface science of titanium dioxide. Surf Sci Rep 48:53–229
146. Yamada Y, Segawa M, Sato F, Kojima T, Sato S (2011) Catalytic performance of rare earth oxides in ketonization of acetic acid. J Mol Catal A 346:79–86
147. Kuriacose JC, Jewur SS (1977) Studies on the surface interaction of acetic acid on iron oxide. J Catal 50:330–341
148. Snell RW, Shanks BH (2013) Insights into the ceria-catalyzed ketonization reaction for biofuels applications. ACS Catal 3:783–789
149. Nagashima O, Sato S, Takahashi R, Sodesawa T (2005) Ketonization of carboxylic acids over CeO2-based composite oxides. J Mol Catal A 227:231–239
150. Ignatchnko AV (2011) Density functional theory study of carboxylic acids adsorption and enolization on monoclinic zirconia surfaces. J Phys Chem 115:16012–16018
151. Pulido A, Oliver-Tomas B, Renz M, Boronat M, Corma A (2013) Ketonic decarboxylation reaction mechanism: a combined experimental and DFT study. ChemSusChem 6:141–151
152. Gaertner CA, Serrano-Ruiz JC, Braden DJ, Dumesic JA (2009) Catalytic coupling of carboxylic acids by ketonization as a processing step in biomass conversion. J Catal 266:71–78

153. Dooley KM, Bhat AK, Plaisance CP, Roy AD (2007) Ketones from acid condensation using supported CeO_2 catalysts: effect of additives. Appl Catal A 320:122–133
154. Pestman R, Koster RM, Pieterse JAZ, Ponec V (1997) Reactions of carboxylic acids on oxides: 1. Selective hydrogenation of acetic acid to acetaldehyde. J Catal 168:255–264
155. Snell R, Hakim SH, Dumesic JA, Shanks BH (2013) Catalysis with ceria nanocrystals: bio-oil model compound ketonization. Appl Catal A 464:288–295
156. Lercher JA, Gründling C, Eder-Mirth G (1996) Infrared studies of the surface acidity of oxides and zeolites using adsorbed probe molecules. Catal Today 27:353–376

Chapter 6
Progress in the Development of Mesoporous Solid Acid and Base Catalysts for Converting Carbohydrates into Platform Chemicals

Zhijun Tai, Adam F. Lee, and Karen Wilson

Abstract This chapter provides a general overview of recent studies on catalytic conversion of fructose, glucose, and cellulose to platform chemicals over porous solid acid and base catalysts, including zeolites, ion-exchange resins, heteropoly acids, as well as structured carbon, silica, and metal oxide materials. Attention is focused on the dehydration of glucose and fructose to HMF, isomerization of glucose to fructose, hydrolysis of cellulose to sugar, and glycosidation of cellulose to alkyl glucosides. The correlation of porous structure, surface properties, and the strength or types of acid or base with the catalyst activity in these reactions is discussed in detail in this chapter.

Keywords Mesoporous material • Solid acid (base) catalyst • Catalysis • Carbohydrates • Platform chemicals

6.1 Introduction

Mounting concerns over dwindling petroleum oil reserves, in concert with growing governmental and public acceptance of the anthropogenic origin of rising CO_2 emissions and associated climate change, are driving academic and commercial routes to utilize renewable feedstocks as sustainable sources of fuel and chemicals [1]. Biomass conversion is proposed as the most readily implemented, and low-cost, solution for transportation fuels [2] and the only nonpetroleum route to organic molecules for the manufacture of bulk, fine, and speciality chemicals and polymers [3] required to meet future societal demands [4, 5]. However, in order to be considered truly sustainable, biomass feedstocks must be derived from sources which do

Z. Tai • A.F. Lee • K. Wilson (✉)
European Bioenergy Research Institute, School of Engineering & Applied Science, Aston University, Aston Triangle, Birmingham B4 7ET, UK
e-mail: k.wilson@aston.ac.uk

M. Schlaf, Z.C. Zhang (eds.), *Reaction Pathways and Mechanisms in Thermocatalytic Biomass Conversion I*, Green Chemistry and Sustainable Technology, DOI 10.1007/978-981-287-688-1_6

not compete with agricultural land use for food production or compromise the environment, e.g., via deforestation [6].

Potential feedstocks include cellulosic or oil-based materials derived from plant or aquatic sources, with the so-called biorefinery concept offering the coproduction of fuels, chemicals, and energy from these resources [7], analogous to today's petroleum refineries which deliver high-volume/low-value (e.g., fuels and commodity chemicals) and low-volume/high-value (e.g., fine/speciality chemicals) products in tandem [8]. Unlike fossil fuels, which comprise predominantly unfunctionalized hydrocarbons, carbohydrates derived from sugars, starches, or lignocellulose are highly functionalized, thus requiring new conversion technologies to yield useful chemicals [9, 10]. The high oxygen content of carbohydrates means transformations such as dehydration, condensation, esterification, or etherification which can be readily facilitated by solid acid or base catalysts will be important components in the biorefining tool kit. Solid acid and base catalysts were first defined and developed early in the 1920s by French chemist – Eugene Houdry [11]. Comparing traditional to homogeneous liquid acids and bases, solid acid and base catalysts offer considerable advantages, such as easy separation and recyclability, low cost, and improved process safety by virtue of being less corrosive towards materials used for reactor construction. More importantly, they have shown excellent activities in many catalytic reactions, such as esterification, hydration and dehydration, hydrolysis, alkylation, and polymerization reactions, and thus widely applied in the industry [12]. For instance, zeolites, a major family of solid acid and base catalysts, play a critical important role in underpinning transformations of crude oil in the petrochemical industry as illustrated in Table 6.1 which shows the value of the refining catalyst market for 1999 and 2005 [13].

Over the past decade there has been growing interest in the utilization of biomass as a promising sustainable alternative to fossil resources for the production of fuels and chemicals [14], with much focus on the conversion of biomass using heterogeneous catalyzed routes. Cellulose, a biopolymer of D-glucose linked by β-1, 4-glycosidic bonds, is the most abundant source of biomass. However, cellulose conversion is challenging due to it having a recalcitrant 3D bulk structure arising

Table 6.1 The refining catalyst market in ton and $ by application for 1999 and 2005 (2)

	1999			2005		
Processes	10^3 tons	%	G ($)	10^3 tons	%	G ($)
Cracking	495	77	0.7	560	73.6	0.83
Hydrotreatments	100	15.5	0.72	135	17.7	0.96
Hydrocracking	7	1.1	0.10	9	1.2	0.12
Reforming	6	0.9	0.12	7	0.9	0.15
Others[a]	~35	5.5	0.56	~50[b]	6.6	0.64
Total solids	~640–650	100	2.2	~760	100	2.7
Alkylation	3100[b]	–	0.85	3700[b]	–	1

Reprinted from ref. [13], with kind permission from Elsevier

[a]Catalysts for H_2 production, polymerization, etherification, Claus, lubes, etc.

[b]Approximate values

from the abundant intra- and intermolecular hydrogen bonds, which protect the β-1,4-glycosidic bonds from attack by foreign molecules [15]. Traditional routes to catalytically convert cellulose involve the use of homogeneous acid or base catalysts, such as HCl, H_2SO_4, and NaOH, with the small homogeneous ions (H^+ and OH^-) able to permeate into the structure to catalytically hydrolyze the β-1,4-glycosidic bonds. Although traditional liquid acid or bases are efficient in the hydrolysis of cellulose, the strong acidity or basicity results in poor selectivity towards desired monomeric products with numerous side reactions leading to undesired by-products. Moreover, the separation and recovery of homogeneous acid and associated waste generated is also problematic for biomass conversion processes. In contrast, the application of solid acid catalysts would not only overcome the above problems but would also allow for greater control over the strength and types of the acidity or basicity, which in turn would improve selectivity to the target products. The production of sugars such as glucose, fructose, and xylose offers a platform for the production of many valuable bulk and fine chemicals using heterogeneous acid or basic catalysts. This chapter will survey the development of solid acid and base catalysts for the conversion of carbohydrates (glucose and fructose) and cellulose to platform chemicals using case studies of the hydrolysis of cellulose to glucose, production of 5-HMF from the isomerization and dehydration of glucose, and the Fischer glycosidation of cellulose to alkyl glycosides.

6.2 Catalytic Conversion of Fructose and Glucose Over Solid Acid or Base Catalysts

Hexoses, such as fructose and glucose, possess multiple hydroxyl groups and are considered to be a very promising biomass resource for the synthesis of fine, bulk, and platform chemicals in place of traditional fossil resources. Many papers have reported on the conversion of sugars over solid acid and base catalysts since 2000, most notably of which are silica-supported sulfonic acid, heteropoly acids, ion-exchanged resins, functionalized zeolites, metal oxides, and carbon-based solid acid catalysts. The progress in development of these catalysts for the dehydration of fructose, isomerization of glucose, and dehydration of glucose will be summarized in the following section.

6.2.1 Dehydration of Fructose into HMF

6.2.1.1 Silica-Based Solid Acid Catalyst

SiO_2 is frequently employed as an “inert” support for syntheses of solid acid and base catalyst, with much interest in the development of ordered mesoporous materials such as SBA-15 attracting much interest for its uniform mesoporous structure with well-defined pore dimensions, high surface area, and excellent hydrothermal

stability. SBA-15 was first synthesized in 1998 by Zhao [16] and has subsequently become very popular in both catalysis and materials research as it is readily functionalized by grafting acidic or basic functional groups to impart catalytic utility.

The synthesis of 3-(Butylthio) propane-1-sulfonic acid (BTPSA)-functionalized SiO_2 catalysts, TAA-A380, and TAA-SBA-15, was reported by Scott et al. [17] using post-grafting and co-condensation methods, respectively, as shown in Fig. 6.1 for TAA-SBA-15. The sulfur loading of the post-grafted synthetic TAA-A380 material was only 0.38 mmol/g, which was much lower than that of TAA-SBA-15 material (2.3 mmol/g). In addition, the functional acidic groups incorporated by co-condensation were found to be more robust under reaction conditions (180 °C) than those by post-grafting. The activities of two materials were investigated for the dehydration of fructose to HMF in biphasic solvent (water–MIBK/2-butanol) with TAA-SBA-15 catalyst found to afford a 74 % selectivity to HMF at 66 % fructose conversion.

Despite being moderately stable, the modified SBA-15 material prepared by co-condensation was found to suffer from collapse of the ordered mesoporous structure and loss of functionality at these elevated temperatures. To overcome these problems [18], an alternative one-pot synthetic route was developed to prepare bifunctional silicas (TESAS-SBA-15 and SSA-SBA-15) with higher functional group loadings using a novel silane (TESAS, 3-((3-(trimethoxysilyl)propyl)thio)propane-1-sulfonic acid). The structure of TESAA is shown in Fig. 6.2.

TESAS-SBA-15 and SSA-SBA-15 have perfect 2D ordered hexagonal mesoporous structure with an average diameter of 4.7 nm, the morphology of which is shown in Fig. 6.3. These two functionalized SBA-15 catalysts have high acidic functional group loadings of 1.25 mmol/g and 0.82 mmol/g in the TESAS-SBA-15 and SSA-SBA-15 catalysts, respectively. Reaction at 130 °C in water–MIBK/2-butanol gave fructose conversions and selectivity to HMF as high as 84 % and 71 % over TESAS-SBA-15 catalyst, while an 81 % fructose conversion and 65 % selectivity to HMF were obtained over SSA-SBA-15, both of which were higher than for a commercial Amberlyst-70 catalyst.

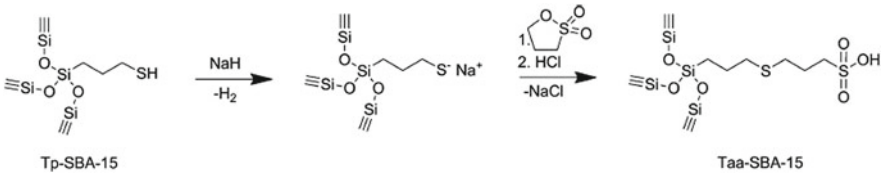

Fig. 6.1 Proposed synthetic scheme for a bifunctional acid catalyst supported on silica (Reprinted from ref. [17], with kind permission from Springer Science+Business Media)

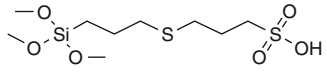

Fig. 6.2 The molecular structure of TESAS (3-((3-(trimethoxysilyl)-propyl)-thio)-propane-1-sulfonic acid) (Reprinted from ref. [18], with kind permission from American Chemical Society)

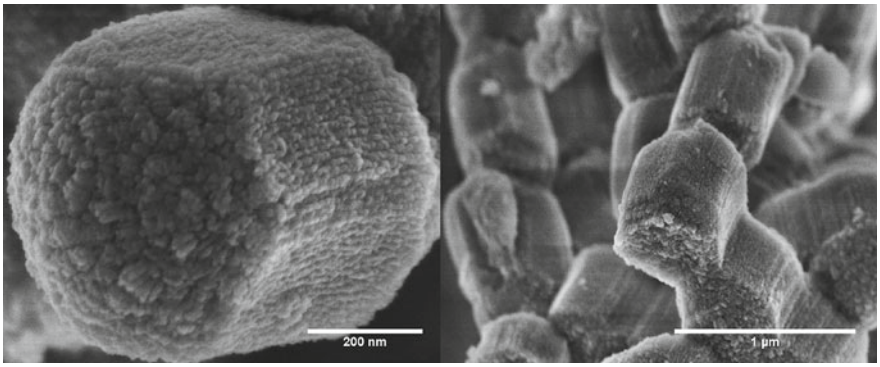

Fig. 6.3 SEM images of TESAS-SBA-15 (Reprinted from ref. [18], with kind permission from American Chemical Society)

The choice of solvent is crucial for the selective conversion of fructose into HMF; thus Mu et al. [19] explored the application of BMIMCl ionic liquid instead of using conventional organic solvents or water, with mesoporous SBA-15-SO_3H catalysts prepared by conventional one-pot routes with varying MPTMS loadings. As expected, sulfonic acid SBA-15 exhibited a high activity and HMF selectivity in BMIMCl at 120 °C, with an 81 % yield of HMF observed at 99 % fructose conversion when using SBA-15-SO_3H-10 catalysts (where 10 represented the MPTMS–(TEOS + MPTMS) ratio). Unfortunately, the SBA-15-SO_3H showed poor stability in the BMIMCl solvent, with activity decreasing steadily over four recycled runs.

As mentioned above, the hydrothermal stability of mesoporous SBA-SO_3H is a problem at elevated temperatures, which is generally attributed to the solvation of –SO_3H sites in water. The use of framework-substituted periodic mesoporous organosilicas (PMOs) synthesized by condensation of organic-linker-bridged disilanes, $(RO)_3Si–R–Si(OR)_3$, is proposed as a route to improve the hydrothermally stability of mesoporous silicas [20, 21]. Dumesic and coworkers [22] prepared two propylsulfonic acid-functionalized ethane-bridged PMOs (where E90 and E45 represent the mol % bridged silane incorporated) with SBA-15-type structures via traditional co-condensation method with different contents of BTME (1,2-bis(trimethoxysilyl)-ethane) in the hybrid organic–inorganic framework. E90 and E45 have typical hexagonal ordered mesoporous structure, high surface area (548 and 559 m^2/g), and well-defined mesoporosity having diameters of 4.2 nm and 4.5 nm. When evaluated in a continuous tubular reactor for the dehydration of fructose at 130 °C, all these ordered mesoporous catalysts (E0, E45, and E90) showed much higher activities and stabilities than commercial materials, with the initial fructose conversion >80 % and 65–75 % HMF selectivity. E0, E45, and E90 catalysts were found to be more stable than commercial silica-supported propylsulfonic acid catalysts, with the selectivity to HMF remaining at >60 %, even after 24 h reaction at 130 °C in steam. Interestingly, E45 had much lower deactivation rate constants (0.032 h^{-1}) than E90 (0.053 h^{-1}), which indicated that E45 had a better stability than E90.

Further improvements in HMF selectivity during fructose dehydration are often reported for biphasic systems in which the produced HMF could be removed immediately from the reactive aqueous phase, thus minimizing side reactions and over-conversion to levulinic acid and formic acid. Jérôme et al. [23] explored sulfonic acid-functionalized periodic mesoporous organosilica (PMO) materials for the dehydration of fructose using such an approach. The synthetic route of the materials was shown in Fig. 6.4, with catalysts possessing a high acid functional loading varying from 0.25 to 1.11 mmol/g. PMO-1 c catalyst with 0.36 mmol/g H^+ sites produced the highest TOF (945 h^{-1}) for fructose dehydration in water–MIBK/2-butanol at 160 °C. Jérôme et al. attributed the highest activity to a combination of: (1) phenyl rings on the pore wall creating a micro hydrophobic environment which prevents the solvation of sulfonic sites by water, (2) improved anchorage of sulfonic sites on a propyl chain, and (3) a moderate sulfonic site loading. Overall PMO materials offer improved stability than Amberlyst-15 or purely siliceous acid-functionalized materials such as SBA-SO_3H and are promising materials for selectively converting fructose to 5-HMF.

The stability and the activity of mesoporous SBA-15-type catalysts have been studied in detail by Hensen et al. [24] who compared sulfonic acid-modified mesoporous SBA-15-type silica and hybrid organosilica catalysts via the co-condensation and grafting functionalization methods. Sulfur leaching was examined by treatment at 120 °C under hydrothermal condition for 7 days which revealed that the sulfonic functional groups on the co-condensed materials were much more stable than those on post-grafted synthetic materials. However, the fructose conversion and HMF selectivity obtained over these catalysts in aqueous solvent were quite low but could be improved significantly by the addition of DMSO solvent. The highest activity

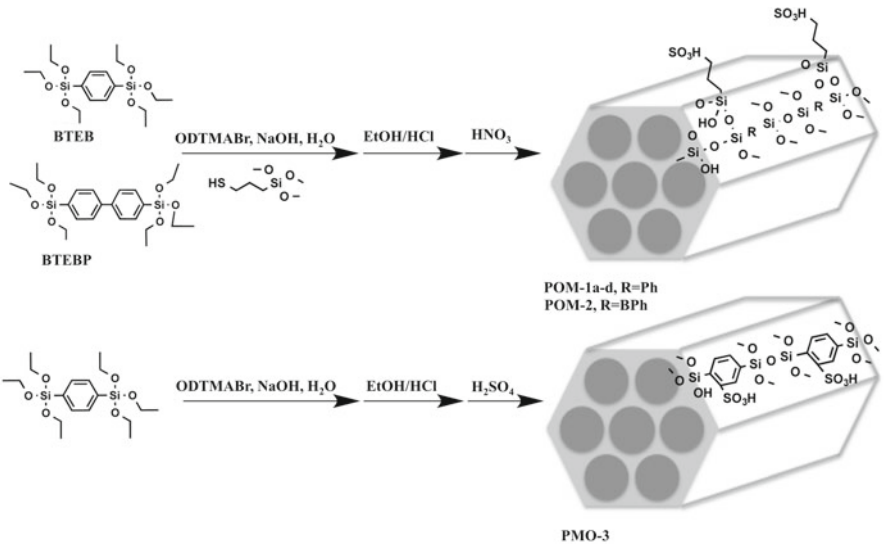

Fig. 6.4 Schematic representation of sulfonic acid-functionalized PMO materials (Reprinted from ref. [23], with kind permission from the Royal Society of Chemistry)

was observed over the co-condensed hybrid organosilica-based catalyst SBA-C_2Ph, which gave an 88 % yield of HMF at 99 % fructose conversion.

Other mesoporous solid acids derived from SBA-15 were prepared by Chilukuri et al. [25] who designed a series of mesoporous aluminum-incorporated SBA-15 catalysts (AlSBA-15) by post-synthesis methods. The loading of acid sites of the AlSBA-15 could be increased with Al content over the range 0.147–0.267 mmol/g. However, when high loadings of Al were incorporated (the ratio of Si/Al over 10), there was an increase in octahedral coordinated Al^{3+} species rather than desired tetrahedral coordinated sites and an increase in non-framework Al species. According to the literature [26–29], only the tetrahedral Al sites introduce Brønsted acidity, which is required for selectivity dehydration of fructose into HMF. Non-framework aluminum cations were suggested to direct the formation of humins from the carbohydrate and furan compounds. This is clearly demonstrated for Al-SBA15 (Si/Al = 40) which exhibited a high selectivity to HMF (89 %) but with a lowest fructose conversion (59 %), whereas Al-SBA15 (Si/Al = 10) having the higher non-framework Al, exhibited the lowest selectivity to HMF (59 %) but with a highest fructose conversion (68 %).

In order to readily separate the solid catalyst and minimize handling losses, Fu et al. [30] prepared a novel magnetic SBA-15-SO_3H material by incorporating magnetic Fe_3O_4 nanoparticles into the mesoporous SiO_2 wall. The average pore diameter of Fe_3O_4–SBA–SO_3H was 4.8 nm, the average pore volume was 0.49 $cm^3\ g^{-1}$, and the BET surface area was 464 m^2g^{-1}. Owing to the above properties, the magnetic Fe_3O_4–SBA-15–SO_3H catalyst exhibited a good activity together with K-OMS-2 catalyst (oxidation catalyst) for the one-pot conversion of fructose into 2, 5-diformylfuran, with an 80 % yield of 2, 5-diformylfuran obtained at 99 % fructose conversion.

A Nafion resin-modified mesocellular silica foam catalyst has also been developed for the dehydration of fructose [31], which was prepared by impregnating Nafion solution onto a mesocellular silica foam, which had well-defined ultra-large mesopores connected with uniformly sized windows. The parent MCF has a large BET surface area of 323 m^2/g which decreased to 298 m^2/g after loading 15 wt.% Nafion. The strong acidity of Nafion and ultra-large mesopores of MCF were beneficial for both the dehydration of fructose and the transformation of the organic molecule. TEM images of mesocellular silica foam and Nafion-modified mesocellular silica foam are shown in Fig. 6.5. Comparison of Nafion/MCF with other solid acid catalysts such as Amberlyst-15, SO_4^{2-}/ZrO_2, and SAC-13 for the catalytic dehydration of fructose in DMSO revealed the high yields (89.3 %) and selectivity (95 %) of HMF to be observed at 90 °C. This is despite Nafion(15)/MCF having a lower acid density (0.142 mmol/g) compared to Amberlyst-15 (3.897 mmol/g) and SO_4^{2-}/ZrO_2 (0.339 mmol/g), suggesting there is an improvement in acid site accessibility imparted from the MCF support. In addition, the stability of this material was examined by recycling for five runs, with only a slight decrease of activity (≈6 %) observed. While clear enhancements in HMF selectivity are achieved using non-protic solvents such as DMSO, the practical application of this solvent for large-scale operation is however questionable, and efforts to avoid such harmful solvents should be encouraged.

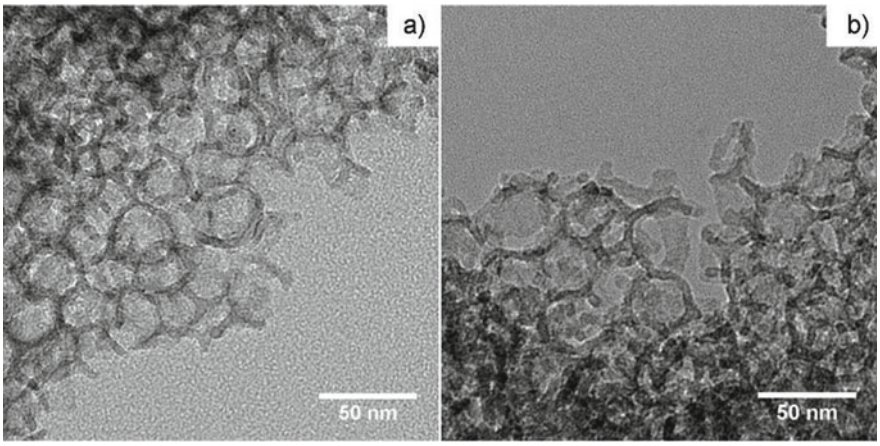

Fig. 6.5 TEM images of (**a**) MCF and (**b**) Nafion(15)/MCF (Reprinted from ref. [31], with kind permission from John Wiley & Sons Ltd)

6.2.1.2 Carbon-Based Solid Acid Catalysts

Compared to SiO_2, carbon-based materials have a higher hydrothermal stability owing to their robust carbon framework. Carbon-based solid acid catalysts are typically prepared by sulfonation of carbon materials with concentrated sulfonic acid at high temperature, which is a corrosive and energy-intensive process. In light of this, Wang et al. [32] developed a facile and eco-friendly approach for preparation of carbon-based solid acid (Glu–TsOH) from glucose and p-toluene sulfonic acid (TsOH). The resulting carbonaceous solid acid Glu–TsOH has a high acid density (2.0 mmol/g) comprising a few strong-acid sites and lots of weak to moderate acid sites, which represents a lower density of –OH groups (0.1 mmol/g) but a higher density of $–SO_3H$ groups (1.3 mmol/g) and –COOH groups (0.6 mmol/g) than the reference material AC–SO_3H. For the dehydration of fructose to HMF in DMSO as solvent, Glu–TsOH exhibited an excellent catalytic performance with an HMF yield as high as 91.2 % at >99 % fructose conversion achieved at 130 °C, which was considerably higher than for AC–SO_3H, H-BEA zeolite, and even Amberlyst-15. Wang et al. attributed this performance to the synergic effect between carboxylic acid groups for the adsorption/orientation of fructose and sulfonic acid groups for the dehydration step. Glu–TsOH also showed a good reusability under the reaction conditions with the conversion kept constant at >99 %, and the selectivity to HMF remained around 90 % over five recycles.

To further probe such effects, Qi et al. [33] prepared two kinds of carbonaceous catalysts functionalized with $–SO_3H$, –COOH, and phenolic –OH groups by incomplete hydrothermal carbonization of cellulose, followed either by sulfonation with H_2SO_4 (CSS) or by chemical activation with KOH and subsequent sulfonation (A-CSS). Through pretreatment with KOH, the surface morphology of CS changes drastically, as shown in Fig. 6.6, with the A-CSS material found to have increased

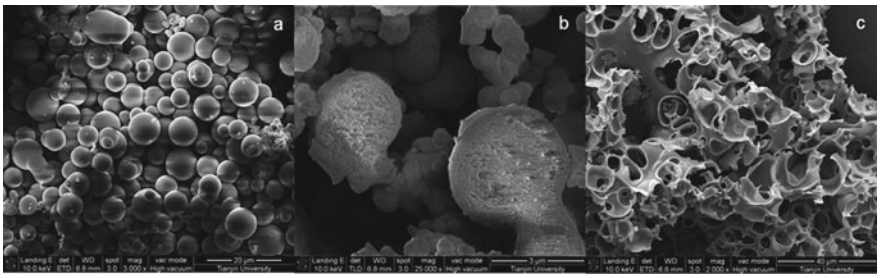

Fig. 6.6 Typical SEM images of carbon materials obtained by hydrothermal treatment of cellulose: (**a**) product without posttreatment, carbonaceous solid (CS); (**b**) product with H_2SO_4 posttreatment, carbonaceous sulfonated solid (CSS); and (**c**) product with KOH and H_2SO_4 posttreatment, activated carbonaceous sulfonated solid (A-CSS) (Reprinted from ref. [33], with kind permission from John Wiley & Sons Ltd)

surface area of 514 m^2/g compared to only <0.5 m^2/g for CSS. However, despite this, the loading of $–SO_3H$ groups on the A-CSS material was quite low (0.172 mmol/g) compared to that of the CSS material (0.953 mmol/g), which led to CSS exhibiting superior conversion of fructose into HMF. An 83 % yield of 5-HMF yield could be obtained at 80 °C for CSS materials using [BMIM][Cl] ionic liquid as the solvent. The CSS material also exhibited a good reusability, which could be recycled at least five times in this ionic liquid reaction system without any obvious deactivation.

The carbonaceous materials derived from incomplete carbonization of biomass usually have amorphous structures, low BET surface, and disordered pores which are readily destroyed by sulfonation treatment at high temperature [33–36]. To overcome this limitation CMK-3 has been developed as an ordered mesoporous carbon material which has a large surface area and excellent accessibility of substrates to the active sites within the well-defined mesopores of the carbon materials. Ma et al. [37] selected the ordered mesoporous carbon materials such as CNTs, carbon nanofibers (CNFs), and hexagonal tube like CMK-5 as supports to prepare a series of sulfonic acid-functionalized carbon materials ($C–SO_3H$), such as poly (p-styrenesulfonic acid)-grafted carbon nanotubes (CNT-PSSA), poly(p-styrenesulfonic acid)-grafted carbon nanofibers (CNF-PSSA), benzene sulfonic acid-grafted CMK-5 (CMK-5-BSA), and benzene sulfonic acid-grafted carbon nanotubes (CNT-BSA). The loadings of $–SO_3H$ group of the above four $C–SO_3H$ materials were in the order 5.67, 4.26, 2.89, and 1.75 mmol/g, with the acid strength found to increase with $–SO_3H$ loading. The activities of the four $C–SO_3H$ materials were investigated in the catalytic conversion of fructose into HMF in DMSO solvent which showed the activity of $C–SO_3H$ materials was dependent on the sulfonic acid density. The highest yield of HMF (89 %) was obtained over CNT-PSSA catalyst at 120 °C, higher than that of commercial Amberlyst-15. In contrast, the HMF yield was only 69 % over CNT-BSA due to its lower sulfonic acid loading (1.75 mmol/g). The application of these $C–SO_3H$ catalysts was also explored for one-pot conversion of fructose into alkyl levulinate in alcohol solvent at 120 °C. While an 86 %

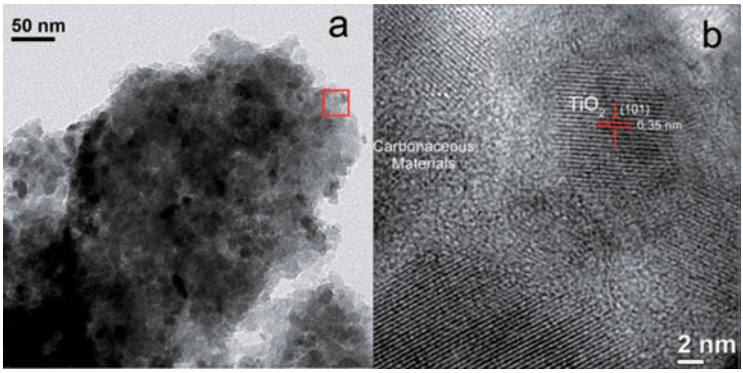

Fig. 6.7 (**a**) HRTEM images of Glu–TsOH–Ti that show its nanostructure and (**b**) a magnified view of this nanostructure that shows the lattice fringes of TiO_2 (Reprinted from ref. [38], with kind permission from John Wiley & Sons Ltd)

yield of alkyl levulinate was obtained over the CNT-PSSA catalyst, the reusability of CNT-PSSA was poor with activity gradually decreasing in five recycles.

In addition to pure carbon catalysts [38], porous sulfonated carbonaceous TiO_2 materials have also been investigated (Glu–TsOH–Ti), which were prepared by the thermal treatment of TsOH, glucose, and titanium (IV) isopropoxide at 180 °C to generate materials with BET surface area of 42.5 m^2/g and average pore size of 4.5 nm (Fig. 6.7). These materials contain both Brønsted acid and Lewis acid sites, having a Brønsted–Lewis acid sites ratio of 1.2 and total acid site density 1.03 mmol/g (evaluated by NH_3 temperature-programmed desorption) lower than that of Glu–TsOH catalyst (2.0 mmol/g evaluated by titration). The catalysts were evaluated in the dehydration of fructose, for which a 60 % yield of HMF can be obtained in MeTHF/H_2O biphasic solvent at 180 °C. Glu–TsOH–Ti was also able to operate as a bifunctional catalyst for the dehydration of glucose to HMF with a 38 % yield of HMF obtained at 200 °C. While these results are promising, some care must be taken when operating at such elevated temperatures (>150 °C) which inevitably lead to large quantities of humins being formed in aqueous media.

6.2.1.3 Zeolite-Based Solid Acid Catalysts

Zeolites are widely used for solid acid- or base-catalyzed transformations by the petrochemical industry. Due to its uniform pore structure, controlled acid and base active sites, and tunable acidic or basic character, they were considered to be promising monofunctional or bifunctional solid catalysts for conversion of carbohydrate into platform molecules.

Moreau et al. [39] studied the selective dehydration of fructose to HMF over microporous H-type zeolites, including H-Y faujasites, H-mordenites, H-beta, and H-ZSM-5 at 165 °C in a mixed solvent of water and MIBK. It was found that the

fructose conversion and selectivity to HMF were closely dependent on the acidic property and pore structure. While for H-Y faujasites and H-mordenites, the conversion of fructose increased with changing the Si/Al ratio from 15 to 11, the selectivity to HMF decreased with increasing Si/Al ratio due to strong-acid sites promoting secondary reactions of HMF to form formic and levulinic acids or even humins. In addition to the acidic properties, the structure of zeolites also has an impact on HMF selectivity. The bidimensional channel structure in H-mordenites showed preferable shape selective to 5-hydroxymethylfurfural compared to tridimensional channel structure in H-Y faujasites, H-beta, and H-ZSM-5. A particularly high selectivity (>90–95 %) to 5-hydroxymethylfurfural was reported over H-mordenites, which was correlated with the shape-selective properties.

Subsequently, Moreau et al. [40] investigated the activities of a series of dealuminated H-mordenites for the dehydration of fructose into HMF in mixed water/MIBK solvent at 165 °C. Fructose conversion and HMF selectivity were closely dependent on not only the acidic properties and structural properties but also micropore vs. mesopore volume distribution. As shown in Fig. 6.8, relatively low selectivity to HMF was observed over the dealuminated H-mordenite catalyst with higher mesoporous volume, which was probably because the formation of hydronium species within mesopores causes the further degradation of HMF. Overall, a 92 % selectivity to 5-hydroxymethylfurfural at 54 % fructose conversion was obtained over H-mordenite with a Si/A1 ratio of 11. By prolonging the reaction time to 60 min, the selectivity remained at 91 % but with a higher fructose conversion of 76 %.

Cation-exchanged montmorillonite K-10 clay [41] with a series of cations (Cr^{3+}, Al^{3+}, Zn^{2+}, Cu^{2+}, and Fe^{3+}) have also been explored for the conversion of carbohydrates into HMF. Chromium-exchanged K-10 clay (K-10 clay-Cr) was found to be the best catalyst for fructose dehydration, with a high HMF yield of ~95 % reported in either DMSO or [BMIM]Cl solvent at 120 °C. In addition cation-exchanged [42] K-10 clay-supported dodecatungstophosphoric acid catalyst (K-10 clay-HPW) was utilized for the one-pot conversion of fructose to EMF by coupling the dehydration of fructose and etherification of HMF with ethanol. Catalyst activity for the

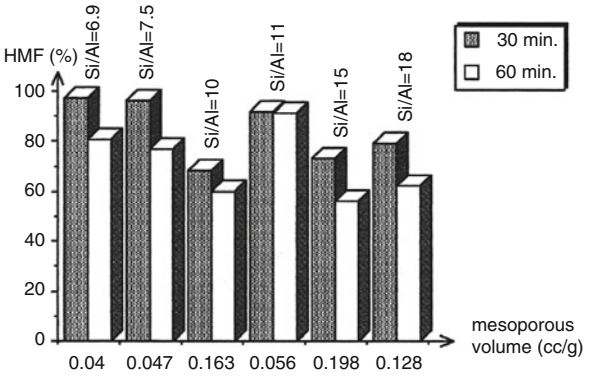

Fig. 6.8 Effect of mesoporous volume on the selectivity to 5-HMF over dealuminated H-mordenites (Reprinted from ref. [40], with kind permission from Elsevier)

production of EMF was found to be dependent on the amount of acid sites, with the highest yield of 61.5 % of EMF from fructose obtained over the 30 wt.% K-10 clay-HPW catalyst at 100 °C following 24 h reaction in ethanol.

H-beta-18 (SiO_2/Al_2O_3 ratio of 18) has also been investigated in the dehydration of fructose [43] and was found to not only catalyze the dehydration of fructose but also catalyze fructose isomerization to glucose as well as decomposition of HMF to formic and levulinic acids. The isomerization between fructose and glucose is mainly caused by octahedral aluminum atoms at lattice defect sites and extra-framework Al atoms, which act as Lewis acid sites. In addition, it was found that some organic acids produced from HMF via rehydration would contribute to the leaching of aluminosilicate species from the zeolite. Unfortunately, the dissolved aluminosilicate species promoted some undesired side reactions.

When water is used as the solvent, the yield and selectivity of HMF from fructose are often quite low as there are competing side reactions, notable of the rehydration of fructose over the hydrophilic acid sites. Nijhuis et al. [44] studied the effect of organic solvent addition on the dehydration of fructose over zeolite catalysts, including MOR, ZSM-5, BEA, and amorphous aluminosilicate. Among them, MOR zeolite exhibited the highest selectivity, with the addition of MIBK significantly increasing the initial selectivity of HMF. It was hypothesized that MIBK fills the zeolite pores, interacting strongly with the acid sites, which helps with the displacement of reactively formed HMF from the zeolite surface, preventing further oligomerization. Silylated zeolite catalysts were also investigated, which afforded an increased selectivity at higher conversion in a biphasic system due to the deactivation of unselective external acid sites for fructose conversion.

The catalytic behaviors of zeolite catalysts for the conversion of fructose to HMF have been studied widely in water solvent or organic-water mixed solvents. Although some zeolites, such as H-mordenites and H-Y faujasites, showed a high selectivity to HMF (>90 %), potential structural collapse of zeolites has to be considered when these materials are used for aqueous-phase conversion of biomass. Lercher et al. have studied the stability of zeolites including different kinds of zeolites Y and ZSM-5 in hot water (150–200 °C). The results indicated that the hydrothermal stability of zeolites was strongly dependent on their framework type. ZSM-5 is stable at 150 °C and 200 °C, whereas the structures of Y typed zeolites are damaged to some extent at the same conditions, which was dependent on the Si/Al ratio. When the Si/Al ratio was increased to 41, zeolite Y was totally transformed into an amorphous structure after hydrothermal treatment at 200 °C for 6 h. The suggested deactivation reason is due to hydrolysis of the siloxane bonds (Si–O–Si) with OH^- from hot water as opposed to dealumination.

6.2.1.4 Ion-Exchange Resin Solid Acid Catalysts

Acidic ion-exchange resin was one of the earliest classes of catalysts to be utilized as a solid acid catalyst for the dehydration of fructose [45, 46], with its strong acidity believed to be beneficial for dehydration of fructose to HMF. High selective

conversions of fructose into HMF with nearly quantitative results with or without ion-exchanged resins have been done.

The dehydration of fructose over Amberlyst-15 [47] was studied by Moreau et al. in two commercially available ionic liquid solvents: a hydrophilic one, 1-butyl 3-methyl imidazolium tetrafluoroborate ($BMIM^+BF_4^-$), and a hydrophobic one, 1-butyl 3-methyl imidazolium hexafluorophosphate ($BMIM^+PF_6^-$). While using the hydrophilic $BMIM^+BF_4^-$ solvent was found to produce a 52 % yield of HMF over Amberlyst-15 at 80 °C, addition of DMSO improved the yield of HMF to 87 %. Similar results were also obtained in $BMIM^+PF_6^-$/DMSO solvent, however, where a yield of HMF slightly lower than 80 % was obtained, suggesting that the hydrophilic properties of $BMIM^+BF_4^-$ solvent were preferable for HMF production over Amberlyst-15.

The use of 1-butyl-3-methyl imidazolium chloride ([BMIM][Cl]) as the solvent was found to give rise to more efficient conversion of fructose to HMF over Amberlyst-15 catalyst [48], with an 83.3 % yield of 5-HMF and a 98.6 % fructose conversion obtained. This activity is superior to that of homogeneous acid catalysts, such as H_3PO_4, HCl, H_2SO_4, and acetic acid as well as $PdCl_2$, under the same conditions. Compared with the above process, this system also remarkably shortened the reaction time while improved the catalytic efficiency. Moreover, this catalytic system (ionic liquid and catalyst) could be reused for seven runs. Satsuma et al. [49] found that decreasing the Amberlyst-15 bead size could further increase the yield of HMF when working in DMSO, with a 100 % yield of HMF that was produced from high fructose concentration (50 wt.% in DMSO) at 120 °C after 4 h using Amberlyst-15 with a bead size of 0.15–0.053 mm. This highlights the problem of accessibility of active sites within ion-exchange resins and the need for catalysts with improved pore architectures that reduce diffusion limitation. In this respect, the use of hierarchical macroporous–mesoporous SBA-15 or pore-expanded SBA-15 sulfonic acid silicas, which are found to be beneficial for improving acid site accessibility for biodiesel synthesis [50, 51], could be of interest to explore.

Water is favored as ecological and green solvent, but unfortunately, the selectivity to HMF from fructose dehydration in water is relatively low due to the high temperatures employed and further conversion to levulinic and formic acid. Moreover, strong-acid resin catalysts are considered to be unstable over 100 °C in water, so in light of this problem, Qi et al. [52] investigated the catalytic dehydration of fructose into 5-HMF in a mixed acetone/water solvent system using a strong-acid cation-exchange resin (Dowex® 50wx8) under microwave heating. A 73.4 % yield of HMF at 95.1 % fructose conversion was obtained at 150 °C with an acetone–H_2O ratio of 7:3. Although the yield of HMF obtained in the acetone/water cosolvent was satisfactory, the existence of water (30 %) still resulted in the degradation of HMF to levulinic and formic acid with increasing reaction time. By replacing H_2O with DMSO so an acetone/DMSO (70:30) biphasic solvent was employed, Qi et al. [53] was able to increase the yield of HMF to 89.8 % with 97.9 % of fructose conversion. Even with a high fructose concentration (10 wt.%), an 83.2 % yield of HMF with 99 % fructose conversion could be maintained.

Despite all the interest in the application of ion-exchange resins in fructose or glucose conversion, few studies seek to correlate the physicochemical properties of ion-exchange resins with their catalytic activities. Han et al. [54] reported on one such study which explored the effects of porosity and acid strength in ionic liquid solvent by employing three different types of ion-exchange resin: a macroporous strong-acid resin, a macroporous weak-acid resin, and a gel strong-acid resin. [BMIM]Cl ionic liquid proved to be the preferred solvent for dehydration of fructose compared with other ILs, because Cl^- can form stronger hydrogen bonds with fructose. In [BMIM]Cl ionic liquid, the macroporous strong-acid resin (D001-cc) exhibited the best catalytic activity for fructose dehydration with a 93.0 % yield of HMF obtained at 75 °C. From these screening results, it was concluded that ion-exchange resins having high surface area, strong acidity, and a large number of macropores were preferential for the efficient production of HMF from fructose.

A comparison of batch and continuous production of HMF from fructose was undertaken by Hermans et al. [55] using Amberlyst-15 to obtain kinetic parameters of the dehydration of fructose. In the batch reactor at 100 °C, the yield of HMF can be up to 75 % when working 1,4-dioxane solvent with a small addition of DMSO. For the batch reactor, the HMF product will undergo consecutive dehydration and/or polymerization reactions due to the high residence time (180 min), resulting in a decreased selectivity with increasing conversion. However, the side reaction could be inhibited in continuous flow conditions by lowing the residence time. As expected, in the continuous fix-bed reactor, the yield of HMF was enhanced to 92 % at 110 °C (only 3 min residence times) and with at least 96 h of catalyst life.

6.2.1.5 Ionic Liquid-Based Solid Acid Catalysts

Ionic liquids are considered as promising catalysts and solvents for the conversion of fructose into HMF. However, as a solvent, the amount of ionic liquid employed is often high, which would have an important impact on the economic cost. Moreover, homogeneous catalysts have obviously process limitations, such as corrosive nature, difficult separation, recovery, and isolation of HMF requiring use of ion-exchange resins to recover the ionic liquid [56]. In view of these issues, the development of heterogeneous supported ionic liquid catalysts has also attracted interest for the production of HMF.

Yokoyama et al. [57] prepared silica gel-immobilized acidic ionic liquid catalysts – ILIS-SO_3H (Brønsted acid) and ILIS-SO_2Cl (Lewis acid) – as shown in Fig. 6.9 which afforded a 70 % and 67 % yield of HMF at 100 % of fructose conversion in DMSO under microwave irradiation for 4 min.

Sidhpuria et al. [58] also developed a new class of silica-immobilized acidic ionic liquids that were prepared on nano-sized amorphous silica-immobilized sulfated ionic liquid 1-(tri-ethoxy silyl-propyl)-3-methyl-imidazolium hydrogen sulfate (IL-HSO4) by grafting method, as shown in Fig. 6.10. Catalysts with different particle sizes (214–504 nm) and IL loading were prepared, with >60 % yield of HMF obtained at 99.9 % fructose conversion that can be obtained over these SILnP

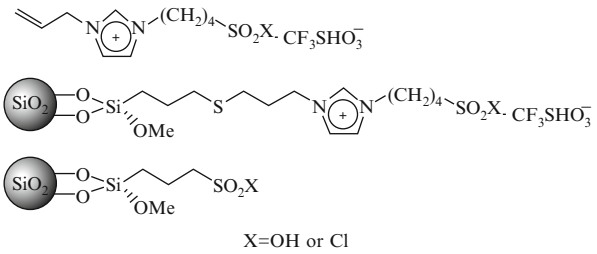

Fig. 6.9 The structure of the SiO_2-supported acidic ionic liquid catalysts (Reprinted from ref. [57], with kind permission from Elsevier)

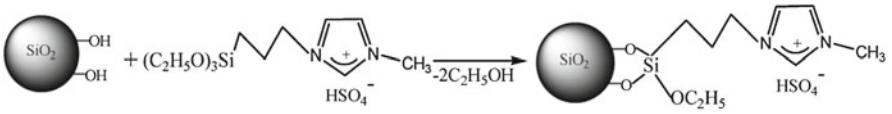

Fig. 6.10 Synthetic route of 1-(tri-ethoxy silyl-propyl)-3-methyl-imidazolium hydrogen sulfate (IL-HSO4) immobilization on silica nanoparticles (Reprinted from ref. [58], with kind permission from the Royal Society of Chemistry)

catalysts in DMSO at 130 °C for 30 min. When less catalyst (20.0 mg) was used, the fructose conversion and HMF yield was found to increase with the size of the silica nanoparticles, which may be a reflection of variation in IL loading. The bigger particles were found to result in higher IL-HSO_4 loadings. Under the same reaction, their performances were more competitive than H-form of Na(H)-ZSM-5, Na-β zeolites, and SiO_2–SO_3H. Most importantly, SILnP catalysts also exhibited a good reusability for this reaction, with no leaching of the ionic liquid and deactivation that were observed on Si-3-IL-HSO_4 in seven repeat reactions.

In addition to monofunctionalized catalysts, Wu et al. [59] developed a bifunctional material comprising both sulfonic acid (HSO_3) and ionic liquid (ILs) functionality on mesoporous SiO_2 nanoparticles. Using DMSO as the solvent, it produced a 72.5 % yield of HMF with a 97 % fructose conversion. Recycling tests indicated that this bifunctional catalyst could be reused four times without any deactivation; unfortunately, in the fifth run, some activity loss was observed, which indicated the stability of this material is still a problem.

Zhang et al. [60] developed a novel material based upon a polypropylene fiber (PPF)-supported pyridinium ionic liquid (PPFPy-IL) using a three-step preparation of: (1) grafting of 4-vinylpyridine (4-VP), (2) surface reaction with 1,3-propanesultone, and (3) acidification with various acids. The SEM images of these materials are shown in Fig. 6.11. FT-IR and elemental analyses indicated that ~4 wt.% sulfonic functional groups could be successfully attached to the PPF surface. Among the various PPFPy-ILs derivatized with different acid functionalities, [PPFPy][HSO_4] was shown to be the best catalyst for HMF production giving 86.2 % yield when working in DMSO at 100 °C. The reusability of [PPFPy][HSO_4] also showed excellent recyclability with the HMF yield maintained around 83 % over ten cycles with no apparent deactivation.

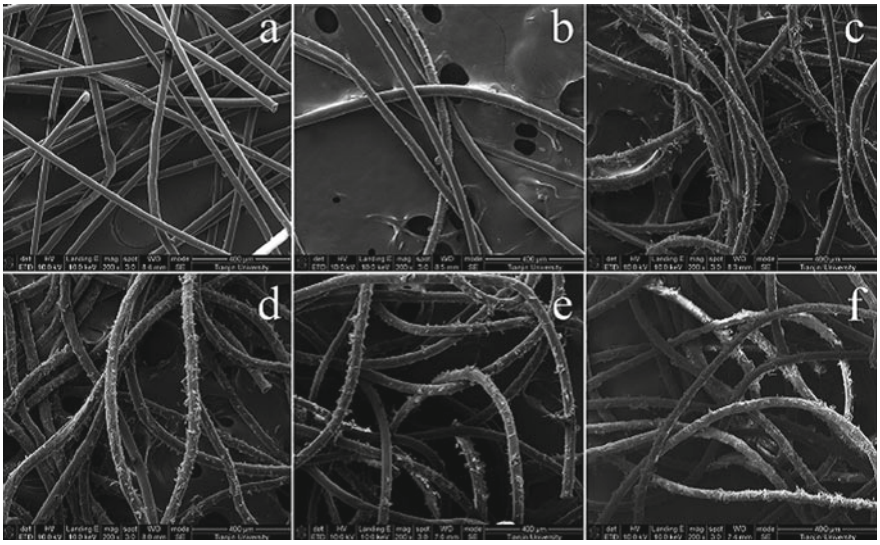

Fig. 6.11 SEM images of (**a**) p-PPF, (**b**) PPF-Py, (**c**) PPF-Py-Ps, (**d**) [PPFPy][HSO4], (**e**) [PPFPy][HSO4]-1, and (**f**) [PPFPy][HSO4]-10 (Reprinted from ref. [60], with kind permission from the Royal Society of Chemistry)

Given the apparent success of ionic derivatized ionic polymers for the dehydration of fructose [61], Yang et al. [62] synthesized two types of SO_3H-functionalized polymeric ionic liquids which were acidified with $H_3PW_{12}O_{40}$ and HCl (FPIL1a and 1b). Both FPIL1a and 1b catalyst types exhibited high activity for the dehydration of fructose to HMF in DMSO with HMF yields of 88–91 % reported at ~98 % fructose conversion.

6.2.1.6 Metal Oxide-Based Solid Acid Catalyst

Metal oxides and mixed oxide catalysts with controlled acidity and basicity as well as a high density of surface oxygen vacancies find wide application as catalysts or supports for oxidation, dehydrogenation, and polymerization reactions. Recently, more and more researchers involved in such materials have explored their application for the catalytic conversion of biomass and in particular the dehydration of fructose.

TiO_2 (anatase or rutile) and m/c-ZrO_2 are the most two common metal oxides catalysts which possess controlled bifunctional active sites with acidic and basic character. In 2005, Watanabe et al. [63] studied the effects of TiO_2 (anatase or rutile) and m/c-ZrO_2 on the conversion of glucose and fructose to HMF in hot-compressed water (200 °C and 2.5 MPa) in a batch reactor. Under these conditions, TiO_2 was found to enhance the yield of HMF from fructose compared with the blank reaction. In contrast m/c-ZrO_2 was found to inhibit the background rate of HMF formation

due to the high loading of base sites over m/c-ZrO_2 catalysts (550 μmol/g, according to CO_2-TPD characterization) leading base-catalyzed transformation of fructose to side products.

Hot-compressed water is a particularly harsh condition, which is sufficiently acidic to facilitate the rapid rehydration of HMF; thus Watanabe et al. [64] chose to study the conversion of fructose and glucose to HMF under microwave irradiation in place of a traditional sand bath to improve the heating and cooling efficiency of the reaction. In contrast to conventional heating, HMF yields were found to be enhanced under microwave irradiation (200 °C for 5 min) over both anatase TiO_2 and ZrO_2 catalysts. A 38 % yield of HMF at 83.6 % fructose conversion was obtained over anatase TiO_2 while a 30.6 % yield of 5-HMF with a fructose conversion of 65.3 % was obtained in the presence of ZrO_2. If the reaction time for the TiO_2 catalyst was increased to 10 min, the fructose conversion was as high as 90.4 % while the yield of HMF rose to 41.2 %. Thus it was confirmed that microwave irradiation could efficiently promote the production of HMF from fructose.

Fedie et al. [65] designed a fixed-bed reactor (Fig. 6.12) for the continuous production of 5-hydroxymethylfurfural (HMF) from sugars such as fructose, glucose, sucrose, and starch over metal oxides including spherical, porous ZrO_2 and TiO_2. An 18 % yield of HMF was obtained from a 23 % aqueous solution of fructose using the TiO_2 catalyst at 200 °C in 3 min contact time with extraction of n-BuOH (the ratio of n-BuOH/H_2O was 1:3). Compared with ionic liquids, hot-compressed

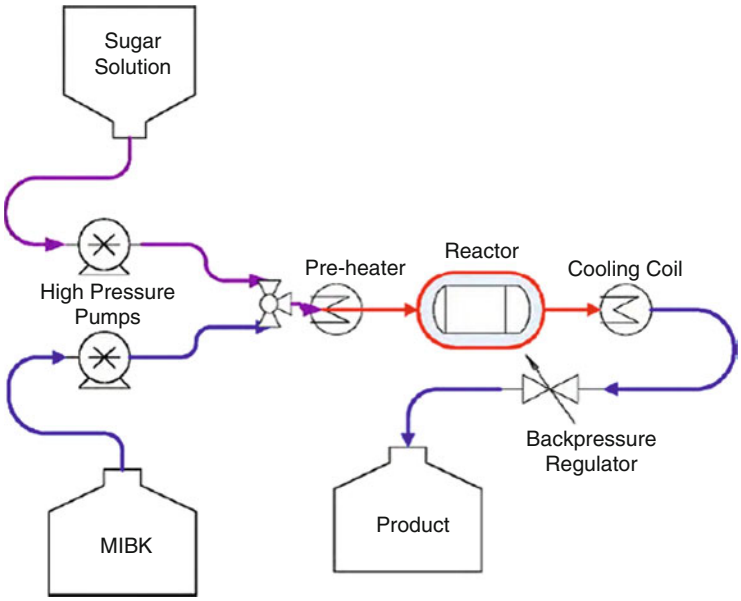

Fig. 6.12 Diagram of a continuous flow system for the production of HMF from simple and complex carbohydrates (*MIBK* methyl isobutyl ketone) (Reprinted from ref. [65], with kind permission from Elsevier)

water is a very harsh condition for selective production of HMF from fructose, because of the instability of fructose and HMF in 200 °C water. When the conversion of fructose proceeds in the ionic liquid solvent, it does so not only under relatively low temperature (<120 °C) in a strong polar environment. This offers excellent capability for dehydration of sugar molecules, largely avoiding the production of by-products even after long reaction time, thereby giving significantly higher yields of HMF.

SO_4^{2-}/ZrO_2 and SO_4^{2-}/ZrO_2–Al_2O_3 catalysts, which are considered to be traditional super strong solid acid catalysts, have also been explored for the dehydration of fructose into HMF. Hu et al. [66] prepared SO_4^{2-}/ZrO_2 (CSZ) and SO_4^{2-}/ZrO_2–Al_2O_3 (CSZA) catalysts by impregnation of $Zr(OH)_4$ and $Zr(OH)_4$–$Al(OH)_3$ with an ethylene dichloride solution of chlorosulfonic acid. The CSZA is a typically amphoteric catalyst, containing both acid sites and Lewis basic sites. With increasing of Al content, the amount of acid sites decreased while the amount of base sites increased. The production of HMF from fructose was found to be closely dependent on the amount of acid sites, with a 68.2 % yield of HMF observed at 100 % fructose conversion over the CSZ catalyst in DMSO.

Although DMSO was the best organic solvent for dehydration of fructose to HMF, its high boiling caused the separation of HMF to be more difficult. Therefore, Qi et al. [67] also tested the SO_4^{2-}/ZrO_2 catalyst in a low-boiling mixture of DMSO/acetone as well as water with microwave heating. The SO_4^{2-}/ZrO_2 catalyst was prepared by sulfation of zirconium hydroxide with H_2SO_4 solution and then calcination at high temperature (500, 600, and 700 °C) for 3 h. In the aqueous phase, SO_4^{2-}/ZrO_2 catalysts were reported to show a lower activity for HMF production than untreated ZrO_2 catalysts, whereas in nonaqueous DMSO/acetone mixed solvent, the activities of SO_4^{2-}/ZrO_2 catalyst were improved dramatically with both the fructose conversion and HMF yield higher than for untreated ZrO_2. The highest HMF yield obtained was 72.8 % at 93.6 % fructose conversion at 180 °C after 20 min reaction over SO_4^{2-}/ZrO_2.

Although aqueous phase is not an ideal solvent for high yield production of HMF as discussed above, H_2O is a preferable candidate for industrial application because of its low boiling and easily separation; furthermore, sugar solution produced from biomass processing is likely to be obtained in aqueous media. Osatiastiani et al. [68] investigated the catalytic properties and behavior of SO_4^{2-}/ZrO_2 catalysts in H_2O for the dehydration of both glucose and fructose to understand the critical balance of acid and base properties in HMF formation. SO_4^{2-}/ZrO_2 catalysts with submonolayer SO_4 coverages were found to possess an amphoteric surface, with Lewis basicity as well as Lewis and Brønsted acidity. The Brønsted acidity was found to increase with the SO_4, with the ZrO_2 surface found to be covered by monolayer of SO_4 corresponding to a maximum acid density of 0.37 mmol/g. The HMF yield from fructose was found to correlate directly with the concentration of Brønsted acid sites, with the highest HMF yield of 32 % obtained over the 0.8 ML of SO_4/ZrO_2 at only 100 °C. The effect of SO_4^{2-}/ZrO_2 catalyst on the production of HMF from glucose was found to be highly sensitive to acid–base ratio and will be further discussed in Sect. 6.2.3.

Nijhuis et al. [69] conducted a comprehensive study of different heterogeneous acid catalysts, including alumina, aluminosilicate, zirconium phosphate, niobic acid, ion-exchange resin Amberlyst-15, and zeolite MOR in the dehydration of fructose to HMF with and without the presence of an organic cosolvent. The transformation of fructose proceeds over both Brønsted and Lewis acid sites over these heterogeneous catalysts. Notably, the activity in the transformation of fructose was dependent on the acidic strength that followed the sequence: $Nb_2O_5 > ZrPO_4 > Al_2O_3 > SiO_2\text{-}Al_2O_3$. However, the activity over MOR catalyst was lower than others, even though it exhibited a highest acidic strength, which may be explained by serious diffusion limitations for fructose inside the zeolite's narrow pores. Besides that, the selectivity to HMF was found to be closely dependent on the number of Brønsted acid sites, that is, ratio of Brønsted–Lewis acid sites, as shown in Fig. 6.13. The highest selectivity (about 60 %) to HMF was obtained over Amberslyst-15 and MOR, which had the higher ratio of Brønsted/Lewis acid sites (ration >5).

Moreover, the addition of MIBK into the water solvent led to an increase in HMF selectivity over Amberlyst-15, which was ascribed to suppression of the rehydration reaction of HMF and primary fructose condensation with HMF by the acid sites over Amberlyst-15 catalyst. The addition of MIBK means that the produced HMF could be consecutively extracted by MIBK from water during the reaction, avoiding the contact with the active sites. As expected, 73 % of the produced HMF could be extracted into MIBK phase according to the partition ratio (0.9) for HMF between water and MIBK at the reaction temperature. Zirconium phosphate and titanium phosphate are also typical solid acid or base catalysts, which have comparable activity with sulfated zirconia and titania. Carlini et al. [70] investigated the activities of zirconium (titanium) phosphate or pyrophosphate catalysts in the conversion of fructose to HMF (Table 6.2). These catalysts possessed low surface areas in range of 1.5–12 m^2/g. The highest activity (TON = 8.9 and 99.8 % selectivity to HMF) was obtained over C-ZrP_2O_7, which was attributed to strong Lewis acid sites from unsaturated octahedral Zr^{4+} species produced upon thermal treatment at 950 °C and the cubic zirconium-pyrophosphate phase. In addition, the γ-TiP catalyst was also

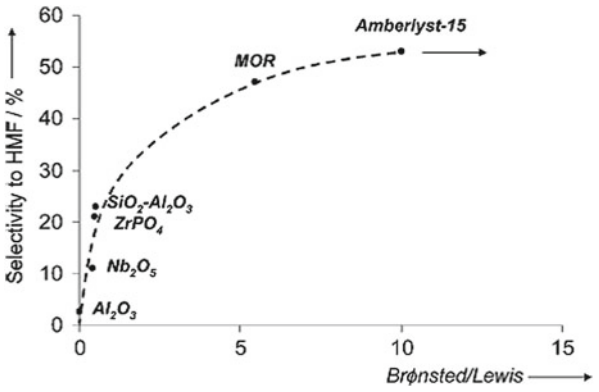

Fig. 6.13 Selectivity towards HMF at fructose conversion of 10 % versus Brønsted/Lewis ratio determined by Py adsorption (Reprinted from ref. [69], with kind permission from John Wiley & Sons Ltd)

Table 6.2 Properties of zirconium and titanium phosphates as well as pyrophosphates

Sample	Structure	Interlayer distance (Å)	Surface area (m^2/g)
α-Zirconium phosphate $(\alpha\text{-ZrP})_{HF}$	$\alpha\text{-Zr(HPO}_4)_2\cdot H_2O$	7.56	1.5
α-Zirconium phosphate $(\alpha\text{-ZrP})_{10/100}$	$\alpha\text{-Zr(HPO}_4)_2\cdot H_2O$	7.56	9.0
Layered α-zirconium-pyrophosphate	$\alpha\text{-L-ZrP}_2O_7$	6.10	10.0
γ-Zirconium phosphate (γ-ZrP)	$\gamma\text{-Zr(PO}_4)(H_2PO_4)\cdot H_2O$	12.20	6.0
Layered γ-zirconium-pyrophosphate	$\gamma\text{-L-ZrP}_2O_7$	9.50	8.0
Cubic zirconium- pyrophosphate	$C\text{-ZrP}_2O_7$	–	12.0
α-Titanium phosphate (α-TiP)10/100	$\alpha\text{-Ti(HPO}_4)\cdot 2H_2O$	7.56	8.7
γ-Titanium phosphate (γ-TiP)	$\gamma\text{-Ti(PO}_4)(H_2PO_4)\cdot 2H_2O$	11.60	4.5
Cubic titanium-pyrophosphate	$C\text{-TiP}_2O_7$	–	10.5

Reprinted from ref. [70], with kind permission from Elsevier

found to afford a high activity (TON = 6.1 and 96.1 % selectivity to HMF), with comparison of all the catalysts suggesting that the yield of HMF was dependent on the Lewis acid strength and ability to prevent formation of levulinic and formic acid.

Although some metal oxides catalysts have showed good performances in selective dehydration of fructose to HMF, there is a need to improve their physical properties such as BET surface area, pore size, and acid site density. Therefore, new types of metal oxide acid or base catalysts with high special surface, stronger acidity (and basicity), as well as high acid site loading have been developed and utilized for the selective dehydration of fructose to HMF.

Saha et al. [71, 72] prepared a series of new types of mesoporous TiO_2 by different methods, including using DL-aspartic acid as template agent to prepare nanoparticulate TiO_2 [71]. This material was comprised of uniform anatase TiO_2 particles with an average particle size ca. 10.6 nm, as shown in Fig. 6.14. Although the BET surface area was only 51.5 m^2g^{-1}, this material showed a high efficiency for HMF production, which was attributed to its strong acidity and high acid site loading (0.27 mmol/g). In biphasic DMA–LiCl solvent, a maximum HMF yield as high as 82.3 % can be obtained at 120 °C under microwave heating with the additive of 20 % [BMIM]Cl. Furthermore, by replacing DL-aspartic acid with a sodium salicylate template, Saha et al. [72] was able to synthesize another type of mesoporous TiO_2 catalyst which was mesoporous and was composed of very tiny uniform spherical nanoparticles (12–20 nm) but has a BET surface area and acidity which were significantly enhanced to 326 m^2/g and 0.4 mmol/g, respectively. A 36 % HMF yield was achieved in aqueous phase over this mesoporous TiO_2 catalyst at 120 °C (microwave heating) which was further enhanced to 54.1 % in the DMSO. Based on above work, Saha et al. considered whether framework acid sites of mesoporous titanium phosphate genuinely play a crucial role for the selective production of HMF by preparation of a hierarchical macro-/mesoporous titanium phosphate catalyst (MTiP-1) [73]. MTiP-1 was a typical amorphous mesoporous material with BET surface area of 193 m^2/g and an average pore dimension of ca. 7 nm. By comparison to other solvents, the highest yield of HMF (44 %) was obtained at 140 °C in

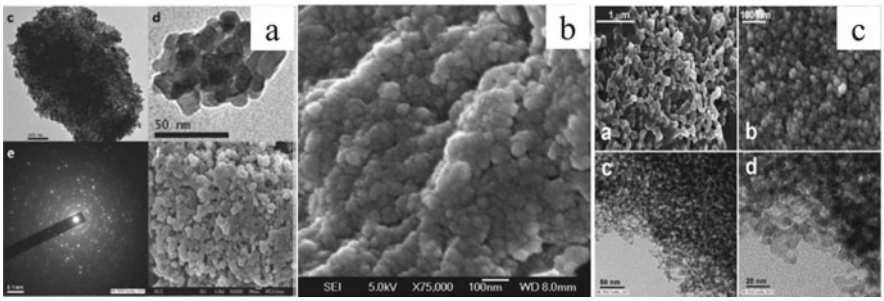

Fig. 6.14 (**a**) (*c*) TEM image of typical TiO_2 nanostructure; (*d*) TEM image of calcined (500 °C) TiO_2 sample; (*e*) selected area electron diffraction (SAED) pattern of the calcined mesoporous TiO_2 sample; (*f*) FE-SEM image of the self-assembled mesoporous TiO_2 nanoparticles (Reprinted from ref. [71], with kind permission from the Royal Society of Chemistry). (**b**) The FE-SEM images of mesoporous TiO_2 nanospheres after first catalytic cycles for the microwave-assisted dehydration of fructose (Reprinted from ref. [72], with kind permission from Elsevier). (**c**) SEM images (*a*) and (*b*) and TEM images (*c*) and (*d*) of MTiP-1 (Reprinted from ref. [73], with kind permission from the Royal Society of Chemistry)

DMA–LiCl solvent. While the mesoporous TiO_2 catalysts could be recycled for at least four cycles without appreciable deactivation, the MTiP-1 catalyst exhibited slight deactivation (about 8 %) in five runs.

Compounds containing niobium are another interesting and important class of catalysts that show excellent activity in many acid-catalyzed reactions in aqueous media. Carlini et al. [74, 75] and Carniti et al. [75] investigated the activities of various niobium-based catalysts for the dehydration of carbohydrate to HMF in both batch reactor and flow reactor, using $Nb_2O_5{\cdot}xH_2O$, H_3PO_4-treated niobic acid and niobium phosphate catalysts. In the batch reactor, all the niobium catalysts display certain activities; however, in contrast, the niobium phosphate catalysts gave a higher activity than H_3PO_4-treated niobic acid catalyst. Furthermore, in the preliminary flow reactor, a packed bed of niobium phosphate also afforded a good performance (81.9 % selectivity with 26.5 % conversion) at 85 °C in aqueous medium.

Du et al. [76] applied H_3PO_4-pretreated $Nb_2O_5{\cdot}nH_2O_2$ catalyst (NA-p) in the conversion of fructose, glucose, inulin, and Jerusalem artichoke juice to HMF. After pretreatment with H_3PO_4, the BET surface area of NA-p increased to 214 m^2/g, but the pore diameter decreased to 4.27 nm which was smaller than for the parent Nb_2O_5. FT-IR results showed evidence for the P-O vibration in the NA-p material frame, which indicated phosphate groups have penetrated to inner layer of niobic acid, and afforded a broad distribution of heterogeneous acid sites. Owing to the above properties, the NA-p showed high catalytic activities for dehydration of mono- and polysaccharides to HMF at 160 °C in water/2-butanol (2:3 v/v) biphasic system, giving a high HMF yield of 89 % and 54 % from fructose and inulin, respectively.

Subsequently, Du et al. [77] investigated the application of tantalum compounds as solid acid catalysts for HMF production, because of its similar chemical properties

to Nb_2O_5. Although tantalum compounds have lower BET surface areas (~141 m^2/g) and fewer acidic sites (1.5 mmol/g) than the niobium catalysts, tantalum compounds were found to exhibit higher activity and better stability in aqueous conversion of fructose to HMF. H_3PO_4-modified hydrated tantalum oxide (TA-p) catalyst was found to give the yields of HMF as high as 90 % at 94 % conversion in water/2-butanol mixed solvent and was possible to be reused for 14 runs without any deactivation.

Recently, Saha et al. [78] also synthesized a large-pore mesoporous tin phosphate (LPSnP-1), by a hydrothermally method using Pluronic P123 as the structure-directing agent. Similarly to mesoporous TiO_2 material, LPSnP-1 was composed of aggregated tin phosphate nanoparticles, whose diameter sizes were in range of 10–15 nm, as shown in Fig. 6.15. This mesoporous tin phosphate has a large BET surface area (216 m^2g^{-1}) and large-pore structure with an average diameter of 10.4 nm and a high loading of acid sites (2.2 $mmolg^{-1}$). For the dehydration of fructose, the LPSnP-1 material gave the best activity with a yield of 77 % HMF in H_2O/MIBK cosolvent.

Dai et al. [79] prepared VPO–MCF (vanadium phosphate and mesostructured cellular foam) hybrid materials, with an abundance of weak to moderate acid sites, and applied them in the three-phase catalytic system (aqueous phase, ionic liquid phase, and catalyst) for production of HMF from fructose. Vanadium phosphate was well dispersed on the surface of MCF in the form of nanocrystals rather than bulk VPO crystals and was found to afford a high activity for fructose dehydration with a 91 mol% selectivity to HMF with 89 % fructose conversion obtained in biphasic H_2O/[BMIM][Tf_2N] system.

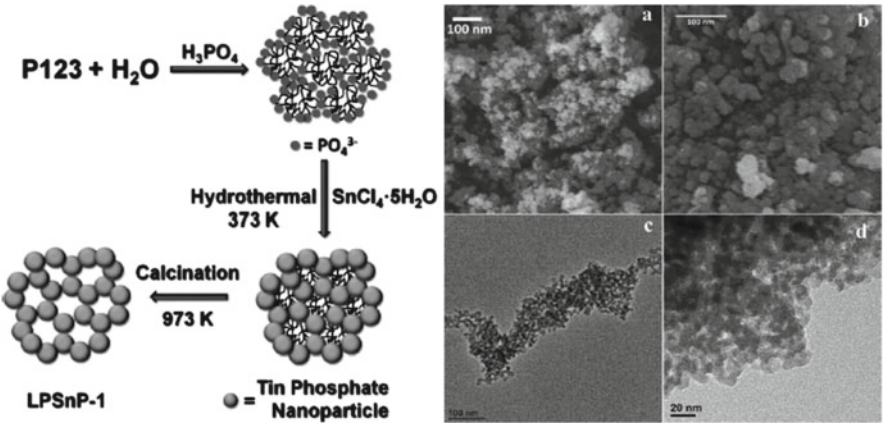

Fig. 6.15 Schematic representation of the synthesis of LPSnP-1 and SEM and TEM images of LPSnP-1 (Reprinted from ref. [78], with kind permission from John Wiley & Sons Ltd)

6.2.1.7 Heteropoly Acid Solid Acid Catalysts

Heteropoly acids or heteropoly acid salts were also considered to be important strong-acid catalysts, because of strong acidity and high proton mobility, which were very appropriate for dehydration reaction. Shimizu et al. [49] has already proven that $H_3PW_{12}O_{40}$, $Cs_{2.5}H_{0.5}PW_{12}O_{40}$, and $FePW_{12}O_{40}$ performed very well for the dehydration of fructose to HMF in DMSO under evacuation conditions, with >90 % yield of HMF possible.

Considering the insolubility and micropore characters of $Ag_3PW_{12}O_{40}$, Wang et al. [80] used $Ag_3PW_{12}O_{40}$ as a solid acid catalyst for production of HMF, which gave a 93.8 % selectivity with 77.7 % yield of HMF in water/MIBK and could be reused for 6 runs without an obvious deactivation. However, leaching of $Ag_3PW_{12}O_{40}$ in the biphasic water/MIBK solvent was inevitable with 5.1 % of the starting catalyst amount lost after six reactions.

The MOF-based MIL-101 material has also been used as heterogeneous catalyst as well as a support for some moderate reactions, because of its large pore size and large surface area facilitating the transformation of reactant molecules in the pores. PTA/MIL-101 catalyst, in that MIL-101 encapsulated phosphotungstic acid (PTA), was prepared by Hensen et al. [81]. The PTA/MIL-101 material has an extra large BET surface area (1352–2508 m^2/g), the microscopic structure of which is shown in Fig. 6.16. A 77 % selectivity to HMF at 82 % fructose conversion was obtained in DMSO over PTA (3.0)/MIL-101.

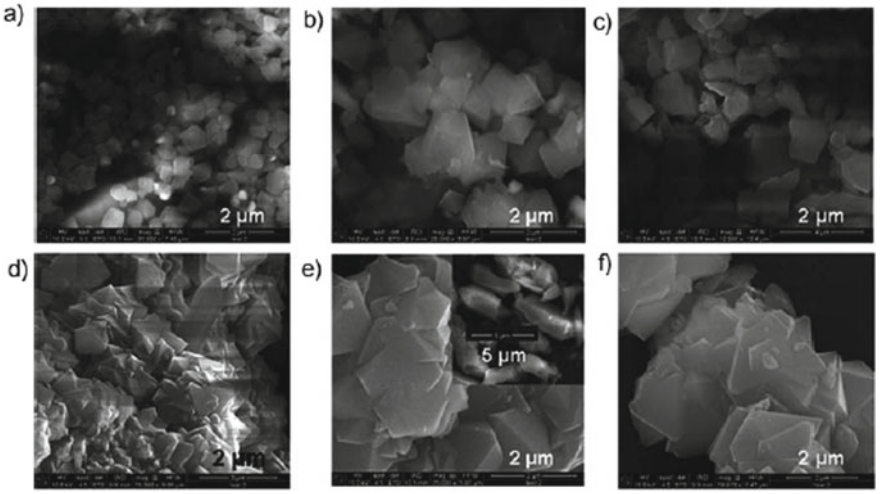

Fig. 6.16 Scanning electron micrographs of: (**a**) MIL-101; (**b**) PTA(0.5)/MIL-101; (**c**) PTA(1.0)/MIL-101; (**d**) PTA(1.5)/MIL-101; (**e**) PTA(2.0)/MIL-101; (**f**) PTA(3.0)/MIL-101 (Reprinted from ref. [81], with kind permission from John Wiley & Sons Ltd)

6.2.2 *Isomerization of Glucose to Fructose*

Isomerization of glucose to fructose is a crucial step for the industrial production of high-fructose corn syrup, which was usually biologically catalyzed by immobilized enzymes [82]. This is also a key step for direct production of the platform molecule HMF from glucose-based biomass. Studies of the isomerization of glucose to fructose have mainly focused on catalysis by enzymes (xylose isomerase), basic catalysts [83, 84], and Lewis acid catalysts, with the earliest studies dating back to the work of Lobry de Bruyn et al. who in 1895 studied the isomerization of hexoses in alkaline medium [85]. More recently in the 1980s, van Bekkum et al. reported the efficacy of potassium hydroxide for the catalytic isomerization of glucose to fructose in water, with a 61 % selectivity to fructose at 18 % glucose conversion reported [86, 87].

While homogeneous basic catalysts have a good selectivity, heterogeneous basic catalysts are more preferred for large-scale application. Moreau et al. [88] investigated cation-exchanged A, X, Y zeolites and hydrotalcites for the aqueous isomerization of glucose to fructose. Monovalent cation-exchanged A, X, Y zeolite catalysts, such as NaA, KX, and CsY, were found to be efficient for fructose formation, with 80 % selectivity to fructose at 23 % glucose conversion obtained over KX zeolites, which was the highest selectivity among the cation-exchanged A, X, Y zeolites. Unfortunately, the leaching of cation over the zeolites in water is dramatic, which was reported to be in the range of 25–30 % after reaction at 95 °C water over the A- series of zeolites. However, basic hydrotalcite (Mg/Al) catalysts showed extraordinary high hydrothermal stability under these conditions with negligible metal leaching reported.

Jung et al. [89] investigated the effect of calcination (HT_C) and calcination/rehydration (HT_R) of a parent Mg–Al hydrotalcite (HT_A) (Mg/Al = 3) for the isomerization of glucose to fructose. It was found that rehydration treatment improved the activity of Mg–Al hydrotalcite (HT_R) catalyst for the conversion of fructose giving the highest yield of fructose. The high yield of fructose was attributed to the abundant weak base sites that existed over HT_R catalyst, which were formed during rehydration process. The comparison of catalytic performances over Mg–Al hydrotalcite was shown in Fig. 6.17.

Normally, Lewis acid catalysts are not considered a good catalyst for isomerization in protic polar solvents, because Lewis acidity was easily suppressed by hindering coordination or irreversible decomposition [90]. However, Davis et al. [82] found that a large-pore zeolite containing tin (Sn-Beta) as a Lewis catalyst exhibited a remarkable activity in water solvent for the isomerization, which was even analogous to the performance of enzymatic catalysts. Ten percent glucose aqueous solution catalyzed by Sn-Beta at 110 °C for 30 min can transfer into 45 % (wt⁄wt) glucose, 32 % (wt⁄wt) fructose, and 9 % (wt⁄wt) mannose. In addition, Davis et al. also investigated the conversion of concentrated glucose solution (45 wt.%) over Sn-Beta catalyst. Surprisingly, a product distribution of 46 % (wt⁄wt) glucose, 29 % (wt⁄wt) fructose, and 8 % (wt⁄wt) mannose was obtained after reacting at 110 °C for

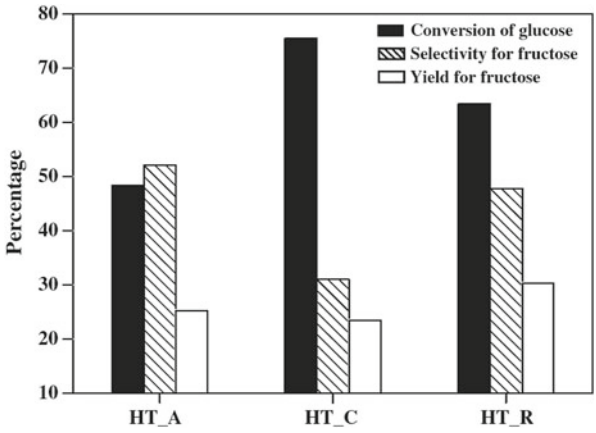

Fig. 6.17 Catalytic performance of hydrotalcite catalysts (HT_A, HT_C, and HT_R) in the isomerization of glucose into fructose at 100 °C for 5 h (Reprinted from ref. [89], with kind permission from Elsevier)

60 min. The remarkably high-fructose yield catalyzed by this catalyst was near to the reaction equilibrium as well as approaching the typical yield from the industrial enzymatic process. Sn-Beta could also be readily reused over three cycles without any deactivation. More importantly, this catalytic process proceeded even in acidic environment (pH = 1), which provided the opportunities for coupling of hydrolysis, dehydration, and hydrogenation reactions for the biomass conversions.

Based on above hypothesis, Davis et al. [91] combined Sn-Beta catalyst with acid catalysts in a biphasic reactor system for production of HMF from glucose, cellobiose, and starch. A H_2O/THF or H_2O/1-butanol biphasic solvent was investigated for the reaction, with H_2O/THF biphasic solvent proven to be preferable for the production of HMF because of improved partitioning of HMF from the aqueous to the organic phase. The addition of NaCl into the biphasic solvent also improved the yield of HMF due to its high efficient extraction. In the H_2O(1)/THF(3)/NaCl biphasic system, an HMF yield of 72 % at 79 % glucose conversion was obtained at 180 °C over the binary Sn-Beta and HCl catalyst.

Davis et al. [90, 92–94] and Bell et al. [95] subsequently investigated the mechanism of catalytic isomerization of glucose to fructose over Sn-Beta catalysts (or other metal-substituted beta zeolite) in water by using ^{1}H and ^{13}C NMR spectroscopy on isotopically labeled glucose, enthalpy computations, and QM/MM computational and density functional calculations. The results indicated it was definitely a Lewis acid-mediated isomerization of glucose; although Lewis acidity was usually considered to be suppressed in the presence of water, it was suggested that the Lewis acidity sites in framework positions were located in a hydrophobic environment [96]. The isolated tin tetrahedral sites coordinated to the crystalline zeolite framework proved to be the actual active sites for the isomerization of glucose to fructose. Davis et al. also demonstrate that the isomerization of glucose to fructose in water proceeds via intramolecular hydride shift way rather than proton transfer way normally catalyzed over base catalyst. The proposed Meerwein–Ponndorf–Verley reaction mechanism is shown in Fig. 6.18 [97].

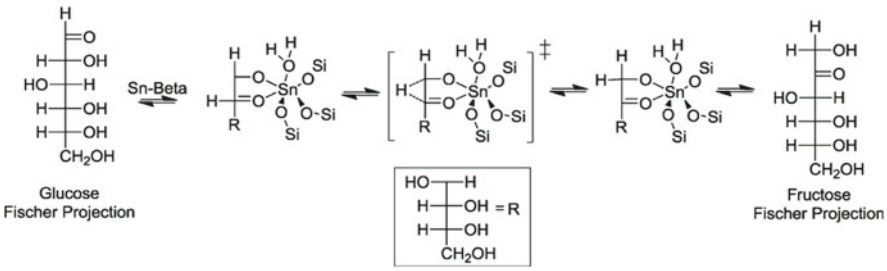

Fig. 6.18 Proposed glucose isomerization reaction mechanism catalyzed by Sn-Beta (Reprinted from ref. [90], with kind permission from American Chemical Society)

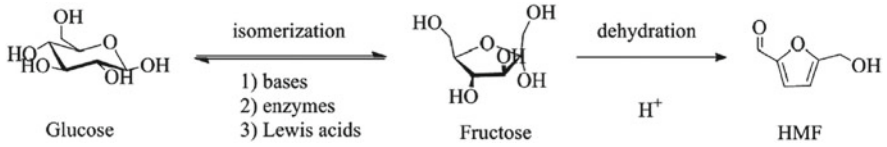

Fig. 6.19 Catalytic conversion of glucose to HMF over combined isomerization and dehydration catalysts (Reprinted from ref. [98], with kind permission from the Royal Society of Chemistry)

6.2.3 Dehydration of Glucose to HMF

In contrast to fructose, glucose is a preferred feedstock for production of HMF due to its wide availability from lignocellulose, which would make the production of HMF from glucose a much more desirable process. However, achieving high catalytic conversion of HMF from glucose is still a challenge, because this process needs to couple both isomerization of glucose and dehydration of fructose, as shown in Fig. 6.19. As discussed above, Lewis acid sites and base sites were considered to be efficient for isomerization of glucose to HMF while Brønsted acid sites were efficient for dehydration of fructose to HMF. Thus, traditional monofunctional solid acid catalysts cannot meet the multi-reactions' demand, stimulating the development of new types of highly efficient bifunctional catalysts for the production of HMF from glucose. This section will review progress that has been made for the one-pot conversion of glucose to HMF.

6.2.3.1 Metal Oxide-Based Catalysts

Saha et al. [71–73, 78] investigated self-assembled mesoporous TiO_2 materials synthesized with different templates (discussed in Sect. 6.2.1.6) for the conversion of glucose to HMF. The highest yields of HMF were up to 30.2 % in DMA–LiCl at 130 °C and 37.2 % in DMSO at 140 °C, respectively. These MTiP-1 (macro-/mesoporous titanium phosphate) and LPSnP-1 (large-pore mesoporous tin phosphate)

materials were also tested for the conversion of glucose producing a 22 % yield of HMF in DMA–LiCl at 140 °C and a 62 % yield of HMF in H_2O/MIBK at 150 °C.

Hot-compressed water, including hydrothermal and supercritical water conditions ($T_c = 374.2$ °C, $P_c = 22.1$ MPa, and $\rho_c = 0.323$ g/cm^3), can be considered a green solvent for biomass refining. Watanabe et al. [63] used TiO_2 and ZrO_2 catalysts (discussed in Sect. 6.2.1.6) for the conversion of glucose in hot-compressed water (200 °C). Anatase TiO_2 was found to produce a high yield of HMF and glucose conversion while ZrO_2 afforded a high yield of fructose from the isomerization of glucose owing to their different proportions and properties of acid and base sites. In contrast, rutile TiO_2 (r-TiO_2) is inactive due to its low density of acid and base sites. Furthermore, with microwave irradiation heating, isomerization of glucose to fructose can be promoted over ZrO_2 and TiO_2 catalysts [64]. In the absence of catalyst, only a 7 % yield of HMF can be obtained in hot-compressed water alone.

Besides hot-compressed H_2O and organic solvent, ionic liquid systems have also been considered as a promising solvent for the production of HMF from glucose. Qi et al. [99] investigated the catalytic activity of ZrO_2 in the conversion of glucose in ionic liquid ([HexylMIM][Cl]). At 200 °C in [HexylMIM][Cl]–water (50:50 w/w%) mixed solvent, a yield of HMF as high as 53 % was obtained over ZrO_2. Moreover, the addition of protic solvents (such as methanol and ethanol) in this system could also promote the production of HMF. McNeff et al. [65] also employed the conversion of glucose in the continuous flow reactor, with a 29 % and 26 % yield of HMF obtained in MIBK at 180 °C over TiO_2 and ZrO_2 catalysts, respectively.

From the above results, we can make a conclusion that the bare TiO_2 or ZrO_2 were active for the production of HMF from fructose, but their low density and weak strength of acidic and basic sites limit the overall yield of HMF produced from the glucose. In contrast, H_2SO_4- or H_3PO_4-treated metal oxides, such as SO_4^{2-}/ZrO_2 and SO_4^{2-}/Al_2O_3, have more strong-acid sites and controlled base sites and could be more promising catalyst for the production of HMF from glucose [66]. As discussed in Sect. 6.2.1.6, the bifunctional SO_4^{2-}/ZrO_2–Al_2O_3 catalyst, prepared by impregnation of $Zr(OH)_4$ and $Zr(OH)_4$–$Al(OH)_3$ with ethylene dichloride solution of chlorosulfonic acid, has both Brønsted acid sites and base sites but without Lewis acid sites. With addition of Al, the density of acid sites gradually decreased but the density of basic sites (middle strength base) slightly increased. Over CSZA-3 with Zr–Al mole ratio of 1:1, 48 % yield of HMF at 99 % glucose conversion was acquired in DMSO at 130 °C which is attributed to the desirable balance of acid and base sites.

Osatiashtiani et al. [68] have also studied bifunctional catalytic behavior of SO_4^{2-}/ZrO_2 for the conversion of glucose to HMF in water. SO_4^{2-}/ZrO_2 catalysts have Lewis base (and acid) and Brønsted acid sites, the ratio of which could be controlled by tuning the SO_4 loading from submonolayer to monolayer coverages. The Lewis acid or base sites originating from the monoclinic ZrO_2 surface were favorable for the isomerization of glucose, while the Brønsted acid sites produced by sulfation and stabilization of the tetragonal phase could catalyze the dehydration of fructose to HMF. The high selectivity to HMF was closely dependent on balance of basic and Lewis–Brønsted acid sites. The best activity (TOF of HMF formation)

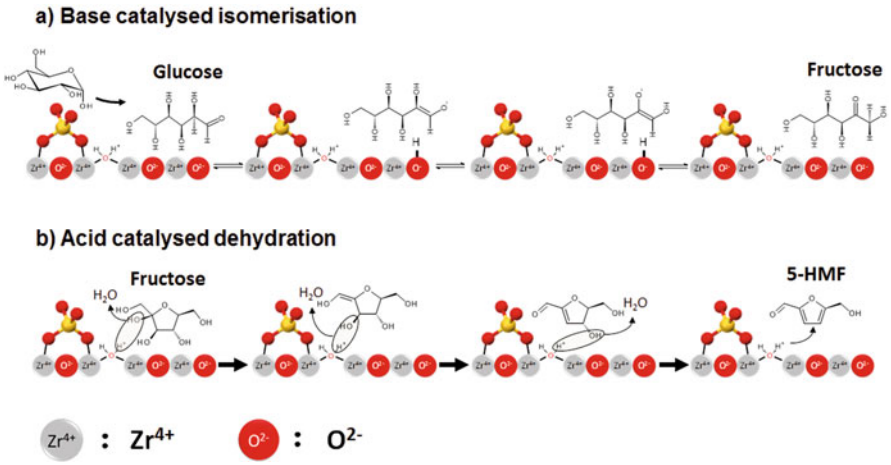

Fig. 6.20 Bifunctional surface-catalyzed mechanism for (**a**) isomerisation of glucose to fructose over basic O^{2-} sites of monoclinic ZrO_2 (Lewis acidic Zr^{4+} may help stabilize the enolate intermediate) and (**b**) dehydration of fructose to 5-HMF over Brønsted acid sites present in submonolayer SO_4/ZrO_2 catalysts (Reprinted from ref. [68], with kind permission from the Royal Society of Chemistry)

was obtained over SO_4^{2-}/ZrO_2 catalyst with sulfate coverages of approximately 0.3 ML, with the bifunctional catalytic mechanism over SO_4^{2-}/ZrO_2 proposed as shown in Fig. 6.20.

Nijhuis et al. [100] also correlated the properties of metal phosphate catalysts, including AlPO, TiPO, ZrPO, and NbPO prepared via coprecipitation, with the catalytic activity in the dehydration of glucose to 5-hydroxymethylfurfural in water. Experimental results suggest that the conversion of glucose decreases in the order NbPO > ZrPO > TiPO > AlPO, which was corresponding to the amount of strong-acid sites over these catalysts, while the selectivity to HMF increased with the ratio of Brønsted to Lewis acid sites. In addition, high loadings of isolated Lewis acid sites were found to be unfavorable for the selective formation of HMF, because of unselective conversion of sugars into humins and other side products. Treatment of phosphates with TEOS was found to deactivate unselective Lewis acid sites and increase the selectivity to HMF. The highest selectivity to HMF in range of 55–60 % was obtained over the silylated phosphates, which have the best balance between protonated phosphate groups and nearby metal Lewis acid sites. Moreover, Nijhuis et al. [101] synthesized a zirconium phosphate-coated aluminum foam catalyst (ZrP-f/Al) by washcoating ZrPO onto the anodized aluminum foam and found a similar correlation between the activity of the catalyst and its acidic properties.

Analogous to ZrO_2- and TiO_2-based solid acid catalysts, the solid acidic niobium and tantalum oxides have attracted growing attention for catalytic dehydration of glucose. Besides fructose, Hara et al. [102] used $Nb_2O_5{\cdot}nH_2O$- and H_3PO_4-treated $Nb_2O_5{\cdot}nH_2O$ heterogeneous catalyst for the conversion of glucose into HMF.

A 12.1 % selectivity to HMF at 100 % conversion was obtained over $Nb_2O_5 \cdot nH_2O$ catalyst in water at 120 °C. When $Nb_2O_5 \cdot nH_2O$ was treated by H_3PO_4, the selectivity sharply increased to 52.1 % with 92 % conversion. Hara et al. [103] also employed titanate nanotubes for the catalytic conversion of glucose to HMF in water, with a yield of HMF as high as 14 % observed at 120 °C.

Phosphoric acid-treated niobic acid (NA-p) catalysts have also been investigated by Yang et al. [76, 77] for the dehydration of glucose at 160 °C with a 49 % yield of HMF obtained in water/2-butanol solvent. In comparison phosphoric acid-treated hydrated tantalum oxide (TA-p) was found to exhibit better activity and stability than NA-p, giving a 58 % yield of HMF from fructose in water/2-butanol mixture.

Carbon-supported niobia catalyst was employed for the conversion of glucose to HMF in biphasic system, and although carbon-supported niobia catalyst has an improved stability compared with pure niobia [104], the carbon-supported catalyst tends to be located in the organic phase due to its hydrophobic nature, resulting in a low activity for the conversion of glucose. In light of this Shanks et al. [105] prepared three kinds of niobia/carbon black catalysts (Nb/CB-1-DP, Nb/CB-2-DP, and Nb/CS-HT) via deposition precipitation and deposition precipitation–carbonization. Due to their different surface properties controlled by the preparation method, the three catalysts existed in the organic phase, aqueous phase, and interface phase, respectively. As expected, the hydrophilic Nb/CB-2-DP was most active and afforded a 20 % HMF yield in sec-butyl phenol/water at 170 °C. While there are clear differences in performance of the carbon-supported catalysts, the lack of characterization of the acid sites and cluster sizes of niobia and varied reaction conditions hinder any understanding of structure activity relationships in the literature.

6.2.3.2 Zeolite-Based Catalysts

As traditional solid acid and base catalysts, zeolites have been widely used for the dehydration of glucose to HMF as similar as fructose. The controlled acidic types (Brønsted or Lewis) and acidic or basic strength were very appropriate to be bifunctional catalyst for the conversion of glucose to HMF. However, it should be borne in mind that the microporous nature of zeolites makes them prone to diffusional limitation in liquid-phase reactions as well as being unstable in hydrothermal conditions.

Liu et al. [106] investigated the activities of various commercial zeolite catalysts, including HY-zeolite, H-mordenite, Hβ-zeolite, and HZSM-5, for the conversion of glucose to HMF in ionic liquid ([BMIM]Cl) system. Hβ-zeolite with Si/Al ratio of 25 exhibited the best catalytic activity among above zeolites. At 150 °C, a glucose conversion of 81 % and HMF yield of 50 % were obtained. Good synergistic effects between surface Brønsted acid sites and Lewis acid sites over Hβ-zeolite were claimed to be essential for good activity as shown in Fig. 6.21. While the Hβ-zeolite catalyst exhibited a decreased HMF yield upon reuse, regeneration was possible by calcination.

As discussed in Sect. 6.2.2, Sn-substituted β-zeolite exhibited a remarkable activity for the isomerization of glucose to fructose; thus Wang et al. [107] prepared a Sn-Mont bifunctional catalyst by ion exchange of natural calcium montmorillonite (Ca-Mont) with an aqueous tin tetrachloride solution. The Sn-Mont material had

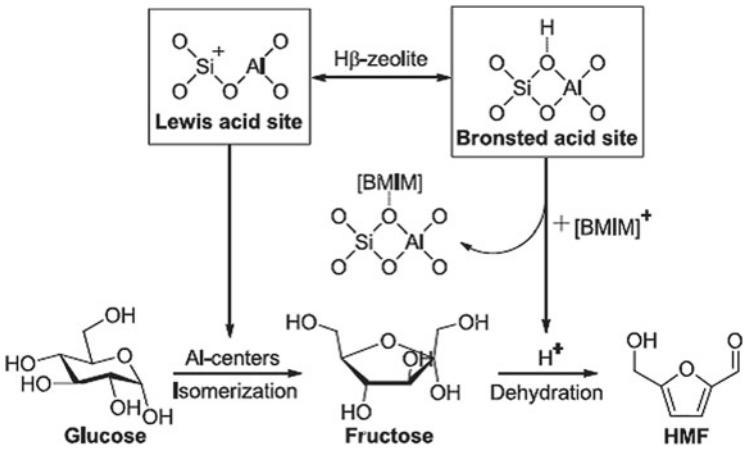

Fig. 6.21 The proposed mechanism for the conversion of glucose into HMF over Hβ-zeolite catalyst in [BMIM]Cl (Reprinted from ref. [106], with kind permission from Elsevier)

a BET surface area of 149.1 m^2g^{-1} and possessed both Lewis acid sites and Brønsted acid sites, which were in the range of weak to moderate strength. Over this catalyst, a 53.5 % yield of HMF with 98.4 % glucose conversion was obtained at 160 °C in a biphasic solvent THF/DMSO (v/v, 70/30), which was attributed to the synergistic effect of tin ions (Lewis acid sites for isomerization of aldose to ketose) and Sn–OH (Brønsted acid sites for dehydration of fructose to HMF) as outlined in Fig. 6.22.

Sels et al. [108] developed a novel bifunctional Sn-doped carbon–silica catalyst (Sn-Si-CSM, carbon-modified Sn-Si-MCM-41). The Sn-Si-CSM material exhibited both Brønsted and Lewis acid sites, with the latter originating from Sn (IV) sites, while the weak Brønsted acid groups were associated with oxygen-containing functional groups in carbon framework. These bifunctional materials were applied for catalytic esterification of mono- and disaccharides with methanol to methyl lactate using methanol as both solvent and reactant. The highest yield of methyl lactate from glucose was 17 %, which was obtained over Sn-Si-CSM-773-20.4 catalyst, which was an Sn-Si-CSM material, prepared via carbonization at 500 °C with a 20.4 wt.% carbon content.

6.2.3.3 Carbon-Based Catalysts and Other Bifunctional Catalysts

Sulfonation of incompletely carbonized biomass, such as glucose, starch, and cellulose by concentrated or fuming sulfuric acid, can be used to produce carbon materials functionalized with $–SO_3H$, –COOH, and phenolic –OH groups, which can be utilized as effective solid catalyst for the hydrolysis of cellulose and dehydration of fructose or glucose to HMF.

Hu et al. prepared such carbonaceous solid acid catalysts by incomplete carbonization of glucose, starch, or cellulose, followed by sulfonation, denoted as GCC, SCC, and CCC, respectively [109], whose surfaces comprised $–SO_3H$, –COOH, and

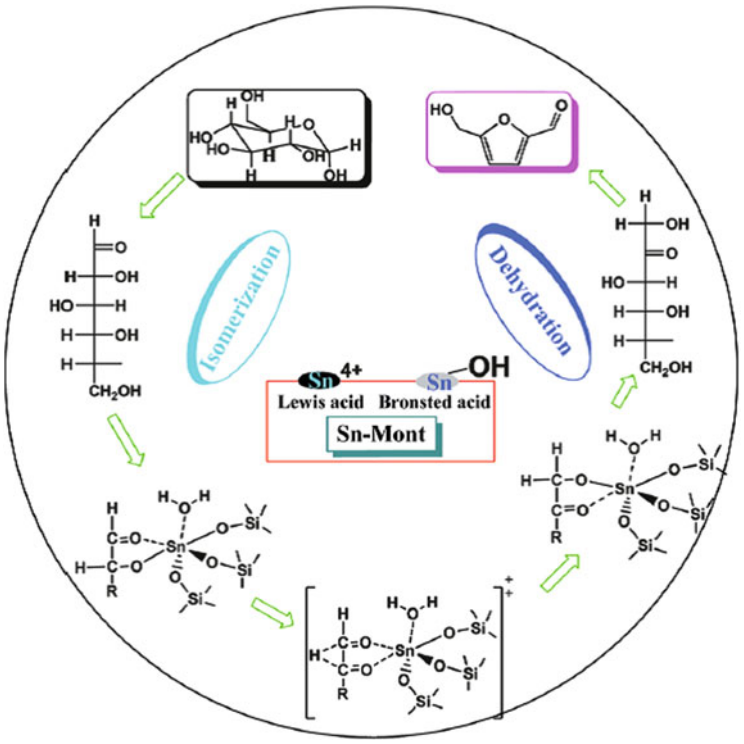

Fig. 6.22 Proposed reaction mechanism for the conversion of glucose to HMF catalyzed over Sn-Mont catalyst (Reprinted from ref. [107], with kind permission from the Royal Society of Chemistry)

phenolic –OH functional groups originating from the oxygen-containing functional groups in the biomass precursors and H_2SO_4. While the densities of –COOH and phenolic –OH functional groups were found to be much higher than $–SO_3H$ on the solid catalysts, these carbonaceous catalysts were found to be more active for the production of HMF than conventional solid acid catalysts, such as HZSM-5, $SO_4^{2-}/TiO_2–ZrO_2$, Amberlyst-15, and even H_2SO_4 (Table 6.3). At 140 °C a 41.2 % yield of HMF at 60.7 % conversion was obtained in 30 min using the CCC catalyst in [BMIM]Cl. However, the CCC catalyst could be reused only for three times and required regeneration by re-carbonization and sulfonation. In this process, Hu et al. proposed that [BMIM]Cl also played an important role that includes promoting the isomerization of glucose into fructose and stabilizing the generated HMF.

Wang et al. [80] employed heteropoly acid and heteropoly acid salts ($Ag_3PW_{12}O_{40}$) as bifunctional solid acid catalysts for the conversion of glucose and fructose into HMF. $Ag_3PW_{12}O_{40}$ exhibited good catalytic activity for the conversion of glucose into HMF with a 76.3 % yield of HMF obtained in water/MIBK at 130 °C. $Ag_3PW_{12}O_{40}$ could be reused for 6 runs without obvious deactivation; however, leaching of $Ag_3PW_{12}O_{40}$ in biphasic solvent of water/MIBK was inevitable with ~5 % of $Ag_3PW_{12}O_{40}$ lost after six runs.

Table 6.3 Conversion of glucose into HMF using various acid catalysts[a]

Entry	Catalyst	HMF yield (%)	Glucose conversion (%)
1	No catalyst	1.5	2.7
2	H-mordenite	14.3	29.5
3	HZSM-5(30)	16.2	35.6
4	$Ag_3PW_{12}O_{40}$	17.5	31.7
5	$Cs_{2.5}H_{0.5}PW_{12}O_{40}$	28.4	50.0
6	SO_4^{2-}/ZrO_2	15.3	29.8
7	SO_4^{2-}/TiO_2-ZrO_2	25.0	49.2
8	Amberlyst-15	25.6	48.8
9	Amberlite IRN-77	30.7	51.5
10	HCl[b]	18.3	39.4
11	H_2SO_4[c]	21.6	44.9
12	ICC[d]	2.1	3.8
13	CCC	41.2	60.7
14	GCC	37.8	55.2
15	SCC	35.3	54.3

Reprinted from ref. [109], with kind permission from Elsevier

[a]Reaction conditions: 40 mg different acid catalysts, 100 mg glucose, 1 g [BMIM]Cl, 140 °C, 30 min

[b]0.0236 mmol HCl (corresponding to 40 mg CCC)

[c]0.0168 mmol H_2SO_4 (corresponding to 40 mg CCC)

[d]Incompletely carbonized cellulose without the sulfonation

By coupling with Cr^{3+} ion, the FPIL (functional polymeric ionic liquids) became bifunctional catalysts (FPIL2, as discussed in Sect. 6.2.1.5). Yang et al. [62] also investigated the activities of FPIL2 materials in the conversion of glucose. The FPIL 2a catalyst afforded a 48.7 % yield of HMF in aqueous/organic mixed solvent (H_2O–DMSO (1:4)/MIBK–n-BuOH (3:7)) after 120 min reaction at 150 °C.

6.2.3.4 Binary Solid Acid and Base Catalyst

The process of converting glucose to HMF can be divided into two steps: (1) isomerization of glucose into fructose over solid base or Lewis acid catalyst and (2) dehydration of fructose into HMF over solid acid catalyst. In light of this Ebitani et al. [110] developed a process utilizing a mixture of solid acid and base catalysts for the one-pot reaction to selectively produce HMF from glucose. Basic Mg–Al hydrotalcite ($Mg_6Al_2(OH)_{16}CO_3$) was chosen for isomerization of glucose to fructose step, with various solid acid catalysts, including Amberlyst-15, Nafion NR50, SO_4^{2-}/ZrO_2, $Nb_2O_5{\cdot}nH_2O$, H-ZSM5, and H-beta, screened for the dehydration of fructose to HMF, with Amberlyst-15 that proved to be the most active acid catalyst for dehydration of fructose. The binary system of HT and Amberlyst was able to convert glucose to HMF in a one-pot approach at 100 °C, giving a HMF selectivity as high as 58 % when working in DMF solvent. Moreover, the binary catalysts also

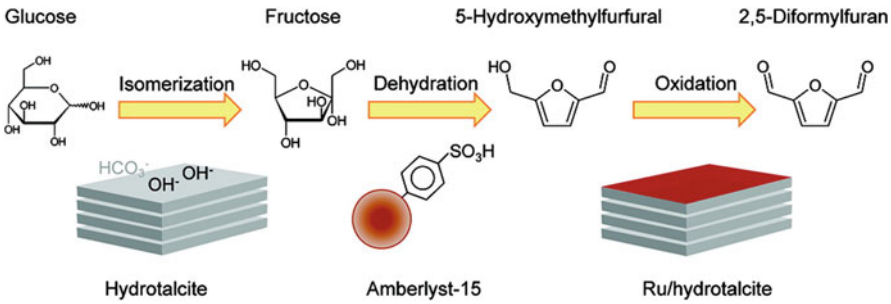

Fig. 6.23 Synthetic route of 2,5-diformylfuran from glucose over solid acid, basic, and oxidative catalysts (Reprinted from ref. [111], with kind permission from American Chemical Society)

afforded good performances for the conversion of disaccharide, sucrose, and cellobiose to HMF. Ebitani et al. [111] also developed a tandem catalytic process for direct production of 2,5-diformylfuran (DFF) from glucose, as shown in Fig. 6.23. For this reaction, three types of catalysts were involved, such as basic hydrotalcite, acidic Amberlyst-15, and oxidative Ru/hydroltalcite. At 100 °C a 25 % yield of DFF was obtained at 98 % glucose conversion via two-step reaction without catalyst separation.

Recently, Xiao et al. [112] also developed polymeric binary solid acid and solid base-catalyzed system for the conversion of glucose to HMF. A super hydrophobic mesoporous polymer acid catalyst (PSO_3H-154) was prepared by copolymerization of divinylbenzene and sodium p-styrene sulfonate, which exhibited an excellent activity for the dehydration of fructose into HMF. For instance, the yield of HMF was as high as 99.0 % over PSO_3H-154 catalyst at 100 °C for 10 h in DMSO solvent or THF–DMSO mixed solvent, which was much higher than that over H_2SO_4 catalyst (53.8–62 %) and Amberlyst-15 acid catalyst (45.7–66.0 %). This was employed in conjunction with a super hydrophilic solid base catalyst (P-VI-0) prepared by copolymerization of divinylbenzene, 1-vinylimidazole, and N,N-methylenediacrylamide. The hydrophobic PSO_3H-154 and hydrophilic P-VI-0 exhibited a perfect synergistic effect for the one-pot catalytic conversion of glucose to HMF, with a 96 % yield of HMF obtained in THF–DMSO solvent at 100 °C, which was mainly attributed to the higher activity of PVI-0 for isomerization of glucose to fructose.

6.3 Conversion of Cellulose Over Solid Acid Catalyst

Cellulose, a biopolymer of d-glucose linked by β-1,4-glycosidic bonds, has a robust 3D bulk structure because of its abundant intra- and intermolecular hydrogen bonds, which protect the β-1,4-glycosidic bonds from attack by foreign molecules. Therefore, the catalytic conversion of cellulose under mild conditions remains a

grand challenge. This section will focus on the introduction about hydrolysis reaction and glycosidation reaction of cellulose over solid acid catalysts.

6.3.1 Hydrolysis of Cellulose into Monosaccharide or Polysaccharides

6.3.1.1 Sulfated Carbon Catalysts

In 2008, Hara et al. [36] demonstrated the efficacy of amorphous carbon-bearing SO_3H, COOH, and OH function catalyst for the one-pot hydrolysis of cellulose. This functionalized amorphous carbon originated from partial carbonization of cellulose and then sulfonation and was a typical Brønsted acid catalyst whose structure is shown in Fig. 6.24. The functional groups of $–SO_3H$, –COOH, and –OH made the amorphous carbon more hydrophilic, which facilitated incorporation of large amounts of hydrophilic molecules. Compared to the traditional solid acid catalyst, such as Nb acid, H-mordenite, Nafion, and Amberlyst-15, this carbon material showed an excellent catalytic activity with a 64 % yield of water-soluble β-1,4-glucan and 4 % yield of glucose obtained from crystalline cellulose at 100 °C for 3 h. The high hydrolysis activity was attributed to the synergistic effect between $–SO_3H$ and –OH functional groups, because –OH functional groups have a strong ability to absorb β-1,4-glucan and then the $–SO_3H$ as active acid sites efficiently break down β-1,4-glycosidic bond. A study of various reaction parameters (the amount of water and cellulose, the speed of stirring, and the temperature) on cellulose hydrolysis using an artificial neural network and response surface methodology indicated that the amount of H_2O was the key factor and the adsorption of cellulose over the catalyst surface was a rate-determining step [113]. In addition to cellulose-derived carbon catalysts, functionalized carbon material that originated from partial carbonization of polyvinyl chloride material (PVC) was also prepared [114]. A Brønsted acid catalyst was generated, which exhibited good activity in cellobiose hydrolysis (model molecule), yielding 30.1 % glucose (>91 % selectivity) over a PVC-AC673 catalyst at 100 °C.

Unfortunately the preparation of cellulose- or PVC-derived amorphous carbon solid acid catalysts was not easy at large scale due to high energy cost by carbonization. In contrast, functionalization of commercial activated carbon with $–SO_3H$ functional group may be more suitable for practical utilization. Yanagisawa et al. [115, 116] adopted this approach and prepared a AC-SO_3H catalyst by sulfonation of activated carbon with concentrated H_2SO_4 under an argon environment at 150 °C. The resulting AC-SO_3H catalyst gave a 40.5 % yield of glucose with 95 % selectivity following reaction at 150 °C of cellulose pretreated by ball milling for 24 h, which is much higher than those over other solid acid catalysts as shown in Fig. 6.25.

Preparation conditions have an important effect on the properties of AC-SO_3H catalyst, which was corresponding to its hydrolysis activity. By investigation of

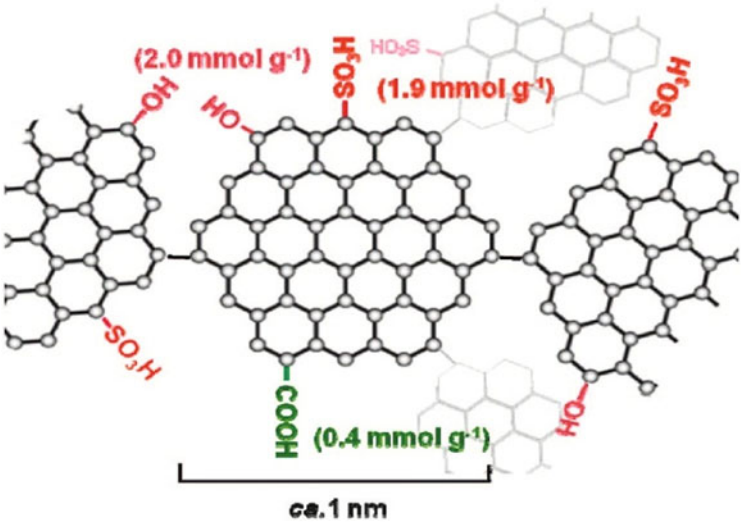

Fig. 6.24 Proposed schematic structure of the prepared carbon material (Reprinted from ref. [36], with kind permission from American Chemical Society)

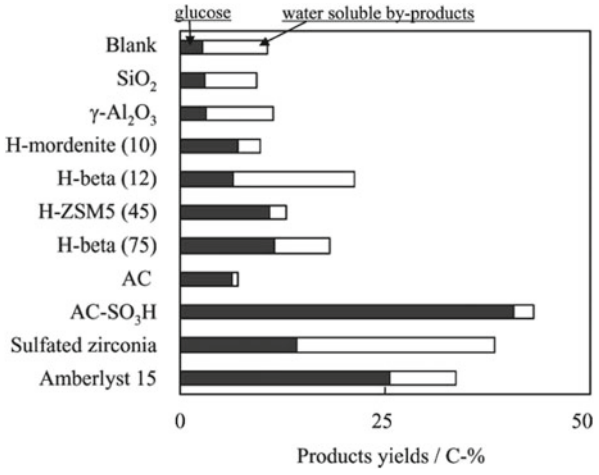

Fig. 6.25 Cellulose hydrolysis over solid acid catalysts at 150 °C (Reprinted from ref. [116], with kind permission from the Royal Society of Chemistry)

sulfonation temperature and pretreatment method, Pang et al. [117] found that the AC-SO_3H prepared by pretreatment with concentrated nitric acid and then sulfonation of concentrated sulfonic acid at 250 °C showed the best activity for hydrolysis of ball-mill-pretreated cellulose. After 24 h reaction at 150 °C, the conversion of cellulose was 74.3 % with a glucose yield of 62.6 %. Pang et al. also investigated the effects of different carbon materials on the hydrolysis activity and found that sulfonated CMK-3, ordered mesoporous carbon, was an excellent material for cellulose hydrolysis. CMK-3-SO_3H exhibited a conversion of cellulose ~94.4 % with

a glucose yield of 74.5 %, which was attributed the high BET surface area, large mesoporous pore architecture, and high –SO_3H group density of this material.

6.3.1.2 Silica-Based Solid Acid Catalysts

In addition to sulfonated carbon materials, early in 2005, Fukuoka et al. [118] employed sulfonated mesoporous silicas catalyst (Et-HMM-SO_3H, Ph-HMM-SO3H, and FSM-SO_3H) for the hydrolysis of sucrose and starch. Et-HMM-SO_3H and FSM-SO_3H, synthesized by a one-pot method or post-grafting method, respectively, exhibited much higher activities and turnover frequency in hydrolysis of both sucrose and starch than Nafion–silica, HZSM-5, and H_2SO_4 catalyst. For the hydrolysis of sucrose, a 90 % yield of glucose with 90 % conversion was obtained over both catalysts following reaction at 80 °C for 4 h; for the hydrolysis of starch, a 39 % yield of glucose was obtained over FSM-SO_3H at 130 °C after 6 h reaction.

As discussed above, solid acid catalysts having a magnetic response offer the potential for facile separation from the liquid phase. Magnetic sulfonic acid-functionalized variants of mesoporous SBA-15 silicas in which magnetic Fe_3O_4 nanoparticles were embedded in the ordered silica matrix have been explored for the hydrolysis of cellulose (Fig. 6.26) [119]. While a yield of glucose as high as 50 % can be obtained following the hydrolysis of amorphous cellulose over Fe_3O_4–SBA–SO_3H following reaction at 150 °C, the hydrolysis of crystalline cellulose yields only 26 % glucose due to recalcitrant nature of the microcrystalline region. The performance of Fe_3O_4–SBA–SO_3H was however superior to other solid acid catalysts, such as AC-SO_3H and Amberlyst-15, under the same conditions.

Zhang et al. [120] explored the synthesis of sulfonic acid-functionalized magnetic core–shell materials (Fe_3O_4@SiO_2–SO_3H) for the hydrolysis of cellulose, which were prepared by two steps: (1) synthesis of magnetic Fe_3O_4@SiO_2 nanoparticles and (2) grafting the sulfonic functional group on SiO_2 surface via the reaction of sulfonic acid chlorides with the surface hydroxyl groups. The density of acid sites over Fe_3O_4@SiO_2–SO_3H material was as high as 2.48 mmol/g. The hydrolysis of cellulose catalyzed by Fe_3O_4@SiO_2–SO_3H catalyst was investigated in ionic liquid [Bmim]Cl, which was in favor of the dissolving of cellulose and access to the active acid sites. Under relatively mild reaction conditions (130 °C for 8 h), a 51.4 % yield of glucose with a 73.2 % yield of reducing sugar (RS) was obtained. Moreover, Fe_3O_4@SiO_2–SO_3H catalyst could be efficiently recovered and reused for five times without any loss in activity. Similar magnetic materials have been synthesized based upon $CoFe_2O_4$@SiO_2–SO_3H catalysts by Takagaki et al. [121], which afforded a high performance for hydrolysis of disaccharides (sucrose and cellobiose) and polysaccharides (starch and cellulose).

In addition to pure silica or carbon materials, Sels et al. [122] prepared sulfonated silica/carbon nanocomposite material for the hydrolytic degradation of cellulose into glucose. Over Si33C66-673-SO_3H (calcination at 400 °C) catalyst a 38 % glucose yield with 98 % selectivity was obtained from cellulose. While increasing silica–carbon ratio results in decreased glucose yield and cellulose con-

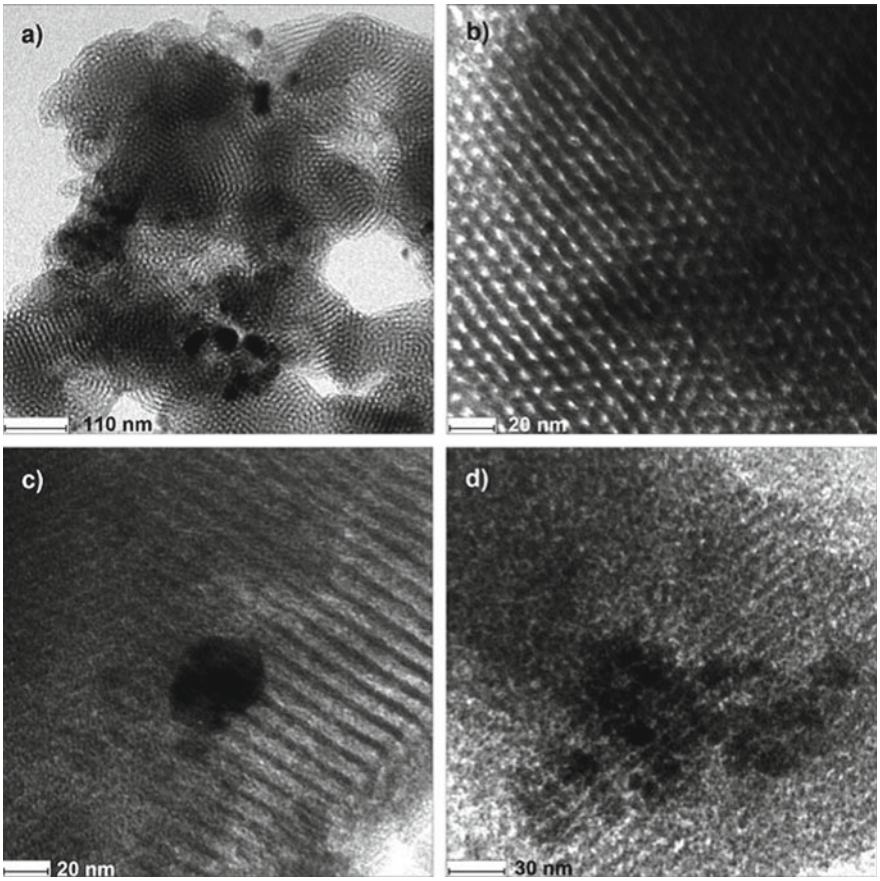

Fig. 6.26 TEM images of fresh (**a**, **b**, and **c**) and spent (**d**) Fe_3O_4–SBA–SO_3H catalysts (Reprinted from ref. [119], with kind permission from John Wiley & Sons Ltd)

version, glucose yield was found to increase with the carbonization temperature. The increase of calcination temperature will result in the pore expansion in bulk structure as shown in Fig. 6.27, causing increased micrometer-scaled cellulose particles to penetrate to the active catalytic sites. The optimum catalyst was found to be Si33C66-823-SO_3H prepared by calcination at 550 °C which afforded a yield of glucose of 50 % (83 % yields) at 150 °C after 24 h reaction.

6.3.1.3 Metal Oxide-Based Solid Acid Catalysts

Metal oxide solid acid catalysts have been widely used in the dehydration of fructose and glucose as discussed in Sects. 6.2.1.6 and 6.2.3.1. Metal oxide solid acid catalysts could be also utilized as a solid acid catalyst for hydrolysis of cellulose due to its strong acidity and water tolerance.

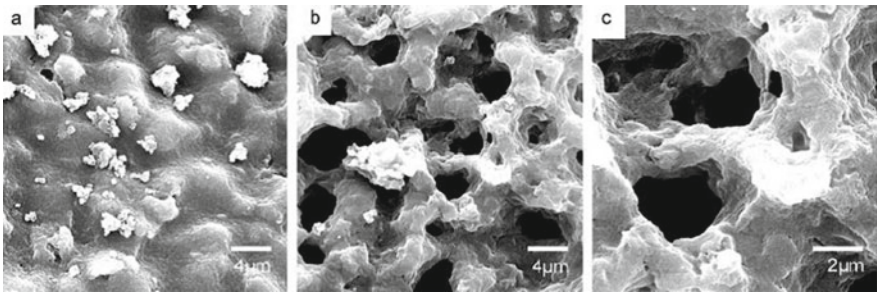

Fig. 6.27 SEM micrographs of the Si33C66-550-SO_3H catalyst system (Reprinted from ref. [122], with kind permission from the Royal Society of Chemistry)

Takagaki et al. [123] developed a series of acidic metal oxide materials, such as $H_{1-x}Nb_{1-x}Mo_{1+x}O_6$, $HNbMoO_6$, Nb–W oxides, and Ta_xW_{10-x}, for the hydrolysis of saccharides, starch, and cellulose. For layered $H_{1-x}Nb_{1-x}Mo_{1+x}O_6$ material, the acid strength increased with Mo concentration in the layer, but the acid amount increased with Nb concentration. For the hydrolysis of cellobiose at 95 °C, the activities of $H_{1-x}Nb_{1-x}Mo_{1+x}O_6$ catalysts were in following order: $H_{0.9}Nb_{0.9}Mo_{1.1}O_6 > HNbMoO_6 > H_{1.1}Nb_{1.1}Mo_{0.9}O_6$, with the TOF and the hydrolysis rate of $H_{0.9}Nb_{0.9}Mo_{1.1}O_6$ reported to be 0.22 h^{-1} and 0.34 mmol g^{-1} h^{-1}, respectively. Replacement of Nb with Ta was investigated by Takagaki et al. [124] who explored the activities of nanosheet and layered $HTaMoO_6$ for the hydrolysis of disaccharides. Although $HTaMoO_6$ nanosheet has a lower acid amount than layered $HTaMoO_6$ and $HNbMoO_6$, it exhibited a higher reaction rate and TOF, which was possibly attributed to the additional strong-acid sites on the oxide formed by exposure of a single layer.

In addition, mesoporous Nb–W and Ta_xW_{10-x} oxides have also been employed and afford good activities in the hydrolysis of sucrose and cellobiose because of its strong-acid sites, large surface area, and easy reactant accessibility [125, 126].

6.3.2 Glycosidation of Cellulose to Alkyl Glucosides

Alkyl glycosides are a class of biodegradable nonionic surfactants with wide applications in the cosmetic, detergent, food, and pharmaceutical industries [127, 128]. Normally, alkyl glycosides were prepared through the Fischer glycosidation of carbonate with an alcohol, which is a simple and low-cost route [129–131]. For example, alkyl glucosides can be synthesized by reacting glucose with an alcohol over acid catalyst under mild condition. Cellulose, an abundant biopolymer existing in nature with D-glucose linked by β-1,4-glycosidic bonds, was a promising alternative to glucose for preparation of alkyl glycoside surfactants. Although the one-pot catalytic transformation of cellulose to alkyl glucosides is possible, obtaining a high yield of alkyl glucosides is still a huge challenge due to the difficulty in selectively hydrolyzing cellulose.

The production of alkyl glucosides from cellulose needs two steps: glucose productions by the hydrolysis of cellulose and then subsequent reaction of released glucose with the alcohol to form the alkyl glucosides, with the hydrolysis of cellulose in alcohol being the rate-determining step. To overcome the rate-determined step, Ishikawa et al. [132] studied the conversion of cellulose under super critical methanol conditions ($T = 200–450$ °C, $P = 14–72$ MPa). Reaction under conditions of 350 °C and 43 MPa completely converted the microcrystalline cellulose into products spanning methylated oligomer, methylated cellobiose, methyl α-and β-d-glucosides, levoglucosan, and other-soluble products. The selectivity to monomeric compounds, such as methyl glucosides, was however quite low, which was a result of the rather harsh hydrothermal conditions employed.

Wang et al. [133] explored the application of an acid catalyst in this process. Fortunately, it was found that the acid catalysts not only afforded good performances for the production of methyl glucosides from cellulose in methanol solvent but also allowed the use of more moderate reaction conditions (<200 °C). Many acid catalysts, including mineral acids, organic acids, and heteropoly acids, as well as solid acids, were investigated. While dilute H_2SO_4 of concentration 6.7 mmol/L produced a 48 % yield of methyl glucosides when operating at 200 °C, under the same conditions, the conversion of cellulose was nearly negligible for other mineral and organic acid catalysts. In contrast phosphotungstic acid and silicotungstic acid catalyst were found to give promising yields of methyl glucosides as high as 43 % and 48 %, respectively. In addition, Wang et al. also investigated the activities of heterogeneous acid solid catalyst for the transformation of cellulose. Traditional solid catalysts, such as zeolite and sulfated ZrO_2, did not show good activity because of their small pore size and low specific surface area. In contrast, commercial sulfated resins (Nafion and Amberlyst-15) and sulfonated carbon exhibited good activities. Over the cellulose-derived carbon solid catalyst, 44 % yield of alkyl glucosides with 90 % conversion of cellulose was obtained at 195 °C for 1 h. Moreover, the yield could be further enhanced to 62 % with 90 % cellulose conversion by using the sulfonated lignin-derived carbon catalyst. Unfortunately, when cellulose reacted with longer chain alcohols, a low yield of longer alkyl glycosides was acquired in this system.

Longer chain alkyl glucosides were biodegradable nonionic surfactants and could be used in cosmetics, detergents, food emulsifiers, and pharmaceutical dispersing agents. In order to synthesize longer chain alkyl glucosides from cellulose, Corma et al. [134] coupled the hydrolysis of the cellulose with the Fischer glycosidation with C4–C8 alcohols in ionic liquid (BMIMCl). This overcame the problems of cellulose hydrolysis at very mild condition and gave much higher yields of alkyl glycoside products. The whole process of this reaction was divided into two parts. Firstly, the cellulose was hydrolyzed in ionic liquid (BMIMCl) at 100 °C for a certain time with a small amount of H_2O and Amberlyst-15 acid catalyst. Secondly, the alcohol, such as n-butanol, n-hexanol, and n-octanol, was added into reaction system and the temperature decreased to 90 °C. Hydrolysis time was found to be an important factor for the Fischer glycosidation step, with 1.5 h hydrolysis of cellulose shown to be the optimum hydrolysis time with a yield ~82 % of n-octanol-α,β-glucosides, and 98 % conversion of cellulose was obtained. Interestingly Ignatyev

et al. also finished a similar work using BMIMCl which produced an 86 % yield of butyl glycosides from the reaction of n-butanol with cellulose over an Amberlyst-15 catalyst [135]. The effect of hydrolysis time was also investigated but found that 4 h was the optimal hydrolysis time for cellulose, which may be due to the different reaction conditions. In addition, the synthesis of longer chain dodecyl glucosides was realized via a transalkylation reaction over Amberlyst-15 catalysts in ionic liquid. By reaction of α-BGP (a-D-glucopyranoside) with n-octanol in BMIMCl, 64 % yield of total octylated compounds was obtained at 110 °C within 24 h.

6.4 Concluding Remarks

This chapter has highlighted the significant progress made in recent years towards the development of solid acids for the valorization of cellulose-derived sugars. The development of heterogeneous catalysts and process engineering hold the key to realizing the potential of cellulose for the production of such renewable chemicals, and catalytic chemists and engineers need to emulate the successes of heterogeneous catalysis in petroleum refining. Advances in chemistry, nanotechnology, and spectroscopy will aid catalyst design, but overall process development requires an improved understanding of biomass properties and its impact on catalyst deactivation in order to accelerate biomass-to-chemical and fuel production. Commercial heterogeneously catalyzed processes will require a better understanding of individual reactant interactions with the active catalyst phase, particularly when dealing with bulky polar molecules such as those found in biorefinery feeds. Most crucially, however, widespread uptake and the development of next-generation chemical feedstocks requires progressive government policies and incentive schemes to place biomass-derived chemicals on a comparable economic footing with cheaper fossil fuel-derived resources [4, 136].

Biomass pretreatment to obtain sugars is one of the most wasteful steps in biorefineries, and new approaches are required to improve the processing of lignocellulose such that the initial acid hydrolysis/extraction to fractionate lignocellulose can be performed more efficiently. Cellulose stability itself presents a major hurdle, with environmentally friendly and energy-efficient means to break up this biopolymer an ongoing challenge. The exciting discovery that ionic liquids can dissolve cellulose and when coupled with acidic reagents also generate selected platform chemicals will, as cheaper more economically viable ILs become available, help hopefully advance this area [137–140].

The development of new catalysts and overall process optimization requires collaboration between catalytic chemists, chemical engineers, and experts in molecular simulation to take advantage of innovative reactor designs; the future of renewable feedstock utilization requires a concerted effort from chemists and engineers to develop catalysts and reactors and overall processes in tandem. Current political concerns over the “food versus fuel” debate and societal issues also require the use of waste-derived feedstocks while being mindful of the necessity to balance current

use of such waste (e.g., in animal feed or for returning to the land). Most crucially, however, if technical advances are to be made, the catalytic community needs to look carefully at the accuracy of analysis and determine mass balances when reporting findings for catalytic biomass conversion. The unrealistically high and varied 5-HMF yields often reported in the literature following elevated temperature (>140 °C) sugar processing no doubt neglect humin and by-product formation, which is not quantifiable by HPLC, leading to unreliable claims of catalyst performance in many studies. Furthermore, the use of sustainable solvents for biomass processing should be encouraged which avoid the use of, e.g., DMSO or other expensive/hazardous solvents. While in the case of HMF production such approaches may furnish an improved selectivity, these do nothing to advance catalyst development when using media that would not be viable on a commercial scale. Such changes in approach by the community are essential if catalytic routes to convert biomass to chemicals and fuels become viable processes in the renewable sector during the twenty-first century.

References

1. Walter B, Gruson JF, Monnier G (2008) Diesel engines and fuels: a wide range of evolutions to come – general context and research themes. Oil Gas Sci Technol Rev D Ifp Energ Nouv 63:387–393
2. Armaroli N, Balzani V (2007) The future of energy supply: challenges and opportunities. Angew Chem Int Ed 46:52–66
3. Chen G-Q, Patel MK (2011) Plastics derived from biological sources: present and future: a technical and environmental review. Chem Rev 112:2082–2099
4. Azadi P, Inderwildi OR, Farnood R, King DA (2013) Liquid fuels, hydrogen and chemicals from lignin: a critical review. Renew Sust Energ Rev 21:506–523
5. Bozell JJ, Petersen GR (2010) Technology development for the production of biobased products from biorefinery carbohydrates-the US Department of Energy's "Top 10" revisited. Green Chem 12:539–554
6. Danielsen F, Beukema H, Burgess ND, Parish F, Bruehl CA, Donald PF, Murdiyarso D, Phalan B, Reijnders L, Struebig M (2009) Biofuel plantations on forested lands: double jeopardy for biodiversity and climate. Conserv Biol 23:348–358
7. Kamm B, Kamm M (2007) The concept of biorefinery – production of platform chemicals and final products. Chem Ing Tech 79:592–603
8. Kamm B (2007) Production of platform chemicals and synthesis gas from biomass. Angew Chem Int Ed 46:5056–5058
9. Corma A, Iborra S, Velty A (2007) Chemical routes for the transformation of biomass into chemicals. Chem Rev 107:2411–2502
10. Gallezot P (2007) Catalytic routes from renewables to fine chemicals. Catal Today 121:76–91
11. Roberts MW (2006) Solid state chemistry and the design of heterogeneous catalysts. Catal Lett 67:55–61
12. Sharma YC, Singh B, Korstad J (2011) Advancements in solid acid catalysts for ecofriendly and economically viable synthesis of biodiesel. Biofuels Bioprod Bioref 5:69–92
13. Galarneau A, Renzo FD, Fajula F, Vedrine J (2001) Zeolites and mesoporous materials at the dawn of the 21st century. In: Galarneau A, Renzo FD, Fajula F, Vedrine J (eds) The 13th international zeolite conference. Elsevier, Montpellier

14. Climent MJ, Corma A, Iborra S (2011) Converting carbohydrates to bulk chemicals and fine chemicals over heterogeneous catalysts. Green Chem 13:520–540
15. Wang A, Zhang T (2013) One-pot conversion of cellulose to ethylene glycol with multifunctional tungsten-based catalysts. Acc Chem Res 46:1377–1386
16. Zhao D, Feng J, Huo Q, Melosh N, Fredrickson GH, Chmelka BF, Stucky GD (1998) Triblock copolymer syntheses of mesoporous silica with periodic 50 to 300 angstrom pores. Science 279:548–552
17. Crisci AJ, Tucker MH, Dumesic JA, Scott SL (2010) Bifunctional solid catalysts for the selective conversion of fructose to 5-hydroxymethylfurfural. Top Catal 53:1185–1192
18. Crisci AJ, Tucker MH, Lee MY, Jang SG, Dumesic JA, Scott SL (2011) Acid-functionalized SBA-15-type silica catalysts for carbohydrate dehydration. ACS Catal 1:719–728
19. Guo X, Cao Q, Jiang Y, Guan J, Wang X, Mu X (2012) Selective dehydration of fructose to 5-hydroxymethylfurfural catalyzed by mesoporous SBA-15-SO_3H in ionic liquid BmimCl. Carbohydr Res 351:35–41
20. Wang W, Lofgreen JE, Ozin GA (2010) Why PMO? Towards functionality and utility of periodic mesoporous organosilicas. Small 6:2634–2642
21. Burleigh MC, Markowitz MA, Jayasundera S, Spector MS, Thomas CW, Gaber BP (2003) Mechanical and hydrothermal stabilities of aged periodic mesoporous organosilicas. J Phys Chem B 107:12628–12634
22. Tucker MH, Crisci AJ, Wigington BN, Phadke N, Alamillo R, Zhang J, Scott SL, Dumesic JA (2012) Acid-functionalized SBA-15-type periodic mesoporous organosilicas and their use in the continuous production of 5-Hydroxymethylfurfural. ACS Catal 2:1865–1876
23. Bispo C, De Oliveira VK, Sardo M, Bion N, Mafra L, Ferreira P, Jerome F (2014) Catalytic dehydration of fructose to HMF over sulfonic acid functionalized periodic mesoporous organosilicas: role of the acid density. Catal Sci Technol 4:2235–2241
24. van der Graaff WNP, Olvera KG, Pidko EA, Hensen EJM (2014) Stability and catalytic properties of porous acidic (organo)silica materials for conversion of carbohydrates. J Mol Catal A Chem 388–389:81–89
25. Lucas N, Kokate G, Nagpure A, Chilukuri S (2013) Dehydration of fructose to 5-hydroxymethyl furfural over ordered AlSBA-15 catalysts. Microporous Mesoporous Mater 181:38–46
26. Kuehl GH, Timken HKC (2000) Acid sites in zeolite beta: effects of ammonium exchange and steaming. Microporous Mesoporous Mater 35–36:521–532
27. de Lucas A, Canizares P, Durán A, Carrero A (1997) Dealumination of HZSM-5 zeolites: effect of steaming on acidity and aromatization activity. Appl Catal Gen 154:221–240
28. Poh NE, Nur H, Muhid MNM, Hamdan H (2006) Sulphated AlMCM-41: mesoporous solid Brønsted acid catalyst for dibenzoylation of biphenyl. Catal Today 114:257–262
29. Weingarten R, Tompsett GA, Conner WC Jr, Huber GW (2011) Design of solid acid catalysts for aqueous-phase dehydration of carbohydrates: the role of Lewis and Brønsted acid sites. J Catal 279:174–182
30. Yang ZZ, Deng J, Pan T, Guo QX, Fu Y (2012) A one-pot approach for conversion of fructose to 2,5-diformylfuran by combination of Fe_3O_4-SBA-SO_3H and K-OMS-2. Green Chem 14:2986–2990
31. Huang Z, Pan W, Zhou H, Qin F, Xu H, Shen W (2013) Nafion-resin-modified mesocellular silica foam catalyst for 5-hydroxymethylfurfural production from D-fructose. ChemSusChem 6:1063–1069
32. Wang J, Xu W, Ren J, Liu X, Lu G, Wang Y (2011) Efficient catalytic conversion of fructose into hydroxymethylfurfural by a novel carbon-based solid acid. Green Chem 13:2678–2681
33. Qi X, Guo H, Li L, Smith RL Jr (2012) Acid-catalyzed dehydration of fructose into 5-hydroxymethylfurfural by cellulose-derived amorphous carbon. ChemSusChem 5:2215–2220
34. Guo F, Fang Z, Zhou TJ (2012) Conversion of fructose and glucose into 5-hydroxymethylfurfural with lignin-derived carbonaceous catalyst under microwave irradiation in dimethyl sulfoxide-ionic liquid mixtures. Bioresour Technol 112:313–318

35. Toda M, Takagaki A, Okamura M, Kondo JN, Hayashi S, Domen K, Hara M (2005) Green chemistry: biodiesel made with sugar catalyst. Nature 438:178–178
36. Suganuma S, Nakajima K, Kitano M, Yamaguchi D, Kato H, Hayashi S, Hara M (2008) Hydrolysis of cellulose by amorphous carbon bearing SO_3H, COOH, and OH groups. J Am Chem Soc 130:12787–12793
37. Liu R, Chen J, Huang X, Chen L, Ma L, Li X (2013) Conversion of fructose into 5-hydroxymethylfurfural and alkyl levulinates catalyzed by sulfonic acid-functionalized carbon materials. Green Chem 15:2895–2903
38. Mazzotta MG, Gupta D, Saha B, Patra AK, Bhaumik A, Abu-Omar MM (2014) Efficient solid acid catalyst containing Lewis and Brønsted acid sites for the production of furfurals. ChemSusChem 7:2342–2350
39. Moreau C, Durand R, Pourcheron C, Razigade S (1994) Preparation of 5-hydroxymethylfurfural from fructose and precursors over H-form zeolites. Ind Crop Prod 3:85–90
40. Moreau C, Durand R, Razigade S, Duhamet J, Faugeras P, Rivalier P, Ros P, Avignon G (1996) Dehydration of fructose to 5-hydroxymethylfurfural over H-mordenites. Appl Catal A Gen 145:211–214
41. Fang Z, Liu B, Luo J, Ren Y, Zhang Z (2014) Efficient conversion of carbohydrates into 5-hydroxymethylfurfural catalyzed by the chromium-exchanged montmorillonite K-10 clay. Biomass Bioenergy 60:171–177
42. Liu A, Liu B, Wang Y, Ren R, Zhang Z (2014) Efficient one-pot synthesis of 5-ethoxymethylfurfural from fructose catalyzed by heteropolyacid supported on K-10 clay. Fuel 117(Part A):68–73
43. Kruger JS, Choudhary V, Nikolakis V, Vlachos DG (2013) Elucidating the roles of zeolite H-BEA in aqueous-phase fructose dehydration and HMF rehydration. ACS Catal 3:1279–1291
44. Ordomsky VV, van der Schaaf J, Schouten JC, Nijhuis TA (2012) The effect of solvent addition on fructose dehydration to 5-hydroxymethylfurfural in biphasic system over zeolites. J Catal 287:68–75
45. Seri K, Inoue Y, Ishida H (2001) Catalytic activity of lanthanide (III) ions for the dehydration of hexose to 5-hydroxymethyl-2-furaldehyde in water. Bull Chem Soc Jpn 74:1145–1150
46. Nakamura Y, Morikawa S (1980) The dehydration of D-fructose to 5-hydroxymethyl-2-furaldehyde. Bull Chem Soc Jpn 53:3705–3706
47. Lansalot-Matras C, Moreau C (2003) Dehydration of fructose into 5-hydroxymethylfurfural in the presence of ionic liquids. Catal Commun 4:517–520
48. Qi X, Watanabe M, Aida TM, Smith JRL (2009) Efficient process for conversion of fructose to 5-hydroxymethylfurfural with ionic liquids. Green Chem 11:1327–1331
49. Shimizu K, Uozumi R, Satsuma A (2009) Enhanced production of hydroxymethylfurfural from fructose with solid acid catalysts by simple water removal methods. Catal Commun 10:1849–1853
50. Dacquin JP, Lee AF, Pirez C, Wilson K (2012) Pore-expanded SBA-15 sulfonic acid silicas for biodiesel synthesis. Catal Commun 48:212–214
51. Dhainaut J, Dacquin J-P, Lee AF, Wilson K (2010) Hierarchical macroporous–mesoporous SBA-15 sulfonic acid catalysts for biodiesel synthesis. Green Chem 12:296–303
52. Qi X, Watanabe M, Aida TM, Smith JRL (2008) Catalytic dehydration of fructose into 5-hydroxymethylfurfural by ion-exchange resin in mixed-aqueous system by microwave heating. Green Chem 10:799–805
53. Qi X, Watanabe M, Aida TM, Smith RL (2008) Selective conversion of D-fructose to 5-hydroxymethylfurfural by ion-exchange resin in acetone/dimethyl sulfoxide solvent mixtures. Ind Eng Chem Res 47:9234–9239
54. Li Y, Liu H, Song C, Gu X, Li H, Zhu W, Yin S, Han C (2013) The dehydration of fructose to 5-hydroxymethylfurfural efficiently catalyzed by acidic ion-exchange resin in ionic liquid. Bioresour Technol 133:347–353
55. Aellig C, Hermans I (2012) Continuous D-fructose dehydration to 5- hydroxymethylfurfural under mild conditions. ChemSusChem 5:1737–1742

56. Binder JB, Raines RT (2010) Fermentable sugars by chemical hydrolysis of biomass. Proc Natl Acad Sci U S A 107:4516–4521
57. Bao Q, Qiao K, Tomida D, Yokoyama C (2008) Preparation of 5-hydroxymethylfurfural by dehydration of fructose in the presence of acidic ionic liquid. Catal Commun 9:1383–1388
58. Sidhpuria KB, Daniel da Silva AL, Trindade T, Coutinho JAP (2011) Supported ionic liquid silica nanoparticles (SILnPs) as an efficient and recyclable heterogeneous catalyst for the dehydration of fructose to 5-hydroxymethylfurfural. Green Chem 13:340–349
59. Lee YY, Wu KCW (2012) Conversion and kinetics study of fructose-to-5-hydroxymethylfurfural (HMF) using sulfonic and ionic liquid groups bi-functionalized mesoporous silica nanoparticles as recyclable solid catalysts in DMSO systems. PCCP 14:13914–13917
60. Shi XL, Zhang M, Li Y, Zhang W (2013) Polypropylene fiber supported ionic liquids for the conversion of fructose to 5-hydroxymethylfurfural under mild conditions. Green Chem 15:3438–3445
61. Yuan J, Antonietti M (2011) Poly (ionic liquid) s: polymers expanding classical property profiles. Polymer 52:1469–1482
62. Li H, Zhang Q, Liu X, Chang F, Zhang Y, Xue W, Yang S (2013) Immobilizing Cr^{3+} with SO_3H-functionalized solid polymeric ionic liquids as efficient and reusable catalysts for selective transformation of carbohydrates into 5-hydroxymethylfurfural. Bioresour Technol 144:21–27
63. Watanabe M, Aizawa Y, Iida T, Nishimura R, Inomata H (2005) Catalytic glucose and fructose conversions with TiO_2 and ZrO_2 in water at 473 K: relationship between reactivity and acid–base property determined by TPD measurement. Appl Catal Gen 295:150–156
64. Qi X, Watanabe M, Aida TM, Smith RL Jr (2008) Catalytical conversion of fructose and glucose into 5-hydroxymethylfurfural in hot compressed water by microwave heating. Catal Commun 9:2244–2249
65. McNeff CV, Nowlan DT, McNeff LC, Yan B, Fedie RL (2010) Continuous production of 5-hydroxymethylfurfural from simple and complex carbohydrates. Appl Catal Gen 384:65–69
66. Yan H, Yang Y, Tong D, Xiang X, Hu C (2009) Catalytic conversion of glucose to 5-hydroxymethylfurfural over SO_4^{2-}/ZrO_2 and SO_4^{2-}/ZrO_2–Al_2O_3 solid acid catalysts. Catal Commun 10:1558–1563
67. Qi X, Watanabe M, Aida TM, Smith RL Jr (2009) Sulfated zirconia as a solid acid catalyst for the dehydration of fructose to 5-hydroxymethylfurfural. Catal Commun 10:1771–1775
68. Osatiashtiani A, Lee AF, Brown DR, Melero JA, Morales G, Wilson K (2014) Bifunctional SO_4/ZrO_2 catalysts for 5-hydroxymethylfurfural (5-HMF) production from glucose. Catal Sci Technol 4:333–342
69. Ordomsky VV, van der Schaaf J, Schouten JC, Nijhuis TA (2012) Fructose dehydration to 5-hydroxymethylfurfural over solid acid catalysts in a biphasic system. ChemSusChem 5:1812–1819
70. Benvenuti F, Carlini C, Patrono P, Raspolli Galletti AM, Sbrana G, Massucci MA, Galli P (2000) Heterogeneous zirconium and titanium catalysts for the selective synthesis of 5-hydroxymethyl-2-furaldehyde from carbohydrates. Appl Catal Gen 193:147–153
71. De S, Dutta S, Patra AK, Bhaumik A, Saha B (2011) Self-assembly of mesoporous TiO_2 nanospheres via aspartic acid templating pathway and its catalytic application for 5-hydroxymethyl-furfural synthesis. J Mater Chem 21:17505–17510
72. Dutta S, De S, Patra AK, Sasidharan M, Bhaumik A, Saha B (2011) Microwave assisted rapid conversion of carbohydrates into 5-hydroxymethylfurfural catalyzed by mesoporous TiO_2 nanoparticles. Appl Catal Gen 409–410:133–139
73. Dutta A, Patra AK, Dutta S, Saha B, Bhaumik A (2012) Hierarchically porous titanium phosphate nanoparticles: an efficient solid acid catalyst for microwave assisted conversion of biomass and carbohydrates into 5-hydroxymethylfurfural. J Mater Chem 22:14094–14100
74. Carlini C, Giuttari M, Maria Raspolli Galletti A, Sbrana G, Armaroli T, Busca G (1999) Selective saccharides dehydration to 5-hydroxymethyl-2-furaldehyde by heterogeneous niobium catalysts. Appl Catal Gen 183:295–302

75. Armaroli T, Busca G, Carlini C, Giuttari M, Raspolli Galletti AM, Sbrana G (2000) Acid sites characterization of niobium phosphate catalysts and their activity in fructose dehydration to 5-hydroxymethyl-2-furaldehyde. J Mol Catal A Chem 151:233–243
76. Yang F, Liu Q, Bai X, Du Y (2011) Conversion of biomass into 5-hydroxymethylfurfural using solid acid catalyst. Bioresour Technol 102:3424–3429
77. Yang F, Liu Q, Yue M, Bai X, Du Y (2011) Tantalum compounds as heterogeneous catalysts for saccharide dehydration to 5-hydroxymethylfurfural. Chem Commun 47:4469–4471
78. Dutta A, Gupta D, Patra AK, Saha B, Bhaumik A (2014) Synthesis of 5-hydroxymethylfurfural from carbohydrates using large-pore mesoporous tin phosphate. ChemSusChem 7:925–933
79. Tian C, Zhu X, Chai SH, Wu Z, Binder A, Brown S, Li L, Luo H, Guo Y, Dai S (2014) Three-phase catalytic system of H_2O, ionic liquid, and $VOPO_4$–SiO_2 solid acid for conversion of fructose to 5-hydroxymethylfurfural. ChemSusChem 7:1703–1709
80. Fan C, Guan H, Zhang H, Wang J, Wang S, Wang X (2011) Conversion of fructose and glucose into 5-hydroxymethylfurfural catalyzed by a solid heteropolyacid salt. Biomass Bioenergy 35:2659–2665
81. Zhang Y, Degirmenci V, Li C, Hensen EJM (2011) Phosphotungstic acid encapsulated in metal–organic framework as catalysts for carbohydrate dehydration to 5-hydroxymethylfurfural. ChemSusChem 4:59–64
82. Moliner M, Roman-Leshkov Y, Davis ME (2010) Tin-containing zeolites are highly active catalysts for the isomerization of glucose in water. Proc Natl Acad Sci U S A 107:6164–6168
83. Yang BY, Montgomery R (1996) Alkaline degradation of glucose: effect of initial concentration of reactants. Carbohydr Res 280:27–45
84. De Wit G, Kieboom APG, van Bekkum H (1979) Enolisation and isomerisation of monosaccharides in aqueous, alkaline solution. Carbohydr Res 74:157–175
85. de Bruyn CAL, van Ekenstein WA (1895) Action des alcalis sur les sucres, II. Transformation réciproque des uns dans les autres des sucres glucose, fructose et mannose. Recl Trav Chim Pays-Bas 14:203–216
86. de Bruijn JM, Kieboom APG, van Bekkum H (1987) Alkaline degradation of monosaccharides V: kinetics of the alkaline isomerization and degradation of monosaccharides. Recl Trav Chim Pays-Bas 106:35–43
87. De Bruijn JM, Kieboom APG, van Bekkum H (1987) Alkaline degradation of monosaccharides part VII. A mechanistic picture. Starch – Stärke 39:23–28
88. Moreau C, Durand R, Roux A, Tichit D (2000) Isomerization of glucose into fructose in the presence of cation-exchanged zeolites and hydrotalcites. Appl Catal Gen 193:257–264
89. Yu S, Kim E, Park S, Song IK, Jung JC (2012) Isomerization of glucose into fructose over Mg–Al hydrotalcite catalysts. Catal Commun 29:63–67
90. Román-Leshkov Y, Davis ME (2011) Activation of carbonyl-containing molecules with solid Lewis acids in aqueous media. ACS Catal 1:1566–1580
91. Nikolla E, Román-Leshkov Y, Moliner M, Davis ME (2011) "One-Pot" synthesis of 5-(Hydroxymethyl)furfural from carbohydrates using tin-beta zeolite. ACS Catal 1:408–410
92. Yuriy Roman-Leshkov MM, Labinger JA, Davis ME (2010) Mechanism of glucose isomerization using a solid Lewis acid catalyst in water. Angew Chem Int Ed 49:8954–8957
93. Bermejo-Deval R, Assary RS, Nikolla E, Moliner M, Román-Leshkov Y, Hwang S-J, Palsdottir A, Silverman D, Lobo RF, Curtiss LA, Davis ME (2012) Metalloenzyme-like catalyzed isomerizations of sugars by Lewis acid zeolites. Proc Natl Acad Sci U S A 109:9727–9732
94. Rai N, Caratzoulas S, Vlachos DG (2013) Role of silanol group in Sn-beta zeolite for glucose isomerization and epimerization reactions. ACS Catal 3:2294–2298
95. Li Y-P, Head-Gordon M, Bell AT (2014) Analysis of the reaction mechanism and catalytic activity of metal-substituted beta zeolite for the isomerization of glucose to fructose. ACS Catal 4:1537–1545
96. Gounder R, Davis ME (2013) Monosaccharide and disaccharide isomerization over Lewis acid sites in hydrophobic and hydrophilic molecular sieves. J Catal 308:176–188

97. Nagorski RW, Richard JP (2001) Mechanistic imperatives for aldose–ketose isomerization in water: specific, general base- and metal ion-catalyzed isomerization of glyceraldehyde with proton and hydride transfer. J Am Chem Soc 123:794–802
98. Wang T, Nolte MW, Shanks BH (2014) Catalytic dehydration of C6 carbohydrates for the production of hydroxymethylfurfural (HMF) as a versatile platform chemical. Green Chem 16:548–572
99. Qi X, Watanabe M, Aida TM, Smith RL (2012) Synergistic conversion of glucose into 5-hydroxymethylfurfural in ionic liquid–water mixtures. Biomass Bioenergy 109:224–228
100. Ordomsky VV, Sushkevich VL, Schouten JC, van der Schaaf J, Nijhuis TA (2013) Glucose dehydration to 5-hydroxymethylfurfural over phosphate catalysts. J Catal 300:37–46
101. Ordomsky VV, van der Schaaf J, Schouten JC, Nijhuis TA (2013) Glucose dehydration to 5-hydroxymethylfurfural in a biphasic system over solid acid foams. ChemSusChem 6:1697–1707
102. Nakajima K, Baba Y, Noma R, Kitano M, N. Kondo J, Hayashi S, Hara M (2011) $Nb_2O_5{\cdot}nH_2O$ as a heterogeneous catalyst with water-tolerant lewis acid sites. J Am Chem Soc 133:4224–4227
103. Kitano M, Nakajima K, Kondo JN, Hayashi S, Hara M (2010) Protonated titanate nanotubes as solid acid catalyst. J Am Chem Soc 132:6622–6623
104. Xiong H, Pham HN, Datye AK (2013) A facile approach for the synthesis of niobia/carbon composites having improved hydrothermal stability for aqueous-phase reactions. J Catal 302:93–100
105. Xiong H, Wang T, Shanks BH, Datye AK (2013) Tuning the location of niobia/carbon composites in a biphasic reaction: dehydration of d-glucose to 5-hydroxymethylfurfural. Catal Lett 143:509–516
106. Hu L, Wu Z, Xu J, Sun Y, Lin L, Liu S (2014) Zeolite-promoted transformation of glucose into 5-hydroxymethylfurfural in ionic liquid. Chem Eng J 244:137–144
107. Wang J, Ren J, Liu X, Xi J, Xia Q, Zu Y, Lu G, Wang Y (2012) Direct conversion of carbohydrates to 5-hydroxymethylfurfural using Sn-Mont catalyst. Green Chem 14:2506–2512
108. de Clippel F, Dusselier M, Van Rompaey R, Vanelderen P, Dijkmans J, Makshina E, Giebeler L, Oswald S, Baron GV, Denayer JF, Pescarmona PP, Jacobs PA, Sels BF (2012) Fast and selective sugar conversion to alkyl lactate and lactic acid with bifunctional carbon-silica catalysts. J Am Chem Soc 134:10089–10101
109. Hu L, Zhao G, Tang X, Wu Z, Xu J, Lin L, Liu S (2013) Catalytic conversion of carbohydrates into 5-hydroxymethylfurfural over cellulose-derived carbonaceous catalyst in ionic liquid. Bioresour Technol 148:501–507
110. Takagaki A, Ohara M, Nishimura S, Ebitani K (2009) A one-pot reaction for biorefinery: combination of solid acid and base catalysts for direct production of 5-hydroxymethylfurfural from saccharides. Chem Commun 41:6276–6278
111. Takagaki A, Takahashi M, Nishimura S, Ebitani K (2011) One-pot synthesis of 2, 5-diformylfuran from carbohydrate derivatives by sulfonated resin and hydrotalcite-supported ruthenium catalysts. ACS Catal 1:1562–1565
112. Wang L, Wang H, Liu F, Zheng A, Zhang J, Sun Q, Lewis JP, Zhu L, Meng X, Xiao FS (2014) Selective catalytic production of 5-hydroxymethylfurfural from glucose by adjusting catalyst wettability. ChemSusChem 7:402–406
113. Yamaguchi D, Kitano M, Suganuma S, Nakajima K, Kato H, Hara M (2009) Hydrolysis of cellulose by a solid acid catalyst under optimal reaction conditions. J Phys Chem C 113:3181–3188
114. Suganuma S, Nakajima K, Kitano M, Hayashi S, Hara M (2012) sp(3) -linked amorphous carbon with sulfonic acid groups as a heterogeneous acid catalyst. ChemSusChem 5:1841–1846
115. Onda A, Ochi T, Yanagisawa K (2009) Hydrolysis of cellulose selectively into glucose over sulfonated activated-carbon catalyst under hydrothermal conditions. Top Catal 52:801–807
116. Onda A, Ochi T, Yanagisawa K (2008) Selective hydrolysis of cellulose into glucose over solid acid catalysts. Green Chem 10:1033–1037

117. Pang J, Wang A, Zheng M, Zhang T (2010) Hydrolysis of cellulose into glucose over carbons sulfonated at elevated temperatures. Chem Commun 46:6935–6937
118. Dhepe PL, Ohashi M, Inagaki S, Ichikawa M, Fukuoka A (2005) Hydrolysis of sugars catalyzed by water-tolerant sulfonated mesoporous silicas. Catal Lett 102:163–169
119. D-m L, Deng L, Li J, Liao B, Guo Q-x, Fu Y (2011) Hydrolysis of cellulose into glucose by magnetic solid acid. ChemSusChem 4:55–58
120. Xiong Y, Zhang Z, Wang X, Liu B, Lin J (2014) Hydrolysis of cellulose in ionic liquids catalyzed by a magnetically-recoverable solid acid catalyst. Chem Eng J 235:349–355
121. Takagaki A, Nishimura M, Nishimura S, Ebitani K (2011) Hydrolysis of sugars using magnetic silica nanoparticles with sulfonic acid groups. Chem Lett 40:1195–1197
122. Van de Vyver S, Peng L, Geboers J, Schepers H, de Clippel F, Gommes CJ, Goderis B, Jacobs PA, Sels BF (2010) Sulfonated silica/carbon nanocomposites as novel catalysts for hydrolysis of cellulose to glucose. Green Chem 12:1560–1563
123. Tagusagawa C, Takagaki A, Takanabe K, Ebitani K, Hayashi S, Domen K (2009) Effects of transition-metal composition of protonated, layered nonstoichiometric oxides $H_{1-x}Nb_{1-x}Mo_{1+x}O_6$ on heterogeneous acid catalysis. J Phys Chem C 113:17421–17427
124. Tagusagawa C, Takagaki A, Takanabe K, Ebitani K, Hayashi S, Domen K (2010) Layered and nanosheet tantalum molybdate as strong solid acid catalysts. J Catal 270:206–212
125. Tagusagawa C, Takagaki A, Iguchi A, Takanabe K, Kondo JN, Ebitani K, Hayashi S, Tatsumi T, Domen K (2010) Highly active mesoporous Nb–W oxide solid-acid catalyst. Angew Chem Int Ed 49:1128–1132
126. Tagusagawa C, Takagaki A, Iguchi A, Takanabe K, Kondo JN, Ebitani K, Tatsumi T, Domen K (2010) Synthesis and characterization of mesoporous Ta–W oxides as strong solid acid catalysts. Chem Mater 22:3072–3078
127. von Rybinski W, Hill K (1998) Alkyl polyglycosides—properties and applications of a new class of surfactants. Angew Chem Int Ed 37:1328–1345
128. Jeffrey GA (1986) Carbohydrate liquid crystals. Acc Chem Res 19:168–173
129. Fischer E (1893) Ueber die Glucoside der Alkohole. Eur J Inorg Chem 26:2400–2412
130. van der Heijden AM, Lee TC, van Rantwijk F, van Bekkum H (2002) Glycosidation of fructose-containing disaccharides using MCM-41 material as the catalyst. Carbohydr Res 337:1993–1998
131. Biermann M, Schmid K, Schulz P (1993) Alkylpolyglucoside – technologie und eigenschaften. Starch – Stärke 45:281–288
132. Ishikawa Y, Saka S (2001) Chemical conversion of cellulose as treated in supercritical methanol. Cellulose 8:189–195
133. Deng W, Liu M, Zhang Q, Tan X, Wang Y (2010) Acid-catalysed direct transformation of cellulose into methyl glucosides in methanol at moderate temperatures. Chem Commun 46:2668–2670
134. Villandier N, Corma A (2010) One pot catalytic conversion of cellulose into biodegradable surfactants. Chem Commun 46:4408–4410
135. Ignatyev IA, Mertens PGN, Van Doorslaer C, Binnemans K, de Vos DE (2010) Cellulose conversion into alkylglycosides in the ionic liquid 1-butyl-3-methylimidazolium chloride. Green Chem 12:1790–1795
136. Pinzi S, Garcia I, Lopez-Gimenez F, Luque de Castro M, Dorado G, Dorado M (2009) The ideal vegetable oil-based biodiesel composition: a review of social, economical and technical implications. Energy Fuels 23:2325–2341
137. Binder JB, Raines RT (2009) Simple chemical transformation of lignocellulosic biomass into furans for fuels and chemicals. J Am Chem Soc 131:1979–1985
138. Brandt A, Hallett JP, Leak DJ, Murphy RJ, Welton T (2010) The effect of the ionic liquid anion in the pretreatment of pine wood chips. Green Chem 12:672–679
139. Zhao H, Holladay JE, Brown H, Zhang ZC (2007) Metal chlorides in ionic liquid solvents convert sugars to 5-hydroxymethylfurfural. Science 316:1597–1600
140. Rinaldi R, Palkovits R, Schuth F (2008) Depolymerization of cellulose using solid catalysts in ionic liquids. Angew Chem Int Ed 47:8047–8050

Chapter 7
Catalytic Oxidation Pathways for the Production of Carboxylic Acids from Biomass

Lisha Yang, Ji Su, Xiaokun Yang, and Hongfei Lin

Abstract The transition from a fossil chemical industry to a renewable chemical industry depends on breakthroughs in the research and development on the most promising alternatives. Biomass is such a class of renewable raw carbon materials for the production of fuels and chemicals, with growing interest among researchers aiming to achieve global sustainability. Catalytic oxidation of biomass can lead to multiple products, and the challenge is to direct the reaction pathways to the desired products. Organic acids are among the listed "platform molecules," which have the potential to be further converted into high-value-added chemicals. In this chapter, various pathways are reviewed for catalytic oxidation of a variety of biomass to produce value-added organic acids.

Keywords Catalytic oxidation • Carboxylic acids • Biomass conversion • Heterogeneous catalyst • Reaction pathway

7.1 Introduction

In 2004, the US Department of Energy issued a report which listed 12 sugar-derived chemicals as potential building blocks for future biorefineries [1]. Bozell et al. provided a dynamic guide to technology development that could realize commercial success through the proper integrated coproduction of biofuels and bio-based products [2]. In both reports, C3–C5 carboxylic acids (e.g., lactic, succinic, malic, maleic, levulinic, etc.) are among the widely spread "platform molecules."

Considerable progress has been made in industry in the use of carbohydrates as starting materials for chemical production. Four leading biochemical companies, Myriant, BioAmber, BASF-Purac, and Reverdia, have started or are building and

L. Yang • J. Su • X. Yang • H. Lin (✉)
Department of Chemical and Materials Engineering, University of Nevada, Reno, NV 89557, USA
e-mail: HongfeiL@unr.edu

M. Schlaf, Z.C. Zhang (eds.), *Reaction Pathways and Mechanisms in Thermocatalytic Biomass Conversion I*, Green Chemistry and Sustainable Technology, DOI 10.1007/978-981-287-688-1_7

expanding their production facilities to produce bio-based organic acids that have the potential to replace their petroleum-derived counterparts. For instance, high-purity bio-succinic acid has been demonstrated to be a drop-in replacement for petroleum-based succinic acid while also being more environmentally friendly and cost advantaged without government subsidies. Difunctional carboxylic acids are excellent platform building blocks for synthesizing a variety of plastic, polymer, and resin products. Today the global market for bio-based organic acids and their derived commodity chemicals is still at the infancy stage, but this market is gaining momentum. The worldwide production capacity for bioplastics is projected to increase sixfold from ~1.0 million tons in 2010 to approximately 5.8 million tons by 2016. By far the strongest growth will be the so-called "drop-in" bio-based plastics, which merely differ from their conventional counterparts in terms of their renewable raw material base. However, the transition from a fossil chemical industry to a renewable chemical industry will likewise depend on the progress of research and development. Herein, we summarize the recent publications in the literature on the catalytic oxidation reaction pathways for the production of carboxylic acids from various types of biomass feedstocks.

7.2 Oxidation of Glycerol

Glycerol, also called glycerine or glycerin (GLY), is a simple C3 polyol compound. It is a colorless, odorless, viscous liquid that is widely used in pharmaceutical formulations. Glycerol has three hydroxyl groups that are responsible for its solubility in water and its hygroscopic nature. The glycerol backbone is central to all lipids known as triglycerides. GLY is a by-product of the production of biodiesel via transesterification and also a coproduct in the production of long-chain carboxylate salts used as soaps. Approximately 950,000 tons of glycerol were produced per year in the United States and Europe, among which 350,000 tons of glycerol were produced per year in the United States alone. It is projected that by the year 2020, production will be six times more than demand.

The conversion of glycerol to value-added chemicals has attracted much attention in recent years due to the projected oversupply in the market (Fig. 7.1). The oxidation of glycerol usually follows complex reaction pathways yielding various C3 (glyceraldehyde, dihydroxyacetone, glyceric acid, tartronic acid, hydroxypyruvic acid, lactic acid, mesoxalic acid) together with C2 (oxalic and glycolic acids) and C1 (formic acid) products, as shown in Table 7.1. These products are potentially valuable chelating agents and useful intermediates in organic synthesis, but presently they have a limited market because they are produced by costly stoichiometric chemical oxidation or enzymatic processes. Thus, new processes based on glycerol oxidation with oxygen or air over metal catalysts might be promising. A relatively complete review of glycerol oxidation reactions in the presence of metal catalysts was published recently [3].

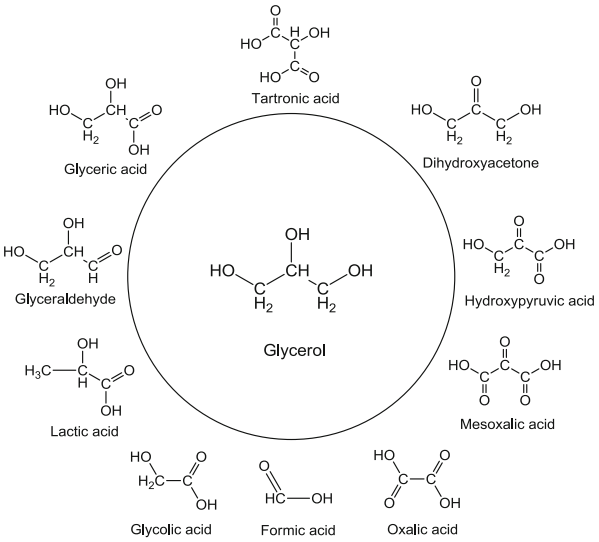

Fig. 7.1 The oxidation products of glycerol

7.2.1 Oxidation of Glycerol to Dihydroxyacetone

Dihydroxyacetone, the oxidation product of the secondary hydroxyl group of glycerol, was first prepared by fermentation (Fig. 7.2). The first catalytic synthesis of dihydroxyacetone directly from glycerol was reported in 1993 [4]. In this work, charcoal-supported platinum showed weak catalytic activity for oxidation of the secondary hydroxyl group of glycerol especially in an acidic media (pH 2–4) with a dihydroxyacetone yield of 4 %. However, incorporation of bismuth in platinum (weight ratio of bismuth to platinum = 0.2) increased the dihydroxyacetone selectivity from 10 to 80 %. A bismuth sub-monolayer on Pt (111) with (x/3 × v/3) R30° structure was proposed for the catalytic oxidation of the secondary hydroxyl group of glycerol molecules. It is postulated that bismuth adatoms function as site blockers on Pt (111), controlling the glycerol orientation toward dihydroxyacetone formation. The application of a fixed-bed reactor increased the glycerol conversion as well as the dihydroxyacetone yield.

The catalytic method showed a much higher productivity than the conventional fermentation process. For instance, the continuous oxidation of 50 wt.% glycerol solutions yielded 52 % of dihydroxyacetone at 50 °C in a fixed-bed reactor with a bimetallic 3 wt.% Pt–0.6 wt.% Bi catalyst (Pt/Bi = 5) supported on a granular carbon [5]. On a Pt/C catalyst, glyceric acid was still the main product (55 % selectivity); but the deposition of bismuth on platinum particles orientates the selectivity toward the oxidation of the secondary hydroxyl group to yield dihydroxyacetone with a selectivity of 50 % at 70 % conversion [6]. The optimization of the bimetallic Pt–Bi

Table 7.1 Selective oxidation of glycerol to different products (reproduced)

		Reaction conditions			Result			Ref
Target products	Catalyst	*T* (°C)	pH	Oxidant	Conversion (%)	Selectivity (%)	Yield (%)	
Dihydroxyacetone	5 wt.% Pt–1 wt.% Bi/C	50	2–4	Air	30	67	20	[4]
Dihydroxyacetone	3 wt.% Pt–0.6 wt.% Bi/C	50	4–8	Air	75	70	52	[5]
Dihydroxyacetone	7.4 wt.% Pt–2.9 wt.% Bi/C	60	2	Air	75	49	37	[6]
Dihydroxyacetone	5 wt.% Pt–5.4 wt.% Bi/C	120	4	0.1 MPa O_2	59	51	30	[7]
Dihydroxyacetone	3 wt.% Pt–0.6 wt.% Bi/C	80	2	O_2	80	60	48	[8]
Dihydroxyacetone	5 wt.% Pt–5 wt.% Bi/C	60		flowing O_2	91.5	49	45	[9]
Dihydroxyacetone	Au/C	60	12	0.1 MPa O_2	50	26		[10]
Dihydroxyacetone	Au–Pt/C (Pt 0.25–0.33)	60	12	0.1 MPa O_2	50	36		
Dihydroxyacetone	1 wt.% Au/C	60	NaOH 0.6 M	0.28 MPa O_2,	30	53	16	[11]
Dihydroxyacetone	Pd–Ag/C (Ag/Pd = 1)	60		Flowing O_2	52	85	44	[12]
Dihydroxyacetone	4.9 wt.% Pt/C	80		0.3 MPa O_2	90	13		
Dihydroxyacetone	4.6 wt.% Pt–5.2 wt.% Bi/C	60		Flowing O_2	90	36		
Dihydroxyacetone	3.8 wt.% Pt–3 wt.% Sb/C	60		Flowing O_2	90	51		[13]
Lactic acid	Au–Pt/TiO2	90	NaOH/GLY = 4	Flowing O_2		85.6		[14]
Lactic acid	Au–Pd/TiO2 with AlCl3	160		2.5 MPa O_2	26	58		[15, 16]
Formic acid	V-substituted phosphomolybdic acid	150		2.0 MPa O_2	100	60		[17]
Glyceric acid	1 wt.% Au/graphite	60	NaOH/GLY = 1	0.3 MPa O2	54	100	54	[18]
Glyceric acid	1 wt.% Au/C (>20 nm)	30	NaOH/GLY = 4	0.3 MPa O2	100	92	92	[19]

Glyceric acid	1 wt.% (Au–Pd)/C (2–3 nm)	30	NaOH/GLY = 4	0.3 MPa O2	90	69		[20]
Glyceric acid	1 wt.% Pd/graphite	30	NaOH/GLY = 4	0.3 MPa O2	90	62		[21]
Glyceric acid	1 wt.% Au/C (45 nm)	60	NaOH/GLY = 2	0.5 MPa O2	50	83		[22]
Glyceric acid	Au/C	60	NaOH/GLY = 2	0.1 MPa O_2	30	75		[23]
Glyceric acid	1.6 wt.% Au/TiO2	60	NaOH/GLY = 2	1 MPa O_2	83	61		[24]
Glyceric acid	2.5 wt.% Au–2.5 wt.% Pd/TiO2	60	NaOH/GLY = 2	1 MPa O_2	90	74		[25]
Glyceric acid	1 wt.% Au/C	60	NaOH/GLY = 2	0.6 MPa O_2	76	36		[26, 27]
Glyceric acid	1 wt.% Au/TiO2	60	NaOH/GLY = 2	0.6 MPa O_2	91	38		
Glyceric acid	1 wt.% Au/Al2O3	60	NaOH/GLY = 2	0.6 MPa O_2	28	28		
Glyceric acid	1 wt.% Au/Nb2O5	60	NaOH/GLY = 2	0.6 MPa O_2	67	47		
Glyceric acid	3.1 wt.% Au/MgAl2O4	50	NaOH/GLY = 4	0.3 MPa O_2	50	61		[28]
Glyceric acid	1 wt.% Au/Dowex M-43	50	NaOH/GLY = 4	0.3 MPa O_2	90	60		[29]
Glyceric acid	0.5 wt.% Pt/carbon spherules	70	NaOH/GLY = 0.8	1 MPa O_2	66	85		[30]
Glyceric acid	5 wt.% Pt/C	60	Base free	O_2	50	47	24	[31]
Glyceric acid	5 wt.% Pt/MWNTs	60	Base free	0.1 MPa O_2	48	66	32	[32, 33]
Glyceric acid	5 wt.% Pt/H2O2-MWNTs	60	Base free	0.1 MPa O_2	70	70	49	
Glyceric acid	5 % Pt/S-MWNTs	60	Base free	0.1 MPa O_2	90	68	62	
Glyceric acid	1 wt.% Au–Pt (6:4)/mordenite	100	Base free	0.3 MPa O_2	70	83		[34]
Glyceric acid	1 wt.% Au–Pt (1:3)/MgO	25	Base free	0.3 MPa O_2	42.5	85		[35]
Glyceric acid	5 wt.% Pt–Cu/C	60	Base free	1 bar O_2	86	71	61	[36]
Glyceric acid	0.7 wt.% Pt/HT	50	Base free	Flowing O_2	63	68		[37]

Reprinted with the permission from ref. [3], Copyright 2014, American Chemical Society

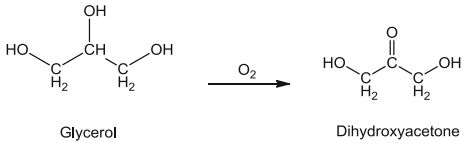

Fig. 7.2 Oxidation of glycerol to dihydroxyacetone

catalyst and reaction conditions for high conversion of glycerol along with high dihydroxyacetone selectivity and yield were studied by several groups. Hu et al. [8] used 3 wt.% Pt–0.6 wt.% Bi supported on a Norit Darco activated carbon, prepared by impregnation of a Pt/C catalyst and reduced with $NaBH_4$, as the catalyst, and yielded 48 % of dihydroxyacetone at a 80 % glycerol conversion in a semi-batch reactor at 80 °C, 0.21 MPa O_2 pressure, and pH 2. Liang et al. [9] reported that the yield of dihydroxyacetone reached 49.0 % at a 91.5 % conversion of glycerol over the 5 % Pt–5 %Bi/C catalyst, and the X-ray diffraction and transmission electron microscopy analysis revealed that the specially configured Pt–Bi nanoparticles (~3.8 nm) were highly dispersed over the active carbon support; however, the stability of Pt–Bi bimetallic catalyst was not satisfactory. For instance, in a continuous trickle-bed reactor, the initial selectivity of 80 % dihydroxyacetone decreased to 40 % after 1000 h on stream [7]. Nie et al. prepared multiwall carbon nanotube (MWCNT)-supported Pt–Sb alloy nanoparticles for the selective oxidation of glycerol to dihydroxyacetone in a base-free aqueous solution. The structure and morphology of the prepared Pt–Sb/MWCNT catalyst were found to be very different from that of Pt–Bi/MWCNTs. Sb homogenously entered into the lattice of Pt and Pt–Sb alloy nanoparticles formed in Pt–Sb/MWCNTs, but Pt particles in Pt–Bi/MWCNTs were wrapped by a layer of $Bi_2O_2CO_3$. The turnover frequency of surface Pt atoms in Pt–Sb/MWCNTs increased from 341.5 (of Pt/MWCNTs) to 878.1 h^{-1}. At the same time, dihydroxyacetone was relatively "stable" over the homogenous Pt–Sb alloy nanoparticles, which depressed the cleavage of C–C bond [13].

Other than Pt catalysts, an Au nanoparticle catalyst was also used for the selective oxidation of glycerol. The nanosized gold catalysts were highly active, so that the reaction could be performed under atmospheric pressure. The influence of the preparation method and the support effect of the Au catalysts have been investigated. The presence of Pt as the promotor was found to increase the selectivity to dihydroxyacetone from 26 % (Au/C) to 36 % (Au–Pt/C) [10]. Recently, Pd-based catalysts for glycerol oxidation to dihydroxyacetone were also developed. It was found that Pd–Ag/C showed higher selectivity to dihydroxyacetone and higher activity than Pd/C: the dihydroxyacetone yield reached 44 % at a 52 % glycerol conversion over Pd–Ag/C (Ag/Pd = 1) [12].

7.2.2 Oxidation of Glycerol to Glyceric Acid

The selective oxidation of glycerol to glyceric acid was usually carried out on supported Pt and Pd catalysts at basic pH [6]. Without adding base, the main reaction products were non-desired C1 by-products, e.g., CO_2, HCHO, and HCOOH. The

formation of C1 by-products was eliminated by adding a base such as NaOH. A high yield (70 %) of glycerate was obtained using a 5 wt.% Pd/C catalyst (Table 7.1) [4]. Since Pt-group metal catalysts suffered from oxygen poisoning at high oxygen partial pressures, gold nano-catalysts that had a better resistance to oxygen poisoning were employed extensively during the last decade. The selective oxidation of glycerol to glycerate over carbon-supported Au catalysts required operation at high pH to reach the optimum performance. The presence of OH^- is essential to observe any glycerol oxidation for Au/C catalysts. Glycerol is oxidized to glyceric acid with 100 % selectivity using either 1 % Au/charcoal or 1 % Au/graphite catalyst under mild reaction conditions (60 °C, 3 h, in aqueous NaOH solution) [38]. In another report, increasing the ratio of NaOH to glycerol to 4, a 92 % selectivity to glycerate at 100 % conversion was obtained by oxidizing 0.3 M glycerol solution at 30 °C over a 1 wt.% Au/C catalyst [19]. It is believed that the base aids the initial dehydrogenation via H-abstraction of one of the primary OH groups of glycerol, and, in this way, the rate-limiting step in the oxidation process is overcome [18].

The size of the metal particles has a profound effect on the selectivity and conversion of glycerol oxidation (Fig. 7.3). It was found that the selectivity to glyceric acid increased with increasing the gold nanoparticle size because the consecutive oxidation reaction to tartronate was minimized at large Au sizes [19, 22]. However, gold particles larger than 50 nm were inactive, and a compromise between activity and selectivity was achieved at ~20 nm [39]. In another study, oxidation of glycerol in the aqueous phase at 333 K and high pH over the Au catalysts revealed a similar influence of particle size, with the 5-nm Au particles giving a TOF of 17 s^{-1} at pH 13.8, and bulk Au was nearly an order of magnitude less active. However, large Au particles (>20 nm) were more selective to glyceric acid. The lower selectivity of small Au particles was attributed to a higher formation rate of H_2O_2 during glycerol oxidation, because peroxide promotes C–C cleavage reaction [22]. Similarly, it was also found that bigger-sized Pt particles (>10 nm) were less active and smaller-sized ones (<6 nm) exhibited higher glycerol conversion and selectivity, as well as good recycled activity [31].

It was found that bimetallic catalysts were more active than monometallic catalysts, indicating that a synergetic effect exists between Au and M (Pd or Pt). This effect was especially significant in that Pt as the monometallic was poisoned before the reaction reached full conversion. In terms of selectivity to glyceric acid, (Au–Pd) catalysts showed in general better selectivity than (Au–Pt) catalysts, while monometallic Pd and Pt mainly promote the formation of tartronic acid and glycolic acid, respectively. The overall selectivity to glyceric acid increased using bimetallic (Au–Pd)/C catalysts with respect to monometallics [20]. It also showed that the use

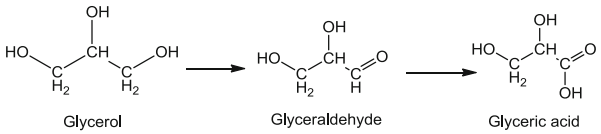

Fig. 7.3 Oxidation of glycerol to glyceric acid

of a bimetallic system of Au and Pd supported on graphite significantly improved the activity with respect to the monometallic system, whereas the selectivity to glyceric acid showed to be dependent upon the reaction temperature and the catalyst preparation method [21].

The support effect was also studied, and no glycerol conversion could be detected with pure carbon or metal oxide supports, while gold nanoparticles supported on different carbons (carbon black, activated carbon, and graphite), and oxides (TiO_2, MgO, and Al_2O_3) were active. For the monometallic catalysts prepared by impregnation, similar activities were observed for Au and Pd, but the carbon-supported monometallic catalysts were more active than those on TiO_2. Glycerate was the major product, and lesser amounts of tartronate, glycolate, oxalate, and formate were observed, suggesting a sequential oxidation pathway. A 1 wt.% Au/Nb_2O_5 catalyst, prepared by gold sol method on a crystalline niobia support, was slightly less active than Au/C and Au/TiO_2 catalysts, but was more selective to glycerate [26, 27]. Also, the selectivity to glycerate over gold catalysts on different $MgAl_2O_4$ spinels was mainly determined by the Al/Mg ratio at the surface as Al-rich surfaces enhanced the C–C bond cleavage [28]. Gold nanoparticles stabilized by THPC (tetrahydroxymethyl phosphonium chloride) deposited on the weak base Dowex M-43 resin and on activated carbon provided a 60 % and 50 % selectivity to glycerate, respectively [29]. A strong effect of the surface chemistry of supporting carbon materials on the selectivity to glycerate was observed, showing particularly that the presence of surface oxygenated groups was unfavorable. A selectivity of 85 % to glycerate was observed at 66 % conversion using Pt particles supported on carbon spherules [30]. The Pt/MWNT catalyst was more active than Pt/AC for glycerol oxidation with oxygen in a base-free aqueous solution at 60 °C. Upon functionalization of the MWNTs by thiolation, free glyceric acid was obtained with a 68 % selectivity at 90 % conversion [32, 33].

The bimetallic Au–Pt nano-catalysts supported on zeolite H-mordenite were able to selectively oxidize glycerol directly to glyceric acid without the use of bases. Au–Pt on activated carbon showed similar initial activity, but the major effect of using mordenite as the support lies in the enhanced selectivity that allows the production of glyceric acid with a selectivity of 81 % at full conversion. The H-mordenite support may prevent H_2O_2 formation that leads to C–C bond scission, thus improving selectivity and material utilization [34]. The selectivity to glyceric acid over a bimetallic Pt–Cu catalyst reached 71 % [36]. When prepared with soluble starch as a reducing and stabilizing agent, the hydrotalcite-supported Pt catalyst afforded the selectivity of 68 % at 63 % conversion and was reused at least three times [37]. Thus, by combining proper bimetallic alloy nanoparticles and support materials, it is possible to prepare an active and durable catalyst that is highly selective toward the formation of oxidized C3 molecules from glycerol under acidic conditions.

In addition, the product selectivity of glycerol oxidation was also affected by the reactor system used to perform the reaction, which can be attributed to the difference in gas–liquid–solid contacting between a batch reactor and a fixed-bed reactor. The higher selectivity to the secondary oxidation products, oxalic and tartronic acids, in the fixed-bed system was likely the result of direct gas–solid contact which

allowed for a higher inventory of dioxygen on the catalyst compared to a batch system. Tartronic acid was formed from oxidizing glyceric acid. Oxalic acid could be produced from both glyceric and glycolic acids. Conditions were selected to minimize the effects of mass transfer on the reaction rates since highly active gold catalysts can be very easily operated in a transport-limited regime [24].

7.2.3 *Oxidation of Glycerol to Lactic Acid*

Lactic acid is an important platform chemical with many applications in the food, pharmaceutical, and chemical industries [40–42]. Lactic acid is currently manufactured mainly by fermentation of carbohydrates. However, the amount of waste generated in the fermentative process is significant and requires costly environmental remediation. It has been reported that lactate could be produced by a hydrothermal reaction of glycerol in the solution of base [43–45]. These studies have shown the potential of glycerol as an alternative reactant for the synthesis of lactic acid, irrespective of their low efficiencies or harsh reaction conditions, which may present significant hurdles to their industrial practice. Moreover, these studies proposed that the formation of lactic acid in the presence of bases was via a glyceraldehyde intermediate formed from glycerol dehydrogenation [43–45] (Fig. 7.4), which appears to be thermodynamically more favorable under oxidation conditions. This proposition is in accordance with the known isomerization of glyceraldehyde and its isomer dihydroxyacetone to lactic acid [46, 47]. Recently, a one-pot approach to the efficient conversion of glycerol into lactic acid at atmospheric pressure by a combination of glycerol oxidation with O_2 on Au–Pt/TiO_2 to glyceraldehyde and dihydroxyacetone intermediates and their instantaneous reactions with NaOH in water was reported [14]. The selective oxidation of glycerol was also investigated using Au–Pd/TiO_2 as the catalyst in the presence of $AlCl_3$, and lactic acid was obtained as the predominant product. It was demonstrated that Au–Pd/TiO_2 and $AlCl_3$ played synergistic roles in the production of lactic acid. A possible reaction pathway was proposed, in which glycerol was first oxidized to glyceraldehyde and dihydroxyacetone, catalyzed by Au–Pd/TiO_2, followed by the formation of lactic acid, catalyzed by $AlCl_3$ [15, 16].

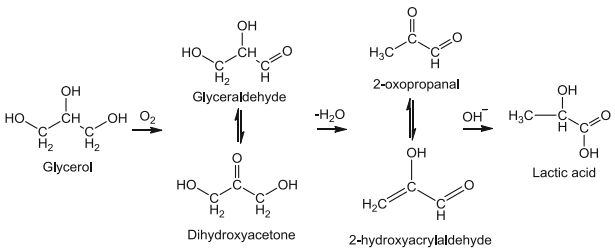

Fig. 7.4 Oxidation of glycerol to lactic acid

7.3 Oxidation of HMF, Furfural, and Glyoxal

7.3.1 Selective Oxidation of 5-Hydroxymethylfurfural (HMF)

5-Hydroxymethylfurfural (HMF), which is derived from the dehydration of fructose, is a potential chemical building block for fuels and chemicals. This yellow low-melting solid is highly water soluble. The molecule consists of a furan ring, containing both aldehyde and alcohol functional groups. HMF has been identified in a wide variety of baked goods. In the Department of Energy (DOE) top 10 list of bio-based chemicals, furan molecules such as 5-hydroxymethylfurfural (HMF), furfural, and 2,5-furandicarboxylic acid are mentioned in the "Top 10 + 4" as additions to the original DOE list [48]. Reviews were published on the preparation of 5-hydroxymethylfurfural (HMF) by acid-catalyzed dehydration of fructose and glucose or hydrolysis/dehydration of polysaccharides and on its use as platform molecule for organic synthesis [48–50]. A relatively complete review of HMF oxidation reactions in the presence of metal catalysts was published recently [3].

HMF oxidation is usually performed in aqueous solutions with variable amounts of liquid bases to neutralize the acidic functions. Relatively dilute solutions were used because of the low solubility of the 2,5-furandicarboxylic acid (FDCA) formed in aqueous solutions, and high catalyst loadings were employed to achieve a rapid oxidation, thus avoiding HMF degradation in the presence of strong bases [3, 48, 51]. The oxidation of HMF was first reported using a Pt/Al_2O_3 catalyst at 60 °C and pH 9 under 0.2 MPa of O_2 oxygen resulted in a complete conversion to FDCA [52, 53]. A basic pH was maintained by continuous addition of KOH (Fig. 7.5). 5-Formyl-2-furancarboxylic acid (FFCA) was the main intermediate, indicating that the hydroxymethyl group was oxidized first, likely by oxidative dehydrogenation, in preference to the aldehyde group. FDCA was formed at longer reaction times. The authors suggested that a strong interaction of the furan with the catalyst prevented deactivation by oxygen, as seen in other Pt-catalyzed oxidations. In the presence of a bimetallic Pb–Pt/C catalyst with a high HMF/Pt molar ratio (18:50), a FDCA yield at higher than 80 % was obtained in a highly alkaline medium (NaOH/HMF = 8) [54]. Metallic salts were added to the reaction medium to act as promoters, but only $PbCl_2$ improved significantly the catalytic activity, and the hydroxyl bases were more effective than

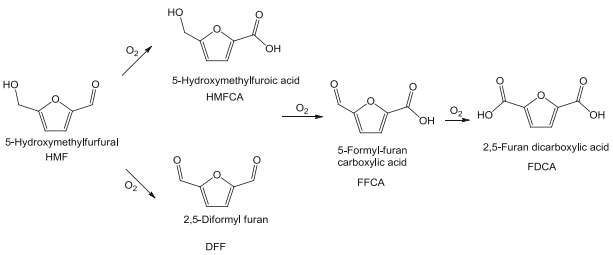

Fig. 7.5 The oxidation products of HMF (reproduced) (Reprinted with the permission from ref. [3]. Copyright 2014 American Chemical Society)

carbonate bases. Homogeneous metal bromide (Co/Mn) catalyst systems, like those used for the industrial synthesis of terephthalic acid, used air to oxidize HMF to DFF and FDCA [55]. DFF has been prepared from HMF by oxidation with air in a non-aqueous solvent over supported vanadium oxides by stoichiometric BaMnO4 oxidation and by Mn(II)–salen-catalyzed hypochlorite oxidation [56].

The feasibility of performing oxidation reactions in neutral medium has been demonstrated using a Pt/ZrO_2 catalyst in a fixed-bed continuous flow reactor (LHSV = 3 h^{-1}) at 100 °C under 1 MPa of air with a 98 % selectivity to FDCA at complete conversion. Conversions and selectivity to these products depended on oxidant, pH, catalyst, and reactor operating conditions. The feasibility of producing these species in a flow reactor was demonstrated [57]. In the presence of Pt/C or Pt/Al_2O_3 catalysts and stoichiometric amounts of sodium carbonate with respect of HMF, the reaction was fast affording a quantitative yield to FDCA, but the selectivity rapidly shifted to FFCA upon additional time on stream due to the adsorption of reaction products onto the catalysts. In acidic conditions (40 % acetic acid, 60 % water), at 100 °C under air, diformylfuran (DFF) was the major product, while at 140 °C and using O_2, an 85 % selectivity to FDCA at 100 % conversion was attained with a LHSV of 7.5 h^{-1}.

The aerobic oxidation of HMF was also examined in water with the Au/TiO_2 nano-catalyst at near-ambient temperature (30 °C). The selectivity of the reaction toward FDCA and the intermediate oxidation product 5-hydroxymethyl-2-furancarboxylic acid (HMFCA) was found to depend on the amount of added base and the oxygen partial pressure, suggesting that the reaction proceeds via initial oxidation of the aldehyde moiety followed by oxidation of the hydroxymethyl group of HMFCA. Under optimized reaction conditions, the oxidation of HMF in 2 M NaOH solutions over the commercial 1 wt.% Au/TiO_2 catalyst afforded a maximum yield of 71 % to FDCA at 25 °C under 2 MPa of O_2 [58]. Using four equivalents of NaOH at 65 °C under 1 MPa of O_2, a 99 % selectivity to FDCA was obtained at total conversion over the Au/CeO_2 nano-catalyst; however, a significant deactivation was observed [59]. The rate-limiting step of the reaction is the alcohol oxidation of HMFCA into FDCA. The absence of metal leaching was verified by chemical analysis of the reaction solution and by confirming that the reaction did not occur after catalyst removal by filtration. A two-step oxidation reaction at different temperatures was thus performed whereby HMF was first oxidized at 25 °C to HMFCA avoiding the HMF degradation in basic medium at high temperature. Then the temperature was raised to 130 °C to oxidize the more stable HMFCA intermediate to FDCA. Gold catalysts supported on hydrotalcite yielded >99 % of FDCA at 95 °C under atmospheric O_2 pressure (HMF/Au = 40) without the addition of a soluble base [60]. In addition, supported Pt, Pd, and Au catalysts were compared under the same conditions at 22 °C under 0.7 MPa of O_2 in basic conditions (NaOH/HMF = 2); Au/C and Au/TiO_2 catalysts were less active for the oxidation of the alcohol group of HMF than Pt/C and Pd/C catalysts which afforded 79 % and 71 % yields to FDCA, respectively, while under the same conditions, the Au/TiO_2 catalyst led to a high-yield production of HMFCA. In general, gold catalysts required higher oxygen pressures and higher base concentrations to obtain a >80 % yield to FDCA at near-ambient temperatures [61].

The detailed mechanism of selective oxidation of aqueous HMF at high pH was studied over supported Pt and Au catalysts. The results of isotope labeling experiments conducted with $^{18}O_2$ and $H_2{}^{18}O$ indicated that water was the source of oxygen atoms during the oxidation of HMF to 2-hydroxymethylfurancarboxylic acid (HFCA) and further to FDCA, presumably through direct participation of hydroxide in the catalytic cycle [62]. The oxidation of HMF to FDCA in aqueous solution at high pH is a sequential reaction in which the aldehyde side chain is first rapidly oxidized by the solvent. In a subsequent reaction, hydroxide ions from water in the presence of Au or Pt metal catalysts promote O–H and C–H bond activation of the alcohol side chain of HMF, converting HMF directly to aldehyde intermediates and eventually to form FDCA. Molecular oxygen was essential for the production of FDCA and played an indirect role during oxidation by removing electrons deposited into the supported metal particles. Different supported metals were also compared at 50 °C, 1 MPa of O_2, HMF/metal = 10 in strongly basic solutions (pH 13) [63]. Au showed better catalytic activity than Pt, Pd, Ru, and Rh at pH 13. The heterogeneously catalyzed oxidation of HMF was then compared to the corresponding electrochemical oxidation catalysis. Electrochemical catalysis offers an added advantage by providing the electrode potential and the faradaic current as two additional external control parameters. These are helpful to tune the thermodynamic driving force, activation energy, and thus the reaction rate and selectivity of complex reaction processes. The electrochemical activation of water at anodic electrode potentials results in the in situ generation of reactive oxygenated surface species from the aqueous solvent and thus eliminates the use of molecular oxygen. The electrocatalytic oxidation of HMF was found very selective for the formation of 2,5-furandicarbaldehyde [63].

The oxidation of HMF at 95 °C under 2 MPa of O_2 in NaOH solution (NaOH/HMF = 4) over Au–Cu bimetallic nanoparticles immobilized on TiO_2 resulted in 99 % yield to FDCA. The excellent performances were attributed to isolation effects of gold by copper in the alloyed particles. Moreover, reusability tests show that the Au–Cu/TiO_2 catalysts are significantly more stable than their monometallic samples. In fact Au–Cu/TiO_2 can be easily recovered and reused without significant leaching and agglomeration of the metal nanoparticles [64]. A strong synergistic effect was evident with the addition of Cu to Au, especially in terms of increasing resistance of Au poisoning. Well-defined Au–Cu alloy nanoparticles supported on anatase TiO_2 are considerably more active and selective toward hydroxymethyl-2-furfural oxidation than their monometallic counterparts (i.e., Au/TiO_2 and Cu/TiO_2), which may be ascribed to Au site isolation effects caused by alloying.

7.3.2 Selective Oxidation of Furfural

Furfural was oxidized to furoic acid completely in the presence of a bimetallic Pb–Pt deposited on charcoal catalyst under oxygen stream, at 65 °C, pH 8 of a 0.36 M solution of aqueous solution within 1 h [65]. Gold-based catalysts over different

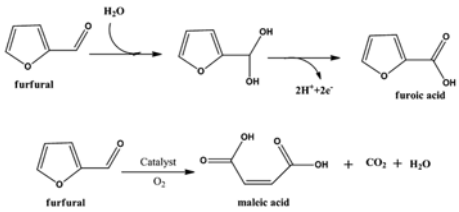

Fig. 7.6 Oxidation of furfural to furoic acid and maleic acid (reproduced) [70, 73]

supports (Au/ZrO_2, Au/CeO_2, and Au/TiO_2) were investigated in the oxidative esterification of furfural [66]. Furfural could be oxidized to methyl furoate using Au/TiO_2 as catalyst in methanol at room temperature with 1 bar oxygen [67]. Compared to Au/TiO_2 and Au/CeO_2, Au/ZrO_2 catalyst showed better catalytic performance on the conversion of furfural into methyl furoate by oxidative esterification with O_2 and methanol [68, 69]. Furfural oxidation in aqueous medium on noble (Au and Pt) and non-noble (Pb, Cu, and Ni) metal electrodes showed that the rate of furfural oxidation was controlled by diffusion on Pt and Ni anodes. A yield of 80 % furoic acid was obtained on Ni anodes in a strong alkaline medium of 0.5 M NaOH [70]. Vapor-phase oxidation of furfural over V_2O_5 catalyst was studied using an isothermal flow reactor in the temperature range of 220–280 °C with maleic anhydride, carbon dioxide, and water as the products by a parallel reaction scheme (Fig. 7.6) based on a two-stage redox mechanism [71, 72]. Small amounts of 6 % maleic acid can be obtained in aqueous-phase oxidation of furfural under an oxygen stream at 98 °C by a V_2O_5 catalyst [73]. A yield of 74.2 % succinic acid was obtained by oxidizing furfural in H_2O_2 solutions using Amberlyst-15 as the reusable solid acid catalyst at 80 °C; meanwhile, 24.6 % and 16.6 % yields of succinic acid were produced using Nb_2O_5 and ZrO_2 as the catalyst, respectively [74].

7.3.3 Selective Oxidation of Glyoxal into Glyoxylic Acid

Glyoxylic acid can be synthesized by catalytic oxidation of aqueous glyoxal solution over carbon-supported platinum metals in air slightly above room temperature [75]. The oxidation of glyoxal in acidic media like $HClO_4$, H_2SO_4, or KNO_3 on a platinum anode led mainly to the formation of glyoxylic acid and then to breaking of the C–C bond, giving formic acid or formaldehyde. The addition of metal salts (Ag, Sn, Pb, Ti) favors the latter reaction [76, 77]. It has been found that glyoxal can be adsorbed strongly on platinum, losing its hydrogen atom, which is the important step for its transformation into glyoxylic acid [78]. The formation of glycolic acid was reported to depend only on the pH [79], while Glaaezot et al. reported a 70 % high yield of glyoxylic acid obtained with 85.5 % glyoxal conversion in near-neutral pH solutions [80]. The oxidation mechanism involves an end-on adsorption of the glyoxal dihydrate molecule on the metal surface followed by dehydrogenation. The initial rate of glyoxylic acid formation increases in the order of 0=Ru < Rh < Pd < Ir < Pt,

similar to the series of the redox potentials of these elements. Ruthenium is totally inactive because it is covered with hydroxyl groups that catalyze side reactions such as dismutation (Cannizzaro reaction) and direct oxidation of glyoxal into formic acid (C–C bond rupture). Various bi- and tri-metallic associations have been tested as catalysts for the selective oxidation of glyoxal into glyoxylic acid in aqueous phase [81]. All catalysts were supported on carbon and consisted of a noble metal (Pd or Pt) in association with a second (or third) metal acting as promoter (Ru or Bi). Out of all the possible combinations, some families of catalysts were selected as interesting candidates, and a detailed kinetic study was undertaken, in order to determine the rate constant associated with the formation of glyoxylic acid. In particular, the Bi–Pt/C catalysts gave very high activity, but low selectivity (due to over-oxidation to oxalic acid), the Pd–Ru/C catalysts gave the highest yields in glyoxylic acid, but with long reaction times and a marked sensitivity to the preparation procedure, while the tri-metallic catalysts gave high yields in relatively short periods of time. The incorporation of Bi or Pb as promoting elements in carbon-supported Pd-based catalysts can significantly increase the catalytic activity in the selective oxidation of glyoxal into glyoxylic acid [82]. The heavy elements could play their promoter role when introduced in solution in combination with a monometallic Pd/C catalyst. The incorporation of bismuth in carbon-supported Pd-based catalysts can achieve 45 % yield glyoxylic acid with main side products, e.g., glycolic acid resulting from Cannizzaro dismutation and oxalic acid, generated by further oxidation of glyoxylic acid [83]. The catalytic performances of Pd–Bi/C catalysts were found to depend upon the composition of the catalyst, yield, and selectivity into glyoxylic acid being simultaneously optimized for a composition characterized by molar ratios of Bi/Pd between 0.5 and 1.0. It was also found that a novel V_2O_5 catalyst supported on active carbon prepared by an incipient wetness impregnation method exhibited obvious activity for liquid-phase oxidation of glyoxal with a yield 13.6 % glyoxylic acid on the conversion of 29.2 % at 313 K in oxygen (0.1 L/min) after reaction for 10 h (Fig. 7.7) [84]. The precursor of V_2O_5/C catalyst was obtained from oxalic acid aqueous solutions of NH_4VO_3.

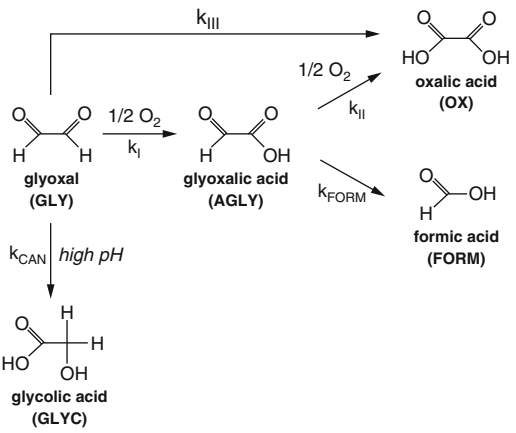

Fig. 7.7 Overall reaction scheme for the liquid-phase oxidation of glyoxal (reprint) (Reprinted from ref. [79], Copyright 2005, with permission from Elsevier)

7.4 Oxidation of Sugars into Chemicals

Gluconic, glucaric, and 2-ketogluconic acids and their salts can be obtained by oxidation of glucose with oxygen, air, or hydrogen peroxide in aqueous solutions (Fig. 7.8) in the presence of supported metal catalysts [3]. Most of the investigations were oriented toward the selective oxidation of glucose to gluconic acid and gluconate, which are used in pharmaceutical and food applications and as water-soluble cleaner for removing calcareous and rust deposits. The glucose oxidation catalyzed by supported metal catalysts is a three-phase process, which includes not only a surface reaction but also interfacial gas–liquid and liquid–solid mass transfers along with internal diffusion of reactants into the inner pore surface of the catalyst. Any of these processes may influence the overall reaction kinetics if its rate is lower or comparable to the rate of the surface glucose oxidation. For this reason, the reactant-to-catalyst ratio and catalyst morphology (size and porosity of the catalyst particles, etc.) may strongly affect the apparent reaction rate of glucose oxidation [85]. Other aldonic acids, produced from different sugars, e.g., arabinose, galactose, lactose, and their derivatives, have numerous applications in the food, pharmaceutical, and cosmetic industries. Selective oxidation of these sugars over supported metal catalysts has also been investigated [86–93].

7.4.1 Selective Oxidation of Glucose to Gluconic Acid

Glucose is often oxidized by oxygen or air at atmospheric pressure in the presence of Pd or Pt catalysts at mild temperatures of 30–80 °C [94–96]. The conversion of glucose on monometallic Pd or Pt catalysts is limited by the strong adsorption of oxygen on the metal surface, followed by primary and secondary alcohol functions oxidized to carbonyl and carboxylic functions via an oxidative dehydrogenation mechanism whereby oxygen reacted with dissociated hydrogen adsorbed on metal

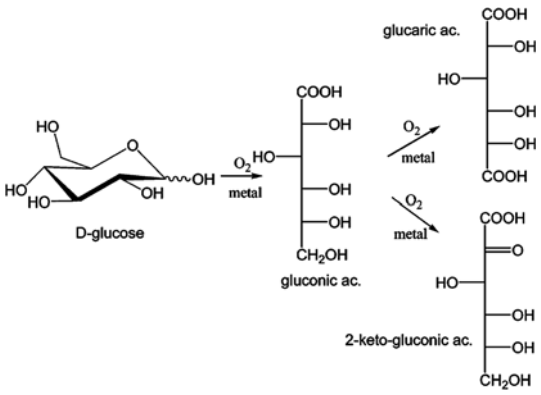

Fig. 7.8 Oxidation of glucose (reprint) (Reprinted with the permission from ref. [3], Copyright 2014, American Chemical Society)

surfaces [3]. The metal particles were usually supported on active carbons, which present the advantage of a high stability under reaction conditions, particularly at low pH and in the presence of chelating carboxylates. The TOFs of the glucose oxidation for the Pt/C catalysts were found to be independent of the mean platinum particle size in the 1–5-nm range, and the selectivity to gluconic acid did not exceed 80 %, while, for Pd/C catalysts, an increase of size from 3 to 6 nm was found to boost the TOF due to the deceleration of the oxidative deactivation of the catalyst, yielding over 95 % of gluconic acid at the 90 % conversion of the substrate under controlled O_2 diffusion [95].

The pH has a profound effect on the platinum-catalyzed oxidation of glucose to gluconic acid. Poisoning of the catalyst by the reaction products in neutral and acidic medium was observed, and the degree of the inhibition of the catalytic activity was pH dependent. D-Gluconic acid in its "free" form is considered to be the main inhibiting species of the Pt catalyst during the oxidation of glucose in acidic medium. When the temperature was increased the inhibition effect was delayed. The presence of bismuth as the promotor suppressed the physical poisoning of the Pt catalyst while promoting selective oxidation of the gluconic acid formed in situ to 2-ketogluconic acid [94]. The process combining alkaline degradation and air oxidation of D-glucose can produce useful carboxylic acids with a high atom efficiency. Yields of 47 % of lactic acid and 46 % of gluconic acid were achieved with a one-pot reaction of D-glucose using the Pt/C catalysts in 1 M NaOH at 80 °C under flowing air [97]. The product ratio of lactic acid to gluconic acid changed with the reaction temperature and the Pt/C content. The NaOH concentration affects the alkaline degradation into lactic acid and the oxidation into gluconic acid. Higher NaOH concentrations (>1.0 M) favored high yields of lactic and gluconic acids and inhibited the production of by-products including lower carboxylic acids. Also, the Pd/γ-Al_2O_3 used for selective oxidation of glucose prepared by room-temperature plasma reduction followed by a treatment under argon at 500 °C exhibits a higher activity than that prepared by the hydrogen thermally reduced one [98].

The use of promoters can enhance the activity and the selectivity in glucose oxidation. Metal promoters such as bismuth or lead were added to Pd or Pt particles by impregnation with a solution of promoter salt or by redox surface reactions [99–103]. Bimetallic catalysts Pd–Bi/SiO_2 containing a high amount of bismuth (5–8 wt.%) were found more effective in the oxidation of glucose [99]. The rate of glucose oxidation to gluconate was much higher on the Pd–Bi/C, with a 99 % yield of gluconate, than on the Pd/C catalyst [100]. The high activity of Pd–Bi/C catalysts was attributed to the promoting effect of bismuth deposited on the surface of Pd particles acting as cocatalysts preventing the over-oxidation of Pd [3]. Thallium was also found to be a "promoter" for the catalytic activity and selectivity of monometallic Pd/SiO_2 catalysts for glucose oxidation [104]. Monometallic Ru/C catalysts were found to be inactive for the oxidation of glucose, but acting as a "promoter" in the Ru–Pd/C catalysts (Fig. 7.9), which was active and selective for the transformation of glucose to gluconic acid even at temperatures as low as 50 °C and especially when the two metals were present in a 1:1 ratio [96]. The activity and selectivity of bimetallic Pd–Te/SiO_2 and Pd–Te/Al_2O_3 catalysts containing 5 wt.% of Pd and

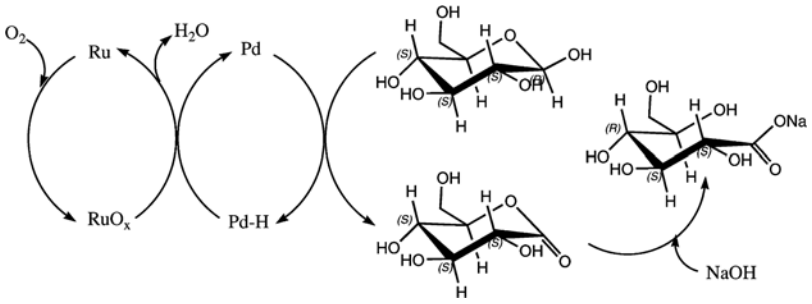

Fig. 7.9 Suggested catalytic cycle for the oxidation of glucose into gluconic acid with a Ru–Pd/C catalysts (reprint) (Reprinted from ref. [96], Copyright 2002, with permission from Elsevier)

0.3–5 wt.% Te also showed high catalytic activities in the oxidation of glucose to gluconic acid [105].

Platinum and other noble metals have also been found to be effective catalysts for the complete oxidation of sugars by vanadium(IV) in acidic solutions [106]. A redox type of sugar-powered fuel cell could be established by vanadium(IV)/vanadium(III) differing substantially from that of dioxygen/water. It has been demonstrated that most sugars can reduce vanadium(IV) to vanadium(III) under suitable conditions, favorably a suitable ratio of oxidant to sugar, and for most parts, the reaction steps are irreversible in the sense that the reconstruction of the ordered structure of the starting material is very unlikely. It is suggested that, in order to reach 100 % combustion, the sugar concentration must not be higher than that at least two surface sites per adsorbed carbon residue are always free and available. The formate ion adsorbed on the platinum surface is oxidized by a VO^{2+} ion to form CO_2 which is thought to be the rate-determining step.

A renewed interest has been given to supported gold catalysts as an alternative to palladium-based catalysts because of their higher activity and selectivity to gluconate from glucose with unique properties, e.g., they operate without the external control of pH, thus ensuring total conversion at all pH values [107–113]. It is well accepted that the catalytic performance of supported gold catalysts in glucose oxidation depends primarily on the dispersion and electronic state of gold, which in turn can be affected by the catalyst preparation techniques, as well as by chemical nature of the catalyst supports [85]. The highest catalytic activity was observed for Au particles of few nanometers in size supported on certain metal oxides, e.g., Al_2O_3, TiO_2, CeO_2, ZrO_2, SiO_2, and carbon supports [114–121]. The selective oxidation of D-glucose to D-gluconic acid was performed at both controlled (7–9.5) and free pH values in an aqueous solution in the presence of the Au/C catalyst usiJ22ng dioxygen as the oxidant under mild conditions (323–373 K, 100–300 kPa O_2) [107]. No isomerization of glucose to fructose was observed during the reaction, and higher activity and stability toward deactivation were observed on gold on carbon catalyst than commercial palladium and platinum-derived catalysts. Active Au/Al_2O_3 catalysts for glucose oxidation were prepared by deposition–precipita-

tion methods, and a 100 % selectivity toward D-gluconate was obtained [122]. Additionally, they have an excellent long-term stability. The Au/Al_2O_3 catalysts were found to be more active than the Au/C catalysts at high glucose: Au molar ratios with the highest TOF on the Au nanoparticles of 1–5 nm in size [85]. While at a low glucose/Au molar ratio, the reaction rate was limited by oxygen dissolution in the aqueous phase. In this mass transfer control regime, the rate of glucose oxidation over the carbon-supported Au catalysts exceeds the reaction rate over the alumina-supported Au catalysts, which was attributed to a higher adhesion of the hydrophobic carbon support to the gas–liquid interface facilitating the oxygen mass transfer toward catalytic sites. Hydrogen peroxide (H_2O_2) was also been used for the oxidation of D-glucose to sodium d-gluconate using a 0.3 % Au/Al_2O_3 catalyst with a selectivity of 99 % at D-glucose conversions >99 % [120]. The 1 wt.% Au/SiO_2 catalyst suspended in 30 % H_2O_2 using ultrasound was highly active and selective for D-glucose oxidation at room temperature with an 85 % selectivity to gluconate at 100 % conversion under pH 9 [116]. A catalyst with 0.45 wt.% Au supported on TiO_2 yielded 95 % of gluconate from the oxidation of glucose at 40–60 °C and pH 9, and the Au/TiO_2 catalyst was reused at least 17 times without loss of activity or change of the gold particle size [117]. Among a variety of support materials, carbon supports exhibit excellent catalytic performance in the oxidation of glucose [114]. Au/ZrO_2 catalysts prepared by the solid grinding method exhibited extremely high catalytic activity at 50 °C with the TOFs of 45 s^{-1} and 56 s^{-1} at pH 9.0 and 9.5, respectively. The activity of $Au/CeO_2–Al_2O_3$ catalysts in glucose oxidation with oxygen as oxidant was found to be even higher than that of the Au/Al_2O_3 catalyst [115]. Glucose oxidation over polymer-supported gold nanoparticles has attracted limited interest due to lower catalytic activity than Au supported on carbon or metal oxides [123]. Biffis et al. reported that gold nanoclusters of small size (2.5 nm) stabilized by polymer microgel supports exhibited high TOF of 450 h^{-1} on glucose oxidation at 50 °C and pH 9.5, nearly one-fifth of that of Au/C in spite of the small size of Au NPs [124]. However, Haruta's group [123] found that gold nanoparticles on strongly basic anion-exchange resins such as quaternary ammonium salt ($–N^+Me_3$) exhibited remarkable catalytic activity, up to TOF of 27,000 h^{-1} (7.5 s^{-1}) for glucose oxidation at 60 °C and pH 9.5. The catalytic activity for the oxidation of glucose with molecular oxygen was more greatly influenced by the basic nature of polymer supports than by the size of gold nanoparticles. The catalytic performance of Au on polymer beads for glucose oxidation with H_2O_2 was in the order of PMMA > PS > PVC > PANI > MF. The moderate interaction between Au NPs and supports such as oxygen atoms of PMMA might contribute to the catalytic properties of Au/polymers.

Bi- or tri-metallic catalysts (Ag, Au, Pt, Pd, and Rh) in the form of supported particles or colloidal dispersions were compared with the monometallic catalysts in the aerobic oxidation of D-glucose in water solution under mild conditions [125]. Under acidic conditions, the activity of single metals either was weak (TOF = 51–60 h^{-1} on Au or Pt and TOF < 2 on Rh or Pd), while the activity was enhanced by combining Au with Pd or Pt with high TOFs up to 924 h^{-1} for the synthesis of gluconic

acid [126]. A series of nonsupported, PVP-protected colloids of bi- or tri-metallic Au nanoparticles, e.g., Au–Ag, Au–Pt, and Au–Pd, were synthesized by reduction of the corresponding metal ions with rapid injection of $NaBH_4$ [127–130]. The PVP-protected Ag_{core}/Au_{shell} bimetallic nanoparticles exhibited not only a high catalytic activity but also a high longtime stability for the aerobic glucose oxidation with the highest activity of 16,890 mol-glucose h^{-1} mol-metal^{-1} at the Ag to Au atomic ratio of 2:8 [130]. The tri-metallic Au–Pt–Ag (70:20:10) colloidal nanoparticles with an average diameter of 1.5 nm were also demonstrated to have an excellent catalytic activity and durability for aerobic glucose oxidation [131].

7.4.2 Selective Oxidation of Other Pentoses or Hexoses to Aldonic Acids

Other aldonic acids can also be produced from the oxidation of various pentoses (arabinose, ribose, lyxose, and xylose) or hexoses (acetylated glucosamine, galactose, mannose, and rhamnose) over Au, Pd, and Pt catalysts [132]. Various supported gold catalysts (Au–Al_2O_3, Au–SiO_2, Au–TiO_2, Au–Fe_2O_3, Au–Fe_3O_4, and Au–ZrO_2) were utilized in aerobic oxidation of lactose (Fig. 7.10). Gold catalysts were sensitive to the type of support: the Au/Al_2O_3 catalyst exhibited the highest activity at 60 °C and pH 8 [89]. Selective oxidation of arabinose to arabinonic acid was carried out over Pd–Au/Al_2O_3 and Pd–Au/CeO_2 catalysts, prepared by deposition–precipitation method using $HAuCl_4$ and urea with subsequent chemisorption of palladium using $PdCl_2$, at moderate conditions of 60 °C and pH 8; gold metallic species seemed to be responsible for the arabinose activation, while Pd species effected oxygen activation [93]. Higher catalyst activity and selectivity to arabinonic acid were achieved with Au/Al_2O_3 than Pd/Al_2O_3 due to the increase of the amount of by-products on the Pd catalyst [133]. An oxidative dehydrogenation mechanism was proposed, and a kinetic model taking into account the catalyst potential changes was developed for the selective oxidation of L-arabinose over Au/Al_2O_3 catalysts [134]. Au supported on Al_2O_3 was revealed to be an effective catalyst for the oxidation of D-galactose to galactonic acid with molecular oxygen at 60 °C and a slightly alkaline pH value (8–10) [135].

Gold and palladium catalysts were successfully applied in aerobic D-lactose oxidation [136]. A 100 % selectivity to lactobionate at 95 % conversion of lactose was achieved with the in situ Bi promotion of a commercial Pd–C catalyst with the ratio of Bi/Pd being 0.50:0.67, at a maximum reaction rate of 0.47 mol kg^{-1} s^{-1} in the pH range 7–10 and at 60 °C [87]. The lactobionate yielded from the oxidation of lactose with air over a Pt–Bi/C catalyst can be further oxidized to 2-keto-lactobionic acid. The oxidation of lactobionic acid was performed with selectivity >95 % toward 2-keto-lactobionic acid without pH control, but the reaction stopped at 50 % conversion due to catalyst poisoning [92]. When lactose was used as the substrate, the conversion of lactobionic acid formed in situ was extended to 83 %, and the catalyst

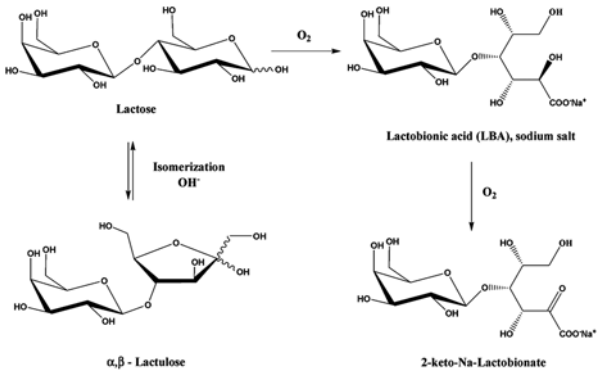

Fig. 7.10 Proposed mechanism for the oxidation of lactose (reprint) (Reprinted from ref. [89], Copyright 2008, with permission from Elsevier)

selectivity toward 2-keto-lactobionic acid was maintained. Lactobionic acid was obtained with a 100 % selectivity of 96 % lactose conversion from the direct aerobic oxidation of lactose under a very low O_2 concentration at pH 9 over low loadings (1.02–0.64 %) of bimetallic Pd–Bi supported on mesoporous SBA-15 silica [101]. It was observed that, with a selective deposition of bismuth on palladium, as well as adequate alkaline pH processing, the redox reaction chain performed efficiently and maintained the continuous dehydrogenation of lactose while avoiding poisoning of the catalyst. Lactose oxidation to lactobionic acid was also investigated over Pd on zeolite β and MCM-22 and it was found that the catalyst preparation methods, as well as acidity, influenced the activity and selectivity. The Pd–H-MCM-22 catalysts were more active than Pd on SiO_2 and Al_2O_3 or zeolite β [137]. Among different supported metal catalysts (Pt, Pd, Au, Ru, Ni), the optimum pH for lactose oxidation was between eight and nine, and lactose oxidation catalysts deactivate rapidly at low pH and at high oxygen concentrations. The highest lactobionic acid yield (99.1 %) was obtained of 100 % conversion with a 2 wt.% Au/CeO_2 catalyst at 60 °C and pH 8 [90]. A 0.7 wt.% Au/SiO_2 catalyst using a silane coupling agent performed a 100 % conversion and selectivity to lactobionic acid with a catalyst to lactose ratio of 0.2 after 100 min of reaction at pH 9.0 and a mild reaction temperature of 65 °C [86].

The oxidative degradation of D-fructose was catalyzed by vanadium(V) catalysts in the presence of H_2SO_4 (Fig. 7.11). The Michaelis–Menten type of kinetics suggested the possibility of the formation of an intermediate complex between the reactive species of vanadium(V) and D-fructose. A probable mechanism was proposed for the low-acidity region with 0.40–1.12 M H_2SO_4 (Fig. 7.12) [91]. Cobalt acetylacetonate encapsulated in sol–gel silica yielded FDCA with a 99 % selectivity directly from fructose at a conversion of 72 %. There are two steps for forming FDCA, the dehydration of fructose and the oxidation of HMF as shown in Fig. 7.13 [88].

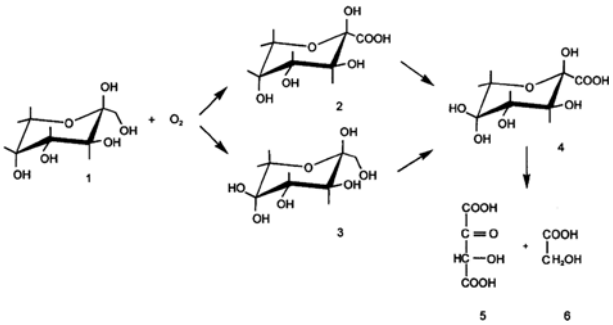

Fig. 7.11 Oxidation products of fructose (*1*), 2-ketogluconic acid (*2*), D-threo-hexo-2,5-diulose (*3*), 2,5-diketogluconic acid *(4)*, 2-hydroxy-3-butanedioic acid (*5*), and glycolic acid (*6*) (Reprinted from ref. [138], Copyright 1997, with permission from Elsevier)

7.5 Oxidation of Cellulose into Carboxylic Acids

As the most abundant biomass on earth, cellulose forms the primary component of terrestrial plants [139–142]. Cellulose is a water-insoluble biopolymer composed of D-glucose units linked by β-1,4-glycosidic bonds [143]. For the conversion of cellulose, hydrolysis can be combined with oxidation to produce gluconic acid, glycolic acid, lactic acid, levulinic acid, or formic acid [140, 144].

Many studies reported the production of gluconic acid by the selective oxidation of glucose by O_2 using supported Au, Pt, and Pd catalysts [94, 105, 146]. Thus, bifunctional catalysts possessing both hydrolysis and oxidation abilities can perform the direct transformation of cellulose into gluconic acid, as shown in Fig. 7.14 [147]. It was reported that the $Au/Cs_xH_{3.0-x}PW_{12}O_{40}$ catalysts with small Au particles (~3 nm) could catalyze the oxidative conversion of ball-milled cellulose into gluconic acid in water. The gluconic acid yields of 47–60 % were achieved with the selectivity of 79–87 % depending on the Cs content of the supported Au catalysts after 11 h at 145 °C and 1.0 MPa O_2 [145]. Cellobiose, a dimer of glucose, was also selectively oxidized to gluconic acid over Pt and Au catalysts on various supports. Onda and co-workers showed that a 46 % yield of gluconic acid was obtained from cellobiose oxidation at 120 °C under 0.1 MPa air over a bifunctional sulfonated carbon-supported Pt catalyst (Pt/AC-SO_3H) [148]. A gluconic acid yield of 97 % was achieved over an $Au/Cs_{1.2}H_{1.8}PW_{12}O_{40}$ catalyst with a mean particle size of 2.7 nm at 145 °C under 0.5 MPa of O_2 after 3 h [149]. Gold nanoparticles loaded on nitric acid-pretreated carbon nanotubes (Au/CNT) were also efficient for the selective oxidation of cellobiose to gluconic acid in aqueous medium. And a gluconic acid yield of 80 % was obtained at 145 °C under 0.5 MPa of O_2 pressure without pH control over a 0.5 wt.% Au/CNT catalyst at 98 % conversion [150].

Levulinic acid derived from cellulose is considered a suitable building block for synthesizing hydrocarbon liquid fuels or valeric esters as fuel additives, as well as a variety of chemicals [151]. Typically, equivalent molar amounts of levulinic acid

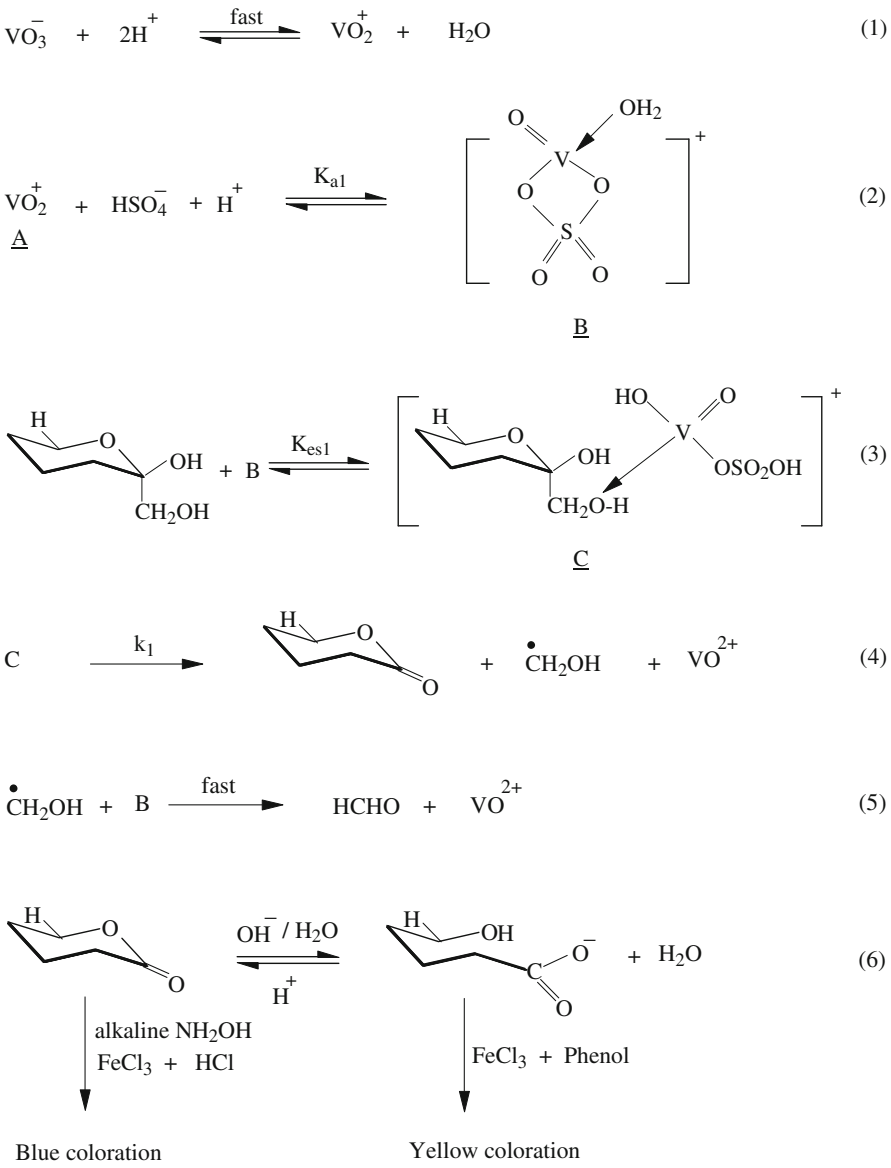

Fig. 7.12 A probable mechanism for the low-acidity region oxidative degradation of D-fructose (reprint) (Reprinted from ref. [91], Copyright 2004, with permission from Elsevier)

and formic acid can be generated in the acid-catalyzed conversion of cellulose without oxygen participation in the overall reactions [152]. Recently, Lin's group developed a nontraditional pathway, aqueous-phase partial oxidation (APPO), for the direct conversion of cellulose into levulinic acid with air and water in the presence of ZrO_2 catalyst [151]. The maximum yield of levulinic acid in the APPO

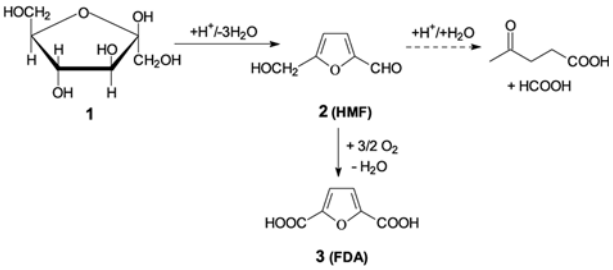

Fig. 7.13 Synthetic route from fructose to FDA via HMF (reprint) (Reprinted from ref. [88], Copyright 2003, with permission from Elsevier)

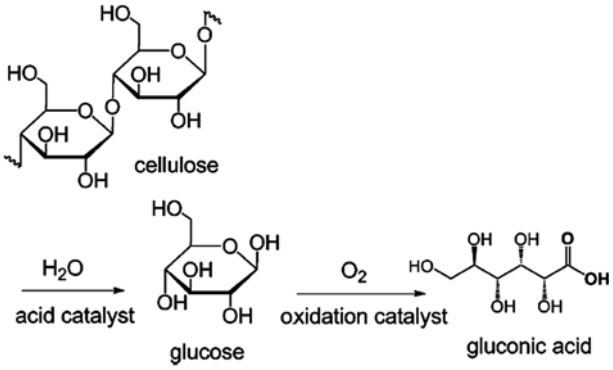

Fig. 7.14 Direct conversion of cellulose into gluconic acid by using hydrolysis and oxidation reactions (reprint) (Reproduced from ref. [145] by permission of John Wiley & Sons Ltd)

process was ~50 % at 240 °C in the presence of lean air with 2.8 % O_2. It was proposed that the formation of superoxide species on ZrO_2 surfaces might play the central role in the oxidative deconstruction of cellulose in the APPO reactions. Gluconic acid, rather than HMF, is the key intermediate to produce levulinic acid, and the addition of a radical scavenger (ascorbic acid) into the APPO system inhibited the yield of levulinic acid, further indicating that the in situ generation of $O_2^{\cdot-}$ in the reaction system contributed to the high selectivity toward levulinic acid (Fig. 7.15) [151].

Other carboxylic acids such as malic acid, acetic acid, and oxalic acids can also be produced directly from cellulose over supported Pt or Pd catalysts [153, 154]. It was found that the supported Pt catalyst was more active toward the oxidation of cellulose, promoting a greater yield of deep oxidation products such as oxalic acid, while the supported Pd catalyst gave a higher selectivity to malic and acetic acid [154]. Acetic acid could be obtained from the oxidation of cellulose in subcritical water (150 °C) using alkali and H_2O_2; however, the use of catalysts (i.e., TiO_2) and additives (i.e., H_2SO_4) did not enhance the overall yields of organic acids [155]. A two-step hydrothermal process was developed to improve the production of acetic acid from cellulose by Jin et al. [156]. In the first step, cellulose was mainly

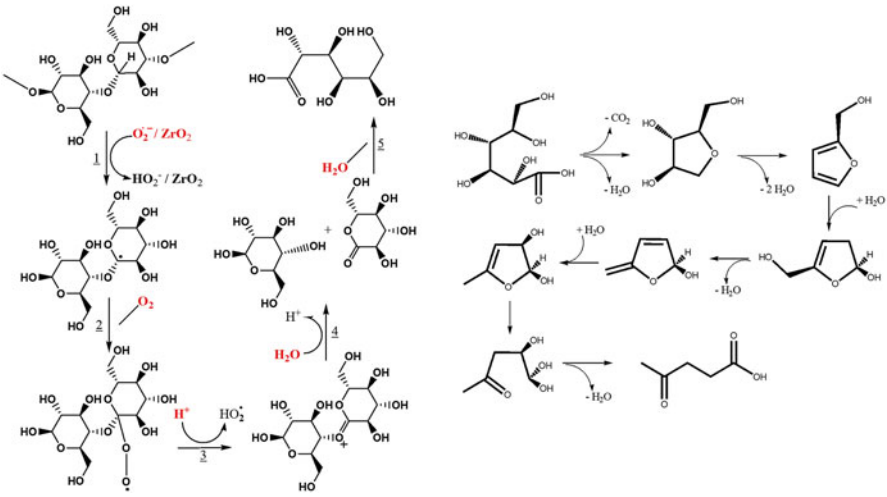

Fig. 7.15 Reaction pathway for converting a cellobiose unit in cellulose to glucose and gluconic acid by superoxide radical anions (*left*); proposed reaction pathway of converting gluconic acid to levulinic acid by a Hofer–Moest-type decarboxylation reaction followed by consecutive dehydration/rehydration reactions (*right*) (reprint) (Reproduced from Ref. [151] by permission of The Royal Society of Chemistry)

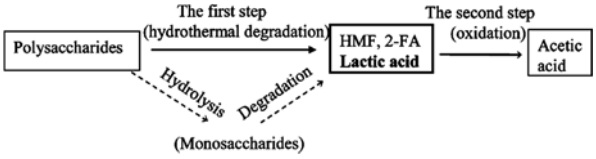

Fig. 7.16 Proposed two-step process for enhancing acetic acid yield (reprint) (Reprinted with the permission from ref. [156], Copyright 2005, American Chemical Society)

transformed to HMF, 2-furaldehyde, and lactic acid, and the second step was to further convert the furans (HMF, 2-FA) and lactic acid to acetic acid by oxidation with newly supplied oxygen (Fig. 7.16). The contribution of two pathways via furans and lactic acid in the two-step process to convert carbohydrates into acetic acid was approximately 85–90 %, and the ratio of the contributions of furans and lactic acid to yield acetic acid was estimated at 2:1. The fact that wet oxidation of carbohydrates is not capable of producing a large amount of acetic acid, while the two-step process can enhance the acetic acid yield, is because formic acid is the end product of direct oxidation of carbohydrates, while acetic acid in wet oxidation of carbohydrates may come from the oxidation of dehydration products of aldoses (Fig. 7.17). Xue's group found that formic and acetic acids were the main products in the chemical conversion of corncobs over nanosized ceria, alumina, titania, or zirconia catalysts with gaseous oxygen as the oxidant at 180 °C, and ceria and zirconia showed relatively high yields of formic acid under oxidative conditions (Fig. 7.18) [157].

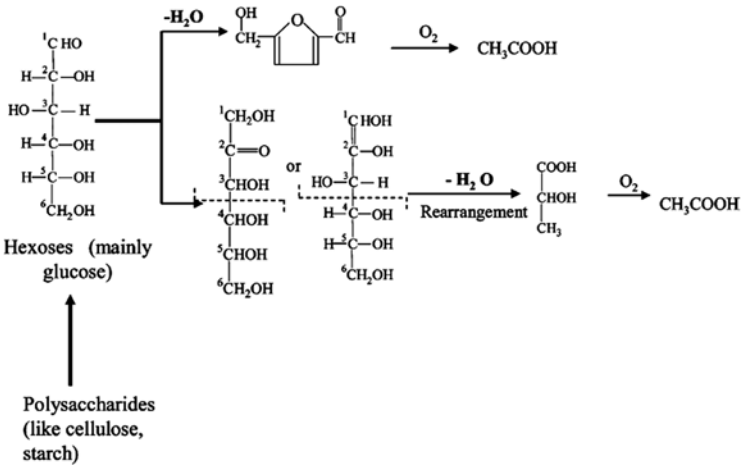

Fig. 7.17 Mechanism of two-step process for carbohydrates (reprint) (Reprinted with the permission from ref. [156], Copyright 2005, American Chemical Society)

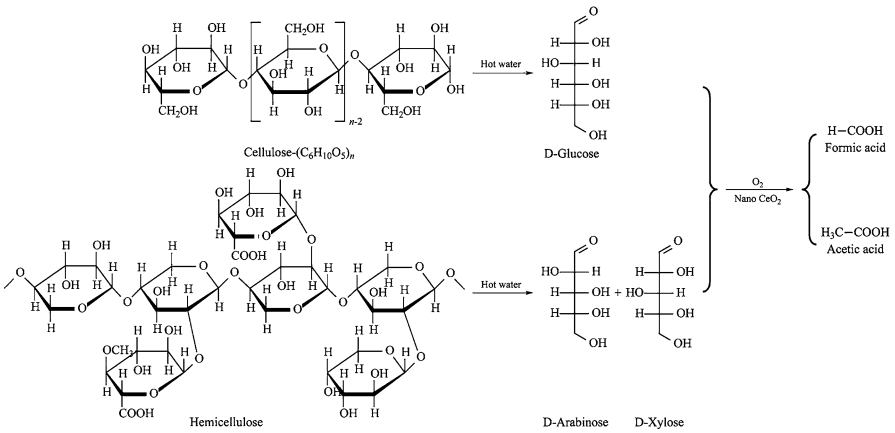

Fig. 7.18 Catalytic conversion of corncob to oxygenates over nano-oxides in aqueous media at high temperature (reprint) (Reprinted from ref. [157], Copyright 2014, with permission from Elsevier)

References

1. Werpy T, Petersen G, Aden A, Bozell J, Holladay J, White J, Amy M, Eliot D, Lasure L, Jones S (2004) Top value added chemicals from biomass volume I – results of screening for potential candidates from sugars and synthesis gas. U.S. Department of Energy, Washington, DC
2. Bozell JJ, Petersen GR (2010) Technology development for the production of biobased products from biorefinery carbohydrates—the US Department of Energy's "Top 10" revisited. Green Chem 12:539–554
3. Besson M, Gallezot P, Pinel C (2014) Conversion of biomass into chemicals over metal catalysts. Chem Rev 114:1827–1870

4. Kimura H, Tsuto K (1993) Selective oxidation of glycerol on a platinum-bismuth catalyst. Appl Catal A Gen 96:217–228
5. Kimura H (1993) Selective oxidation of glycerol on a platinum-bismuth catalyst by using a fixed bed reactor. Appl Catal A Gen 105:147–158
6. Garcia R, Besson M, Gallezot P (1995) Chemoselective catalytic oxidation of glycerol with air on platinum metals. Appl Catal A Gen 127:165–176
7. Brandner A, Lehnert K, Bienholz A et al (2009) Production of biomass-derived chemicals and energy: chemocatalytic conversions of glycerol. Top Catal 52:278–287
8. Hu W, Knight D, Lowry B, Varma A (2010) Selective oxidation of glycerol to dihydroxyacetone over Pt- Bi/C catalyst: optimization of catalyst and reaction conditions. Ind Eng Chem Res 49:10876–10882
9. Liang D, Cui S, Gao J et al (2011) Glycerol oxidation with oxygen over bimetallic Pt-Bi catalysts under atmospheric pressure. Chin J Catal 32:1831–1837
10. Demirel S, Lehnert K, Lucas M, Claus P (2007) Use of renewables for the production of chemicals: glycerol oxidation over carbon supported gold catalysts. Appl Catal B Environ 70:637–643
11. Pollington SD, Enache DI, Landon P et al (2009) Enhanced selective glycerol oxidation in multiphase structured reactors. Catal Today 145:169–175
12. Hirasawa S, Nakagawa Y, Tomishige K (2012) Selective oxidation of glycerol to dihydroxyacetone over a Pd–Ag catalyst. Catal Sci Technol 2:1150–1152
13. Nie R, Liang D, Shen L et al (2012) Selective oxidation of glycerol with oxygen in base-free solution over MWCNTs supported PtSb alloy nanoparticles. Appl Catal B Environ 127:212–220
14. Shen Y, Zhang S, Li H et al (2010) Efficient synthesis of lactic acid by aerobic oxidation of glycerol on Au-Pt/TiO2 catalysts. Chemistry 16:7368–7371
15. Li Y, Chen S, Xu J et al (2014) Ni promoted Pt and Pd catalysts for glycerol oxidation to lactic acid. Clean Soil Air Water 42:1140–1144
16. Xu J, Zhang H, Zhao Y et al (2013) Selective oxidation of glycerol to lactic acid under acidic conditions using AuPd/TiO2 catalyst. Green Chem 15:1520–1525
17. Zhang J, Sun M, Han Y (2014) Selective oxidation of glycerol to formic acid in highly concentrated aqueous solutions with molecular oxygen using V-substituted phosphomolybdic acids. RSC Adv 4:35463–35466
18. Carrettin S, McMorn P, Johnston P et al (2003) Oxidation of glycerol using supported Pt, Pd and Au catalysts. Phys Chem Chem Phys 5:1329–1336
19. Porta F, Prati L (2004) Selective oxidation of glycerol to sodium glycerate with gold-on-carbon catalyst: an insight into reaction selectivity. J Catal 224:397–403
20. Bianchi CL, Canton P, Dimitratos N et al (2005) Selective oxidation of glycerol with oxygen using mono and bimetallic catalysts based on Au, Pd and Pt metals. Catal Today 102–103:203–212
21. Dimitratos N, Porta F, Prati L (2005) Au, Pd (mono and bimetallic) catalysts supported on graphite using the immobilisation method synthesis and catalytic testing for liquid phase oxidation of glycerol. Appl Catal A Gen 291:210–214
22. Ketchie W, Fang Y, Wong M et al (2007) Influence of gold particle size on the aqueous-phase oxidation of carbon monoxide and glycerol. J Catal 250:94–101
23. Demirel-Gülen S, Lucas M, Claus P (2005) Liquid phase oxidation of glycerol over carbon supported gold catalysts. Catal Today 102–103:166–172
24. Zope BN, Davis RJ (2009) Influence of reactor configuration on the selective oxidation of glycerol over Au/TiO2. Top Catal 52:269–277
25. Dimitratos N, Lopez-Sanchez JA, Anthonykutty JM et al (2009) Oxidation of glycerol using gold-palladium alloy-supported nanocrystals. Phys Chem Chem Phys 11:4952–4961
26. Sobczak I, Jagodzinska K, Ziolek M (2010) Glycerol oxidation on gold catalysts supported on group five metal oxides—a comparative study with other metal oxides and carbon based catalysts. Catal Today 158:121–129

27. Musialska K, Finocchio E, Sobczak I et al (2010) Characterization of alumina- and niobia-supported gold catalysts used for oxidation of glycerol. Appl Catal A Gen 384:70–77
28. Villa A, Gaiassi A, Rossetti I et al (2010) Au on MgAl2O4 spinels: the effect of support surface properties in glycerol oxidation. J Catal 275:108–116
29. Villa A, Chan-Thaw CE, Prati L (2010) Au NPs on anionic-exchange resin as catalyst for polyols oxidation in batch and fixed bed reactor. Appl Catal B Environ 96:541–547
30. Huang Z, Li F, Chen B et al (2011) Efficient and recyclable catalysts for selective oxidation of polyols in H2O with molecular oxygen. Green Chem 13:3414–3422
31. Liang D, Gao J, Wang J et al (2009) Selective oxidation of glycerol in a base-free aqueous solution over different sized Pt catalysts. Catal Commun 10:1586–1590
32. Gao J, Liang D, Chen P et al (2009) Oxidation of glycerol with oxygen in a base-free aqueous solution over Pt/AC and Pt/MWNTs catalysts. Catal Lett 130:185–191
33. Liang D, Gao J, Sun H et al (2011) Selective oxidation of glycerol with oxygen in a base-free aqueous solution over MWNTs supported Pt catalysts. Appl Catal B Environ 106:423–432
34. Villa A, Veith GM, Prati L (2010) Selective oxidation of glycerol under acidic conditions using gold catalysts. Angew Chem Int Ed Engl 49:4499–4502
35. Brett GL, He Q, Hammond C et al (2011) Selective oxidation of glycerol by highly active bimetallic catalysts at ambient temperature under base-free conditions. Angew Chem Int Ed Engl 50:10136–10139
36. Liang D, Gao J, Wang J et al (2011) Bimetallic Pt——Cu catalysts for glycerol oxidation with oxygen in a base-free aqueous solution. Catal Commun 12:1059–1062
37. Tongsakul D, Nishimura S, Thammacharoen C et al (2012) Hydrotalcite-supported platinum nanoparticles prepared by a green synthesis method for selective oxidation of glycerol in water using molecular oxygen. Ind Eng Chem Res 51:16182–16187
38. Carrettin S, McMorn P, Johnston P, et al (2002) Selective oxidation of glycerol to glyceric acid using a gold catalyst in aqueous sodium hydroxide. Chem Commun 2002:696–697
39. Carrettin S, Mcmorn P, Johnston P et al (2004) Oxidation of glycerol using supported gold catalysts. Top Catal 27:131–136
40. West RM, Holm MS, Saravanamurugan S et al (2010) Zeolite H-USY for the production of lactic acid and methyl lactate from C3-sugars. J Catal 269:122–130
41. Lunt J (1998) Large-scale production, properties and commercial applications of polylactic acid polymers. Polym Degrad Stab 59:145–152
42. Fukushima K, Kimura Y (2006) Stereocomplexed polylactides (Neo-PLA) as high-performance bio-based polymers: their formation, properties, and application. Polym Int 55:626–642
43. Maris E, Ketchie W, Murayama M, Davis R (2007) Glycerol hydrogenolysis on carbon-supported PtRu and AuRu bimetallic catalysts. J Catal 251:281–294
44. Maris E, Davis R (2007) Hydrogenolysis of glycerol over carbon-supported Ru and Pt catalysts. J Catal 249:328–337
45. Kishida H, Jin F, Zhou Z et al (2005) Conversion of glycerin into lactic acid by alkaline hydrothermal reaction. Chem Lett 34:1560–1561
46. Machell G, Richards GN (1960) Mechanism of saccharinic acid formation. Part I. Competing reactions in the alkaline degradation of 4-O-Methyl-D-glucose, maltose, amylose, and cellulose. J Chem Soc 17:1924–1931
47. Sowden JC, Pohlen KE (1958) The reaction of D-Glycerose-3-C14 with alkali. J Am Chem Soc 80:242–244
48. Van Putten R-J, van der Waal JC, de Jong E et al (2013) Hydroxymethylfurfural, a versatile platform chemical made from renewable resources. Chem Rev 113:1499–1597
49. Rosatella AA, Simeonov SP, Frade RFM, Afonso CAM (2011) 5-Hydroxymethylfurfural (HMF) as a building block platform: biological properties, synthesis and synthetic applications. Green Chem 13:754–793
50. Hu L, Zhao G, Hao W et al (2012) Catalytic conversion of biomass-derived carbohydrates into fuels and chemicals via furanic aldehydes. RSC Adv 2:11184–11206

51. Moreau C, Naceur M, Gandini A (2004) Recent catalytic advances in the chemistry of substituted furans from carbohydrates and in the ensuing polymers. Top Catal 27:11–30
52. Vinke P, van Dam HE, van Bekkum H (1991) On the oxygen tolerance of noble metal catalysts in liquid phase alcohol oxidations the influence of the support on catalyst deactivation. Stud Surf Sci Catal 59:327–335
53. Vinke P, van Dam HE, van Bekkum H (1990) Platinum catalyzed oxidation of 5-hydroxymethylfurfural. Stud Surf Sci Catal 55:147–158
54. Verdeguer P, Merat N, Gaset A (1993) Oxydation catalytique du HMF en acide 2,5-furane dicarboxylique. J Mol Catal 85:327–344
55. Partenheimer W, Grushin VV (2001) Synthesis of 2,5-diformylfuran and furan-2,5-dicarboxylic acid by catalytic air-oxidation of 5-hydroxymethylfurfural. Unexpectedly selective aerobic oxidation of benzyl alcohol to benzaldehyde with metal/bromide catalysts. Adv Synth Catal 343:102–111
56. Amarasekara AS, Green D, McMillan E (2008) Efficient oxidation of 5-hydroxymethylfurfural to 2,5-diformylfuran using Mn(III)–salen catalysts. Catal Commun 9:286–288
57. Lilga MA, Hallen RT, Gray M (2010) Production of oxidized derivatives of 5-Hydroxymethylfurfural (HMF). Top Catal 53:1264–1269
58. Gorbanev YY, Klitgaard SK, Woodley JM et al (2009) Gold-catalyzed aerobic oxidation of 5-hydroxymethylfurfural in water at ambient temperature. ChemSusChem 2:672–675
59. Casanova O, Iborra S, Corma A (2009) Biomass into chemicals: aerobic oxidation of 5-hydroxymethyl-2-furfural into 2,5-furandicarboxylic acid with gold nanoparticle catalysts. ChemSusChem 2:1138–1144
60. Gupta NK, Nishimura S, Takagaki A, Ebitani K (2011) Hydrotalcite-supported gold-nanoparticle-catalyzed highly efficient base-free aqueous oxidation of 5-hydroxymethylfurfural into 2,5-furandicarboxylic acid under atmospheric oxygen pressure. Green Chem 13:824
61. Davis SE, Houk LR, Tamargo EC et al (2011) Oxidation of 5-hydroxymethylfurfural over supported Pt, Pd and Au catalysts. Catal Today 160:55–60
62. Davis SE, Zope BN, Davis RJ (2012) On the mechanism of selective oxidation of 5-hydroxymethylfurfural to 2,5-furandicarboxylic acid over supported Pt and Au catalysts. Green Chem 14:143–147
63. Vuyyuru KR, Strasser P (2012) Oxidation of biomass derived 5-hydroxymethylfurfural using heterogeneous and electrochemical catalysis. Catal Today 195:144–154
64. Pasini T, Piccinini M, Blosi M et al (2011) Selective oxidation of 5-hydroxymethyl-2-furfural using supported gold–copper nanoparticles. Green Chem 13:2091–2099
65. Verdeguer P, Merat N, Gaset A (1994) Lead/platinum on charcoal as catalyst for oxidation of furfural. Effect of main parameters. Appl Catal A Gen 112:1–11
66. Menegazzo F, Signoretto M, Pinna F et al (2014) Oxidative esterification of renewable furfural on gold-based catalysts: which is the best support? J Catal 309:241–247
67. Taarning E, Nielsen IS, Egeblad K et al (2008) Chemicals from renewables: aerobic oxidation of furfural and hydroxymethylfurfural over gold catalysts. ChemSusChem 1:75–78
68. Pinna F, Olivo A, Trevisan V et al (2013) The effects of gold nanosize for the exploitation of furfural by selective oxidation. Catal Today 203:196–201
69. Signoretto M, Menegazzo F, Contessotto L et al (2013) Au/ZrO2: an efficient and reusable catalyst for the oxidative esterification of renewable furfural. Appl Catal B Environ 129:287–293
70. Parpot P, Bettencourt A, Chamoulaud G et al (2004) Electrochemical investigations of the oxidation–reduction of furfural in aqueous medium application to electrosynthesis. Electrochim Acta 49:397–403
71. Murthy MS, Rajamani K (1974) Kinetics of vapour phase oxidation of furfural on vanadium catalyst. Chem Eng Sci 29:601–609
72. Murthy M, Rajamani K, Subramanian P (1975) Mechanism of vapour phase oxidation of furfural on vanadium catalyst. Chem Eng Sci 30:1529–1533
73. Shi S, Guo H, Yin G (2011) Synthesis of maleic acid from renewable resources: catalytic oxidation of furfural in liquid media with dioxygen. Catal Commun 12:731–733

74. Choudhary H, Nishimura S, Ebitani K (2012) Highly efficient aqueous oxidation of furfural to succinic acid using reusable heterogeneous acid catalyst with hydrogen peroxide. Chem Lett 41:409–411
75. Pierre G, Kordi MEL, Cauquis G (1985) Electrochemical synthesis of glyoxylic acid from glyoxal Part I. Role of the electrolyte, temperature and electrode material. J Electroanal Chum 186:167–177
76. Pierre G, Ziade A, Kordi MEL (1987) The oxidation of glyoxal and ethylene glycol on platinum in aqueous acid mediums containing some metal salts. Electrochim Acta 32:601–606
77. Pierre G, El Kordi M, Cauquis G (1985) Electrochemical synthesis of glyoxylic acid from glyoxal—III. Influence of the adatoms on the yields of the reaction on platinum and vitreous carbon electrodes. Electrochim Acta 30:1227–1230
78. Formaro L, Castelli G (1970) Glyoxal adsorption on smooth platinum electrodes. J Electroanal Chem 28:363–374
79. Alardin F, Wullens H, Hermans S, Devillers M (2005) Mechanistic and kinetic studies on glyoxal oxidation with Bi- and Pb-promoted Pd/C catalysts. J Mol Catal A Chem 225:79–89
80. Glaaezot P, de Mesanstoume R, Christidist Y et al (1992) Catalytic oxidation of glyoxal to glyoxylic acid on platinum metals. J Catal 133:479–485
81. Deffernez A, Hermans S, Devillers M (2005) Bimetallic Bi–Pt, Ru–Pt and Ru–Pd and trimetallic catalysts for the selective oxidation of glyoxal into glyoxylic acid in aqueous phase. Appl Catal A Gen 282:303–313
82. Alardin F, Delmon B, Ruiz P, Devillers M (2000) Stability of bimetallic Bi–Pd and Pb–Pd carbon-supported catalysts during their use in glyoxal oxidation. Catal Today 61:255–262
83. Alardin F, Ruiz P, Delmon B, Devillers M (2001) Bismuth-promoted palladium catalysts for the selective oxidation of glyoxal into glyoxylic acid. Appl Catal A Gen 215:125–136
84. Niu YL, Xu Z, Li M, Li RF (2008) Oxidation of glyoxal to glyoxylic acid by oxygen over V2O5/C catalyst. Chin Chem Lett 19:245–248
85. Delidovich IV, Moroz BL, Taran OP et al (2013) Aerobic selective oxidation of glucose to gluconate catalyzed by Au/Al2O3 and Au/C: impact of the mass-transfer processes on the overall kinetics. Chem Eng J 223:921–931
86. Gutierrez L-F, Hamoudi S, Belkacemi K (2011) Selective production of lactobionic acid by aerobic oxidation of lactose over gold crystallites supported on mesoporous silica. Appl Catal A Gen 402:94–103
87. Hendriks HEJ, Kuster BFM, Marin GB (1990) The effect of bismuth on the selective oxidation of lactose on supported palladium catalysts. Carbohydr Res 204:121–129
88. Ribeiro ML, Schuchardt U (2003) Cooperative effect of cobalt acetylacetonate and silica in the catalytic cyclization and oxidation of fructose to 2,5-furandicarboxylic acid. Catal Commun 4:83–86
89. Murzina EV, Tokarev AV, Kordás K et al (2008) D-Lactose oxidation over gold catalysts. Catal Today 131:385–392
90. Kuusisto J, Tokarev AV, Murzina EV et al (2007) From renewable raw materials to high value-added fine chemicals—catalytic hydrogenation and oxidation of D-lactose. Catal Today 121:92–99
91. Khan Z, Babu PSS (2004) Kinetics and mechanism of the oxidation of d-fructose by vanadium(V) in H2SO4 medium. Carbohydr Res 339:133–140
92. Abbadi A, Gotlieb KF, Meiberg JB, van Bekkum H (1997) Selective chemo-catalytic oxidation of lactose and/of lactobionic acid towards 1-carboxylactulose (2-keto-lactobionic acid). Appl Catal A Gen 156:105–115
93. Smolentseva E, Kusema BT, Beloshapkin S et al (2011) Selective oxidation of arabinose to arabinonic acid over Pd–Au catalysts supported on alumina and ceria. Appl Catal A Gen 392:69–79
94. Abbadi A, van Bekkum H (1995) Effect of pH in the Pt-catalyzed oxidation of D-glucose to d-gluconic acid. J Mol Catal A Chem 97:111–118
95. Delidovich IV, Taran OP, Matvienko LG et al (2010) Selective oxidation of glucose over carbon-supported Pd and Pt catalysts. Catal Letters 140:14–21

96. Hermans S, Devillers M (2002) On the role of ruthenium associated with Pd and/or Bi in carbon-supported catalysts for the partial oxidation of glucose. Appl Catal A Gen 235:253–264
97. Onda A, Ochi T, Kajiyoshi K, Yanagisawa K (2008) A new chemical process for catalytic conversion of D-glucose into lactic acid and gluconic acid. Appl Catal A Gen 343:49–54
98. Liang X, Liu C, Kuai P (2008) Selective oxidation of glucose to gluconic acid over argon plasma reduced Pd/Al2O3. Green Chem 10:1318
99. Karski S (2006) Activity and selectivity of Pd–Bi/SiO2 catalysts in the light of mutual interaction between Pd and Bi. J Mol Catal A Chem 253:147–154
100. Besson M, Lahmer F, Gallezot P et al (1995) Catalytic oxidation of glucose on Bismuth-promoted palladium catalysts. J Catal 152:116–121
101. Belkacemi K, Hamoudi S, La V (2010) Chemocatalytic oxidation of lactose to lactobionic acid over Pd–Bi/SBA-15: reaction kinetics and modeling. Ind Eng Chem Res 49:6878–6889
102. Abbadi A, Van Bekkum H (1995) Highly selective oxidation of aldonic acids to 2-keto-aldonic acids over Pt—Bi and Pt—Pb catalysts. Appl Catal A Gen 124:409–417
103. Wenkin M, Ruiz P, Delmon B, Devillers M (2002) The role of bismuth as promoter in Pd–Bi catalysts for the selective oxidation of glucose to gluconate. J Mol Catal A Chem 180:141–159
104. Karski S, Witońska I, Gołuchowska J (2006) Catalytic properties of Pd–Tl/SiO2 systems in the reaction of liquid phase oxidation of aldoses. J Mol Catal A Chem 245:225–230
105. Witońska I, Frajtak M, Karski S (2011) Selective oxidation of glucose to gluconic acid over Pd–Te supported catalysts. Appl Catal A Gen 401:73–82
106. Larsson R, Folkesson B (2005) A catalytic oxidation of sugar by vanadium(IV). J Mol Catal A Chem 229:183–190
107. Biella S, Prati L, Rossi M (2002) Selective oxidation of D-glucose on gold catalyst. J Catal 206:242–247
108. Beltrame P, Comotti M, Della Pina C, Rossi M (2006) Aerobic oxidation of glucose II. Catalysis by colloidal gold. Appl Catal A Gen 297:1–7
109. Ishida T, Watanabe H, Bebeko T et al (2010) Aerobic oxidation of glucose over gold nanoparticles deposited on cellulose. Appl Catal A Gen 377:42–46
110. Okatsu H, Kinoshita N, Akita T et al (2009) Deposition of gold nanoparticles on carbons for aerobic glucose oxidation. Appl Catal A Gen 369:8–14
111. Önal Y, Schimpf S, Claus P (2004) Structure sensitivity and kinetics of D-glucose oxidation to D-gluconic acid over carbon-supported gold catalysts. J Catal 223:122–133
112. Prüße U, Herrmann M, Baatz C, Decker N (2011) Gold-catalyzed selective glucose oxidation at high glucose concentrations and oxygen partial pressures. Appl Catal A Gen 406:89–93
113. Thielecke N, Aytemir M, Prüsse U (2007) Selective oxidation of carbohydrates with gold catalysts: continuous-flow reactor system for glucose oxidation. Catal Today 121:115–120
114. Ishida T, Kinoshita N, Okatsu H et al (2008) Influence of the support and the size of gold clusters on catalytic activity for glucose oxidation. Angew Chem Int Ed Engl 47:9265–9268
115. Gaweł B, Lambrechts K, Øye G (2012) Preparation and characterization of Au/CeO2-Al2O3 monoliths. Mater Sci Eng B 177:575–580
116. Bujak P, Bartczak P, Polanski J (2012) Highly efficient room-temperature oxidation of cyclohexene and D -glucose over nanogold Au/SiO2 in water. J Catal 295:15–21
117. Mirescu A, Berndt H, Martin A, Prüße U (2007) Long-term stability of a 0.45 % Au/TiO2 catalyst in the selective oxidation of glucose at optimised reaction conditions. Appl Catal A Gen 317:204–209
118. Thielecke N, Vorlop K-D, Prüße U (2007) Long-term stability of an Au/Al2O3 catalyst prepared by incipient wetness in continuous-flow glucose oxidation. Catal Today 122:266–269
119. Hermans S, Deffernez A, Devillers M (2011) Au–Pd/C catalysts for glyoxal and glucose selective oxidations. Appl Catal A Gen 395:19–27
120. Saliger R, Decker N, Prüße U (2011) D-Glucose oxidation with H2O2 on an Au/Al2O3 catalyst. Appl Catal B Environ 102:584–589

121. Zhang M, Zhu X, Liang X, Wang Z (2012) Preparation of highly efficient Au/C catalysts for glucose oxidation via novel plasma reduction. Catal Commun 25:92–95
122. Baatz C, Thielecke N, Prüße U (2007) Influence of the preparation conditions on the properties of gold catalysts for the oxidation of glucose. Appl Catal B Environ 70:653–660
123. Ishida T, Okamoto S, Makiyama R, Haruta M (2009) Aerobic oxidation of glucose and 1-phenylethanol over gold nanoparticles directly deposited on ion-exchange resins. Appl Catal A Gen 353:243–248
124. Biffis A, Cunial S, Spontoni P, Prati L (2007) Microgel-stabilized gold nanoclusters: powerful "quasi-homogeneous" catalysts for the aerobic oxidation of alcohols in water. J Catal 251:1–6
125. Comotti M, Pina C, Della RM (2006) Mono- and bimetallic catalysts for glucose oxidation. J Mol Catal A Chem 251:89–92
126. Hermans S, Deffernez A, Devillers M (2010) Preparation of Au–Pd/C catalysts by adsorption of metallic species in aqueous phase for selective oxidation. Catal Today 157:77–82
127. Zhang H, Toshima N (2012) Fabrication of catalytically active AgAu bimetallic nanoparticles by physical mixture of small Au clusters with Ag ions. Appl Catal A Gen 447–448:81–88
128. Zhang H, Toshima N (2013) Synthesis of Au/Pt bimetallic nanoparticles with a Pt-rich shell and their high catalytic activities for aerobic glucose oxidation. J Colloid Interface Sci 394:166–176
129. Zhang H, Watanabe T, Okumura M et al (2012) Catalytically highly active top gold atom on palladium nanocluster. Nat Mater 11:49–52
130. Zhang H, Okuni J, Toshima N (2011) One-pot synthesis of Ag-Au bimetallic nanoparticles with Au shell and their high catalytic activity for aerobic glucose oxidation. J Colloid Interface Sci 354:131–138
131. Zhang H, Toshima N (2011) Preparation of novel Au/Pt/Ag trimetallic nanoparticles and their high catalytic activity for aerobic glucose oxidation. Appl Catal A Gen 400:9–13
132. Mirescu A, Prüße U (2007) A new environmental friendly method for the preparation of sugar acids via catalytic oxidation on gold catalysts. Appl Catal B Environ 70:644–652
133. Kusema BT, Campo BC, Mäki-Arvela P et al (2010) Selective catalytic oxidation of arabinose—a comparison of gold and palladium catalysts. Appl Catal A Gen 386:101–108
134. Kusema BT, Mikkola J-P, Murzin DY (2012) Kinetics of l-arabinose oxidation over supported gold catalysts with in situ catalyst electrical potential measurements. Catal Sci Technol 2:423
135. Kusema BT, Murzin DY (2013) Catalytic oxidation of rare sugars over gold catalysts. Catal Sci Technol 3:297–307
136. Tokarev AV, Murzina EV, Mikkola JP et al (2007) Application of in situ catalyst potential measurements for estimation of reaction performance: lactose oxidation over Au and Pd catalysts. Chem Eng J 134:153–161
137. Tokarev AV, Murzina EV, Seelam PK et al (2008) Influence of surface acidity in lactose oxidation over supported Pd catalysts. Microporous Mesoporous Mater 113:122–131
138. Heinen AW, Peters JA, van Bekkum H (1997) The oxidation of fructose on Pt/C catalysts: the formation of d-threo-hexo-2,5-diulose and the effect of additives. Carbohydr Res 304:155–164
139. Yang P, Kobayashi H, Fukuoka A (2011) Recent developments in the catalytic conversion of cellulose into valuable chemicals. Chin J Catal 32:716–722
140. Deng W, Zhang Q, Wang Y (2015) Catalytic transformations of cellulose and its derived carbohydrates into 5-hydroxymethylfurfural, levulinic acid, and lactic acid. Sci China Chem 58:29–46
141. Collinson SR, Thielemans W (2010) The catalytic oxidation of biomass to new materials focusing on starch, cellulose and lignin. Coord Chem Rev 254:1854–1870
142. Hegner J, Pereira KC, DeBoef B, Lucht BL (2010) Conversion of cellulose to glucose and levulinic acid via solid-supported acid catalysis. Tetrahedron Lett 51:2356–2358
143. Kobayashi H, Komanoya T, Guha SK et al (2011) Conversion of cellulose into renewable chemicals by supported metal catalysis. Appl Catal A Gen 409–410:13–20

144. Deng W, Zhang Q, Wang Y (2014) Catalytic transformations of cellulose and cellulose-derived carbohydrates into organic acids. Catal Today 234:31–41
145. An D, Ye A, Deng W et al (2012) Selective conversion of cellobiose and cellulose into gluconic acid in water in the presence of oxygen, catalyzed by polyoxometalate-supported gold nanoparticles. Chem A Eur J 18:2938–2947
146. Prüße U, Jarzombek P, Vorlop K-D (2012) Gold-catalyzed glucose oxidation using novel spherical sol–gel derived alumina supports produced via the JetCutter. Top Catal 55:453–459
147. Deng W, Zhang Q, Wang Y (2012) Polyoxometalates as efficient catalysts for transformations of cellulose into platform chemicals. Dalton Trans 41:9817–9831
148. Onda A, Ochi T, Yanagisawa K (2011) New direct production of gluconic acid from polysaccharides using a bifunctional catalyst in hot water. Catal Commun 12:421–425
149. Zhang J, Xu X, Hedhili MN, Yihan Zhu YH (2011) Highly selective and complete conversion of cellobiose to gluconic acid over Au/Cs2HPW12O40 nanocomposite catalyst. ChemCatChem 3:1294–1298
150. Tan X, Deng W, Liu M et al (2009) Carbon nanotube-supported gold nanoparticles as efficient catalysts for selective oxidation of cellobiose into gluconic acid in aqueous medium. Chem Commun (Camb) 2009:7179–7181
151. Lin H, Strull J, Liu Y et al (2012) High yield production of levulinic acid by catalytic partial oxidation of cellulose in aqueous media. Energy Environ Sci 5:9773–9777
152. Braden DJ, Henao CA, Heltzel J et al (2011) Production of liquid hydrocarbon fuels by catalytic conversion of biomass-derived levulinic acid. Green Chem 13:1755–1756
153. Patrick TA, Abraham MA (2000) Evaluation of a monolith-supported Pt/Al2O3 catalyst for wet oxidation of carbohydrate-containing waste streams. Environ Sci Technol 34:3480–3488
154. Schutt BD, Serrano B, Cerro RL, Abraham MA (2002) Production of chemicals from cellulose and biomass-derived compounds through catalytic sub-critical water oxidation in a monolith reactor. Biomass Bioenergy 22:365–375
155. Calvo L, Vallejo D (2002) Formation of organic acids during the hydrolysis and oxidation of several wastes in sub-and supercritical water. Ind Eng Chem Res 41:6503–6509
156. Jin F, Zhou Z, Moriya T et al (2005) Controlling hydrothermal reaction pathways to improve acetic acid production from carbohydrate biomass. Environ Sci Technol 39:1893–1902
157. Cheng L, Liu H, Cui Y et al (2014) Direct conversion of corn cob to formic and acetic acids over nano oxide catalysts. J Energy Chem 23:43–49

Chapter 8
New Reaction Schemes for the Production of Biomass-Based Chemicals Created by Selective Catalytic Hydrogenolysis: Catalysts with Noble Metal and Tungsten

Yoshinao Nakagawa, Masazumi Tamura, and Keiichi Tomishige

Abstract Bimetallic catalysts containing noble metal and tungsten are effective in C-O hydrogenolysis reactions. Three types of C-O hydrogenolysis reactions have been reported: one is the direct hydrogenolysis of C-O bond neighboring a terminal OH group such as tetrahydrofurfuryl alcohol to 1,5-pentanediol. This catalysis is common for Rh-MO_x (M = Mo, Re, and W) catalysts. Water solvent and low reaction temperature (~393 K) are applied. Another is deoxydehydration + hydration of vicinal *cis*-diols to mono-alcohols such as 1,4-anhydroerythritol to 3-hydroxytetrahydrofuran. The combination of WO_3 and noble metal, especially Pd, is effective in this reaction. The reaction proceeds in non-water solvent (1,4-dioxane) and at high temperature (453–473 K). The other is selective production of 1,3-propanediol from glycerol over Pt-W catalysts. The combination of Pt and W is specifically effective. The reaction is operated in the presence of water at high temperature (~453 K). The proposed mechanism is a variant of dehydration + hydrogenation, and the intermediate of 1,3-propanediol formation is stabilized by W species.

Keywords Hydrogenolysis • Noble metal • Tungsten • Rhenium • Alcohol

8.1 Introduction

Biomass contains much amount of oxygen atoms, and typically the oxygen content is larger than that of fuels and chemicals. C-O hydrogenolysis, which is composed of dissociation of C-O bonds and insertion of hydrogen atoms, is a key reaction in

Y. Nakagawa (✉) • M. Tamura • K. Tomishige (✉)
Department of Applied Chemistry, School of Engineering, Tohoku University, Aoba 6-6-07, Aramaki, Aoba-ku, Sendai, Japan
e-mail: yoshinao@erec.che.tohoku.ac.jp; tomi@erec.che.tohoku.ac.jp

M. Schlaf, Z.C. Zhang (eds.), *Reaction Pathways and Mechanisms in Thermocatalytic Biomass Conversion I*, Green Chemistry and Sustainable Technology, DOI 10.1007/978-981-287-688-1_8

biomass conversion [1, 2]. C-O hydrogenolysis requires hydrogen activation, and therefore, it is necessary to use metal catalysts, especially noble metal catalysts. However, using noble metal catalysts alone does not give satisfactory results in most cases, i.e., low conversion of substrate and low selectivity to target product. To improve the performance, noble metal catalysts are frequently combined with a component that can activate substrate molecule. Acid is one of typical additives. Acid catalyzes dehydration of alcohol to alkenes, and hydrogenation of produced alkenes with noble metal catalysts gives alkanes (Fig. 8.1) [3]. This two-step reaction formally dissociates C-O bond of alcohol and inserts hydrogen; it is one typical mechanism of C-O hydrogenolysis. As a variant of this two-step mechanism, acid-catalyzed dehydration of vicinal diols gives keto compounds via keto-enol tautomerism, and mono-alcohol can be produced by hydrogenation of the keto intermediate. Hydrogenolysis of glycerol to 1,2-propanediol is known to proceed via acetol (hydroxyacetone) intermediate over noble metal + acid catalyst systems [4–7]. Hydrogenolysis of ethers is also possible by noble metal + acid systems in water solvent, although more difficult than that of alcohols: hydration of ether to alcohols followed by dehydration and hydrogenation.

Selective C-O hydrogenolysis by this two-step indirect mechanism is rather difficult except limited cases such as glycerol to 1,2-propanediol, because the first dehydration step is catalyzed by structure-insensitive Brønsted acids. Usually, the selectivity is governed by the relative thermodynamic stability among possible intermediates: in the case of glycerol, acetol is thermodynamically more stable than 3-hydroxypropanal which is the intermediate of 1,3-propanediol formation. If the target product requires less stable intermediate, the selective production is almost impossible by this two-step mechanism.

Therefore, other types of C-O hydrogenolysis reaction are needed to produce a wide variety of chemicals from poly-functionalized biomass-derived feedstock. Instead of simple acids, metal oxides have been frequently selected as additives to noble metal catalysts in C-O hydrogenolysis systems [8–11]. Typical oxides are those of group 6 or 7 metals such as molybdenum, tungsten, and rhenium. Among these metals, tungsten is relatively inexpensive and has a rich chemistry in solid oxides such as mixed oxides, tungsten bronze, and polyoxometalates. This chapter focuses on the addition effect of tungsten to noble metal catalysts for C-O hydrogenolysis reactions.

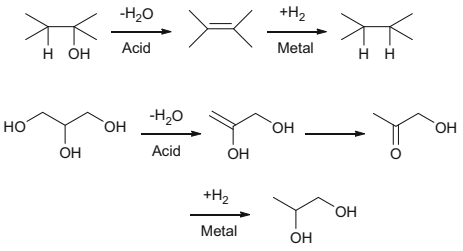

Fig. 8.1 C-O hydrogenolysis via dehydration and hydrogenation

8.2 Addition Effect Common to Group 6–7 Metal Oxides

The addition effect of tungsten can be classified into two categories: (i) effect similar to those observed in the additions of other group 6–7 metal oxides and (ii) unique effect for tungsten addition. This section focuses on the category (i). In this category, the noble metal plays the leading role of the catalysis, and the catalytic performance much depends on the type of noble metal.

8.2.1 Rh-W Catalysts and the Differences to Rh-Re and Rh-Mo Catalysts

Among monometallic noble metal catalysts, Rh catalysts have relatively high C-O hydrogenolysis activity. Figure 8.2 shows the results of glycerol conversion over carbon-, silica-, and alumina-supported noble metal catalysts in water [12]. Rh/SiO_2 with high surface area shows the highest activity and good selectivity to C-O hydrogenolysis products. Rh/C shows also good activity and selectivity although the activity is lower than Rh/SiO_2. The activity of Rh/Al_2O_3 is very low, and this behavior can be explained by low reducibility of Rh species on Al_2O_3 support.

Because of the intrinsic activity of Rh for C-O hydrogenolysis, Rh has been frequently selected as the main component for bimetallic C-O hydrogenolysis catalysts [13–27]. Various additives including tungsten have been tested for Rh-based catalysts. Figure 8.3 shows the comparison of the glycerol hydrogenolysis over modified Rh/SiO_2 catalysts with various metals [16]. In these experiments, the catalysts were prepared by sequential impregnation with aqueous $RhCl_3$ and then with

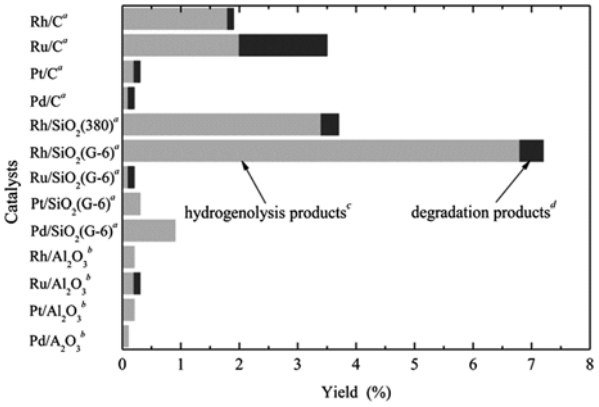

Fig. 8.2 Glycerol hydrogenolysis over noble metal catalysts. Conditions: glycerol 4 g, water 16 g, catalyst (5 wt.%) 150 mg, H_2 8 MPa, 393 K, 10 h. [a]Pre-reduced in situ at 393 K. [b]Pre-reduced externally at 573 K. [c]Propanediols and propanols. [d]C1 and C2 compounds (Reproduced from ref. [12] with permission from The Royal Society of Chemistry)

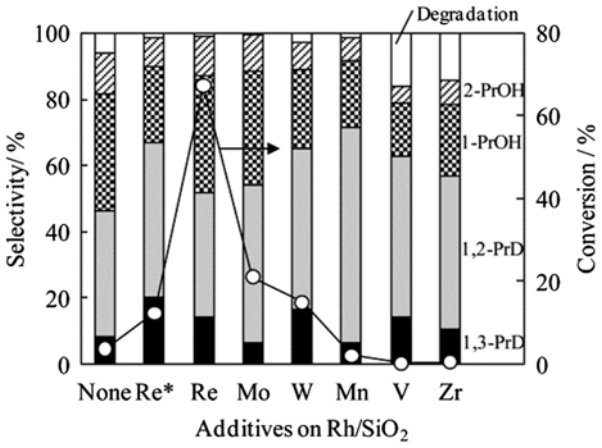

Fig. 8.3 Comparison of the catalytic performances in the glycerol hydrogenolysis over modified Rh/SiO_2. Conditions: glycerol 4 g, water 16 g, catalyst (4 wt.% Rh, additive/Rh = 0.25) 150 mg, H_2 8 MPa, 393 K, 5 h. *PrD* propanediol, *PrOH* propanol. *: Re/Rh = 0.5 (Reprinted with permission from ref. [16] Copyright 2010 by Elsevier)

aqueous solution of additive precursor. Increase in activity is observed for Re-, Mo-, and W-based catalysts. In terms of selectivity, addition of Re and W increases the selectivity to 1,3-propanediol, which is the most valuable product in glycerol hydrogenolysis, to almost the same extent, while addition of Mo does not increase the selectivity. Although the activity increase by tungsten addition is smaller than those by molybdenum and rhenium, the lower cost of tungsten than rhenium is attractive in view of production of 1,3-propanediol.

There is also a report for glycerol hydrogenolysis to 1,3-propanediol over supported Rh catalysts in combination with external H_2WO_4 [28]. The maximum reported selectivity to 1,3-propanediol is 26 %, whose value is similar to that obtained over $Rh\text{-}WO_x/SiO_2$. Figure 8.4 shows the effect of addition amount of W, Mo, and Re on the catalysis of $Rh\text{-}MO_x/SiO_2$ for glycerol hydrogenolysis [16]. The activity of $Rh\text{-}WO_x/SiO_2$ is increased with increasing W amount up to W/Rh = 0.13, and then it is decreased when W/Rh is >0.13 (Fig. 8.4c). Similar volcano-type dependences of activity on additive amount are observed for Re and Mo (Fig. 8.4a, b), while the optimum additive amount of Re is significantly larger than those of W and Mo.

These $Rh\text{-}MO_x/SiO_2$ (M = W, Mo, and Re) catalysts have been also applied to C-O hydrogenolysis reactions of tetrahydrofurfuryl alcohol and 1,2-propanediol to 1,5-pentanediol and 1-propanol, respectively (Table 8.1). All modified catalysts show similar selectivity patterns: ≥84 % selectivity to 1,5-pentanediol from tetrahydrofurfuryl alcohol and >70 % selectivity to 1-propanol from 1,2-propanediol. The activity dependences in these reactions on type and amount of additive are very similar to those in glycerol hydrogenolysis: volcano-type dependence on additive amount, optimum additive amount 0.13, 0.06–0.13, and 0.5 for W, Mo, and Re, respectively, and higher activity of Re-added catalyst than Mo- or W-added ones at the optimum additive amount. ReO_x/SiO_2, MoO_x/SiO_2, and WO_x/SiO_2 catalysts without Rh are totally inactive.

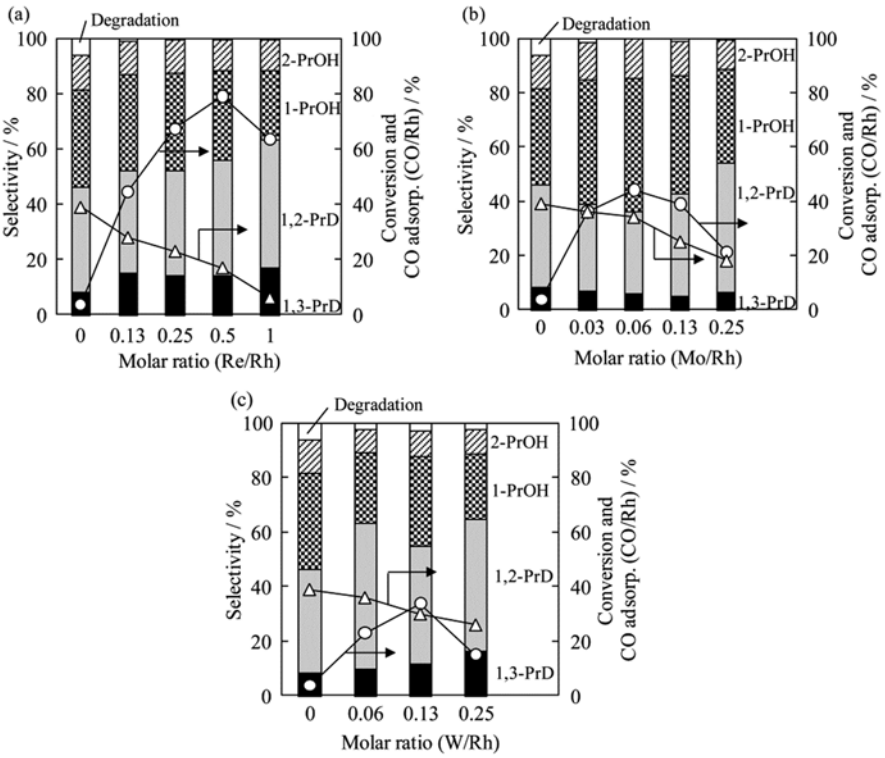

Fig. 8.4 Dependence of catalytic performance on additive amount (**a** Re, **b** Mo, **c** W). Conditions: glycerol 4 g, water 16 g, catalyst (4 wt.% Rh/SiO2) 150 mg, H2 8 MPa, 393 K, 5 h. *PrD* propanediol, *PrOH* propanol. *Circles* and *triangles* represent conversion and CO adsorption amount, respectively (Reprinted with permission from ref. [16] Copyright 2010 by Elsevier)

Table 8.1 C-O hydrogenolysis reactions over Rh-MO_x/SiO_2 catalysts [15, 18]

Substrate	M (M/Rh ratio)	Conv. [%]	Product (selectivity [%])
Tetrahydrofurfuryl alcohol[a]	Re (0.5)	56.9	1,5-Pentanediol (94), 1-pentanol (4)
Tetrahydrofurfuryl alcohol[a]	Mo (0.13)	50.1	1,5-Pentanediol (96), 1-pentanol (4)
Tetrahydrofurfuryl alcohol[a]	W (0.13)	30.4	1,5-Pentanediol (85), 1-pentanol (6)
1,2-Propanediol[b]	Re (0.5)	35.3	1-Propanol (79), 2-propanol (18), propane (3)
1,2-Propanediol[b]	Mo (0.13)	20.0	1-Propanol (76), 2-propanol (21), propane (3)
1,2-Propanediol[b]	W (0.13)	25.1	1-Propanol (74), 2-propanol (21), propane (5)

Conditions: catalyst (Rh 4 wt.%) [a]50 mg or [b]150 mg, [a]tetrahydrofurfuryl alcohol aq. (5 %) or [b]1,2-propanediol aq. (20 %) 20 g, H_2 8 MPa, 393 K, [a]6 h or [b]4 h

Rh-MO_x/SiO_2 (M = W, Mo, and Re) catalysts have been characterized with various techniques [14–16, 20, 29]. XRD patterns of all catalysts after reduction show Rh metal phase as well as SiO_2 phase, and the average particle size of Rh metal is calculated to be about 3 nm from the width of the peak for all catalysts. The shift of the Rh peaks is not observed, suggesting that alloy is not formed. The peaks of additive metal or metal oxides are not observed, indicating that the species of additive are amorphous or highly dispersed. The amount of CO adsorption on the catalyst is shown in Fig. 8.4 as well as the results of catalysis. The amount of CO adsorption is decreased gradually with increasing additive amount for all additives. Considering that CO can be adsorbed on surface Rh atoms and not on MO_x species (M = W, Mo, and Re), the surface of Rh particles is partially covered with MO_x species. Rh-MoO_x/SiO_2 and Rh-ReO_x/SiO_2 catalysts have been further characterized by temperature-programmed reduction (TPR) and XAFS. Based on the results, MO_x species (M = Mo or Re) are reduced to low-valent oxide, and direct bonds between Rh and M are present with coordination number (CN) ≈ 3. On lower M/Rh ratio (M/Rh = 0.13), almost all the M species interact with Rh metal surface. On higher M/Rh ratio (M/Rh ≥0.25), the direct bonds between Rh and Mo become fewer (CN 3→1.4 from Mo/Rh = 0.13 to 0.5), while those between Rh and Re are not decreased. In the case of Rh-MoO_x/SiO_2, the structure of $Rh_{surface}$-O-Mo might appear instead of Rh-Mo direct bond. Comparison between the structures and activity trends suggests that the Rh-M direct bond is a key structure in the C-O hydrogenolysis catalysis. Rh-WO_x/SiO_2 catalyst has been less characterized in comparison with Mo or Re counterparts. The similar catalysis of Rh-WO_x/SiO_2 to Mo or Re counterparts with small additive amount (Figs. 8.3 and 8.4) suggests the similar structure for these catalysts: Rh particles covered with MO_x species via direct Rh-M bonds. The rapid decrease in the activity by increasing W amount suggests the formation of Rh-O-W structure. The reducibility of tungsten oxide is generally lower than that of molybdenum oxide or rhenium oxide. Therefore, larger amount of W addition can lead to the formation of higher-valent (+5 or +6) tungsten oxide which does not form direct W-noble metal bonds. In addition, the amount of CO adsorption on Rh-WO_x/SiO_2 is slightly larger than those on Rh-MoO_x/SiO_2 or Rh-ReO_x/SiO_2 with the same amount of M/Rh (M = W, Mo, and Re), while those on Rh-MoO_x/SiO_2 and Rh-ReO_x/SiO_2 are almost the same (Fig. 8.4). This trend can be explained by the formation of three-dimensional WO_x species rather than monomeric or planar MO_x species. The interaction between Rh-M becomes weaker in the following order: Rh-Re > Rh-Mo > Rh-W.

The reaction mechanism of Rh-ReO_x/SiO_2 and Rh-MoO_x/SiO_2 for selective C-O hydrogenolysis has been proposed based on kinetic analysis and reactivity trends of various substrates (“direct” mechanism; Fig. 8.5) [14–19]. The reaction mechanism of Rh-WO_x/SiO_2 is probably the same as that of Re or Mo counterparts. First, the substrate molecule with terminal OH group is adsorbed on MO_x site which is directly bonded to noble metal surface to form alkoxide species. The strong adsorption on MO_x site is shown by the lower reaction order with respect to substrate concentration for Rh-MO_x/SiO_2 than Rh/SiO_2. Group 5–7 metal oxides are well known to form alkoxide species by the reaction of alcohols [30]. H_2 molecule is

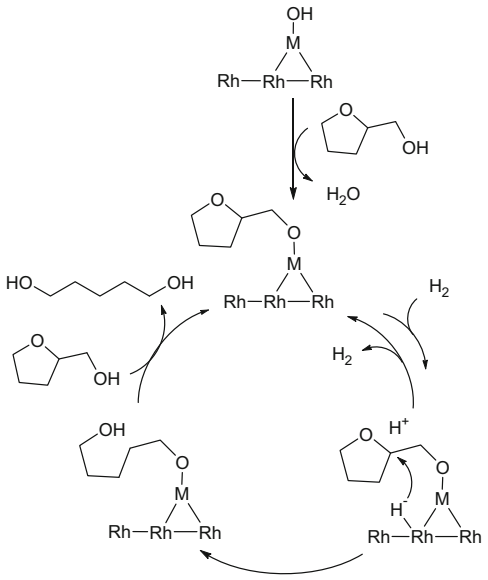

Fig. 8.5 "Direct" mechanism of hydrogenolysis of tetrahydrofurfuryl alcohol to 1,5-pentanediol over Rh-MO_x catalysts

activated on Rh metal surface. The substrate bound on the interface between Rh and MO_x reacts with the activated hydrogen species. This reaction can be regarded as S_N2, and the activated hydrogen species should have ionic nature (hydride species). In fact, Rh-MO_x/SiO_2 catalysts are very effective in ketone hydrogenation, which is known to proceed by hydride transfer. The reaction order with respect to H_2 is one for these C-O hydrogenolysis reactions, and this value is consistent with the formation of one hydride species from one H_2 molecule ($H_2 \rightarrow H^+ + H^-$). Finally, the hydrolysis or alcoholysis of produced alkoxide releases product molecule. This mechanism dissociates C-O bond neighboring to terminal $–CH_2OH$ group: 1,2-alkanediol to 1-alcohol, tetrahydrofurfuryl alcohol to 1,5-pentanediol, tetrahydropyran-2-methanol to 1,6-hexanediol, and 2-alkoxyethanol to 1:1 mixture of ethanol and alcohol. Substrates without this structure are much less reactive such as tetrahydrofuran, 2-methyltetrahydrofuran, and tetrahydrofuran-3-methanol. In the case of 1,2-alkanediol, when the substrate is adsorbed with the OH group at 2-position, the hydride attack to the neighboring C-O bond produces 2-alcohol instead of 1-alcohol. The observed selectivity ratio of 1-alcohol/2-alcohol is around 80/20, and therefore, the adsorption with 2-position is minor. The difference can be explained by the steric hindrance around the OH group. In the case of glycerol, this mechanism should produce mainly 1,3-propanediol. However, in fact there are more amount of other products such as 1,2-propanediol and 1-propanol. Two mechanisms for production of 1,2-propanediol from glycerol are known for conventional catalysts: dehydration-hydrogenation (Fig. 8.1) and dehydrogenation-dehydration-hydrogenation (Fig. 8.6) [4]. The former mechanism is proposed for noble metal + acid systems as discussed in Sect. 8.1. The latter one is typically proposed for Cu catalyst, and the key of this mechanism is the activation of α-hydrogen of aldehyde

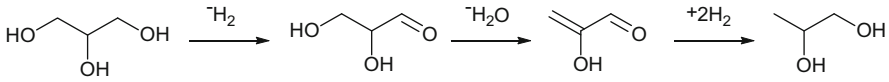

Fig. 8.6 Dehydrogenation-dehydration-hydrogenation of glycerol to 1,2-propanediol

group. Even though the first dehydrogenation step is strongly limited by equilibrium in the presence of excess hydrogen, elimination of α-hydrogen and β-OH group in the aldehyde intermediate (glyceraldehyde) quickly proceeds to give α,β-unsaturated aldehyde (2-hydroxyacrolein). Total hydrogenation of the unsaturated aldehyde gives the final product. This mechanism is specific to α,γ-diols. Rh-MO_x/SiO_2 can catalyze either mechanism in addition to the "direct" mechanism shown in Fig. 8.5. 1-Propanol can be formed from 1,2-propanediol via "direct" mechanism.

In the literature another mechanism has been proposed for hydrogenolysis of tetrahydrofurfuryl alcohol to 1,5-pentanediol over Rh-MO_x-type catalysts based on DFT calculations [21–23, 27]: protonation of the ether oxygen of tetrahydrofurfuryl alcohol, rearrangement of the cationic intermediate to 5-hydroxypentanal, and then hydrogenation to 1,5-pentanediol. The M-OH species attached to Rh metal particles work as strong Brønsted acids [23]. The reactivity of various substrates and the selectivity from them were explained by the relative stability of the cationic intermediate [21]. However, the reactivity order of ethylene glycol >1,2-alkanediols with shorter chains >1,2-alkanediols with longer chains [21] is more reasonably explained by the "direct" mechanism (S_N2 at 2-position). The higher selectivity to 1-ol than that to 2-ol from 1,2-alkanediol contradicts the relative stability of cationic intermediates: protonated ketones are more stable than protonated aldehydes. We conducted deuterium-label experiments for hydrogenolysis of tetrahydrofurfuryl alcohol to 1,5-pentanediol over Ir-ReO_x/SiO_2 catalyst, and the results showed that the rearrangement did not proceed [31].

8.2.2 Ir-Based Catalysts

Iridium is located just under rhodium in the periodic table, and the chemical properties of iridium and rhodium are similar. Similarly to rhodium, iridium catalysts combined with oxides of group 6 and 7 metal and vanadium have been investigated for C-O hydrogenolysis [31–47]. The combination of iridium and rhenium has by far the best performance [31–42]. Figure 8.7 shows the substrate scope of Ir-ReO_x/SiO_2 for C-O hydrogenolysis. The selectivity is similar to that of Rh-MO_x/SiO_2: dissociation of C-O bond neighboring terminal OH group. The largest difference between Ir-ReO_x/SiO_2 and Rh-MO_x/SiO_2 catalysts is the result of glycerol hydrogenolysis: Ir-ReO_x/SiO_2 catalyst shows much higher selectivity to 1,3-propanediol. These results show that the "direct" mechanism as shown in Fig. 8.5 proceeds and the conventional indirect mechanisms (Figs. 8.1 and 8.6) hardly proceed over Ir-ReO_x/SiO_2. Another feature of Ir-ReO_x/SiO_2 catalyst is the very low activity in

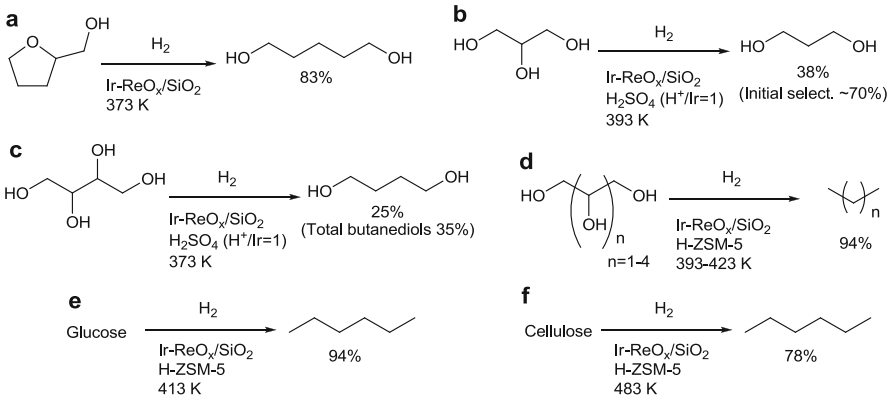

Fig. 8.7 C-O hydrogenolysis catalyzed by Ir-ReO_x/SiO_2. (**a**) Ref. [31]; (**b**) ref. [32]; (**c**) ref. [34]; (**d**, **e**) ref. [37]; (**f**) ref. [41]

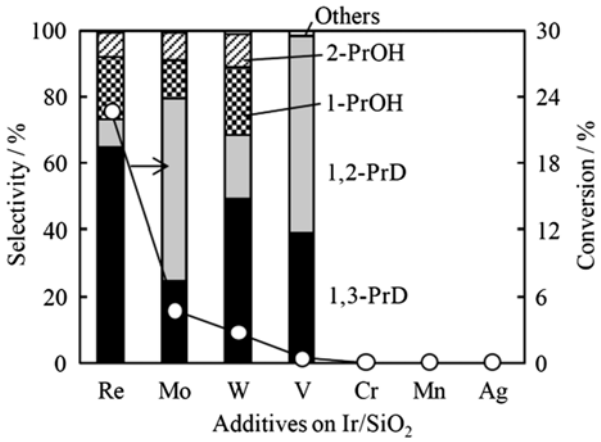

Fig. 8.8 Comparison of the catalytic performances in the glycerol hydrogenolysis over modified Ir/SiO_2. Conditions: glycerol 4 g, water 2 g, catalyst (4 wt.% Ir, additive/Ir = 0.25) 150 mg, H_2SO_4 $H^+/Ir = 1$, H_2 8 MPa, 393 K, 12 h. *PrD* propanediol, *PrOH* propanol (Reprinted with permission from ref. [33] Copyright 2011 by Elsevier)

C-C dissociation. The Ir-ReO_x/SiO_2 catalyst can be also used for total hydrodeoxygenation reactions maintaining carbon chain of the substrate, such as sugar alcohols to *n*-alkanes [37]. In total hydrodeoxygenation reactions, H-ZSM-5 as an acid is used to help the conversion of mono-alcohols to which the "direct" mechanism cannot be applied. Ir-ReO_x/SiO_2 has C = O hydrogenation activity, and it is possible to directly convert sugars or even cellulose to *n*-hexane over Ir-ReO_x/SiO_2 in combination with H-ZSM-5 [37, 41, 42].

Figure 8.8 shows the effect of the addition of various metal oxides to Ir/SiO_2 in glycerol hydrogenolysis [33]. The Ir-WO_x/SiO_2 catalyst has some activity and good

Table 8.2 Hydrogenolysis of tetrahydrofurfuryl alcohol over Ir-MO_x/SiO_2 catalysts [31]

M (M/Ir ratio)	Temp. [K]	Conv. [%]	Product (selectivity [%])
None[a]	413	1.6	1,5-Pentanediol (99), 1-pentanol (1)
Re (0.5)	373	33.3	1,5-Pentanediol (96), 1-pentanol (4)
Re (1)	373	43.3	1,5-Pentanediol (95), 1-pentanol (4)
Re (2)	373	58.2	1,5-Pentanediol (96), 1-pentanol (4)
Mo (0.06)	393	24.5	1,5-Pentanediol (96), 1-pentanol (4)
Mo (0.13)	393	30.6	1,5-Pentanediol (93), 1-pentanol (7)
Mo (0.25)	393	25.1	1,5-Pentanediol (94), 1-pentanol (6)
W (0.13)	393	2.8	1,5-Pentanediol (92), 1-pentanol (5)
W (0.25)	393	5.1	1,5-Pentanediol (97), 1-pentanol (1)
W (0.5)	393	1.0	1,5-Pentanediol (99), 1-pentanol (1)

Conditions: catalyst (Ir 4 wt.%) 150 mg, tetrahydrofurfuryl alcohol 1 g, water 4 g, H_2 8 MPa, 2 h
[a]Catalyst 300 mg, 48 h

1,3-propanediol selectivity, although both the activity and selectivity are lower than those of Ir-ReO_x/SiO_2. In the hydrogenolysis of tetrahydrofurfuryl alcohol, all Ir-MO_x/SiO_2 catalysts (M = W, V, Mo, and Re) showed good selectivity to 1,5-pentanediol, similarly to Rh-MO_x/SiO_2 catalysts (Table 8.2) [31, 46, 47]. The Ir-WO_x/SiO_2 catalyst has not been characterized at all, while Ir-ReO_x/SiO_2 catalyst has been well characterized by XRD, TEM, TPR, adsorption studies, XPS, and XAFS: iridium metal particles (~2 nm) covered with low-valent rhenium oxide clusters via direct Ir-Re bonds are dynamically formed by calcination-reduction treatments [32, 33, 48]. Compared with rhenium oxides, many tungsten-containing oxides have more stable structure in redox reactions such as Keggin-type polyoxometalate. With the optimization of the structure of Ir-WO_x, the catalyst may improve the catalytic performance.

8.3 The Unique Addition Effect of Tungsten

This category focuses on the catalysts whose performance is much different from catalysts containing other group 6–7 metal oxides. This situation is realized by the mechanism where tungsten is the active center of catalysis.

8.3.1 Pd-W Catalysts for the Partial C-O Hydrogenolysis of Diols

Palladium is a very active catalyst for hydrogenation of C-C bonds, indicating that it is very effective in activating hydrogen molecule. On the other hand, Pd has a very low catalytic activity in C-O hydrogenolysis reactions when used alone. Therefore,

Table 8.3 Hydrogenolysis of 1,4-anhydroerythritol over various catalysts [49]

Entry	Catalyst	Temp. [K]	Time [h]	Conv. [%]	Product (selectivity [%])
1	Pd/WO_3	473	16	10	3-HTHF (65), THF (8), AHT (9)
2	Pd/NH_4ReO_4	473	16	20	3-HTHF (20), THF (40), AHT (31)
3	Pd/MoO_3	473	16	2	3-HTHF (24), THF (31), AHT (17)
4	Pd/V_2O_5	473	16	19	3-HTHF (13), THF (40), AHT (41)
5	Pd/Nb_2O_5	473	16	9	3-HTHF (30), THF (10), AHT (45)
6	Pt/WO_3	473	16	12	3-HTHF (54), THF (14), AHT (9)
7	Rh/WO_3	473	16	24	3-HTHF (29), THF (46), AHT (9), BuD + BuOH (7)
8	Ir/WO_3	473	16	17	3-HTHF (24), THF (32), AHT (2), BuD + BuOH (22)
9	Ru/WO_3	473	4	23	3-HTHF (33), THF (25), AHT (19), BuD + BuOH (14)
10	WO_3	473	16	3	3-HTHF (45), THF (6), AHT (2)
11	WO_x-Pd/ZrO_2	453	16	7	3-HTHF (71), THF (3), AHT (5)
12	WO_x-Pd/C	453	16	44	3-HTHF (69), THF (8), AHT (1)
13	WO_x-Pd/SiO_2	453	16	36	3-HTHF (69), THF (2), AHT (<1)
14	WO_x-Pd/Al_2O_3	453	16	22	3-HTHF (65), THF (8), AHT (8)
15	WO_x-Pd/TiO_2	453	16	30	3-HTHF (51), THF (19), AHT (3)
16	WO_x-Pd/CeO_2	453	16	25	3-HTHF (47), THF (9), AHT (30)
17	WO_x-Pd/MgO	453	16	3	3-HTHF (45), THF (3), AHT (31)
18	WO_x/ZrO_2	453	16	4	3-HTHF (59), THF (5), AHT (2)
19	Pd/ZrO_2	453	16	1	3-HTHF (25), THF (19), AHT (32)

HTHF hydroxytetrahydrofuran, *THF* tetrahydrofuran, *AHT* 1,4-anhydrothreitol, *BuD + BuOH* butanediols + butanols. Conditions: catalyst 50 mg (entries 1–10) or 150 mg (entries 11–19), 1,4-anhydroerythritol 1 g, 1,4-dioxane 4 g, H_2 8 MPa. Loading amount: 5 wt.% for entries 1–9 and 19; 9.9 wt.% W and 1.4 wt.% Pd for entries 11–18

Pd is an ideal component for hydrogen activation. We tested Pd catalysts supported on various group 5–7 metal oxides for hydrogenolysis of 1,4-anhydro-erythritol (*cis*-3,4-dihydroxytetrahydrofuran) (Table 8.3) [49]. 1,4-Anhydroerythritol is easily produced by dehydration of erythritol, which is derived from glucose by fermentation [50]. The reaction temperature (473 K) is significantly higher than that for Rh- or Ir-based hydrogenolysis systems as described in Sect. 8.2 (~393 K). 1,4-Dioxane is used as the solvent. Among the Pd/MO_x catalysts, Pd/WO_3 gives the highest selectivity to 3-hydroxytetrahydrofuran (mono-deoxygenation product). Main products of other Pd/MO_x catalysts are tetrahydrofuran (THF; di-deoxygenation product) and 1,4-anhydrothreitol (*trans* isomer of substrate). Interestingly, WO_3 alone has some catalytic activity in the production of 3-hydroxytetrahydrofuran. The activities of Rh, Ir, and Ru catalysts supported on WO_3 are higher than that of Pd/WO_3; however, the selectivities to 3-hydroxytetrahydrofuran are lower. Butanols and butanediols are formed as by-products in addition to THF over these three catalysts, indicating that unselective C-O hydrogenolysis proceeds. These side reactions

can be caused by the intrinsic activity of Rh, Ir, and Ru in C-O hydrogenolysis. On the other hand, Pt/WO_3 catalyst shows comparably high selectivity to 3-hydroxytetrahydrofuran. Nevertheless, Pd/WO_3 shows the highest selectivity to 3-hydroxytetrahydrofuran. Supported Pd-W catalysts (WO_x-Pd/support) have been also investigated to increase the catalytic activity, and the results are also shown in Table 8.3. Most supported catalysts show good selectivity to 3-hydroxytetrahydrofuran. WO_x-Pd/C has the highest activity among the tested supports. The difference of activity among various supports is relatively small except the very low activity of WO_x-Pd/MgO. The low activity of WO_x-Pd/ZrO_2 in Table 8.3 is due to the small surface area of used ZrO_2, which is calcined at 1,273 K. When high-surface-area ZrO_2 is used as support, the activity of WO_x-Pd/ZrO_2 becomes similar to other supported catalysts (conversion = 31 %). This weak dependence of catalytic performance on the type of support is in contrast to Rh-MO_x and Ir-MO_x catalysts, which are only active when silica or carbon is used as the support.

Figure 8.9 shows the time course of C-O hydrogenolysis of 1,4-anhydroerythritol over WO_x-Pd/C catalyst. The selectivity to 3-hydroxytetrahydrofuran is almost unchanged even when the conversion reaches >99 %. The highest yield of 3-hydroxytetrahydrofuran is 72 %. The low reactivity of 3-hydroxytetrahydrofuran is also confirmed by the reaction test using 3-hydroxytetrahydrofuran as the substrate. The reaction results of various substrates over WO_x-Pd/C are shown in Table 8.4. The main product from *cis*-1,2-cycloalkanediol is the corresponding cycloalkanol. The reactivity of 1,4-anhydrothreitol is much lower than that of 1,4-anhydroerythriol. Similarly, the reactivity of *trans*-1,2-cyclopentanediol and *trans*-1,2-cyclohexanediol is much lower than that of the corresponding *cis* isomer.

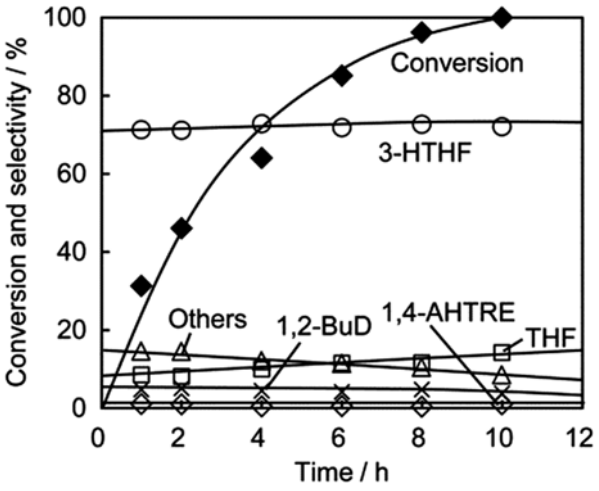

Fig. 8.9 Time course of the hydrogenolysis of 1,4-anhydroerythritol over WO_x-Pd/C (9.9 wt.% W, Pd/W = 0.25). *HTHF* hydroxytetrahydrofuran, *THF* tetrahydrofuran, *BuD* butanediol, *AHTRE* anhydrothreitol. Conditions: substrate 1 g, 1,4-dioxane 4 g, catalyst 50 mg, H_2 8 MPa, 493 K (Reprinted with permission from ref. [49] Copyright 2014 by Wiley-VCH Verlag GmbH & Co)

Table 8.4 Hydrogenolysis of various substrates over WO_x-Pd/C [49]

Entry	Substrate	Conv. [%]	Product (selectivity [%])
1	1,4-Anhydroerythritol	44	3-Hydroxytetrahydrofuran (69), THF (8)
2	1,4-Anhydrothreitol	4	3-Hydroxytetrahydrofuran (39), THF (14)
3	*cis*-1,2-Cyclopentanediol	16	Cyclopentanol (66), *trans*-1,2-cyclopentanediol (7)
4	*trans*-1,2-Cyclopentanediol	6	Cyclopentanol (11), *cis*-1,2-cyclopentanediol (48)
5	*cis*-1,2-Cyclohexanediol	9	Cyclohexanol (42), cyclohexane (22), *trans*-1,2-cyclohexanediol (3)
6	*trans*-1,2-Cyclohexanediol	2	Cyclohexanol (27), *cis*-1,2-cyclohexanediol (55)
7	2,3-Butanediol	5	2-Butanol (66)
8	1,2-Propanediol	6	1-Propanol (61), 2-propanol (15)
9	Ethylene glycol	3	Ethanol (58)
10	Glycerol	14	1,2-Propanediol (41), 1,3-propanediol (31)

Conditions: catalyst (9.9 wt.% W, Pd/W = 0.25) 150 mg, substrate 1 g, 1,4-dioxane 4 g, H_2 8 MPa, 453 K, 16 h

The reaction of straight-chain alkanediols also produces mainly mono-alcohols, although the reactivity is lower than *cis*-1,2-cycloalkanediols.

In the case of 1,2-propanediol, the selectivity to 1-propanol is higher than that to 2-propanol. However, from glycerol, the selectivity to 1,3-propanediol is lower than that of 1,2-propanediol. The selectivity may be influenced by the indirect mechanisms as shown in Figs. 8.1 and 8.6. According to Table 8.4, WO_x-Pd catalysts have some activity in *trans*/*cis* isomerization of cycloalkanediols. The isomerization proceeds by dehydrogenation to 2-ketocycloalkanol and subsequent hydrogenation, indicating that this catalyst has some activity in dehydrogenation. Dehydrogenation is the first step of the three-step indirect mechanism as shown in Fig. 8.6, and therefore, the three-step indirect mechanism of glycerol hydrogenolysis to 1,2-propanediol (Fig. 8.6) may proceed over WO_x-Pd/C catalyst.

Characterization of WO_x-Pd/C has been carried out by TPR, XRD, and TEM. The TPR profile of WO_x-Pd/C shows a broad large signal with a peak at around 900 K. The reduction started below the reaction temperature (453 K), indicating that WO_3 is partly reduced during the reaction. The XRD pattern of WO_x-Pd/C after catalytic use shows only peaks for Pd metal and carbon support. The estimated particle size of Pd is 9 nm from the linewidth of the XRD peak. The TEM image and EDX elemental mapping are shown in Fig. 8.10. The image is vague, probably because of dispersed tungsten species. Pd particles with around 10 nm size are observed in the area where WO_x species condensed. From these results, the WOx--Pd/C catalyst has amorphous WO_x species and Pd particles. Characterization of WO_x-Pd/ZrO_2 has been also carried out, and the results of catalysts with different W amount are compared with those of reaction tests. The XRD and Raman data show that crystalline WO_3 phase is formed in the sample with ≥2.5 wt.% W. On the other hand, the catalytic activity is increased with increasing W amount up to 2.5 wt.%,

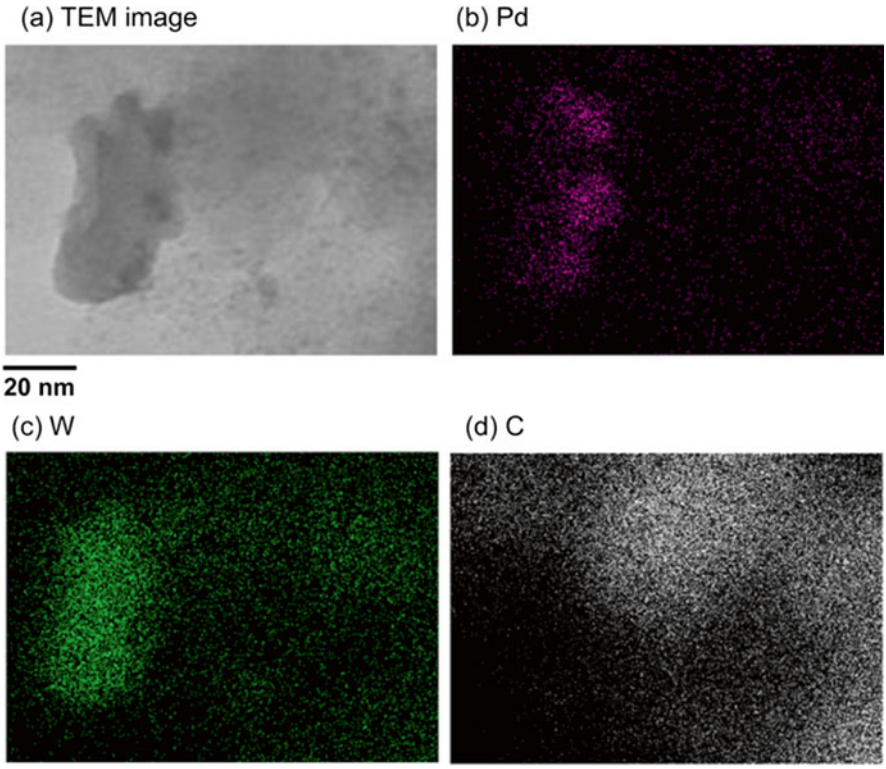

Fig. 8.10 (**a**) TEM image and (**b**–**d**) elemental mapping by TEM-EDX of WO_x-Pd/C after catalytic use. The reaction conditions were the same as those for Table 8.4, entry 1 (Reprinted with permission from ref. [49] Copyright 2014 by Wiley-VCH Verlag GmbH & Co)

and the increase is almost stopped at the amount. These data agree with the idea that the active phase is amorphous WO_x species.

The "direct" mechanism like Fig. 8.5 can be excluded in this system, because S_N2 reaction of substituents that are directly bonded to the ring is prohibited by the steric hindrance [36]. The used solvent (1,4-dioxane) is different from that used in the systems of Rh or Ir catalysts modified with group 6–7 metals (water; Sect. 8.2). In fact, when water solvent is used for WO_x-Pd/C catalyst, the hydrogenolysis is totally suppressed. The reaction order of WO_x-Pd/C catalyst system with respect to H_2 pressure is zero, and it is different from that of the "direct" mechanism. We propose the reaction mechanism of WO_x-Pd-catalyzed partial hydrodeoxygenation, referring the reports for reaction mechanism of Re-catalyzed deoxydehydration [51–54]. Re-catalyzed deoxydehydration produces alkenes from vicinal diols and will be explained in detail in another chapter. This reaction can be regarded as the reverse reaction of *cis*-dihydroxylation of alkenes (e.g., osmium oxidation), and *trans*-1,2-cycloalkanediol is not reactive, similarly to our WO_x-Pd catalyst system. The key step of deoxydehydration is the reduction of coordinated substrate as

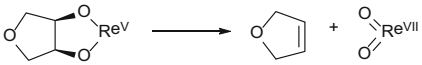

Fig. 8.11 Key step in deoxydehydration of 1,4-anhydroerythritol with Re catalyst

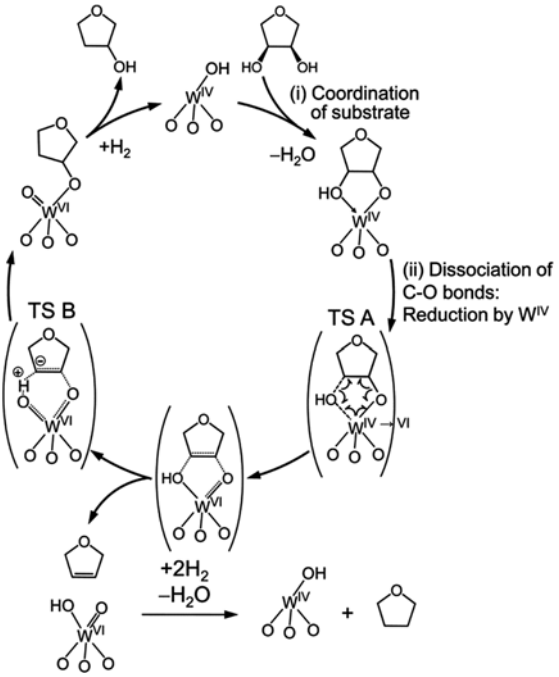

Fig. 8.12 Proposed reaction mechanism (deoxydehydration + hydration) for hydrogenolysis of 1,4-anhydroerythritol over WO_x-Pd catalysts (Reprinted with permission from ref. [49] Copyright 2014 by Wiley-VCH Verlag GmbH & Co)

diolate by Re^V center, as shown in Fig. 8.11. The Re-catalyzed deoxydehydration also uses non-water solvents such as alcohols, aromatics, and 1,4-dioxane. While the reason why water cannot be used in deoxydehydration has not been discussed in the literature, one explanation is that the formation of diolate is suppressed by the hydrolysis of diolate. The main product of WO_x-Pd catalyst system is the same as the hydration product of alkenes which are formed by deoxydehydration. Therefore, the WO_x-Pd-catalyzed hydrodeoxygenation can be formally described as deoxydehydration + hydration.

The proposed mechanism is shown in Fig. 8.12. The reduced W center is the active site. The reduction of W is promoted by Pd metal, and this step is fast. The fast reduction of W gives the zero-order kinetics with respect to H_2 pressure. The substrate is coordinated to the reduced W center through the two hydroxyl groups as the diolate. The next step is the dissociation of the C-O bonds and the reduction by W^{IV}. After the transition state (TS A), two reaction paths exist: one is the removal of alkene as normal deoxydehydration reaction. The produced alkene is quickly converted to alkane by Pd-catalyzed hydrogenation. This path is a side reaction, and

THF is produced from 1,4-anhydroerythritol. The other path involves the protonation of adsorbed alkene precursor before formation of free alkene (TS B). This step gives alkoxide and will be desorbed as a mono-alcohol product. The protonation of adsorbed alkene precursor and the subsequent desorption as alcohol can be together regarded as "hydration." TS A and TS B represent the transition states of "deoxydehydration" and "hydration," respectively, in this deoxydehydration + hydration mechanism. The difference between the WO_x-Pd-catalyzed system and Re-catalyzed one may include the acidity of the W center. The Re^V center may have lower acidity, and the substrate reduced by Re^V is desorbed as an alkene without protonation.

8.3.2 Pt-W Catalysts for the Hydrogenolysis of Glycerol to 1,3-Propanediol

The combination of Pt and W has been intensively investigated by several research groups for catalytic hydrogenolysis of glycerol to 1,3-propanediol [55–68]. Used W species in the literature include supported WO_x, WO_3 support, mixed oxide supports containing W, and polyoxometalates. Although most catalysts using Pt and W show around 40 % selectivity to 1,3-propanediol (Table 8.5), Kaneda et al. reported impressive 66 % yield of 1,3-propanediol using Pt/WO_x/AlOOH catalyst. This is the highest value of 1,3-propanediol yield in all the reported systems of glycerol hydrogenolysis up to now [69]. However, the activity of Pt-W-based catalysts should be improved for practical use: in the typical reported cases, comparable or even larger amount of catalyst in weight was used in comparison with the glycerol amount. The reaction temperature is typically around 453 K, which is much higher than that of Rh- and Ir-based direct hydrogenolysis catalysts (Sect. 8.2). Water has been typically used as a solvent, and in the flow systems, water is usually co-fed. On the other hand, systems using an aprotic polar solvent such as 1,3-dimethyl-2-imidazolidinone (DMI) have been also reported.

The activity and selectivity pattern is very sensitive to the loading amounts of Pt and W, and volcano-type trends in activity/selectivity have been reported for some systems [58, 60]. Typically, in water solvent, the Pt-W catalysts with optimized W amount have about three times higher activity than the catalysts without W (Table 8.6, entries 2 and 6) [59–61, 63]. The catalysts without Pt have lower activity than Pt-W catalysts or even Pt catalysts without W (entries 1, 2, 6, and 7) [61, 67]. The catalyst containing Pd instead of Pt has also lower activity (entry 3) than the Pt-W catalyst, whose trend is different from deoxydehydration + hydration in 1,4-dioxane solvent where Pd/WO_3 and Pt/WO_3 show similar catalytic performance. In view of selectivity, the presence of both Pt and W is necessary to obtain significant selectivity to 1,3-propanediol. The Pt catalysts without W give 1,2-propanediol or 1-propanol, and the W catalysts without Pt give acrolein as a main product [61, 67, 70, 71]. The complex dependences on the loading metals and amounts suggest that only the site with a very specific structure containing both Pt and W can work as the

Table 8.5 Hydrogenolysis of glycerol to 1,3-propanediol over Pt-W catalysts

Catalyst	Solvent	Glycerol/catalyst/solvent [g]	$P(H_2)$ [MPa]	Temp. [K]	Time [h]	Conv. [%]	Select. [%]	Ref.
Pt-W/Al_2O_3	Water	12/4/120	5.5	433	3	23	65	[55]
Pt-W/ZrO_2	DMI	0.3/0.1/0.2	8	443	18	86	28	[56]
Pt/WO_3/ZrO_2	DMI-water	4/1 mL/36	5.5	443	12	31.6	34.9	[57]
Pt/WO_3-ZrO_2	Water	Flow, 60 % glycerol	4	403	LHSV 0.25 h^{-1}	70.2	45.6	[58]
Pt/WO_3/TiO_2/ SiO_2	Water	4/2 mL/36	5.5	453	12	15.3	50.5	[59]
Pt-$H_4SiW_{12}O_{40}$/ SiO_2	Water	Flow, 10 % glycerol	5	473	WHSV 0.045 h^{-1}	63.8	34.5	[60]
Pt-$H_4SiW_{12}O_{40}$/ ZrO_2	Water	Flow, 10 % glycerol	5	433	WHSV 0.045 h^{-1}	56.1	44	[61]
Pt/WO_3	Water	4/1/36	5.5	453	12	18.0	39.3	[62]
Pt/Al_2O_3 + H_2WO_4	Water	0.05/0.1 + 0.05/5	4	473	18	43	28	[63]
Pt-$Li_2H_2SiW_{12}O_{40}$ /ZrO_2	Water	Flow, 10 % glycerol	5	453	WHSV 0.09 h^{-1}	43.5	53.6	[64]
Pt/TiO_2-WO_3	Water	4/1/36	5.5	453	12	24.2	33.5	[65]
Pt-AlO_x/WO_3	Water	0.09/0.1/3	3	453	10	90	44	[66]
Pt-W/AlOOH	Water	0.09/0.1/3	5	453	12	100	66	[67]
Pt-W/ZrO_2-SiO_2	Water	Flow, 10 % glycerol	5	453	WHSV 1 h^{-1}	54.3	52.0	[68]

DMI 1,3-dimethyl-2-imidazolidinone

Table 8.6 Hydrogenolysis of glycerol over Pt-$H_4SiW_{12}O_{40}/ZrO_2$ or the related catalysts [61]

Entry	Catalyst	WHSV [h^{-1}]	Conv. [%]	Product (selectivity [%])
1	Pt-$H_4SiW_{12}O_{40}/ZrO_2$	0.045	>99	1-PO(80), 2-PO(11), 1,3-PD (1), 1,2-PD (5)
2	Pt-$H_4SiW_{12}O_{40}/ZrO_2$	0.17	47	1-PO(37), 2-PO(5), 1,3-PD (25), 1,2-PD (24)
3	Pd-$H_4SiW_{12}O_{40}/ZrO_2$	0.045	25	1-PO(27), 2-PO(3), 1,3-PD (11), 1,2-PD (49)
4	Pt-WO_3/ZrO_2	0.045	91	1-PO(64), 2-PO(12), 1,3-PD (9), 1,2-PD (9)
5	Pt-MoO_3/ZrO_2	0.045	60	1-PO(41), 2-PO(6), 1,3-PD (5), 1,2-PD (37)
6	Pt/ZrO_2	0.045	52	1-PO(8), 2-PO(1), 1,3-PD (1), 1,2-PD (75)
7	$H_4SiW_{12}O_{40}/ZrO_2$	0.045	11	1-PO(5), 2-PO(1), 1,3-PD (3), 1,2-PD (9), acrolein (65), acetol (12)

PO propanol, *PD* propanediol. Conditions: catalyst (2 wt.% noble metal, 15 % additive), glycerol 10 % aq., H_2 5 MPa, H_2/glycerol = 137, 473 K

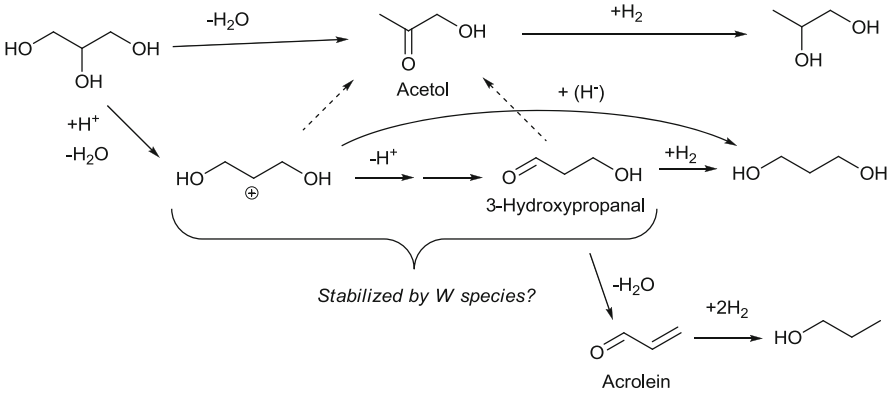

Fig. 8.13 Proposed reaction routes of glycerol hydrogenolysis over Pt-W catalysts

catalytic center for 1,3-propanediol formation. However, the catalyst characterization is rather difficult for systems using Pt and W: XRD patterns have sometimes no peaks, and TEM images usually only detect Pt particles. The precise control of structure will improve the catalytic performance.

The reaction mechanism for Pt-W-based catalysts has not been clearly determined. The reaction mechanism of systems with apolar solvent may be the deoxydehydration + hydration which is discussed in Sect. 8.3.1; however, most systems use water solvent that is not favorable to deoxydehydration + hydration. Several research groups proposed that the reaction is composed of dehydration of glycerol to 3-hydroxypropanal and subsequent hydrogenation to 1,3-propanediol

(Fig. 8.13) [56, 59–61, 63, 64, 67]. The former reaction at the acidic W site is the key step. The correlation between 1,3-propanediol yield and number of Brønsted acid site has been pointed out. As a closely related mechanism, the direct reduction of cationic intermediate with hydrogen species to 1,3-propanediol has been also proposed [58, 62, 66]. However, the large difference in the glycerol conversions over catalysts with and without Pt indicates that Pt has another role in addition to hydrogenating the intermediates. One explanation is that Pt promotes the reduction of hexavalent W species with H_2, and this reaction produces acidic protons ($2W^{6+} + H_2 \rightarrow 2W^{5+} + 2H^+$) [65, 69]. As discussed in Sect. 8.2.1, reaction orders with respect to H_2 pressure can give information in the determination of reaction mechanism. Various reaction orders of glycerol conversion with respect to H_2 from negative [66] to >1 [58, 60] were reported for Pt-W catalysts. Even volcano-type dependencies on H_2 pressure were reported [59]. The selectivity to 1,3-propanediol is generally increased with increasing H_2 pressure. The kinetics may be related to the formation of two equiv. of acidic protons per one H_2 molecule in low H_2 pressure and the deactivation by deep reduction of W species in too high H_2 pressure. The roles of W species may include stabilization of the cationic intermediate and/or 3-hydroxypropanal because acetol, which is also a dehydration product of glycerol, is thermodynamically more stable than 3-hydroxypropanal. The "soft" nature of acidity of polyoxotungstate may affect the stability of cationic intermediate. The increase in 1,3-propanediol selectivity by increase of H_2 pressure may be due to the faster hydrogenation of the cationic intermediate or 3-hydroxypropanal before interconversion to acetol or further dehydration of 3-hydroxypropanal to acrolein. However, why Pt works better than other noble metals is still an unexplained point. The Pt-W-based catalysts have been mainly applied to only glycerol hydrogenolysis. The investigation of the reactivity of various related substrates will give useful information for the determination of the reaction mechanism.

8.4 Conclusions

The three reaction mechanisms introduced in this chapter are summarized in Table 8.7: (a) direct C-O hydrogenolysis, (b) deoxydehydration + hydration, and (c) dehydration + hydrogenation with stabilization of intermediate. For (a), the rate-determining step is the attack of hydride-like species on noble metal to the adsorbed substrate. The activity much depends on the type of noble metal – Rh > Ir > other noble metals ~ 0 – and performances of Rh-MO_x (M = Mo, W, and Re) catalysts are similar. For (b), reduced W is the active species, and the performances of M′-WO_3 (M′ = noble metal) catalysts are similar. For (c), both Pt and W are essential in the catalysis. Each mechanism has unique selectivity and can be used in selective production of bio-related chemicals. However, there is a room for improvement in the activity and selectivity. The characterization of catalysts has been also insufficient. The elucidation of the structure of the active site and the precise structure control of the catalysts will improve the performance.

Table 8.7 Summary of proposed reaction mechanisms of C-O hydrogenolysis over W catalysts combined with a noble metal

Mechanism	Effective noble metal	Reaction	Rate-determining step	Solvent	Temp. [K]	Dependence on $P(H_2)$
(a) Direct C-O hydrogenolysis	Rh, Ir	Dissociation of C-O bond neighboring terminal CH_2OH group	Hydride attack	Water	~393	First order (2–8 MPa)
(b) Deoxydehydration + hydration	Any	Vicinal *cis*-diol → mono-alcohol	Reduction of coordinated substrate with reduced W species	Non-water (1,4-dioxane)	~453	Zero order (2–12 MPa)
(c) Dehydration + hydrogenation with stabilization of intermediate	Pt	Glycerol → 1,3-propanediol	Dehydration of substrate	Water	~453	Volcano curve (1–6 MPa)

References

1. Ruppert AM, Weinberg K, Palkovits R (2012) Hydrogenolysis goes bio: from carbohydrates and sugar alcohols to platform chemicals. Angew Chem Int Ed 51:2564–2601
2. Besson R, Gallezot P, Pinel C (2014) Conversion of biomass into chemicals over metal catalysts. Chem Rev 114:1827–1870
3. Schlaf M (2006) Selective deoxygenation of sugar polyols to α,ξ-diols and other oxygen content reduced materials—a new challenge to homogeneous ionic hydrogenation and hydrogenolysis catalysis. Dalton Trans :4645–4653
4. Nakagawa Y, Tomishige K (2011) Heterogeneous catalysis of the glycerol hydrogenolysis. Catal Sci Technol 1:179–190
5. Miyazawa T, Koso S, Kunimori K, Tomishige K (2007) Development of a Ru/C catalyst for glycerol hydrogenolysis in combination with an ion-exchange resin. Appl Catal A 318:244–251
6. Miyazawa T, Koso S, Kunimori K, Tomishige K (2007) Glycerol hydrogenolysis to 1,2-propanediol catalyzed by a heat-resistant ion-exchange resin combined with Ru/C. Appl Catal A 329:30–35
7. Miyazawa T, Kusunoki Y, Kunimori K, Tomishige K (2006) Glycerol conversion in the aqueous solution under hydrogen over Ru/C + an ion-exchange resin and its reaction mechanism. J Catal 240:213–221
8. Alonso DM, Wettstein SG, Dumesic JA (2012) Bimetallic catalysts for upgrading of biomass to fuels and chemicals. Chem Soc Rev 41:8075–8098
9. Nakagawa Y, Tomishige K (2011) Catalyst development for the hydrogenolysis of biomass-derived chemicals to value-added ones. Catal Surv Asia 15:111–116
10. Tomishige K, Tamura M, Nakagawa Y (2014) Role of Re species and acid cocatalyst on Ir-ReO_x/SiO_2 in the C-O hydrogenolysis of biomass-derived substrates. Chem Rec 14:1041–1054
11. Tomishige K, Nakagawa Y, Tamura M (2014) Selective hydrogenolysis of C-O bonds using the interaction of the catalyst surface and OH groups. Top Curr Chem 353:127–162
12. Furikado I, Miyazawa T, Koso S, Shimao A, Kunimori K, Tomishige K (2007) Catalytic performance of Rh/SiO_2 in glycerol reaction under hydrogen. Green Chem 9:582–588

13. Shimao A, Koso S, Ueda N, Shinmi Y, Furikado I, Tomishige K (2009) Promoting effect of Re addition to Rh/SiO_2 on glycerol hydrogenolysis. Chem Lett 38:540–541
14. Koso S, Furikado I, Shimao A, Miyazawa T, Kunimori K, Tomishige K (2009) Chemoselective hydrogenolysis of tetrahydrofurfuryl alcohol to 1,5-pentanediol. Chem Commun :2035–2037
15. Koso S, Ueda N, Shinmi Y, Okumura K, Kizuka T, Tomishige K (2009) Promoting effect of Mo on the hydrogenolysis of tetrahydrofurfuryl alcohol to 1,5-pentanediol over Rh/SiO_2. J Catal 267:89–92
16. Shinmi Y, Koso S, Kubota T, Nakagawa Y, Tomishige K (2010) Modification of Rh/SiO_2 catalyst for the hydrogenolysis of glycerol in water. Appl Catal B 94:318–326
17. Chen K, Koso S, Kubota T, Nakagawa Y, Tomishige K (2010) Chemoselective hydrogenolysis of tetrahydropyran-2-methanol to 1,6-hexanediol over rhenium-modified carbon-supported rhodium catalysts. ChemCatChem 2:547–555
18. Amada Y, Koso S, Nakagawa Y, Tomishige K (2010) Hydrogenolysis of 1,2-propanediol for the production of biopropanols from glycerol. ChemSusChem 3:728–736
19. Koso S, Nakagawa Y, Tomishige K (2011) Mechanism of the hydrogenolysis of ethers over silica-supported rhodium catalyst modified with rhenium oxide. J Catal 280:221–229
20. Koso S, Watanabe H, Okumura K, Nakagawa Y, Tomishige K (2012) Comparative study of $Rh\text{-}MoO_x$ and $Rh\text{-}ReO_x$ supported on SiO_2 for the hydrogenolysis of ethers and polyols. Appl Catal B 111–112:27–37
21. Chia M, Pagán-Torres YJ, Hibbitts D, Tan Q, Pham HN, Datye AK, Neurock M, Davis RJ, Dumesic JA (2011) Selective hydrogenolysis of polyols and cyclic ethers over bifunctional surface sites on rhodium-rhenium catalysts. J Am Chem Soc 133:1275–12689
22. Chia M, O'Neill BJ, Alamillo R, Dietrich PJ, Ribeiro FH, Miller JT, Dumesic JA (2013) Bimetallic RhRe/C catalysts for the production of biomass-derived chemicals. J Catal 308:226–236
23. Hibbitts D, Tan Q, Neurock M (2014) Acid strength and bifunctional catalytic behavior of alloys comprised of noble metals and oxophilic metal promoters. J Catal 315:48–58
24. Buntara T, Noel S, Phua PH, Melián-Cabrera I, de Vries JG, Heeres HJ (2012) From 5-hydroxymethylfurfural (HMF) to polymer precursors: catalyst screening studies on the conversion of 1,2,6-hexanetriol to 1,6-hexanediol. Top Catal 55:612–619
25. Buntara T, Melián-Cabrera I, Tan Q, Fierro JLG, Neurock M, de Vries JG, Heeres HJ (2013) Catalyst studies on the ring opening of tetrahydrofuran-dimethanol to 1,2,6-hexanetriol. Catal Today 210:106–116
26. Checa M, Auneau F, Hidalgo-Carrillo J, Marinas A, Marinas JM, Pinel C, Urbano FJ (2012) Catalytic transformation of glycerol on several metal systems supported on ZnO. Catal Today 196:91–100
27. Guan J, Peng G, Cao Q, Mu X (2014) Role of MoO_3 on a rhodium catalyst in the selective hydrogenolysis of biomass-derived tetrahydrofurfuryl alcohol into 1,5-pentanediol. J Phys Chem C 118:25555–25566
28. Chaminand J, Djakovitch L, Gallezot P, Marion P, Pinel P, Rosier C (2004) Glycerol hydrogenolysis on heterogeneous catalysts. Green Chem 6:359–361
29. Koso S, Watanabe H, Okumura K, Nakagawa Y, Tomishige K (2012) Stable low-valence ReO_x cluster attached on Rh metal particles formed by hydrogen reduction and its formation mechanism. J Phys Chem C 116:3079–3090
30. Weldon MK, Friend CM (1996) Probing surface reaction mechanisms using chemical and vibrational methods: alkyl oxidation and reactivity of alcohols on transitions metal surfaces. Chem Rev 96:1391–1411
31. Chen K, Mori K, Watanabe H, Nakagawa Y, Tomishige K (2012) C-O bond hydrogenolysis of cyclic ethers with OH groups over rhenium-modified supported iridium catalysts. J Catal 294:171–183
32. Nakagawa Y, Shinmi Y, Koso S, Tomishige K (2010) Direct hydrogenolysis of glycerol into 1,3-propanediol over rhenium-modified iridium catalyst. J Catal 272:191–194
33. Amada Y, Shinmi Y, Koso S, Kubota T, Nakagawa Y, Tomishige K (2011) Reaction mechanism of the glycerol hydrogenolysis to 1,3-propanediol over $Ir\text{-}ReO_x/SiO_2$ catalyst. Appl Catal B 105:117–127

34. Amada Y, Watanabe H, Hirai Y, Kajikawa Y, Nakagawa Y, Tomishige K (2012) Production of biobutanediols by the hydrogenolysis of erythritol. ChemSusChem 5:1991–1999
35. Nakagawa Y, Ning X, Amada Y, Tomishige K (2012) Solid acid co-catalyst for the hydrogenolysis of glycerol to 1,3-propanediol over Ir-ReO_x/SiO_2. Appl Catal A 433–434:128–134
36. Nakagawa Y, Mori K, Chen K, Amada Y, Tamura K, Tomishige K (2013) Hydrogenolysis of CO bond over Re-modified Ir catalyst in alkane solvent. Appl Catal A 468:418–425
37. Chen K, Tamura M, Yuan Z, Nakagawa Y, Tomishige K (2013) One-pot conversion of sugar and sugar polyols to *n*-alkanes without C-C dissociation over the Ir-ReO_x/SiO_2 catalyst combined with H-ZSM-5. ChemSusChem 6:613–621
38. Liu S, Amada Y, Tamura M, Nakagawa Y, Tomishige K (2014) One-pot selective conversion of furfural into 1,5-pentanediol over a Pd-added Ir-ReO_x/SiO_2 bifunctional catalyst. Green Chem 16:617–626
39. Tamura M, Amada Y, Liu S, Yuan Z, Nakagawa Y, Tomishige K (2014) Promoting effect of Ru on Ir-ReO_x/SiO_2 catalyst in hydrogenolysis of glycerol. J Mol Catal A 388–389:177–187
40. Liu S, Amada Y, Tamura M, Nakagawa Y, Tomishige K (2014) Performance and characterization of rhenium modified Rh-Ir alloy catalyst for one-pot conversion of furfural into 1,5-pentanediol. Catal Sci Technol 4:2535–2549
41. Liu S, Tamura M, Nakagawa Y, Tomishige K (2014) One-pot conversion of cellulose into *n*-hexane over the Ir-ReO_x/SiO_2 catalyst combined with HZSM-5. ACS Sustain Chem Eng 2:1819–1827
42. Liu S, Okuyama Y, Tamura M, Nakagawa Y, Imai A, Tomishige K (2015) Production of renewable hexanols from mechanocatalytically depolymerized cellulose by using Ir-ReO_x/SiO_2 catalyst. ChemSusChem 8:628–635
43. Li F, Xue F, Chen B, Huang Z, Yuan Y, Yuan G (2012) Direct catalytic conversion of glycerol to liquid-fuel classes over Ir-Re supported on W-doped mesostructured silica. Appl Catal A 449:163–171
44. Deng C, Duan X, Zhou J, Zhou X, Yuan X, Scott SL (2015) Ir-Re alloy as a highly active catalyst for the hydrogenolysis of glycerol to 1,3-propanediol. Catal Sci Technol 5:1540–1547
45. Mascal M, Dutta S, Gandarias I (2014) Hydrodeoxygenation of the angelica lactone dimer, a cellulose-based feedstock: simple, high-yield synthesis of branched C7-C10 gasoline-like hydrocarbons. Angew Chem Int Ed 53:1854–1857
46. Wang Z, Pholjaroen B, Li M, Dong W, Li N, Wang A, Wang X, Cong Y, Zhang T (2014) Chemoselective hydrogenolysis of tetrahydrofurfuryl alcohol to 1,5-pentanediol over Ir-MoO_x/SiO_2 catalyst. J Energy Chem 23:427–434
47. Pholjaroen B, Li N, Huang Y, Li L, Wang A, Zhang T (2015) Selective hydrogenolysis of tetrahydrofurfuryl alcohol to 1,5-pentanediol over vanadium modified Ir/SiO_2 catalyst. Catal Today 245:93–99
48. Amada Y, Watanabe H, Tamura M, Nakagawa Y, Okumura K, Tomishige K (2012) Structure of ReO_x clusters attached on the Ir metal surface in Ir-ReO_x/SiO_2 for the hydrogenolysis reaction. J Phys Chem C 116:23503–23514
49. Amada Y, Ota N, Tamura M, Nakagawa Y, Tomishige K (2014) Selective hydrodeoxygenation of cyclic vicinal diols to cyclic alcohols over tungsten oxide-palladium catalysts. ChemSusChem 7:2185–2192
50. Childers KG, Dreher SD, Lee J, Williams JM (2006) A practical and scaleable preparation of 1,4-anhydroerythritol. Org Process Res Dev 10:934–936
51. Shiramizu M, Toste FD (2012) Deoxygenation of biomass-derived feedstocks: oxorhenium-catalyzed deoxydehydration of sugars and sugar alcohols. Angew Chem Int Ed 51:8082–8086
52. Dethlefsen JR, Fristrup P (2015) Rhenium-catalyzed deoxydehydration of diols and polyols. ChemSusChem 8:767–775
53. Raju S, Moret M, Gebbink RJMK (2015) Rhenium-catalyzed dehydration and deoxydehydration of alcohols and polyols: opportunities for the formation of olefins from biomass. ACS Catal 5:281–300

54. Ota N, Tamura M, Nakagawa Y, Okumura K, Tomishige K (2015) Hydrodeoxygenation of vicinal OH groups over heterogeneous rhenium catalyst promoted by palladium and ceria support. Angew Chem Int Ed 54:1897–1900
55. Suzuki N, Yoshikawa Y, Takahashi M, Tamura M (2007) Process for producing product of hydrogenolysis of polyhydric alcohol using heterogeneous-system catalysts with high selectivity. WO Patent 2,007,129,560 15 Nov 2007
56. Kurosaka T, Maruyama H, Naribayashi I, Sasaki Y (2008) Production of 1,3-propanediol by hydrogenolysis of glycerol catalyzed by $Pt/WO_3/ZrO_2$. Catal Commun 9:1360–1363
57. Gong L, Lü Y, Ding Y, Lin R, Li J, Dong W, Wang T, Chen W (2009) Solvent effect on selective dehydroxylation of glycerol to 1,3-propanediol over a $Pt/WO_3/ZrO_2$ catalyst. Chin J Catal 30:1189–1191
58. Qin L, Song M, Chen C (2012) Aqueous-phase deoxygenation of glycerol to 1,3-propanediol over $Pt/WO_3/ZrO_2$ catalysts in a fixed-bed reactor. Green Chem 12:1466–1472
59. Gong L, Lu Y, Ding Y, Lin R, Li J, Dong W, Wang T, Chen W (2010) Selective hydrogenolysis of glycerol to 1,3-propanediol over a $Pt/WO_3/TiO_2/SiO_2$ catalyst in aqueous media. Appl Catal A 390:119–126
60. Zhu S, Zhu Y, Hao S, Chen L, Zhang B, Li Y (2012) Aqueous-phase hydrogenolysis of glycerol to 1,3-propanediol over $Pt\text{-}H_4SiW_{12}O_{40}/SiO_2$. Catal Lett 142:267–274
61. Zhu S, Zhu Y, Hao S, Zheng H, Mo T, Li Y (2012) One-step hydrogenolysis of glycerol to biopropanols over $Pt\text{-}H_4SiW_{12}O_{40}/ZrO_2$ catalysts. Green Chem 14:2607–2616
62. Liu L, Zhang Y, Wang A, Zhang T (2012) Mesoporous WO_3 supported Pt catalyst for hydrogenolysis of glycerol to 1,3-propanediol. Chin J Catal 33:1257–1261
63. ten Dam J, Djanashvili K, Kapteijn F, Hanefeld U (2013) Pt/Al_2O_3 catalyzed 1,3-propanediol formation from glycerol using tungsten additives. ChemCatChem 5:497–505
64. Zhu S, Gao X, Zhu Y, Zhu Y, Xiang X, Hu C, Li Y (2013) Alkaline metals modified $Pt\text{-}H_4SiW_{12}O_{40}/ZrO_2$ catalysts for the selective hydrogenolysis of glycerol to 1,3-propanediol. Appl Catal B 140–141:60–67
65. Zhang Y, Zho X, Wang Y, Zhou L, Zhang J, Wang J, Wang A, Zhang T (2013) Mesoporous Ti-W oxide: synthesis, characterization, and performance in selective hydrogenolysis of glycerol. J Mater Chem A 1:3724–3732
66. Mizugaki T, Yamakawa T, Arundhathi R, Mitsudome T, Jitsukawa K, Kaneda K (2012) Selective hydrogenolysis of glycerol to 1,3-propanediol catalyzed by Pt nanoparticles AlO_x/WO_3. Chem Lett 41:1720–1722
67. Arundhathi R, Mizugaki T, Mitsudome T, Jitsukawa K, Kaneda K (2013) Highly selective hydrogenolysis of glycerol to 1,3-propanediol over a boehmite-supported platinum/tungsten catalyst. ChemSusChem 6:1345–1347
68. Zhu S, Gao X, Zhu Y, Cui J, Zheng H, Li Y (2014) SiO_2 promoted $Pt/WO_x/ZrO_2$ catalysts for the selective hydrogenolysis of glycerol to 1,3-propanediol. Appl Catal B 158–159:391–399
69. Nakagawa Y, Tamura M, Tomishige K (2014) Catalytic materials for the hydrogenolysis of glycerol to 1,3-propanediol. J Mater Chem A 2:6688–6702
70. Daniel OM, DeLaRiva A, Kunkes EL, Datye AK, Dumesic JA, Davis RJ (2010) X-ray absorption spectroscopy of bimetallic Pt-Re catalysts for hydrogenolysis of glycerol to propanediols. ChemCatChem 2:1107–1114
71. Delgado SN, Yap D, Vivier L, Especel C (2013) Influence of the nature of the support on the catalytic properties of Pt-based catalysts for hydrogenolysis of glycerol. J Mol Catal A 367:89–98

Chapter 9
Mechanism and Kinetic Analysis of the Hydrogenolysis of Cellulose to Polyols

Mingyuan Zheng, Aiqin Wang, Jifeng Pang, Ning Li, and Tao Zhang

Abstract The catalytic hydrogenolysis of cellulose to polyols represents an attractive process for biomass conversion to value-added products with a high atom economy. In the past decade, extensive studies have been conducted and promptly accumulated a rich knowledge in this field. In this chapter, we focus on the review of reaction mechanisms and kinetics after a brief description of the catalyst development for this process. In view of the different polyol products, the present review is mainly composed of two parts: cellulose conversion to sugar alcohols and cellulose hydrogenolysis to ethylene glycol and 1,2-propylene glycol. The reaction mechanisms are discussed and summarized to obtain general rules in terms of the specific performance of various catalysts. The reaction kinetics of cellulose hydrogenolysis are analyzed on the basis of the kinetics of the individual reaction steps and their correlations in the whole route covering in detail the reactions of cellulose hydrolysis, sugar hydrogenation, retro-aldol condensation, and sugar condensations. Finally, the prospective for the reaction mechanism and kinetics study of cellulose hydrogenolysis is presented.

Keywords Cellulose • Hydrogenolysis • Polyols • Hexitol • Sugar alcohol • Ethylene glycol • Propylene glycol • Kinetics • Reaction mechanism

9.1 Introduction

Cellulosic biomass has been used as a fuel for millions of years. Also, as a fiber-rich material, it is widely applied to the production of cloth, paper, ropes, vessels, and buildings, thanks to its high tension strength and hardness. Most of these applications are of still in use today. Beyond these traditional uses, daily life demands ever more high-quality building blocks for material synthesis and convenient fuels for

M. Zheng • A. Wang • J. Pang • N. Li • T. Zhang (✉)
State Key Laboratory of Catalysis, Dalian Institute of Chemical Physics, Chinese Academy of Sciences, 110, Dalian 116023, China
e-mail: taozhang@dicp.ac.cn

M. Schlaf, Z.C. Zhang (eds.), *Reaction Pathways and Mechanisms in Thermocatalytic Biomass Conversion I*, Green Chemistry and Sustainable Technology, DOI 10.1007/978-981-287-688-1_9

use [1–3]. In the past century, petroleum, coal, and natural gas supplied the world with tremendous amounts of energy and materials to achieve the current prosperity. However, this situation is facing increasing challenges due to the depletion of fossil energy resources and pressing environmental issues. To meet the long-term demand of sustainable development, it is necessary to explore cellulose transformation into a large variety of platform chemicals and fuels by chemical and biological techniques [1–6].

Differing from the fossil energy resources of petroleum and coal, cellulose contains rather high content of oxygen up to ca. 50 wt.% besides carbon and hydrogen elements. The abundant oxygen in cellulose is of some disadvantage for the transformation to fuels. However, if considered for the synthesis of chemicals, particularly oxygen-containing compounds such as polyols, prominent advantages can be shown over fossil resources. First, the transformation theoretically possesses a high atom economy since most hydroxyl groups of cellulose can be preserved in the target polyol products. Second, the value of polyol products is generally high, offering conversions with a good economic viability. Third, the market capacity of polyols is significant (30–40 million ton/a) but not too large, well fitting the moderate availability of biomass in view of the scales of collection, transportation, and storage.

The conversion of cellulosic biomass to polyols can be traced back to the 1930s [7, 8]. Because cellulose has a crystalline structure which strongly inhibits its degradation, conventional methods for polyol production from cellulose generally comprise two separated steps, i.e., hydrolysis of cellulose to soluble sugars with concentrated mineral acids and followed by hydrogenation or hydrogenolysis of polyols with transition metal catalysts. It is therefore highly desirable to develop novel green techniques for the direct hydrolytic hydrogenolysis of cellulose.

Recently, a one-pot catalytic hydrolytic hydrogenolysis of cellulose to polyols has been developed and was the target of intensive investigations [6, 9–33]. Heterogeneous catalysts are employed to take advantage of the convenience in recycling after reaction. Water is used as a green reaction medium, which not only participates in the hydrolysis reaction but also generates protons in situ at high temperatures to promote the cellulose hydrolysis. Reactions are conducted at temperatures of 423–523 K, at which cellulose is activated by subcritical water. Multiple reactions are coupled in one pot, involving polysaccharides hydrolysis, sugar isomerization, hydrogenation, retro-aldol condensation, decarbonylation, polymerization, and some other side reactions. The polyol products vary from C_6 to C_2 polyols, including sorbitol, mannitol, erythritol, glycerol, 1,2-propylene glycol, and ethylene glycol. The polyol distributions are highly dependent on the type of catalysts, reaction conditions, and reaction kinetics of the major reactions involved.

Significant progress has been made in cellulose hydrogenolysis to polyols in many aspects, including polyol production with high yields, reaction efficiency promotion, product selectivity control, development of less expensive catalysts, reaction-environment endurable catalysts, and raw biomass conversion. Nevertheless, a complete and insightful understanding of the reaction mechanism and kinetics is not yet available, and it is not an easy task to clearly identify the

reaction mechanism and kinetics in the hydrogenolysis of cellulose although they are of paramount importance for the design of more efficient catalysts and processes. The obstacles are mainly set by the harsh reaction environment where most characterization techniques are not feasible for an in situ detection of reaction intermediates and active sites on catalysts. In addition, the multiple active components of catalysts strongly interact with each other, further increasing the complexity of studying the reaction kinetics. Considering that the reaction mechanisms are closely dependent on the catalyst, reaction conditions, and target products, in this chapter, we discuss and summarize the reaction mechanisms and kinetics following a brief description of catalysts for cellulose hydrogenolysis.

9.2 Cellulose Hydrogenolysis to Sugar Alcohols

9.2.1 Catalysts and Reaction Mechanisms

Sugar alcohols, mainly referring to sorbitol and mannitol, are high-value commodity chemicals widely used in drugs, food, and cosmetics [30]. Cellulose is composed of C_6 glucan units and it should certainly be possible to use it for the production of sugar alcohols through a direct hydrolytic hydrogenation process. Glucan units in cellulose are linked via 1,4-glycosidic bonds and protected by the crystalline structure of cellulose. Accordingly, the catalysts must fulfill two functions for the cellulose hydrolytic hydrogenation: (1) the catalytic hydrolysis of cellulose to release glucose and soluble oligosaccharides and (2) the catalytic hydrogenation of sugars to form polyols [34]. The sugars formed during the reaction are metastable, i.e., they readily to undergo condensation to form humins under harsh reaction conditions. Therefore, for the production of hexitols from cellulose in high yields, the essential questions are how to realize cellulose hydrolysis without using a conventional mineral acid and how to keep the rates of tandem reactions in a suitable balance.

In 2006, Fukuoka and coworkers reported one-pot catalytic transformation of cellulose to sugar alcohols in hot water with heterogeneous catalysts, involving noble metal catalysts consisting of Pt/Al_2O_3, $Pt/SiO_2–Al_2O_3$, Pt/HUSY, and Ru/HUSY [9]. After reaction at 463 K and 5 MPa H_2 for 24 h, hexitols were obtained at a yield of 31 %. The researchers proposed that the Pt catalysts participate in the hydrogenation and also play a solid acid role in promoting cellulose hydrolysis. The acidic sites of catalysts on one hand originate from the acidic supports. On the other hand, they were generated by hydrogen atoms spilling over from metallic Pt sites to the support surface [9, 19]. The remarkable activity of noble metal sites for cellulose hydrolysis was further identified in later studies [35, 36]. For instance, over a mesoporous carbon-supported Ru catalyst, glucose was obtained at a yield of 34.2 %. The Ru sites were also found to be very active for the hydrolysis of oligosaccharides, which result from the preliminary degradation of cellulose [35]. The reaction mechanism of cellulose transformation over Pt/Al_2O_3 is presented in Fig. 9.1, wherein cellulose hydrolysis and sugar hydrogenation reactions are coupled in one pot.

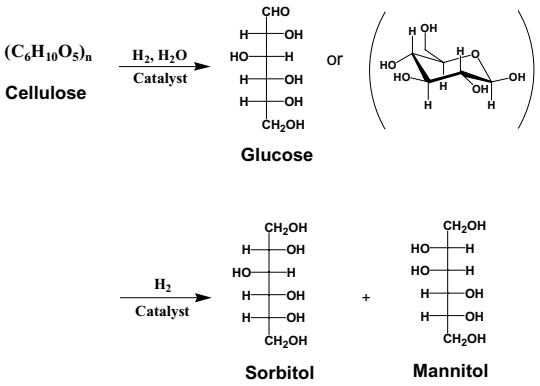

Fig. 9.1 Catalytic conversion of cellulose into sugar alcohols (Reprinted with permission from Ref. [9] Copyright 2006 by John Wiley & Sons Ltd)

Compared to the conventional transformation of cellulose to polyols using mineral acids and by multiple steps, the one-pot hydrolytic hydrogenation process with solid catalysts has several attractive features: (1) heterogeneous catalysts are less corrosive to the reaction equipment and can readily be recycled after the reaction, (2) the reaction process is simplified by coupling multiple reactions in one pot, and (3) the aqueous reaction medium is nontoxic to the environment. However, problems are also evident from the early work, e.g., a low efficiency of reaction, low selectivity to hexitols, and high cost of noble metal catalysts. Bearing in mind the potential advantages of this process and the known challenges for cellulose conversion, great endeavors were further made in the following years to obtain a more encouraging catalytic performance.

The active components of catalysts and reaction conditions for cellulose transformation to hexitols described in the literature vary over a wide range. The approaches to promote the catalytic performance can be largely ascribed to the following aspects: (1) reaction condition optimization, (2) novel acidic supports, (3) different hydrogenation components, (4) combining homogeneous and heterogeneous catalysis, (5) pretreatment of cellulose, and (6) hydrogen source alternatives to H_2. In the following context, detailed discussions on the catalysts and reaction mechanisms will be presented along this classification.

As shown by Liu and coworkers, the reaction temperature has remarkable effects on the reaction efficiency [12]. When the reaction was performed at 518 K, its efficiency was significantly improved with 100 % cellulose conversion in 30 min, in contrast to a 24 h reaction at 463 K [9]. They proposed that protons are generated from subcritical water and act as acid to promote cellulose hydrolysis. The resulting sugars then undergo hydrogenation over transition metal catalysts to form hexitols. The reaction mechanism is shown in Fig. 9.2.

For a good heterogeneous catalyst for cellulose hydrolytic hydrogenation, its support should not only fulfill the function of dispersing metallic active components but also afford acidic sites to compose a bifunctional catalyst. Various acidic supports were employed, including Al_2O_3 [9, 19, 37], SiO_2-Al_2O_3 [9], ZSM-5 [25], MCM-41 [38], MCM-48 [38], H-USY [9], $Cs_3PW_{12}O_{40}$ [21], AC-SO_3H [39],

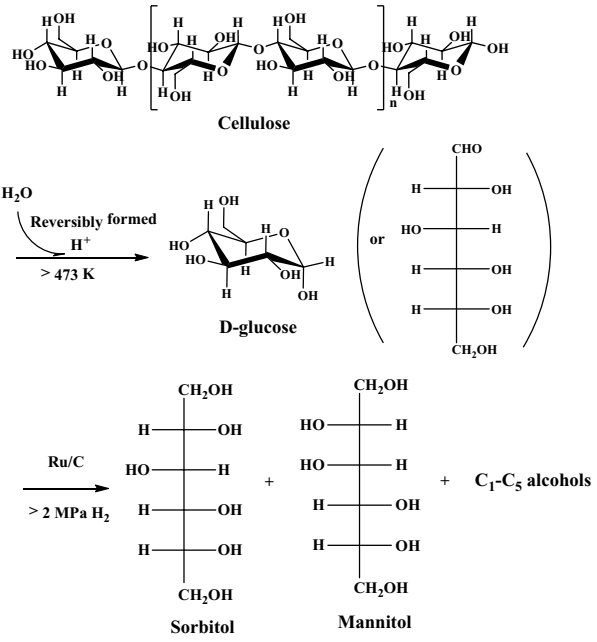

Fig. 9.2 Catalytic conversion of cellulose into hexitols with the aid of in situ formed proton acid (Reprinted with permission from Ref. [12] Copyright 2007 by John Wiley & Sons Ltd)

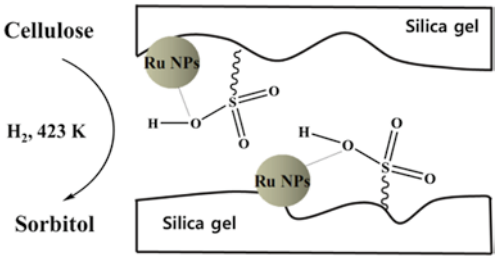

Fig. 9.3 Cellulose conversion over Ru/SiO_2–SO_3H catalyst (Reprinted with permission from Ref. [41] Copyright 2014 by the Royal Society of Chemistry)

MCM-41-n-SO_3H [40], SiO_2–SO_3H [41], Zr-SBA-15 [42], zirconium phosphate (ZrP) [31, 43], PTA/MIL-100(Cr) [44], and $NbOPO_4$ [45]. These supports possess Brønsted acid sites for cellulose hydrolysis and sometimes also afford Lewis acid sites for cellulose activation and sugar isomerization [31, 46]. After loading with transition metals Ru, Pt, Ni, Rh, or Ir, bifunctional catalysts were obtained and exhibited enhanced performance with hexitols yields reaching 60–90 %. Following this strategy, modification of a neutral support with acidic groups is feasible to improve the reaction rate of cellulose hydrolysis [41]. Also, the product selectivity can be modified to some extent with suitable interactions between the modifier and metal sites on the support. In one instance, Hou et al. showed that the sulfonic groups on SiO_2–SO_3H changed the electronic property of Ru nanoparticles, consequently improving the selectivity to sorbitol by inhibiting its further degradation (as shown in Fig. 9.3) [41].

The oxide-based bifunctional catalysts have reasonably good stability and can be reused for several times in the one-pot process. However, in a long-term operation, they still suffer from activity decay. The Brønsted acid sites on the oxide support surface gradually leach into the hot aqueous solution. Otherwise, the oxide support itself is transformed into hydroxide by the hot water, leading to the collapse of the pristine structure and the loss of acidic sites. Using carbon materials as catalyst carriers is a promising alternative approach to resolve this problem. Carbons are hydrothermally stable under the reaction conditions typically at temperatures of 423–573 K. Moreover, the surface of carbon materials can be furnished with plenty of OH and carboxyl groups. Such weak acidic sites have been found to contribute to the activation of the glycosidic bonds in cellulose and consequently promote the hydrolysis of cellulose [27, 35, 47–51]. Conversely, strong acid sites on carbon materials are unequivocally effective for cellulose hydrolysis [52–54]. In one instance, a 65 % hexitols yield was obtained over a 10 % Ru/AC-SO_3H catalyst [39]. But unfortunately, SO_3H groups on the activated carbon are not stable enough under the harsh reaction conditions required for crystalline cellulose conversion; they still suffered from gradual leaching during the reaction.

Besides the support, the hydrogenating metal is another important factor determining the hexitols yields in cellulose hydrolytic hydrogenation. Zhao and coworkers investigated nickel catalysts supported on a series of carriers, including Al_2O_3, SiO_2, ZSM-5, bentonite, kieselguhr, and TiO_2 [55]. They found that high activity for hydrogenation and inferior activity for dehydrogenation of Ni catalysts were essential for obtaining high yields of hexitols. The synergistic effect between Ni and acid–base sites of the support could accelerate the dehydrogenation of sorbitol to form glucose, which further undergoes retro-aldol condensation, hydrogenation, and dehydration to form small polyols at the expense of the hexitols yield. The proposed reaction pathway is depicted in Fig. 9.4.

The ratio of hydrogenation sites and hydrolysis active sites affects the hexitols yield [44, 48]. Huang et al. found that to obtain a high yield of hexitols over a Ru-PTA/MIL-100(Cr) catalyst, the optimal quantity ratio of two catalytic functions should be kept in a range of $8.84 < n_{Acid}/n_{Ru} < 12.90$ [44].

Hydrolytic transformation of cellulose is normally conducted in compressed hot water, in which metallic particles of catalysts are liable to sinter during the reaction as a result of the so-called Ostwald ripening. The particles of transition metal, in particular non-precious metal such as Ni and Cu, slowly release metal ions into the hot aqueous solution, and the metal ions are then reduced to the metallic state over the hydrogenation sites and deposited there. The overall effect is that the small metal particles minimize and eventually disappear, while the large metal particles grow to larger ones parallel to the reaction running. The essential reason is associated with the difference in the relative surface free energy between metal particles of different sizes. Increasing metal loadings can increase the particle size and accordingly improve the catalyst stability. Fukuoka et al. showed that larger crystalline Ni particles were more resistant to sintering and to oxidation on the surface [56]. Another way to improve the stability of a metallic catalyst is modifying it with a second metal to form a bimetallic catalyst [27, 57]. Zhang and coworkers synthe-

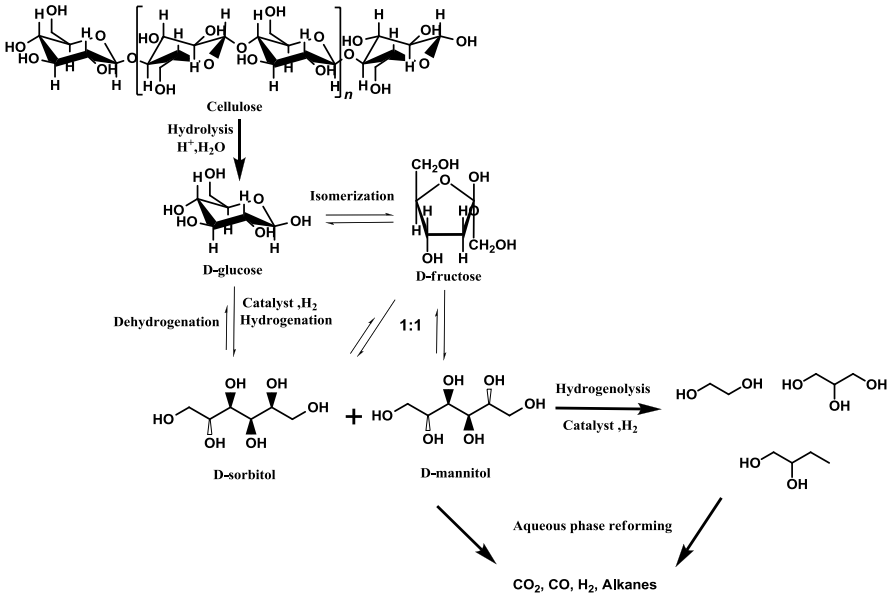

Fig. 9.4 The proposed reaction pathways for the cellulose hydrogenolysis over Ni catalysts (Reprinted from Ref. [55], Copyright 2014, with permission from Elsevier)

sized bimetallic catalysts, e.g., 1 %Rh-5 %Ni/MC and 4 %Ir-4 %Ni/MC, with a mesoporous carbon support and obtained 58 % hexitols yield [27]. The catalysts endured reactions at 518 K for at least four recycles without decay in the catalytic activity. Similarly, Zhao et al. synthesized a PtNi/ZSM-5 catalyst for cellulose hydrogenolysis [57]. Compared to the monometallic catalyst Ni/ZSM-5 [25], the bimetallic catalyst showed much better reuse stability, which was attributed to the formation of Pt-enriched alloy surface [57].

Besides noble metal catalysts, transition metal phosphide catalysts, e.g., Ni_2P, are also suitable candidates to be used as bifunctional catalysts for cellulose hydrolytic hydrogenation [14, 58]. The nickel phosphide catalysts are prepared by impregnation of Ni phosphates on the supports followed by reduction in hydrogen. However, a small portion of Ni phosphate species cannot be completely reduced to nickel phosphides due to the strong interaction between Ni phosphate and the support. Thus, the reserved Ni phosphate provides acidic sites for the cellulose hydrolysis, cooperating with the reduced Ni phosphides for the hydrogenation of sugars to form hexitols in cellulose hydrogenolysis.

In summary, although a solid catalyst possesses advantages in separation and recycling after reaction, it must be pointed out that its effectiveness is much lower than that of a homogeneous catalyst. The reason lies in the interaction opportunities between the solid catalyst and water-insoluble cellulosic reactant, which is several orders of magnitude lower than that of a homogeneous catalyst [59]. Only the surface acid sites of the catalyst can be accessed at the beginning of the reaction because the dimensional size of cellulose fibers is some hundreds times larger than

the pore size in the solid acid catalyst [59]. This greatly hinders cellulose depolymerization with high efficiency. In some cases, H_3O^+ species can be released from the solid acid into the reaction medium, such as an ionic liquid, leading to high reaction rates essentially due to the homogeneous catalysis [60, 61].

To achieve high reaction efficiency, many studies attempted to use water-soluble acids in combination with hydrogenation catalysts [18, 62–64]. Sels and coworkers combined a soluble heteropoly acid, i.e., $H_4SiW_{12}O_{40}$, with a heterogeneous Ru/C catalyst for cellulose hydrolytic hydrogenation [63]. After 0.33 h reaction at 363 K, the ball-milled cellulose at 10 % concentration was almost completely converted with a 65 % hexitols yield. The reaction efficiency was increased by several orders of magnitude in comparison with that over typical solid catalysts [9, 12], even at the much milder reaction temperature. Besides the contribution of soluble heteropoly acid, the ball-milling pretreatment on cellulose also greatly enhanced reaction efficiency. In a control experiment, the cellulose conversion was lower than 80 % even after 4 h reaction if carried out without ball-milling pretreatment [63]. Another alternative way to improve the reaction efficiency is pre-depolymerizing cellulose with an acid [65]. Schüth, Rinaldi, and coworkers pretreated cellulosic feedstock by impregnating catalytic quantities of H_2SO_4 and subsequent ball milling for 2 h. In this way, cellulose was totally converted to water-soluble oligosaccharides and gave a 94.3 % hexitols yield through reaction at 423 K over a Ru/C catalyst. The reaction rate was 18–27 times faster than the best examples reported in literatures [65].

For the cellulose hydrolytic hydrogenation reaction, hydrogen is evidently required for sugar hydrogenation to form polyols. Fukuoka and coworkers studied the possibility to utilize in situ generated hydrogen for this process. They used 2-propanol as hydrogen resource instead of H_2 gas in cellulose transformation [20, 66]. Over Ru/C catalysts, a higher hexitols yield was obtained in the presence of 2-propanol than that under 0.8 MPa H_2 (46.9 % vs. 37.8 %). The reaction route is presented in Fig. 9.5.

Ma and coworkers tested cellulose hydrolytic hydrogenation using CO as a substitute for H_2. The reaction was conducted under 4.5 MPa CO at 523 K for 30 min

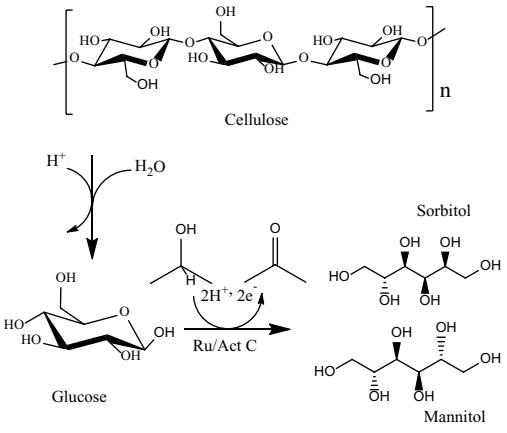

Fig. 9.5 Cellulose transformation over Ru/AC to hexitols with 2-propanol as a hydrogen donor (Reprinted with permission from Ref. [20] Copyright 2011 by the Royal Society of Chemistry)

and produced hexitols at a yield of 25 % over a 7 %Pt–40 %Mo_2C/C catalyst [67]. The Pt–Mo_2C/C was deemed to act as a tandem catalyst, where the Pt–Mo_2C domains were responsible for hydrogen generation via water-gas shift reaction and the Pt–C domains were responsible for the subsequent hydrogenation reaction.

9.2.2 Reaction Kinetics

As discussed above, different catalysts have been developed for cellulose hydrogenolysis to sugar alcohols. The detailed mechanisms to achieve high catalytic performance are not all the same and need to be discussed case by case. However, there are still some common rules followed in these reactions. It has been popularly accepted that the cellulose hydrolytic hydrogenation process is mainly composed of two consecutive reactions: cellulose hydrolysis to sugars and the sugars hydrogenation to hexitols, accompanied by some side reactions. This suggests that the study on the reaction kinetics of cellulose hydrogenolysis can be largely divided into two parts, i.e., hydrolysis reaction and hydrogenation reaction. A whole expression for the reaction kinetics of cellulose hydrogenolysis can be obtained according to the kinetics of individual reactions and their correlation in a model.

For the first reaction step, i.e., cellulose hydrolysis, there have been a plenty of studies conducted because this is a really important topic for biomass utilizations [35, 51, 59, 68–95]. Several recent reviews presented very comprehensive summary on the reaction kinetics for cellulose hydrolysis [59, 75, 76, 82, 85, 94]. As shown therein and the literatures cited, Saeman described the kinetics of cellulose hydrolysis with a model involving two consecutive pseudo-first-order reactions with respect to H^+ concentration (Eq. 9.1) [68, 88]:

$$\text{Cellulose} \xrightarrow{k_2} \text{Glucose} \xrightarrow{k_2} \text{Degradation products} \tag{9.1}$$

The reaction rate k can be represented by an Arrhenius equation modified with acid concentration (Eq. 9.2) [88]:

$$k = k_{i0} \times A^{m_i} \times e^{(E_i/RT)} \quad i = 1, 2 \tag{9.2}$$

wherein k_{i0} is the pre-exponential factor, A is the concentration of acid, m_i is the power of acid concentration, E_i is the activation energy, T is the temperature, R is the universal gas constant, and m_1 and m_2 are the slopes of cellulose and glucose hydrolysis profiles, respectively [88]. Table 9.1 lists a series of parameter values obtained from acid hydrolysis of cellulose according to Saeman's model. One notices that the apparent activation energies for cellulose hydrolysis to glucose are ca. 120–180 kJ/mol, but pre-exponential factors and acid exponents vary over a very wide range, i.e., 10^{10}–10^{19} min^{-1} and 1.0 – 6.0, respectively [88].

Table 9.1 Overview of kinetic parameters of cellulose acid hydrolysis reported in the literatures

Substrate	Reaction conditions[a]	K_{10} (min^{-1})	E_{a1} (kJ/mol)	m_1	K_{20} (min^{-1})	E_{a2} (kJ/mol)	m_2
Cellulose pulp from sugarcane bagasse	Acid: 0.07–0.28 wt.%	1.3×10^{19}	184.9		3×10^{12}	124.5	
	Temp: 453–503 K						
Douglas fir	Acid: 0.4–1.0 wt.%	1.73×10^{19}	179.5	1.34	2.38×10^{14}	137.5	1.02
	Temp: 443–463 K						
Microcrystalline cellulose	Acid: 30–70 wt.%	2.946×10^{10}	127.2	6.0	7.98×10^{26}	166.9	0.77
	Temp: 298–313 K						
Paper refuse	Acid: 0.2–1.0 wt.%	29×10^{19}	188.7	1.78	4.9×10^{14}	137.2	0.55
	Temp: 453–513 K						
Municipal solid wastes	Acid: 1.3–4.4 wt.%	1.94×10^{16}	171.61	1.0	1.148×10^{12}	142.3	0.66
	Temp: 473–513 K						
α-Cellulose	Acid: 0.2–1.0 wt.%	1.2×10^{19}	177.6	1.3	3.8×10^{14}	136.7	0.7
	Temp: 493–513 K						
Solka-floc	Acid: 0.5–2.0 wt.%	1.22×10^{19}	177.8	1.16	3.79×10^{14}	136.8	0.69
	Temp: 453–513 K						
Filter paper	Acid: 0.4–1.5 wt.%	1.22×10^{19}	178.9	1.16	3.79×10^{14}	137.2	0.69
	Temp: 473–513 K						
Hardwood	Acid: 4.41–12.2 wt.%	6.6×10^{16}	165.34	1.64	6.4×10^{12}	128.9	1.10
	Temp: 443–463 K						

[a]Acid used in all the experiments was H_2SO_4. The kinetic parameters correspond to Eqs. 9.1 (reaction) and 9.2 (Arrhenius expression)

The big discrepancy in the parameter values is caused by the different reaction conditions under which the Saeman's model is invalid to describe the kinetics. Equation 9.1 was obtained at 443–463 K and acid concentrations in 0.2–2 %. However, if the reaction is conducted under conditions significantly different from those in Saeman's study, the cellulose morphology, crystallinity, structure, and solubility would be remarkably changed and accordingly affect the validity of the reaction model [96]. For instance, the crystallinity of cellulose can be disrupted to amorphism by subcritical or supercritical water [91, 94], and the resulting amorphous cellulose is much easier to be hydrolyzed [59]. Cellulose has different types of crystallinity including celluloses I, II, III_I, III_{II}, IV_I, and IV_{II}. It was found that the rate of cellulose decomposition depended on the types of crystalline cellulose and reaction temperatures when the hydrolytic reaction was conducted in at 503–543 K and 10 MPa [95]. Celluloses I, III_I, and IV_I were easier than celluloses II, III_{II}, and IV_{II} to be degraded, and the E_a for cellulose degradation were in a range of 50–70 kJ/mol. The difference of the E_a values from those reported in other literatures were ascribed to definitions of decomposition processes and treatment conditions used [95].

In general, cellulose hydrolysis is unlikely to directly generate monosaccharides. Rather, as shown in Eq. 9.3, it typically comprises consecutive steps of cellulose hydrolysis to oligosaccharides and the further hydrolysis to glucose [82]:

$$\begin{array}{l}\text{Polysaccharides} \xrightarrow{k_1} \text{Oligosaccharides} \xrightarrow{k_2} \text{Monosaccharides(sugars)} \xrightarrow{k_3} \\ \quad \text{Dehydration products}\end{array} \tag{9.3}$$

The values of the kinetic constants (k_1, k_2) are correlated to the acid sites available and accessible in aqueous medium [97], the diffusion limitations of poly/oligosaccharides [98], and polymerization degrees of oligosaccharides [99]. The second step of oligosaccharides hydrolysis takes place more rapidly than the first one. Overend et al. observed the formation of sugar oligomers in the hydrolysis of α-cellulose, and the rate of glucose formation from oligomers was three times faster than the glucose formation from cellulose [100]. Therefore, the first step is the rate-determining step, and the overall reaction kinetics still follows Seaman's equation in most cases.

The cellulose hydrolysis is possibly following two routes, i.e., one dominant route involving cleavage at the glycosidic bond and the other minor route involving cleavage at the ring oxygen [88]. As shown in Fig. 9.6 using a cellobiose molecule to represent cellulose, the attack of an acid proton happens at either glycosidic oxygen or ring oxygen, resulting in a cyclic or a noncyclic carbonium ion, respectively. The protonation of the glycosidic oxygen atom forms a cyclic carbonium cation and glucose, followed with further addition of water to form a saccharide and a proton. In the minor pathway, a proton attacks the ring oxygen to form a noncyclic carbonium cation. After the addition of water to the carbonium intermediate, two glucose molecules are produced [59, 88]. Regarding the protonation of the glycosidic oxy-

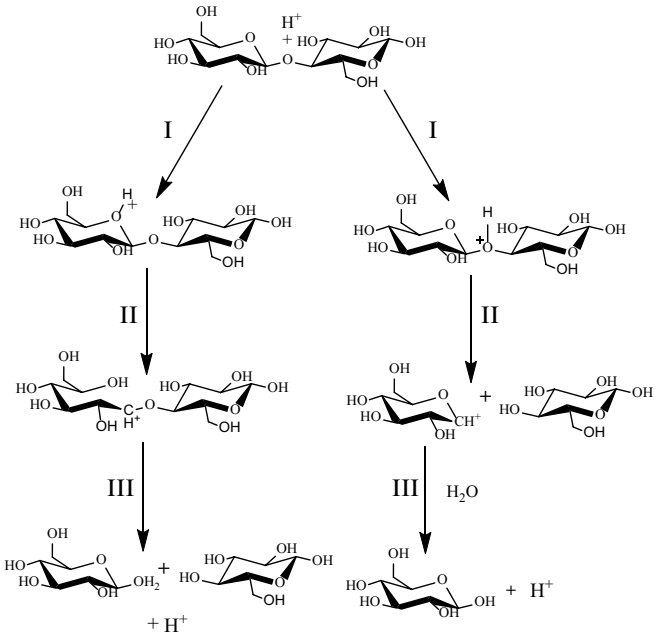

Fig. 9.6 Mechanism of acid hydrolysis of cellobiose (Reprinted with permission from Ref. [88] Copyright 2014 by the American Chemical Society)

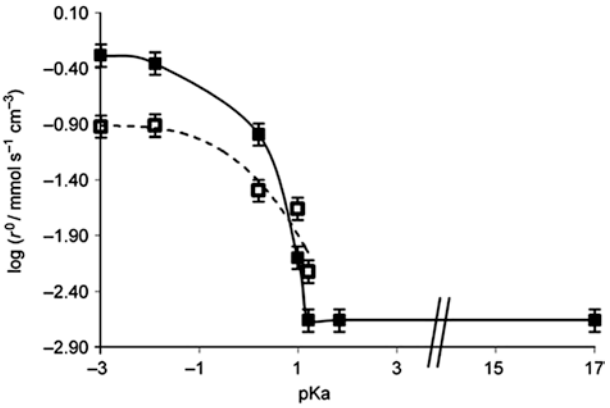

Fig. 9.7 The initial rates of cellobiose hydrolysis in ionic liquid as a function of pKa of the acid for glucose formation (■) and glucose degradation (□) (Reprinted with permission from Ref. [101] Copyright 2009 by the Royal Society of Chemistry)

gen, strong Brønsted acid sites are required (pK= <4). Vanoye et al. disclosed that the hydrolysis rate of cellobiose in ionic liquid shows an evident dependence on the pK_a of the acid used in the reaction, as shown in Fig. 9.7 [101].

As for the cellulose hydrolysis over solid acid catalysts, numerous studies have been performed. As reviewed in a literature and papers cited therein [85], the solid

acids involved metal oxides, polymer-based acids, sulfonated carbon-based acids, heteropoly acids, H-form zeolites, and supported metal catalysts. The reaction efficiency of cellulose hydrolysis over solid acid catalyst is determined by acid strength, acid density, surface polarity, functional groups on the surface, pore size of solids, and solvents. However, few of these studies provided the reaction kinetic data. Rinaldi and coworkers investigated the cellulose hydrolysis in ionic liquid [BMIM]Cl with the acid catalyst Amberlyst 15DRY [102]. They found that cellulose hydrolysis still follows a first-order reaction with respect to the amount of solid acid. The activation energy for cellulose hydrolysis was 108 kJ mol^{-1}, which is lower than that with liquid acids (e.g., 170–180 kJ mol^{-1} in H_2SO_4).

Synergistic effects between the functional groups on the surface of solid acids could substantially decrease the activation energy of cellulose hydrolysis [103]. Pan et al. introduced $–SO_3H$ to partially replace –Cl groups in chloromethyl polystyrene (CP) resin and used it for the catalytic hydrolysis of crystalline cellulose. The best yield of glucose reached 93 % over CP–SO_3H, in contrast to no hydrolysis of cellulose occurred when using sulfuric acid. The activation energy of cellulose hydrolysis was merely 83 kJ mol^{-1} at 373–413 K, which is much lower than that for sulfuric acid (170 kJ mol^{-1}). The authors proposed that the chlorine (–Cl) groups play roles in binding cellulose via hydrogen bonds and the sulfonic acid groups ($–SO_3H$) function as the hydrolytic sites. A similar synergistic effect was also observed on sulfonated carbon materials. Hara et al. studied cellulose hydrolysis over a sulfonated carbon catalyst and obtained 110 kJ mol^{-1} activation energy, which is again notably lower than that for sulfuric acid [53]. The decrease in E_a was ascribed to phenolic groups (pK_a of ca. 10) and carboxylic acid groups (pK_a of ca. 4.7) coexisting with strong acid sites $–SO_3H$ (pK_a ca. −2.8) on the sulfonated carbon surface. The weak acid sites adsorbed soluble oligosaccharides onto the surface of carbon material and promoted the overall reaction rate [104]. Katz et al. further manifested the promoting function of weak acidic OH-defect sites on the surface of supports for cellulose hydrolysis by comparatively studying the performance of modified silica and alumina in β-glucan hydrolysis [51]. The authors concluded that (1) OH-defect sites on the surface favored adsorption of the β-glu strand in highly constrained environment and (2) OH-defect sites activated glycosidic bonding for hydrolysis via hydrogen bonding.

As for the side reactions, typically sugar decomposition, its apparent activation energy is similar to that of cellulose hydrolysis, and the rates of sugar degradation and cellulose hydrolysis are also in the same order of magnitude under the harsh reaction conditions [59]. This is one reason why it is favorable to hydrogenate sugars in situ into stable sugar alcohols with high yields in the cellulose conversion.

The hydrogenation of glucose to sorbitol follows a Langmuir–Hinshelwood mechanism where the surface reaction is the rate-determining step (as shown in Table 9.2) [105–111]. Kapteijn et al. carried out a detailed study on the reaction kinetics of D-glucose hydrogenation over a 5 % Ru/C catalyst at 373–403 K, 4.0–7.5 MPa H_2, and glucose concentration of 0.56–1.39 mol/L [108]. Three plausible models were used based on Langmuir–Hinshelwood–Hougen–Watson (LHHW) kinetics, i.e., Model (1) noncompetitive adsorption of hydrogen and glucose, Model

Table 9.2 Overview of model equations presented in literatures and the obtained kinetic parameters

Model by	Mechanism	Model equation	Parameter estimation	Remarks
Brahme and Doraiswamy	Reaction between molecularly adsorbed hydrogen and D-glucose in liquid phase	$r = \frac{kK_{H_2}C_G C_{H_2}}{1 + K_{H_2}C_{H_2}}$	$k = 6.2\times10^{8}\,e^{-62.760/RT}\,(h^{-1})$ $K_{H_2} = 4.5\times10^{-4}\,e^{38.493/RT}\,(1/mol)$	
Wisniak and Simon	Reaction between atomically adsorbed hydrogen and adsorbed D-glucose	$r = \frac{kK_H C_G P_H}{(1 + K_S C_S + \sqrt{K_H P_H})^2}$		Valid for Raney Ni and Ru/C at pressures below 3.5–4.0 MPa
	Reaction between atomically chemisorbed hydrogen and adsorbed D-glucose	$r = \frac{kK_H K_G C_G P_H}{(1 + K_G C_G + K_S C_S + \sqrt{K_H P_H})^3}$		Valid for Ru/C at pressures high than 3.5–4.0 MPa
Turek et al.	Reaction between molecularly adsorbed hydrogen and adsorbed D-glucose taking place on different sites	$r = \frac{kK_{H_2}K_G C_{H_2} C_G}{(1 + K_{H_2}C_{H_2})(1 + K_G C_G)}$	$k = 1.62e^{-38.500/RT}\,(mol/gs)$ $K_{H_2} = 2.8e^{11798/RT}\,(1/mol)$ $K_G = 1.7e_{3850/RT}\,(1/mol)$	
Déchamp et al.	Reaction between molecularly adsorbed hydrogen and adsorbed D-glucose	$r = \frac{kK_G K_{H_2} C_G P_{H_2}}{(1 + K_G C_G + K_{H_2}P_{H_2})^2}$	At 403 K, k=497 mmol/(gNi h) K_G=0.87 (1/mol) K_{H2} = 0.07 MPa-^{1}	

Reprinted with permission from Ref. [108] Copyright 2003 by Elsevier

(2) competitive adsorption of molecular hydrogen and glucose, and Model (3) competitive adsorption of dissociatively chemisorbed hydrogen and glucose. They found that hydrogenation rate was first order with respect to H_2 pressure. But the reaction order with respect to glucose shifted from first order to zero order when the sugar concentrations increased from 0.3 mol/L to higher concentrations. The three models described the data satisfactorily. No inhibition by sorbitol or mannitol was observed. The activation energy of glucose hydrogenation over the Ru catalyst was 55 kJ/mol, which is well consistent with the values of ~60 kJ/mol in other studies [106, 108, 112]. Besides Ru catalysts, Ni catalysts are also extensively considered for glucose hydrogenation. The E_a values of glucose hydrogenation over Ni are determined to be in a range of 63–82 kJ/mol [106, 107, 111].

For the hydrolytic hydrogenation of saccharide oligomers, two competing pathways were found to occur concurrently. Negahdar et al. conducted a kinetic study of the catalytic conversion of cellobiose to sorbitol by using a binary catalyst of silicotungstic acid and Ru/AC [112]. As shown in Fig. 9.8, they found that the cellobiose hydrogenolysis either follows a first step of hydrolytic reaction (route I) to form glucose or a first step of hydrogenation (route II) to form 3-D-glucopyranosyl-D-glucitol (cellobitol), which is subsequently hydrolyzed to sorbitol and glucose. Which route is to be followed is determined by the reaction temperature. At a moderate temperature, e.g., 393 K, cellobitol is the main product with a maximum selectivity of 81 %. Conversely, at notably higher temperatures, the cellobitol selectivity decreased to 1 % but with sorbitol selectivity rising up to 75 %. The results were ascribed to the different activation energies of the two reactions. Kinetic modeling showed that the E_a for cellobiose hydrolysis was 115 kJ mol^{-1}, in contrast to 76 kJ mol^{-1} for cellobiose hydrogenation to cellobitol. The subsequent hydrolysis of cellobitol and hydrogenation of glucose had E_a values of 103 kJ mol^{-1} and 69 kJ mol^{-1}, respectively. Therefore, route II, i.e., direct hydrogenation, is more preferable at lower temperatures. In addition, the hydrolysis of cellobitol is slightly easier than the hydrolysis of cellobiose (E_a = 103 vs. 115 kJ mol^{-1}). If one extends this conclusion to the hydrolytic hydrogenation of cellulose, the direct hydrogenation of terminal sugars of cellulose macromolecules could promote cellulose degradation to some extent.

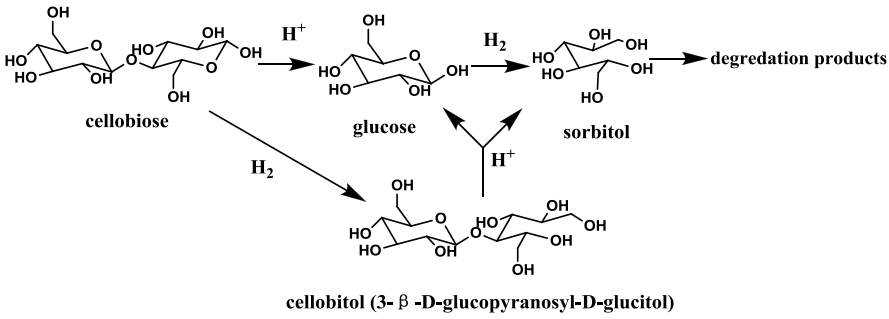

Fig. 9.8 Proposed reaction pathways for the conversion of cellobiose with silicotungstic acid and Ru/C (Reprinted with permission from Ref. [112]. Copyright 2014 by Elsevier Inc)

Taken all together, it is evident that the E_a of sugar hydrogenation is much lower than that of cellulose hydrolysis, and the reaction rate of the former is rather faster than that of cellulose hydrolysis. In particular over a solid catalyst, the rate of cellulose hydrolysis is further decreased by orders of magnitude. In addition, as mentioned above, the side reaction of sugar degradation has activation energy and reaction rate comparable to that of cellulose hydrolysis. Therefore, the rate of hexitols production in cellulose hydrogenolysis is dominantly determined by the low rate of cellulose hydrolysis. This makes it relatively easier to model the reaction kinetics and control the reaction selectivity as compared with the production of smaller C_2–C_3 polyols, which will be discussed in the following section.

9.3 Cellulose Hydrogenolysis to Ethylene Glycol and 1,2-Propylene Glycol

9.3.1 Catalysts and Reaction Mechanism

Ethylene glycol (EG) and 1,2-propylene glycol (1,2-PG) are the two most produced man-made polyols, with global production reaching more than 30 million tons per year. They are widely used for the synthesis of fibers, package articles, antifreeze agent, unsaturated resins, and other commodity chemicals. Currently, EG and 1,2-PG are dominantly synthesized from ethylene and propylene via an epoxidation and hydration process. Using biomass, in particular the nonedible, cellulosic materials are of great attractiveness to prepare EG and 1,2-PG because of many merits inherent in this process, such as the high value of products, large market demand, and the renewability of feedstock.

In the last decade, catalytic hydrogenolysis of cellulose to EG and 1,2-PG has made significant progresses. One of the representative works is the direct catalytic conversion of lignocellulose to ethylene glycol (DLEG), which was first disclosed by Zhang, Chen, and coworkers in 2008 [13]. The tungsten carbide catalysts were initially used to substitute noble metal catalysts for cellulose hydrogenolysis to hexitols. However, the dominant product over the carbide catalyst was unexpectedly EG, not the conventional hexitols. The EG yield was 27 % over a W_2C/AC catalyst and further improved to 61 % by introducing small amount of nickel to the tungsten carbide catalyst [13]. In the following years, higher EG yields up to 72–76 % were achieved by optimizing the preparation method of catalyst or using novel catalyst supports [15, 17, 23]. Besides tungsten carbides, the active components of catalysts were extended to tungsten phosphide [16], metallic tungsten-based binary catalysts [17, 113, 114], and tungsten oxide-based binary catalysts [26, 28, 115–118]. The cost of catalysts was greatly reduced due to the convenience in the preparation and the better reusability of catalysts without decay in the performance [28, 115]. The feedstock involved microcrystalline cellulose and raw biomass, in detail including corn stover [22], birch wood [24], miscanthus [119], concentrated glucose [116,

120], and Jerusalem artichoke [121]. The product distributions were tuned between EG, erythritol, and hexitols by varying the ratio of tungsten and hydrogenation metals [88]. Alternatively, the dominant product was altered from EG to 1,2-PG by changing the feedstock from glucose-based biomass to fructose-rich biomass such as Jerusalem artichoke [121]. On the basis of extensive studies, the reaction route and mechanism of this process were identified [17, 28, 29, 115, 122], and reaction kinetics are preliminarily modeled for the essential reactions [123–125]. All these progresses not only accumulate much valuable knowledge for academic interest but also provide a good foundation for the potential application of DLEG process in the future.

The reaction pathway and mechanism of DLEG are depicted in Fig. 9.9. Cellulose is first hydrolyzed into oligosaccharides and glucose by catalysis by Brønsted acids generated in subcritical hot water and by acid sites provided by the catalyst. The resulting glucose undergoes retro-aldol condensation (RAC) catalyzed by the tungsten species to form glycol aldehyde and eventually produce EG via hydrogenation over the metal sites of catalyst. The homogenous tungsten species (such as tungsten bronze H_xWO_3) are found to be uniquely active for the RAC reaction. Besides the major route for EG production, glucose isomerization happens in a minor route to form fructose, which produces 1,2-PG after a series of reactions involving RAC reaction, dehydration, rearrangement, and hydrogenation. For instance, Liu et al. employed basic active carbon as a secondary catalyst to enhance the isomerization of glucose to fructose. As a result, the product distribution was dramatically changed with 1,2-PG selectivity overwhelming that of EG (30.7 % vs. 16.6 %) in the presence of an optimal catalyst (50 %WO_3/Al_2O_3 + C_{act}) [26].

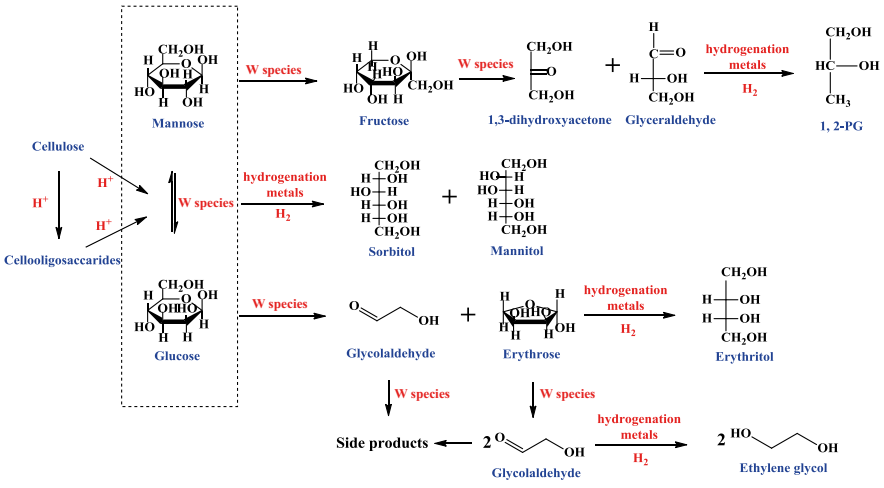

Fig. 9.9 The reaction network of cellulose hydrogenolysis in the presence of tungstenic binary catalysts (Reprinted with permission from Ref. [125] Copyright 2014 by the American Chemical Society)

In addition, and quite different from many previous studies in which hexitols were used as feedstock or reaction intermediates for the hydrogenolysis to form 1,2-PG and EG [55, 126–133], hexitols formation is competing with the glucose degradation in the DLEG process. The hexitols formed are found to be stable under the reaction conditions and cannot be further converted into EG and 1,2-PG [17, 115]. Accordingly, the balance between the rates of hydrogenation and RAC reaction of glucose largely determines the ratio of EG and hexitols yields [17, 29]. Apart from the activity for RAC reactions, the tungsten species can also play a role of heterogeneous acid sites for cellulose hydrolysis when they are highly dispersed on the alumina support and strongly interacting with it [26].

Besides tungstenic catalysts, some other effective binary catalysts have been developed for cellulose hydrogenolysis to EG and 1,2-PG. These catalysts include Ni/ZnO [134], Cu/CrO_x-$Ca(OH)_2$ [135], Pt–Sn/Al_2O_3 [136], Ni–La_2O_3 [32], Ru/C--NaOH [137], CuO/ZnO/Al_2O_3 [138], and Ru/$NbOPO_4$ [139]. With respect to the catalytic performance, they are generally less selective to the EG formation but give remarkably higher yields of 1,2-PG in contrast to the tungstenic catalysts.

Some of amphoteric oxide-supported transition metal catalysts were also effective for the cellulose hydrogenolysis to glycols. Liu et al. investigated the catalytic performance of Ni–Sn/Al_2O_3 in the conversion of cellulose and obtained 53.9 % selectivity to acetol (the precursor of 1,2-PG) over a catalyst with Sn/Ni ratio of 0.5 [140]. The authors proposed that the SnO_x domains catalyzed the isomerization of glucose to fructose and the C–C bond cleavage by retro-aldol condensation. In comparison with other basic sites of CeO_x, ZnO_x, and AlO_x supported on Al_2O_3, the SnO_x presented a larger concentration of stronger basic sites which facilitated the isomerization of glucose to fructose and its subsequent C–C bond cleavage. In a later study, the authors obtained hexitols and 1,2-PG from cellulose conversion by using a bimetallic catalyst of Pt–SnO_x/Al_2O_3 which had enhanced hydrogenation activity as compared to the previously employed Ni–Sn/Al_2O_3 [136].

In another instance, amphoteric ZnO was used as a support for Ni and Ni–Cu catalysts. The overall yield of glycols (including EG, 1,2-PG, and butanediols) reached ca. 70 % [134, 141]. The authors proposed that it is the basic sites but not the acidic sites on the support surface play a critical role for the activity and selectivity of the catalysts.

Cu–Cr catalysts in the presence of $Ca(OH)_2$ were studied for the production glycols, and 42.6 % yield of 1,2-PG and 31.6 % yield of EG were obtained with 10 % concentration of cellulose [135]. The reaction mechanism mainly involves hydrolytic hydrogenation of cellulose to hexitols and the subsequent hydrogenolysis of hexitols to 1,2-PG and EG. As shown in many other extensive studies, the basic sites and metallic dehydrogenation and hydrogenation sites play synergistic roles in polyol conversion to 1,2-PG and EG [55, 126–133].

As shown in Fig. 9.10, the first step of the reaction is sugar alcohol dehydrogenation over metallic sites to form glucose, fructose, and some other sugar isomers, followed by base-catalyzed retro-aldol condensation (RAC) to form glycolaldehyde and glyceraldehyde. After hydrogenation of the intermediates, EG, 1,2-PG, and glycerol are produced. The primary dehydrogenation step limits the rate of sugar

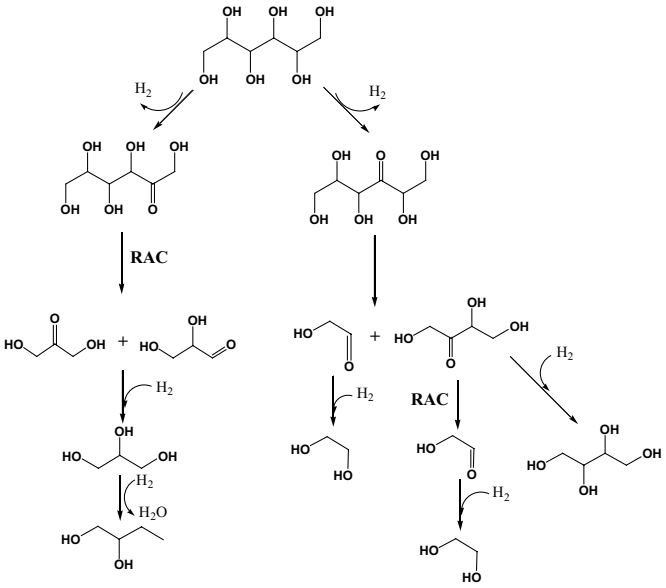

Fig. 9.10 Reaction pathways for sorbitol conversion to EG and 1,2-PG, RAC represents retro-aldol condensation (Reprinted with permission from Ref. [142] Copyright 2010 by the Elsevier)

alcohol hydrogenolysis, and the product distributions are determined by the competition between the hydrogenation steps and the RAC reaction [126]. Besides the RAC reaction accounting for the C–C bond breakage, Shanks et al. found that a decarbonylation reaction takes place and leads to the scission of the terminal C–C bond in polyol hydrogenolysis [143]. The reaction rates depended on the configuration of the polyol stereoisomers but not the carbon chain length. In addition, the primary hydroxyl groups of a polyol were more readily dehydrogenated than internal hydroxyl groups.

Different from the catalysts mentioned above, a La-based binary catalyst Ni–La_2O_3 presented versatile behaviors following a dual-route mechanism for EG production [32]. The main route is similar to that of tungsten-based catalysts, where cellulose is first hydrolyzed to glucose, followed by degradation to glycol aldehyde by the catalysis of La ions and hydrogenation over metallic Ni sites into EG. The other minor route is similar to that of the basic binary catalysts, such as Cu/CrOx-$Ca(OH)_2$, where glucose is first hydrogenated to hexitols and then hydrogenolyzed to 1,2-PG and EG. The theoretical calculation showed glucose was activated by La–OH species to form a mannose complex via an epimerization reaction. The C2–C3 bond in the sugar complex was then broken through a 2,3-hydride shift reaction to form glycol aldehyde, the precursor of EG. Comparative studies showed that the E_a for glucose degradation was lower than that for fructose, which could account for the higher yield of EG than 1,2-PG in the reaction. The catalyst was very efficient for cellulose hydrogenolysis even at a very low concentration of 0.2 mmol/L La (III). The highest combined yield of EG and 1,2-PG reached 63.7 %. The reaction mechanism is presented in Fig. 9.11.

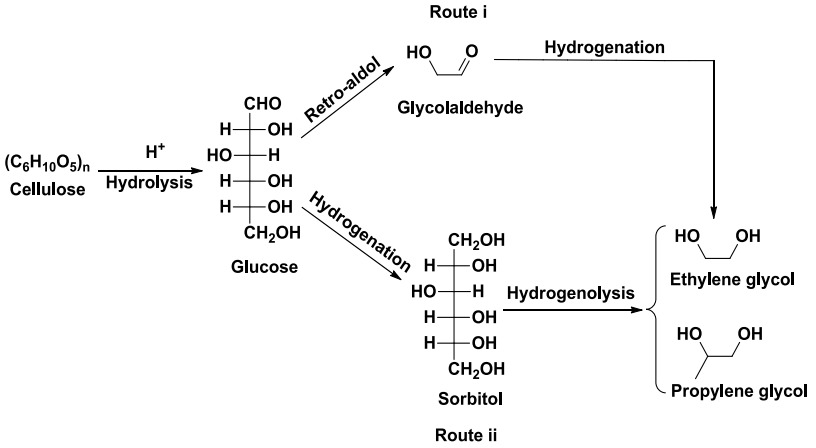

Fig. 9.11 Proposed reaction pathways for the conversion of cellulose to ethylene glycol and propylene glycol with the Ni-La(III) catalyst (Reprinted with permission from Ref. [32] Copyright 2014 by the American Chemical Society)

Besides cellulose hydrogenolysis in aqueous solution, Wang et al. reported their work using methanol as a solvent for cellulose hydrogenolysis [139]. The cellulose was converted to EG and ethylene glycol monoether (EGME) with an overall yield of 64 % over a Ru/$NbOPO_4$ catalyst. The methanol was found to not only serve as a solvent for the reaction but also participated in glucose acetalization so that the C=O bond was protected for the next step reaction. The $NbOPO_4$ promoted the cleavage of C–C bond in glucose, followed by hydrogenation by supported Ru particles to form the final EG-based products. In comparison with different dopants (W, Sn, Ni, Cu) in the catalyst, only the Ru–Ni/$NbOPO_4$ catalyst was effective due to the suppression of further hydrogenolysis of products (EG and EGME) to CO and alkanes.

Palkovits and coworkers investigated hydrolytic hydrogenation of cellulose over a CuO/ZnO/Al_2O_3 catalyst at 518 K and 50 bar H_2 and proposed a unified reaction mechanism according to the observed product distribution [144]. As shown in Fig. 9.12, there are many elementary transformations, including dehydration, dehydrogenation/hydrogenation, Lobry de Bruyn–van Ekenstein isomerization, and retro-aldol condensation, which play important roles in controlling the selectivity to simple polyols and carbohydrates. Besides the hydrolysis of glycosidic bond usually mentioned as the first step in the cellulose hydrogenolysis, an additional depolymerization mechanism involving only the reducing ends of cellulose and oligomers was proposed in this work. In this pathway, cellulose could directly release C_2 and C_4 molecules from the end of polysaccharides in the catalytic reaction. This is consistent with the results recently reported by Zhang and Wang [123]. They studied the cellobiose hydrogenolysis to EG with a tungstenic catalyst and found that cellobiose can be directly degraded to glycol aldehyde and glucosyl-erythrose via the RAC reaction prior to the hydrolysis to form glucose. But the activity of cellobiose in the RAC reaction is lower than that of glucose. In addition, the RAC reaction of cellobiose could promote the hydrolysis of cellobiose.

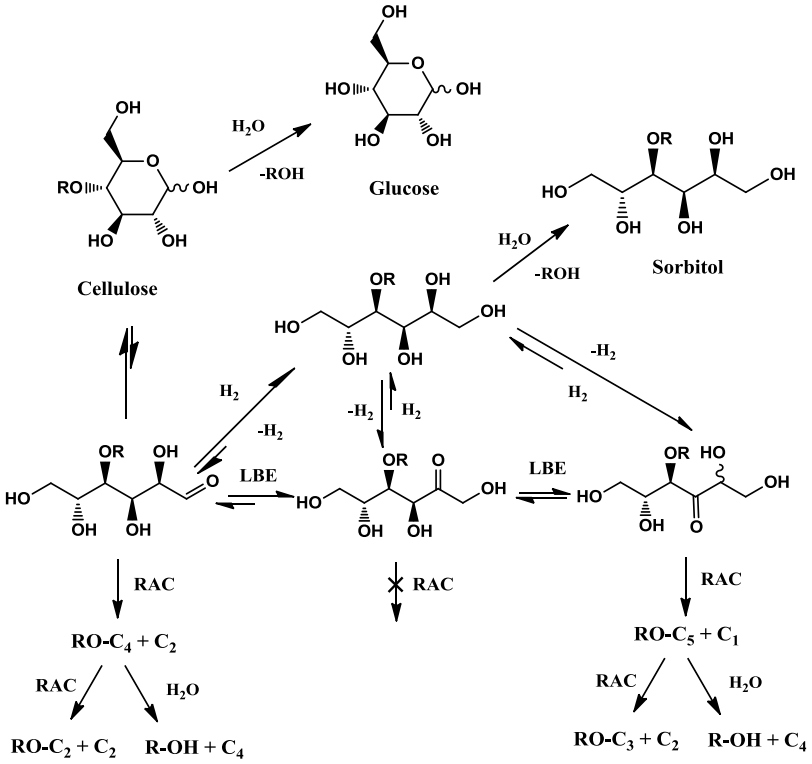

Fig. 9.12 Depolymerization and degradation pathways of terminal glucose units in cellulose, ROH = cellulose, LBE represents Lobry de Bruyn–van Ekenstein isomerization, and RAC represents retro-aldol condensation (Reprinted with permission from Ref. [144] Copyright 2014 by John Wiley & Sons Ltd)

In summary, regardless of whether the reactants of hydrogenolysis are sugar oligomers, polysaccharides, or sugar alcohols, the sugar formation is the critical step in most of the reaction mechanisms. The C–C bond breakage takes place mainly via retro-aldol condensation through catalysis by transition metal species or bases. In addition, the degradation to monosaccharides, i.e., the direct degradation of cellulose and oligosaccharides from the reducing end sugar, also contributes to the EG and 1,2-PG formation as well as cellulose degradation. However, the relative contributions from different routes are still uncertain due to the lack of reaction kinetic data for each route.

9.3.2 Reaction Kinetics

Extensive studies have been performed in developing novel catalysts and processes for cellulose hydrolytic hydrogenolysis to polyols. However, few of them focused on the essential reaction kinetics, in particular for the formation of C_2 and C_3

glycols. This might be related to higher difficulty of studying reaction kinetics of cellulose hydrogenolysis to EG and 1,2-PG as compared to that of cellulose degradation to glucose and hexitols. Not only are the reaction conditions for the former usually harsher than the latter, but also more reactions are involved in this process, including retro-aldol condensation, isomerization, epimerization, hydrogenation, and condensation catalyzed by multifunctional active components in the catalysts (Fig. 9.9). One feasible strategy to obtain in-depth knowledge of the reaction kinetics is studying each elementary transformation individually and then integrating them into complete reaction kinetics on the basis of their relationship. To this end, using model reactants to replace recalcitrant solid cellulose and conducting the reactions at moderate conditions are necessary to obtain useful information. Moreover, because of the complexity of the reaction system, establishing reasonable kinetic models and making suitable presumptions and omission are required for overcoming obstacles in arriving at meaningful results.

Zhang, Wang, and coworkers conducted detailed investigations on the reaction kinetics of cellulose hydrolytic hydrogenation to EG in the presence of tungsten-based binary catalysts. According to the reaction mechanism discussed above, they resolved the process of cellulose hydrogenolysis to EG into three consecutive reactions: (1) hydrolysis of cellulose to glucose, (2) retro-aldol condensation (RAC) of glucose to glycolaldehyde (GA), and (3) hydrogenation of GA to EG. As shown in Fig. 9.13, to simplify the reaction network, glucose was used as a substituted reactant for cellulose based on the consideration that glucose is the critical intermediate for the RAC reaction to form GA. Soluble ammonia metatungstate (AMT) was used as a homogeneous catalyst for the RAC reaction. Glucose isomerization reaction to fructose (accounting for 1,2-PG formation) was omitted according to the experi-

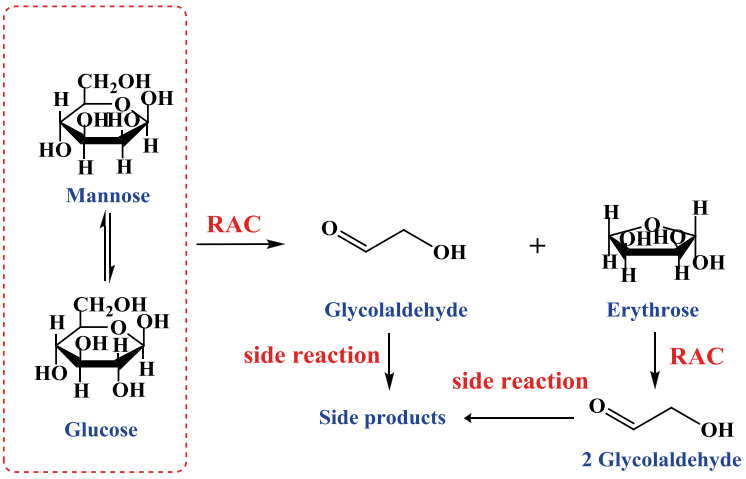

Fig. 9.13 The simplified kinetic model for glucose conversion to glycolaldehyde by catalysis of ammonium metatungstate. RAC refers to retro-aldol condensation (Reprinted with permission from Ref. [125]. Copyright 2014 by the American Chemical Society)

mental results that the ratio of EG to 1,2-PG yields is very high (10:1–20:1) in the reaction. The reactions were conducted at milder temperatures of 423–503 K so that the reactant and products could be quantified more accurately.

The Arrhenius equation obtained for the RAC reaction shows that it is a first-order reaction with respect to glucose. The activation energy E_a for the RAC reaction is in the range of 141.3–148.8 kJ/mol, which is much higher than that of the sugar hydrogenation [116, 125]. This indicates that RAC is much more sensitive to the reaction temperature as compared to the sugar hydrogenation [115]. A high temperature would favor GA and EG formation. The pre-exponential coefficient was found to be as high as 5.39×10^{13}, which is in good agreement with the features of a homogeneous catalytic reaction. Interestingly, the reaction order with respect to the concentration of AMT is 0.257 for the RAC reaction. This indicates that one AMT molecule might complex four molecules of glucose. At present, no characterization technique is available to identify the coordination numbers of tungsten in the sugar complex in the hot and compressed aqueous environment. Thus, the result of this kinetic study provides a valuable clue for the deeper investigations on the tungsten–sugar interactions with development of in situ measurement techniques in the future.

As the precursor of EG, GA readily undergoes side reactions, typically condensations, with a low E_a of 52.7 kJ/mol and at reaction orders of 2–2.5 [116, 124]. This suggests that it is important to keep the GA concentration at a low level during the reaction so that EG can be obtained with high selectivity. Employing a semicontinuous reaction system has been proven to be a feasible way in practice, as shown in the studies of high concentration glucose conversion to EG [116, 120].

The catalytic behavior of metastable reaction intermediates was also tentatively analyzed in the kinetic study. In detail, the RAC reaction of glucose forms an equimolar amount of GA and erythrose, and the latter can be further degraded into two molecules of GA. Zhang and coworkers deduced the E_a value of the erythrose RAC reaction by decoupling the dual reactions in the kinetic model equations. The obtained E_a was 79.9 kJ/mol, notably lower than that of glucose RAC reaction (141.3 kJ/mol). This indicates that the C_4 sugar is more reactive than glucose in the RAC reaction, which accounts for the experimental result that only a small amount of C_4 polyols was formed in the reaction.

As for the kinetics study of GA hydrogenation to EG, Zhang and coworkers employed a Langmuir–Hinshelwood–Hougen–Watson (LHHW) model, which has been popularly accepted in the kinetic study of sugar hydrogenation over heterogeneous catalysts [106–108]. As elucidated in the reaction network (Fig. 9.9), the GA formation from glucose confronts a competitive reaction of glucose hydrogenation, which generates chemically stable hexitols at the expense of GA and EG production. Tables 9.3, 9.4, and 9.5 list the results of the kinetic studies. It was found that the E_a values for GA and glucose hydrogenation are very similar (42.6 kJ/mol vs. 49.6 kJ/mol) over the Ru/AC catalyst. However, a detailed study disclosed that GA hydrogenation is still much favored over glucose hydrogenation due to several aspects. First, the adsorption equilibrium constant of GA (K_{GA}) is twice as large as that of glucose (K_G), suggesting that GA molecules are preferentially adsorbed on

Table 9.3 Modeling results for individual hydrogenation of glucose and glycolaldehyde over Ru/C in the absence of ammonium metatungstate

Model equation	Parameter	Estimated values			
		373 K	383 K	393 K	403 K
$r_G = k_G \frac{K_H P_H K_G C_G}{(1+K_G C_G)}$	$\boldsymbol{k_G K_H}$(mol/g_{cat}bar s)	1.01E-06	1.54E-06	2.28E-06	3.33E-06
	$\boldsymbol{K_G}$(m^3/mol)	3.19E-01	2.78E-01	2.43E-01	2.15E-01
$r_{GA} = k_{GA} \frac{K_H P_H K_{GA} C_{GA}}{(1+K_{GA} C_{GA})}$	$\boldsymbol{k_{GA} K_H}$(mol/g_{cat}bar s)	2.20E-06	3.14E-06	4.42E-06	6.11E-06
	$\boldsymbol{K_{GA}}$(m^3/mol)	6.32E-01	5.79E-01	5.33E-01	4.93E-01

Reprinted with permission from Ref. [124] Copyright 2015 by the American Chemical Society

the Ru surface than glucose. Second, the rate constant of GA hydrogenation (k_{GA}) is also twice as that of glucose (k_G). Taken together, the rate of GA hydrogenation is therefore ca. four times faster than that of the glucose hydrogenation. Moreover, experimental results for the competitive hydrogenation of GA and glucose showed that the presence of GA significantly inhibited glucose hydrogenation. Glucose hydrogenation only starts to occur when GA has been almost consumed in the reaction.

Another important finding in the kinetics study is that tungsten species not only take charge of the catalysis of the RAC reaction to form GA but also impose a remarkable inhibitive effect on hydrogenation reactions over metallic Ru sites. Tungsten species strongly adsorbed on the Ru surface and poisoned the catalyst for hydrogenation, but the effect varies with reactants. The reaction order of AMT was −0.238 for GA hydrogenation and −0.691 for glucose hydrogenation, respectively. This indicates that the inhibitive effect of AMT is much more pronounced for glucose hydrogenation than GA hydrogenation. In other words, the presence of AMT further improves the priority of GA hydrogenation over glucose hydrogenation and ensures the high selectivity to EG in the reaction.

In conclusion, the reaction kinetics of the one-pot hydrogenolysis of cellulose to EG have been primarily identified by studying the kinetics of glucose conversion. Except for the first step of cellulose hydrolysis, the reaction kinetics were systematically investigated for the essentially important elemental reactions, including the RAC reaction, hydrogenation, and the side reaction of GA condensation. A series of reaction kinetics data have been obtained on the basis of the deep understanding of the reaction mechanism, rational models, and kinetics. The reaction behaviors of cellulose and sugars can be qualitatively explained or partially quantitatively predicted in terms of the kinetic results. These studies will provide valuable guidance for the design of more effective catalysts and catalytic processes with better controlled reaction selectivity.

Table 9.4 Modeling results of glucose hydrogenation over Ru/C in the presence of ammonium metatungstate

Model equation	T (K)	Parameters				
		$k_G K_H$ (mol/g_{cat} bar s)	K_G (m^3/mol)	$K_{G\text{-}AMT}$ (m^3/mol)^5	K_{AMT} (m^3/mol)	R^2
$r_{G?AMT} = k_G \frac{K_H P_H (K_{G?AMT} C_{AMT} C_G{}^4 + K_G C_G)}{1 + K_{G?AMT} C_{AMT} C_G{}^4 + K_G C_G + K_{AMT} C_{AMT}}$	373	1.01E-06	3.19E-01	4.52E-02	2.60E+02	0.977
	383	1.54E-06	2.78E-01	2.57E-02	2.39E+02	0.977
	393	2.28E-06	2.43E-01	1.50E-02	2.21E+02	0.974
	403	3.33E-06	2.15E-01	8.99E-03	2.05E+02	0.979

Reprinted with permission from Ref. [124] Copyright 2015 by the American Chemical Society

Table 9.5 Modeling results of glycolaldehyde hydrogenation over Ru/C in the presence of ammonium metatungstate

Model equation	T (K)	Parameters				
		$k_{GA}K_H$ (mol/g_{cat} bar s)	K_{GA} (m^3/mol)	$K_{GA\text{-}AMT}$ (m^3/mol)^2	K_{AMT} (m^3/mol)	R^2
$r_{GA?AMT} = k_{GA}\frac{K_H P_H (K_{GA?AMT}C_{AMT}C_{GA} + K_{GA}C_{GA})}{1 + K_{GA?AMT}C_{AMT}C_{GA} + K_{GA}C_{GA} + K_{AMT}C_{AMT}}$	373	2.20E-06	6.32E-01	1.92E+01	2.60E+02	0.972
	383	3.14E-06	5.79E-01	1.42E+01	2.39E+02	0.975
	393	4.42E-06	5.33E-01	1.07E+01	2.21E+02	0.979
	403	6.11E-06	4.93E-01	8.14	2.05E+02	0.971

9.4 Outlook

Catalytic hydrogenolysis of cellulose to polyols represents a green and promising process for the production of high-value commodity chemicals. In comparison with the traditional synthesis processes in petroleum industry, the biomass conversion possesses notable advantages, thanks to the renewability of feedstock, the high atom economy of the process, and the increasing economic viability conditioned by the rapid development of low-cost catalysts. After extensive investigations in the past decade, various effective catalysts have been developed and several different polyols have been obtained with high selectivity. The rules of "green chemistry" have been followed in designing the catalysts and exploring reaction processes for biomass conversion, as embodied by the convenience of reaction operation and smaller footprints of chemical processes in the environment. The reaction mechanisms for polyols formation are becoming deeply understood and some of reaction kinetics has been largely determined. However, because the cellulose hydrogenolysis is usually conducted in compressed hot water and high pressure H_2, the reaction conditions are still harsh and many reactions are coupled in one pot. This greatly increases the difficulty in in situ monitoring the reaction intermediates, probing the catalytic active sites, and disclosing the reaction mechanisms at molecular levels. Future development of characterization techniques such as NMR, FTIR, Raman spectra, and HPLC would provide powerful support for such studies. In addition, more attention should be paid to the kinetic study of raw biomass conversion, by which the influence of impurities in biomass can be concurrently considered for the purpose of practical applications. With more progress in the understanding of reaction mechanism and kinetics, the process of cellulose hydrogenolysis could be better utilized for polyol production and eventually contribute to a sustainable bio-economy.

References

1. Delidovich I, Leonhardb K, Palkovits R (2014) Cellulose and hemicellulose valorisation: an integrated challenge of catalysis and reaction engineering. Energy Environ Sci 7:2803–2830
2. Chatterjee C, Pong F, Sen A (2014) Chemical conversion pathways for carbohydrates. Green Chem 17(1):40–71
3. Liu X, Wang X, Yao S, Jiang Y, Guan J, Mu X (2014) Recent advances in the production of polyols from lignocellulosic biomass and biomass-derived compounds. RSC Adv 4:49501–49520
4. Ruppert AM, Weinberg K, Palkovits R (2012) Hydrogenolysis goes bio: from carbohydrates and sugar alcohols to platform chemicals. Angew Chem Int Ed 51(11):2564–2601
5. Gallezot P (2012) Conversion of biomass to selected chemical products. Chem Soc Rev 41(4):1538–1558
6. Climent MJ, Corma A, Iborra S (2011) Converting carbohydrates to bulk chemicals and fine chemicals over heterogeneous catalysts. Green Chem 13(3):520–540
7. Improvements in or relating to the manufacture of glycerol and glycols (1933). Du Pont Patent GB19330035971

8. Method of converting aliphatic polyhydric alcohols to alcohols of lower molecular weight (1937). Ass of American Soap And Glyce Patent GB19370003458
9. Fukuoka A, Dhepe PL (2006) Catalytic conversion of cellulose into sugar alcohols. Angew Chem Int Ed 45(31):5161–5163
10. Rinaldi R, Schüth F (2009) Design of solid catalysts for the conversion of biomass. Energy Environ Sci 2(6):610–626
11. Dhepe PL, Fukuoka A (2008) Cellulose conversion under heterogeneous catalysis. ChemSusChem 1(12):969–975
12. Luo C, Wang S, Liu H (2007) Cellulose conversion into polyols catalyzed by reversibly formed acids and supported ruthenium clusters in hot water. Angew Chem Int Ed 46(40):7636–7639
13. Ji N, Zhang T, Zheng M, Wang A, Wang H, Wang X, Chen JG (2008) Direct catalytic conversion of cellulose into ethylene glycol using nickel-promoted tungsten carbide catalysts. Angew Chem Int Ed 47(44):8510–8513
14. Ding L, Wang A, Zheng M, Zhang T (2010) Selective transformation of cellulose into sorbitol by using a bifunctional nickel phosphide catalyst. ChemSusChem 3(7):818–821
15. Zhang Y, Wang A, Zhang T (2010) A new 3D mesoporous carbon replicated from commercial silica as a catalyst support for direct conversion of cellulose into ethylene glycol. Chem Commun 46(6):862–864
16. Zhao G, Zheng M, Wang A, Zhang T (2010) Catalytic conversion of cellulose to ethylene glycol over tungsten phosphide catalysts. Chin J Catal 31(8):928–932
17. Zheng M, Wang A, Ji N, Pang J, Wang X, Zhang T (2010) Transition metal-tungsten bimetallic catalysts for the conversion of cellulose into ethylene glycol. ChemSusChem 3(1):63–66
18. Geboers J, Van de Vyver S, Carpentier K, Jacobs P, Sels B (2011) Hydrolytic hydrogenation of cellulose with hydrotreated caesium salts of heteropoly acids and Ru/C. Green Chem 13(8):2167–2174
19. Kobayashi H, Ito Y, Komanoya T, Hosaka Y, Dhepe PL, Kasai K, Hara K, Fukuoka A (2011) Synthesis of sugar alcohols by hydrolytic hydrogenation of cellulose over supported metal catalysts. Green Chem 13(2):326–333
20. Kobayashi H, Matsuhashi H, Komanoya T, Hara K, Fukuoka A (2011) Transfer hydrogenation of cellulose to sugar alcohols over supported ruthenium catalysts. Chem Commun 47(8):2366–2368
21. Liu M, Deng W, Zhang Q, Wang Y (2011) Polyoxometalate-supported ruthenium nanoparticles as bifunctional heterogeneous catalysts for the conversions of cellobiose and cellulose into sorbitol under mild conditions. Chem Commun 47(34):9717–9719
22. Pang J, Zheng M, Wang A, Zhang T (2011) Catalytic hydrogenation of corn stalk to ethylene glycol and 1,2-propylene glycol. Ind Eng Chem Res 50(11):6601–6608
23. Ji N, Zheng M, Wang A, Zhang T, Chen JG (2012) Nickel-promoted tungsten carbide catalysts for cellulose conversion: effect of preparation methods. ChemSusChem 5(5):939–944
24. Li C, Zheng M, Wang A, Zhang T (2012) One-pot catalytic hydrocracking of raw woody biomass into chemicals over supported carbide catalysts: simultaneous conversion of cellulose, hemicellulose and lignin. Energy Environ Sci 5(4):6383–6390
25. Liang G, Cheng H, Li W, He L, Yu Y, Zhao F (2012) Selective conversion of microcrystalline cellulose into hexitols on nickel particles encapsulated within ZSM-5 zeolite. Green Chem 14(8):2146–2149
26. Liu Y, Luo C, Liu H (2012) Tungsten trioxide promoted selective conversion of cellulose into propylene glycol and ethylene glycol on a ruthenium catalyst. Angew Chem Int Ed 51(13):3249–3253
27. Pang J, Wang A, Zheng M, Zhang Y, Huang Y, Chen X, Zhang T (2012) Catalytic conversion of cellulose to hexitols with mesoporous carbon supported Ni-based bimetallic catalysts. Green Chem 14(3):614–617
28. Tai Z, Zhang J, Wang A, Zheng M, Zhang T (2012) Temperature-controlled phase-transfer catalysis for ethylene glycol production from cellulose. Chem Commun 48(56):7052–7054

29. Wang A, Zhang T (2013) One-pot conversion of cellulose to ethylene glycol with multifunctional tungsten-based catalysts. Acc Chem Res 46(7):1377–1386
30. Zhang J, Li J, Wu S, Liu Y (2013) Advances in the catalytic production and utilization of sorbitol. Ind Eng Chem Res 52(34):11799–11815
31. Liu Q, Liao Y, Wang T, Cai C, Zhang Q, Tsubaki N, Ma L (2014) One-pot transformation of cellulose to sugar alcohols over acidic metal phosphates combined with Ru/C. Ind Eng Chem Res 53(32):12655–12664
32. Sun R, Wang T, Zheng M, Deng W, Pang J, Wang A, Wang X, Zhang T (2014) Versatile Nickel–Lanthanum(III) catalyst for direct conversion of cellulose to glycols. ACS Catal 5(2):874–883
33. Pang J, Zheng M, Sun R, Song L, Wang A, Wang X, Zhang T (2015) Catalytic conversion of cellulosic biomass to ethylene glycol: effects of inorganic impurities in biomass. Bioresour Technol 175:424–429
34. Deng W, Wang Y, Zhang Q, Wang Y (2012) Development of bifunctional catalysts for the conversions of cellulose or cellobiose into polyols and organic acids in water. Catal Surv Asia 16(2):91–105
35. Kobayashi H, Komanoya T, Hara K, Fukuoka A (2010) Water-tolerant mesoporous-carbon-supported ruthenium catalysts for the hydrolysis of cellulose to glucose. ChemSusChem 3(4):440–443
36. Komanoya T, Kobayashi H, Hara K, Chun WJ, Fukuoka A (2014) Kinetic study of catalytic conversion of cellulose to sugar alcohols under low-pressure hydrogen. ChemCatChem 6(1):230–236
37. Shrotri A, Tanksale A, Beltramini JN, Gurav H, Chilukuri SV (2012) Conversion of cellulose to polyols over promoted nickel catalysts. Catal Sci Technol 2(9):1852
38. Käldström M, Kumar N, Tenho M, Mokeev MV, Moskalenko YE, Murzin DY (2012) Catalytic transformations of birch kraft pulp. ACS Catal 2(7):1381–1393
39. Han JW, Lee H (2012) Direct conversion of cellulose into sorbitol using dual-functionalized catalysts in neutral aqueous solution. Catal Commun 19:115–118
40. Wu Z, Ge S, Ren C, Zhang M, Yip A, Xu C (2012) Selective conversion of cellulose into bulk chemicals over Brønsted acid-promoted ruthenium catalyst: one-pot vs. sequential process. Green Chem 14(12):3336–3343
41. Zhu W, Yang H, Chen J, Chen C, Guo L, Gan H, Zhao X, Hou Z (2014) Efficient hydrogenolysis of cellulose into sorbitol catalyzed by a bifunctional catalyst. Green Chem 16(3):1534–1542
42. Niu Y, Wang H, Zhu X, Song Z, Xie X, Liu X, Han J, Ge Q (2014) Ru supported on zirconia-modified SBA-15 for selective conversion of cellobiose to hexitols. Microporous Mesoporous Mater 198:215–222
43. Liao Y, Liu Q, Wang T, Long J, Ma L, Zhang Q (2014) Zirconium phosphate combined with Ru/C as a highly efficient catalyst for the direct transformation of cellulose to C6 alditols. Green Chem 16(6):3305–3312
44. Chen J, Wang S, Huang J, Chen L, Ma L, Huang X (2013) Conversion of cellulose and cellobiose into sorbitol catalyzed by ruthenium supported on a polyoxometalate/metal-organic framework hybrid. ChemSusChem 6(8):1545–1555
45. Xi J, Zhang Y, Xia Q, Liu X, Ren J, Lu G, Wang Y (2013) Direct conversion of cellulose into sorbitol with high yield by a novel mesoporous niobium phosphate supported Ruthenium bifunctional catalyst. Appl Catal A Gen 459:52–58
46. Roman-Leshkov Y, Moliner M, Labinger JA, Davis ME (2010) Mechanism of glucose isomerization using a solid Lewis acid catalyst in water. Angew Chem Int Ed 49(47):8954–8957
47. Van de Vyver S, Geboers J, Dusselier M, Schepers H, Vosch T, Zhang L, Van Tendeloo G, Jacobs PA, Sels BF (2010) Selective bifunctional catalytic conversion of cellulose over reshaped Ni particles at the tip of carbon nanofibers. ChemSusChem 3(6):698–701
48. Van de Vyver S, Geboers J, Schutyser W, Dusselier M, Eloy P, Dornez E, Seo JW, Courtin CM, Gaigneaux EM, Jacobs PA, Sels BF (2012) Tuning the acid/metal balance of carbon

nanofiber-supported nickel catalysts for hydrolytic hydrogenation of cellulose. ChemSusChem 5(8):1549–1558
49. Park DS, Yun D, Kim TY, Baek J, Yun YS, Yi J (2013) A mesoporous carbon-supported Pt nanocatalyst for the conversion of lignocellulose to sugar alcohols. ChemSusChem 6(12):2281–2289
50. Wang H, Zhu L, Peng S, Peng F, Yu H, Yang J (2012) High efficient conversion of cellulose to polyols with Ru/CNTs as catalyst. Renew Energy 37(1):192–196
51. Gazit OM, Katz A (2013) Understanding the role of defect sites in glucan hydrolysis on surfaces. J Am Chem Soc 135(11):4398–4402
52. Onda A, Ochi T, Yanagisawa K (2008) Selective hydrolysis of cellulose into glucose over solid acid catalysts. Green Chem 10(10):1033–1037
53. Suganuma S, Nakajima K, Kitano M, Yamaguchi D, Kato H, Hayashi S, Hara M (2008) Hydrolysis of cellulose by amorphous carbon bearing SO_3H, COOH, and OH groups. J Am Chem Soc 130(38):12787–12793
54. Pang J, Wang A, Zheng M, Zhang T (2010) Hydrolysis of cellulose into glucose over carbons sulfonated at elevated temperatures. Chem Commun 46(37):6935–6937
55. Liang G, He L, Cheng H, Li W, Li X, Zhang C, Yu Y, Zhao F (2014) The hydrogenation/dehydrogenation activity of supported Ni catalysts and their effect on hexitols selectivity in hydrolytic hydrogenation of cellulose. J Catal 309:468–476
56. Kobayashi H, Hosaka Y, Hara K, Feng B, Hirosaki Y, Fukuoka A (2014) Control of selectivity, activity and durability of simple supported nickel catalysts for hydrolytic hydrogenation of cellulose. Green Chem 16(2):637
57. Liang G, He L, Arai M, Zhao F (2014) The Pt-enriched PtNi alloy surface and its excellent catalytic performance in hydrolytic hydrogenation of cellulose. ChemSusChem 7(5):1415–1421
58. Yang P, Kobayashi H, Hara K, Fukuoka A (2012) Phase change of nickel phosphide catalysts in the conversion of cellulose into sorbitol. ChemSusChem 5(5):920–926
59. Rinaldi R, Schuth F (2009) Acid hydrolysis of cellulose as the entry point into biorefinery schemes. ChemSusChem 2(12):1096–1107
60. Rinaldi R, Palkovits R, Schüth F (2008) Depolymerization of cellulose using solid catalysts in Ionic Liquids. Angew Chem Int Ed 47(42):8047–8050
61. Cai H, Li C, Wang A, Xu G, Zhang T (2012) Zeolite-promoted hydrolysis of cellulose in ionic liquid, insight into the mutual behavior of zeolite, cellulose and ionic liquid. Appl Catal B Environ 123:333–338
62. Palkovits R, Tajvidi K, Ruppert AM, Procelewska J (2011) Heteropoly acids as efficient acid catalysts in the one-step conversion of cellulose to sugar alcohols. Chem Commun 47(1):576–578
63. Geboers J, Van de Vyver S, Carpentier K, de Blochouse K, Jacobs P, Sels B (2010) Efficient catalytic conversion of concentrated cellulose feeds to hexitols with heteropoly acids and Ru on carbon. Chem Commun 46(20):3577–3579
64. Palkovits R, Tajvidi K, Procelewska J, Rinaldi R, Ruppert A (2010) Hydrogenolysis of cellulose combining mineral acids and hydrogenation catalysts. Green Chem 12(6):972–978
65. Hilgert J, Meine N, Rinaldi R, Schüth F (2013) Mechanocatalytic depolymerization of cellulose combined with hydrogenolysis as a highly efficient pathway to sugar alcohols. Energy Environ Sci 6(1):92–96
66. Shrotri A, Kobayashi H, Tanksale A, Fukuoka A, Beltramini J (2014) Transfer hydrogenation of cellulose-based oligomers over carbon-supported Ruthenium catalyst in a fixed-bed reactor. ChemCatChem 6:1349–1356
67. Li J, Liu L, Liu Y, Li M, Zhu Y, Liu H, Kou Y, Zhang J, Han Y, Ma D (2014) Direct conversion of cellulose using carbon monoxide and water on a Pt–Mo_2C–C catalyst. Energy Environ Sci 7(1):393–398
68. Saeman JF (1945) Kinetics of wood saccharification hydrolysis of cellulose and decomposition of sugars in dilute acid at high temperature. Ind Eng Chem Res 37(1):43–52

69. Amarasekara AS, Wiredu B (2012) Aryl sulfonic acid catalyzed hydrolysis of cellulose in water. Appl Catal A Gen 417–418:259–262
70. Stephens CH, Whitmore PM, Morris HR, Bier ME (2008) Hydrolysis of the amorphous cellulose in cotton-based paper. Biomacromolecules 9:1093–1099
71. Tolonen LK, Zuckerstatter G, Penttila PA, Milacher W, Habicht W, Serimaa R, Kruse A, Sixta H (2011) Structural changes in microcrystalline cellulose in subcritical water treatment. Biomacromolecules 12(7):2544–2551
72. Adel AM, Abd El-Wahab ZH, Ibrahim AA, Al-Shemy MT (2010) Characterization of microcrystalline cellulose prepared from lignocellulosic materials. Part I. Acid catalyzed hydrolysis. Bioresour Technol 101(12):4446–4455
73. Al-Zuhair S (2008) The effect of crystallinity of cellulose on the rate of reducing sugars production by heterogeneous enzymatic hydrolysis. Bioresour Technol 99(10):4078–4085
74. Ni J, Wang H, Chen Y, She Z, Na H, Zhu J (2013) A novel facile two-step method for producing glucose from cellulose. Bioresour Technol 137:106–110
75. Sun Y, Cheng J (2002) Hydrolysis of lignocellulosic materials for ethanol production: a review. Bioresour Technol 83:1–11
76. Abdul KHP, Davoudpour Y, Islam MN, Mustapha A, Sudesh K, Dungani R, Jawaid M (2014) Production and modification of nanofibrillated cellulose using various mechanical processes: a review. Carbohydr Polym 99:649–665
77. Adel AM, Abd El-Wahab ZH, Ibrahim AA, Al-Shemy MT (2011) Characterization of microcrystalline cellulose prepared from lignocellulosic materials. Part II: Physicochemical properties. Carbohydr Polym 83(2):676–687
78. Guo J, Catchmark JM (2012) Surface area and porosity of acid hydrolyzed cellulose nanowhiskers and cellulose produced by Gluconacetobacter xylinus. Carbohydr Polym 87(2):1026–1037
79. Testova L, Nieminen K, Penttila PA, Serimaa R, Potthast A, Sixta H (2014) Cellulose degradation in alkaline media upon acidic pretreatment and stabilisation. Carbohydr Polym 100:185–194
80. Zhang J, Wu S, Li B, Zhang H (2012) Direct conversion of cellobiose into sorbitol and catalyst deactivation mechanism. Catal Commun 29:180–184
81. Gazit OM, Charmot A, Katz A (2011) Grafted cellulose strands on the surface of silica: effect of environment on reactivity. Chem Commun 47(1):376–378
82. Vilcocq L, Castilho PC, Carvalheiro F, Duarte LC (2014) Hydrolysis of oligosaccharides over solid acid catalysts: a review. ChemSusChem 7(4):1010–1019
83. Wuttke S, Negoi A, Gheorghe N, Kuncser V, Kemnitz E, Parvulescu V, Coman SM (2012) Sn-doped hydroxylated MgF(2) catalysts for the fast and selective saccharification of cellulose to glucose. ChemSusChem 5(9):1708–1711
84. Zakzeski J, Grisel RJ, Smit AT, Weckhuysen BM (2012) Solid acid-catalyzed cellulose hydrolysis monitored by in situ ATR-IR spectroscopy. ChemSusChem 5(2):430–437
85. Huang Y, Fu Y (2013) Hydrolysis of cellulose to glucose by solid acid catalysts. Green Chem 15(5):1095–1111
86. Kunov-Kruse AJ, Riisager A, Saravanamurugan S, Berg RW, Kristensen SB, Fehrmann R (2013) Revisiting the Brønsted acid catalysed hydrolysis kinetics of polymeric carbohydrates in ionic liquids by in situ ATR-FTIR spectroscopy. Green Chem 15(10):2843–2848
87. Mohd SZ, Yu Y, Wu H (2014) Insights into the primary decomposition mechanism of cellobiose under hydrothermal conditions. Ind Eng Chem Res 53(38):14607–14616
88. SriBala G, Vinu R (2014) Unified kinetic model for cellulose deconstruction via acid hydrolysis. Ind Eng Chem Res 53(21):8714–8725
89. Yu Y, Shafie ZM, Wu H (2013) Cellobiose decomposition in hot-compressed water: importance of isomerization reactions. Ind Eng Chem Res 52(47):17006–17014
90. Chundawat SP, Bellesia G, Uppugundla N, da Costa Sousa L, Gao D, Cheh AM, Agarwal UP, Bianchetti CM, Phillips GN Jr, Langan P, Balan V, Gnanakaran S, Dale BE (2011)

Restructuring the crystalline cellulose hydrogen bond network enhances its depolymerization rate. J Am Chem Soc 133(29):11163–11174
91. Cantero DA, Bermejo MD, Cocero MJ (2013) Kinetic analysis of cellulose depolymerization reactions in near critical water. J Supercrit Fluids 75:48–57
92. Rogalinski T, Ingram T, Brunner G (2008) Hydrolysis of lignocellulosic biomass in water under elevated temperatures and pressures. J Supercrit Fluids 47(1):54–63
93. Rogalinski T, Liu K, Albrecht T, Brunner G (2008) Hydrolysis kinetics of biopolymers in subcritical water. J Supercrit Fluids 46(3):335–341
94. Schacht C, Zetzl C, Brunner G (2008) From plant materials to ethanol by means of supercritical fluid technology. J Supercrit Fluids 46(3):299–321
95. Abdullah R, Ueda K, Saka S (2014) Hydrothermal decomposition of various crystalline celluloses as treated by semi-flow hot-compressed water. J Wood Sci 60(4):278–286
96. Higgins HG, Goldsmith V, McKenzie AW (1958) The reactivity of cellulose. IV. The activation energy for heterogeneous acid hydrolysis. J Polym Sci 32(124):247–252
97. Xu C, Pranovich A, Vahasalo L, Hemming J, Holmbom B, Schols HA, Willfor S (2008) Kinetics of acid hydrolysis of water-soluble spruce o-acetyl galactoglucomannans. J Agric Food Chem 56(7):2429–2435
98. Carniti P, Gervasini A, Marzo M (2010) Silica-niobia oxides as viable acid catalysts in water: effective vs. intrinsic acidity. Catal Today 152(1–4):42–47
99. Lee YY, Iyer P, Torget RW (1999) Dilute-acid hydrolysis of lignocellulosic biomass. Adv Biochem Eng Biotechnol 65:93–115
100. Abatzoglou N, Bouchard J, Chornet E, Overend RP (1986) Dilute acid depolymerization of cellulose in aqueous phase: experimental. Can J Chem Eng 64(5):781–786
101. Vanoye L, Fanselow M, Holbrey JD, Atkins MP, Seddon KR (2009) Kinetic model for the hydrolysis of lignocellulosic biomass in the ionic liquid, 1-ethyl-3-methyl-imidazolium chloride. Green Chem 11(3):390–396
102. Rinaldi R, Meine N, vom Stein J, Palkovits R, Schüth F (2010) Which controls the depolymerization of cellulose in ionic liquids: the solid acid catalyst or cellulose? ChemSusChem 3(2):266–276
103. Shuai L, Pan X (2012) Hydrolysis of cellulose by cellulase-mimetic solid catalyst. Energy Environ Sci 5(5):6889–6894
104. Kitano M, Yamaguchi D, Suganuma S, Nakajima K, Kato H, Hayashi S, Hara M (2009) Adsorption-enhanced hydrolysis of beta-1,4-Glucan on graphene-based amorphous carbon bearing SO_3H, COOH, and OH groups. Langmuir 25(9):5068–5075
105. Gallezot P, Nicolaus N, Fleche G, Fuertes P, Perrard A (1998) Glucose hydrogenation on ruthenium catalysts in a trickle-bed reactor. J Catal 180:51–55
106. Wisniak J, Simon R (1979) Hydrogenation of glucose, fructose, and their mixtures. Ind Eng Chem Prod Res Dev 18(1):50–57
107. Brahme PH, Doralswamy LK (1976) Modelling of a slurry reaction. Hydrogenation of glucose on Raney nickel. Ind Eng Chem Process Des Dev 15(1):130–137
108. Crezee E, Hoffer BW, Berger RJ, Makkee M, Kapteijn F, Moulijn JA (2003) Three-phase hydrogenation of D-glucose over a carbon supported ruthenium catalyst—mass transfer and kinetics. Appl Catal A Gen 251(1):1–17
109. Hoffer B (2003) The role of the active phase of Raney-type Ni catalysts in the selective hydrogenation of D-glucose to D-sorbitol. Appl Catal A Gen 253(2):437–452
110. McManus JR, Salciccioli M, Yu W, Vlachos DG, Chen JG, Vohs JM (2012) Correlating the surface chemistry of C2 and C3 aldoses with a C6 sugar: reaction of glucose, glyceraldehyde, and glycolaldehyde on Pd(111). J Phys Chem C 116(35):18891–18898
111. Dechamp N, Gamez A, Perrard A, Gallezot P (1995) Kinetics of glucose hydrogenation in a trickle-bed reactor. Catal Today 24:29–34
112. Negahdar L, Oltmanns JU, Palkovits S, Palkovits R (2014) Kinetic investigation of the catalytic conversion of cellobiose to sorbitol. Appl Catal B Environ 147:677–683

113. You SJ, Baek IG, Park ED (2013) Hydrogenolysis of cellulose into polyols over Ni/W/SiO_2 catalysts. Appl Catal A Gen 466:161–168
114. Fabičovicová K, Malter O, Lucas M, Claus P (2014) Hydrogenolysis of cellulose to valuable chemicals over activated carbon supported mono- and bimetallic nickel/tungsten catalysts. Green Chem 16(7):3580–3588
115. Tai Z, Zhang J, Wang A, Pang J, Zheng M, Zhang T (2013) Catalytic conversion of cellulose to ethylene glycol over a low-cost binary catalyst of Raney Ni and tungstic acid. ChemSusChem 6(4):652–658
116. Zhao G, Zheng M, Zhang J, Wang A, Zhang T (2013) Catalytic conversion of concentrated glucose to ethylene glycol with semicontinuous reaction system. Ind Eng Chem Res 52(28):9566–9572
117. Cao Y, Wang J, Kang M, Zhu Y (2014) Efficient synthesis of ethylene glycol from cellulose over Ni–WO_3/SBA-15 catalysts. J Mol Catal A Chem 381:46–53
118. Chambon F, Rataboul F, Pinel C, Cabiac A, Guillon E, Essayem N (2013) Cellulose conversion with tungstated-alumina-based catalysts: influence of the presence of platinum and mechanistic studies. ChemSusChem 6(3):500–507
119. Pang J, Zheng M, Wang A, Sun R, Wang H, Jiang Y, Zhang T (2014) Catalytic conversion of concentrated miscanthus in water for ethylene glycol production. AlChE J 60(6):2254–2262
120. Ooms R, Dusselier M, Geboers JA, Beeck BO, Verhaeven R, Gobechiya E, Martens JA, Redl A, Sels BF (2014) Conversion of sugars to ethylene glycol with nickel tungsten carbide in a fed-batch reactor: high productivity and reaction network elucidation. Green Chem 16(2):695–707
121. Zhou L, Wang A, Li C, Zheng M, Zhang T (2012) Selective production of 1,2-propylene glycol from Jerusalem artichoke tuber using Ni-W_2C/AC catalysts. ChemSusChem 5(5):932–938
122. Zheng M, Pang J, Wang A, Zhang T (2014) One-pot catalytic conversion of cellulose to ethylene glycol and other chemicals: from fundamental discovery to potential commercialization. Chin J Catal 35(5):602–613
123. Zhang J, Yang X, Hou B, Wang A, Li Z, Wang H, Zhang T (2014) Comparison of cellobiose and glucose transformation to ethylene glycol. Chin J Catal 35(11):1811–1817
124. Zhang J, Hou B, Wang A, Li Z, Wang H, Zhang T (2015) Kinetic study of the competitive hydrogenation of glycolaldehyde and glucose on Ru/C with or without AMT. AlChE J 61(1):224–238
125. Zhang J, Hou B, Wang A, Li Z, Wang H, Zhang T (2014) Kinetic study of retro-aldol condensation of glucose to glycolaldehyde with ammonium metatungstate as the catalyst. AlChE J 60(11):3804–3813
126. Sun J, Liu H (2011) Selective hydrogenolysis of biomass-derived xylitol to ethylene glycol and propylene glycol on supported Ru catalysts. Green Chem 13(1):135–142
127. Zhang J, Lu F, Yu W, Chen J, Chen S, Gao J, Xu J (2014) Selective hydrogenative cleavage of C–C bonds in sorbitol using Ni–Re/C catalyst under nitrogen atmosphere. Catal Today 234:107–112
128. Xiao Z, Jin S, Sha G, Williams CT, Liang C (2014) Two-step conversion of biomass-derived glucose with high concentration over Cu–Cr catalysts. Ind Eng Chem Res 53(21):8735–8743
129. Huang Z, Chen J, Jia Y, Liu H, Xia C, Liu H (2014) Selective hydrogenolysis of xylitol to ethylene glycol and propylene glycol over copper catalysts. Appl Catal B Environ 147:377–386
130. Soták T, Schmidt T, Hronec M (2013) Hydrogenolysis of polyalcohols in the presence of metal phosphide catalysts. Appl Catal A Gen 459:26–33
131. Jin X, Roy D, Thapa PS, Subramaniam B, Chaudhari RV (2013) Atom economical aqueous-phase conversion (APC) of biopolyols to lactic acid, glycols, and linear alcohols using supported metal catalysts. ACS Sustain Chem Eng 1(11):1453–1462

132. Ye L, Duan X, Lin H, Yuan Y (2012) Improved performance of magnetically recoverable Ce-promoted Ni/Al_2O_3 catalysts for aqueous-phase hydrogenolysis of sorbitol to glycols. Catal Today 183(1):65–71
133. Zhao L, Zhou J, Sui Z, Zhou X (2010) Hydrogenolysis of sorbitol to glycols over carbon nanofiber supported ruthenium catalyst. Chem Eng Sci 65(1):30–35
134. Wang X, Meng L, Wu F, Jiang Y, Wang L, Mu X (2012) Efficient conversion of microcrystalline cellulose to 1,2-alkanediols over supported Ni catalysts. Green Chem 14(3):758–765
135. Xiao Z, Jin S, Pang M, Liang C (2013) Conversion of highly concentrated cellulose to 1,2-propanediol and ethylene glycol over highly efficient Cu–Cr catalysts. Green Chem 15(4):891–895
136. Deng T, Liu H (2013) Promoting effect of SnOx on selective conversion of cellulose to polyols over bimetallic Pt–SnOx/Al_2O_3 catalysts. Green Chem 15(1):116–124
137. Liu M, Wang H, Han J, Niu Y (2012) Enhanced hydrogenolysis conversion of cellulose to C2-C3 polyols via alkaline pretreatment. Carbohydr Polym 89(2):607–612
138. Tajvidi K, Pupovac K, Kukrek M, Palkovits R (2012) Copper-based catalysts for efficient valorization of cellulose. ChemSusChem 5(11):2139–2142
139. Xi J, Ding D, Shao Y, Liu X, Lu G, Wang Y (2014) Production of ethylene glycol and its monoether derivative from cellulose. ACS Sustain Chem Eng 2(10):2355–2362
140. Deng T, Liu H (2014) Direct conversion of cellulose into acetol on bimetallic Ni-SnOx/Al_2O_3 catalysts. J Mol Catal A Chem 388–389:66–73
141. Wang X, Wu F, Yao S, Jiang Y, Guan J, Mu X (2012) Ni–Cu/ZnO-catalyzed hydrogenolysis of cellulose for the production of 1,2-alkanediols in hot compressed water. Chem Lett 41(5):476–478
142. Li N, Huber GW (2010) Aqueous-phase hydrodeoxygenation of sorbitol with Pt/SiO_2-Al_2O_3: identification of reaction intermediates. J Catal 270(1):48–59
143. Deutsch KL, Lahr DG, Shanks BH (2012) Probing the ruthenium-catalyzed higher polyol hydrogenolysis reaction through the use of stereoisomers. Green Chem 14(6):1635–1642
144. Tajvidi K, Hausoul PJ, Palkovits R (2014) Hydrogenolysis of cellulose over Cu-based catalysts-analysis of the reaction network. ChemSusChem 7(5):1311–1317